

TID-24342

# EVALUATION OF EXPERIMENTAL AND THEORETICAL DATA ON RADIAL NOZZLES IN PRESSURE VESSELS

FACILITY FORM 602

**N 68-30578**  
(ACCESSION NUMBER)

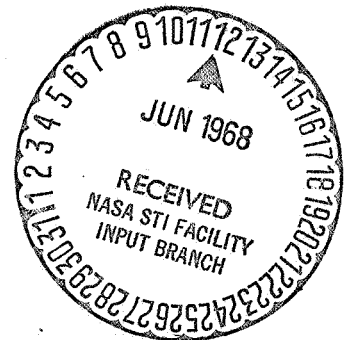
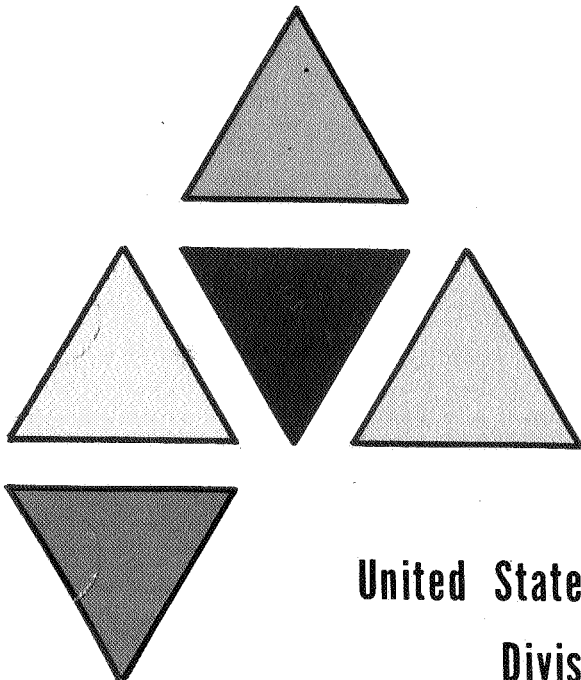
**239**  
(PAGES)

**CR-95896**  
(NASA CR OR TMX OR AD NUMBER)

**1**  
(THRU)

**32**  
(CODE)

**32**  
(CATEGORY)



United States Atomic Energy Commission  
Division of Technical Information

## LEGAL NOTICE

This report was prepared as an account of Government sponsored work. Neither the United States, nor the Commission, nor any person acting on behalf of the Commission:

A. Makes any warranty or representation, expressed or implied, with respect to the accuracy, completeness, or usefulness of the information contained in this report, or that the use of any information, apparatus, method, or process disclosed in this report may not infringe privately owned rights; or

B. Assumes any liabilities with respect to the use of, or for damages resulting from the use of any information, apparatus, method, or process disclosed in this report.

As used in the above, "person acting on behalf of the Commission" includes any employee or contractor of the Commission, or employee of such contractor, to the extent that such employee or contractor of the Commission, or employee of such contractor prepares, disseminates, or provides access to, any information pursuant to his employment or contract with the Commission, or his employment with such contractor.

This report has been reproduced directly from the best available copy.

Printed in USA. Price \$3.00. Available from the Clearinghouse for Federal Scientific and Technical Information, National Bureau of Standards, U. S. Department of Commerce, Springfield, Virginia 22151.

EVALUATION OF  
EXPERIMENTAL AND THEORETICAL DATA ON RADIAL NOZZLES  
IN PRESSURE VESSELS

by

E. C. Rodabaugh<sup>(1)</sup>

T. J. Atterbury<sup>(1)</sup>

R. L. Cloud<sup>(2)</sup>

F. J. Witt<sup>(3)</sup>

to

UNITED STATES ATOMIC ENERGY COMMISSION

Battelle Memorial Institute, Columbus, Ohio

Contract No. W-7405-eng-92, Task 16

(1) Battelle Memorial Institute, Columbus, Ohio

(2) Westinghouse Electric Corp., Bettis Atomic Power Lab., Pittsburgh Pa.

(3) Oak Ridge National Laboratory, Oak Ridge, Tenn.

## ACKNOWLEDGEMENTS

Preparation of this report was sponsored by the United States Atomic Energy Commission, Battelle Contract No. W-7405-eng-92, Task 16. Major financial contributions to development of theoretical and experimental work used in the report were made by the American Gas Association, U. S. Atomic Energy Commission, U. S. Navy, National Aeronautics and Space Administration, and the Pressure Vessel Research Committee.

Technical guidance and reviews were provided by a Steering Task Group of the Pressure Vessel Research Committee, Subcommittee on Reinforced Openings and External Loadings. This group consisted of J. L. Mershon (Chairman), W. E. Cooper, J. R. Farr, B. L. Greenstreet, B. F. Langer, and E. O. Waters. Major contributions to experimental data were developed by S. C. Grigory, D. E. Hardenbergh, N. C. Lind, M. M. Leven, A. G. Pickett, W. F. Riley and C. E. Taylor; major contributions to theoretical data were made by A. C. Eringen, S. E. Moore and E. O. Waters. The contributions of those listed, as well as the many other contributions indicated by the references in the report, are gratefully acknowledged. The authors also wish to express their appreciation for computer program results furnished by Oak Ridge National Laboratory and by Westinghouse Electric Co., Bettis Atomic Power Laboratory.

## ABSTRACT

The six sections of this Report were originally issued as six phase reports. the first three (Sections 1, 2, and 3) are on nozzles in spherical shells. the last three (Sections 4, 5, and 6) are on nozzles in cylindrical shells.

Sections 1 and 4 contain proposed design procedures for nozzles with internal pressure loading. The procedures are relatively concise, being contained on pp. 3, 4, and 5 of Section 1, pp. 6, 7, and 8 of Section 4. The remainder of these two sections contains a brief description of the development of the design procedures and comparisons with other design procedures.

Sections 2 and 5 cover external loadings as well as internal pressure. Comparisons are made between a number of theories and between those theories and test data. Section 2 includes an Appendix giving graphs for obtaining stresses for nozzles in spherical shells due to internal pressure, external loads or combinations thereof. Section 5 includes an Appendix giving tables of stresses for nozzles in cylindrical shells due to internal pressure loading.

Sections 3 and 6 cover the subject of flexibility of nozzles in pressure vessels. The flexibility of the nozzle is significant where the nozzle is attached to a piping system and the external loads on the nozzle arise from piping expansion.

## TABLE OF CONTENTS

(Tables of Contents for each Section are given at the beginning of each Section.)

### Section 1

Proposed Reinforcement Design Procedure for Radial Nozzles in Spherical Shells  
with Internal Pressure

### Section 2

Stresses at Nozzles in Spherical Shells Loaded with Pressure, Moment or Thrust

### Section 3

Flexibility of Nozzles in Spherical Shells

### Section 4

Proposed Reinforcement Design Procedure for Radial Nozzles in Cylindrical  
Shells with Internal Pressure

### Section 5

Stresses at Nozzles in Cylindrical Shells Loaded with Pressure, Moment or Thrust.

### Section 6

Flexibility of Nozzles in Cylindrical Shells

PHASE REPORT NO. 1

on

PROPOSED REINFORCEMENT DESIGN PROCEDURE  
FOR RADIAL NOZZLES IN SPHERICAL  
SHELLS WITH INTERNAL PRESSURE

March 31, 1966

to

UNITED STATES ATOMIC ENERGY COMMISSION

by

R. L. Cloud  
(Westinghouse Electric Corporation,  
Bettis Atomic Power Laboratory  
Pittsburgh, Pennsylvania)

and

E. C. Rodabaugh  
(Battelle Memorial Institute  
Columbus, Ohio  
Battelle Contract No. W-7405-eng-92)

### DISCLAIMER

The work covered by this report was sponsored under contract with the Atomic Energy Commission in cooperation with the Pressure Vessel Research Committee. Although this report is intended to be the first of a series of reports summarizing the results of PVRC research on reinforced openings, it is issued at this time primarily for informational purposes, indicating current thinking concerning development of design procedures for reinforced openings. It has not yet been approved for publication by PVRC, nor has it been submitted for review and consideration by ASME Code Groups. Therefore, it should be understood that it has no status whatever insofar as the ASME Code is concerned.



TABLE OF CONTENTS

	<u>Page</u>
INTRODUCTION . . . . .	1
DESIGN PROCEDURE FOR RADIAL NOZZLES IN SPHERICAL SHELLS UNDER INTERNAL PRESSURE . . . . .	3
DESIGN CRITERIA . . . . .	6
DEVELOPMENT OF DESIGN PROCEDURE . . . . .	8
Uniform Wall Designs . . . . .	10
Inwardly Protruding Nozzles . . . . .	16
Compact Reinforcing . . . . .	16
Radii and Transition Sections . . . . .	17
DISCUSSION . . . . .	18
Uniform Wall Reinforcing . . . . .	18
Basic Elastic Analysis . . . . .	18
Lengths of Uniform Thickness Reinforcing . . . . .	19
Reinforcing on Nozzle and Shell . . . . .	22
Limit Pressure Analysis . . . . .	22
Inwardly Protruding Nozzles . . . . .	26
Compact Reinforcing . . . . .	26
Elastic Analysis and Test Data . . . . .	26
Area and Boundary for Compact Reinforcing . . . . .	29
Radii and Transition Sections . . . . .	34
COMPARISON WITH OTHER DESIGN PROCEDURES . . . . .	41
Current American Practice . . . . .	41
Leckie and Penny Analysis . . . . .	45
German Practice . . . . .	45
REFERENCES . . . . .	52

LIST OF FIGURES

	<u>Page</u>
FIGURE 1. REINFORCED NOZZLES DETAILS. . . . .	4
FIGURE 2. GRAPHS FOR OBTAINING g- AND h- FACTORS. . . . .	5
FIGURE 3. BASIC NOZZLE-TO-SPHERE CONFIGURATION. . . . .	9
FIGURE 4. REQUIRED REINFORCING ON SPHERE FOR $\bar{\sigma} = 3S$ , WATERS' ANALYSIS. . . . .	11
FIGURE 5. REQUIRED REINFORCING ON NOZZLE FOR $\bar{\sigma} = 3S$ , WATERS' ANALYSIS. . . . .	12
FIGURE 6. REQUIRED REINFORCING ON SPHERE BY LIMIT ANALYSIS. . . . .	14
FIGURE 7. REQUIRED REINFORCING ON NOZZLE BY LIMIT ANALYSIS. . . . .	15
FIGURE 8. COMPARISON OF REINFORCING ON SPHERE FOR $\bar{\sigma}_m = 1.5S$ WITH LIMIT PRESSURE ANALYSIS. . . . .	24
FIGURE 9. COMPARISON OF REINFORCING ON NOZZLE FOR $\bar{\sigma}_m = 1.5S$ WITH LIMIT PRESSURE ANALYSIS. . . . .	25
FIGURE 10. COMPARISON OF FLUSH WITH INWARDLY PROTRUDING NOZZLES, LECKIE-PENNY ANALYSIS AT $\sigma = 2.25S$ . . . . .	27
FIGURE 11. FILLET RADIUS REINFORCING AREA REQUIRED BY ELASTIC ANALYSIS, $\bar{\sigma} = 2.0S$ . . . . .	30
FIGURE 12. REINFORCING REQUIRED TO OBTAIN AN AVERAGE NORMAL STRESS EQUAL TO $1.0S$ . . . . .	31
FIGURE 13. REINFORCING AREAS FOR REINFORCING ON THE SPHERE AND COMPACT REINFORCING. . . . .	32
FIGURE 14. REINFORCING AREAS FOR REINFORCING ON THE NOZZLE AND COMPACT REINFORCING . . . . .	33
FIGURE 15. REINFORCING LENGTHS FOR UNIFORM WALL AND COMPACT REINFORCING . . . . .	35
FIGURE 16. SPACE AVAILABLE FOR COMPACT REINFORCING . . . . .	36
FIGURE 17. COMPARISON OF COMPACT REINFORCING AREA REQUIRED BY PROPOSED RULES WITH THE REINFORCING AREA FOR A FILLET RADIUS, ELASTIC ANALYSIS, $\bar{\sigma} = 2.0S$ . . . . .	37

LIST OF FIGURES (contd)

	<u>Page</u>
FIGURE 18. EXAMPLE OF VARIATION IN STRESS WITH NOZZLE THICKNESS. . . . .	39
FIGURE 19. REINFORCEMENT ZONE, CURRENT AMERICAN PRACTICE EXCEPT THE ASME NUCLEAR VESSEL CODE . . . . .	42
FIGURE 20. REINFORCEMENT ZONE, ASME NUCLEAR VESSEL CODE. . . . .	43
FIGURE 21. NOZZLES NOT REQUIRING REINFORCING IN ACCORDANCE WITH THE ASME NUCLEAR VESSEL CODE . . . . .	44
FIGURE 22. COMPARISON OF REINFORCEMENT ZONES . . . . .	46
FIGURE 23. SHELL REINFORCING AS REQUIRED BY LECKIE-PENNY ANALYSIS WITH A MAXIMUM STRESS IN THE SPHERE OF 2.25S. . . . .	47
FIGURE 24. NOZZLE REINFORCING AS REQUIRED BY LECKIE-PENNY ANALYSIS WITH A MAXIMUM STRESS IN THE SPHERE OF 2.25S. . . . .	48
FIGURE 25. SHELL REINFORCING AS REQUIRED BY GERMAN PRACTICE, DESIGN CRITERIA OF 0.2% MAXIMUM STRAIN. . . . .	50
FIGURE 26. NOZZLE REINFORCING AS REQUIRED BY GERMAN PRACTICE, DESIGN CRITERIA OF 0.2% MAXIMUM STRAIN. . . . .	51

PROPOSED DESIGN PROCEDURE FOR RADIAL  
NOZZLES IN SPHERICAL SHELLS WITH INTERNAL PRESSURE

INTRODUCTION

In the past, openings in pressure vessels have been reinforced according to the area replacement rule. Vessels so designed have, by and large, performed satisfactorily; however, in the relatively few cases where problems have developed in pressure vessels, those problems have often been associated with the nozzles or openings. Prior to the work of the past few years, the stress levels, fatigue loading resistance, and maximum pressure capacities of nozzles in pressure vessels were known only very roughly.

The trend towards the use of higher strength materials and higher nominal stresses in pressure vessel design, along with the advent of nuclear vessels with their very high reliability requirements, intensified the need for better knowledge of the behavior of reinforced openings in pressure vessels. In recognition of this need, the Sub-committee on Reinforced Openings of the Pressure Vessel Research Committee has sponsored a broad program of both experimental and analytical work directed towards the determination of the behavior of reinforced openings in pressure vessels, considering both the effects of internal pressure and external loads. A summary of this work, as of the time of publication, is given by J. L. Mershon<sup>(1,2)\*</sup>.

This report covers one phase of the overall problem of reinforced openings in pressure vessels; specifically, the development of a design procedure for radial nozzles in spherical shells loaded with internal pressure. The design procedure is intended to define acceptable reinforcing details for radial nozzles in spherical vessels, hemispherical heads, torispherical heads provided the opening is in the spherical section sufficiently away from the toroidal section, and ellipsoidal heads in the central section. Reinforcing, if any is required, is assumed to be continuous

---

\* Numbers refer to the list of references.

with the shells, as contrasted to "welded-on" pads. Since limit analysis is used to establish the design procedure, an implied assumption is that the material of the shells and the weld metal is ductile, e.g., is capable of withstanding several percent of local strain in a complex stress field at all temperatures at which the vessel may be loaded.

The design procedure covers isolated nozzles in which the edge of the opening is remote from any other significant local stress discontinuity. It is suggested that the design of closely spaced nozzles be guided by the existing rules given in the ASME Boiler and Pressure Vessel Code, Section III, ("Rules for the Construction of Nuclear Vessels").

The "Design Procedure", in a brief form suitable for use in design work, is presented in the following section. The remainder of the report provides the background and basis of the design procedure along with comparison with other design procedures.

It is emphasized that this design procedure covers internal pressure loading only, and that additions or modifications may be necessary to accommodate other super-imposed loadings; particularly, external loadings from an attached piping system and thermally induced stresses. The elastic stress criterion chosen (maximum stress intensity  $\leq 3S$ ) is the limit which, under the rules of the Nuclear Vessel Code, applies to the sum of the primary and secondary stresses, including pressure, thermal and external loading effects. Since the limit analysis criterion controls almost throughout the dimensional range covered herein, the design procedure inherently contains at least a small margin to accommodate stresses from such additional sources. This general problem will be the subject of further study and recommendations.

DESIGN PROCEDURE FOR RADIAL NOZZLES IN  
SPHERICAL SHELLS UNDER INTERNAL PRESSURE

1. Nozzles may be reinforced by increasing the thickness of the nozzle and/or sphere near the nozzle-to-sphere juncture according to Paragraph 3, or by applying extra material around the nozzle-to-sphere juncture according to Paragraph 4. These rules apply to isolated nozzles in which the edge of the opening is at least a distance equal to  $2.5 \sqrt{DT}/2$  from the nearest edge of any other local stress discontinuity.
2. Dimension T is the required\* thickness of the unperforated sphere for the design pressure; t is the required\* thickness of the nozzle (as a cylindrical shell) for the design pressure. Other dimensions and symbols are defined in the following text and Figure 1. All dimensions shall be taken in the "corroded" condition. For elliptical heads, D/2 shall be taken as the largest radius of curvature of the head. It is assumed that the materials used in the sphere, nozzle, weld metal, and reinforcement section (if any) are of equal strength.

3. (a) Uniformly thickened nozzle wall, Figure 1a

$$t' \geq gt, \quad l \geq \sqrt{dgt}, \quad g \text{ obtained from Figure 2a.}$$

- (b) Uniformly thickened sphere wall, Figure 1b

$$T' \geq hT, \quad L \geq 0.7 \sqrt{DhT}, \quad h \text{ obtained from Figure 2b.}$$

- (c) Uniformly thickened nozzle and sphere wall, Figure 1c

$$\text{Determine } g' \text{ and } h' \text{ according to: } \frac{g' - 1}{g - 1} + \frac{h' - 1}{h - 1} = 1$$

g and h obtained from Figures 2a and 2b, respectively.

$$t' \geq g't, \quad l \geq \sqrt{dg't}$$

$$T' \geq h'T, \quad L \geq .7 \sqrt{Dh'T}$$

- (d) Uniformly thickened nozzle wall protruding through sphere, Figure 1d

$$t' \geq \text{larger of } t \text{ or } 2gt/3 \quad l \geq \sqrt{dt''}, \quad g \text{ from Figure 2a.}$$

$$t'' = \text{larger of } t \text{ or } 2gt/3$$

4. Compact reinforcements, Figures 1e, 1f, 1g

$A_r$  is the required cross-sectional area of reinforcement. The reinforcement must be uniform around the nozzle axis. Only the area within the circle defined by the radius  $L_c$  may be taken as contributing to  $A_r$ .

$$\text{For: } d/D \leq \sqrt{0.02/(D/T)}; \quad A_r = 0$$

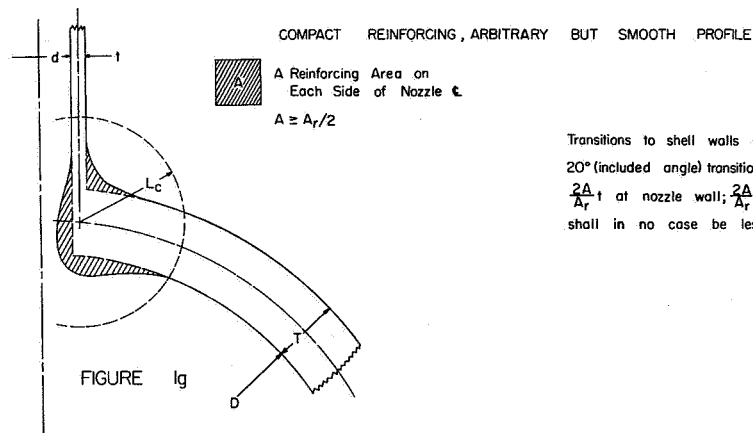
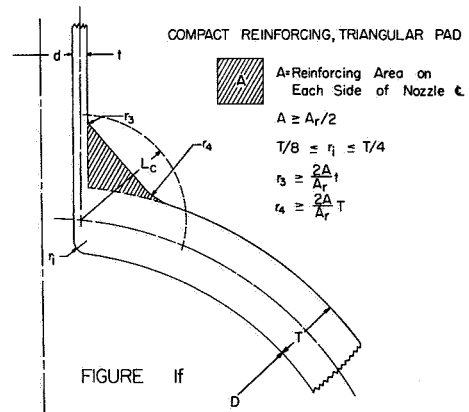
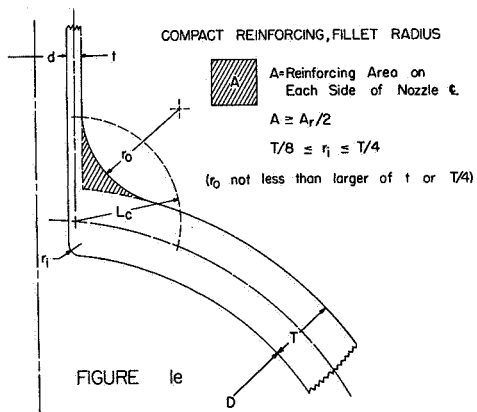
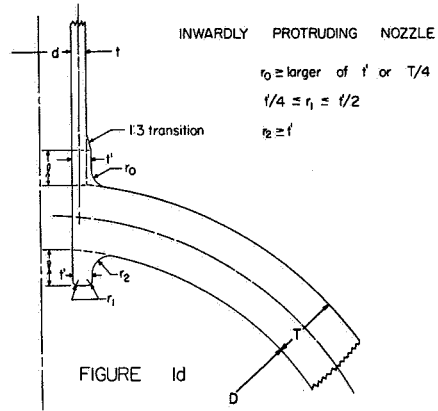
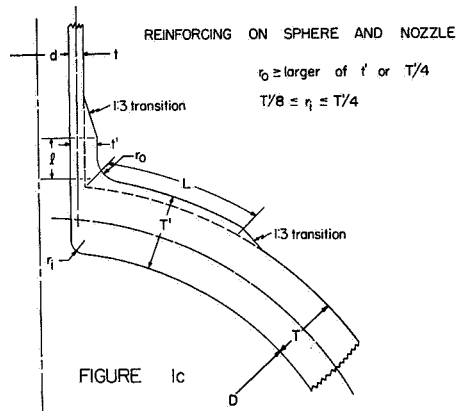
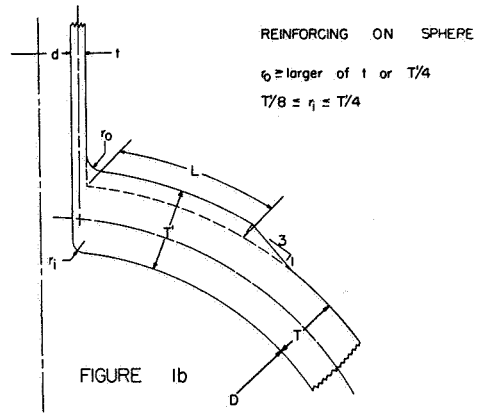
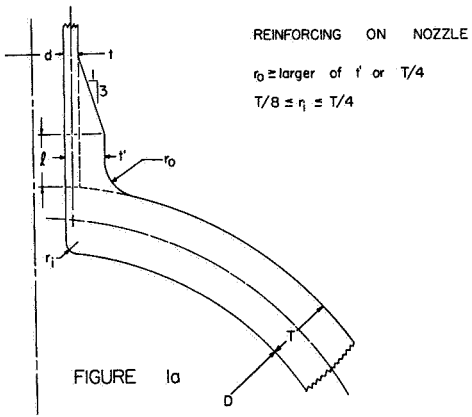
$$\text{For: } \sqrt{0.02/(D/T)} \leq d/D \leq \sqrt{0.08/(D/T)}; \quad A_r = (dT)(d/D \sqrt{50D/T - 1})^{1/2}$$

$$\text{For: } \sqrt{0.08/(D/T)} \leq d/D; \quad A_r = dT \cos \phi$$

$$\phi = \sin^{-1} d/D$$

$$L_c = 1.5 (T/D)^{(2/3)} D$$

\* Required thickness according to the appropriate design code; e.g., for the ASME Boiler Code, Section VIII:  $T = PD/(4S E - 0.4P)$ , where P = internal pressure, D = sphere inside diameter,  $S_a$  = allowable stress, E = joint efficiency of welded joint in the sphere.



Transitions to shell walls shall be equivalent to not more than 20° (included angle) transition sections or by radii not less than  $\frac{2A}{A_r} t$  at nozzle wall;  $\frac{2A}{A_r} T$  at sphere wall. Outside fillet radii shall in no case be less than the larger of  $t$  or  $T/4$ .

FIGURE 1: REINFORCED NOZZLE DETAILS

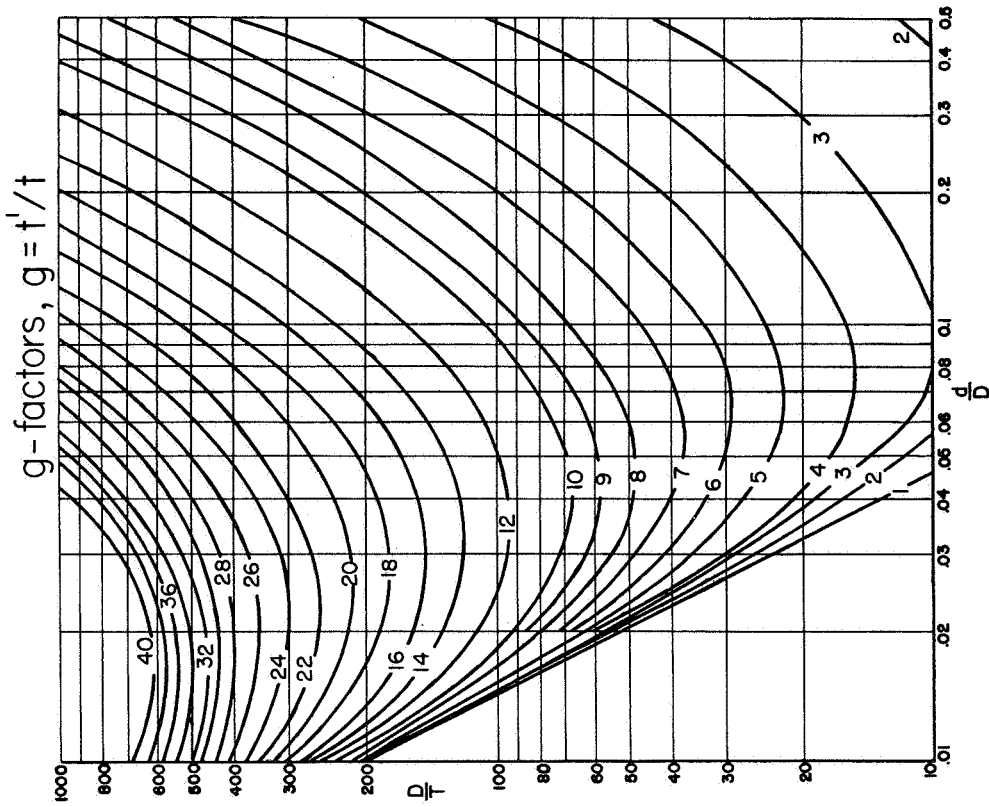


FIGURE 2a

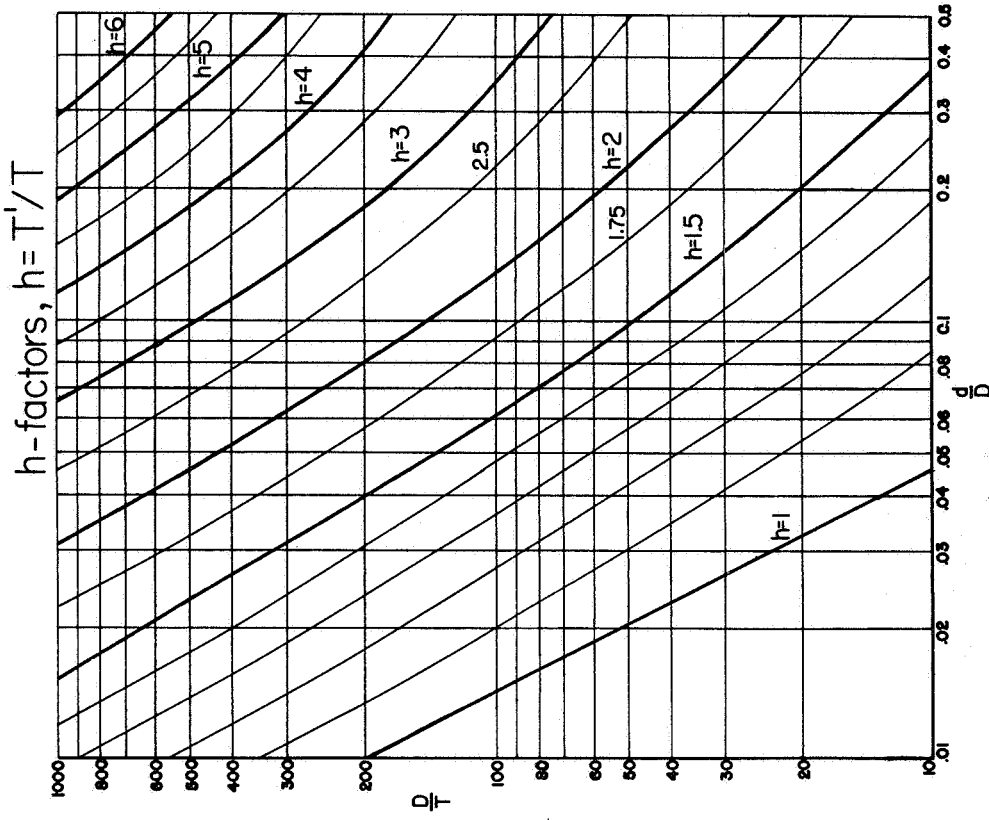


FIGURE 2b



DESIGN CRITERIA

The basic problem in determining the proper proportions of a structure is twofold. First, the stresses must be found, and second, allowable values of the stresses must be prescribed. Present day techniques of stress analysis--analytical, numerical, and experimental--are normally sufficient for the determination of stresses in pressure vessels. However, a certain amount of arbitrariness is still exercised in fixing allowable values of elastic stresses.

Static failure of a ductile material is a plastic process, and a rational basis for determining allowable stresses will necessarily involve plasticity considerations. The principles of plastic limit design were used to set allowable stresses in Section III of the ASME Boiler and Pressure Vessel Code, Nuclear Vessels<sup>(3,4)</sup>. Conservative simplifications and generalizations were made to achieve complete stress limits for all parts of a nuclear vessel. In particular, the  $1.5 S_m$  limit on local membrane stress was set to insure against local plastic collapse. A satisfactory, consistent nozzle design procedure cannot be constructed with this limit as a basis because it is too restrictive. This can be readily seen by considering very small nozzles, which should require no reinforcement, yet produce local membrane stresses of  $2 S_m$  in the shell. Therefore, the  $1.5 S_m$  limit of Section III is replaced in the proposed procedure by an actual limit analysis.

The design procedure presented herein results from a direct application of limit design principles to a specific geometry when subjected to internal pressure. The design philosophy is therefore the same as that of the ASME Nuclear Vessels Code.

It is the intent of the Nuclear Vessels Code to (1) provide a safety margin of 1.5 against plastic collapse when strain-hardening is neglected and (2) to insure shakedown to elastic action. In accordance with this intent, the proposed reinforcements were proportioned so that (1) the collapse pressure is at least 1.5 times the design pressure and

(2) so that the most highly stressed regions of the nozzle will shakedown to elastic action. The collapse limit was established using the results of the plastic-limit analysis described in Reference 5. The shakedown criteria used was that of limiting the maximum elastic stress intensity\* to three times the nominal stress in the unperforated sphere; for materials with design stress intensity values established by the limit of two-thirds of the yield strength, this is the equivalent of limiting the maximum stress intensity,  $\bar{\sigma}$ , to twice\*\* the yield strength of the material. Elastic stresses were calculated according to Reference 6, with the addition of a local flexibility factor at the nozzle-sphere juncture and approximate "thick-wall" shell correction factors. It is re-emphasized that both criteria mentioned, the collapse pressure and the  $3 S_m$  limit, are met for all nozzle designs recommended by the present design procedure.

---

\* Stress intensity at a point is defined as twice the maximum shear stress at that point.

\*\* For vessel materials in which the ratio of ultimate strength to yield strength is less than two, the design stress intensity is one-third of the ultimate strength. For such materials the margins against plastic collapse or continued nonelastic straining are greater than indicated.

DEVELOPMENT OF DESIGN PROCEDURE

This section briefly describes how the design procedure was developed. Detailed discussion of the development is given in the subsequent section entitled "Discussion".

The design of a cylindrical nozzle in a spherical shell may be considered as consisting of a basic configuration plus reinforcement. The basic configuration is defined as an outwardly protruding nozzle and spherical shell segment, as shown in Figure 3, in which the nozzle and spherical shell have the same nominal stress for a given pressure. Specifically

$$\text{For the nozzle: } s = Pd/2t$$

$$\text{For the sphere: } S = PD/4T$$

where  $P$  = internal pressure

$d$  = inside diameter of nozzle

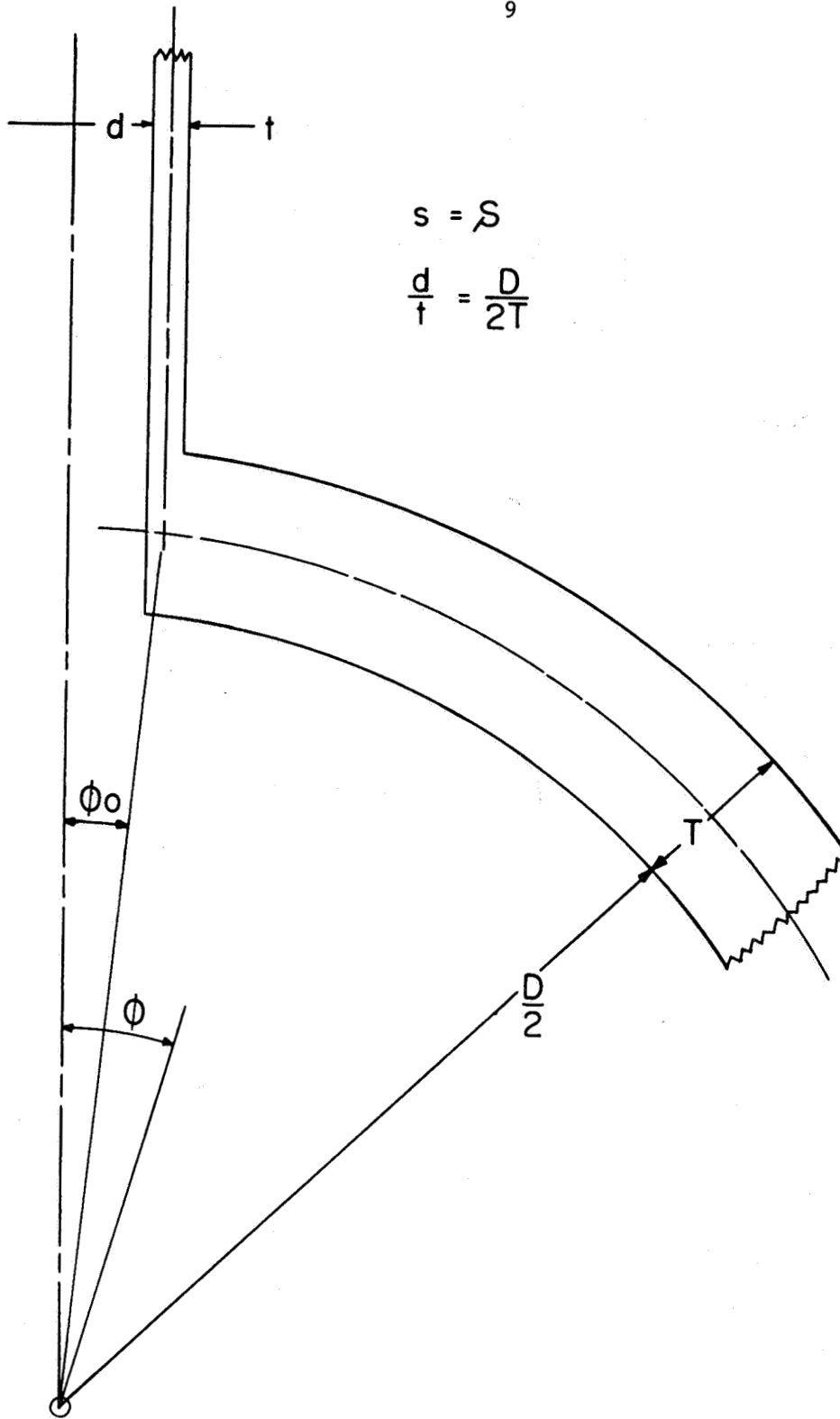
$t$  = wall thickness of nozzle

$D$  = inside diameter of sphere

$T$  = wall thickness of sphere.

For the basic configuration, by definition,  $s = S$  = allowable design stress intensity for the material used in the nozzle and sphere--assumed to be made of equal strength materials.

The design procedure consists of specifications of the dimensions of reinforcing required, if any, in order to meet the design criteria described above.



$$s = S$$

$$\frac{d}{t} = \frac{D}{2T}$$

Uniform Wall Designs

A nozzle-shell junction may be reinforced either by using a nozzle and/or sphere with wall thickness increased over the basic configuration, as shown in Figures 1a and 1b. As a first step in deriving the design procedure, an extensive parametric study was made based on E. O. Waters' elastic analysis and covering the parameter ranges:  $.01 \leq \frac{d}{D} \leq .5$ ,  $10 \leq \frac{D}{T} \leq 1000$ ,  $.0625 \leq s/S \leq 8$ . The stresses obtained in this parametric study indicated which basic configurations required reinforcing in order to meet the elastic stress criteria  $\bar{\sigma} = 3S$  and how much reinforcing would be required if:

- (1) Reinforcing consisted only of an increase in wall thickness or the sphere, or
- (2) Reinforcing consisted only of an increase in wall thickness of the nozzle.

Figure 4 shows the reinforcement required on the sphere only, in terms on the parameters  $d/D$ ,  $D/T$  and  $h = T'/T$ . The line marked  $h = 1$  indicates those combinations of  $D/T$  and  $d/D$  for which the maximum shear stress in the basic configuration (with an adequate fillet radius,  $r_o$ ) does not exceed  $3.0 S$ . The lines marked  $h > 1$  indicates the thickness required in the sphere so that  $\bar{\sigma} = 3.0 S$ . Note that  $S = PD/4T$ , not  $PD/4T'$ ; i.e., the index stress is that of the unreinforced sphere.

Figure 5 shows the reinforcement required on the nozzle only, in terms of the parameters  $d/D$ ,  $D/T$  and  $g = t'/t$ . The line marked  $g = 1$  is the same as on Figure 4; higher values of  $g$  indicate the thickness required in the nozzle for  $\bar{\sigma} = 3.0 S$ .

Using the limit pressure analysis for cylindrical nozzles in spheres developed by R. L. Cloud<sup>(5)</sup>, the necessary increase in wall thickness of nozzle or sphere was calculated, based on the criteria  $P^L = 0.98 P^*$ , where:

$P^L$  = limit pressure

$P^*$  = nominal yield pressure of sphere =  $4\sigma_o T/D$

$\sigma_o$  = yield strength of material

$T$  = wall thickness of sphere

$D$  = inside diameter of sphere.

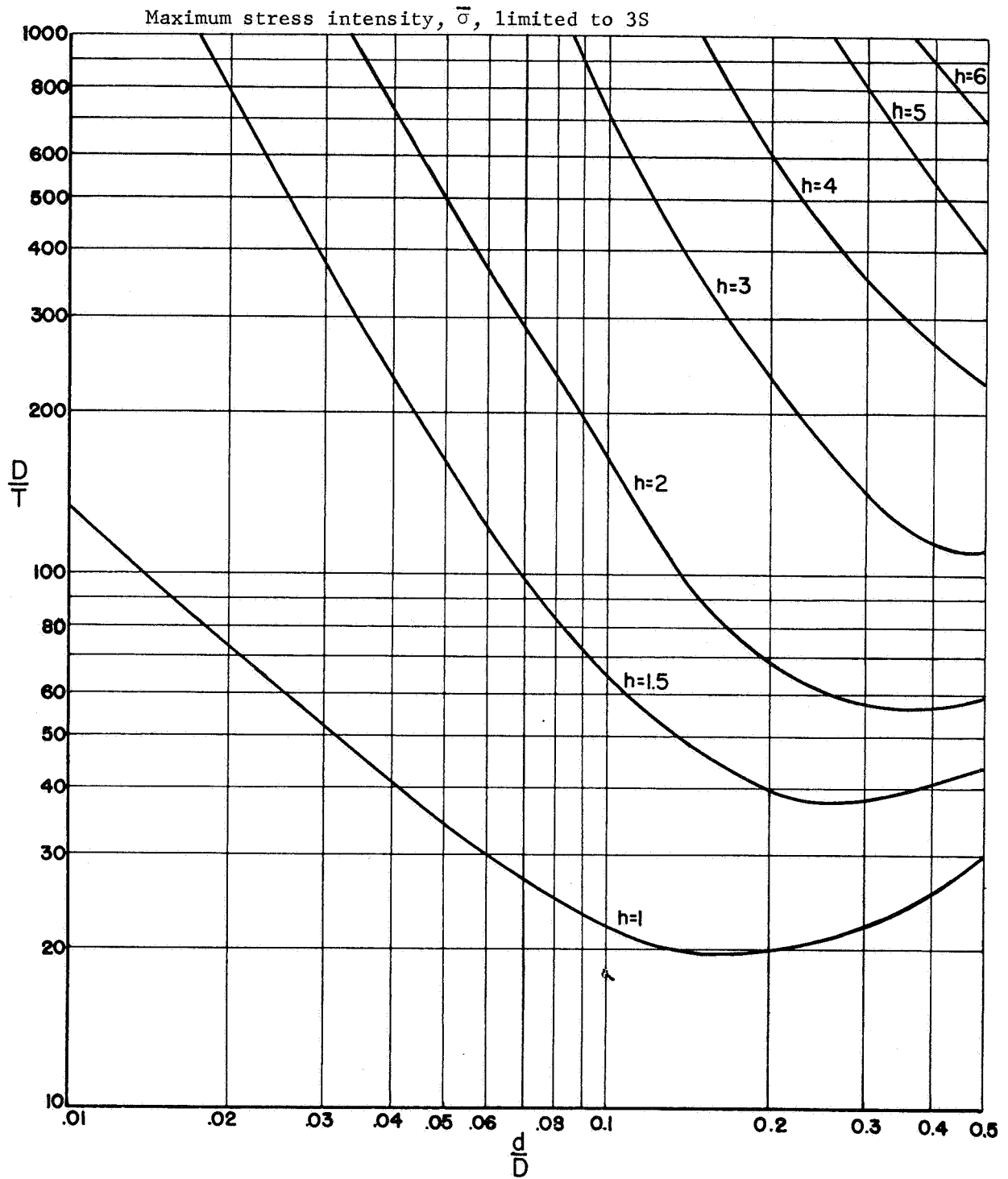


FIGURE 4. REQUIRED REINFORCING ON SPHERE  
FOR  $\bar{\sigma} = 3S$ , WATERS' ANALYSIS

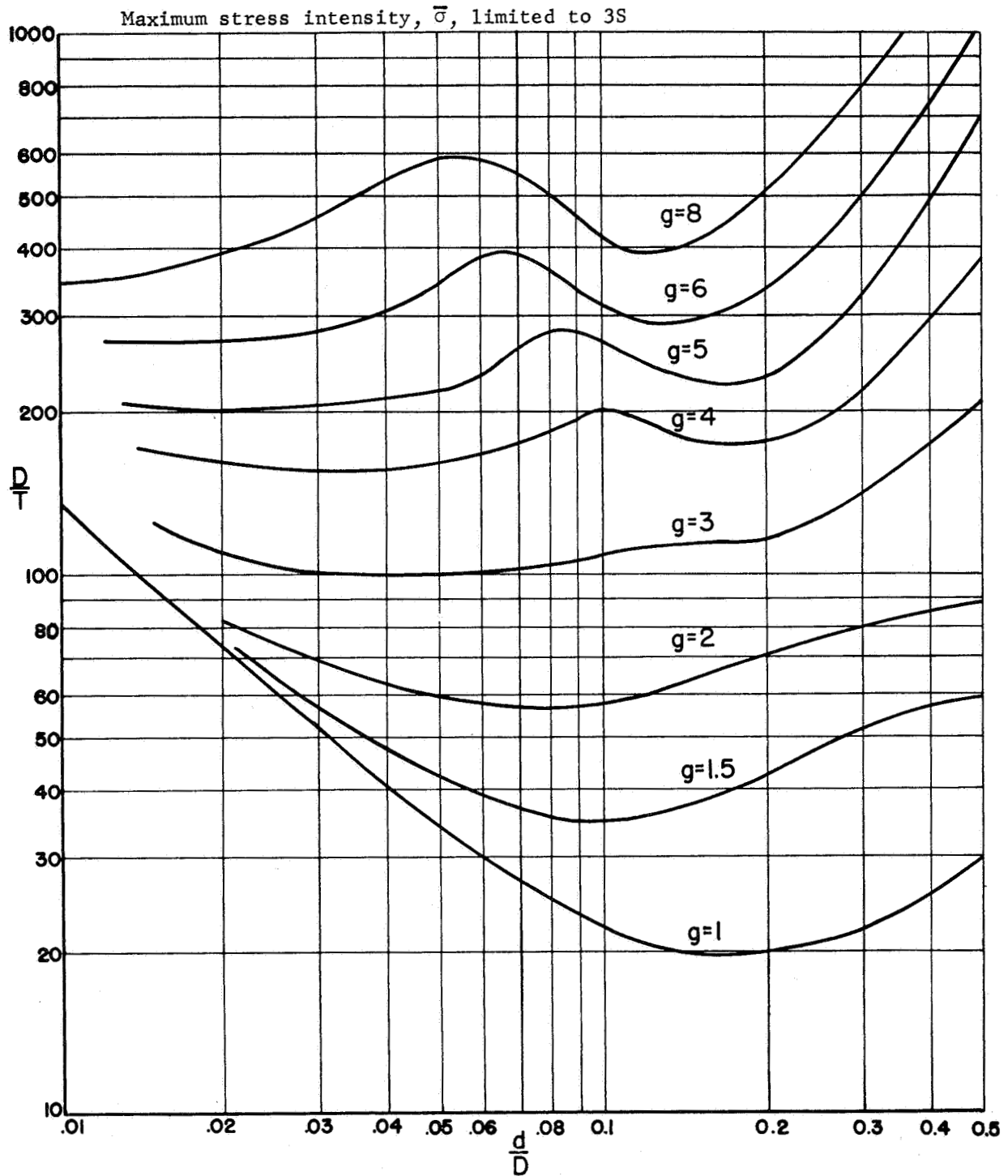


FIGURE 5. REQUIRED REINFORCING ON NOZZLE FOR  $\bar{\sigma} = 3S$ , WATERS' ANALYSIS

The curves resulting from the limit analysis are shown as dashed lines in Figures 6 and 7, and are superimposed over the analogous curves based on elastic analysis. The design graphs (Figures 2a and 2b) were obtained by using the limit pressure curves; the limit pressure curves are more conservative almost\* throughout the range of parameters covered herein †.

The length of reinforcement, as indicated by Figures 1a and 1b must be at least equal to  $\sqrt{DT'}/2$  on the sphere or  $\sqrt{dt'}$  on the nozzle. These lengths are based on elastic theory, limit analysis, evaluation of the attenuation of stresses obtained in tests and comparison of test data with and without finite-length reinforcement on the nozzle or sphere.

The requirements given above relate to either a reinforced sphere or a reinforced nozzle. In many practical designs, it may be desirable to use a combination of reinforcing on the sphere and nozzle, as shown in Figure 1c. While it is possible to construct a number of graphs similar to Figures 2a and 2b which, with interpolation, would cover these cases, in the interest of simplicity a linear relationship was developed, i.e.:

$$\frac{g' - 1}{g - 1} + \frac{h' - 1}{h - 1} = 1 \quad (1)$$

where  $g = t'/t$  from Figure 2a

$g' =$  partial nozzle reinforcement,  $1 < g' < g$

$h = T'/T$  from Figure 2b

$h' =$  partial sphere reinforcement,  $1 < h' < h$ .

---

\* For the dimensional parameter range near  $h = g = 1$  with small  $d/D$ , the elastic criteria is slightly more conservative than the limit pressure criteria, however, the elastic stress, using the dimensions obtained from the limit pressure analysis, is not more than 3.2 S.

† The lines for  $h = 1$  and  $g = 1$  were adjusted slightly downward from the limit pressure analysis so as to agree with the Nuclear Vessel Code equation in Par N-452(a)(1):  $d = 0.1414 \sqrt{DT}$ . A comparison of these lines is shown on Figure 21.



———— Elastic Analysis,  $\bar{\sigma} = 3S$   
 - - - - - Limit Pressure Analysis

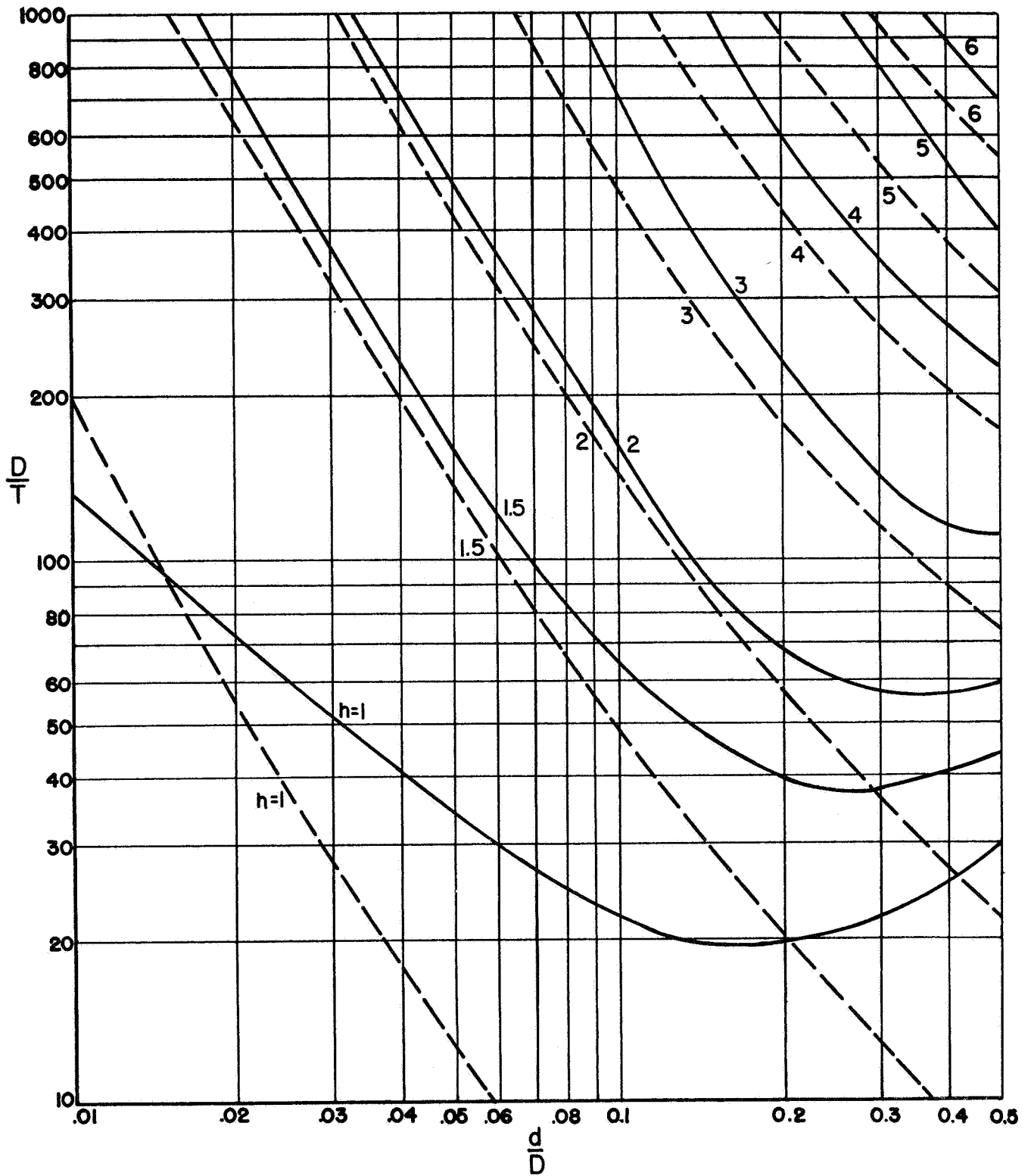


FIGURE 6. REQUIRED REINFORCING ON SPHERE BY LIMIT ANALYSIS

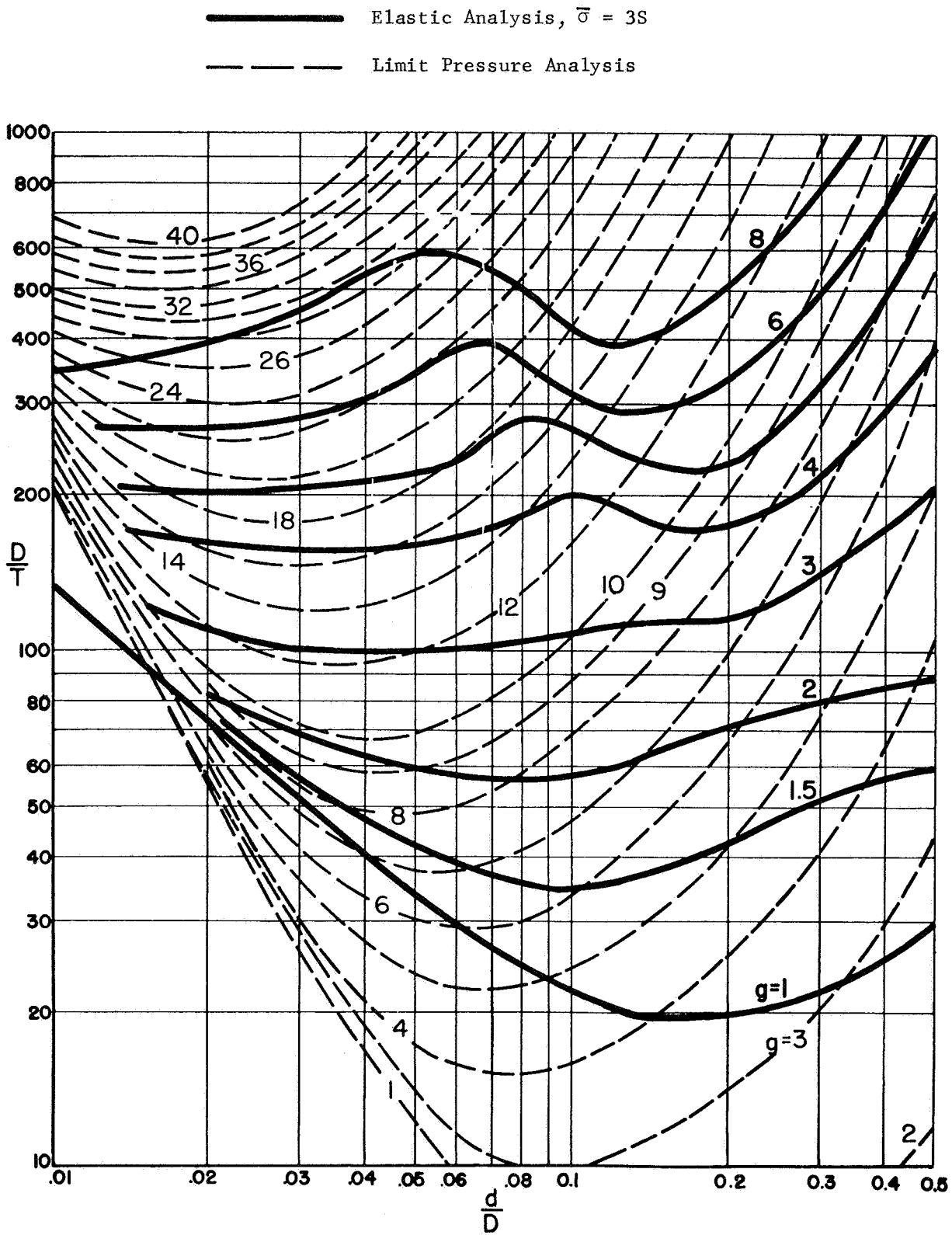


FIGURE 7. REQUIRED REINFORCING ON NOZZLE BY LIMIT ANALYSIS

### Inwardly Protruding Nozzles

Nozzles which protrude inside the vessel, as shown in Figure 1d, have been analyzed by Leckie and Penny<sup>(7)</sup> for elastic stresses. Limit pressure considerations, along with the elastic analysis, indicate the following rule is adequate:

$$t' \geq \text{larger of } t \text{ or } \frac{2gt}{3}; \quad l \geq \sqrt{dt''} \quad (2)$$

$$t'' = \text{larger of } t \text{ or } \frac{2gt}{3}$$

### Compact Reinforcing

Both test data and theoretical analysis has shown that reinforcing material placed close to the nozzle-sphere junction is more efficient than a similar amount of reinforcing material placed away from the junction. For example, a large fillet radius as shown in Figure 1e provides an efficient compact reinforcing. Test data and analysis for nozzles with such reinforcing show that, in the dimensional parameter range covered herein, the reinforcing area required to reduce the maximum stress intensity to  $2.0S^*$  is less than  $0.80 dT$ . The product  $dT$  will be recognized as the area of reinforcing required by existing codes, i.e., the inside diameter of the nozzle times the required wall thickness of the sphere. In contrast, the reinforcing area required for uniform-wall reinforcing is as much as  $2.3 dT$ ; reflecting the effect of the relatively "spread-out" reinforcing.

As in the case of uniform-wall reinforcing, it is necessary to also consider the limit pressure of the reinforced nozzle. From the basic configuration ( $s/S \approx 1.0$ ), it can be shown that reinforcing area,  $A_r$ , equal to  $dT \cos \phi_0$ , if placed close to the nozzle sphere junction, will insure that the limit pressure of the reinforced nozzle is equal to that of the unperforated sphere.

For a small, unreinforced nozzle in a sphere, the shell-theory elastic stress intensity is essentially equal to  $2.0 S$ . This is highly localized stress and will not lead to any significant gross deformation. The reinforcing required to increase the limit pressure to that of the unperforated sphere is small, i.e.,  $A_r = dT \cos \phi_0$  where  $d$  is small.

---

\* The elastic stress limit of  $2.0 S$  was used in this comparison because of the availability of a parametric analysis using the Seal-Shell-2<sup>(15)</sup> computer program.

For small nozzles without reinforcing, the limit pressure is practically equal to that of the unperforated sphere. Accordingly, for small holes in spheres, no reinforcing is required.

On the basis of the above concepts, the following design procedure was developed.

$$\text{For } d/D \leq \sqrt{\frac{0.02}{D/T}} \quad ; \quad A_r = 0. \quad (3)$$

This rule permits the use of the unreinforced basic configuration in essentially the same parameter range as shown by Figures 2a and 2b, i.e., the lower left section of the graphs below  $h = 1$  or  $g = 1$ .

$$\text{For } \sqrt{\frac{0.02}{D/T}} \leq d/D \leq \sqrt{\frac{0.08}{D/T}} \quad ; \quad A_r = dT (d/D \sqrt{50D/T} - 1)^{1/2}. \quad (4)$$

This rule provides a transition between the parametric ranges where no reinforcing is required and those parametric ranges where the full reinforcing,  $A_r = dT \cos \phi_o$ , is required.

$$\text{For } d/D \geq \sqrt{\frac{0.08}{D/T}} \quad ; \quad A_r = dT \cos \phi_o, \quad (5)$$

where

$$\phi_o = \sin^{-1} (d/D).$$

Compact reinforcing, as shown by Figure 1e, 1f, and 1g, is defined as that reinforcing placed inside a circle with center at the midwall junction of nozzle and sphere and with radius equal to  $1.5 (T/D)^{2/3} D$ . The value of the radius of  $1.5 (T/D)^{2/3} D$  was developed by evaluating the reinforcing areas and reinforcing zones of uniform wall reinforcing in relation to the reinforcing area required for compact reinforcing.

#### Radii and Transition Sections

Selection of radii and transition profiles was based on comparisons of theoretical analysis with test data, along with consideration of current practice as given in various pressure vessel design codes.

DISCUSSIONUniform Wall ReinforcingBasic Elastic Analysis

The elastic analysis used is essentially that described in Reference 6, with the addition of the effect of a local flexibility factor<sup>(8)</sup> at the nozzle-sphere junction and an approximate thick-wall correction factor for the stresses.

Test data<sup>(9,10)</sup> are available on 38 photoelastic models of uniform-wall nozzles in spherical shells. Measured stresses are also available<sup>(11,12)</sup> on two steel models of uniform wall nozzles in spherical shells. These models cover the parameter range of  $d/D$  from 0.05 to 0.5;  $D/T$  from 9 to 240,  $s/S$  from 0.39 to 2.0. Comparison of the data with Waters' analysis shows that the analysis is conservative for all models (with one exception) provided the outside fillet radius is equal to or greater than the nozzle wall thickness,  $t$ . Unless the fillet radius is more than two times the nozzle thickness, the degree of conservatism is not large, and, hence, Waters' analysis is deemed to be directly applicable to uniform-wall nozzles in spherical shells with fillet radii about equal to  $t$ .

The one exception occurred on a photoelastic model (S-1G) with  $d/D = 0.05$ ,  $D/T = 23.7$ , and  $s/S = 0.39$ . A high normal stress ( $\sigma/S = 2.60$ ) occurred on the inside corner of the sphere opening; Waters' analysis predicts only 55 per cent of this stress. The maximum measured stress intensity of this model was  $2.78S$  which, in itself, is acceptable under the elastic design criteria; however, because of the limit pressure design criteria, this particular model would not be acceptable; a g-factor (Figure 2a) of about 5.0, corresponding to an  $s/S$  of 0.20, would be required compared to the  $s/S$  of 0.39 used in the model.

Because the design procedure is controlled by limit pressure considerations, it is generally quite conservative with respect to measured elastic stresses in test models.

#### Lengths of Uniform Thickness Reinforcing

It is obvious that the length of uniformly increased wall thickness, integral with the sphere or nozzle wall (hereafter referred to as "pad length" for brevity), need not be very large in order for the local stresses at the nozzle-sphere junction to be the same as if the pad length was infinite. The required minimum pad lengths may be estimated in several ways:

1. Elastic theory used in a two-piece shell analysis of a nozzle in a sphere gives an approximation of an attenuation length; i.e., that distance from the nozzle shell juncture at which loads applied at the juncture produce negligible stresses in the shells.

Edge loading of the nozzle (cylindrical shell) is characterized by linear combinations of exponential trigonometric functions whose behavior is well known<sup>(13)</sup>. Attenuation of stresses is different for a shear edge load as compared to a moment edge load; however, in either case the stresses due to the edge loads are negligible if

$$\beta X > 1.816, \quad (7)$$

where

$$\beta = \sqrt[4]{\frac{12(1 - \nu^2)}{d^2(t')^2}}$$

X = distance from edge.

For a Poisson's ration,  $\nu = 0.3$ , Equation 7 gives

$$X = \sqrt{dt'}. \quad (8)$$

Edge loading on the sphere hole, using the Esslinger approximation, is characterized by linear combinations of Kelvin functions whose characteristics are also well known<sup>(13)</sup>. Determination of a

a suitable attenuation length from the Esslinger approximation is difficult since the attenuation of the Kelvin functions depends upon the angle  $\phi_o$ , defined by  $\sin \phi_o = d/D$ , as well as the unknown angle  $\phi_x$ , which defines the attenuation length. For locations on the sphere near the apex, as may be seen from plotted values of the Kelvin functions (or more directly, Schleicher functions; see page 245 of Reference 13), an increase in the argument of the functions by an increment of 1.816 generally reduces the value of the functions to a relatively negligible value. The argument of the Kelvin functions, as used by Waters, is almost  $\lambda\phi$ , where:

$$\lambda = \sqrt[4]{12(1 - \nu^2) R^2 / (T')^2}$$

$\phi$  = central angle of sphere as shown in Figure 3

$R = D/2 =$  sphere radius.

With  $\Delta(\lambda\phi)$  equal to 1.816 and  $\phi = X/R$ , the attenuation length on the sphere,  $X$ , is found to be  $\sqrt{RT'}$ .

For locations far from the apex,  $X$  becomes larger and approaches  $\sqrt{DT'}$  at 90 degrees from the apex.

Attenuation lengths can also be established by evaluation of parametric studies using an elastic analysis. Available data using Waters' analysis give stresses only at the juncture. A parametric study made by F. J. Witt<sup>(14)</sup>, using the C.E.R.L. computer program, gives stresses at various distances from the juncture. These results indicate that  $\ell = \sqrt{dt'}$  is adequate for all parameters.  $L = \sqrt{RT'}$  is adequate for most parameters, but for large  $D/T$  combined with large  $d/D$ , the attenuation distance is somewhat greater than  $\sqrt{RT'}$ . However, in view of the transition tapers or radii required by the proposed rules, the required length  $L = \sqrt{RT'}$  should be sufficient for all parameters covered by the proposed rules.

3. Attenuation lengths can be determined by evaluation of the pattern of stresses measured on test models. Test results on photoelastic and steel models indicate that, in general, stresses are near their nominal values at distances from the juncture corresponding to  $l = \sqrt{dt'}$  on the nozzle,  $L = \sqrt{RT'}$  on the sphere.
4. Some test data are available<sup>(10)</sup> which compare models with an increased wall thickness section on the nozzle with uniform-wall nozzles (photoelastic models N-1C versus N-1E and N-3B with N-3D). These tests confirm the validity of  $l = \sqrt{dt'}$ , since stress levels for the comparative models were essentially the same.
5. Limit pressure analysis<sup>(5)</sup> also gives minimum required lengths of pads on the sphere or nozzle. These equations are:

$$\text{On sphere: } \phi_o - \phi_x = \sqrt{\frac{4(d/D)^2 + h^2}{D/T(h-1)}} \quad (9)$$

$$\text{On nozzle: } x = \sqrt{\frac{(gd/2)(gt)}{(g-1)}} \quad (10)$$

The pad lengths required by Equations 9 and 10 are less than those given by the elastic analysis ( $L = \sqrt{hRT}$  and  $l = \sqrt{gdt}$ ) provided that  $h$  or  $g$  is more than 2. Hence, use of the elastic analysis lengths is conservative for such structures. As  $h$  or  $g$  approaches 1.0, the lengths required by Equations 9 and 10 approach infinity. At the same time, however, the limit pressure of the unreinforced structure is approaching that of the unperforated sphere. Accordingly, use of the pad lengths given by the elastic analysis along with the transition required by the proposed rules will result in only a small reduction in the theoretical limit pressure of the reinforced structure.



### Reinforcing on Nozzle and Shell

The approximate rule:

$$\frac{g' - 1}{g - 1} + \frac{h' - 1}{h - 1} = 1 \quad (11)$$

gives a simple means of determining the amount of uniform wall reinforcing required when part of the reinforcing is on the sphere and part on the nozzle. This rule is, of course, in agreement with the general analysis at either end of its range; i.e., for either  $g' = g$ ,  $h' = 1$ , or  $h' = h$ ,  $g' = 1$ . This is also a conservative approximation, from an elastic-stress standpoint, throughout the range, as shown by Table 1 wherein the calculated elastic stresses for nozzles reinforced in conformance with the approximate rule, Equation 11, are shown to be less than  $3.0S$ .

### Limit Pressure Analysis

The limit pressure analysis used as the basis of the proposed design procedure was developed by Cloud<sup>(5)</sup>. This reference also gives the results of tests on annealed, carbon steel test models of uniform wall thickness nozzles in spherical shells. The parameters of the test models were:  $D/T = 160$ ;  $d/D = 0.059, 0.119, \text{ and } 0.245$ ;  $s/S = 1.0$ . The test results were in good agreement with the theoretical analyses.

An alternate approach to insure the absence of gross yielding of the nozzle-sphere junction would be to use an additional elastic stress criteria; e.g., the maximum membrane stress intensity limited to  $1.5S$ . Figures 8 and 9 show the resulting shell and nozzle thickening factors, with the limit pressure analysis lines for comparison. For reinforcing on the shell, limiting the elastic membrane stress to  $1.5S$  is more conservative than the limit pressure approach. For reinforcing on the nozzle, however, the elastic limitation is more conservative for small  $d/D$  and less conservative for large  $d/D$  ratios. From a practical standpoint, reinforcing by use of a heavy nozzle will be principally applied for small  $d/D$  ratios. Nozzle-thickening factors of 10 to 50 are not uncommon for small nozzles.

TABLE 1. MAXIMUM STRESS INTENSITY IN NOZZLES DESIGNED  
 ACCORDING TO PAR. 3(c) OF THE DESIGN PROCEDURE,  
 EXAMPLES SELECTED AT MID-RANGES OF EQUATION 1

d/D	D/T	h	g	h'	g'	$\bar{\sigma}/S$
0.02	630	1.5	40	1.25	20.5	1.4
0.05	135	"	14	"	7.5	1.4
0.10	48	"	7.0	"	4.0	1.4
0.20	20	"	3.6	"	2.3	1.5
0.10	140	2.0	11	1.5	6.0	1.4
0.20	57	"	5.6	"	3.3	1.3
0.50	21.5	"	2.5	"	1.75	1.6
0.10	480	3.0	19	2.0	10.0	1.4
0.20	180	"	8.7	"	4.85	1.5
0.50	73	"	3.6	"	2.3	1.5
0.2	420	4.0	11.5	2.5	6.25	1.7
0.5	180	"	4.8	"	1.95	1.8
0.2	910	5.0	15.5	3.0	8.25	1.7
0.5	310	"	5.7	"	3.35	1.7
0.5	550	6.0	6.8	3.5	3.90	1.8
0.5	12	1.65	2	1.32	1.5	2.0
0.1	9.5	1.13	3	1.06	2.0	2.1
0.2	14.0	1.4	"	1.20	"	1.7
0.5	44	2.4	"	1.70	"	1.5
0.02	60	1.02	4	1.01	2.5	2.6
0.05	17.5	1.05	"	1.025	"	1.7
0.10	16.0	1.23	"	1.12	"	1.6
0.20	26	1.65	"	1.32	"	1.5
0.50	107	3.3	"	2.15	"	1.6
0.02	68	1.03	6	1.015	3.5	2.2
0.05	30	1.15	"	1.075	"	1.5
0.1	34	1.4	"	1.2	"	1.5
0.2	69	2.1	"	1.55	"	1.4
0.5	370	5.3	"	3.15	"	1.7
0.01	240	1.05	10	1.025	5.5	2.9
0.02	95	1.09	"	1.045	"	1.8
0.05	69	1.33	"	1.16	"	1.6
0.1	109	1.8	"	1.40	"	1.4
0.2	265	3.4	"	2.20	"	1.7
0.01	290	1.08	16	1.04	8.5	2.6
0.02	155	1.18	"	1.09	"	1.7
0.05	165	1.55	"	1.275	"	1.5
0.10	320	2.6	"	1.80	"	1.4
0.20	1000	5.1	"	3.05	"	1.5
0.01	590	1.21	36	1.10	18.5	1.9
0.02	540	1.46	"	1.23	"	1.8
0.05	970	2.60	"	1.65	"	1.6

\_\_\_\_\_ Elastic Analysis,  $\bar{\sigma}_m = 1.5S$   
 $\bar{\sigma}_m$  = maximum membrane stress intensity  
 - - - - - Limit Pressure Analysis

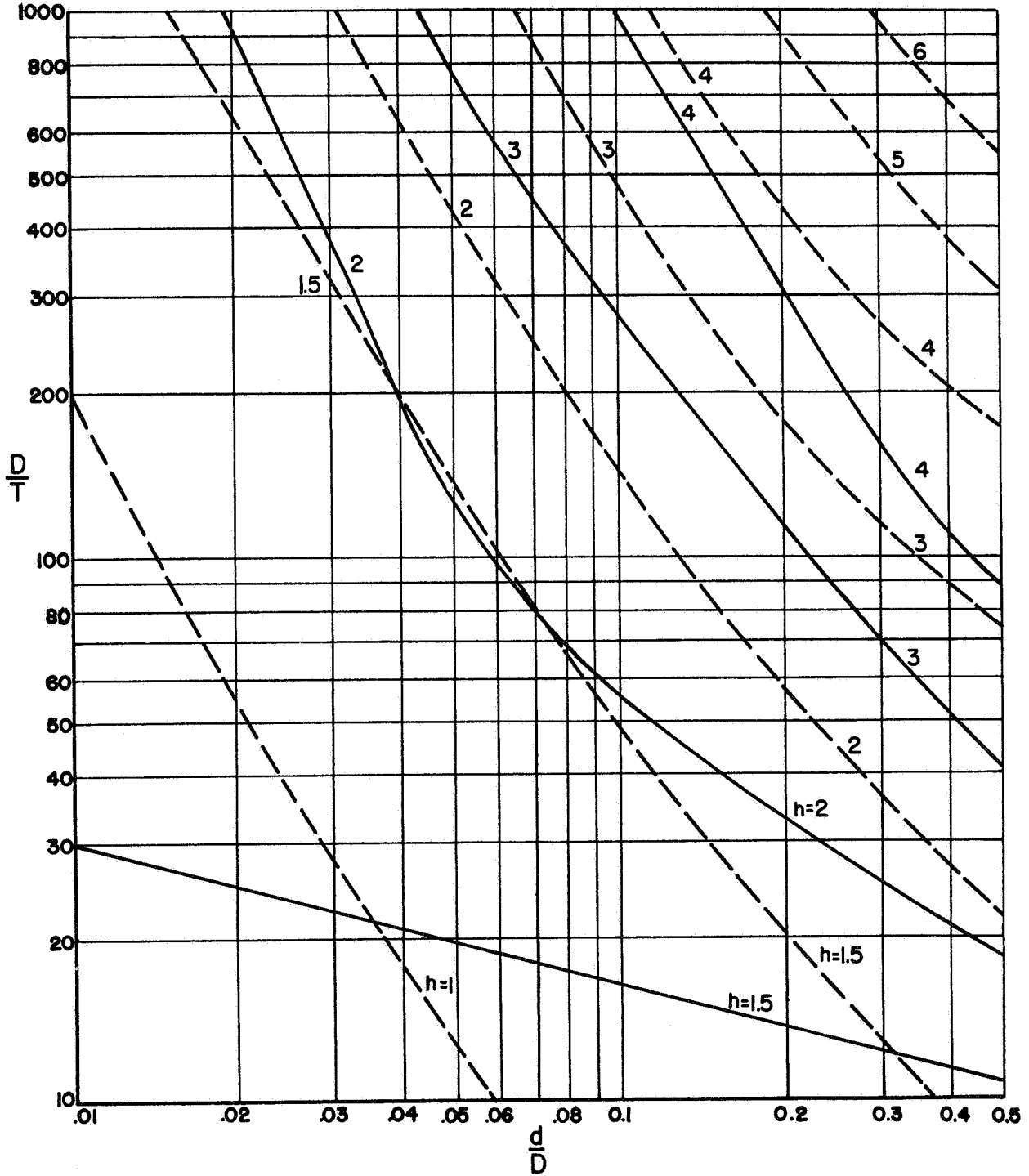


FIGURE 8. COMPARISON OF REINFORCING ON SPHERE FOR  $\bar{\sigma}_m = 1.5S$  WITH LIMIT PRESSURE ANALYSIS

Elastic Analysis,  $\bar{\sigma}_m = 1.5S$

—  $\bar{\sigma}_m$  = maximum membrane stress intensity

- - - Limit Pressure Analysis

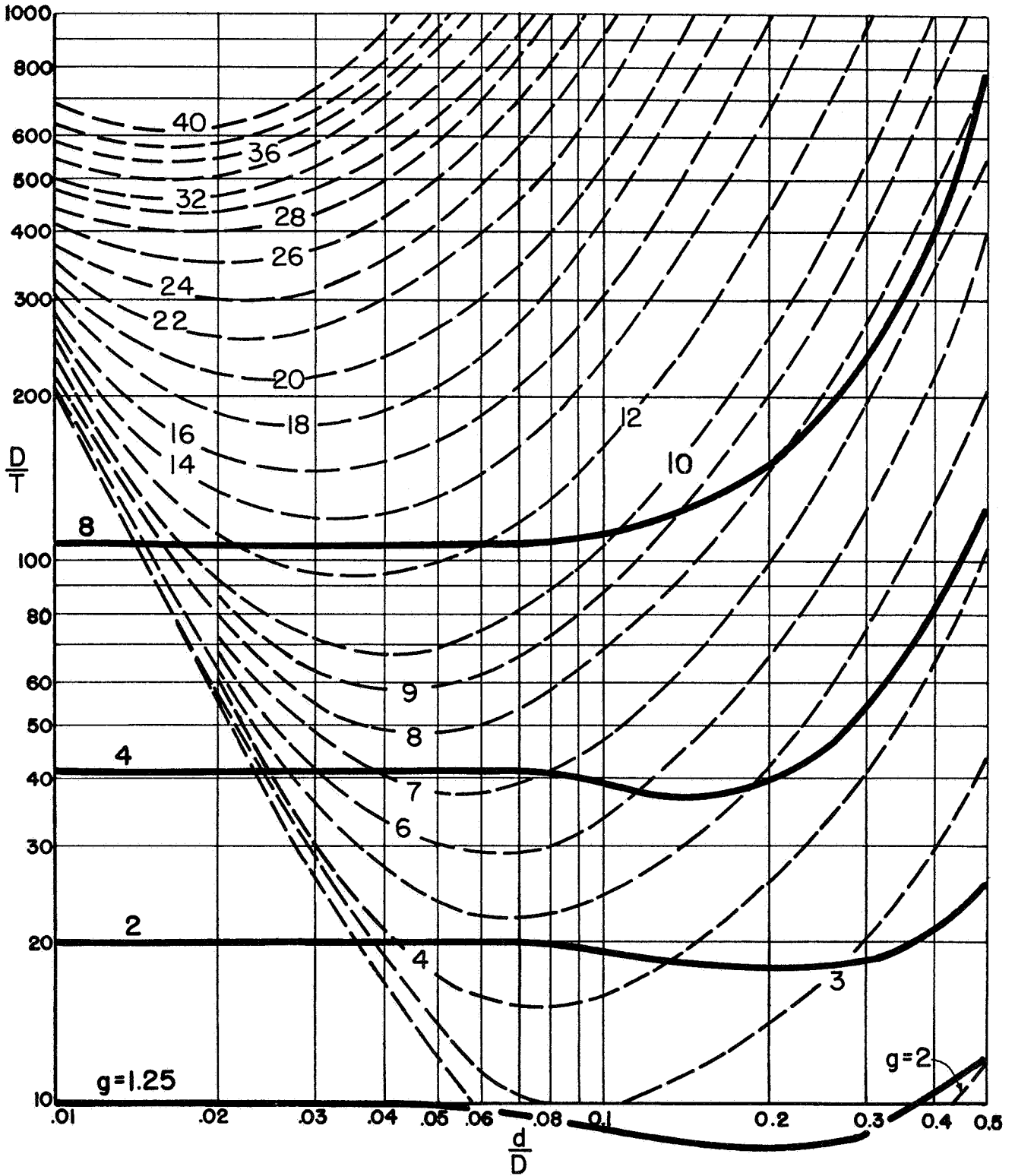


FIGURE 9. COMPARISON OF REINFORCING ON NOZZLE FOR  $\bar{\sigma}_m = 1.5S$  WITH LIMIT PRESSURE ANALYSIS

At a  $d/D$  ratio of 0.5, however, a  $g$ -factor of 3.0 means that the nozzle is three times as thick as the sphere and represents a seldom-used construction.

### Inwardly Protruding Nozzles

For inwardly protruding nozzles, as shown in Figure 1d, the proposed design rule is:

$$\begin{aligned} t' &\geq \text{larger of } t \text{ or } 2gt/3; \quad l \geq \sqrt{dt''}. & (12) \\ t'' &= \text{larger of } t \text{ or } 2gt/3 \end{aligned}$$

From a limit pressure standpoint, the material in the inwardly projecting nozzle with length equal to  $\sqrt{dt'}$  can be considered to be fully effective in restricting gross plastic deformation of the nozzle-sphere junction. Accordingly, the proposed rule requiring that the increase in nozzle thickness for reinforcing be two-thirds as much as for a nozzle protruding outward only is conservative from a limit pressure standpoint.

Leckie and Penny<sup>(7)</sup> elastic analysis may be used to indicate the comparative stresses in flush and inwardly protruding nozzles. Figure 10 gives such a comparison based on the particular stress limit,  $\sigma_{\max} = 2.25S$ . This comparison indicates that the proposed rule gives roughly consistent reinforcing requirements for inwardly protruding nozzles as compared to flush nozzles. While more complex rules could be given to cover the case of inwardly protruding nozzles, the proposed rule is desirable from the standpoint of simplicity.

### Compact Reinforcing

#### Elastic Analysis and Test Data

While Waters' two-piece shell theory applies with sufficient accuracy to uniform-wall nozzles in spheres, where there is a significant

$\sigma = 2.25S$ ;  $\sigma$  = maximum stress in sphere

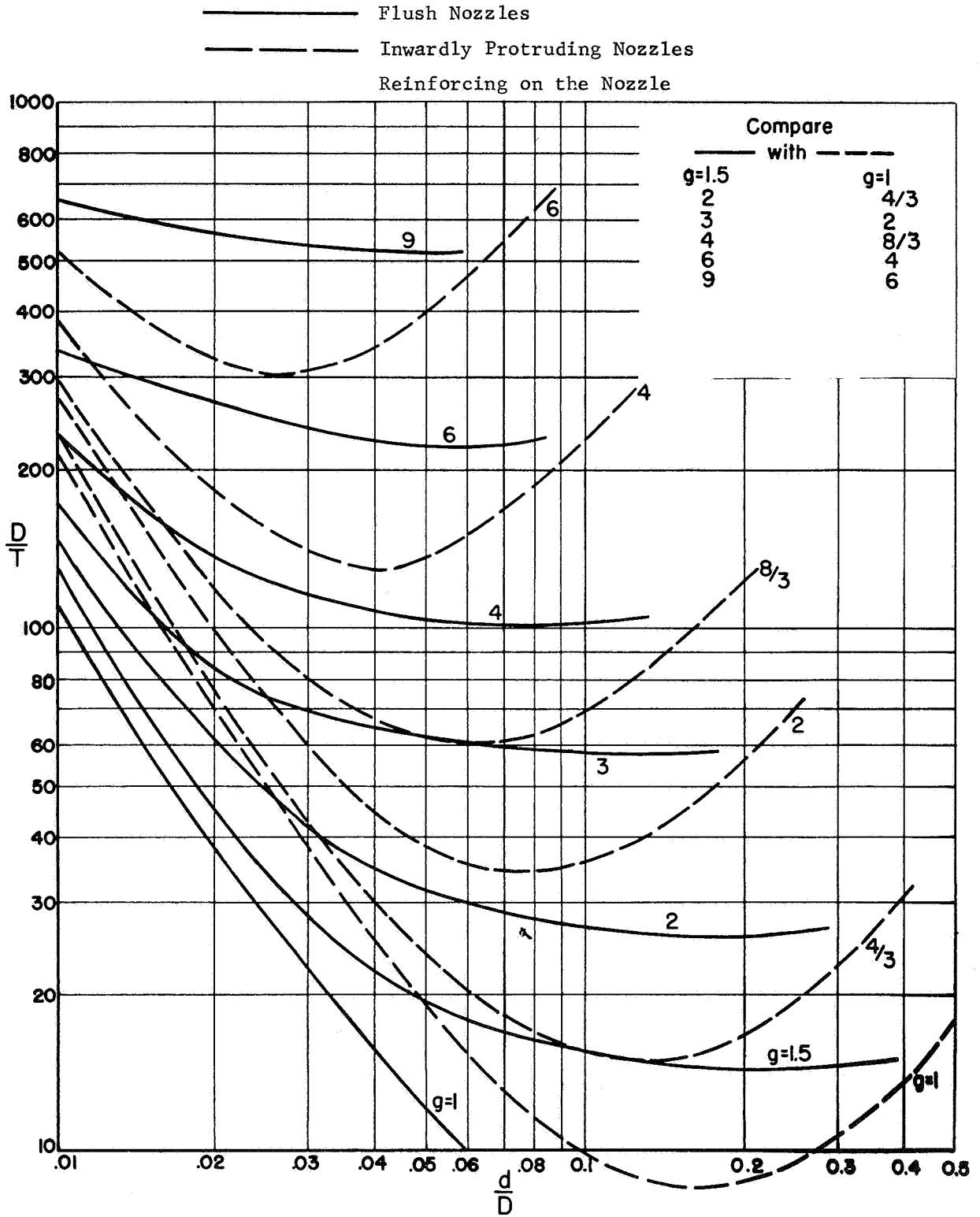


FIGURE 10. COMPARISONS OF FLUSH WITH INWARDLY PROTRUDING NOZZLES, LECKIE-PENNY ANALYSIS AT  $\sigma = 2.25S$

amount of relatively compact reinforcing (such as a large fillet radius or a triangular-shaped pad), Waters' shell theory is not applicable.

C. M. Friedrich<sup>(15)</sup> has developed a computer program (Seal-Shell-2) for determining stresses in axisymmetric shells with axisymmetric loadings based on a multipiece, thick-shell theory. Comparisons between calculated results using the Seal-Shell-2 computer program and test data on photo-elastic models indicate that the Seal-Shell-2 gives accurate results, provided the change in thickness at the juncture is not too abrupt. A limited parametric study was made using the Seal-Shell-2 program for compact reinforcing provided by fillet radii. This study indicates that the value of  $r_o/t$  required to obtain a maximum stress intensity of  $2S^*$  is approximately given by:

$$r_o/t = 0.336 (D/T)^{3/4}, \quad (13)$$

where

$r_o$  = fillet radius at nozzle-to-sphere junction

$t$  = nozzle thickness

$D$  = sphere mean diameter

$T$  = sphere wall thickness.

The requirement for  $r_o/t$  to obtain  $\bar{\sigma} = 2S$ , given by Equation 13, can also be expressed in terms of the area ratio,  $A/dT$ . The relationship is approximately

$$A/dT = 0.23 (D/T)^{1/2} \frac{d/D}{(d/D + 1)^4} \sec \phi_o, \quad (14)$$

where

$A$  = reinforcing area provided by the fillet radii

such that  $\bar{\sigma} = 2S$

$D$  = sphere mean diameter

$d$  = nozzle mean diameter

$T$  = sphere wall thickness

$\phi_o$  = angle whose sin is  $d/D$ .

---

\* The elastic stress limit of  $2.0 S$  was used in this comparison because of the availability of a parametric analysis using the Seal-Shell-2<sup>(15)</sup> computer program.

Equation 14 is plotted in Figure 11. Recalling that the product  $dT$  is the ASME Code replacement area, Figure 11 indicates that a fillet radius with area significantly less than that required by the ASME Code can be used for pressure load reinforcement provided  $\bar{\sigma} = 2S$  is considered as an acceptable design criteria.

The above analysis applies directly to fillet radii reinforcement but might be considered as applicable to other compact reinforcing provided suitable transition sections between reinforcing and shell walls are provided. This type of construction, however, may result in a fairly wide zone in which mean stresses are greater than  $S$ . Accordingly, such designs may have a limit pressure less than that of the unperforated sphere.

#### Area and Boundary for Compact Reinforcing

It is apparent from equilibrium conditions, as shown in Figure 12, that reinforcing area equal to  $dT \cos \phi_0$ , placed close to the nozzle-sphere junction, is sufficient to insure a limit pressure equal to that of the unperforated sphere. This result is derived rigorously from limit analysis by Cloud<sup>(16)</sup>. A suitable rule was developed for defining "close to the nozzle-sphere juncture" as described in the following.

The reinforcement areas required by the uniform wall reinforcing rules are shown in Figures 13 and 14 for reinforcing on the sphere and nozzle, respectively. Also shown on Figures 13 and 14 are the compact reinforcing areas by the proposed design procedure. Figure 15 shows the reinforcing length for uniform wall reinforcements. These graphs show that the relative reinforcing area required on the nozzle as compared to that on the sphere is roughly inversely proportional to the length of reinforcing. For large  $d/D$  the length of reinforcing on nozzle and sphere is about the same, and the area of reinforcing required on the nozzle is also about the same as that required on the sphere. For small  $d/D$  the length of reinforcing on the nozzle is shorter (more compact), and the required area is correspondingly smaller. A relatively simple rule for the length of a compact reinforcing, consistent in area-length requirements with uniform wall reinforcing, is:



Elastic limit criteria:  $\bar{\sigma} = 2S$ , where  $\bar{\sigma}$  = maximum stress intensity

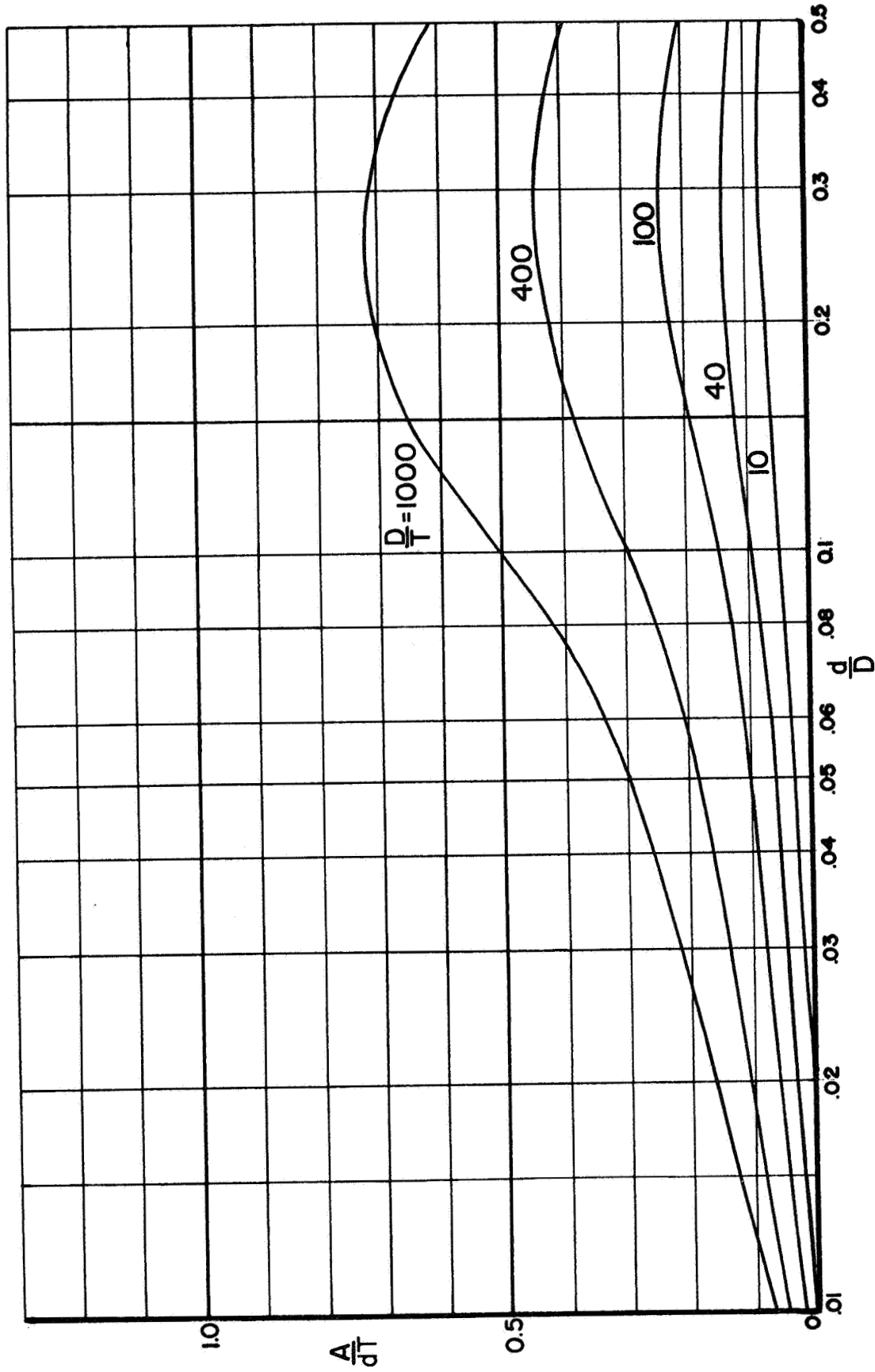
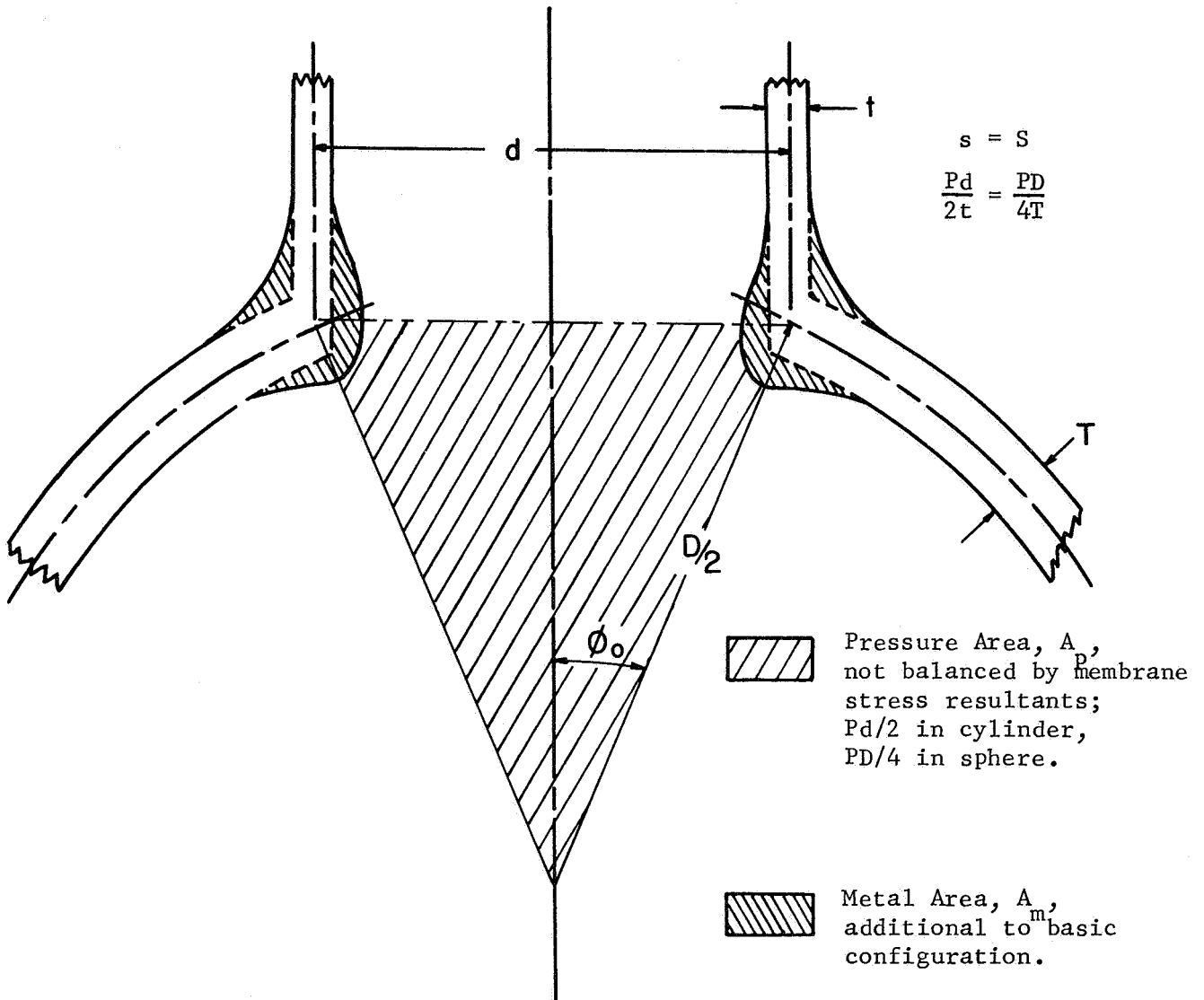


FIGURE 11. FILLET RADIUS REINFORCING AREA REQUIRED BY ELASTIC ANALYSIS,  $\bar{\sigma} = 2.0S$



For force equilibrium normal to plane shown:

$$S A_m = P A_p$$

(Thin Shells Assumed)

$$\frac{PD}{4T} A_m = P \cdot \frac{d}{2} \cdot \frac{D}{2} \cos \phi_0$$

$$A_m = dT \cos \phi_0$$

FIGURE 12. REINFORCING REQUIRED TO OBTAIN AN AVERAGE NORMAL STRESS EQUAL TO 1.0S

Uniform wall reinforcing area on sphere

Compact reinforcing area

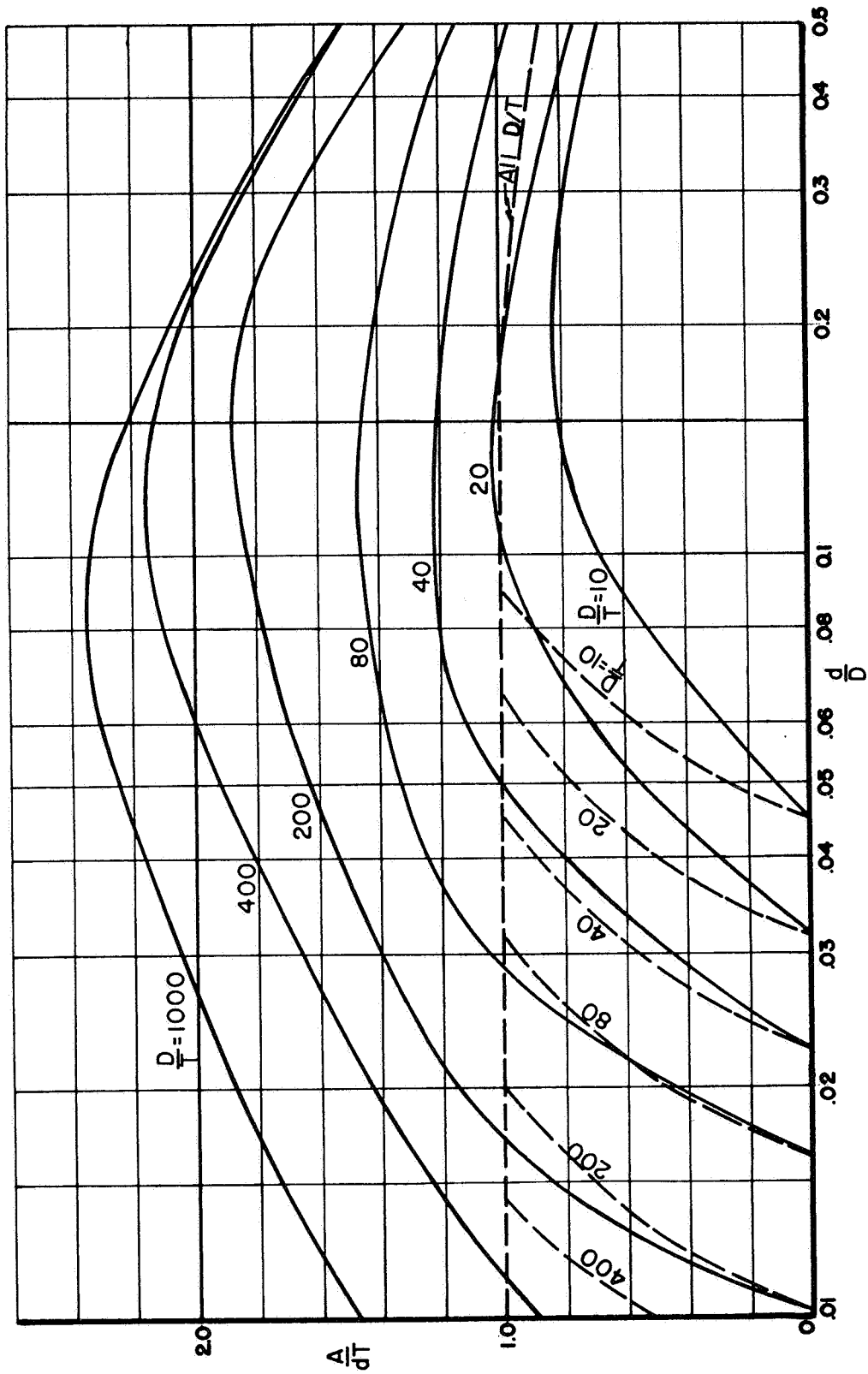


FIGURE 13. REINFORCING AREAS FOR REINFORCING ON THE SPHERE AND COMPACT REINFORCING

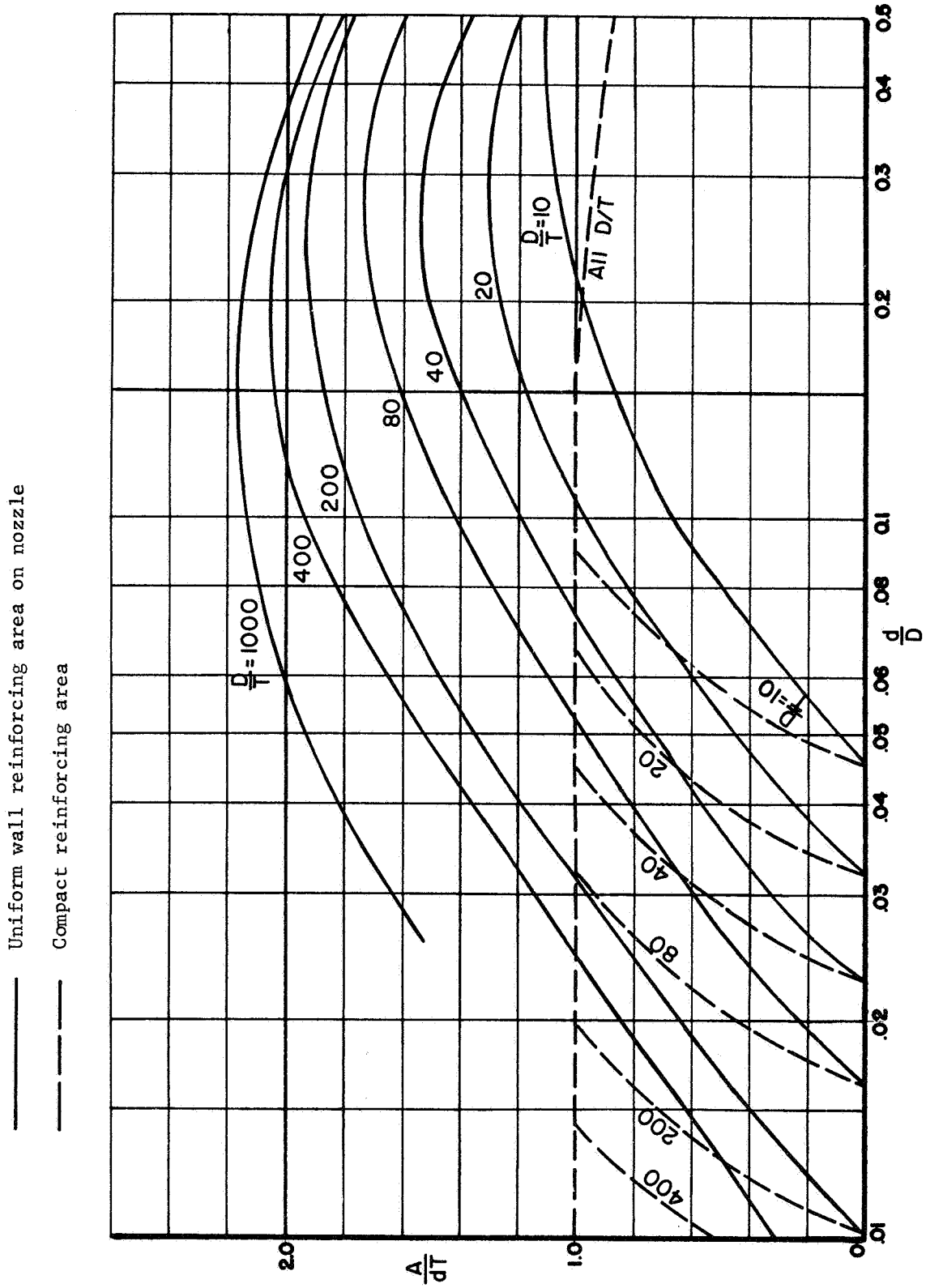


FIGURE 14. REINFORCING AREAS FOR REINFORCING ON THE NOZZLE AND COMPACT REINFORCING

$$L_c/D = 1.5 (T/D)^{2/3}. \quad (15)$$

Figure 15 shows the lengths of uniform wall reinforcing along with the lengths of compact reinforcing as defined by Equation 15. It will be noted that, in general, where the compact reinforcing length is smaller than that required for uniform wall thickness reinforcing, the required area is correspondingly smaller, and vice versa.

From purely geometric considerations, as shown in Figure 16, it is possible to place the required compact reinforcing area entirely outside the shell and within the prescribed zone.

Reinforcing areas required for fillet radii reinforcing, using the Seal-Shell-2 elastic-stress analysis (with  $\bar{\sigma} = 2.0S$ ), are compared with the reinforcing area required by the proposed design procedure for compact reinforcing in Figure 17. It is apparent that the design procedure is conservative with respect to the elastic-stress criteria, except for small  $d/D$  ratios where the elastic analysis would require a small amount of reinforcing. However, in these areas, the required minimum fillet radius for all nozzles ( $r_o \geq$  larger of  $t$  or  $T/4$ ) will be sufficient for pressure loading.

#### Radii and Transition Sections

The elastic analysis used as the basis of the procedure does not include stress concentrations that arise on the outside surface at the nozzle-sphere juncture. Comparison of test data with Waters' analysis indicates that, if the outside fillet radius,  $r_o$ , is about equal to the branch thickness,  $t$ , or larger, the analysis is not unconservative. With a fillet radius about equal to  $t$ , the reinforcing effect of the extra metal roughly compensates for the stress concentration of the notch. Accordingly, the proposed design procedure requires that  $r_o \geq t$  ( $t'$  for a pad on the nozzle).

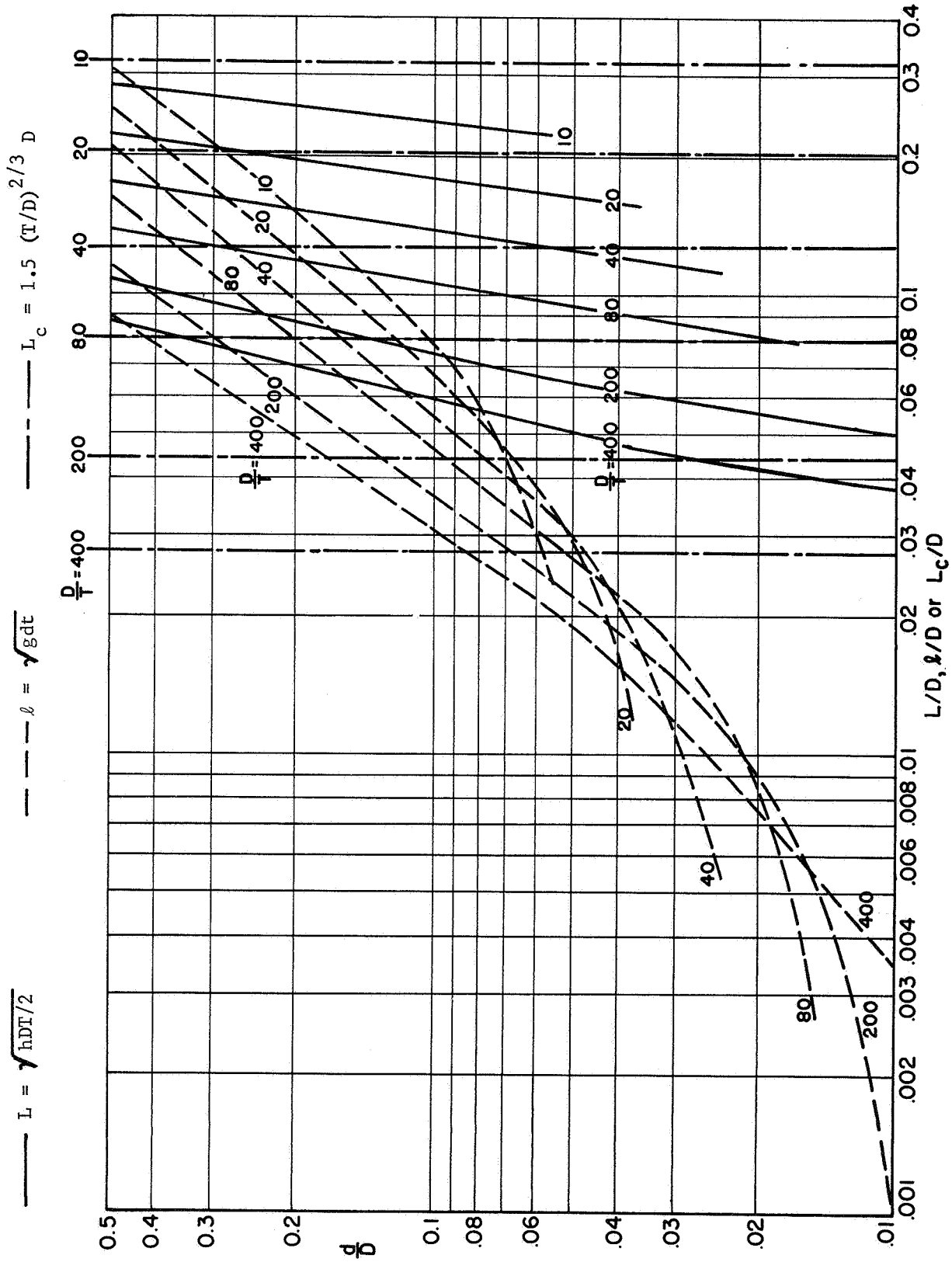
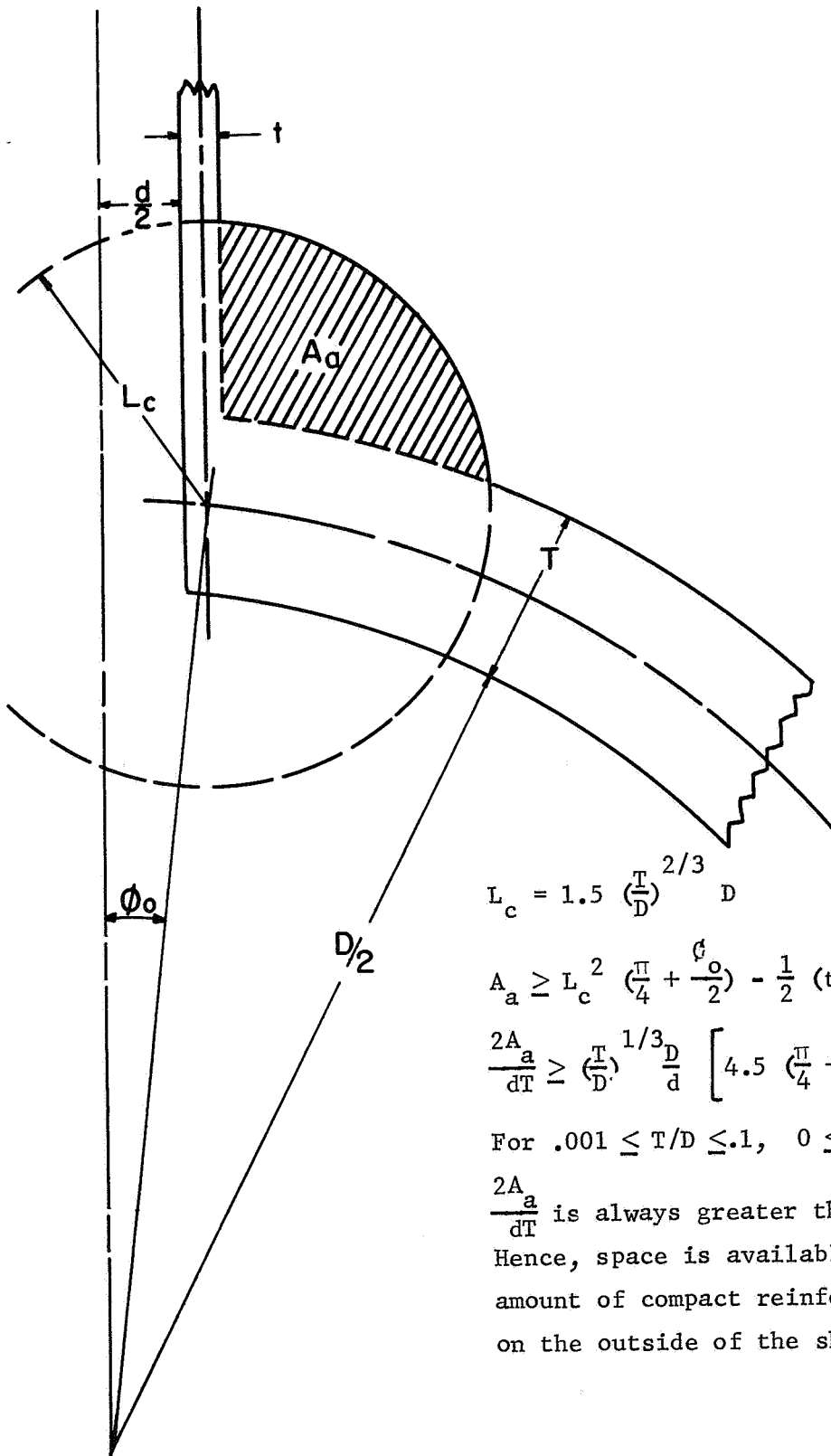


FIGURE 15. REINFORCING LENGTHS FOR UNIFORM WALL AND COMPACT REINFORCING



$$L_c = 1.5 \left(\frac{T}{D}\right)^{2/3} D$$

$$A_a \geq L_c^2 \left(\frac{\pi}{4} + \frac{\phi_0}{2}\right) - \frac{1}{2} (t + T) L_c$$

$$\frac{2A_a}{dT} \geq \left(\frac{T}{D}\right)^{1/3} \frac{D}{d} \left[ 4.5 \left(\frac{\pi}{4} + \frac{\phi_0}{2}\right) - 1.5 \left(2 \frac{d}{D} + 1\right) \left(\frac{T}{D}\right)^{1/3} \right]$$

$$\text{For } .001 \leq T/D \leq .1, \quad 0 \leq \frac{d}{D} \leq .5$$

$\frac{2A_a}{dT}$  is always greater than  $\cos \phi_0$ .

Hence, space is available for the required amount of compact reinforcing placed entirely on the outside of the shell.

FIGURE 16 . SPACE AVAILABLE FOR COMPACT REINFORCING

—— Fillet radii reinforcing,  $\bar{\sigma} = 2.0S$

- - - - Compact reinforcing, proposed rules

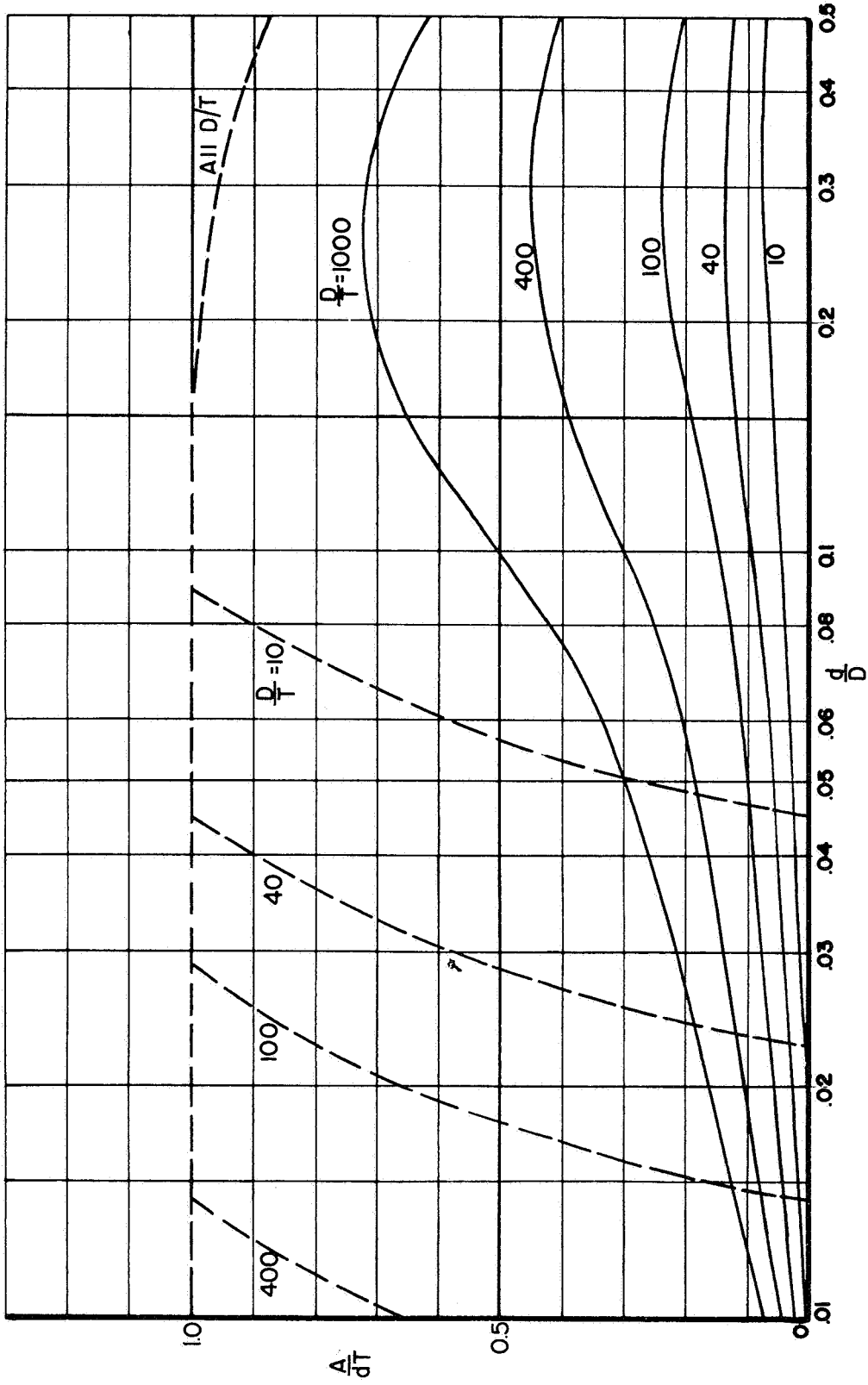


FIGURE 17. COMPARISON OF COMPACT REINFORCING AREA REQUIRED BY PROPOSED RULES WITH THE REINFORCING AREA FOR A FILLET RADIUS, ELASTIC ANALYSIS,  $\bar{\sigma} = 2.0S$



Small variations of the inside corner radius,  $r_i$ , on photoelastic test models had relatively little effect on the stress levels. Some radius on the inside corner is desirable from the standpoint of fatigue strength, and a very large inside corner radius would probably weaken the structure because of the reduction in area. Accordingly, the design procedure includes the somewhat arbitrary rule:

$$T/8 \leq r_i \leq T/4. \quad (16)$$

A change in wall thickness in a cylindrical or spherical shell produces locally increased stresses. This condition exists at the outer edges of the reinforcing prescribed in the design procedure. Design codes prescribe transition tapers between changes in wall thickness; in particular, Figure N-466 of the Nuclear Vessel Code requires a transition with a slope not greater than 1:3. Under the assumption that the stress conditions at the outer edge of the nozzle reinforcing is independent of the opening in the sphere, the same transition taper has been specified in the proposed design procedure.

Compact reinforcing as specified by Figure 1e, using a large outside fillet radius, directly insures good transition between reinforcing and the shells. Compact reinforcing consisting of a triangular external pad (Figure 1f) has transition radii compatible with those specified for uniform wall reinforcing. Compact reinforcing of arbitrary smooth profiles (Figure 1g) has transition and radii requirements that are comparable to those for the more specific shapes covered by the design procedure.

Requirements for reinforcing are specified in terms of minimums. It is possible, under certain conditions, to increase stress levels by adding reinforcement. For example, in certain parameter ranges of uniform-wall nozzle-to-sphere structures, monotonically increasing the nozzle thickness,  $t$ , results in a stress variation as indicated by Figure 18. The minimum value of  $\bar{\sigma}$  marked  $\bar{\sigma}_1$  occurs when the stiffness of the nozzle and sphere are particularly compatible. However, reducing  $\bar{\sigma}$  to  $3S$  generally requires a considerably greater nozzle thickness, as indicated by  $\bar{\sigma}_2$ . It is possible that a similar minimum occurs with compact reinforcing.

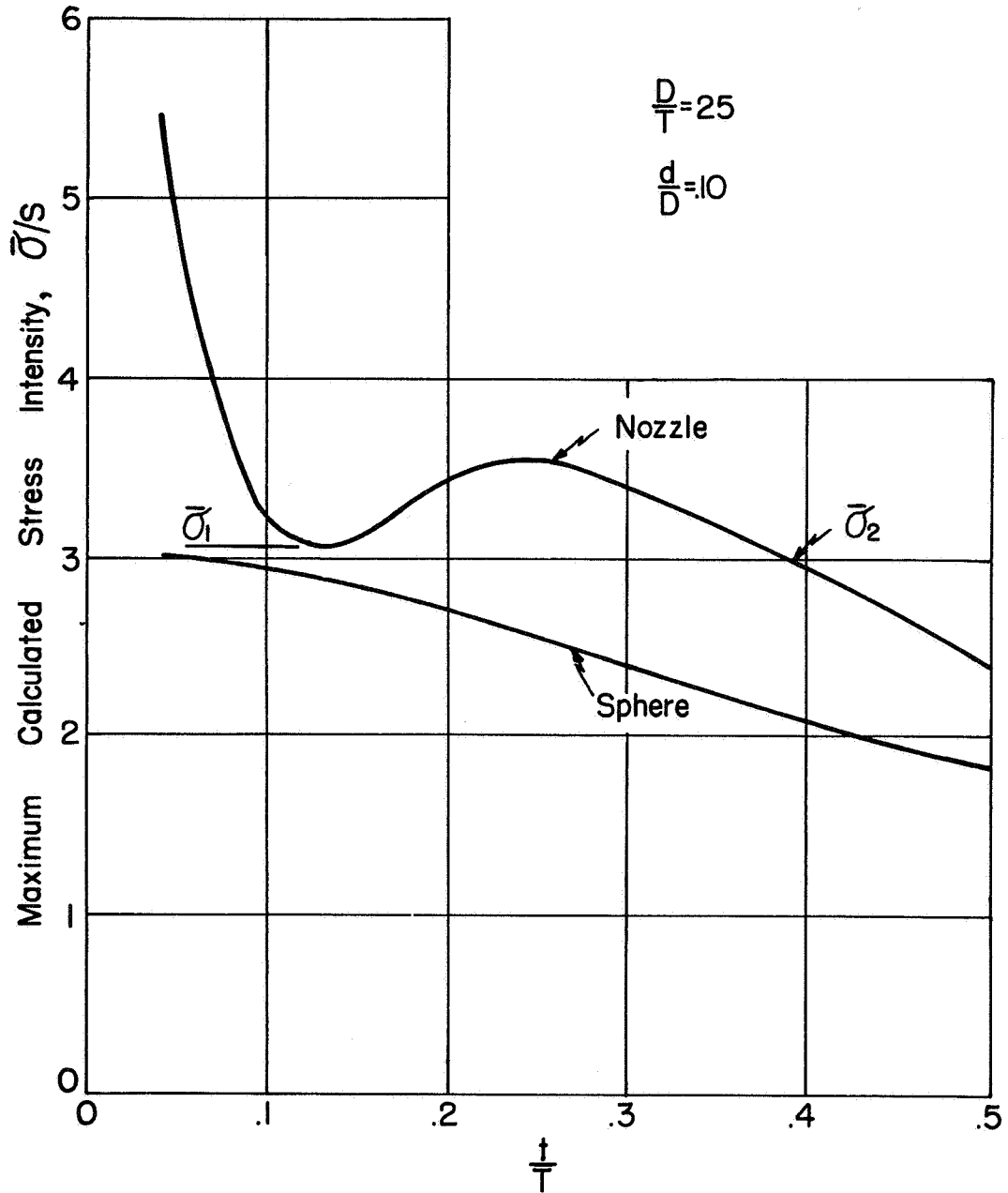


FIGURE 18. EXAMPLE OF VARIATION IN STRESS WITH NOZZLE THICKNESS

More directly, however, increased thickness of reinforcing may result in increased stresses at the outer edges of the reinforcing. Transition sections and radii are specified in the design procedure to minimize this possibility.

The design procedure generally requires increased fillet radii or transition sections in proportion to the amount of over-reinforcing. In Figure 1a, for example,  $r_o$  must be larger than  $t'$  rather than  $gt$ ; if  $t'$  is larger than  $gt$  (over-reinforced), the required fillet radius is proportionally increased. Similarly, the transition section increases in proportion to  $(t' - t)$ , not  $(gt - t)$ . The additional requirement that  $r_o \geq T/4$  insures a transition section reasonably proportioned with respect to the sphere wall, even if the nozzle wall is very thin. Figures 1b, 1c, and 1d are similar, with regard to transitions for over-reinforced designs, to Figure 1a. In Figure 1e the reinforcing area is directly obtained by the fillet radius so that over-reinforcing necessarily requires a larger radius. Transitions in Figures 1f and 1g are directly proportional to the amount of over-reinforcing, i.e., by the factor  $2A/A_r$ , where  $A$  is the actual reinforcing area on each side of the nozzle centerline, and  $A_r$  is the total required reinforcing area.

COMPARISON WITH OTHER DESIGN PROCEDURESCurrent American Practice

Reinforcement of openings is specified in several American Design Codes<sup>(4,17,18,19,20)</sup>. These codes all require that the material cut out by the opening,  $d_i T$ , be replaced around the opening within a specified zone. For all except the Nuclear Vessel Code, the zone of reinforcement is defined as shown in Figure 19. The Nuclear Vessel Code specifies a reinforcing zone in terms of the foundation modulus of the nozzle or shell, as shown in Figure 20. In this respect, the Nuclear Vessel Code is similar to the proposed design procedure.

A comparison between the reinforcing area required by the proposed design procedure and the area  $dT$  is shown in Figure 13, uniform wall reinforcing on shell, and Figure 14, uniform wall reinforcing on nozzle. The required areas of compact reinforcing are also shown on these graphs. Those openings which do not require reinforcing, according to the Nuclear Vessel Code, are shown on Figure 21; these are in general agreement with the proposed rules.

For uniform wall reinforcing, there are combinations of  $d/D$  and  $D/T$  for which the proposed design procedure requires significantly more reinforcing than the current rule of  $dT$ --up to 2.3 times as much. For compact reinforcing, however, the proposed design procedure does not require any more reinforcing than the current rule.

There is, of course, an interdependence between area of reinforcement and the zone in which the reinforcement is placed. Accordingly, whether the current rules are unconservative, as judged by the present analysis, depends upon the "compactness" of the zone of reinforcing specified by the current rules. Since the current rules require a reinforcing area  $dT$ , which is greater than that required for compact reinforcing, the current rules are conservative with respect to the proposed design procedure if the zone of reinforcement is no greater than that specified by Equation 15.

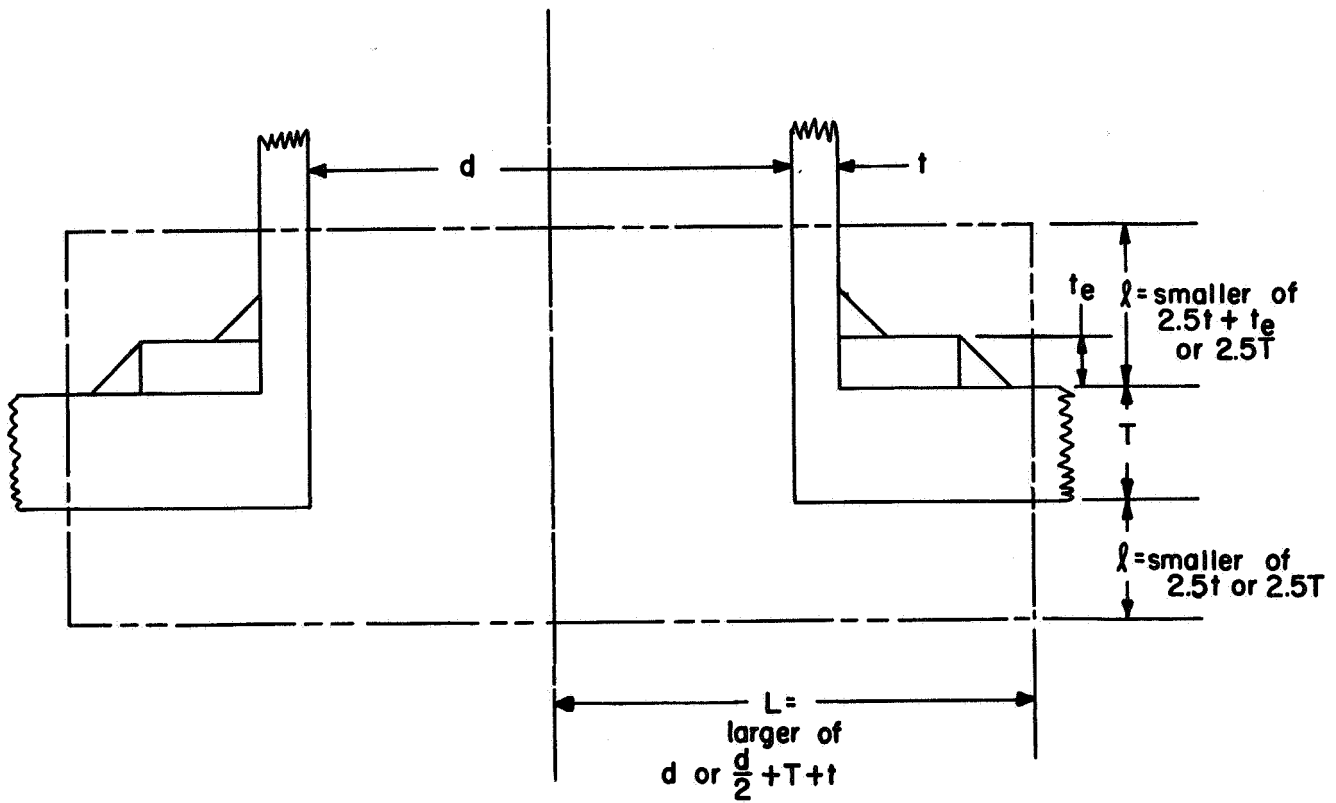


FIGURE 19. REINFORCEMENT ZONE, CURRENT AMERICAN PRACTICE  
EXCEPT THE ASME NUCLEAR VESSEL CODE

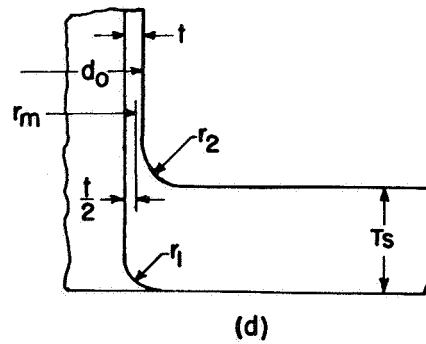
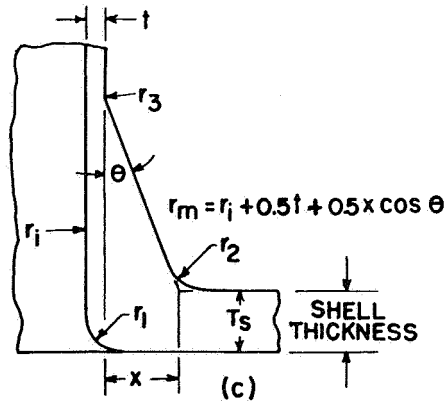
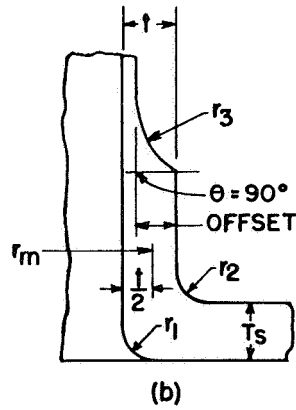
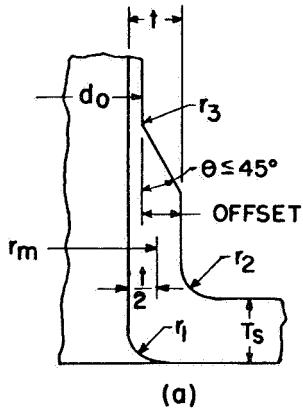
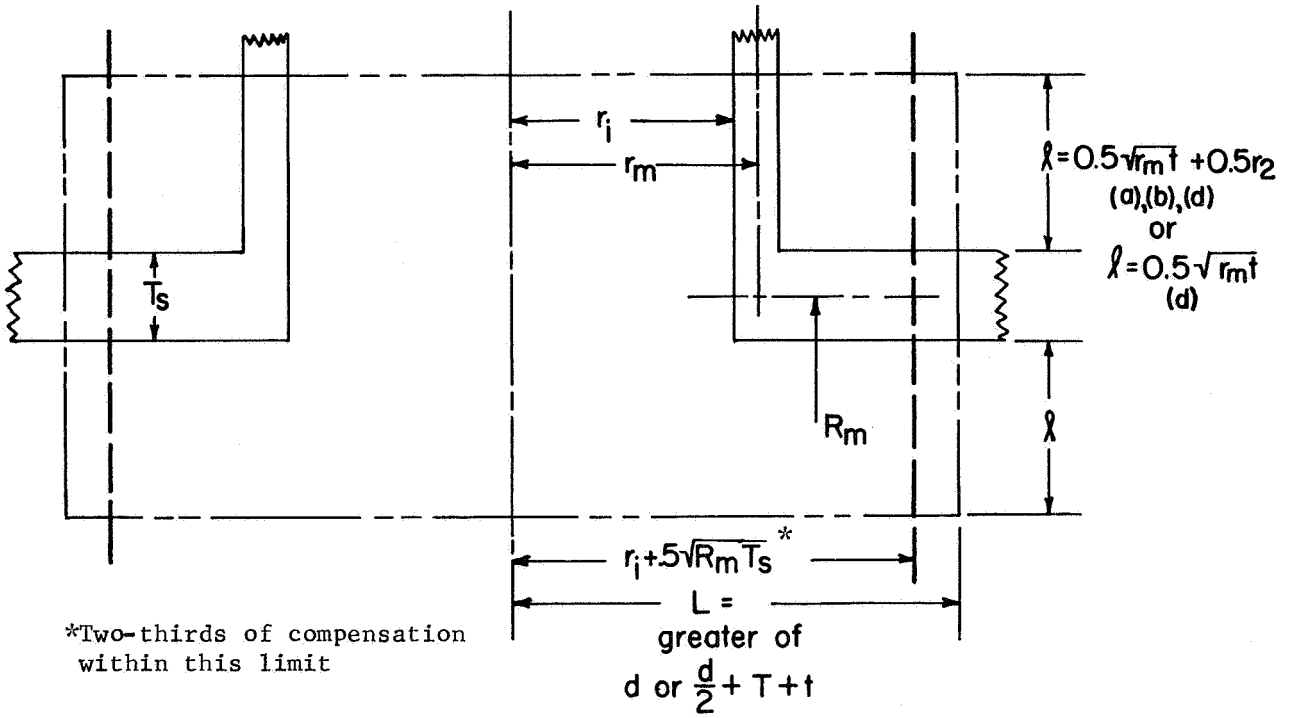
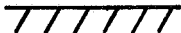
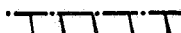



FIGURE 20. REINFORCEMENT ZONE, ASME NUCLEAR VESSEL CODE

 Reinforcing not required, ASME Nuclear Code (1963)  
 Reinforcing not required, ASME Nuclear Code (1965)  
 Limit Pressure Analysis

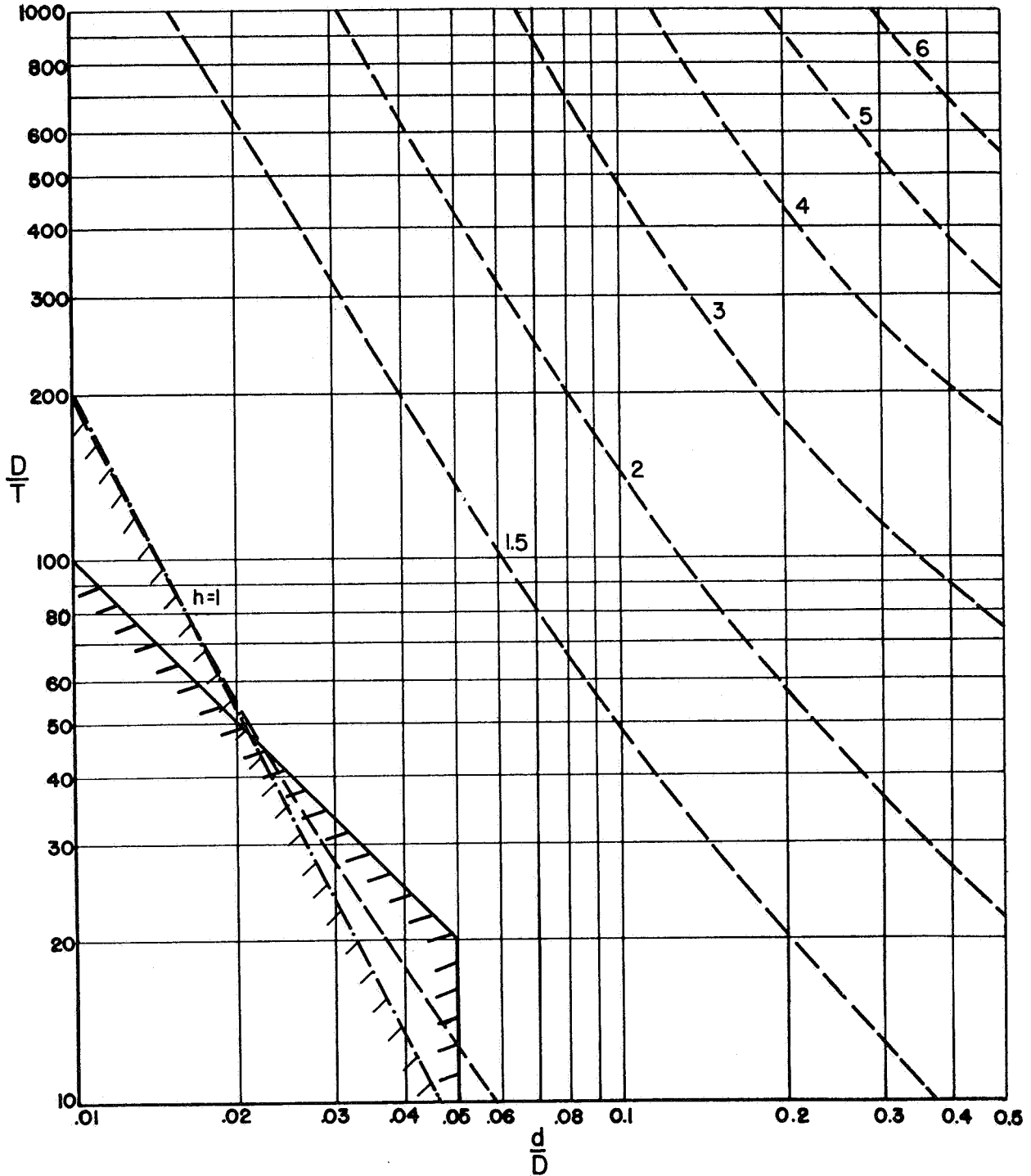


FIGURE 21. NOZZLES NOT REQUIRING REINFORCING IN ACCORDANCE WITH THE ASME NUCLEAR VESSEL CODE

For a pad on the sphere, where current rules specify a zone limit of  $0.5d$ , it may be seen from Figure 22 (compare  $L_2/D$  line with  $L_c/D$  lines) that present rules are unconservative only for combinations of large  $D/T$  with large  $d/D$ -ratios. For reinforcing on the nozzle, where current rules permit a zone limited to  $2.5t$ , Figure 22 shows (compare  $L_1/D$  lines with corresponding  $D/T - L_c/D$  lines) that the current rules are conservative throughout the parameter range covered.

### Leckie and Penny Analysis

Present British practice for reinforcing nozzles (BS-1500) is essentially the same as ASME Boiler Code Section VIII. However, consideration is being given to a nozzle design procedure based on Leckie and Penny's analysis, with a maximum stress concentration factor of 2.25. Figures 23 and 24 show the  $h$ - and  $g$ -factors derived on this basis (flush nozzles) and can be compared with the analogous Figures 6 and 7.

Comparisons in Figures 23 and 24 of the solid lines with the dashed lines show that, except near  $g$  or  $h = 1.0$ , the proposed design procedure requires more reinforcing than the Leckie-Penny analysis with  $\sigma_{\max} = 2.25S$ .

### German Practice

In some design procedures for reinforcements of openings, the German practice is essentially the same as the ASME Code, i.e., replacement of the cutout area  $dT$  in a prescribed zone close to the opening. For uniform wall reinforcing, however, design charts\* are in use which are based on tests to establish the pressure required to produce a permanent strain

---

\* DK 621.642.02.001.24, Design of Pressure Vessels, AD-Note B9, January, 1960. Vereinigung der Technischen Überwachungs-Vereine e.V., Essen, Huysenalle 54/56.



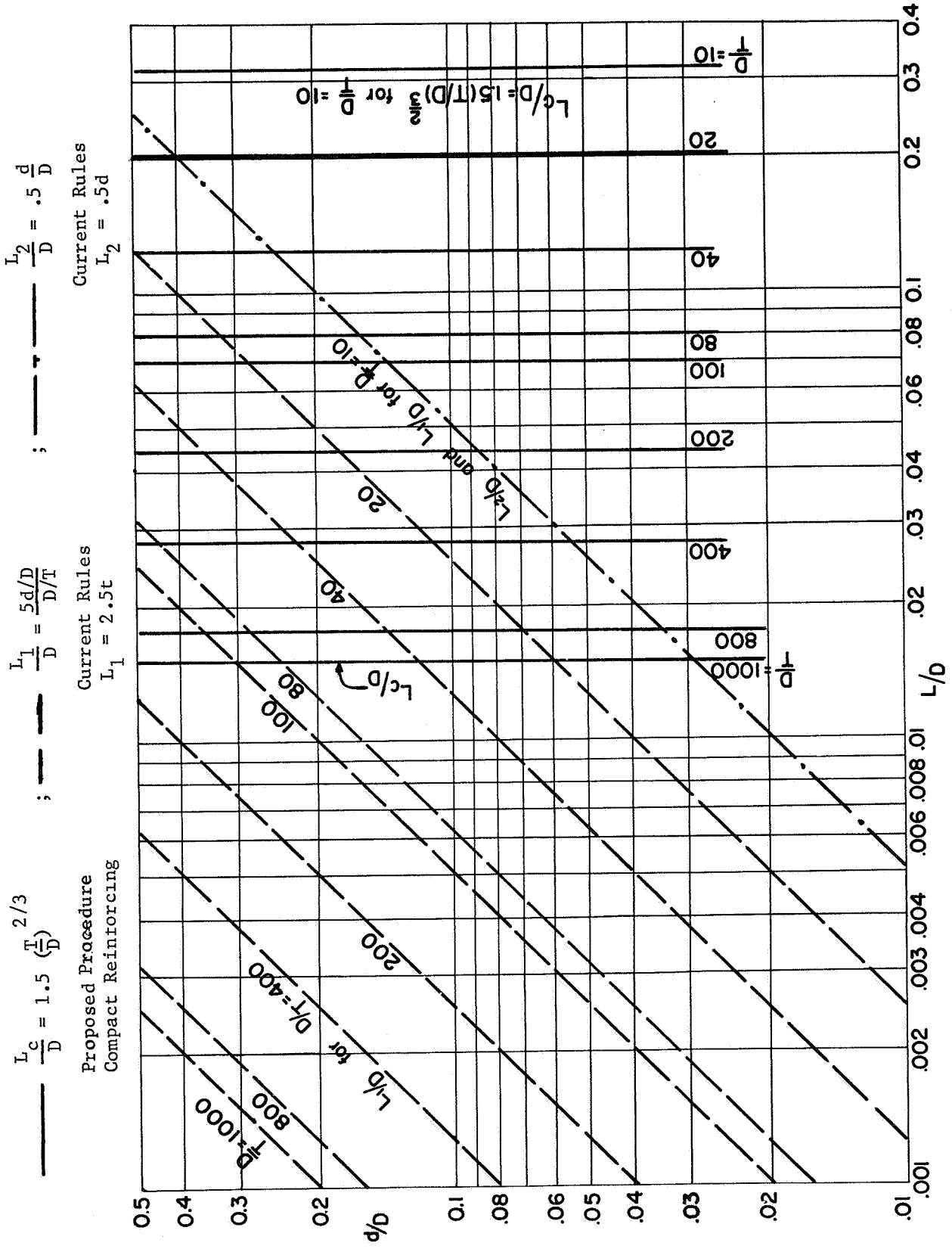


FIGURE 22. COMPARISON OF REINFORCEMENT ZONES

————— Leckie-Penny,  $\sigma = 2.25S$   
 $\sigma =$  maximum stress in sphere  
 - - - - - Limit Pressure Analysis

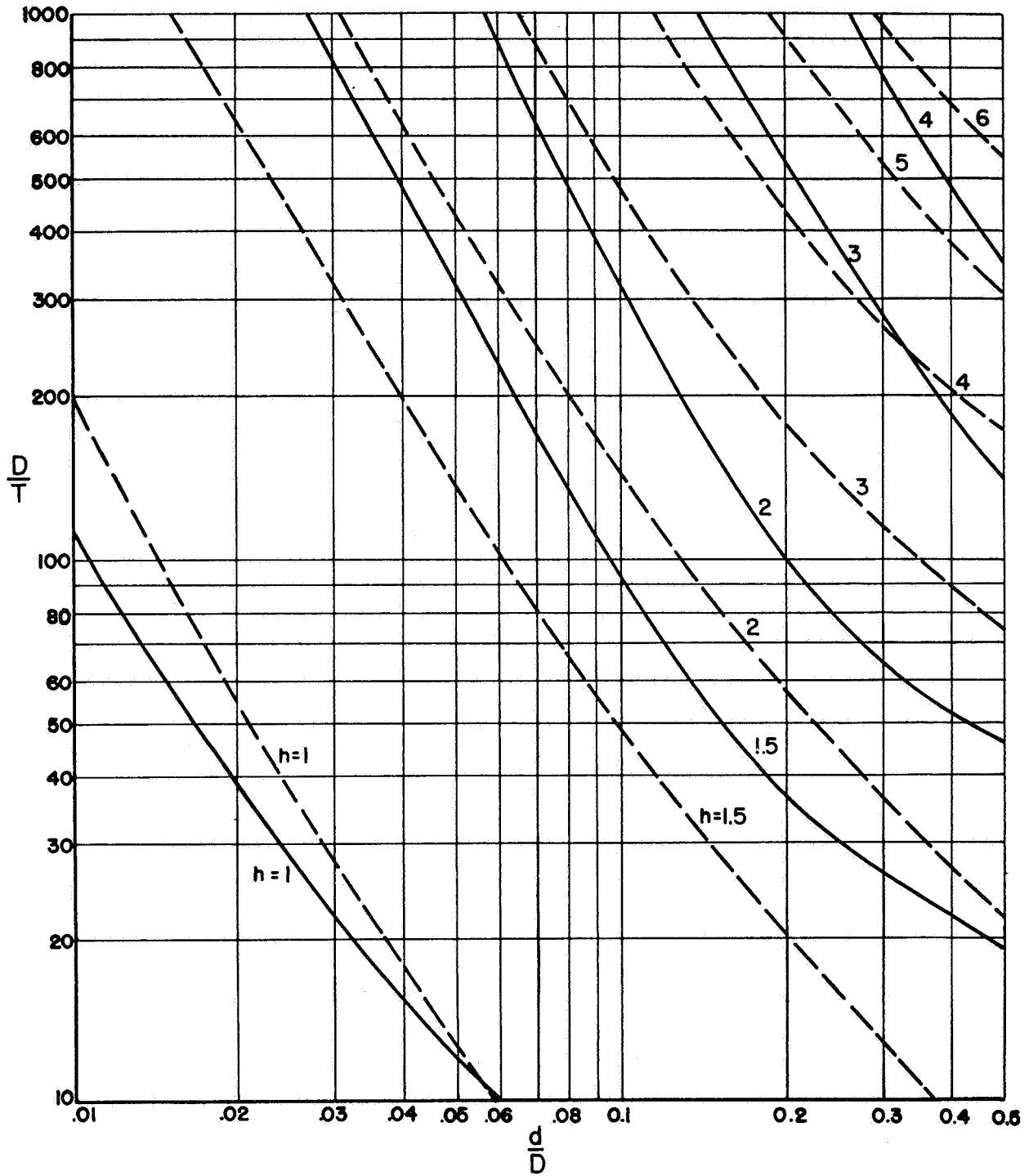


FIGURE 23. SHELL REINFORCING AS REQUIRED BY LECKIE-PENNY ANALYSIS WITH A MAXIMUM STRESS IN THE SPHERE OF 2.25S

Leckie-Penny,  $\sigma = 2.25S$

- $\sigma =$  maximum stress in sphere
- - - Limit Pressure Analysis

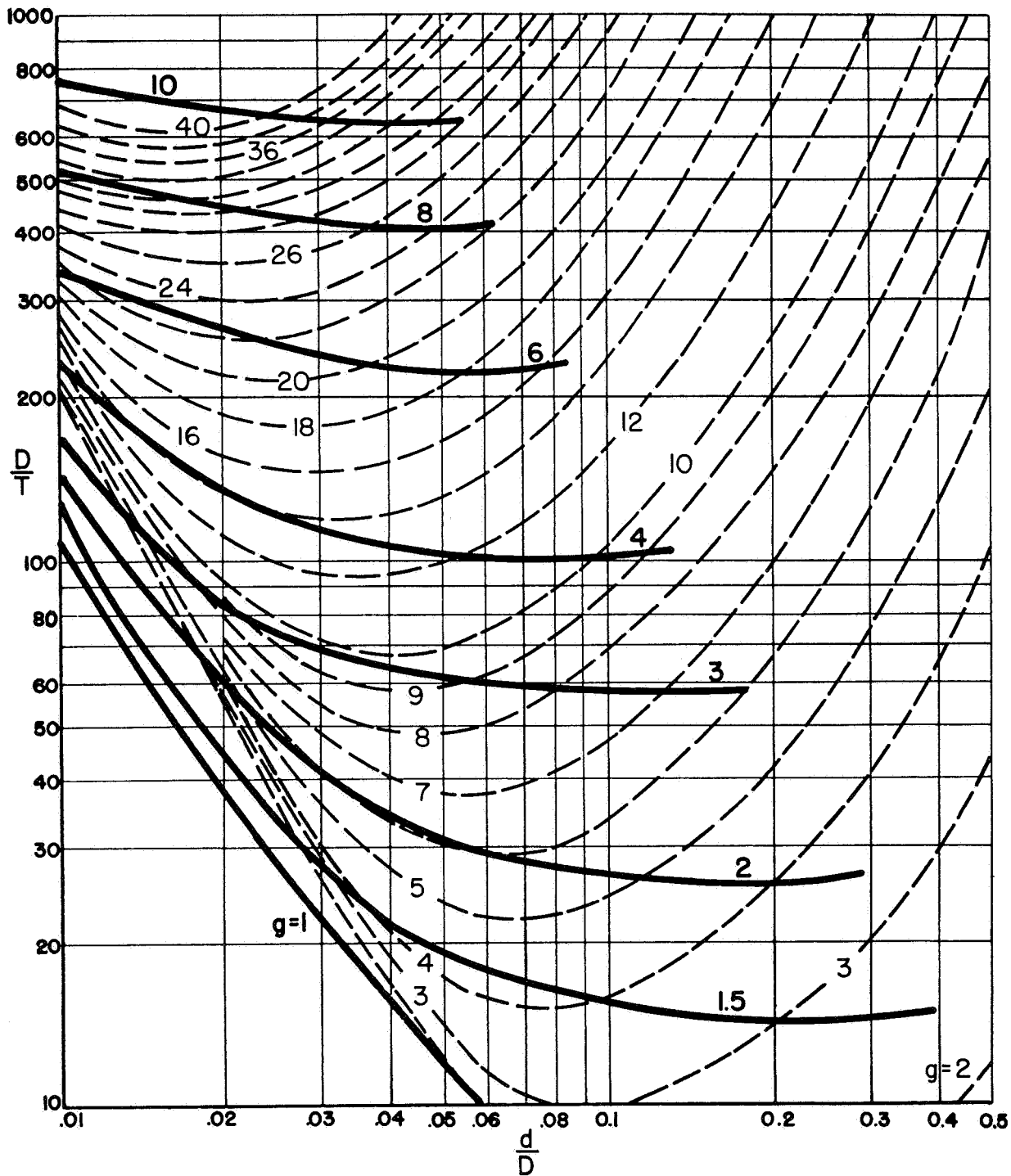


FIGURE 24. NOZZLE REINFORCING AS REQUIRED BY LECKIE-PENNY ANALYSIS WITH A MAXIMUM STRESS IN THE SPHERE OF 2.25S

of 0.2 per cent. In contrast to the purely elastic analysis considered for use in Britain, this German practice corresponds to an experimental limit pressure analysis. The German design chart is apparently based entirely on tests on nozzles in cylindrical shells; however, it is used for nozzles in spherical shells or formed heads. This is analogous to the Leckie-Penny analysis, which is theoretically applicable only to nozzles in spheres but is also used for nozzles in cylinders.

Data given in the German design charts have been converted to h- and g-factors for comparison with the proposed design procedure, as shown in Figures 25 and 26. Figure 25 shows that the German empirically derived limit pressure rules for reinforcing on the sphere are quite similar to the rules derived by a theoretical limit analysis for a nozzle in a sphere, although generally less conservative. Figure 26, for reinforcing on the nozzle, shows that the German rules are different than the analogous curves derived by a limit analysis and that the German rules are less conservative, except for combinations of small  $d/D$  and  $D/T$  ratios.

RLC/ECR:do/mew

June 8, 1965

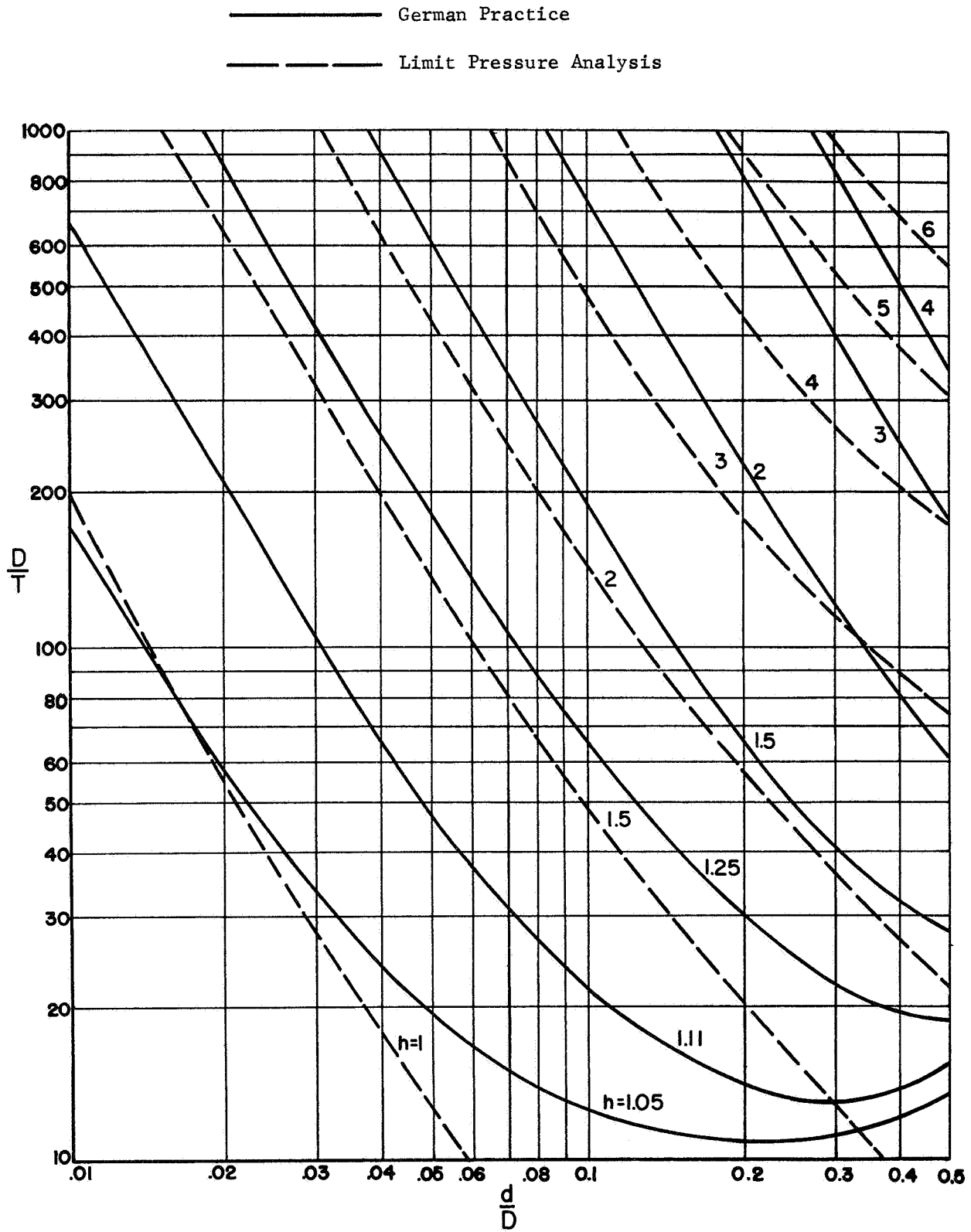


FIGURE 25. SHELL REINFORCING AS REQUIRED BY GERMAN PRACTICE, DESIGN CRITERIA OF 0.2% MAXIMUM STRAIN

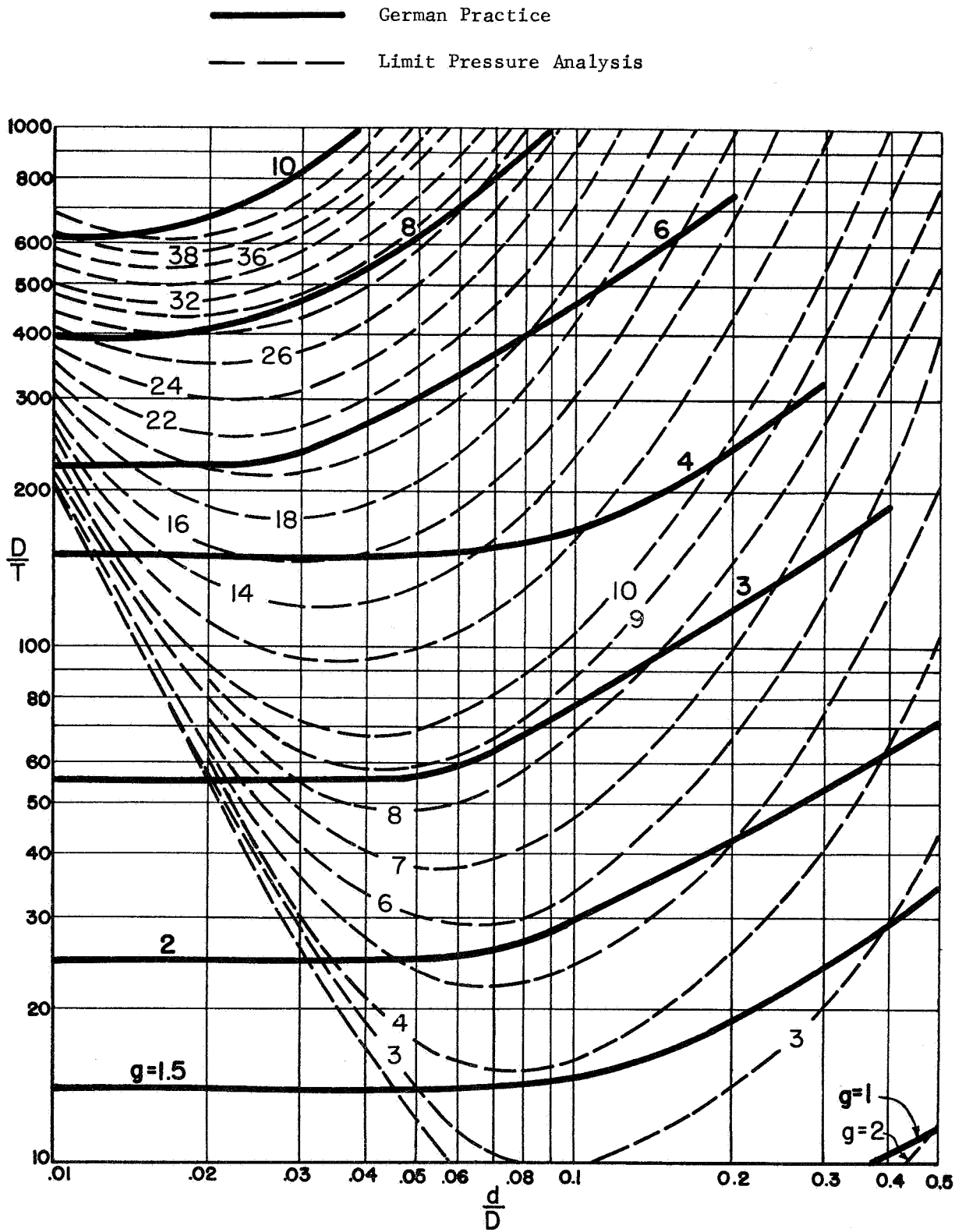


FIGURE 26. NOZZLE REINFORCING AS REQUIRED BY GERMAN PRACTICE, DESIGN CRITERIA OF 0.2% MAXIMUM STRAIN

REFERENCES

1. Mershon, J. L., "PVRC Research on Reinforcement of Openings in Pressure Vessels", Welding Research Council Bulletin No. 77, May, 1962.
2. Mershon, J. L., "PVRC Interpretive Report of Pressure Vessel Research, Section I, Design Considerations, Part 1.6, Reinforcement of Openings Under Internal Pressure", Welding Research Council Bulletin No. 95, April, 1964.
3. "Criteria of Section III of the ASME Boiler and Pressure Vessel Code for Nuclear Vessels", ASME Boiler and Pressure Vessel Code Committee.
4. ASME Boiler and Pressure Vessel Code, Section III, Rules for Construction of Nuclear Vessels, published by the American Society of Mechanical Engineers, 345 East 47th Street, New York, New York.
5. Cloud, R. L., "The Limit Pressure of Radial Nozzles in Spherical Shells", Nuclear Structural Engineering, Vol 1, No. 4.
6. Waters, E. O., "Stresses Near a Cylindrical Outlet in a Spherical Vessel", Welding Research Council Bulletin No. 96, May, 1964.
7. Leckie, F. A., and Penny, R. K., "Stress Concentration Factors for the Stresses at Nozzle Intersections in Pressure Vessels", Welding Research Council Bulletin No. 90, September, 1963.
8. O'Donnell, W. J., "The Additional Deflection of a Cantilever Due to the Elasticity of the Support", Journal of Applied Mechanics, September, 1960.
9. Leven, M. M., "Photoelastic Determination of the Stresses in Reinforced Openings in Pressure Vessels", Westinghouse Electric Corporation Report 64-9D7-514-R1, October 30, 1964.
10. Taylor, C. E., and Lind, N. C., "Photoelastic Study of the Stresses Near Openings in Pressure Vessels", University of Illinois T & AM Report No. 270, March, 1965.
11. Riley, W. F., "Experimental Determination of Stress Distributions in Thin Walled Cylindrical and Spherical Pressure Vessels with Circular Nozzles", IIT Research Inst. Proj. No. M6053, Phase Report No. 1.

12. Pickett, Schmidt, and Gregory, "Studies of the Fatigue Strength of Pressure Vessels", Southwest Research Institute Proj. Nos. 03-1274, 03-1275, and 03-1384, Progress Report No. 8, May, 1964.
13. Hetenyi, M., "Beams on Elastic Foundation", The University of Michigan Press, Ann Arbor, Michigan.
14. Witt, F. J., Oak Ridge National Laboratory, Oak Ridge, Tennessee. A parametric study of nozzles in spheres using a two-piece-shell theory developed by F. A. Leckie and R. K. Penny with modifications. The study covers the parameter ranges  $0.01 \leq d/D \leq 0.5$ ,  $0.01 \leq t/T \leq 3.0$ ,  $10 \leq D/T \leq 1000$ . Stresses due to internal pressure, axial load on the nozzles, and moment on the nozzle are computed.
15. Friedrich, C. M., "Seal-Shell-2, A Computer Program for the Stress Analysis of a Thick Shell of Revolution with Axisymmetric Pressures, Temperatures, and Distributed Loads", Bettis Atomic Power Laboratory Report WAPD-TM-398.
16. Cloud, R. L., "Minimum Weight Design of a Radial Nozzle in a Spherical Shell", Trans. of ASME, Journal of Applied Mechanics, June, 1965, Vol 32, Series E.
17. ASME Boiler and Pressure Vessel Code, Section I, Power Boilers (see Reference 4).
18. ASME Boiler and Pressure Vessel Code, Section VIII, Unfired Pressure Vessels (see Reference 4).
19. Code for Pressure Piping, ASA B31.1, American Standards Association, 10 East 40th Street, New York, New York.
20. API Recommended Rules for Design and Construction of Large, Welded, Low Pressure Storage Tanks, API Standard 620, American Petroleum Institute, 111 West 50th Street, New York, New York.



PHASE REPORT NO. 2

on

STRESSES AT NOZZLES IN SPHERICAL SHELLS  
LOADED WITH PRESSURE, MOMENT OR THRUST

July 15, 1966

to

UNITED STATES ATOMIC ENERGY COMMISSION

by

E. C. Rodabaugh  
Battelle Memorial Institute  
Columbus, Ohio  
(Battelle Contract No. W-7405-eng-92)

F. J. Witt  
Oak Ridge National Laboratory  
Oak Ridge, Tennessee

R. L. Cloud  
Westinghouse Electric Corporation  
Bettis Atomic Power Laboratory  
Pittsburgh, Pennsylvania

Section 2

TABLE OF CONTENTS

	<u>Page</u>
INTRODUCTION . . . . .	1
SCOPE. . . . .	2
SUMMARY. . . . .	4
NOMENCLATURE . . . . .	9
COMPARISON OF THEORIES . . . . .	13
General Comments. . . . .	13
Leckie-Penny Analysis . . . . .	14
CERL Code . . . . .	15
Waters' Analysis. . . . .	23
Bijlaard Analysis . . . . .	34
Kalnins' Analysis and Computer Program . . . . .	36
Seal-Shell-2. . . . .	44
The Battelle Axisymmetric Stress Intensity Code - BASIC . . . . .	51
Use of Computer Programs. . . . .	54
COMPARISON OF THEORIES WITH TEST DATA. . . . .	55
General Comments. . . . .	55
Internal Pressure Loading . . . . .	55
Model BUSHips D . . . . .	55
Uniform Wall Models. . . . .	59
Models with Local Reinforcing. . . . .	93
Moment or Thrust Loading. . . . .	116
Models with Small Fillet Radius. . . . .	116
Models without a Fillet Radius . . . . .	128
Fabricated Models with Local Reinforcing . . . . .	137
DISCUSSION OF RESULTS IN RELATIONSHIP TO PRESENT CODES AND PRACTICES. . . . .	149
Pressure Loading. . . . .	149
Replacement Area, d <sub>i</sub> T. . . . .	149
ASME Section III Stress Indices. . . . .	149
Moment Loading, Comparison with ASA B31.1 . . . . .	154

TABLE OF CONTENTS (contd)

	<u>Page</u>
Combined Pressure and Moment Loading. . . . .	162
Linear Superposition of Stresses . . . . .	162
Location of Maximum Stresses . . . . .	163
Relative Magnitude of Stresses from Pressure or Moment Loading . . . . .	164
Stresses in Phase I Designs . . . . .	172

APPENDIX

DESIGN GRAPHS. . . . .	A-1
------------------------	-----

## INTRODUCTION

Nozzles in pressure vessels may be loaded by external forces as well as internal pressure. To evaluate critical stress conditions at the nozzles, it is necessary to determine the stresses due to each of these loads and combinations thereof.

Several analytical and experimental investigations have been made to assist the pressure vessel designer to determine stresses at nozzles in spherical vessels or heads. Bijlaard<sup>(1-6)\*</sup> developed an analysis for either a rigid plug (references 1, 2, and 5) or a pipe nozzle (references 3, 4, and 6) in a spherical shell, subjected to either moment or thrust loading applied to the plug or pipe nozzle. Graphs were prepared showing stress resultants and displacements for the sphere covering a range of dimensional parameters. The above work by Bijlaard has been replotted in more readable form and presented as a part of a design manual by Wichman, Mershon, and Hopper<sup>(7)</sup>. Since Bijlaard did not compute the stress resultants in the nozzles, the maximum stresses may not be indicated by these references. In addition, the data are somewhat difficult to use in design work because of the required interpolations between graphs.

Leckie and Penny<sup>(8, 9, 10)</sup> developed a somewhat more general analysis for nozzles in spheres, with loadings of internal pressure, moment on the nozzle, thrust on the nozzle or shear on the nozzle. Their Reference 10 presents maximum stresses in the sphere for these three loads. They found it possible to present these maximum stresses as functions of  $t/T$  and  $(r/R) \sqrt{R/T}$  only; thereby providing a major advantage in convenience to the user. This design information, however, is limited in two respects: (1) stresses in the nozzles are not given, and (2) since neither the location or direction of the maximum stress in the sphere is given (and, in general, these are not the same for various loads), it is not possible to find the stresses due to a combination of loads.

---

\* Numbers in raised parentheses refer to list of references at end of Report.

Waters<sup>(11)</sup> developed an analysis for nozzles in spheres subjected to internal pressure, including some boundary conditions not considered by Leckie and Penny. This analysis, with some additional refinements, was used by Cloud & Rodabaugh<sup>(12)</sup> to define elastic stress magnitudes in establishing a design procedure for radial nozzles in spherical vessels loaded with internal pressure.

The analyses described above are essentially "two-piece" shell theories, i.e., a cylindrical nozzle joined to a spherical shell segment. These analyses cannot directly indicate the effect of any local reinforcing, such as a fillet radius at the outside of the nozzle-sphere juncture. Computer programs<sup>(13, 14)</sup> which permit breaking the nozzle-sphere juncture into a "multipiece-shell" of variable midsurface and wall thickness are available; these are useful in evaluating the effect of the local details of the nozzle-sphere juncture. Also, a computer program<sup>(15)</sup> is available which treats the axisymmetric structure with axisymmetric loading as a three-dimensional elastic problem without the simplifications of shell theory.

In addition to the analytical work discussed above, extensive experimental work has been completed; a major part of which is summarized by Mershon<sup>(16, 17, & 35)</sup>.

#### SCOPE

This report presents information on the stresses in the neighborhood of a juncture of a cylindrical nozzle mounted radially on a spherical shell segment. The nozzle is considered to be isolated from other nozzles or geometric discontinuities. Loadings considered are (a) internal pressure, (b) moment applied to the nozzle, and (c) thrust applied to the nozzle. The report consists of:

- (1) A brief discussion and extensive numerical comparisons of various theoretical methods used for calculating stresses for nozzles in spherical shells.

- (2) Comparisons of calculated stresses with measured stresses of nozzles in spheres; these comparisons are made for 70 different test models, involving a wide range of dimensions and details of local reinforcing.
- (3) A discussion of the results of (1) and (2) in relationship to present pressure vessel and piping codes and practices.
- (4) Design Graphs, based on "two-piece" elastic shell theory, from which stresses can be determined at the nozzle-sphere juncture for pressure, moment or thrust loads, or combinations thereof. Examples of the use of the design graphs are included in this part.

Part 4 of the Report is intended to be useable for design work without reference to the remainder of the Report. For this purpose, it is included as an Appendix.

SUMMARYComparison of Theories

The "two-piece" shell theories used in this Report are:

Bijlaard: Moment or thrust loadings

Waters: Internal pressure

Leckie-Penny: Internal pressure, moment or thrust loadings

Kalnins: Internal pressure, moment or thrust loadings

(As a two-piece theory)

The basis of each of these theories is briefly discussed. Within the range of dimensional parameters covered, it was found that Bijlaard, Leckie-Penny and Kalnins theories give essentially the same results. Waters theory gives different results than Leckie-Penny or Kalnins theories; the reasons for these differences are considered and numerical comparisons are given.

"Multi-piece" shell theories used (in the form of computer programs) were those of Kalnins and Seal-Shell-2. The development of these two programs is discussed, along with numerical comparisons: Kalnins theory is based on thin-shell assumptions; Seal-Shell-2 is more applicable to thick shells and, in general, agrees better with test data than Kalnins.

A computer program entitled "BASIC", which uses point matching for axisymmetric bodies of revolution subjected to axisymmetric forces, is briefly discussed and the results for an example are shown.

Comparison of Theories with Test DataInternal Pressure Loading

Comparisons are made between the theories and results from some 55 test models. Most of the test models included a fillet radius at the juncture of nozzle and the sphere; the comparison between two-piece shell theories and test results were, in most cases, strongly dependent upon

the size of the fillet radius,  $r_o$ . For models which were considered as essentially consisting of a uniform-wall nozzle in a uniform-wall sphere, Waters' theory was found to be conservative provided that  $r_o/t$  is greater than about 0.8 and the theory is fairly accurate for predicting the maximum stress for  $r_o/t$  between about 0.5 and 3.

Modifications to Waters' theory involving the actual wall thicknesses at the juncture, "curved-beam" effects and Lamé-type effects brought the modified theory into better agreement with test data, particularly with large fillet radii.

Comparisons of test data with the multipiece shell programs gave, in most cases, quite good agreement. Comparisons are limited to models with  $d/D$  of 0.2 or larger. There are tentative indications that these programs may be of limited applicability to nozzles with small  $d/D$  ratios and an abrupt transition between a small thickness nozzle wall and a large thickness sphere wall.

The significance of stresses at the outer edges of reinforcing is noted; abrupt transitions between heavy reinforcing and thin nozzle or sphere walls can give rise to high stresses, even though the opening, per se, is adequately reinforced.

The Seal-Shell-2 program was used to develop a parametric study of reinforcing provided by a fillet radius. This study results in a simple equation for the size of fillet radius required to achieve a stress intensity index of 2.0. Comparison of this theoretical equation with test data is generally satisfactory. For small  $d/D$  ratios and thick-wall spheres, however, a very large fillet radius apparently is required to reduce the maximum stress intensity index to 2.0.

Variations of the inside corner radius, within the range of the test models, had relatively little effect on the magnitude of the stresses.

#### Moment or Thrust Loading

Comparisons are made between the theories and results of 14 tests with moment loading; 9 tests with thrust loading. A series of 5 tests on



photoelastic models, when compared with two-piece shell theory, again indicate the strong dependence upon the size of the fillet radius. Semi-empirical modifications to two-piece shell theory bring the theory into adequate agreement with the test data. Results from Kalnins' multipiece shell program agree quite well with the test data.

Comparison of two-piece shell theory with two test models with practically zero fillet radius is made, giving generally good agreement between test data and theory at points away from the junctures.

Comparisons are made with six fabricated test models subjected to both moment and thrust loadings. These models had significant reinforcing; adequate agreement between test data and theory is shown at points away from the junctures.

### Discussions

#### Replacement Area, Pressure Loading

Assuming a design stress criterion that the maximum stress intensity index is limited to 3.0 S, Waters' theory indicates that present code rules of replacement area and associated reinforcement zones are conservative except for reinforcing on the sphere where present code rules (except ASME Section III) may be unconservative for large  $d/D$  ratios combined with large  $D/T$  ratios.

#### ASME Section III Stress Indices, Pressure Loading

The stress indices in Par I-612(a) of the above Code are compared with Waters' analysis and, in one case, Kalnins' multipiece shell program. These stress indices are in general agreement with the theories, except for reinforcing on the sphere with large  $d/D$  ratios combined with large  $D/T$  ratios, where it appears that maximum stresses will be some 50% higher than the Code index.

### Moment Loading, Comparison with ASA B31.1

Since nozzles on pressure vessels quite often are at one end of a piping system, the stress intensification factors given in ASA B31.1 for piping components are significant with respect to the design of nozzles. The theoretical elastic stresses for nozzles in spheres are compared with the fatigue-test derived stress intensification factors for other piping components.

### Combined Pressure and Moment

A brief discussion is given on the questions of (1) are the stresses due to pressure linearly superposable on stresses due to moment and (2) are maximum stress locations the same for pressure loading as for moment loading. The answer given to both of these questions is negative. However, the amount of conservatism introduced by assuming linear superposition is small. The amount of conservatism introduced by assuming that maximum stress locations coincide depends upon the dimensional parameters of the nozzles.

### Relative Magnitude of Stresses, Internal Pressure and Moment Loading

Because moment loadings depend upon the piping system, and may not be established in the early design stage, several limitations to moments in piping systems are discussed. Depending upon which moment limitation is assumed, and the particular dimensional parameters at the nozzles, stresses due to moments may be anywhere from 4 or 5 times those due to pressure down to practically negligible magnitudes.

### Stresses in Phase I Designs

Phase I Report<sup>(12)</sup> gives dimensions of nozzles that (1) have a plastic collapse pressure of at least 1.5 times the design pressure and (2) have a maximum stress intensity of not more than 3.0 S. Because the plastic collapse pressure is the controlling limit for almost all dimensional parameters, the maximum stress intensity index in these designs is generally less than 3.0. If a maximum stress intensity index of 3.0 for combined loadings is used as a design criteria, the Phase I designs have some capacity for moment loadings. The stress intensities of Phase I designs are given, along with stress intensities due to moment loadings. The moment load capacity of any Phase I design can be obtained from the data presented; several examples are given.

### Appendix

Design graphs, based on the CERL program results, are given for:

<u>Loadings</u>	<u>Stress Types</u>	<u>Stress Directions</u>	<u>Dimensional Parameters</u>
Internal Pressure	Membrane	Normal	$10 \leq \frac{D}{T} \leq 250$
Moment on Nozzle	Bending	Tangential	$0.01 \leq \frac{d}{D} \leq 0.5$
Thrust on Nozzle			$0.01 \leq \frac{t}{T} \leq 3.0$

The stresses are functions of three independent dimensional parameters. Because three parameters present difficult interpolation problems to the user, the graphs were prepared as functions of two parameters although this entailed some loss in accuracy.

NOMENCLATURE  
(See Figure 1)

Dimensions

$D$  = mean diameter of sphere, inches  
 $d$  = mean diameter of nozzle, inches  
 $R$  = mean radius of sphere, inches  
 $r$  = mean radius of nozzle, inches  
(In some parts of the Report, inside dimensions are used, indicated by a subscript  $i$ )  
 $T$  = wall thickness of sphere, inches }  $T'$  and  $t'$  are used for locally increased  
 $t$  = wall thickness of nozzle, inches } thickness near the nozzle-sphere juncture.  
 $r_o$  = outside fillet radius, inches  
 $r_i$  = inside corner radius, inches  
 $h$  = thickness normal to an assumed neutral surface, inches  
 $h_1$  = normal thickness assumed for nozzle (See Fig. 12)  
 $h_2$  = normal thickness assumed for sphere (See Fig. 12)  
 $R_1$  = local radius assumed for nozzle, inches (See Fig. 12)  
 $R_2$  = local radius assumed for sphere, inches (See Fig. 12)  
 $A_a$  = cross-sectional area of reinforcing, sq in

Co-ordinates

$\phi$  = meridional angle on sphere (See Fig. 1)  
 $\theta$  = latitude angle on sphere  
 $x$  = axial direction on nozzle  
 $y$  = circumferential direction on nozzle

Loads

$P$  = internal pressure, psi  
 $M$  = moment, in lb, positive as shown in Fig. 1  
 $L$  = thrust, lb, positive as shown in Fig. 1

Stress Resultants (See Fig. 1 for positive directions)

$N_\theta$  = force,  $\theta$  - direction, lb/in  
 $M_\theta$  = moment,  $\theta$  - direction, in-lb/in  
 $N_\phi$  = force,  $\phi$  - direction, lb/in  
 $M_\phi$  = moment,  $\phi$  - direction, in-lb/in  
 $N_y$  = force,  $y$  - direction, lb/in  
 $M_y$  = moment,  $y$  - direction, in-lb/in  
 $N_x$  = force,  $x$  - direction, lb/in  
 $M_x$  = moment,  $x$  - direction, in-lb/in

continued on next page

NOMENCLATURE (contd)Stresses

Nominal stresses are designated by  $S$  or  $s$ , measured or calculated stresses by  $\sigma$ ; with appropriate subscripts.

For Pressure Loading

$$S = PD/4T, \text{ psi}$$

$$s = Pd/2t, \text{ psi}$$

(The ratio  $s/S$  is also used as a dimensional parameter,  $s/S = 2 (d/D) (T/t)$ )

For Moment Loading

$$S = 4M/\pi d^2 t, \text{ psi}$$

For Thrust Loading

$$S = L/\pi dt \text{ psi}$$

$\sigma_{n\theta}$  = membrane stress,  $\theta$  - direction, in sphere, psi

$\sigma_{b\theta}$  = bending stress,  $\theta$  - direction, in sphere, psi

$\sigma_{n\phi}$  = membrane stress,  $\phi$  - direction, in sphere, psi

$\sigma_{b\phi}$  = bending stress,  $\phi$  - direction, in sphere, psi

$\sigma_{ny}$  = membrane stress,  $y$  - direction, in nozzle, psi

$\sigma_{by}$  = bending stress,  $y$  - direction, in nozzle, psi

$\sigma_{nx}$  = membrane stress,  $x$  - direction, in nozzle, psi

$\sigma_{bx}$  = bending stress,  $x$  - direction, in nozzle, psi

$\sigma_n$  = stress in  $\theta$  or  $y$  - direction

$\sigma_t$  = stress in  $\phi$  or  $x$  - direction

(Most of the test data gives surface stresses using the  $\sigma_n$ ,  $\sigma_t$  nomenclature. In general, these surface stresses cannot be accurately separated into membrane or bending stresses and, in many cases, the location of maximum stresses cannot be definitely assigned to the sphere or nozzle portion of the test model. In comparison of theory with test data, the stress components listed above are combined to give surface stresses.)

Stress Indices ( $\sigma/S$ )

Stress indices are denoted by the letter  $K$  with suitable subscripts. The nominal stress,  $S$ , depends upon the load as defined above.

$K_{n\theta}$  = stress index, membrane,  $\theta$  - direction, in sphere

$K_{b\theta}$  = stress index, bending,  $\theta$  - direction, in sphere

$K_{n\phi}$  = stress index, membrane,  $\phi$  - direction, in sphere

$K_{b\phi}$  = stress index, bending,  $\phi$  - direction, in sphere

continued on next page

NOMENCLATURE (contd)

$K_{ny}$  = stress index, membrane, y - direction, in nozzle

$K_{by}$  = stress index, bending, y - direction, in nozzle

$K_{nx}$  = stress index, membrane, x - direction, in nozzle

$K_{bx}$  = stress index, bending, x - direction, in nozzle

Material Properties

E = modulus of elasticity, psi

$\nu$  = Poisson's ratio

$S_a$  = allowable stress, psi

$S_o$  = yield strength, psi

Other symbols are defined where used in text.

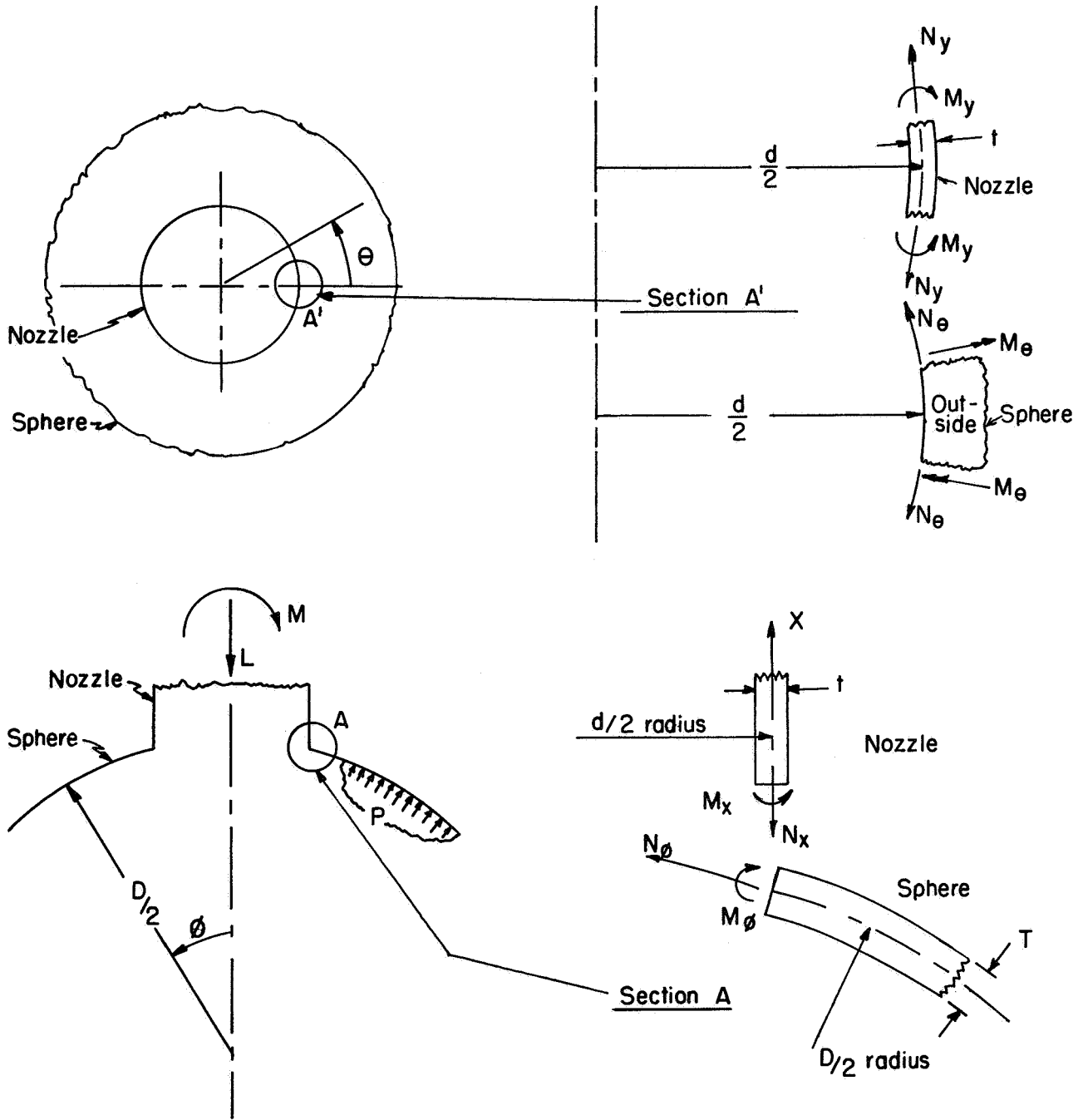


FIGURE 1. NOMENCLATURE ILLUSTRATION

## COMPARISON OF THEORIES

### General Comments

Several analytical developments are used in the subsequent section of this Report, "Comparison of Theories with Test Data". These analytical developments were selected principally because of their availability; no implication is intended that these analyses are necessarily better than other similar analyses.

In this section, an attempt is made to bring out those facets of the analyses which are significant with respect to comparison with test data, and those aspects which differentiate the analyses from each other. No attempt is made to describe these developments completely. A more complete review of some of the analyses used herein, and other similar developments, is given by Kraus<sup>(19)</sup>.



Leckie-Penny Analysis

The Leckie-Penny analysis<sup>(8)</sup> is based on the usual assumptions of thin-shell elastic theory. The most significant of these assumptions, in the present context, is that the shell wall thickness is small compared to the radius of curvature; its significance arising because in most designs of nozzles in spherical shells, this assumption is not valid.

The analysis of the spherical shell is based on asymptotic integration of the basic differential equation of a spherical shell, expressed in terms of a complex stress function. The analysis is applicable either to symmetric loading (e.g., internal pressure, axial thrust on the nozzle) or any loading of the form  $L_n = L \cos n \theta$ . The value of  $n$  in the analysis may be any integer, however, calculated results for a range of dimensional parameters are available only for  $n = 0$  and  $n = 1$ . The loading with  $n = 1$  represents a bending moment applied to the nozzle. The analysis is applicable to any angle  $\theta$ , as contrasted to the Esslinger approximation which is limited to small values of  $\theta$ , or the Geckler approximation for large values of  $\theta$ . The use of asymptotic integration implies a further limitation of the "thinness" of the shell. Leckie and Penny<sup>(10)</sup>, in numerical solutions for cylindrical nozzles in spherical shells, limited themselves to  $D/T$  values of 60 or larger. Thin shell theory itself should be reasonably valid at somewhat smaller  $D/T$  values.

Edge bending solutions for the cylindrical nozzle are given by Hoff<sup>(20)</sup>. For the cases of  $n = 1$ , these were further simplified to give the same results as for the axisymmetric case ( $n = 0$ ). The axisymmetric bending behavior of cylinders is well known<sup>(21)</sup>.

The nozzle in a spherical shell problem was solved<sup>(9)</sup> by the usual technique of requiring that the edge forces (shears and moments) be such that the deflections and rotations of the shell edges are equal.

It should be noted that the edge forces are assumed to be applied at the midsurfaces of the nozzle and sphere; a major point of

difference between this analysis and Water s' analysis discussed later herein. Solutions are included<sup>(10)</sup> for the following type of nozzles:

- (1) Cylindrical nozzle protruding either outward only, inward only or in both directions. The length of the nozzle, inward and/or outward, is assumed to be "semi-infinite".
- (2) Spherical shell of constant thickness or a spherical shell of thickness  $T'$  near the nozzle and a thickness  $T$  away from the nozzle,  $T' \geq T$ .

#### CERL Code

The CERL Code\* is a computer program based on the Leckie-Penny analysis. A parametric study using the CERL Code, for outwardly protruding nozzles, provides some detailed data not available in Reference (10).

- (1) Calculations were made for  $D/T$  values down to 10, as compared to a lower limit of 60 in Reference (10).
- (2) Calculations were made for  $t/T$  values up to 3, as compared to an upper limit of 1.0 in Reference (10).
- (3) Stresses in the nozzles were calculated.

Figure 2 gives the maximum stresses in the sphere with internal pressure loading and corresponds to Figure 2 of Reference (10). The lines for  $t/T \leq 1.0$  are, of course, essentially the same as in Reference (10). The graph also shows the points calculated for each  $D/T$ -value to illustrate the degree of approximation involved in using the two independent variables;  $t/T$  and  $d/D \sqrt{D/2T}$ . Figure 3 gives maximum stresses in the nozzle with internal pressure loading. It is apparent from Figures 2 and 3 that:

- (1) The selection of independent variables of  $t/T$  and  $d/D \sqrt{D/2T}$  does not eliminate  $D/T$  as an independent variable for maximum stresses in the nozzle, see Figure 3.

---

\* This program is identified as the CERL-II Code, See Reference (34).

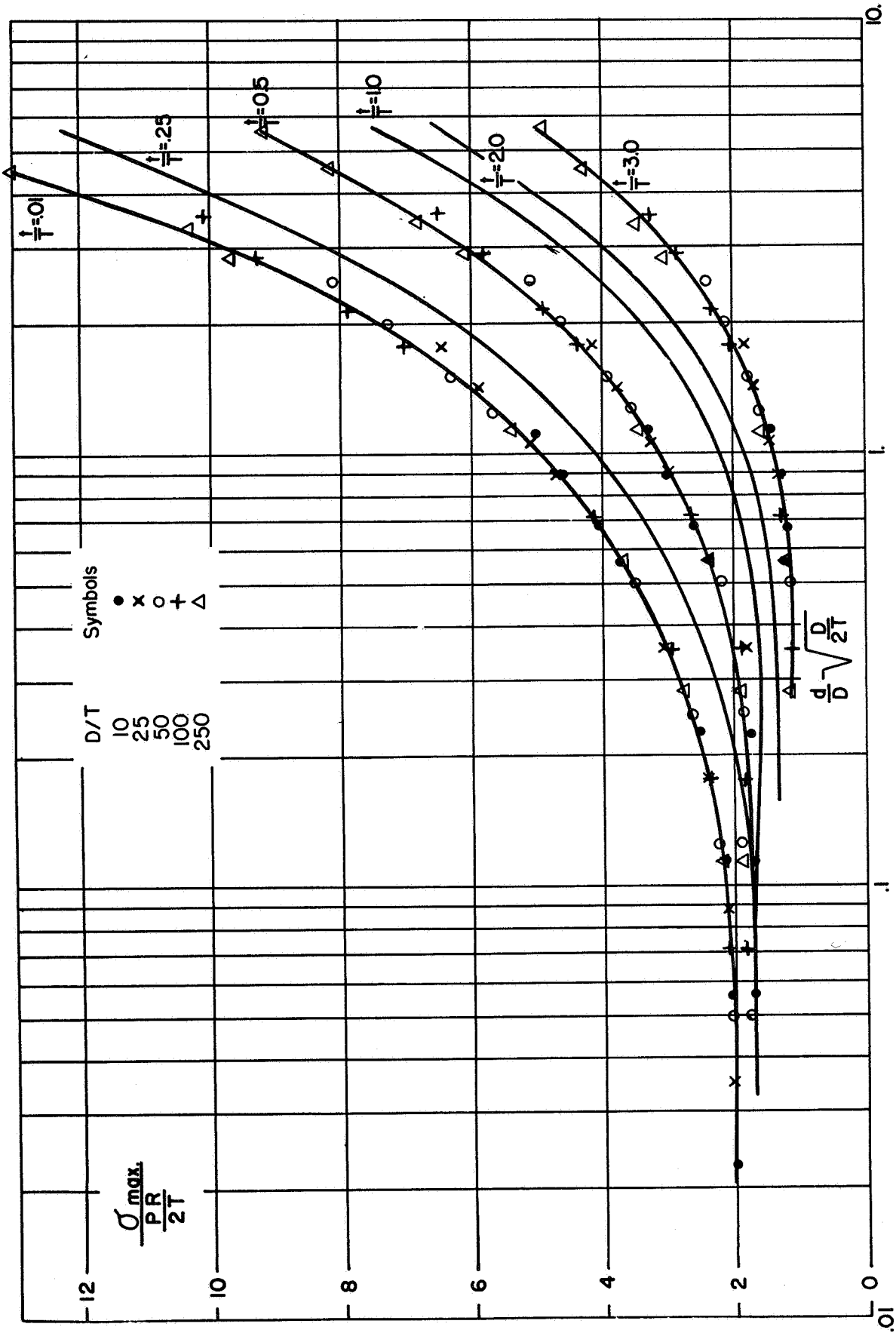


FIGURE 2. MAXIMUM CALCULATED STRESS IN SPHERE BY CERL CODE, PRESSURE LOADING

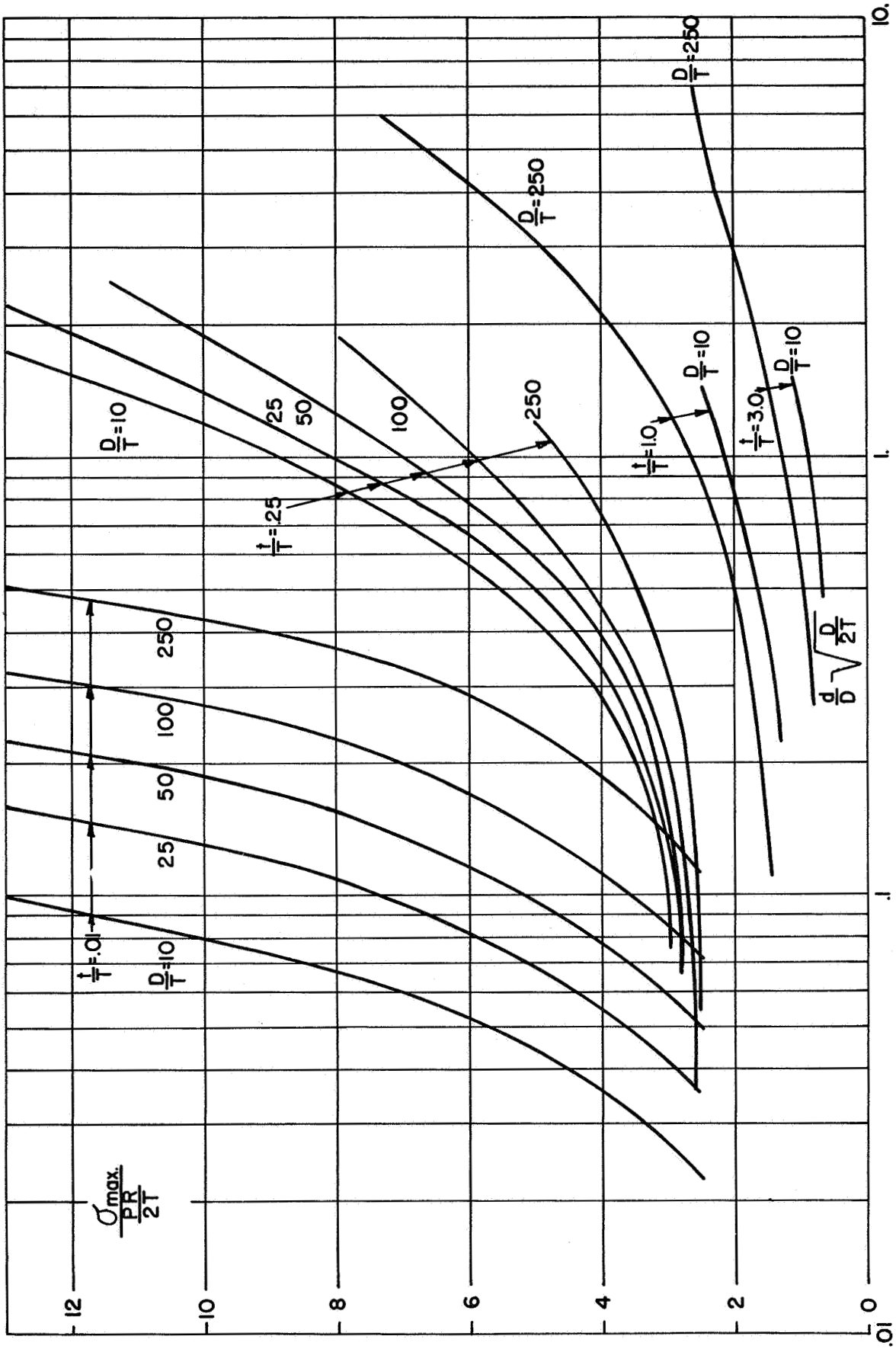


FIGURE 3. MAXIMUM CALCULATED STRESS IN NOZZLE BY CERL CODE, PRESSURE LOADING

(2) The maximum theoretical stress in the nozzle-sphere structure occurs:

in the nozzle for  $t/T < \sim .5$ ;

in the sphere for  $t/T > \sim 1.0$

For a  $d/D$  of 0.01, the transition occurs around  $t/T = .5$ .

For large  $d/D$ , the transition occurs at around  $t/T = 1.0$ .

An exception occurs when the nozzle-sphere dimensions are such that the bending moment in the nozzle is almost zero (see Figure A 5b\*); near these points the maximum stress in the sphere may be about equal to or slightly exceed the maximum stress in the nozzle. For example, for  $D/T = 25$ ,  $d/D = .10$ ,  $t/T = .068$  the maximum stress index in the sphere is about 2.9; that in the nozzle about 2.5.

Figure 4 gives the maximum stresses in the sphere with moment loading and corresponds to Figure 9 of Reference (10). Figure 5 is the analogous graph for stresses in the nozzle. Figures 6 and 7 are corresponding graphs for thrust loading in the sphere and nozzle, respectively. For moment or thrust loads, the maximum stress occurs:

in the nozzle for  $t/T < .8$

in the sphere for  $t/T > 1.0$ .

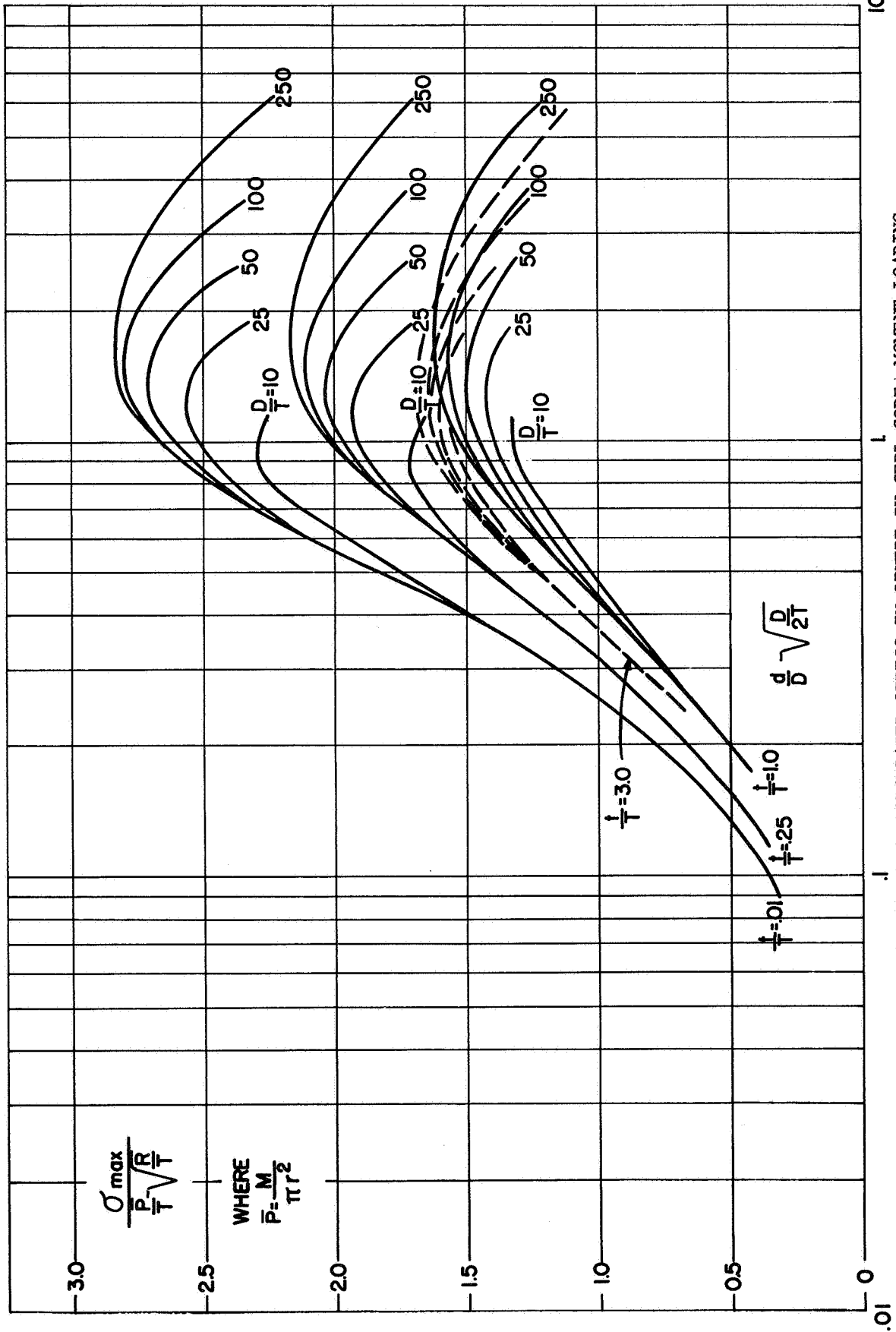


FIGURE 4. MAXIMUM CALCULATED STRESS IN SPHERE BY CERRL CODE; MOMENT LOADING

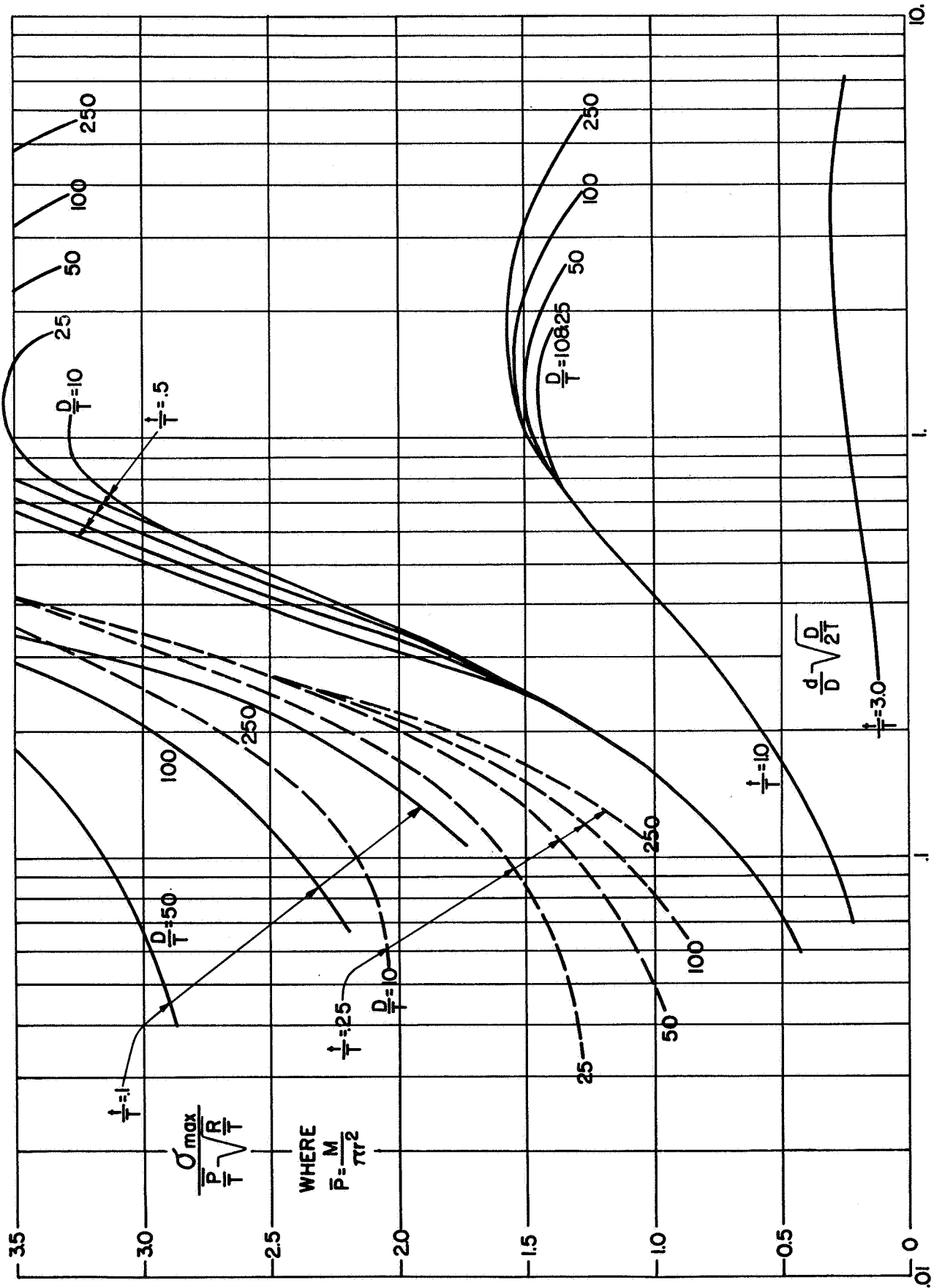


FIGURE 5. MAXIMUM CALCULATED STRESS IN NOZZLE BY CERL CODE, MOMENT LOADING

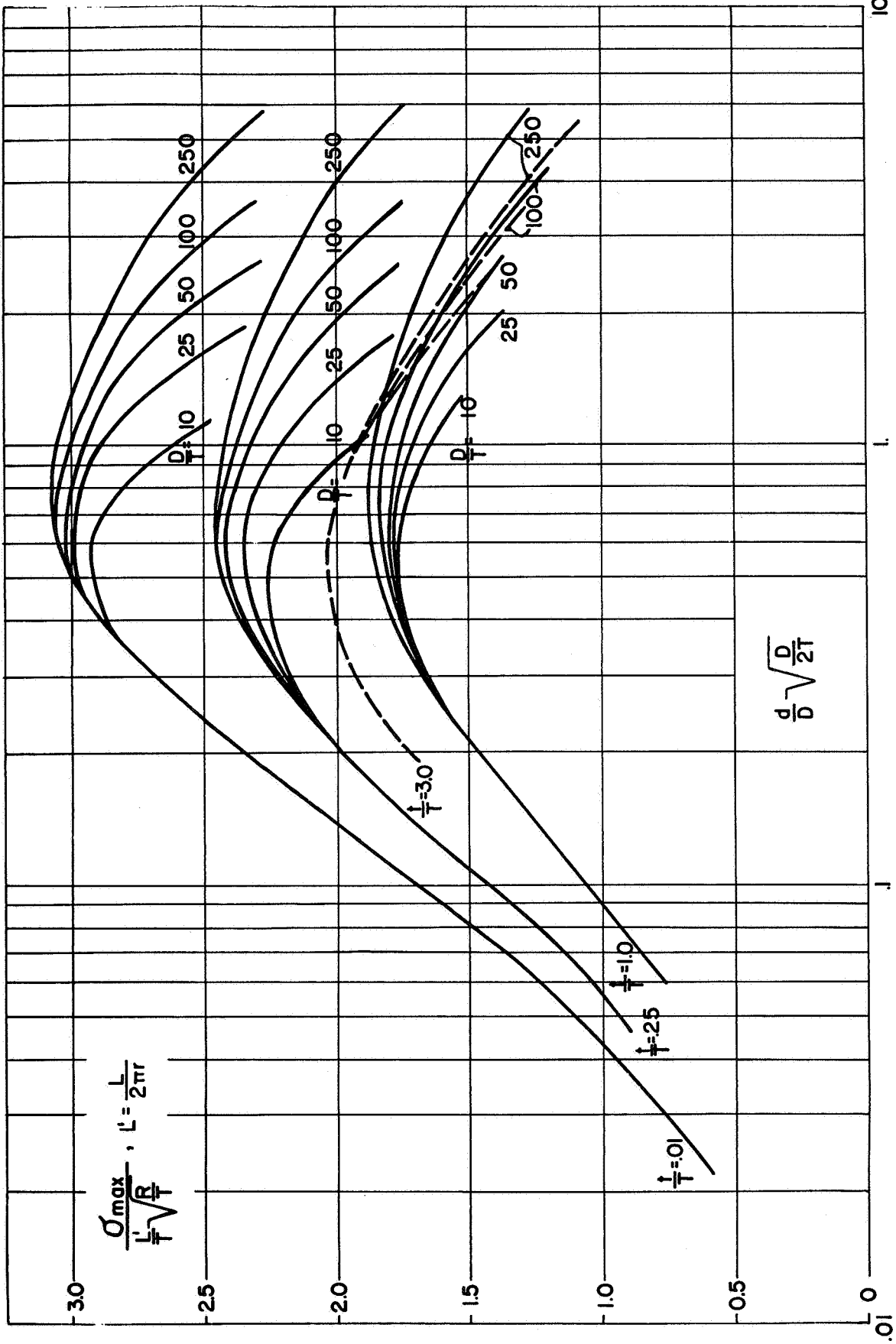


FIGURE 6. MAXIMUM CALCULATED STRESS IN SPHERE BY CERL CODE, THRUST LOADING



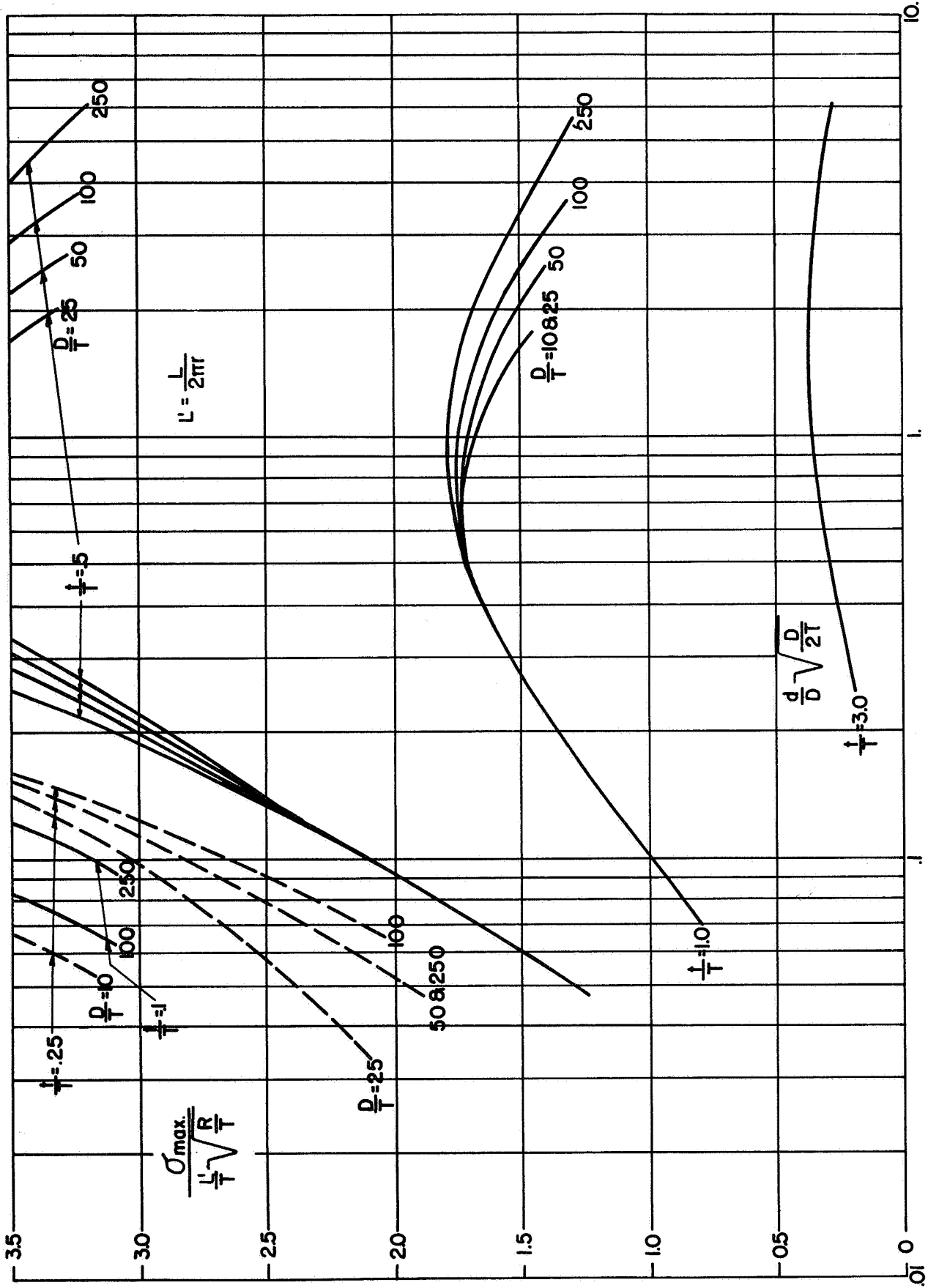


FIGURE 7. MAXIMUM CALCULATED STRESS IN NOZZLE BY CERL CODE, THRUST LOADING

### Waters' Analysis

Waters' analysis was developed for outwardly protruding nozzles in spherical shells with pressure loading. The general basis of the analysis is given in Reference (11). Two refinements were later added by Waters, consisting of:

- (a) A thick-wall (Lame approximation) correction factor, and
- (b) The inclusion of a "local flexibility factor".

A comparison of results obtained from the CERL Code with those obtained from Waters' analysis is given in Table 1. It is apparent from Table 1 that the two analyses give significantly different results throughout the dimensional parameter range covered. The differences between the two analyses are discussed in the following.

#### (1) Local Flexibility Factor

The CERL Code analyses involves the assumption that at the juncture between nozzle and sphere the tangents to the surfaces do not rotate with respect to each other; analogous to the usual engineering assumption that there is no rotation at the "fixed" end of a cantilever beam. A more precise analysis of the juncture area of cantilever beam with an elastic half-plane shows, of course, that absolute rigidity at the joint cannot be obtained and that there are (usually negligible) deflections and rotations due to local strains in the beam and its support. Waters' analysis includes "local flexibility factors" which approximate the effect of these local strains. The plane strain formulas given in Bettis Atomic Power Laboratory Report WAPD-X (CE)-170, p. 40 were used; these formulas are:

$$\left. \begin{aligned}
 \delta_m &= -2.38 (1-\nu-2\nu^2) M_{co}/Et \\
 \psi_m &= -6.36 (1-\nu^2) M_{co}/Et^2 \\
 \delta_v &= 1.408 (1-\nu^2) \Phi Q_{co}/E \\
 \psi_v &= -\delta_m Q_{co}/M_{co} \\
 \Phi &= \ln \frac{r}{t} - \sum_{n=1}^{\infty} \frac{1}{2n(2n+1) (2r/t) 2n + \frac{3}{2}} \\
 &\approx \ln \frac{r}{t} - \frac{1}{24(r/t)^2} + \frac{3}{2}
 \end{aligned} \right\} (1)$$

TABLE 1. COMPARISON OF CALCULATED JUNCTURE STRESSES FOR  
INTERNAL PRESSURE, WATERS AND CERL

$\frac{D}{T}$	$\frac{d}{D}$	$\frac{t}{T}$	$\frac{d}{t}$	$\frac{s}{S}$	Calculation Method	$\sigma/S$ ( $S = PD/4t$ )							
						In Sphere		In Nozzle					
					$K_{n\theta}$	$-K_{b\theta}$	$K_{n\phi}$	$-K_{b\phi}$	$K_{ny}$	$-K_{by}$	$K_{nx}$	$-K_{bx}$	
10	.01	.01	10.	2.0	Waters	1.79	.0094	-.169	.0032	2.22	.0845	.810	.282
					CERL	2.00	.0130	.0011	.00005	2.30	.164	1.00	.547
		.02	5.	1.0	Waters	1.46	-.0014	.163	.0112	1.58	.147	.320	.489
					CERL	1.99	.0121	.0013	.00083	2.14	.620	.50	2.07
		.04	2.5	.5	Waters	1.08	-.0063	.544	.0115	.936	.0728	.090	.243
					CERL	1.96	.0081	.0425	.0044	2.02	.830	.25	2.77
	.10	.04	25.	5.0	Waters	2.23	.500	-.446	-.0232	3.64	-.447	2.30	-1.49
					CERL	2.16	.433	-.0079	-.0058	2.90	-.0348	2.50	-.116
		.10	10.	2.0	Waters	1.88	.318	-.140	.0836	2.51	.203	.810	.678
					CERL	2.12	.405	.0264	.0100	2.40	.625	1.00	2.08
		.25	4.	.8	Waters	1.35	.0912	.335	.120	1.35	.120	.225	.401
					CERL	1.92	.224	.179	.147	1.98	.717	.40	2.39
		.50	2.	.4	Waters	.967	.0164	.673	.0095	.658	.0950	.050	.0316
					CERL	1.61	-.122	.415	.434	1.54	.480	.20	1.60
	.25	.10	25.	5.0	Waters	2.88	1.07	-.429	.0950	4.63	.0950	2.30	.317
					CERL	2.77	.976	.0363	-.0171	3.48	-.513	2.50	-1.71
		.25	10.	2.0	Waters	2.19	.611	-.0311	.340	2.87	.414	.810	1.38
					CERL	2.50	.768	.152	.159	2.73	.762	1.00	2.54
		.50	5.	1.0	Waters	1.58	.285	.329	.401	1.65	.171	.320	.569
					CERL	2.01	.354	.340	.586	2.04	.702	.50	2.34
		2.00	1.25	.25	Waters	.826	.0074	.804	-.0028	.297	-.0109	.005	-.0364
					CERL	1.17	-.0921	.542	.543	.960	.0408	.125	.136
	.50	.25	20.	4.0	Waters	3.64	1.14	-.214	.719	4.95	.781	1.80	2.60
					CERL	3.53	.992	.287	.157	4.00	.756	2.00	2.51
		.50	10.	2.0	Waters	2.50	.662	.167	.856	2.96	.482	.810	1.61
					CERL	2.68	.662	.440	.777	2.82	.934	1.00	3.11

TABLE 1. (contd)

D T	d D	t T	d t	s S	Calculation Method	$\sigma/S$ (S = PD/4T)							
						In Sphere			In Nozzle				
					$K_{n\theta}$	$-K_{b\theta}$	$K_{n\phi}$	$-K_{b\phi}$	K <sub>ny</sub>	$-K_{by}$	K <sub>nx</sub>	$-K_{bx}$	
10	.50	1.0	5.	1.0	Waters	1.65	.323	.510	.470	1.68	.0906	.320	.302
					CERL	1.90	.356	.584	1.34	1.83	.401	.50	1.34
50	.01	.01	50	2.0	Waters	1.97	.0465	.0381	-.0024	2.34	.146	.960	.488
					CERL	2.01	.0490	.00058	.00006	2.31	.169	1.00	.563
		.02	25	1.0	Waters	1.88	.0329	.0422	.0136	2.04	.393	.46	1.31
					CERL	2.00	.0480	.00517	.00084	2.15	.630	.50	2.10
		.04	12.5	.50	Waters	1.74	.0067	1.85	.0353	1.69	.382	.22	1.27
					CERL	1.99	.0437	.0195	.00454	2.06	.853	.25	2.84
		.10	5.	.20	Waters	1.43	-.0343	.498	.0646	1.08	.199	.064	.663
					CERL	1.92	.0139	.0850	.0314	1.93	.944	.10	3.14
	.10	.04	125.	5.0	Waters	2.66	.894	-.0862	.0083	4.30	-.115	2.46	-.385
					CERL	2.64	.876	.00452	-.00343	3.37	-.641	2.50	-2.14
		.10	50.	2.0	Waters	2.49	.765	.0019	.115	3.48	.864	.96	2.88
					CERL	2.59	.838	.0286	.0278	2.88	.835	1.00	2.78
		.25	20.	.8	Waters	2.12	.455	.190	.408	2.40	.722	.36	2.41
					CERL	1.98	.615	.130	.261	2.44	1.25	.40	4.17
		.50	10.	.4	Waters	1.76	.206	.389	.590	1.54	.296	.16	.987
					CERL	1.98	.225	.280	.714	1.95	.858	.20	2.86
	.25	.10	125.	5.0	Waters	4.31	1.29	-.0413	.202	6.22	1.27	2.46	4.23
					CERL	4.31	1.26	.0703	.0295	5.03	.885	2.50	2.95
		.25	50.	2.0	Waters	3.51	.977	.137	.691	4.45	1.66	.96	5.53
					CERL	3.76	1.05	.173	.438	4.00	2.10	1.00	7.00
		.50	25.	1.0	Waters	2.68	.657	.316	1.25	2.87	.927	.46	3.09
					CERL	2.86	.714	.316	1.29	2.90	1.55	.50	5.16
		2.00	6.25	.25	Waters	1.54	.218	.762	.447	1.20	-.0244	.088	-.0814
					CERL	1.61	.239	.451	1.39	1.44	.104	.125	.347

TABLE 1. (contd)

$\frac{D}{T}$	$\frac{d}{D}$	$\frac{t}{T}$	$\frac{d}{t}$	$\frac{s}{S}$	Calculation Method	$\sigma/S$ ( $S = PD/4t$ )								
						In Sphere			In Nozzle					
					$K_{n\theta}$	$-K_{b\theta}$	$K_{n\theta}$	$-K_{b\theta}$	$K_{ny}$	$-K_{by}$	$K_{nx}$	$-K_{bx}$		
50	.50	.25	100.	4.0	Waters	5.73	1.24	.178	1.21	7.06	2.51	1.96	8.38	
					CERL	5.80	1.07	.339	.583	6.28	2.80	2.00	2.00	9.32
					Waters	4.04	1.00	.366	2.08	4.53	1.63	.96	1.00	5.43
					CERL	4.16	.957	.466	1.86	4.30	2.24	1.00	1.00	7.45
50	.50	.50	50.	2.0	Waters	2.87	.770	.532	2.24	2.79	.506	.46	1.69	
					CERL	2.78	.869	.571	2.96	2.74	.888	.50	2.96	
					Waters	1.49	.136	.879	.173	1.36	-.0302	.129	-.101	
					CERL	1.59	.394	.817	1.61	1.38	.0538	.167	.179	
250	.01	.01	250.	2.0	Waters	2.03	.165	-.0074	.0018	2.50	.254	.99	.848	
					CERL	2.04	.167	.00034	.00006	2.34	.198	1.00	.661	
					Waters	2.01	.155	.0108	.0096	2.31	.619	.49	2.06	
					CERL	2.03	.165	.00247	.00089	2.19	.666	.50	2.22	
250	.01	.04	62.5	.5	Waters	1.97	.131	.0473	.0307	2.14	.722	.24	2.40	
					CERL	2.03	.161	.00915	.00408	2.12	.900	.25	3.00	
					Waters	1.86	.046	.155	.106	1.80	.599	.092	2.00	
					CERL	1.99	.128	.0406	.0340	2.01	1.02	.10	3.40	
250	.01	.04	625.	5.0	Waters	4.10	1.28	-.0097	.0328	6.11	1.27	2.49	4.22	
					CERL	4.10	1.28	.0110	.00365	4.85	.685	2.50	2.28	
					Waters	3.91	1.20	.0342	.175	5.32	2.57	.992	8.57	
					CERL	3.99	1.23	.0331	.0800	4.28	2.40	1.00	8.00	
250	.01	.25	100.	.8	Waters	3.31	.926	.147	.768	4.04	2.33	.392	7.76	
					CERL	3.51	1.01	.118	.581	3.60	2.80	.40	9.31	
					Waters	2.67	.633	.263	1.47	2.75	1.22	.192	4.08	
					CERL	2.78	.675	.228	1.48	2.76	1.77	.20	5.91	
250	.25	.10	625.	5.0	Waters	7.89	1.47	.0474	.344	9.95	4.41	2.49	14.7	
					CERL	7.94	1.41	.0864	.137	8.66	4.11	2.50	13.7	

TABLE 1. (contd)

$\frac{D}{T}$	$\frac{d}{D}$	$\frac{t}{T}$	$\frac{d}{t}$	$\frac{s}{S}$	Calculation Method	$\sigma/S (S = PD/4T)$							
						In Sphere			In Nozzle				
					$K_{n\theta}$	$-K_{b\theta}$	$K_{n\phi}$	$-K_{b\phi}$	$K_{ny}$	$-K_{by}$	$K_{nx}$	$-K_{bx}$	
250	.25	.25	250.	2.0	Waters	6.44	1.34	.174	1.36	7.61	4.68	.992	15.6
					CERL	6.71	1.33	.184	1.08	6.96	5.19	1.00	17.3
					Waters	4.67	1.24	.306	2.93	5.05	2.82	.492	9.42
250	.50	.50	125.	1.0	CERL	4.83	1.27	.307	2.90	4.88	3.48	.50	11.6
					Waters	2.64	.737	.622	2.37	2.37	.115	.117	.384
					CERL	2.55	.909	.566	3.47	2.41	.260	.125	.867
250	.50	.25	500.	4.0	Waters	10.8	1.55	.276	2.21	12.1	6.93	1.99	23.1
					CERL	10.9	1.32	.362	1.54	11.4	7.39	2.00	24.6
					Waters	7.34	1.75	.419	4.57	7.91	4.46	.992	14.8
250	.50	.50	250.	2.0	CERL	7.51	1.67	.478	4.30	7.66	5.16	1.00	17.2
					Waters	4.92	1.83	.530	5.95	4.88	1.57	.492	5.23
					CERL	4.79	1.98	.566	6.62	4.76	1.99	.50	6.62
250	.50	1.0	125.	1.0	Waters	2.70	.681	.811	2.11	2.53	.0356	.159	.119
					CERL	2.63	1.16	.773	4.13	2.44	.138	.167	.459

In the above:

$\nu$  = Poisson's ratio

E = modulus of elasticity

Other symbols defined in Figure 8.

In order to determine the magnitude of "local flexibility factor" effects; these factors were eliminated from Waters' analyses and stresses for the dimensional parameters shown in Table 1 were recomputed. Results for typical values of the dimensions covered are shown in Table 1a; identified as "Waters-1". For stresses in the sphere, in general, the effect of the "local flexibility factor" is to decrease the magnitude of the  $\theta$ -stresses and increase the magnitude of the  $\phi$ -stresses. In the nozzle, the y-stresses and the x-bending stresses generally increase due to the "local flexibility factor". The effect of the "local flexibility factor" is generally small in the sphere but can be quite large in the nozzle. For example, with dimensions  $D/T = 250$ ,  $d/D = .10$ ,  $t/T = .10$ , the value of  $K_{bx}$  is 14.7 including the local flexibility effect; 6.89 without the "local flexibility effect".

### (2) Location of Juncture Stresses

Juncture stresses from the CERL Code are located at  $x = 0$  (nozzle) and  $\phi = \phi_a$  (sphere) as shown in Figure 9. In Waters' analysis, the nozzle stress is also located at  $x = 0$ , but the sphere stress juncture location is taken at  $\phi_b$ . To indicate the significance of this difference, the Waters-1 analysis was revised to give the stresses at  $\phi = \phi_a$ . Results for typical values of the dimensions covered are shown in Table 1a; identified as "Waters-2". The effect of this difference depends upon the nozzle thickness  $t$  as compared to the sphere shell decay modulus,  $\sqrt{DT}$ . For large values of  $t/T$ , the stresses are quite different for location  $\phi_a$  as compared with location  $\phi_b$ . For example, with  $D/T = 250$ ,  $d/D = .5$ ,  $t/T = 3.0$ ,  $K_{b\phi} = -6.46$  at  $\phi_a$ ;  $K_{b\phi} = -2.72$  at  $\phi_b$ .

### (3) Thick Wall Effects

The CERL code is based on thin-wall shell theory; the value of  $T/D$  and  $t/d$  are assumed to be negligible as compared to unity. Further,

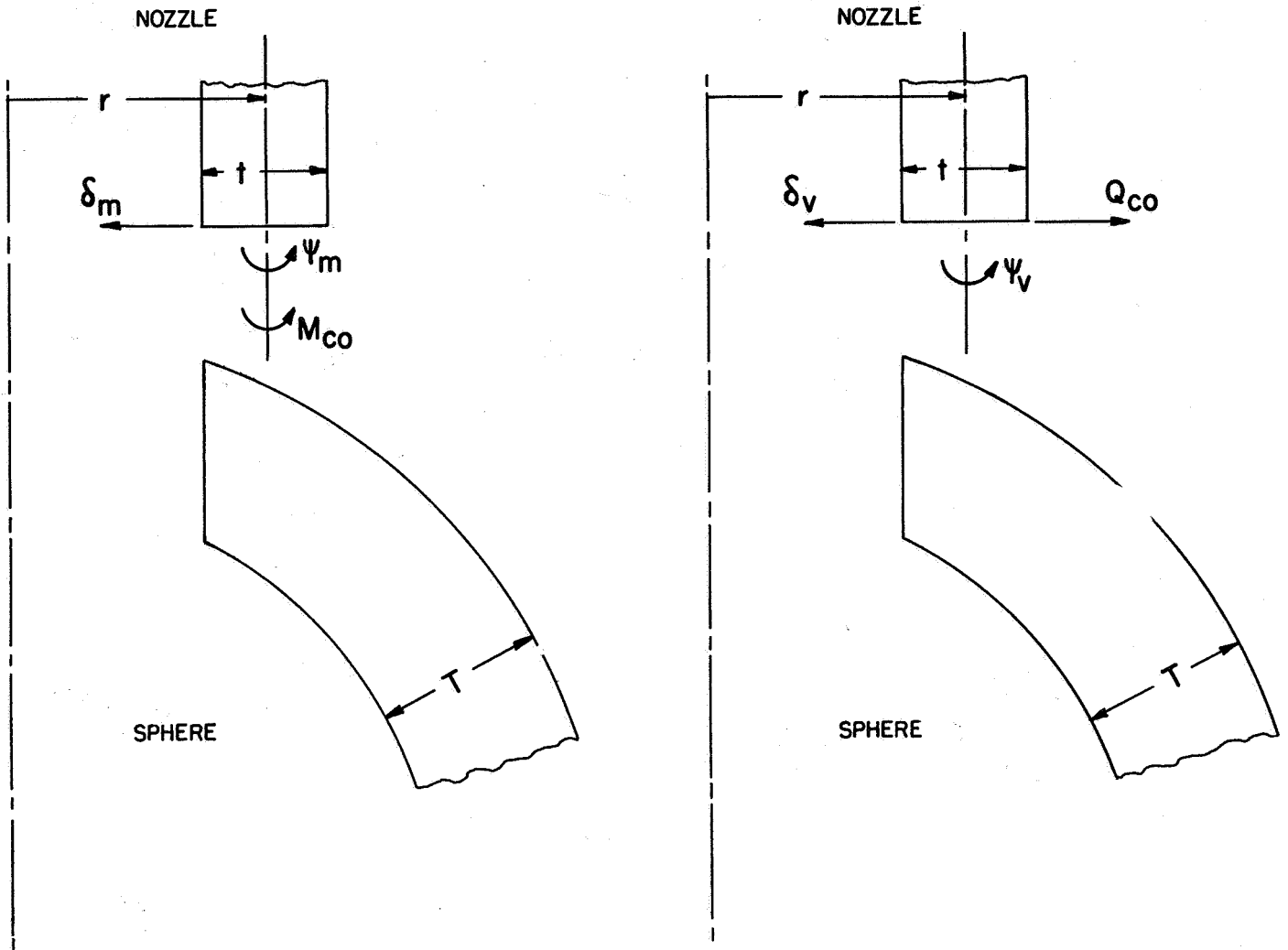


FIGURE 8. DEFINITION OF TERMS IN EQUATION (1), LOCAL FLEXIBILITY EFFECT, WATERS THEORY



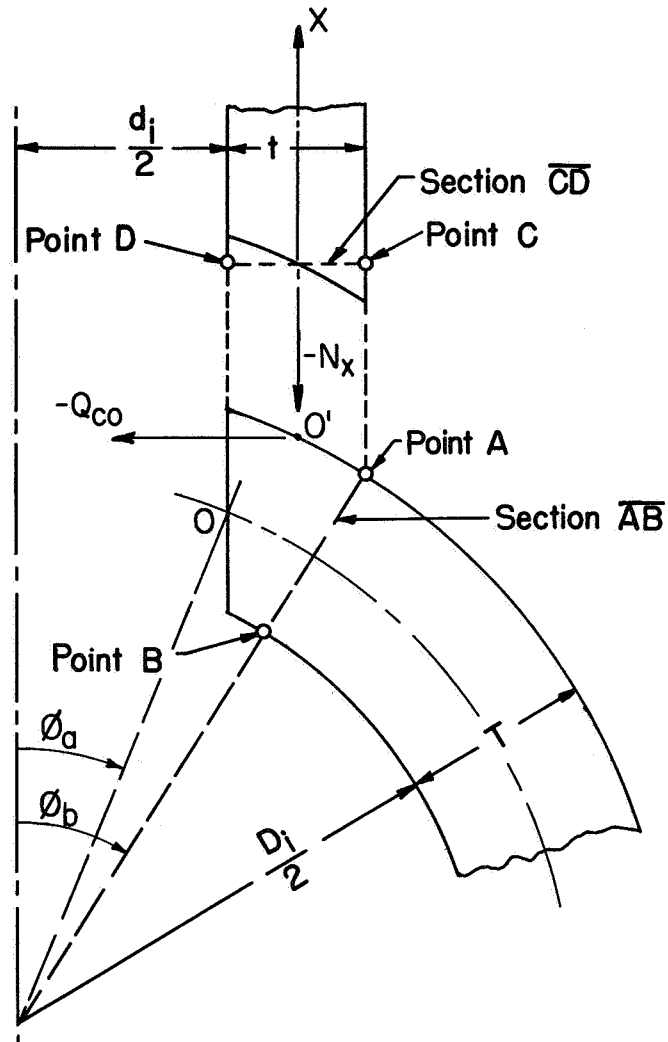


FIGURE 9. DEFINITION OF TERMS USED IN WATERS ANALYSIS

TABLE 1a. EXAMPLES OF THE EFFECT OF MODIFICATIONS TO THIN-WALL SHELL THEORY INTRODUCED IN WATERS' ANALYSIS

D/T	d/D	t/T	d/t	s/s	Calculation Method (1)	$\sigma/S$ (S = PD /4T)									
						In Sphere					In Nozzle				
						$K_{n\theta}$	$-K_{b\theta}$	$K_{n\phi}$	$-K_{b\phi}$	$K_{ny}$	$-K_{by}$	$K_{nx}$	$-K_{bx}$		
10	0.01	0.02	5.0	1.0	Waters Waters-1 Waters-2 Waters-3 CERL	1.46 1.46 2.02 1.99 1.99	-0.0014 0.0028 0.0013 0.0120 0.0121	0.163 0.161 -0.397 0.0112 0.0113	0.0112 0.0069 0.0095 0.00083 0.00083	1.58 1.19 1.19 2.14 2.14	0.147 0.131 0.131 0.619 0.620	0.32 0.32 0.32 0.50 0.50	0.489 0.438 0.438 2.06 2.07		
	0.50	1.0	5.0	1.0	Waters Waters-1 Waters-2 Waters-3 CERL	1.65 1.75 2.51 1.89 1.90	0.323 0.358 0.554 0.329 0.356	0.510 0.490 -0.154 0.548 0.584	0.470 0.415 2.02 1.30 1.34	1.68 1.30 1.30 1.88 1.83	0.0906 0.137 0.137 0.391 0.401	0.32 0.32 0.32 0.50 0.50	0.302 0.460 0.460 1.30 1.34		
250	0.01	0.02	125	1.0	Waters Waters-1 Waters-2 Waters-3 CERL	2.01 2.01 2.03 2.03 2.03	0.155 0.161 0.163 0.165 0.165	0.0108 0.00905 -0.0152 0.00243 0.00247	0.0096 0.0039 0.0029 0.00089 0.00089	2.31 1.32 1.32 2.18 2.19	0.619 0.196 0.196 0.666 0.666	0.49 0.49 0.49 0.50 0.50	2.06 0.653 0.653 2.22 2.22		
	0.50	1.0	125	1.0	Waters Waters-1 Waters-2 Waters-3 CERL	4.92 6.85 7.14 4.79 4.79	1.83 1.96 2.41 1.97 1.98	0.530 0.415 0.328 0.522 0.566	5.95 5.66 7.40 6.61 6.62	4.88 1.66 1.66 4.79 4.76	1.57 1.66 1.66 1.98 1.99	0.49 0.49 0.49 0.50 0.50	5.23 5.55 5.55 6.61 6.62		

(1) Waters = Waters analysis.  
 Waters-1 = Waters analysis with "Local flexibility factor" taken out.  
 Waters-2 = Waters-1 with sphere stresses calculated at  $\phi_a$  instead of  $\phi_b$ .  
 Waters-3 = Waters-2 with "thick-wall" effects taken out.

the CERL code is based on the assumption that the juncture forces and moments are transferred at the intersection of the midwall of the cylindrical shell (nozzle) and the spherical shell. Waters' analysis contains thick-wall effects from two aspects.

- (a) Correction factors are applied to the "membrane stresses". The correction factors are based on Lamé' equations for a sphere or cylinder; approximated by use of a truncated series in  $R/T$  or  $r/t$ . For example, the midwall membrane  $\sigma_\theta$ -stress at section  $\overline{AB}$  (Figure 9) is given by.

$$(\sigma_\theta)_{mm} = \frac{(R - T/2)^2}{2RT} + f(\lambda\theta_b) \quad (2)$$

where  $f(\lambda\theta_b)$  represents the edge-effect solution. In thin-wall shell theory, the first term in equation (2) would be simply  $R/2T$ . At points A and B (Figure 9) the membrane stresses are given by:

$$(\sigma_\theta)_{ma} = \sigma_{mn} \left( \frac{R - T/2}{R} \right) \quad (3)$$

$$(\sigma_\theta)_{mb} = \sigma_{mn} \left( \frac{R}{R - T/2} \right) \quad (4)$$

Analogous corrections are used for the nozzle.

- (b) Waters assumes (See Figure 9) that the shear force produces a moment about point 0 of:

$$M_{\phi_a} = -Q_{co} (T - t \sin \phi_a) r/2 \cos \phi_a \quad (5)$$

and that the force  $N_x$  produces the moment

$$M_{\phi_a} = -N_x (t/2) (r - t/4) \quad (6)$$

further, the rotation at  $\phi_a$  produces a displacement of point 0' with respect to point 0 of:

$$\delta = - \frac{(d\phi_a) (T - t \sin \phi_a)}{2 \cos \phi_a} \quad (7)$$

Where:  $(d\phi_a)$  = rotation at  $\phi_a$

To determine the effect of these assumptions, the Waters-2 computer program was altered to a "thin-shell" program and stresses calculated for the dimensional parameters of Table 1. Results for some typical values are shown in Table 1a: identified as "Waters-3". At this point, the major difference between "Waters-3" and the CERL code is that Waters analysis is based on shallow-shell theory (Esslinger approximation) whereas the CERL code is based on a non-shallow shell theory. As indicated by Table 1a, "Waters-3" and the CERL code results are in good agreement. For  $d/D$  of 0.5; there are small differences, particularly in the values of  $K_{n\phi}$ . It is apparent, however, that the shallow shell theory is of adequate accuracy for  $d/D$  up to 0.50 and  $D/T$  up to 250.

It is apparent by comparing "Waters-2" with "Waters-3" of Table 1a that large differences may arise due to the "thick-wall effects" described above. These are particularly significant in the value of  $K_{bx}$ , the axial bending stress in the nozzle.

The Lamé type thick-wall factors range from 0.9 to 1.1 for stresses in the sphere and do not account for the differences shown in Table 1a (in particular,  $K_{n\phi}$ , which often contains a sign reversal between "Waters-2" and "Waters-3"). The axial membrane stress index,  $K_{nx}$ , is obtained directly from static equilibrium; in the CERL code  $\sigma_{nx} = Pd_m/4t$ ; in Waters analysis the exact equation  $\sigma_{nx} = Pd_i^2/4d_m t$  is used. In general, the more significant differences arise when  $D/T$  and/or  $d/t$  are small.

Some further comparisons between Waters' analysis and the CERL code are made in the subsequent section of this report on "Comparison of Theories with Test Data".

### Bijlaard Analysis

The pertinent work of Bijlaard with respect to nozzles in spherical vessels is given in References 1 through 6. The development is quite general but detailed results are given only for:

- (a) A solid plug nozzle in a spherical shell; the plug being loaded with radial thrust or moment loading.
- (b) A cylindrical shell nozzle protruding outward from a spherical shell, with loading as in (a).
- (c) A solid plug nozzle in a spherical shell with an annular pad around the nozzle, with loading as in (a).

Bijlaard's analysis for the spherical shell starts with Reissner's<sup>(22)</sup> differential equations for a shallow spherical shell. For axisymmetric (thrust) loading, the "edge effect" solution is the same as given by the Esslinger approximation used by Waters. The analysis of the cylindrical shell for thrust loading is the same as that used by Leckie-Penny and Waters and is the well-known<sup>(21)</sup> solution for a cylindrical

shell subjected to symmetric edge loads. Bijlaard used boundary conditions at the nozzle-sphere juncture analogous to Leckie-Penny assumptions, i.e., shears and moments are transferred at the shell mid-walls and the juncture itself is rigid.

Bijlaard's analysis of the spherical shell with non-symmetrical loading is analogous to the Leckie-Penny analysis in that the stress function is assumed to be of the form  $F = F_n \cos n\theta$  and  $w = w_n \cos n\theta$ . However, because of the shallow shell assumption, Bijlaard's analysis is significantly simplified. Bijlaard's analysis of the cylindrical shell is based on Donnell's<sup>(25)</sup> equations which, for the "edge-effect" solution, moment loading ( $n = 1$ ), give:

$$w = e^{-\alpha x} (C_1 \cos \beta x + C_2 \sin \beta x) \cos \theta \quad (8)$$

$$\text{where } \alpha = (1/r) \left\{ 1 - (\nu/2) + \left[ 3(1 - \nu^2)(r/t)^2 + 1 - .75\nu^2 \right]^{1/2} \right\}^{1/2}$$

$$\beta = (1/r) \left\{ -1 + (\nu/2) + \left[ 3(1 - \nu^2)(r/t)^2 + 1 - .75\nu^2 \right]^{1/2} \right\}^{1/2}$$

$C_1$  and  $C_2$  are constants.

It is apparent that for moderately large values of  $r/t$ ,  $\alpha \approx \beta \approx \frac{4}{\sqrt{3(1-\nu^2)}} / \sqrt{rt}$  and Equation (8), except for the  $\cos \theta$  factor, is the same as the symmetrical loaded edge-effect solution. Leckie-Penny used the simplified solution for  $w$ , while Bijlaard retained Equation (8). For small values of  $r/t$ , which are often encountered in pressure vessel nozzles, Bijlaard's analysis may be more accurate in this respect.

Because Bijlaard's published data are somewhat limited in choice of dimensional parameters, a computer program based on Bijlaard's

theoretical development was prepared. This program was used to compute stresses for comparison with CERL results. Table 2 shows this comparison for thrust loading; Table 3 for moment loading. It is apparent that for thrust loading, Bijlaard and CERL results are essentially the same. The differences between the two theories increase slightly with increasing  $d/D$ , but even at  $d/D = 0.5$ , the differences are small in an engineering sense and indicates that the shallow-shell theory is reasonably valid for  $d/D$  up to .5 with  $D/T$  of 100 or less. For moment loading the differences between Bijlaard and CERL are significant when the diameter-to-thickness ratio of the nozzle is small, e.g., 2.5. As discussed above, there is a difference between these two theories in the analysis of the nozzle as a cylindrical shell which may account for the differences in results.

#### Kalnins Analysis and Computer Program

The preceding analyses are applicable to uniform wall thickness, spherical or cylindrical shell segments which geometrically contain an axis of revolution. Kalnins' <sup>(14)</sup> analysis and computer program, along with the "Seal-Shell-2" program discussed later, is more general in that the wall thickness may vary in an arbitrary manner, and the meridian curve is not restricted; provided that the wall thickness is small compared to the radius of curvature.

Two approaches have been taken to the numerical solution of the general shell of revolution.

- (1) Finite difference approach, in which a set of grid points are chosen and the differential equations for the shell are replaced by finite difference equations defined at the grid points.
- (2) Direct numerical integration of the differential equations for the shell by, for example, the Runge-Kutta technique.

TABLE 2. COMPARISON OF CALCULATED JUNCTION STRESSES FOR THRUST LOADING, BIJLAARD AND CERL

$\frac{D}{T}$	$\frac{d}{D}$	$\frac{t}{T}$	$\frac{d}{t}$	$\frac{s}{S}$	Calculation Method	Stress Indices							
						In Sphere			In Nozzle				
						$-K_{n\theta}$	$K_{b\theta}$	$-K_{n\phi}$	$K_{b\phi}$	$-K_{ny}$	$K_{by}$	$-K_{nx}$	$K_{bx}$
25	.01	.10	2.5	.20	Bijlaard CERL	.0097 .0092	.271 .273	.0237 .0242	.0064 .0067	.303 .299	.190 .200	1.00 1.00	.635 .666
		.04	6.25	.50	Bijlaard CERL	.00749 .00747	.110 .111	.00589 .00591	.00092 .00094	.306 .306	.173 .175	1.00 1.00	.577 .582
		.02	12.5	1.0	Bijlaard CERL	.00459 .00459	.0555 .0557	.00210 .00211	.00022 .00022	.304 .303	.168 .168	1.00 1.00	.560 .562
		.01	25.0	2.0	Bijlaard CERL	.00258 .00258	.0278 .0279	.00077 .00077	.00006 .00006	.302 .302	.166 .166	1.00 1.00	.552 .552
	.05	.50	2.5	.20	Bijlaard CERL	.310 .306	2.11 2.11	.465 .469	.935 .964	.470 .434	1.12 1.16	1.00 1.00	3.74 3.85
		.25	5.0	.40	Bijlaard CERL	.298 .299	1.36 1.38	.131 .132	.155 .159	.558 .544	.745 .762	1.00 1.00	2.48 2.54
		.10	12.5	1.0	Bijlaard CERL	.157 .158	.599 .606	.0226 .0226	.0124 .0125	.450 .445	.371 .375	1.00 1.00	1.24 1.25
		.04	31.2	2.5	Bijlaard CERL	.0673 .0677	.244 .247	.00511 .00511	.0012 .0012	.366 .364	.232 .232	1.00 1.00	.773 .775
	.25	2.0	2.5	.25	Bijlaard CERL	2.00 2.12	3.24 3.36	2.35 2.38	10.9 11.4	1.60 1.55	.816 .855	1.00 1.00	2.72 2.85
		1.0	5.0	.50	Bijlaard CERL	1.43 1.49	1.90 1.96	1.11 1.13	4.81 5.02	1.39 1.38	1.44 1.51	1.00 1.00	4.81 5.02
		.50	12.5	1.00	Bijlaard CERL	1.29 1.35	1.35 1.38	.473 .489	1.46 1.53	1.45 1.47	1.75 1.83	1.00 1.00	5.84 6.11
		.25	50.0	2.00	Bijlaard CERL	1.02 1.07	.910 .937	.159 .165	.274 .288	1.27 1.31	1.31 1.38	1.00 1.00	4.38 4.60



TABLE 2. (contd)

$\frac{D}{T}$	$\frac{d}{D}$	$\frac{t}{T}$	$\frac{d}{t}$	$\frac{s}{S}$	Calculation Method	Stress Indices							
						In Sphere			In Nozzle				
						$-K_{n\theta}$	$K_{b\theta}$	$-K_{n\phi}$	$K_{b\phi}$	$-K_{ny}$	$K_{by}$	$-K_{nx}$	$K_{bx}$
25	.50	3.00	4.17	.333	Bijlaard CERL	2.25	3.55	3.05	12.27	1.63	.408	1.00	1.36
		1.00	12.5	1.00	Bijlaard CERL	2.54	3.89	3.26	13.44	1.69	.449	1.00	1.49
		.50	25.0	2.00	Bijlaard CERL	1.33	1.33	.922	3.81	1.35	1.14	1.00	3.81
		.25	50.0	4.00	Bijlaard CERL	1.48	1.43	1.00	4.16	1.42	1.25	1.00	4.16
					Bijlaard CERL	1.23	.772	.416	1.17	1.41	1.40	1.00	4.66
					Bijlaard CERL	1.37	.796	.457	1.29	1.51	1.54	1.00	5.15
					Bijlaard CERL	.982	.465	.167	.227	1.23	1.09	1.00	3.64
					Bijlaard CERL	1.12	.470	.186	.255	1.36	1.22	1.00	4.08
100	.01	.10	10.0	.20	Bijlaard CERL	.118	.830	.0203	.0127	.412	.381	1.00	1.27
		.04	25.0	.50	Bijlaard CERL	.118	.831	.0204	.0128	.410	.386	1.00	1.28
		.02	50.0	1.00	Bijlaard CERL	.0517	.336	.00381	.00123	.351	.231	1.00	.771
		.01	100.0	2.00	Bijlaard CERL	.0517	.337	.00381	.00124	.350	.232	1.00	.774
					Bijlaard CERL	.0265	.168	.00126	.00026	.326	.192	1.00	.640
					Bijlaard CERL	.0265	.169	.00126	.00026	.326	.192	1.00	.640
					Bijlaard CERL	.0134	.0843	.00045	.00006	.313	.176	1.00	.586
					Bijlaard CERL	.0134	.0844	.00045	.00006	.313	.176	1.00	.586
	.05	.5	10.0	.20	Bijlaard CERL	1.74	3.85	.780	3.12	1.81	3.75	1.00	12.49
		.25	20.0	.40	Bijlaard CERL	1.75	3.86	.782	3.14	1.79	3.77	1.00	12.57
		.10	50.0	1.00	Bijlaard CERL	1.34	2.76	.208	.542	1.58	2.60	1.00	8.67
		.04	125.0	2.50	Bijlaard CERL	1.34	2.77	.209	.546	1.57	2.62	1.00	8.73
					Bijlaard CERL	.651	1.27	.0273	.0349	.943	1.05	1.00	3.49
					Bijlaard CERL	.654	1.28	.0273	.0351	.942	1.05	1.00	3.51
					Bijlaard CERL	.271	.520	.00470	.0024	.570	.450	1.00	1.50
					Bijlaard CERL	.272	.523	.00475	.0024	.570	.451	1.00	1.50

TABLE 2. (contd)

				Stress Indices									
				In Sphere					In Nozzle				
$\frac{D}{T}$	$\frac{d}{D}$	$\frac{t}{T}$	$\frac{d}{t}$	$\frac{s}{S}$	Calculation Method	$-K_{n\theta}$	$K_{b\theta}$	$-K_{n\phi}$	$K_{b\phi}$	$-K_{ny}$	$K_{by}$	$-K_{nx}$	$K_{bx}$
100	.25	2.0	10.0	.25	Bijlaard	5.92	6.03	2.97	21.1	5.33	1.58	1.00	5.28
					CERL	6.09	6.18	3.03	21.7	5.41	1.63	1.00	5.42
		1.0	20.0	.50	Bijlaard	4.14	3.34	1.27	10.18	4.06	3.06	1.00	10.18
					CERL	4.26	3.42	1.30	10.46	4.14	3.14	1.00	10.46
100	.50	.50	50.0	1.00	Bijlaard	3.45	1.92	.530	3.29	3.59	3.95	1.00	13.2
					CERL	3.55	1.95	.544	3.39	3.68	4.06	1.00	13.5
		.25	200.0	2.00	Bijlaard	2.65	1.15	.173	.629	2.90	3.02	1.00	10.07
					CERL	2.74	1.16	.179	.652	2.99	3.13	1.00	10.42
100	.50	3.0	16.67	.333	Bijlaard	5.67	6.15	3.57	21.4	4.90	.711	1.00	2.37
					CERL	6.05	6.52	3.78	22.6	5.14	.752	1.00	2.51
		1.0	50.0	1.00	Bijlaard	3.47	2.44	.981	7.79	3.47	2.34	1.00	7.79
					CERL	3.75	2.60	1.06	8.36	3.70	2.51	1.00	8.36
100	.50	.5	100.0	2.00	Bijlaard	3.01	1.16	.433	2.47	3.18	2.97	1.00	9.89
					CERL	3.28	1.19	.472	2.68	3.43	3.22	1.00	10.73
		.25	200.0	4.00	Bijlaard	2.33	.567	.170	.480	2.58	2.30	1.00	7.68
					CERL	2.59	.565	.188	.528	2.83	2.54	1.00	8.45

TABLE 3. COMPARISON OF CALCULATED JUNCTURE STRESSES FOR MOMENT LOADING, BIJLAARD AND CERL

$\frac{D}{T}$	$\frac{d}{D}$	$\frac{t}{T}$	$\frac{d}{t}$	$\frac{s}{S}$	Calculation Method	In Sphere			In Nozzle				
						$-K_{n\theta}$	$K_{b\theta}$	$-K_{n\phi}$	$K_{b\phi}$	$-K_{ny}$	$K_{by}$	$-K_{nx}$	$K_{bx}$
25	.01	.10	2.5	.20	Bijlaard	-.0156	.0378	.0157	.0108	.280	.325	1.00	1.08
					CERL	-.0178	.0447	.0180	.00389	.275	.117	1.00	.389
					Bijlaard	-.00480	.0183	.00487	.00118	.294	.222	1.00	.740
					CERL	-.00532	.0186	.00540	.00081	.292	.152	1.00	.507
		.02	12.5	1.00	Bijlaard	-.00187	.00948	.00191	.00026	.298	.192	1.00	.639
					CERL	-.00199	.00952	.00204	.00021	.296	.158	1.00	.525
					Bijlaard	-.00071	.00481	.00073	.00006	.300	.177	1.00	.591
					CERL	-.00074	.00481	.00075	.00006	.298	.180	1.00	.600
	.05	.50	2.5	.20	Bijlaard	-.0706	.735	.123	.424	.193	.508	1.00	1.70
					CERL	-.0850	.910	.144	.247	.140	.296	1.00	.988
					Bijlaard	-.0205	.505	.0520	.0751	.264	.360	1.00	1.20
					CERL	-.0226	.530	.0552	.0509	.245	.244	1.00	.815
		.10	12.5	1.00	Bijlaard	-.00101	.225	.0145	.00778	.295	.233	1.00	.778
					CERL	-.00125	.227	.0149	.00632	.288	.190	1.00	.632
					Bijlaard	.00116	.0922	.00435	.00099	.300	.187	1.00	.622
					CERL	.00112	.0925	.00440	.00091	.295	.171	1.00	.569
	.25	2.0	2.5	.25	Bijlaard	.829	3.08	1.33	9.65	.731	.724	1.00	2.41
					CERL	.840	3.34	1.49	9.36	.369	.702	1.00	2.34
					Bijlaard	.596	1.89	.738	4.09	.675	1.23	1.00	4.09
					CERL	.600	1.98	.800	4.05	.360	1.21	1.00	4.05
		1.0	5.0	.50	Bijlaard	.668	1.43	.361	1.25	.860	1.49	1.00	4.98
					CERL	.680	1.47	.382	1.27	.625	1.52	1.00	5.07
					Bijlaard	.597	1.01	.134	.237	.857	1.14	1.00	3.79
					CERL	.622	1.04	.140	.244	.756	1.17	1.00	3.90

TABLE 3. (contd)

$\frac{D}{T}$	$\frac{d}{D}$	$\frac{t}{T}$	$\frac{d}{t}$	$\frac{s}{S}$	Calculation Method	In Sphere			In Nozzle				
						$-K_{n\theta}$	$K_{b\theta}$	$-K_{n\theta}$	$K_{b\theta}$	$-K_{ny}$	$K_{by}$	$-K_{nx}$	$K_{bx}$
25	.50	3.00	4.17	.333	Bijlaard	1.64	3.89	2.44	13.1	1.20	.437	1.00	1.46
					CERL	1.89	4.23	2.73	13.3	1.01	.444	1.00	1.48
					Bijlaard	.957	1.43	.803	3.76	1.02	1.13	1.00	3.76
					CERL	1.08	1.54	.882	3.92	.770	1.18	1.00	3.92
100	.01	.50	25.0	2.00	Bijlaard	.981	.883	.385	1.16	1.16	1.39	1.00	4.63
					CERL	1.09	.925	.424	1.24	.985	1.49	1.00	4.96
					Bijlaard	.835	.564	.161	.229	1.09	1.10	1.00	3.66
					CERL	.950	.585	.179	.250	1.04	1.20	1.00	4.00
100	.01	.10	10.0	.20	Bijlaard	-.00862	.186	.0110	.00754	.288	.226	1.00	.754
					CERL	-.00908	.188	.0115	.00576	.286	.173	1.00	.576
					Bijlaard	-.00201	.0765	.00298	.00099	.297	.185	1.00	.617
					CERL	-.00208	.0765	.00304	.00088	.296	.165	1.00	.550
100	.01	.02	50.0	1.00	Bijlaard	-.00063	.0385	.00112	.00023	.299	.173	1.00	.578
					CERL	-.00065	.0386	.00113	.00022	.299	.165	1.00	.550
					Bijlaard	-.00018	.0193	.00043	.00006	.300	.168	1.00	.560
					CERL	-.00019	.0193	.00043	.00005	.300	.150	1.00	.500
100	.05	.50	10.0	.20	Bijlaard	.174	2.47	.333	1.62	.374	1.94	1.00	6.46
					CERL	.146	2.45	.359	1.63	.265	1.96	1.00	6.52
					Bijlaard	.232	1.76	.0890	.281	.502	1.35	1.00	4.50
					CERL	.228	1.76	.103	.283	.460	1.36	1.00	4.53
100	.05	.10	50.0	1.00	Bijlaard	.131	.803	.0161	.0189	.426	.568	1.00	1.89
					CERL	.131	.805	.0187	.0187	.415	.561	1.00	1.87
					Bijlaard	.0561	.328	.00370	.00151	.355	.283	1.00	.943
					CERL	.0564	.330	.00370	.00149	.352	.280	1.00	.932

TABLE 3. (contd)

$\frac{D}{T}$	$\frac{d}{D}$	$\frac{t}{T}$	$\frac{d}{t}$	$\frac{s}{S}$	Calculation Method	In Sphere				In Nozzle			
						$-K_{n\theta}$	$K_{b\theta}$	$-K_{n\phi}$	$K_{b\phi}$	$-K_{ny}$	$K_{by}$	$-K_{nx}$	$K_{bx}$
100	.25	2.0	10.0	.25	Bijlaard	4.11	6.18	2.36	20.8	3.71	1.56	1.00	5.20
					CERL	4.24	6.45	2.43	21.0	3.52	1.57	1.00	5.25
		1.0	20.0	.50	Bijlaard	2.92	3.40	1.07	9.71	2.90	2.91	1.00	9.71
					CERL	2.98	3.64	1.10	9.88	2.63	2.96	1.00	9.88
100	.50	.50	50.0	1.00	Bijlaard	2.67	2.11	.481	3.23	2.83	3.87	1.00	12.9
					CERL	2.74	2.14	.496	3.31	2.60	3.96	1.00	13.2
		.25	100.0	2.00	Bijlaard	2.24	1.37	.167	.643	2.49	3.09	1.00	10.3
					CERL	2.31	1.39	.171	.662	2.40	3.18	1.00	10.6
100	.50	3.0	16.67	.333	Bijlaard	4.98	6.54	3.29	22.5	4.29	.748	1.00	2.49
					CERL	5.40	6.87	3.51	23.3	4.38	.774	1.00	2.58
		1.0	50.0	1.00	Bijlaard	3.03	2.52	.925	7.81	3.05	2.34	1.00	7.81
					CERL	3.30	2.65	.998	8.25	2.95	2.48	1.00	8.25
100	.50	.50	100.0	2.00	Bijlaard	2.75	1.24	.423	2.51	2.92	3.01	1.00	10.0
					CERL	3.00	1.28	.458	2.69	2.85	3.24	1.00	10.8
		.25	200.0	4.00	Bijlaard	2.22	.643	.169	.497	2.47	2.38	1.00	7.93
					CERL	2.46	.650	.181	.540	2.52	2.59	1.00	8.64

The finite difference approach has been used as the basis for a number of computer solutions for axisymmetric shell problems. One problem which arises in this technique is the selection of a grid spacing sufficiently fine so that adequate accuracy is achieved. A fine grid spacing results in the generation of large square matrices which must be inverted.

The numerical integration approach is more directly applicable to initial-value problems rather than shell-of-revolution problem in which it is necessary to take account of boundary loads at both ends of the shell. The integration technique may be applied, however, by assigning an arbitrary (e.g., unity) value to each variable at the starting edge of the shell. The shell equations are then integrated over the shell length to get six (symmetric loading) or eight (non-symmetric loading) equations relating the values of the variables at the remote edge to the (unit) values at the starting edge. Since three (or four for nonsymmetric loading) of the variables are known at each edge of the shell, the remaining six (or eight) unknown values are obtained by solving the six (or eight) simultaneous equations. While this technique works well for "short" shells, a major difficulty develops with "long" shells. In long shells, application of self-equilibrating boundary loads on one edge results in very small effects at the opposite edge. The numerical integration method, in such "long" shells, gives equations which are almost singular and truncation errors completely obliterate the desired answers. Kalnins overcomes this difficulty by applying the numerical technique to a shell broken up into short segments. The solutions for the short segments are then combined so that the continuity conditions at the junctures and the boundary conditions are satisfied. A major advantage is that the size of the matrix required for the final solutions is small as compared to that required in the finite difference approach; at the same time adequate accuracy can be maintained through control of the accuracy of the numerical integration.

While the approach used by Kalnins is different than the analytic approach used by Leckie and Penny, the basic theory, including continuity

conditions at junctures, are the same. The asymptotic integration used by Leckie and Penny might, for small values of  $D/T$  and/or  $d/t$ , lead to some differences between the results. Tables 4, 5, and 6 give comparisons between Kalnins' results and CERL (Leckie-Penny) results for Pressure, Thrust and Moment Loading, respectively. The dimensional parameters were chosen to represent the extremes investigated in this Report. Table 7 gives some comparisons for several test models. It is apparent, from Tables 4 through 7, that Kalnins and CERL computer programs give essentially the same results over the range of dimensional parameters covered.

In the above comparisons, Kalnins' program is used as a "two-piece" shell theory--simply to establish its consistency with respect to the CERL Code. In the subsequent section of this Report, Kalnins' program is used as a "multipiece" shell theory in comparison with results from the Seal-Shell-2 computer program.

### Seal-Shell-2

(13)

The Seal-Shell-2 computer program permits dividing an axisymmetric shell into from 2 to 100 segments. Each segment may have a curved middle surface (considered as part of an ellipsoid) or the middle surface may be straight (part of a plate, cone, or cylinder). Thick shell geometry is used in the analysis, with basic assumptions that plane sections remain plane and the shear stress varies parabolically through the wall thickness. By application of the principle of virtual work to the strain energy of each segment, the forces on each segment are determined in terms of the deflections. Influence coefficients are then obtained and the conditions of continuity at the segment junctures are imposed to obtain a "stiffness matrix"; the solution of which gives the forces connecting the shell segments; the strain energy relationships then give local stresses and strains.

Seal-Shell-2 is similar to CERL, Bijlaard and Kalnins developments in that forces and moments between segments are assumed to be transferred at the shell midsurfaces; it is different than Waters' development in this respect.

TABLE 4. COMPARISON OF KALNINS WITH CERL, PRESSURE LOADING

$\frac{D}{T}$	$\frac{d}{D}$	$\frac{t}{T}$	$\frac{d}{t}$	$\frac{s}{S}$	Calculation Method	Stress Indices									
						In Sphere					In Nozzle				
						$K_{n\theta}$	$K_{b\theta}$	$K_{n\phi}$	$K_{b\phi}$	$K_{ny}$	$K_{by}$	$K_{nx}$	$K_{bx}$		
10	.01	.01	10.	2.00	Kalnins	2.00	.0132	.00118	.00006	2.30	.170	1.04	.568		
					CERL	2.00	.0130	.00114	.00005	2.30	.164	1.00	.547		
	↓	.04	2.5	.50	Kalnins	1.96	.0088	.0425	.0044	2.02	.830	.260	2.77		
					CERL	1.96	.0081	.0425	.0044	2.02	.830	.250	2.77		
	↓	.25	20.	4.00	Kalnins	3.49	.961	.285	.148	4.00	.717	2.00	2.37		
					CERL	3.53	.992	.287	.157	4.00	.756	2.00	2.51		
	↓	1.0	5.0	1.00	Kalnins	1.87	.355	.586	1.32	1.85	.396	.500	1.32		
					CERL	1.90	.356	.584	1.34	1.83	.401	.500	1.34		
250	.01	.01	250.	2.00	Kalnins	2.04	.166	.00034	.00007	2.33	.199	1.00	.661		
					CERL	2.04	.166	.00034	.00007	2.33	.198	1.00	.661		
	↓	1.00	2.5	.02	Kalnins	1.45	.412	.540	.515	1.29	.155	.01	.515		
					CERL	1.45	.412	.540	.515	1.29	.154	.01	.515		
	↓	.25	500.	4.00	Kalnins	10.9	1.32	.362	1.54	11.4	7.38	2.00	24.6		
					CERL	10.9	1.32	.362	1.54	11.4	7.39	2.00	24.6		
	↓	3.00	41.7	.333	Kalnins	2.62	1.16	.772	4.12	2.44	.137	.166	.458		
					CERL	2.63	1.16	.773	4.13	2.44	.137	.166	.459		



TABLE 5. COMPARISON OF KALNINS WITH CERL, THRUST LOADING

				Stress Indices										
				In Sphere					In Nozzle					
$\frac{D}{T}$	$\frac{d}{D}$	$\frac{t}{T}$	$\frac{d}{t}$	$\frac{s}{S}$	Calculation Method	$K_{n\theta}$	$K_{b\theta}$	$K_{n\phi}$	$K_{b\phi}$	$K_{ny}$	$-K_{by}$	$K_{nx}$	$K_{bx}$	
10	.01	.01	10	2.00	Kalnins	.00019	.0130	.00114	.000054	.299	.163	1.00	.544	
					CERL	.00018	.0130	.00114	.000055	.300	.164	1.00	.547	
	.5	.04	.25	20	4.00	Kalnins	.00478	.0515	.00860	.00086	.292	.161	1.00	.547
						CERL	.00344	.0513	.00871	.00088	.292	.166	1.00	.552
250	.01	.01	250	2.00	Kalnins	.566	.411	.182	.151	.815	.727	1.00	2.42	
					CERL	.583	.426	.183	.155	.816	.745	1.00	2.48	
	.5	1.00	1.00	5.0	1.00	Kalnins	.628	1.03	.937	2.56	.647	.767	1.00	2.56
						CERL	.669	1.05	.935	2.62	.598	.787	1.00	2.62
250	.01	.01	250	2.00	Kalnins	.0352	.167	.00035	.00007	.335	.199	1.00	.661	
					CERL	.0354	.167	.00034	.00007	.335	.198	1.00	.661	
	.5	1.00	1.00	2.5	.02	Kalnins	.735	6.29	2.16	10.5	.385	3.16	1.00	10.5
						CERL	.738	6.22	2.17	10.6	.369	3.19	1.00	10.6
250	.5	.25	500.	4.00	Kalnins	4.29	.663	.189	.845	4.54	4.05	1.00	13.5	
					CERL	4.30	.664	.189	.846	4.56	4.06	1.00	13.5	
	.5	3.00	41.7	.333	Kalnins	10.2	9.57	4.00	32.9	9.27	1.10	1.00	3.65	
					CERL	10.2	9.59	3.98	32.9	9.27	1.10	1.00	3.66	

TABLE 6. COMPARISON OF KALNINS WITH CERL, MOMENT LOADING

$\frac{D}{T}$	d/D	t/T	d/t	s/s	Computer Program	Stress Indices									
						In Sphere					In Nozzle				
						-K <sub>nθ</sub>	K <sub>bθ</sub>	-K <sub>nφ</sub>	K <sub>bφ</sub>	-K <sub>ny</sub>	K <sub>by</sub>	-K <sub>nx</sub>	K <sub>bx</sub>		
25	0.10	0.04	62.5	5.0	Kalnins CERL	0.0243 0.0240	0.164 0.163	0.00590 0.00590	0.00110 0.00108	0.322 0.315	0.207 0.202	0.997 1.00	0.689 0.675		
	0.10	0.25	10.0	0.8	Kalnins CERL	0.0915 0.0855	0.895 0.900	0.0784 0.0828	0.120 0.116	0.348 0.315	0.584 0.396	0.937 1.00	1.93 1.32		
	0.50	0.25	50.0	4.0	Kalnins CERL	0.954 0.950	0.567 0.585	0.178 0.179	0.248 0.250	1.20 1.04	1.21 1.20	0.973 0.990	3.96 4.00		
	0.50	1.0	12.5	1.0	Kalnins CERL	1.10 1.08	1.49 1.54	0.870 0.882	3.94 3.92	1.11 0.770	1.25 1.18	0.859 0.974	3.94 3.92		
250	0.10	0.10	250.0	2.0	Kalnins CERL	1.45 1.45	1.46 1.47	0.0305 0.0306	0.0768 <b>0.0773</b>	1.74 1.71	2.31 2.32	0.986 1.00	7.68 7.73		
	0.10	1.00	25.0	0.2	Kalnins CERL	3.66 3.62	5.92 5.92	1.42 1.44	16.2 16.2	3.47 3.27	4.99 4.86	0.782 0.998	16.2 16.2		
	0.5	0.25	500.0	4.0	Kalnins CERL	4.19 4.19	0.723 0.726	0.188 0.188	0.862 0.862	4.43 4.26	4.14 4.14	0.981 0.995	13.8 13.8		
	0.5	3.00	41.7	.33	Kalnins CERL	9.53 9.55	9.89 9.90	3.83 3.83	33.7 33.9	8.67 8.51	1.32 1.13	.970 .983	3.74 3.76		

TABLE 7. COMPARISON OF CALCULATED RESULTS FOR MOMENT LOADING, KALNINS WITH CERL COMPUTER PROGRAM, PHOTOELASTIC TEST MODELS

Model No.	$\frac{r}{R}$	$\frac{R}{T}$	$\frac{r}{t}$	Computer Program	Calculated Stresses* at Juncture											
					In Sphere						In Nozzle					
					$\sigma_{\theta}$		$\sigma_{\theta}$		$\sigma_x$		$\sigma_x$		$\sigma_y$		$\sigma_y$	
					Out	In	Out	In	Out	In	Out	In	Out	In	Out	In
WN50A	.50	25.5	25.0	Kalnins	2.40	-1.49	3.00	.84	8.36	-6.47	4.33	-.19				
					CERL	2.40	-1.50	3.00	.82	8.50	-6.50	4.05	-.47			
WN50B	.27	25.5	14.1	Kalnins	2.55	-1.67	3.34	-.04	9.49	-7.69	4.42	-.85				
					CERL	2.57	-1.68	3.32	-.08	9.66	-7.66	4.10	-1.09			
WN50C	.27	25.9	27.5	Kalnins	.62	-.29	2.63	.23	7.93	-6.01	3.78	-.45				
					CERL	.62	-.29	2.62	.21	8.01	-6.00	3.58	-.59			
WN50D	.13	25.4	13.3	Kalnins	.45	-.20	2.19	-.93	6.17	-4.30	2.48	-.70				
					CERL	.45	-.20	2.18	-.94	6.27	-4.26	2.38	-.79			

\* The magnitude of the moment loading, M, is such that  $M/\pi r^2 t = 1.0$ . The stresses tabulated are therefore also stress indices as defined in the Nomenclature.

Seal-Shell-2 is similar to Kalnins program in that a shell may be broken up into a large number of pieces for a more accurate analysis. However, Seal-Shell-2 includes thick-wall effects which appear to lead to a more accurate solution for the thick-wall nozzle-in-sphere geometry. In Kalnins program, the midsurface is also the neutral surface whereas, in Seal-Shell-2, the midsurface is not necessarily the neutral surface. Seal-Shell-2 should be capable in principle, of directly indicating the non-linear distribution of stress in the transition zone between nozzle and sphere, analogous to the "curved-beam approximation" discussed later herein in comparing test data with Waters' two-piece shell theory. The Seal-Shell-2 computer program is limited to axisymmetric loads; i.e., it is not directly applicable to a bending moment applied to the nozzle.

Table 8 shows some comparisons between Seal-Shell-2 and Kalnins' computer program for internal pressure loading and various amounts of reinforcing supplied by a fillet radius.

TABLE 8. COMPARISON OF KALNINS' AND SEAL-SHELL-2 CALCULATED STRESSES, NOZZLES WITH FILLET RADIUS REINFORCEMENT

$\frac{D}{T}$	$\frac{d}{D}$	$\frac{S}{S}$	$\frac{r_o}{t}$	$\frac{A}{d_i T}$	Computer Program	$\sigma_n/s$		$\sigma_t/s$	
						Outside	Inside	Outside	Inside
25	0.20	1.0	3.75	0.101	Seal-Shell-2 Kalnins	1.47	1.81	1.19	- 0.34
						1.88	1.31	1.14	- 0.45
25	0.50	1.0	3.75	0.079	Seal-Shell-2 Kalnins	1.71	1.64	1.40	- 0.33
						2.05	1.40	1.28	- 0.59
100	0.20	1.0	7.5	0.109	Seal-Shell-2 Kalnins	2.25	1.73	1.78	- 0.38
						2.30	1.54	1.43	- 0.67
100	0.50	1.0	7.5	0.099	Seal-Shell-2 Kalnins	2.61	1.71	2.10	- 0.61
						2.25	1.55	1.65	- 0.64

The Battelle Axisymmetric Stress Intensity Code - BASIC

BASIC<sup>(15)</sup> is a computer program developed to apply the point matching approach to determine the stresses in axisymmetric bodies of arbitrary shape loaded by axisymmetrically distributed forces or with specified axisymmetric boundary displacements. To use the approach, it is first necessary to set up a series solution to the problem. The series is truncated at some finite number of terms. The coefficients of the series are chosen so that the boundary conditions of the problem are satisfied (in the least squares sense) at some large but finite number of boundary points.

The critical part of this approach is the choice of a series solution that converges sufficiently rapidly for the given problem. In BASIC, the solution can be obtained by using a stress function series whose terms are either spherical functions or toroidal functions or both.

The spherical functions give solutions with singularities either on the axis of rotation or at infinity. The ring functions are used when the solution has a ring singularity. These latter singularities exist in the neighborhood of stress raisers such as notches or fillets. By combining a number of series of toroidal and spherical functions, it is generally possible to set up a solution that converges sufficiently well to give an accurate solution to a given problem.

As implied above, the BASIC computer program is not yet developed to the point of routine application to nozzles in spherical shells.

The BASIC computer program was used to compute the stresses in test model WN-7B<sup>(25)</sup>; results are compared with test data in Figure 10; results using the Seal-Shell-2 program for the same test model are shown in Figure 10a. The BASIC program results match the measured peak stresses better than Seal-Shell-2. In this preliminary trial, the length of the sphere section used in the analysis was too short to develop the attenuation effects present in the actual test model.

Model WN-7B was selected for analysis because Seal-Shell-2 did not agree very well with the test results, in contrast to a number of other test

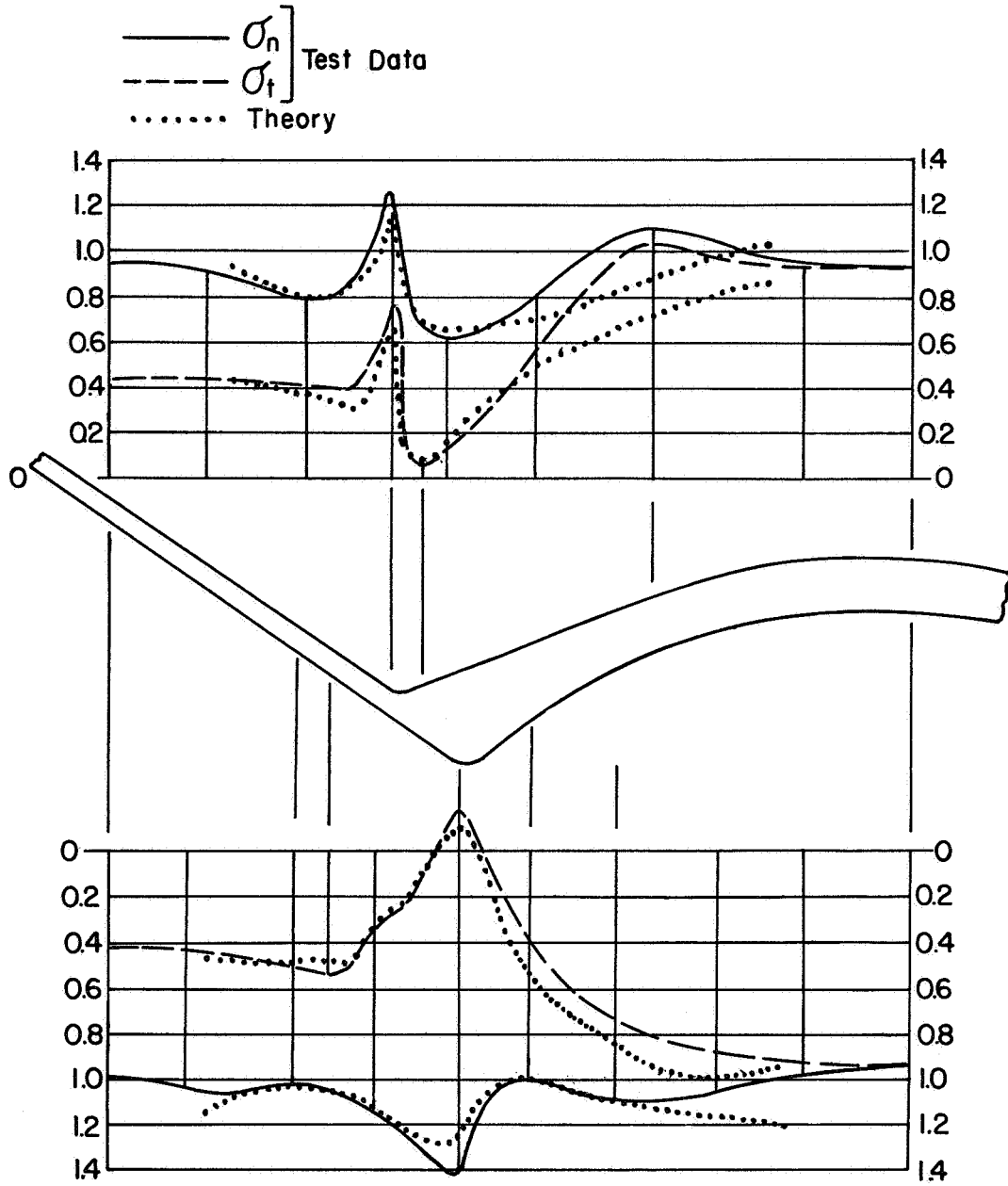


FIGURE 10. COMPARISON OF "BASIC" COMPUTER PROGRAM RESULTS WITH TEST MODEL WN-7B

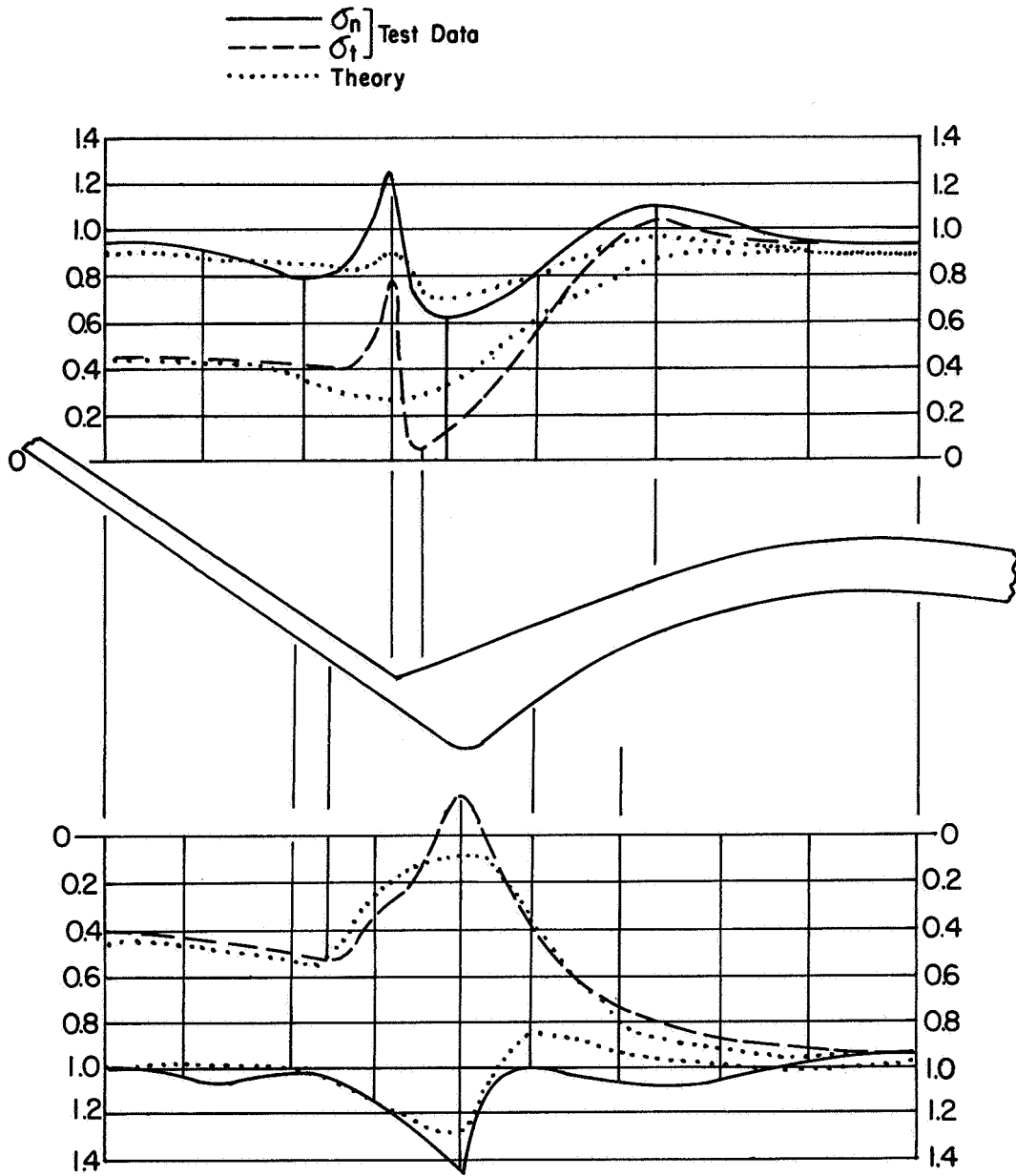


FIGURE 10a. COMPARISON OF "SEAL-SHELL-2" COMPUTER PROGRAM RESULTS WITH TEST MODEL WN-7B



models where Seal-Shell-2 was in good agreement with the test results. It should be noted that Seal-Shell-2 requires a certain amount of judgement in selecting a middle surface and associated normal thicknesses; the data shown possibly does not represent an optimum use of Seal-Shell-2.

#### Use of Computer Programs

Computer programs for the "two-piece" shell theories (CERL, Waters, Bijlaard) require only simple input data, e.g., three dimensional ratios and the load. The computer time, on a Control Data 3400 computer, is very short; around 3 or 4 seconds per model. Accordingly, it is relatively easy to compute an extensive parametric study of nozzles in spheres with such programs.

Both Kalnins' and Seal-Shell-2 programs require considerably more input data. Also, these programs require the selection of a midsurface (or reference surface) and thicknesses normal to that surface. In the transition zone between nozzle and sphere, particularly with a significant amount of local reinforcing, this selection may be somewhat arbitrary, hence, a degree of judgement on the part of the user is required. Both of these programs require boundary condition input data; in some cases, these boundary conditions must be quite accurately calculated in order to get reasonable results. The computer time for Kalnins' program runs about 1 to 2 minutes (CD-3400 computer) for typical models; the Seal-Shell-2 program runs about 20 minutes for the same model on the same computer.

As applied to reinforced nozzles in spheres, insufficient experience exists with the BASIC computer program to generalize the amount of input data and computer time required. For Model WN-7B in particular, the computer time was about 6 minutes.

It is apparent that an extensive parametric study using any of the last three mentioned computer programs would be relatively expensive. However, in view of the more accurate results which apparently can be obtained with these programs, it may be desirable to investigate one or more "standardized-shapes" of nozzle reinforcing--those shapes preferably being such that they would be easy to forge and/or machine and hence, an economical kind of reinforced nozzle detail.

## COMPARISON OF THEORIES WITH TEST DATA

### General Comments

The test data used herein are abstracted from reports by Taylor and Lind<sup>(24)</sup>, Leven<sup>(25)</sup>, Riley<sup>(26)</sup>, Maxwell, Holland, and Cofer<sup>(27)</sup> and Dally<sup>(28)</sup>. The first two references are compilations of extensive tests on photoelastic models, the last three references give data on steel models using strain gages.

The above references describe in considerable detail the test models and test methods, hence this information is not included herein. References (24) and (25) discuss the accuracy of photoelastic test results. The accuracy of strain gage results is well known, as well as the difficulty in accurately determining stresses with such gages in a zone of rapidly varying stress. The photoelastic method is also least accurate in zones of rapidly varying stress. Comparison of theory with test data gives no reason to doubt the accuracy of the test data. In general, as discussed in this section, comparisons between theory and test data indicate that as refinements are made to the theories so that such theories should be more applicable to the test models, the theoretical results tend to agree better with the test results.

In comparisons herein, theoretical results are based on a Poisson's ratio of 0.5 for comparison with photoelastic models; 0.3 for comparison with steel models. For some dimensional parameters, a difference between Poisson's ratio of 0.3 and 0.5 can lead to significant differences in calculated stresses\*.

### Internal Pressure Loading

#### Model BUSHips D

The available test data on stresses at nozzles in spheres includes one model with dimensions such that it does not violate the shell-theory

---

\* See Table 10 of Reference (35) and Appendix B of Reference (36).

assumption that the radius of curvature is everywhere large compared to the thickness; that model being BUShips D shown in Figure 11. The stresses for this model were calculated using Kalnin's Computer Program, the results are shown in Figure 11a along with the test data. The agreement between theory and test data is good; discrepancies that exist are well within the range of experimental data scatter\*. This comparison gives added confidence both in the accuracy of the photoelastic test data and shell theory, where the latter is directly applicable.

---

\* As shown in Figure 11 , the thickness of BUShip D was 0.0615" in the nozzle, 0.057" at the juncture of toroidal section to the sphere and 0.063" in the sphere. Variation of thickness between points indicated is not known. The theoretical stress calculations were based on a constant thickness of 0.062". Thickness variations could account for a major part of the discrepancies between calculated and measured stresses. Also, there was some difference in test data depending upon whether a 60-mil or 12-mil subslice was used in the photoelastic evaluation.

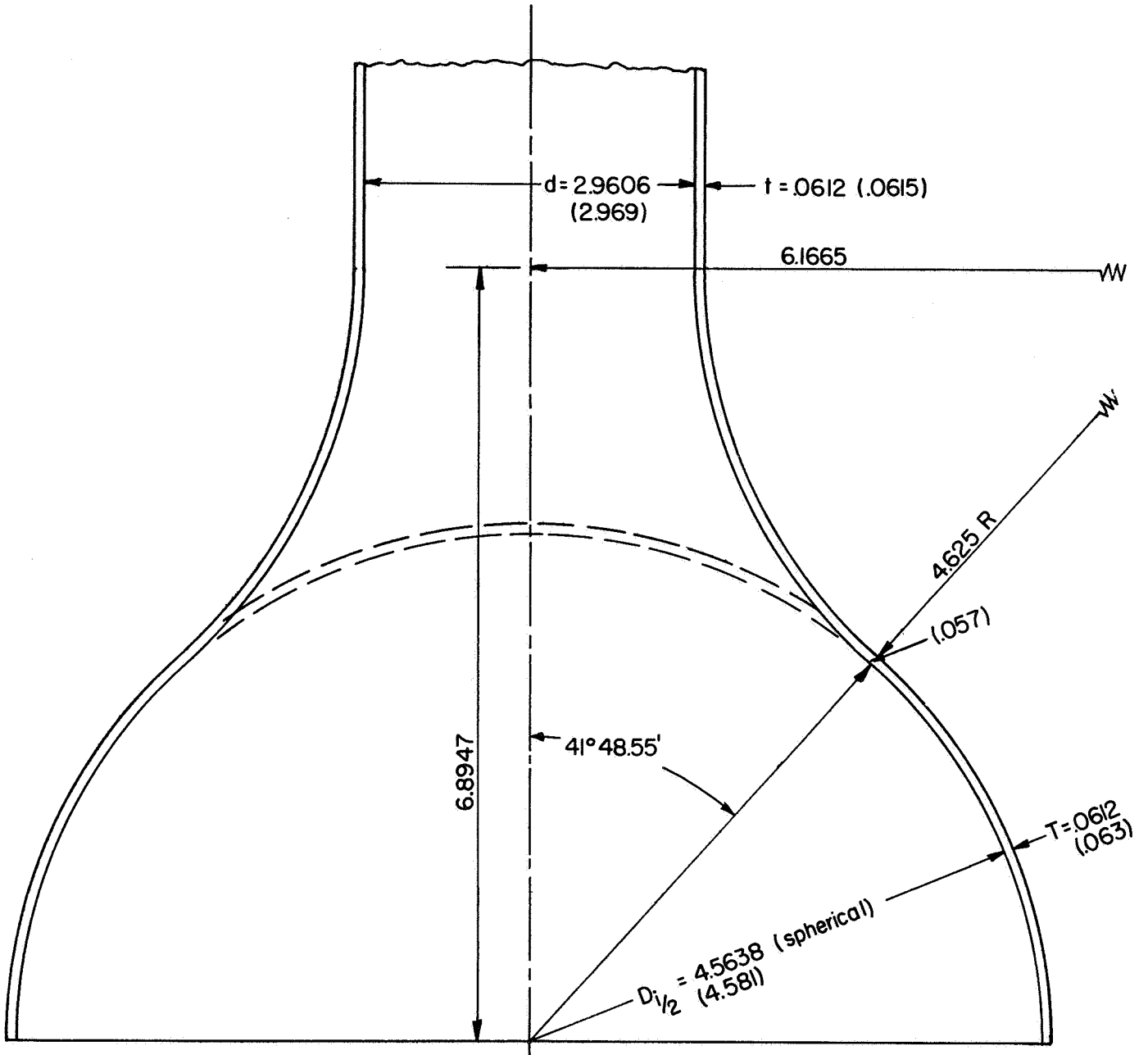


FIGURE 11. PHOTOELASTIC TEST MODEL Bu.S-D

Bu Ships D (contoured): O' Section

--- Calculated Stresses,  $\sigma_t/s$   
 --- Calculated Stresses,  $\sigma_n/s$

o---o Meridian or Tangential Stress Ratio:  $\sigma_t/s$   
 o---o Circumferential or Hoop Stress Ratio:  $\sigma_n/s$  (from 12 mil subslice)  
 o Circumferential stress ratio obtained from entire 60 mil thick section shown without subslicing.

$$d_1/D_1 = 0.324; D_1/T = 145.4$$

$$d_1/s = 48.28; R_0/D_1 = 1.00$$

$$s/s = 0.675$$

$$\sigma_{max} = S \cdot p (D_1 + T)/4T$$

$$s = p (d_1 + 1)/2t$$

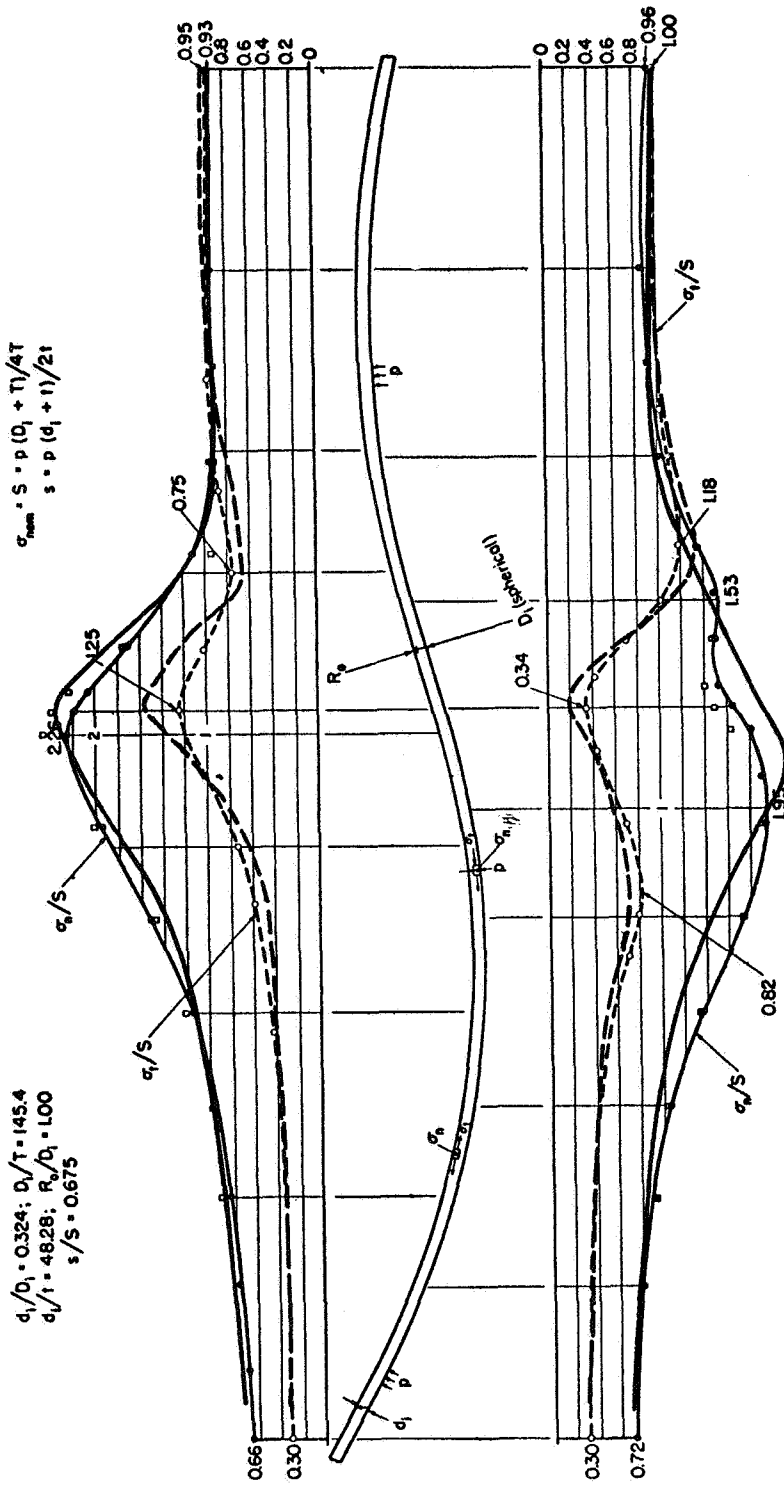


FIGURE 11a. COMPARISON OF SHELL THEORY (KALNINS) WITH TEST DATA,  
 MODEL Bu. S-D

## UNIFORM WALL MODELS

Dimensions and Comparison with Waters' Analysis. Test data considered as "Uniform Wall Models" consist of:

- (1) Photoelastic tests of 42 models, conducted at the University of Illinois<sup>(24)</sup> and Westinghouse Electric Corporation<sup>(25)</sup>.
- (2) Strain gage tests of a steel model, conducted at ITT Research Institute<sup>(26)</sup>.
- (3) Strain gage tests of two steel models, conducted at the University of Tennessee<sup>(27)</sup>.

There are, of course, continuous distributions of stresses occurring in each of these test models. The surface stresses are given, in the above references, in the form of "stress-profiles", i.e., stresses plotted as a function of location in the test model. In the case of nozzles in spheres, because of symmetry, a plane containing the axis of the nozzle represents stresses everywhere in the test model. The four principal surfaces stresses are:

$\sigma_n$  - outside surface

$\sigma_n$  - inside surface

$\sigma_t$  - outside surface

$\sigma_t$  - inside surface

where  $\sigma_n$  is a stress normal to the plane containing the nozzles axis,  $\sigma_t$  is a stress tangential to a surface cut by that plane. References (24) and (25) give experimentally determined stress profiles using the above nomenclature. Reference (26) and (27) use different nomenclature but the correlation is obvious.

From an engineering standpoint, the maximums of these four surface stresses are of greatest interest. Because of this, and in order to more concisely present the significant data, only the maximum measured values of each of the four principal surface stresses are compared with the maximum calculated values of those stresses. Calculated stresses were ob-

tained using Waters' analysis; in this analysis two results are obtained for each of these four surface stresses, i.e., at section  $\overline{AB}$  and  $\overline{CD}$  of Figure 9. The calculated stress, for comparison with test data, is arbitrarily taken as the larger of the stresses at sections  $\overline{AB}$  and  $\overline{CD}$ .

The dimensional parameters of the 45 "uniform wall models" are shown in the left group of columns of Table 9. Measured stresses are shown in the next group of five columns of Table 9;  $\sigma_m$  being the largest measured stress. The next group of five columns of Table 9 shows calculated stresses using Waters' analysis;  $\sigma$  being the largest calculated stress. The column headed  $\sigma/\sigma_m$  gives the ratio of maximum calculated to maximum measured stress.

It is apparent that the size of the fillet radius  $r_o$  is a significant factor in comparing theory with test data. For a very small fillet radius the theory would be expected to be unconservative because of the stress concentration at the juncture; for large fillet radii the theory would be expected to be conservative because of the added thickness of the nozzle and sphere walls at the juncture. Table 9 indicates that, except for Model S-1G, if  $r_o/t$  is greater than about 0.8, the theory is conservative with respect to the test results; i.e.,  $\sigma_c/\sigma_m$  is greater than unity. Where  $0.5 < r_o/t < 3$ , the test results and theory agree in a qualitative sense in that models such as IIT-S1, S-2AZ, and S-3C had relatively high stresses, both theoretically and experimentally. Models such as N-2BM, N-4E, S-5AW, and S-1G theoretically have relatively low stresses; experimentally these models did have relatively low stresses with the exception of Model S-1G.

In a more quantitative sense, Table 9 shows larger discrepancies between theory and test results than indicated by the above comparisons. As shown in Table 9, there are several models in which maximum stresses occurred either at different surfaces or different directions than indicated by the theory. Also, stresses other than the maximums are often in poor agreement, e.g., model N-8G,  $\sigma_t$  - inside, where the test data gives -0.38; theory gives -1.69.

TABLE 9. UNIFORM WALL MODEL DIMENSIONS AND COMPARISONS TEST DATA WITH WATERS' ANALYSIS

Model No.(1)	$\frac{d_i}{D_i}$	$\frac{D_i}{T}$	$\frac{s}{S}$	$\frac{t}{T}$	$\frac{d_j}{t}$	$\frac{r_o}{t}$	$\frac{A_a}{d_i^2}$	$\frac{r_i}{t}$	Measured Stresses(3)				Calculated Stresses (Waters)(3)				$\frac{\sigma_c}{\sigma_m}$ (4)
									$\sigma_n/S$		$\sigma_t/S$		$\sigma_n/S$		$\sigma_t/S$		
									Outside	Inside	Outside	Inside	Outside	Inside	Outside	Inside	
S-1G	0.05	23.7	0.39	0.311	3.82	1.76	0.086	0.80	1.14	1.02	1.38	1.41	0.76	-0.52	1.41	0.54	
S-1A	0.05	23.8	1.01	0.103	11.6	0.81	0.0022	2.42	2.2	1.25	2.79	1.67	2.06	-1.20	2.79	1.27	
S-1AB	0.05	24.0	1.00	0.107	11.2	5.23	0.091	2.34	1.51	1.07	2.75	1.66	2.03	-1.21	2.75	1.27	
S-1C	0.05	11.5	1.96	0.051	11.3	0.79	0.0011	4.9	1.9	1.0	2.81	2.34	1.75	-0.18	2.81	0.97	
WS-1LM	0.05	71.5	1.01	0.100	35.5	47.3	2.00	4.9	1.17	1.20	4.27	1.63	3.65	-2.69	4.27	2.28	
WS-1LB	0.05	24.2	0.99	0.105	11.5	28.0	2.00	2.4	1.07	1.13	2.79	1.67	2.05	-1.21	2.79	1.38	
N-8C	0.129	17.1	0.63	0.471	4.66	0.73	0.015	0.73	1.68	1.39	1.69	1.39	0.94	-0.52	1.69	0.84	
N-8H	0.129	23.7	1.03	0.261	11.7	0.40	0.0011	0.40	3.1	2.06	3.21	1.56	2.56	-1.69	3.21	1.04	
N-8F	0.129	23.6	1.00	0.269	11.3	0.72	0.0037	0.72	2.66	1.90	3.13	1.55	2.49	-1.64	3.13	1.18	
N-8E	0.129	23.9	1.01	0.266	11.5	1.81	0.023	1.81	2.19	1.26	3.17	1.55	2.52	-1.67	3.17	1.45	
N-8G	0.129	24.5	0.99	0.270	11.7	2.53	0.042	2.53	1.96	1.29	3.18	1.55	2.54	-1.69	3.18	1.56	
S-2AZ	0.129	66.4	0.99	0.264	32.5	0.74	0.0013	0.88	4.6	4.0	5.30	1.74	5.00	-4.07	5.30	1.15	
N-8D	0.129	16.3	1.48	0.178	11.8	1.89	0.016	1.89	2.53	1.52	3.44	1.90	2.62	-1.36	3.44	1.36	
N-4F	0.20	24.9	0.38	1.29	3.88	0.45	0.014	0.45	1.70	1.83	1.72	1.45	1.17	0.14	1.72	0.94	
N-1E	0.20	28.0	0.40	1.17	4.80	0.56	0.016	0.56	1.82	1.77	1.88	1.46	1.27	-0.04	1.88	1.03	
N-1EA	0.20	24.0	0.46	1.00	4.81	0.56	0.014	0.56	1.80	1.77	1.88	1.46	1.24	-0.10	1.88	1.04	
N-3D	0.20	25.7	0.55	0.815	6.34	0.73	0.015	0.73	1.91	1.75	2.08	1.44	1.31	-0.39	2.08	1.09	
N-1C*	0.20	26.3	0.42	1.10	4.76	0.55	0.015	0.55	1.80	1.68	1.87	1.46	1.26	-0.06	1.87	1.04	
N-2B*	0.20	25.2	0.44	1.06	4.75	0.55	0.014	0.55	2.00	2.10	1.87	1.46	1.25	-0.07	1.87	0.89	
N-3B*	0.20	24.8	0.57	0.790	6.33	0.73	0.015	0.73	1.96	1.74	2.00	1.42	1.25	-0.36	2.00	1.02	
N-1AA	0.20	24.6	0.98	0.429	11.5	1.33	0.016	1.33	2.55	2.04	3.11	1.53	2.46	-1.63	3.11	1.22	
N-2BM*	0.20	24.7	0.45	1.03	4.80	0.56	0.016	0.56	1.75	1.74	1.88	1.46	1.25	-0.09	1.88	1.07	
N-4E*	0.20	23.8	0.39	1.22	3.90	0.45	0.013	0.45	1.79	1.72	1.72	1.45	1.17	-0.12	1.72	0.96	
N-1A	0.20	25.1	1.13	0.368	13.7	1.59	0.016	1.59	2.72	2.01	3.62	1.60	2.99	-2.01	3.62	1.33	
N-5B	0.20	16.8	1.38	0.304	11.4	2.37	0.034	1.32	2.70	2.23	3.55	1.77	2.83	-1.66	3.55	1.31	
S-3C	0.20	11.6	1.99	0.201	11.5	0.81	0.0029	1.25	4.0	2.60	3.89	2.33	2.94	-1.25	3.89	0.97	
S-3CB	0.20	11.6	1.98	0.202	11.4	2.39	0.024	1.24	2.90	2.62	3.87	2.32	2.92	-1.25	3.87	1.33	
WN-10B	0.20	24.0	1.02	0.412	11.7	10.5	0.67	1.35	1.37	1.22	3.20	1.55	2.56	-1.69	3.20	1.99	
WN-10D	0.20	24.0	1.02	0.412	11.7	3.78	0.086	1.35	1.61	1.15	3.20	1.55	2.55	-1.69	3.20	1.83	
WN-50B	0.27	50.2	1.10	0.500	27.2	1.6	0.013	0.50	3.92	3.06	4.95	1.80	4.45	-3.41	4.95	1.26	
Bu.-S-1	0.27	36.9	0.54	1.10	9.2	1.2	0.071	0.35	2.29	1.96	2.53	1.60	1.75	-0.66	2.53	1.10	
N-9E	0.38	23.7	1.01	0.792	11.5	0.13	0.0002	0.13	4.4	4.3	2.94	1.73	1.85	-0.99	2.94	0.67	
N-9A	0.38	23.6	1.02	0.783	11.6	0.25	0.00059	0.25	4.0	3.8	2.95	1.73	1.88	-1.01	2.95	0.74	
N-9B	0.38	24.4	1.00	0.806	11.6	0.61	0.0035	0.61	3.00	2.74	2.95	1.73	1.85	-0.97	2.95	0.98	
N-9C	0.38	23.7	1.02	0.782	11.6	0.85	0.0064	0.85	2.75	2.40	2.92	1.72	1.85	-1.00	2.92	1.06	
WA1-1	0.38	7.65	1.24	0.675	4.37	3.58	0.15	0.40	1.55	1.32	2.01	2.02	1.17	-0.35	2.02	1.30	
S-5E	0.50	24.1	0.66	1.64	7.35	0.49	0.0039	0.15	2.58	2.45	2.24	1.88	1.44	0.13	2.24	0.87	
S-5AZ	0.50	70.5	1.02	1.00	35.3	0.79	0.0009	0.25	4.9	4.2	4.67	1.93	3.62	-2.55	4.67	0.95	
S-5A	0.50	24.1	1.00	1.04	11.6	0.78	0.0046	0.24	2.87	2.50	3.01	1.93	2.03	-0.95	3.01	1.05	
S-5AW	0.50	9.0	1.10	1.00	4.5	0.55	0.0057	0.55	2.29	1.93	2.03	2.03	1.14	-0.15	2.03	0.89	
S-5C	0.50	11.5	2.00	0.50	11.5	1.10	0.0056	0.50	3.62	2.60	4.05	2.29	3.15	-1.46	4.05	1.12	
WS-5LM	0.50	78.8	0.96	1.01	37.2	20.3	0.72	0.56	1.41	1.12	4.78	2.00	3.80	-2.70	4.78	3.39	
IIT-S1	0.50	240	1.00	0.99	120	~1.4	0.0018	~1.4	5.70	5.68	6.59	3.29	6.30	-5.22	6.59	1.17	
ORNL-5	0.079	80.5	0.49	0.333	19	~0	-	~0	2.98	2.20	2.69	1.72	2.48	-2.03	2.69	(5)	
ORNL-6	0.083	80.5	1.01	0.167	40	~0	-	~0	4.24	3.30	4.06	2.01	4.16	-3.19	4.16	(5)	

(1) Model numbers are the same as in those given in References 24, 25, 26 and 27. \* = The length of nozzle with increased thickness was sufficient to consider models as "uniform wall".

(2)  $A_a$  = cross sectional area of the fillet radius.

(3) Tabulated stresses are maximum significant stresses near the opening; remote from the opening  $\sigma_n/S$  and  $\sigma_t/S$  approaches 0.5 s/s on the nozzle.

(4)  $\sigma_m$  = maximum measured stress,  $\sigma_c$  = maximum calculated stress.

(5) The ORNL models are discussed separately, see Figures 14 through 17.



Semi-Empirical Modifications to Analysis. There are several reasons why the "two-piece" shell theory may not give accurate stresses for the test models. Three of the more important reasons are discussed in the following, along with semi-empirical modifications made in an attempt to bring theory and test data into better agreement.

(1) Normal plane thickness\*

The fillet radius may be considered as altering the thicknesses of the shells at a critical location, i.e., at the juncture between nozzle and sphere. If it is assumed, for relatively small amount of reinforcing added by the fillet, that the "two-piece" shell theory gives a good estimate of the forces and moments at and near the nozzle-sphere juncture, then the stresses are given by the equations:

$$\sigma_m = \frac{N}{h} \quad (9)$$

$$\sigma_b = \frac{6M}{h^2} \quad (10)$$

where:

$\sigma_m$  = membrane stress, psi

N = normal force, lb/in

$\sigma_b$  = bending stress, psi

M = bending moment, in-lb/in

h = normal thickness of section, in.

The value of h is not well defined in the juncture zone; the zone of principal interest since maximum stresses are usually found therein. The thickness h in the transition zone has been somewhat arbitrarily defined as shown by Figure 12. For models under consideration, planes radiating from the fillet radius center appear to be suitable for use as "normal planes" in the transition zone.

---

\* This concept was originally used by Atterbury<sup>(29)</sup> in correlating and interpolating test data on nozzles in cylindrical shells, leading to a development of rules for design of such structures.

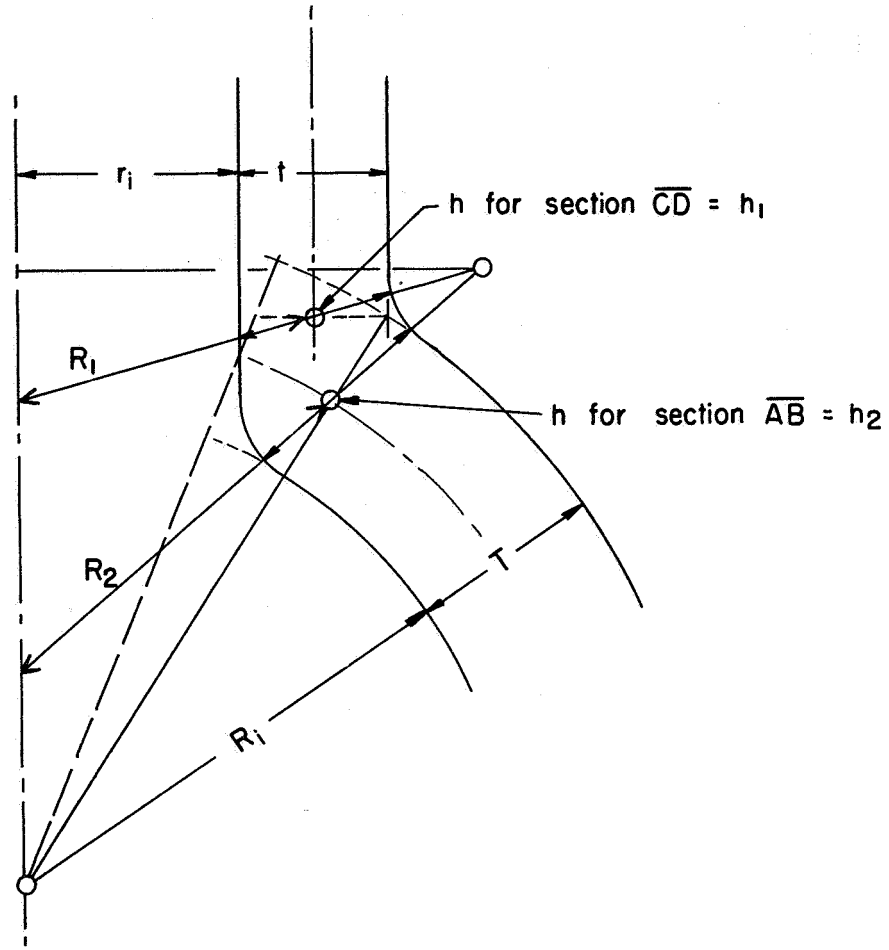


FIGURE 12. DEFINITION OF NORMAL THICKNESSES AND RADII IN THE TRANSITION SECTION

Using the  $h$ -values obtained from large-scale (10 times actual size) drawings of the transition sections, the "two-piece" shell theory was modified by the factors:

$$\begin{aligned} T/h_2 & \text{ for membrane stress at sections } \overline{AB} \\ (T/h_2)^2 & \text{ for bending stress at section } \overline{AB} \\ t/h_1 & \text{ for membrane stress at section } \overline{CD} \\ (t/h_1)^2 & \text{ for bending stress at section } \overline{CD} \end{aligned}$$

where:

$T$  = wall thickness of spherical shell

$t$  = wall thickness of nozzle

$h_1$  and  $h_2$  are normal thicknesses as defined by Figure 12.

$\overline{AB}$  and  $\overline{CD}$  are sections corresponding to Waters' two-piece shell theory, as shown by Figure 12.

The maximum calculated stress  $\sigma'$  is compared with test data in Table 10. By comparing rows marked  $\sigma$  with those marked  $\sigma'$ , it is apparent that the major discrepancies occurring in those models with large fillet radii are significantly reduced; however, in general, this type of correction by itself tends to underestimate the stresses as compared to the test data. Table 11 gives a summary of computed-to-measured stress ratios.

Because of the assumption that the forces and moments are given by "two-piece" shell theory, it is apparent that the empirical modification discussed above is applicable only for small amounts of reinforcing. That is, a large amount of reinforcing would significantly alter the forces and moments. A more direct method of accounting for local reinforcing thickness is available by use of "multi-piece" shell theories such as those contained in Seal-Shell-2 or Kalnins' computer programs. Even with these theories, however, arbitrary selection of a midsurface and normal thicknesses in the juncture zone is required. Comparison of these theories with test data is given later herein.

## (2) Curved Beam Factor

From general considerations of stress concentrations, a high stress would be expected to develop in models with small fillet radii. This effect implies a non-linear distribution of stresses through the wall thickness and cannot be evaluated by thin-shell theory. Taylor and Lind<sup>(24)</sup> show stresses through the wall thickness for models N-1A, S-5C, and N-1EA, illustrating to some extent the non-linear character of stresses as a function of position in the wall.

TABLE 10. COMPARISON OF TEST DATA WITH WATERS' THEORY AND EMPIRICAL MODIFICATIONS, UNIFORM WALL MODELS

Model No.	Stress (1)	Stress Indices			
		$\sigma_n/S$		$\sigma_t/S$	
		Outside	Inside	Outside	Inside
S-1G	Test Data	1.14	2.60	1.02	- .30
	$\sigma$	1.38	1.41	.76	- .52
	$\sigma'$	1.19	1.23	.59	+ .24
	$\sigma''$	1.20	1.23	.69	+ .29
	$\sigma'''$	.83	1.97	.57	- .13
S-1A	Test Data	2.20	2.20	1.25	- .28
	$\sigma$	2.79	1.67	2.06	- 1.20
	$\sigma'$	2.02	1.66	1.31	- .64
	$\sigma''$	2.17	1.71	1.74	- .41
	$\sigma'''$	2.11	2.72	1.74	- .41
S-1AB	Test Data	1.51	2.17	1.07	- .24
	$\sigma$	2.75	1.66	2.03	- 1.21
	$\sigma'$	1.60	1.43	.34	- .05
	$\sigma''$	1.64	1.45	.38	+ .03
	$\sigma'''$	1.01	3.02	.38	- .80
S-1C	Test Data	1.90	2.90	1.00	- .20
	$\sigma$	2.81	2.34	1.75	- .18
	$\sigma'$	2.06	1.87	1.17	- .18
	$\sigma''$	2.21	1.90	1.40	+ .23
	$\sigma'''$	2.10	2.99	1.40	- 1.30
WS-1LM	Test Data	1.17	1.87	1.20	- .06
	$\sigma$	4.27	1.63	3.65	- 2.69
	$\sigma'$	1.21	.97	.07	+ .02
	$\sigma''$	1.22	.98	.08	+ .02
	$\sigma'''$	.83	1.68	.06	- .95
WS-1LB	Test Data	1.07	2.03	1.13	- .17
	$\sigma$	2.79	1.67	2.05	- 1.21
	$\sigma'$	1.55	1.39	.18	+ .03
	$\sigma''$	1.56	1.40	.19	+ .03
	$\sigma'''$	.66	4.21	.13	- .75
N-8C	Test Data	1.68	2.02	1.39	- .34
	$\sigma$	1.69	1.39	.94	- .52
	$\sigma'$	1.55	1.28	.78	- .37
	$\sigma''$	1.63	1.31	1.09	- .23
	$\sigma'''$	1.46	1.93	1.04	- .43

(1) Test Data = measured stresses

$\sigma$  = calculated stresses, Waters' theory

$\sigma'$  = calculated stresses with normal thickness modification

$\sigma''$  = calculated stresses with normal thickness and curved beam modifications

$\sigma'''$  = calculated stresses with normal thickness, curved beam and thick-wall modifications.

TABLE 10 (contd.)

Model No.	Stress (1)	Stress Indices			
		$\sigma_n/S$		$\sigma_t/S$	
		Outside	Inside	Outside	Inside
N-8H	Test Data	3.10	2.06	2.75	- .98
	$\sigma$	3.21	1.56	2.56	- 1.69
	$\sigma'$	2.84	1.54	2.16	- 1.37
	$\sigma''$	3.14	1.64	3.37	- .82
	$\sigma'''$	3.14	2.67	3.37	- .84
N-8F	Test Data	2.66	2.18	1.90	- .68
	$\sigma$	3.13	1.55	2.49	- 1.64
	$\sigma'$	2.51	1.51	1.82	- 1.12
	$\sigma''$	2.67	1.60	2.48	- .75
	$\sigma'''$	2.66	2.63	2.48	- .85
N-8E	Test Data	2.19	2.00	1.26	- .37
	$\sigma$	3.17	1.55	2.52	- 1.67
	$\sigma'$	2.05	1.43	1.21	- .64
	$\sigma''$	2.16	1.48	1.43	- .48
	$\sigma'''$	1.93	2.49	1.43	- .86
N-8G	Test Data	1.96	2.04	1.29	- .38
	$\sigma$	3.18	1.55	2.54	- 1.69
	$\sigma'$	1.93	1.37	.94	- .46
	$\sigma''$	2.01	1.41	1.08	- .35
	$\sigma'''$	1.74	2.37	1.08	- .86
S-2AZ	Test Data	4.60	2.60	4.00	- 2.10
	$\sigma$	5.30	1.74	5.00	- 4.07
	$\sigma'$	4.14	1.68	3.58	- 2.80
	$\sigma''$	4.48	1.82	4.97	- 2.01
	$\sigma'''$	4.48	3.25	4.97	- 2.01
N-8D	Test Data	2.53	2.14	1.52	- .23
	$\sigma$	3.44	1.90	2.62	- 1.36
	$\sigma'$	2.20	1.53	1.25	- .43
	$\sigma''$	2.37	1.60	1.45	- .29
	$\sigma'''$	2.07	2.82	1.45	- 1.03
N-4F	Test Data	1.70	1.58	1.83	- .14
	$\sigma$	1.72	1.45	1.17	.14
	$\sigma'$	1.50	1.41	.99	.18
	$\sigma''$	1.56	1.42	1.21	.30
	$\sigma'''$	1.49	1.51	1.18	.09

TABLE 10 (contd.)

Model No.	Stress (1)	Stress Indices			
		$\sigma_n/S$		$\sigma_t/S$	
		Outside	Inside	Outside	Inside
N-1E	Test Data	1.82	1.80	1.77	- .14
	$\sigma$	1.88	1.46	1.27	- .04
	$\sigma'$	1.60	1.39	1.04	.04
	$\sigma''$	1.66	1.40	1.28	.17
	$\sigma'''$	1.58	1.60	1.25	- .26
N-1EA	Test Data	1.80	1.77	1.67	- .23
	$\sigma$	1.88	1.46	1.24	- .10
	$\sigma'$	1.66	1.39	1.06	- .08
	$\sigma''$	1.74	1.40	1.35	.12
	$\sigma'''$	1.64	1.71	1.31	- .32
N-3D	Test Data	1.91	1.77	1.75	- .40
	$\sigma$	2.08	1.44	1.31	- .39
	$\sigma'$	1.79	1.33	1.08	- .30
	$\sigma''$	1.88	1.36	1.40	- .19
	$\sigma'''$	1.78	1.87	1.37	- .56
N-1C	Test Data	1.80	1.64	1.68	- .15
	$\sigma$	1.87	1.46	1.26	- .06
	$\sigma'$	1.63	1.40	1.06	- .02
	$\sigma''$	1.71	1.41	1.32	.16
	$\sigma'''$	1.62	1.66	1.29	- .27
N-2B	Test Data	2.00	1.70	2.10	- .30
	$\sigma$	1.87	1.46	1.25	- .07
	$\sigma'$	1.64	1.40	1.06	- .04
	$\sigma''$	1.72	1.41	1.33	.14
	$\sigma'''$	1.63	1.68	1.30	- .29
N-3B	Test Data	1.96	1.81	1.74	- .38
	$\sigma$	2.00	1.42	1.25	- .36
	$\sigma'$	1.74	1.32	1.04	- .29
	$\sigma''$	1.82	1.35	1.35	- .18
	$\sigma'''$	1.71	1.84	1.32	- .51
N-1AA	Test Data	2.55	2.04	1.74	- .77
	$\sigma$	3.11	1.53	2.46	- 1.63
	$\sigma'$	2.27	1.38	1.59	- .94
	$\sigma''$	2.36	1.44	1.94	- .71
	$\sigma'''$	2.34	2.35	1.94	- .89

TABLE 10 (contd.)

Model No.	Stress (1)	Stress Indices			
		$\sigma_n / S$		$\sigma_t / S$	
		Outside	Inside	Outside	Inside
N-2BM	Test Data	1.75	1.58	1.54	- .11
	$\sigma$	1.88	1.46	1.25	- .09
	$\sigma'$	1.32	1.19	.80	.07
	$\sigma''$	1.35	1.20	.89	.13
	$\sigma'''$	1.22	1.32	.84	- .38
N-4E	Test Data	1.79	1.77	1.72	- .16
	$\sigma$	1.72	1.45	1.17	.12
	$\sigma'$	1.53	1.42	1.01	.15
	$\sigma''$	1.60	1.42	1.25	.28
	$\sigma'''$	1.52	1.56	1.21	- .10
N-1A	Test Data	2.72	2.01	1.84	- .78
	$\sigma$	3.62	1.60	2.99	- 2.01
	$\sigma'$	2.35	1.47	1.65	- .94
	$\sigma''$	2.45	1.53	1.98	- .72
	$\sigma'''$	2.41	2.60	1.98	- .96
N-5B	Test Data	2.70	2.23	1.55	- .35
	$\sigma$	3.55	1.77	2.83	- 1.66
	$\sigma'$	2.17	1.45	1.34	- .57
	$\sigma''$	2.27	1.51	1.52	- .43
	$\sigma'''$	2.06	2.61	1.52	- 1.00
S-3C	Test Data	4.00	2.60	3.40	- 1.05
	$\sigma$	3.89	2.33	2.94	- 1.25
	$\sigma'$	3.25	2.14	2.30	- .84
	$\sigma''$	3.40	2.23	2.92	- .48
	$\sigma'''$	3.39	3.11	2.92	- 1.25
S-3CB	Test Data	2.90	2.62	1.70	- .25
	$\sigma$	3.87	2.32	2.92	- 1.25
	$\sigma'$	2.36	1.73	1.39	- .32
	$\sigma''$	2.52	1.76	1.56	- .22
	$\sigma'''$	2.23	3.04	1.56	- 1.24
WN-10B	Test Data	1.37	1.61	1.22	- .16
	$\sigma$	3.20	1.55	2.56	- 1.69
	$\sigma'$	1.56	1.15	.51	- .15
	$\sigma''$	1.57	1.16	.55	- .11
	$\sigma'''$	1.32	1.82	.51	- .89

TABLE 10 (contd.)

Model No.	Stress (1)	Stress Indices			
		$\sigma_n/s$		$\sigma_t/s$	
		Outside	Inside	Outside	Inside
WN-10D	Test Data	1.61	1.75	1.51	- .28
	$\sigma$	3.20	1.55	2.55	- 1.69
	$\sigma'$	2.19	1.41	.86	- .39
	$\sigma''$	2.24	1.45	.96	- .32
	$\sigma'''$	2.04	2.48	.96	- .98
WN-50B	Test Data	3.92	2.83	3.06	- 1.62
	$\sigma$	4.95	1.80	4.45	- 3.41
	$\sigma'$	3.22	1.70	2.33	- 1.60
	$\sigma''$	3.37	1.79	2.83	- 1.26
	$\sigma'''$	3.29	3.33	2.83	- 1.34
Bu.S-1	Test Data	2.29	2.06	1.96	- .31
	$\sigma$	2.53	1.60	1.75	- .66
	$\sigma'$	2.22	1.42	1.46	- .48
	$\sigma''$	2.29	1.44	1.70	- .32
	$\sigma'''$	2.22	2.11	1.68	- .80
N-9E	Test Data	4.40	1.88	4.30	- 1.03
	$\sigma$	2.94	1.73	1.85	- .99
	$\sigma'$	2.91	1.73	1.85	- .99
	$\sigma''$	3.64	1.88	4.33	- .41
	$\sigma'''$	3.62	2.87	4.33	- .88
N-9A	Test Data	4.00	1.86	3.80	- 1.00
	$\sigma$	2.95	1.73	1.88	- 1.01
	$\sigma'$	2.87	1.73	1.88	- 1.01
	$\sigma''$	3.32	1.86	3.30	- .51
	$\sigma'''$	3.28	2.84	3.30	- .95
N-9B	Test Data	3.00	1.81	2.74	- .96
	$\sigma$	2.95	1.73	1.85	- .97
	$\sigma'$	2.72	1.72	1.77	- .94
	$\sigma''$	2.92	1.80	2.38	- .60
	$\sigma'''$	2.86	2.68	2.38	- 1.03
N-9C	Test Data	2.95	1.95	2.40	- .83
	$\sigma$	2.92	1.72	1.85	- 1.00
	$\sigma'$	2.64	1.68	1.74	- .92
	$\sigma''$	2.75	1.76	2.20	- .63
	$\sigma'''$	2.76	2.58	2.20	- 1.03



TABLE 10 (contd.)

Model No.	Stress (1)	Stress Indices			
		$\sigma_n/S$		$\sigma_t/S$	
		Outside	Inside	Outside	Inside
WAI-1	Test Data	1.55	1.77	1.32	- .46
	$\sigma$	2.01	2.02	1.17	- .35
	$\sigma'$	1.62	1.54	.74	- .17
	$\sigma''$	1.64	1.55	.81	- .12
	$\sigma'''$	1.41	1.97	.77	- .79
S-5E	Test Data	2.58	1.78	2.45	- .43
	$\sigma$	2.24	1.88	1.45	.13
	$\sigma'$	2.24	1.88	1.45	.13
	$\sigma''$	2.33	1.89	1.72	.17
	$\sigma'''$	2.30	2.31	1.70	.17
S-5AZ	Test Data	4.90	2.34	4.20	- 1.78
	$\sigma$	4.67	1.93	3.62	- 2.55
	$\sigma'$	4.08	1.91	2.94	- 1.99
	$\sigma''$	4.30	2.04	3.91	- 1.42
	$\sigma'''$	4.30	3.47	3.91	- 1.94
S-5A	Test Data	2.87	2.00	2.50	- .60
	$\sigma$	3.01	1.93	2.03	- .95
	$\sigma'$	2.69	1.92	1.75	- .76
	$\sigma''$	2.83	1.97	2.22	- .47
	$\sigma'''$	2.78	2.61	2.21	- .96
S-5AW	Test Data	2.29	1.68	1.93	- .41
	$\sigma$	2.03	2.03	1.14	- .15
	$\sigma'$	1.96	1.95	1.08	- .13
	$\sigma''$	2.07	1.97	1.41	.05
	$\sigma'''$	2.00	2.15	1.39	- .46
S-5C	Test Data	3.62	2.45	2.60	- .66
	$\sigma$	4.05	2.29	3.15	- 1.46
	$\sigma'$	3.69	2.21	2.78	- 1.21
	$\sigma''$	3.83	2.30	3.35	- .83
	$\sigma'''$	3.83	3.41	3.35	- 1.31
WS-5IM	Test Data	1.41	1.16	1.12	- .04
	$\sigma$	4.78	2.00	3.80	- 2.70
	$\sigma'$	1.24	.99	.56	- .19
	$\sigma''$	1.25	.99	.58	- .17
	$\sigma'''$	1.19	1.04	.57	- .97
IIT-s1	Test Data	5.75	3.44	5.72	- 2.02
	$\sigma$	6.59	3.29	6.30	- 5.22
	$\sigma'$	5.66	3.14	4.78	- 3.87
	$\sigma''$	5.75	3.20	5.77	- 3.17
	$\sigma'''$	5.75	3.20	5.77	- 3.17

TABLE 11. RANGES, AVERAGES, AND AVERAGE ERRORS OF THE RATIOS OF  
 COMPUTED MAXIMUM STRESS TO MEASURED MAXIMUM STRESS

Stress Ratio (1)	All Models of Table 9			Models of Table 9 Where $r_0/t < 6$				
	Range		Avg. Error	Range		Avg. Error		
	Min.	Max.		Min.	Max.			
$\sigma/\sigma_m$	0.54	3.39	1.21	0.29	0.54	1.56	1.08	0.17
$\sigma'/\sigma_m$	0.47	1.25	0.87	0.15	0.47	1.04	0.86	0.14
$\sigma''/\sigma_m$	0.47	1.28	0.92	0.11	0.47	1.09	0.92	0.10
$\sigma'''/\sigma_m$	0.76	2.08	1.01	0.14	0.76	1.40	0.98	0.11
	<u>Waters</u>							
	0.86	3.55	1.55	0.55	0.86	2.19	1.40	0.41
	0.65	1.47	1.08	0.17	0.65	1.36	1.09	0.17
	0.78	1.93	1.23	0.29	0.78	1.93	1.24	0.29
	0.89	2.44	1.32	0.33	0.94	1.93	1.30	0.31
	<u>Thin Shell</u>							
	0.86	3.55	1.55	0.55	0.86	2.19	1.40	0.41
	0.65	1.47	1.08	0.17	0.65	1.36	1.09	0.17
	0.78	1.93	1.23	0.29	0.78	1.93	1.24	0.29
	0.89	2.44	1.32	0.33	0.94	1.93	1.30	0.31

(1)  $\sigma$  = stress calculated by indicated theory ("Waters" or "thin shell").

$\sigma'$  = calculated stresses with normal thickness modification.

$\sigma''$  = calculated stresses with normal thickness and curved-beam modifications.

$\sigma'''$  = calculated stresses with normal thickness, curved beam, and Lamé-type modifications.

$\sigma_m$  = maximum measured stress.

It has been suggested by Lind<sup>(30)</sup> that these stress concentration factors might be approximated by analogy with the theory of curved beams. Curved beam theory was used to modify the shell theory by equations of the type:

For tangential stresses

$$\sigma''_t = \sigma'_t \pm (i-1) \sigma'_{tb} \quad (11)$$

For normal stresses

$$\sigma''_n = \sigma'_n \pm \nu (i - 1) \sigma'_{tb} \quad (12)$$

where

$\sigma''_t$  = tangential surface stress with modifications for both normal plane thickness and curved beam factor

$\sigma'_t$  = tangential surface stress with normal plane thickness modification

$\sigma''_n$  = normal surface stress with modifications for both normal plane thickness and curved beam factor

$\sigma'_n$  = normal surface stress with modification for normal plane thickness

$\nu$  = Poisson's ratio

$i$  = stress concentration factor from curved beam theory,  $i_o$  for outside of shell,  $i_i$  for inside of shell.

The stress concentration factor  $i$  is used in the form

$$\sigma = \frac{6M}{h^2} i \quad (13)$$

where  $M$  = moment applied to curved beam

$h$  = thickness of curved beam sections

From the Winkler-Bach theory for curved beams:

$$i_o = \frac{\left[ \frac{\frac{c}{a} - 1}{\log_e c/a} - 1 \right] \left( \frac{c}{a} - 1 \right)}{6 \left[ \frac{1}{2} \left( \frac{c}{a} + 1 \right) - \frac{\frac{c}{a} - 1}{\log_e c/a} \right]} \quad (14)$$

$$i_i = \frac{\left[ -\frac{a}{c} \left( \frac{c}{a} - 1 \right) + 1 \right] \left( \frac{c}{a} - 1 \right)}{6 \left[ \frac{1}{2} \left( \frac{c}{a} + 1 \right) - \frac{\frac{c}{a} - 1}{\log_e c/a} \right]} \quad (15)$$

As applied to nozzles in spheres, in equations (11) and (12):

$$\frac{c}{a} = \frac{r_o + h_1}{r_o} \quad \text{for section } \overline{CD} \text{ of Figure 12.}$$

$$\frac{c}{a} = \frac{r_o + h_2}{r_o} \quad \text{for section } \overline{AB} \text{ of Figure 12.}$$

A graph of the curved beam factors,  $i_o$  and  $i_i$ , is shown as Figure 13. The maximum calculated stress  $\sigma''$ , including both the normal plane thickness and curved beam factor modifications is shown in Table 10 in the rows marked  $\sigma''$ . Some additional improvement in correlation with test data is obtained; as shown in Table 11 the average of  $\sigma''/\sigma_m$  is closer to the ideal value of 1.00.

### (3) Lamé'-type Factor

In several models the normal stress at the inside corner of the juncture was the maximum measured stress, e.g., Model S-1G with a stress concentration factor of 2.6 and Model S-1C with a stress concentration factor of 2.9. Neither the shell theory nor the two modifications discussed above predict these stress concentrations.

If it is assumed that there is a transition in radii through the junction zone from the radius of the cylindrical nozzle to the radius of the sphere, with intermediate radii being normal to the midsurface of the junction zone, significant thick-wall-shell stresses can arise. With "normal radii" defined as shown in Figure 12, the additional stresses due to the thick wall effect was approximated by equations of the type:

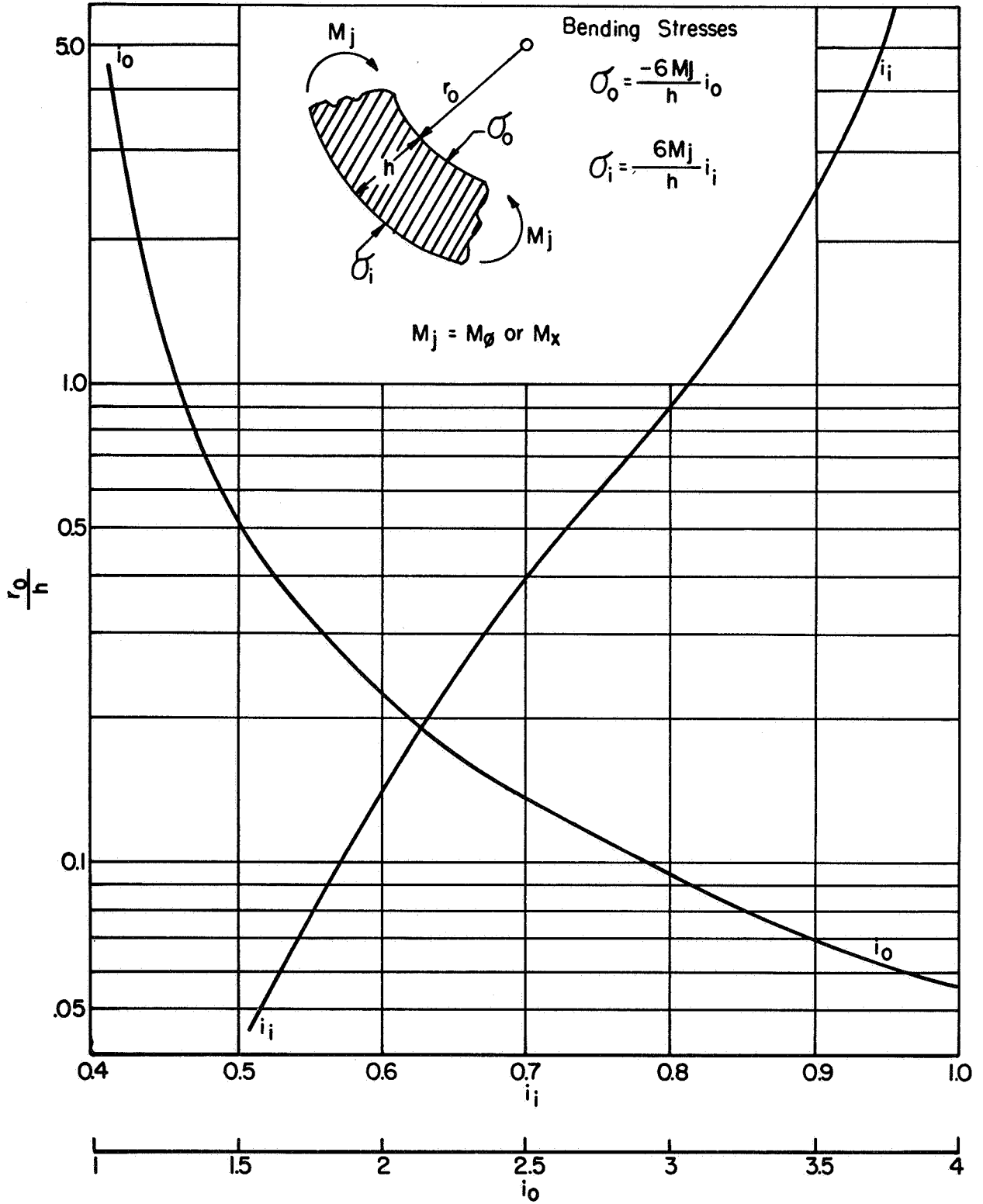


FIGURE 13. STRESS-CONCENTRATION FACTORS, CURVED BEAM THEORY

Section  $\overline{AB}$ , normal stress, outside surface

$$\sigma_n''' = \sigma_n'' + \sigma_{ab}' \left[ (1 + T/D_i) (1 - h_2/2R_2) - 1 \right] \quad (16)$$

where  $\sigma_n''' =$  normal stress at A (Figure 9) with modifications for normal thickness, curved beam factor and Lamé factor.

$\sigma_n'' =$  normal stress at A with modifications for normal thickness and curved beam factor.

$\sigma_{ab}' =$  midwall stress at section  $\overline{AB}$  (Figure 9) with modification for normal plane thickness.

$T =$  wall thickness of sphere.

$D_i =$  inside diameter of sphere.

$h_2, R_2 =$  defined by Figure 12.

The correction factor is obtained by a truncated series expansion of Lamé equations for spheres and cylinders in terms of the thickness-to-radius ratio. Since Waters' equations contain a correction of this type ( $T/2R$  or  $t/2r$ ) the additional correction factor ( $h_2/2R_2$  or  $h_1/2R_1$ ) is included so that when  $T/D = h_2/2R_2$  or  $t/d = h_1/2R_1$ , Waters' stresses are not changed.

Table 10 shows  $\sigma'''$  in the rows so marked. While improved correlation is apparent in some models (S-1G and S-1C in particular), and the average of  $\sigma'''/\sigma_m$  (Table 11) is brought very close to the ideal value of 1.00, the normal stress on the inside corner is grossly overestimated in some models; S-1AB, WS-1LB, WN-10D in particular. Examination of the detailed geometry of these models indicates why this overestimate occurs, however, a general rule for accurate modifications applicable to all test models has not been found.

The series of modifications is more productive than directly indicated in the above discussion in the sense that all four stress groups are usually brought into better agreement by these modifications.

Comparisons with "Thin-Shell" Theory. As pointed out earlier, Waters' analysis contains a number of refinements designed to make thin-shell theory more applicable to nozzles in pressure vessel heads. The Leckie-Penny analysis and CERL computer programs do not include these refinements. The "Waters-3" computer program gives results essentially the same as the CERL computer program (for internal pressure, externally protruding nozzle), hence it was used to obtain a comparison between the Leckie-Penny analysis and the test results. Computed stresses directly from the Waters-3 (thin-shell) program, along with computed stresses including the modifications discussed above, are shown in Table 12 and are summarized in the lower part of Table 11.

In general, the thin-shell theory over-predicts stresses, as compared to test data. In some models, of course, its results are closer to test results than Waters', but in general Waters' analysis is closer to the test results. The thin-shell (Waters-3, Leckie-Penny, CERL) analysis has some advantage in that it is almost always conservative as compared to test results.

TABLE 12. COMPARISON OF TEST DATA WITH THIN-SHELL THEORY AND EMPIRICAL MODIFICATIONS, UNIFORM WALL MODELS

Model No.	Stress (1)	Stress Indices			
		$\sigma_n/s$		$\sigma_t/s$	
		Outside	Inside	Outside	Inside
S-1G	Test Data	1.14	2.60	1.02	- .30
	$\sigma$	3.22	1.70	3.01	- 2.63
	$\sigma'$	1.69	1.48	1.23	- .99
	$\sigma''$	1.76	1.50	1.52	- .79
	$\sigma'''$	1.45	2.87	1.52	- .79
S-1A	Test Data	2.20	2.20	1.25	- .28
	$\sigma$	3.67	1.71	3.29	- 2.27
	$\sigma'$	2.60	1.71	2.07	- 1.28
	$\sigma''$	2.78	1.78	2.79	- .87
	$\sigma'''$	2.62	3.15	2.79	- .92
S-1AB	Test Data	1.51	2.17	1.07	- .24
	$\sigma$	3.68	1.71	3.32	- 2.35
	$\sigma'$	1.95	1.48	.52	- .18
	$\sigma''$	2.02	1.52	.58	- .13
	$\sigma'''$	1.27	3.56	.58	- .13
S-1C	Test Data	1.90	2.90	1.00	- .20
	$\sigma$	3.11	1.92	2.17	- .20
	$\sigma'$	2.26	1.80	1.44	.06
	$\sigma''$	2.65	1.86	1.74	.23
	$\sigma'''$	2.25	3.38	1.74	- .98
WS-1LM	Test Data	1.17	1.87	1.20	- .06
	$\sigma$	4.30	1.62	4.20	- 3.18
	$\sigma'$	1.32	.99	.05	.02
	$\sigma''$	1.33	1.00	.05	.02
	$\sigma'''$	.91	1.82	.05	- .97
WS-1LB	Test Data	1.07	2.03	1.13	- .17
	$\sigma$	3.67	1.71	3.31	- 2.32
	$\sigma'$	1.89	1.45	.09	.02
	$\sigma''$	1.90	1.46	.10	.02
	$\sigma'''$	.85	4.96	.10	- .87
N-8C	Test Data	1.68	2.02	1.39	- .34
	$\sigma$	3.20	1.56	2.94	- 2.31
	$\sigma'$	2.64	1.47	2.26	- 1.71
	$\sigma''$	2.85	1.51	3.11	- 1.23
	$\sigma'''$	2.55	2.63	3.11	- 1.23

(1) Test Data = measured stresses

$\sigma$  = calculated stresses, thin-shell theory.

$\sigma'$  = calculated stresses with normal thickness modification

$\sigma''$  = calculated stresses with normal thickness and curved beam modifications

$\sigma'''$  = calculated stresses with normal thickness, curved beam and thick-wall modifications.



TABLE 12 (contd)

Model No.	Stress (1)	Stress Indices			
		$\sigma_n / S$		$\sigma_t / S$	
		Outside	Inside	Outside	Inside
N-8H	Test Data	3.10	2.06	2.75	- .98
	$\sigma$	4.40	1.61	4.45	- 3.42
	$\sigma'$	3.85	1.60	3.73	- 2.80
	$\sigma''$	4.41	1.73	5.97	- 1.79
	$\sigma'''$	4.24	3.17	5.97	- 1.79
N-8F	Test Data	2.66	2.18	1.90	- .64
	$\sigma$	4.37	1.61	4.41	- 3.41
	$\sigma'$	3.44	1.58	3.21	- 2.37
	$\sigma''$	3.74	1.69	4.45	- 1.68
	$\sigma'''$	3.57	3.13	4.45	- 1.68
N-8E	Test Data	2.19	2.00	1.26	- .37
	$\sigma$	4.39	1.61	4.44	- 3.43
	$\sigma'$	2.51	1.49	2.07	- 1.40
	$\sigma''$	2.66	1.57	2.49	- 1.10
	$\sigma'''$	2.42	2.98	2.49	- 1.10
N-8G	Test Data	1.96	2.04	1.29	- .38
	$\sigma$	4.41	1.61	4.47	- 3.47
	$\sigma'$	2.35	1.44	1.60	- 1.03
	$\sigma''$	2.46	1.50	1.87	- .83
	$\sigma'''$	2.10	2.85	1.87	- .85
S-2AZ	Test Data	4.60	2.60	4.00	- 2.10
	$\sigma$	6.08	1.84	6.81	- 5.81
	$\sigma'$	4.67	1.80	4.85	- 4.02
	$\sigma''$	5.15	1.93	6.79	- 2.93
	$\sigma'''$	5.08	3.63	6.79	- 2.93
N-8D	Test Data	2.53	2.14	1.52	- .23
	$\sigma$	4.15	1.60	3.86	- 2.39
	$\sigma'$	2.69	1.54	1.81	- .84
	$\sigma''$	2.92	1.63	2.12	- .62
	$\sigma'''$	2.47	3.31	2.12	- .87
N-4F	Test Data	1.70	1.58	1.83	- .14
	$\sigma$	2.08	1.23	1.82	- .75
	$\sigma'$	1.81	1.13	1.50	- .55
	$\sigma''$	1.92	1.18	2.02	- .34
	$\sigma'''$	1.76	1.81	1.97	- .74

TABLE 12 (contd.)

Model No.	Stress (1)	Stress Indices			
		$\sigma_n/S$		$\sigma_t/S$	
		Outside	Inside	Outside	Inside
N-1E	Test Data	1.82	1.80	1.77	- .14
	$\sigma$	2.20	1.25	1.87	- .86
	$\sigma'$	1.95	1.14	1.48	- .71
	$\sigma''$	2.06	1.19	1.97	- .47
	$\sigma'''$	1.81	1.85	1.93	- .85
N-1EA	Test Data	1.80	1.77	1.67	- .23
	$\sigma$	2.29	1.30	1.76	- 1.06
	$\sigma'$	2.14	1.22	1.46	- .94
	$\sigma''$	2.28	1.27	2.01	- .63
	$\sigma'''$	2.02	2.03	1.97	- .87
N-3D	Test Data	1.91	1.77	1.75	- .40
	$\sigma$	2.77	1.37	2.19	- 1.64
	$\sigma'$	2.44	1.27	1.83	- 1.33
	$\sigma''$	2.60	1.32	2.47	- .95
	$\sigma'''$	2.37	2.18	2.47	- .95
N-1C	Test Data	1.80	1.64	1.68	- .15
	$\sigma$	2.20	1.27	1.83	- .87
	$\sigma'$	2.03	1.18	1.50	- .79
	$\sigma''$	2.15	1.22	2.02	- .53
	$\sigma'''$	1.89	1.93	1.98	- .87
N-2B	Test Data	2.00	1.70	2.10	- .30
	$\sigma$	2.20	1.28	1.80	- .95
	$\sigma'$	2.07	1.19	1.49	- .85
	$\sigma''$	2.20	1.24	2.02	- .57
	$\sigma'''$	1.94	1.98	1.98	- .87
N-3B	Test Data	1.96	1.81	1.74	- .38
	$\sigma$	2.74	1.40	2.17	- 1.64
	$\sigma'$	2.44	1.29	1.84	- 1.36
	$\sigma''$	2.60	1.34	2.50	- .98
	$\sigma'''$	2.37	2.21	2.50	- .98
N-1AA	Test Data	2.55	2.04	1.74	- .77
	$\sigma$	4.47	1.63	4.55	- 3.57
	$\sigma'$	3.17	1.47	2.90	- 2.13
	$\sigma''$	3.34	1.54	3.59	- 1.66
	$\sigma'''$	3.17	2.79	3.59	- 1.66

TABLE 12 (contd)

Model No.	Stress (1)	Stress Indices			
		$\sigma_n/S$		$\sigma_t/S$	
		Outside	Inside	Outside	Inside
N-2EM	Test Data	1.75	1.58	1.54	- .11
	$\sigma$	2.24	1.29	1.78	- 1.00
	$\sigma'$	1.71	1.05	1.07	- .61
	$\sigma''$	1.76	1.07	1.25	- .48
	$\sigma'''$	1.51	1.59	1.20	- .83
N-4E	Test Data	1.79	1.77	1.72	- .16
	$\sigma$	2.09	1.24	1.80	- .75
	$\sigma'$	1.87	1.16	1.52	- .62
	$\sigma''$	1.99	1.20	2.06	- .39
	$\sigma'''$	1.79	1.87	2.01	- .76
N-1A	Test Data	2.72	2.01	1.84	- .78
	$\sigma$	4.87	1.70	5.07	- 3.94
	$\sigma'$	3.05	1.56	2.73	- 1.93
	$\sigma''$	3.20	1.64	3.33	- 1.52
	$\sigma'''$	3.05	3.07	3.33	- 1.52
N-5B	Test Data	2.70	2.23	1.55	- .35
	$\sigma$	4.68	1.67	4.70	- 3.31
	$\sigma'$	2.63	1.52	2.15	- 1.25
	$\sigma''$	2.75	1.59	2.49	- 1.01
	$\sigma'''$	2.50	3.15	2.49	- 1.01
S-3C	Test Data	4.00	2.60	3.40	- 1.05
	$\sigma$	4.37	1.64	3.98	- 1.98
	$\sigma'$	3.61	1.63	3.10	- 1.37
	$\sigma''$	3.83	1.78	3.98	- .85
	$\sigma'''$	3.63	3.61	3.98	- .85
S-3CB	Test Data	2.90	2.62	1.70	- .25
	$\sigma$	4.37	1.64	3.98	- 2.00
	$\sigma'$	2.85	1.56	1.86	- .59
	$\sigma''$	3.04	1.65	2.10	- .41
	$\sigma'''$	2.51	3.56	2.10	- .85
WN-10B	Test Data	1.37	1.61	1.22	- .16
	$\sigma$	4.55	1.64	4.65	- 3.63
	$\sigma'$	1.83	1.23	.56	- .25
	$\sigma''$	1.85	1.25	.60	- .21
	$\sigma'''$	1.52	2.21	.60	- .88

TABLE 12 (contd.)

Model No.	Stress (1)	Stress Indices			
		$\sigma_n / S$		$\sigma_t / S$	
		Outside	Inside	Outside	Inside
WN-10D	Test Data	1.61	1.75	1.51	- .28
	$\sigma$	4.54	1.64	4.65	- 3.63
	$\sigma'$	2.58	1.51	1.50	- .95
	$\sigma''$	2.64	1.55	1.69	- .81
	$\sigma'''$	2.33	2.95	1.69	- .95
WN-50B	Test Data	3.92	2.83	3.06	- 1.62
	$\sigma$	6.08	1.89	6.55	- 5.44
	$\sigma'$	3.68	1.79	3.39	- 2.60
	$\sigma''$	3.87	1.88	4.16	- 2.08
	$\sigma'''$	3.77	3.66	4.16	- 2.08
Bu.S-1	Test Data	2.29	2.06	<b>1.96</b>	- .31
	$\sigma$	2.82	1.18	2.39	- 1.43
	$\sigma'$	2.47	1.14	1.98	- 1.12
	$\sigma''$	2.55	1.20	2.36	- .86
	$\sigma'''$	2.43	2.13	2.33	- 1.39
N-9E	Test Data	4.40	1.88	4.30	- 1.03
	$\sigma$	3.77	1.39	3.36	- 2.35
	$\sigma'$	3.77	1.39	3.36	- 2.35
	$\sigma''$	4.86	1.58	7.72	- 1.18
	$\sigma'''$	4.67	2.99	7.72	- 1.18
N-9A	Test Data	4.00	1.86	3.80	- 1.00
	$\sigma$	3.80	1.40	3.41	- 2.39
	$\sigma'$	3.80	1.39	3.41	- 2.39
	$\sigma''$	4.47	1.56	6.10	- 1.37
	$\sigma'''$	4.29	2.97	6.10	- 1.37
N-9B	Test Data	3.00	1.81	2.74	- .96
	$\sigma$	3.73	1.37	3.30	- 2.31
	$\sigma'$	3.67	1.34	3.23	- 2.25
	$\sigma''$	3.97	1.46	4.46	- 1.57
	$\sigma'''$	3.80	2.79	4.46	- 1.57
N-9C	Test Data	2.95	1.95	2.40	- .83
	$\sigma$	3.78	1.40	3.38	- 2.38
	$\sigma'$	3.60	1.35	3.17	- 2.20
	$\sigma''$	3.83	1.44	4.09	- 1.63
	$\sigma'''$	3.65	2.72	4.09	- 1.63

TABLE 12 (contd.)

Model No.	Stress (1)	Stress Indices			
		$\sigma_n/S$		$\sigma_t/S$	
		Outside	Inside	Outside	Inside
WAI-1	Test Data	1.55	1.71	1.32	- .46
	$\sigma$	3.19	1.44	2.76	- 1.52
	$\sigma'$	2.12	1.29	1.58	- .67
	$\sigma''$	2.15	1.31	1.71	- .56
	$\sigma'''$	1.78	2.61	1.71	- .74
S-5E	Test Data	2.58	1.78	2.45	- .43
	$\sigma$	2.81	1.32	2.75	- 1.45
	$\sigma'$	2.81	1.32	2.75	- 1.45
	$\sigma''$	2.97	1.37	3.48	- 1.00
	$\sigma'''$	2.86	2.02	3.44	- 1.31
S-5AZ	Test Data	4.90	2.34	4.20	- 1.78
	$\sigma$	4.89	1.19	4.26	- 3.24
	$\sigma'$	4.73	1.24	4.07	- 3.07
	$\sigma''$	5.05	1.41	5.36	- 2.29
	$\sigma'''$	4.98	3.19	5.36	- 2.33
S-5A	Test Data	2.87	2.00	2.50	- .60
	$\sigma$	3.32	1.19	2.78	- 1.68
	$\sigma'$	3.23	1.19	2.53	- 1.54
	$\sigma''$	3.41	1.30	3.27	- 1.09
	$\sigma'''$	3.24	2.46	3.27	- 1.41
S-5AW	Test Data	2.29	1.68	1.93	- .41
	$\sigma$	2.62	1.24	1.98	- .87
	$\sigma'$	2.49	1.22	1.87	- .79
	$\sigma''$	2.64	1.30	2.53	- .44
	$\sigma'''$	2.39	2.44	2.47	- .81
S-5C	Test Data	3.62	2.45	2.60	- .66
	$\sigma$	4.88	1.85	4.72	- 2.72
	$\sigma'$	4.41	1.78	4.15	- 2.29
	$\sigma''$	4.64	1.88	5.06	- 1.69
	$\sigma'''$	4.42	3.78	5.06	- 1.69
WS-5LM	Test Data	1.41	1.16	1.12	- .04
	$\sigma$	5.00	1.26	4.52	- 3.44
	$\sigma'$	1.32	.86	.64	- .28
	$\sigma''$	1.32	.86	.66	- .27
	$\sigma'''$	1.25	.94	.65	- 1.06

TABLE 12 (contd)

Model No.	Stress (1)	Stress Indices			
		$\sigma_n/S$		$\sigma_t/S$	
		Outside	Inside	Outside	Inside
IIT-51	Test Data	5.75	3.44	5.72	- 2.02
	$\sigma$	6.67	2.80	7.04	- 6.03
	$\sigma'$	5.97	2.67	5.96	- 5.04
	$\sigma''$	6.08	2.75	7.22	- 4.15
	$\sigma'''$	6.04	2.79	7.22	- 4.15

ORNL Models. The Oak Ridge National Laboratory models ORNL-5 and ORNL-6\* are particular pertinent in comparing test data with theory because, by elimination of the fillet radius, these test models are geometrically the same as the theoretical models of two-piece shell theories. Figures 14 through 17 compare test data with theory for these two models. The theoretical data was obtained using Kalnins computer program, however, essentially the same results would be expected using the CERL computer program.

In plotting the theoretical data, it has been assumed that the nozzle starts ( $x = 0$ ) at the outer surface of the sphere, the sphere starts ( $\phi = \phi_0$ ) at the outer surface of the nozzle. This leaves a section at the juncture (a rectangle, with dimensions  $t$  by  $T$ ) which is undefined by the theory. One strain gage was placed on this section; on the inside of the nozzle at the mid-surface of the sphere. This test data point is arbitrarily shown in Figures 14 through 17 at a location of  $-t$  on the sphere. One might expect  $\sigma_n$  from this gage would be comparable with the mid-wall  $\sigma_n$  calculated at the opening in the sphere; as can be seen in Figures 14 and 16, agreement does exist. The value of  $\sigma_t$  from this gage, however, is not comparable with shell theory because, as a point on the sphere  $\sigma_t = 0$ , as a point on the nozzle the thickness is indeterminate.

As can be seen in Figures 14 through 17, agreement of test data with theory is good, except for the tangential stresses on the outside of the sphere\*\*. The reason for the disagreement of theory and test data for the tangential stress on the outside of the sphere is not known.

---

\* These are two (configurations 5 and 6) of the six models included in Reference 27. The other models had internally protruding nozzles which are not covered in this report.

\*\* The same discrepancy also occurs for moment or thrust loading.

Presumably there was a high local stress at the nozzle-sphere juncture due to the sharp re-entrant corner. Possibly this high local stress persisted for some distance along the sphere, leading to the high measured tangential stresses on the outer surface of the sphere.

Juncture stresses obtained from Waters' analysis are also shown on Figures 14 through 17. These stresses agree somewhat closer than Kalnins' results with maximum measured stresses, however, since the maximum measured stresses are not exactly at the juncture, the better agreement of Waters' analysis cannot be taken as meaning that the analysis is more accurate. The discrepancy for the tangential stress on the outside surface of the sphere is about the same for Waters' results as for Kalnins' results.



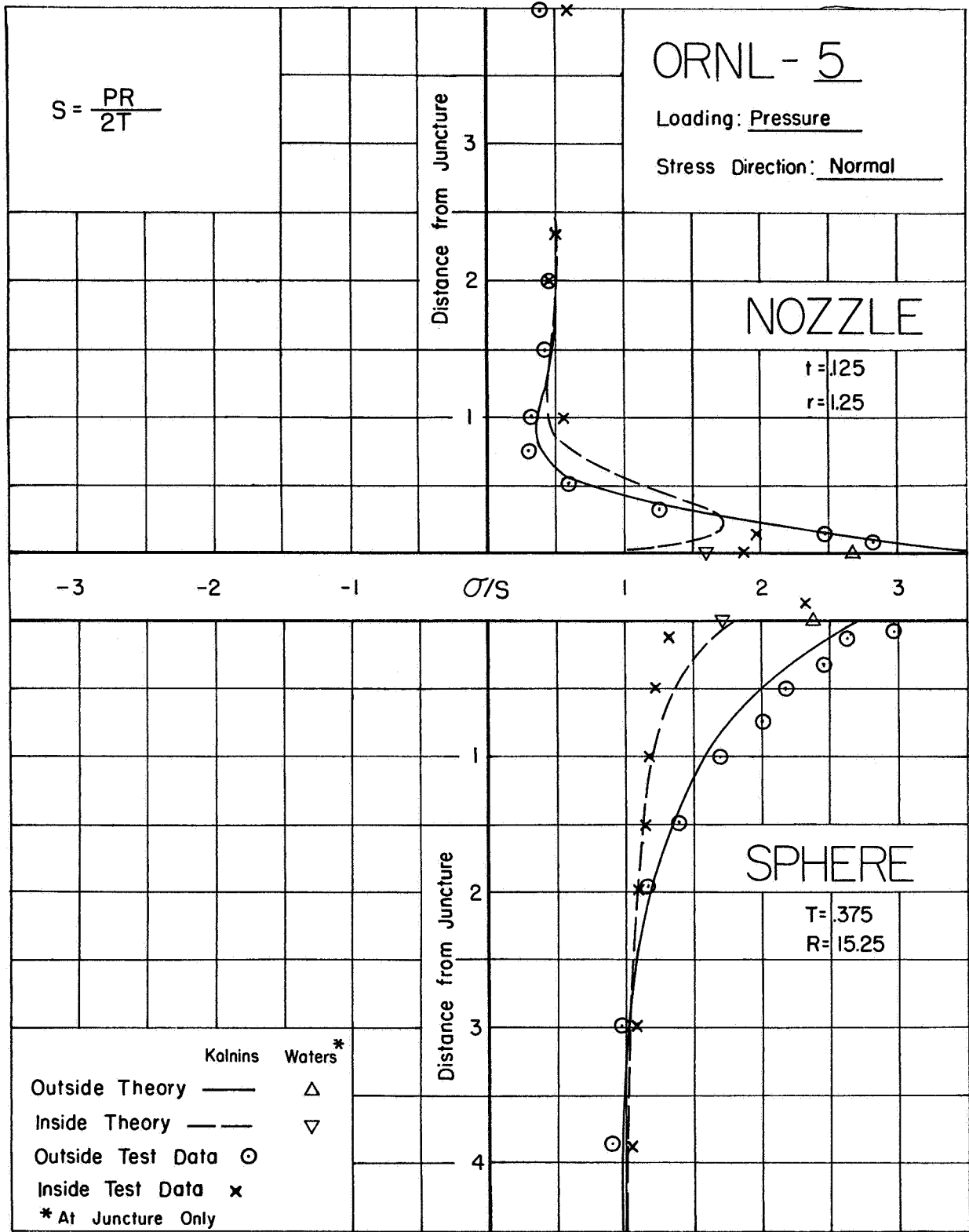


FIGURE 14. NORMAL STRESSES IN MODEL ORNL 5, INTERNAL PRESSURE

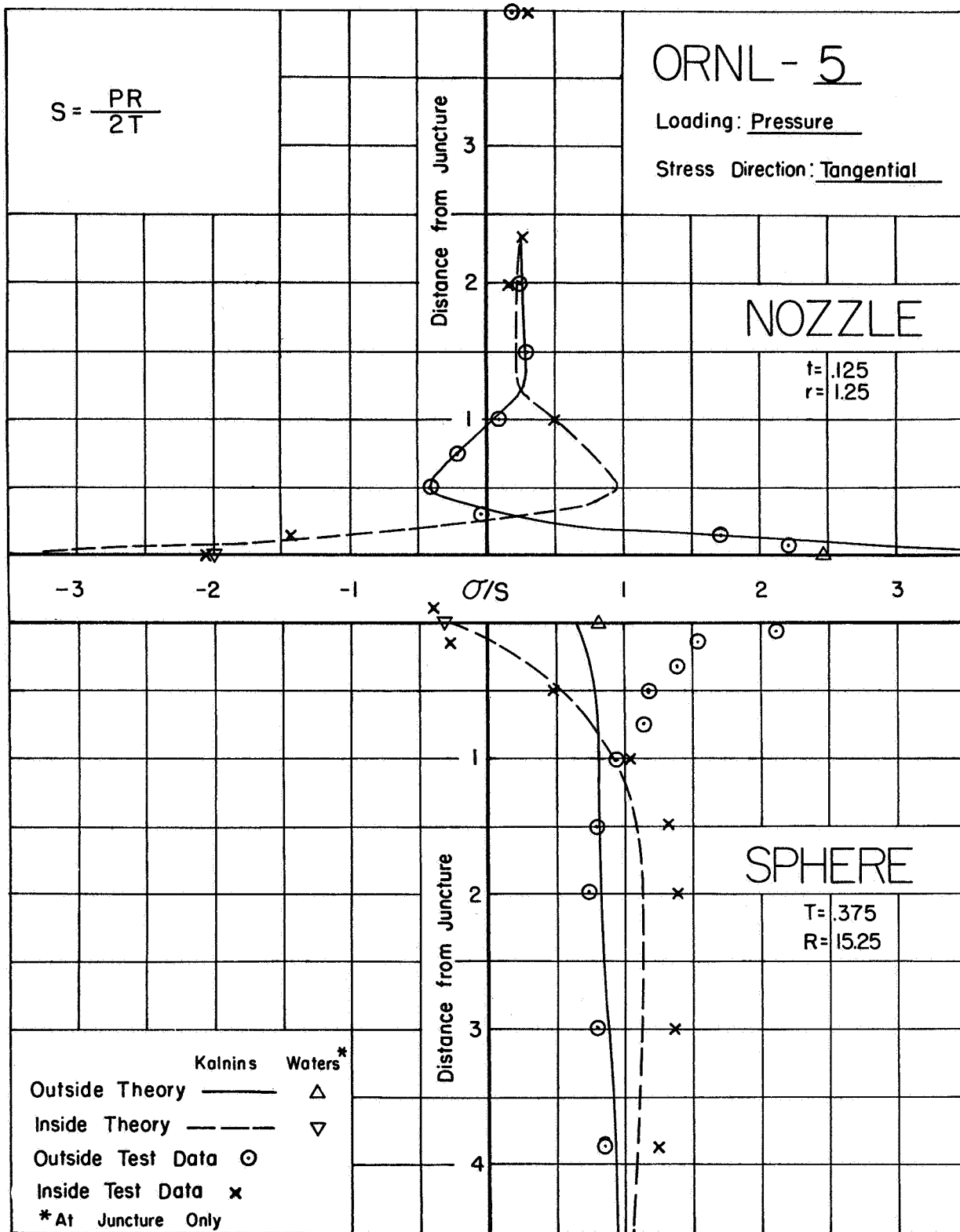


FIGURE 15. TANGENTIAL STRESSES IN MODEL ORNL 5, INTERNAL PRESSURE

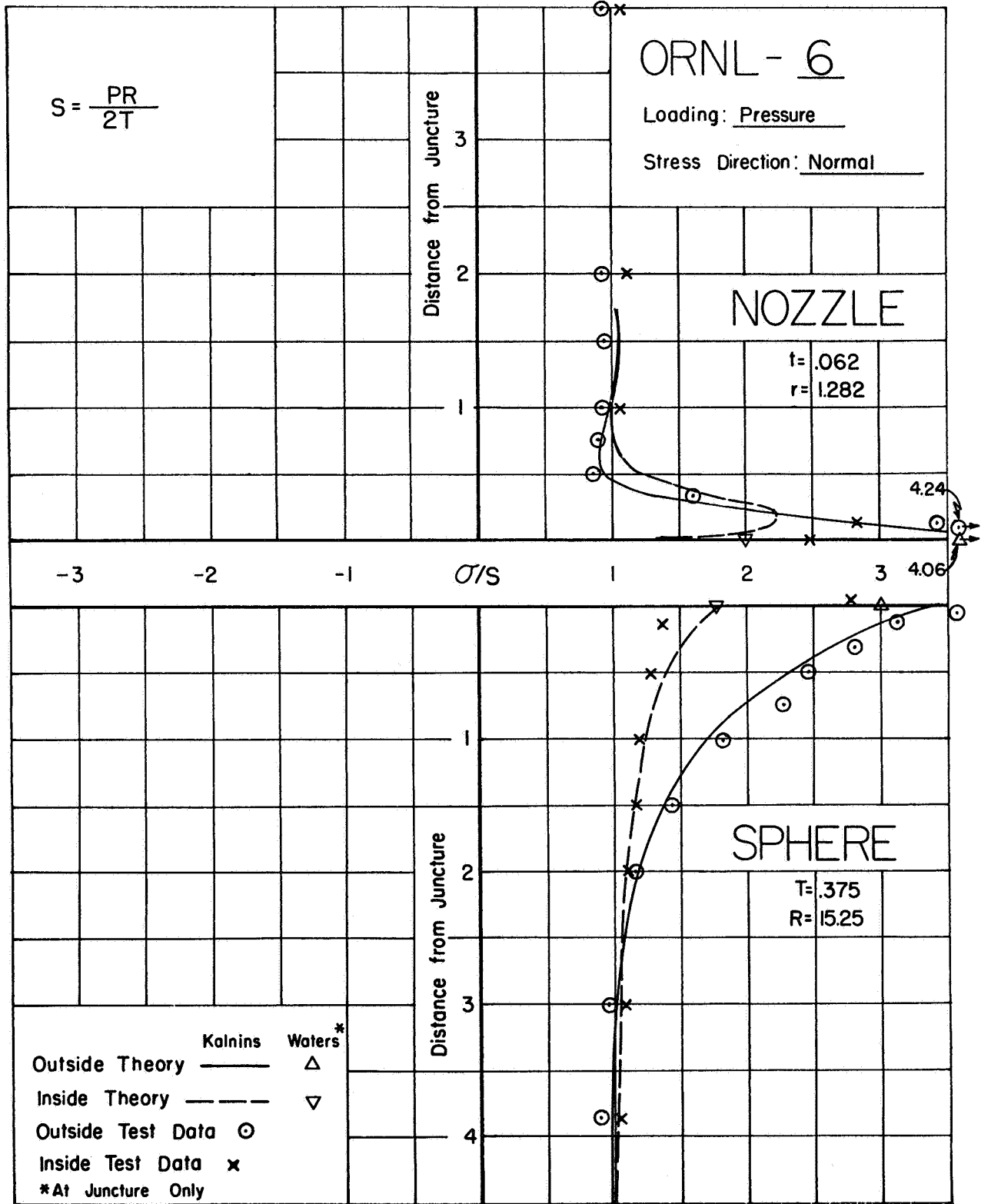


FIGURE 16. NORMAL STRESSES IN MODEL ORNL 6,  
INTERNAL PRESSURE

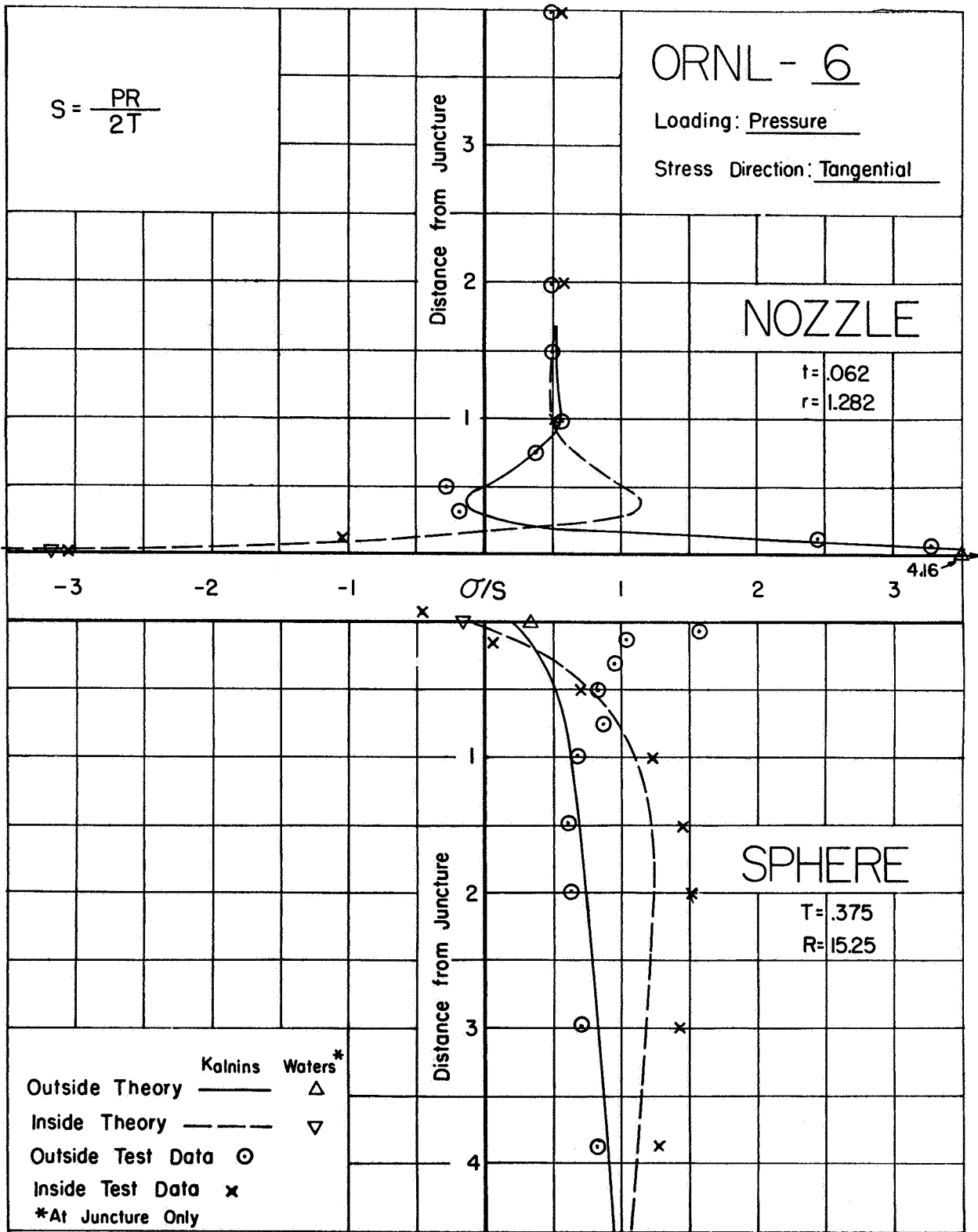


FIGURE 17. TANGENTIAL STRESSES IN MODEL ORNL 6, INTERNAL PRESSURE

Inside Corner Radii. All of the photoelastic test models, as well as model IIT-S1, had inside corner radii as shown in Table 9 as  $r_i/t$ . The test data indicates that variations in the inside corner radius, of the magnitude used in the test models, have relatively little effect on the magnitude of the maximum stress. Some radius on the inside corner is desirable to provide a smooth surface for optimum fatigue strength, and a very large fillet radius would probably weaken the structure because of reduction of reinforcing area at the juncture. Between these rather wide bounds, however, the inside corner radius appears to be relatively insignificant.

Fillet Radii. The significance of the fillet radius has been discussed and illustrated for the test models in the preceding, in which the ratio  $r_o/t$  has been used as a parameter. In References (24) and (25), the ratio  $r_o/T$  is shown. In Reference (16), the effect of the fillet radius is discussed in terms of  $r_o/T$  and some design codes specify the fillet radius in terms of  $T$ . The question arises as to whether  $r_o/t$  or  $r_o/T$  is a more significant parameter. From a theoretical standpoint, either parameter may be more significant because the effect depends upon the relative increase in the nozzle thickness as compared to the increase in the sphere thickness, as well as the relative stress levels of the nozzle and sphere. For the test models considered, the theoretical effect of the fillet radius on the nozzle is almost always much more significant than in the sphere, hence the ratio of  $r_o/t$  appears more significant than  $r_o/T$ . In some extreme cases (not included in the test models), the ratio of  $r_o/\sqrt{rt}$  or  $r_o/\sqrt{RT}$  may be significant because if  $r_o \ll \sqrt{rt}$  or  $\ll \sqrt{RT}$ , the maximum stress may occur at the edge of the fillet radius and be approximately the same as given by the theory for the juncture stress.

Two series of test models were run in which essentially the only variable was the size of the fillet radius. These models are included in Table 10; part of the data is tabulated again below:

Model No.	$\frac{r_o}{t}$	Maximum Stresses on Outside Surface					
		$\sigma_n/S$			$\sigma_t/S$		
		Waters	$\sigma'''$	Test	Waters	$\sigma'''$	Test
N-8H	.40	3.21	3.14	3.10	2.56	3.37	2.75
N-8F	.72	3.13	2.66	2.66	2.49	2.48	1.90
N-8E	1.81	3.17	1.93	2.19	2.52	1.43	1.26
N-8G	2.53	3.18	1.74	1.96	2.54	1.08	1.29
N-9E	.13	2.94	3.62	4.40	1.85	4.33	4.30
N-9A	.25	2.95	3.28	4.00	1.88	3.30	3.80
N-9B	.61	2.95	2.86	3.00	1.85	2.38	2.74
N-9C	.85	2.92	2.76	2.95	1.85	2.20	2.40

Waters analysis is not dependent upon  $r_o$ , hence it gives essentially the same stresses for each set of models. After modifications as discussed previously, however, the  $\sigma'''$  stresses agree reasonably well with the test data and parallel the trends indicated by the test data. Similar comparisons may be made from Table 11 (thin-shell, Waters-3, Kalnins, CERL), however, starting with the thin shell basic theory, the modified ( $\sigma'''$ ) stresses are high with respect to the test data.

Fillet radii reinforcing is considered further in the subsequent section on "Models with Local Reinforcing", wherein certain trends of the effectiveness of fillet radii reinforcing with respect to other dimensional parameters is discussed.

## MODELS WITH LOCAL REINFORCING

The distinction between "Uniform Wall Models" and "Models with Local Reinforcing" is, of course, arbitrary. Uniform Wall Models included only models with reinforcing consisting of a fillet radius. In some models the fillet radius was quite large; these models are discussed again in this section of the report, along with a general study of fillet radius reinforcing. Also, results of tests on Model WN-50B are given in detail along with comparison with Kalnins' computer program results.

Test data is compared with results from Kalnins and Seal-Shell-2 computer programs in the following. Some judgement is required by users of these programs in selecting midsurfaces (or reference surfaces) and appropriate normal thicknesses. While considerable time was expended in preparing input data for the models discussed herein, further refinements in input data would probably give closer agreement between calculated results and test results.

Model WN-50B. Figure 18 gives a comparison of test results for Model WN-50B with calculated results using Kalnins program. The maximum stress, which is the  $\sigma_n$ -stress on the outside surface, is quite closely predicted by the calculations. Kalnins program is based on thin-shell theory and therefore does not include non-linear effects such as represented by the "curved beam effect" discussed previously. Qualitatively, corrections to Kalnins' theory analogous to the "curved beam effect" would bring calculations and test data into better agreement, except for the very sharp peak in the measured normal stress on the inside surface. In this particular respect, Waters' theory with adjustments is closer to the test data; 3.33 calculated vs. 2.83 test (See Table 10).

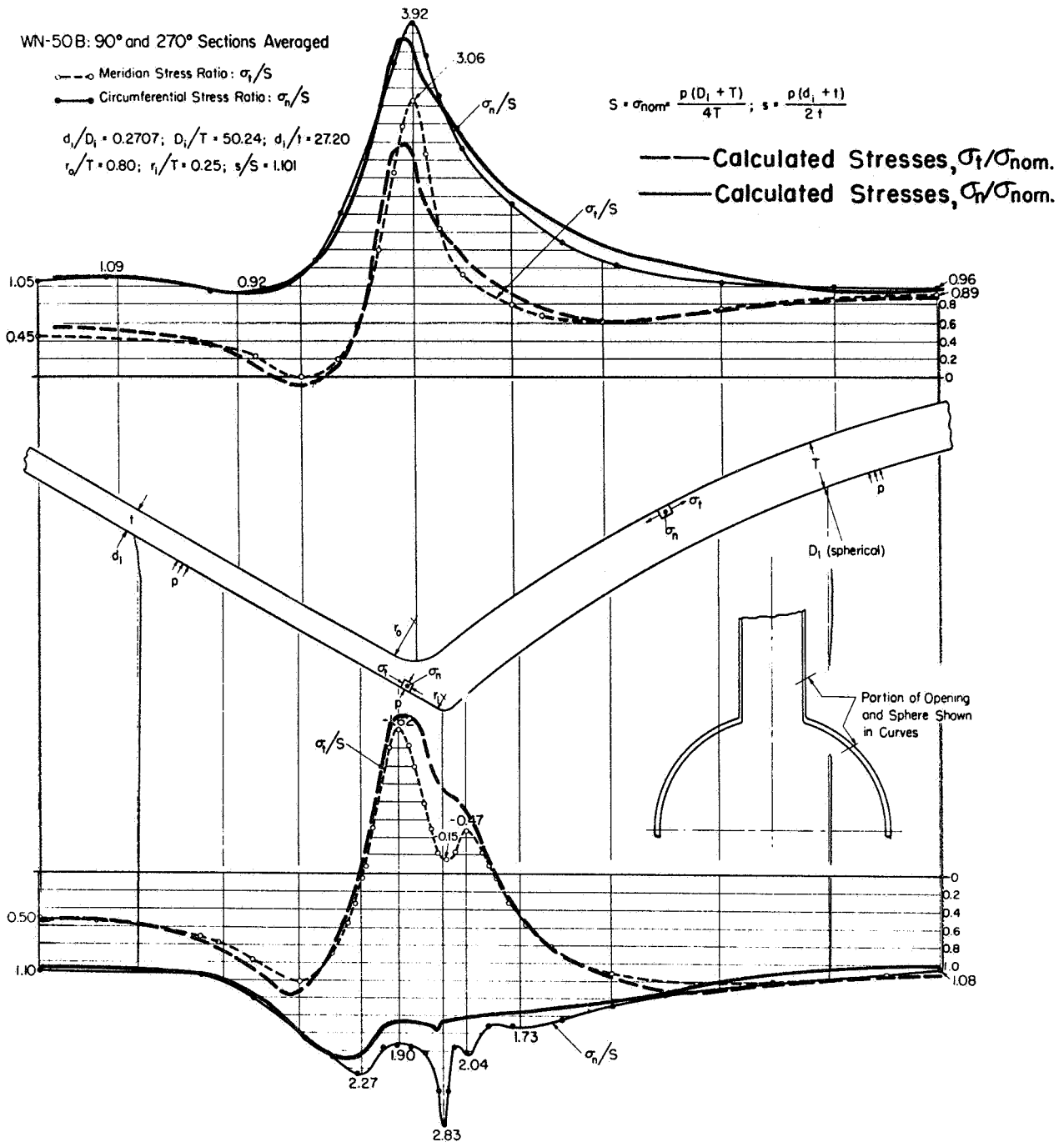


FIGURE 18. TEST DATA AND CALCULATED (KALNINS) RESULTS, MODEL WN-50B, INTERNAL PRESSURE



Comparison with Seal-Shell-2 and Kalnins. Basic dimensions of models with local reinforcing are shown in Table 13, along with a general description of the type of reinforcing. The exact detail of the reinforcing is, of course, important - however, these are shown in References (24) and (25) and hence are not included herein. A summary of maximum measured stresses is given in Table 13 analogous to the summary of Table 9.

Table 14 compares test data with Seal-Shell-2 and Kalnins calculated results for a number of test models with local reinforcing. In general, agreement between these test results and calculated results is quite satisfactory. The number of comparisons made was limited by available time and funds; all models have  $d/D$  ratios of 0.20 or larger. There are tentative indications, however, that these calculation methods may be of limited applicability to small  $d/D$ -ratios where substantial reinforcement is present; or at least considerable more care in setting up the theoretical models will be required. Also, calculation of stresses at abrupt changes in wall thickness (such as in Model N-4G, in the sphere at the toe of the "fillet weld") is impossible with Kalnins' program and difficult, at best, with the Seal-Shell-2 program.

Figures 19 through 22 give "stress-profiles" for Models W-1B and WS-5LB, comparing both Kalnins and Seal-Shell-2 calculated results with the test data. In these comparisons, the developed middle surface is shown as the abscissa, stress index as the ordinate. As noted in discussion of Model WN-5OB, Kalnins results do not include the "curved beam effect" and some better agreement might be obtained by a modification of this type. Figure 10a gives another example of a stress-profile calculated by the Seal-Shell-2 program as compared with test data.

The Seal-Shell-2 program was also used to calculate stresses for a "inverted nozzle", Model WN-6BR. The calculated results and test results compare quite closely, except for the tangential stress in the nozzle. This systematic discrepancy appears to indicate either an error in the input boundary conditions or in the computer program. An attempt

was made to calculate this same model using Kalnins' program, however, certain difficulties arise because of the required direction of integration along the shell. This problem has arisen for other shells using Kalnins' program and can be overcome, in some cases at least, by mapping the actual geometry into an imaginary plane such that the radius of curvature is entered as a negative quantity with appropriate changes in surface forces and boundary conditions. This technique has not yet been attempted for the "inverted nozzle" problem.

TABLE 13. SUMMARY OF DIMENSIONS AND MEASURED STRESSES,  
MODELS WITH LOCAL REINFORCING

Model No. (1)	$\frac{d_i}{D_i}$	$\frac{D_i}{T}$	$\frac{s}{S}$	Type of Reinforcement	$\frac{A_a}{d_i T}$ (3)	Measured Stresses (2)				Comments
						$\sigma_n/S$		$\sigma_t/S$		
						Outside	Inside	Outside	Inside	
WS-1LM	0.05	71.5	1.01	External fillet radius	2.0	1.17*	1.87	1.20*	-0.06	* Stress location near the intersection of the reinforcing with the sphere.
WS-1LB	0.05	24.2	0.99	External fillet radius	2.0	1.07*	2.03	1.13*	-0.17	
WN-6F	0.10	28.7	0.75	Balanced	1.1	1.10*	1.12	1.11*	1.12* a	+ Stress location near the intersection of reinforcing with the nozzle
WN-10B	0.20	24.0	1.02	External fillet radius	0.67	1.37*	1.61	1.22*	-0.16	
WN-10D	0.20	24.0	1.02	External fillet radius	0.09	1.61	1.75	1.15	-0.28	
N-1B	0.20	25.2	0.96	Pad on nozzle	0.55	1.91*	1.80	1.73*	-0.23	
N-4A	0.20	24.8	0.97	Tapered pad on nozzle	0.65	1.77*	1.77	1.76*	-0.15	
N-4D	0.20	23.3	1.03	Tapered pad	0.80	1.62*	1.62	1.73*	-0.08	
N-4G	0.20	23.8	0.99	Pad on nozzle	0.75	2.10*	1.68	2.24*	-0.12	
N-5A	0.20	16.2	1.48	Pad on nozzle	0.35	2.06*	2.13	1.85*	-0.40	
N-6A	0.20	24.3	0.99	Balanced	0.95	1.35*	1.28 <sup>+</sup>	1.26*	-0.15	
N-6D	0.20	23.8	1.00	Balanced	0.65	2.00*	1.35 <sup>+</sup>	1.55*	-0.49	
N-6E	0.20	24.0	1.00	Balanced	1.0	1.90*	1.11 <sup>+</sup>	2.09*	-0.63	
N-7A	0.20	25.2	0.95	Pad on sphere	0.90	1.82 <sup>+</sup>	1.49 <sup>+</sup>	1.25 <sup>+</sup>	-0.21	
WN-6B	0.20	23.9	1.01	Balanced, drainable	0.65	1.18*	1.30	1.03*	-0.35	
WN-6C	0.20	24.7	1.00	Balanced, non-drainable	0.65	2.09*	1.42*	2.24*	1.21* b	
WN-7B	0.20	23.9	1.01	Tapered pad on sphere	0.85	1.26 <sup>+</sup>	1.45	1.03*	-0.17	
BuS.-A	0.34	156.6	1.92	Balanced	1.0	1.96 <sup>+</sup>	1.20*	1.07	1.22* c	
WS-5LB	0.50	24.4	1.00	Compound external fillet radii	0.65	1.26*	1.28	1.13*	-0.15	
WS-5LM	0.50	78.8	0.96	External fillet radius	0.72	1.41*	1.16	1.12*	-0.04	
WS-5LO	0.50	71.5	1.02	Balanced	0.65	1.22* <sup>++</sup>	1.17	0.99*	-0.14	
Inverted Nozzles										
WN-6BR	0.20	23.7	0.98	Balanced	0.65	2.05	-1.45 <sup>+</sup>	-0.54	1.50*	
WN-6CR	0.20	24.0	1.00	Balanced	0.65	1.90*	1.56*	1.90*	1.77*	

(1) Model numbers N- (e.g. N-1B) are from Reference 24; all other models are from Reference 25.

(2) Tabulated stresses are maximum significant stresses due to the opening or reinforcement; remote from the opening  $\sigma_n/S$  and  $\sigma_t/S$  approach 1.0 in the sphere;  $\sigma_n/S$  approaches  $s/S$  and  $\sigma_t/S$  approaches  $0.5 s/S$  in the nozzle.

(3)  $A_a$  = area of reinforcing provided by reinforcement in excess of the basic configuration described by  $d_i/D_i$ ,  $D_i/T$  and  $s/S$ .  $A_a$  is not the same as the reinforcing area computed according to usual code rules because (1) no reinforcing zone limit is used, and (2) reinforcing from an excess nozzle thickness ( $s/S < 1.0$ ) or excess sphere thickness ( $s/S > 1.0$ ) is not included.

TABLE 14: COMPARISON OF TEST DATA WITH THEORY,  
MODELS WITH LOCAL REINFORCING

Model No.	Stress from:	Stress Indices				$\sigma_c/\sigma_m$ (1)
		$\sigma_n/S$		$\sigma_t/S$		
		Outside	Inside	Outside	Inside	
N-1B	Test Data	1.91	1.80	1.73	-0.23	--
	Seal-Shell-2	1.75	1.83	1.50	-0.02	0.96
	Kalnins	1.72	1.21	1.30	-0.48	0.90
N-4A	Test Data	1.77	1.77	1.76	-0.15	--
	Seal-Shell-2	1.68	1.54	1.54	-0.03	0.95
	Kalnins	1.74	1.37	1.46	-0.50	0.98
N-7A	Test Data	1.82	1.49	1.25	-0.21	--
	Seal-Shell-2	1.64	1.51	1.13	-0.23	0.90
	Kalnins	1.75	1.42	1.17	-0.42	0.96
WN-6B	Test Data	1.18	1.30	1.03	-0.35	--
	Seal-Shell-2	1.38	1.44	1.13	-0.19	1.11
	Kalnins	2.04	1.32	0.92	-0.48	1.57
WN-7B	Test Data	1.26	1.45	1.03	-0.17	--
	Seal-Shell-2	1.28	1.27	0.90	0.10	0.88
	Kalnins	1.06	1.87	1.30	-0.03	1.29
WS-5LB	Test Data	1.26	1.28	1.13	-0.15	--
	Seal-Shell-2	1.04	1.07	0.94	0.00	0.84
	Kalnins	1.19	1.06	0.99	-0.17	0.93
WS-5LM	Test Data	1.41	1.16	1.12	-0.04	--
	Seal-Shell-2	1.35	0.96	1.26	0.03	0.96
	Kalnins	1.00	1.00	1.05	-0.23	0.75
WS-5LO	Test Data	1.22	1.17	0.99	-0.14	--
	Seal-Shell-2	1.12	0.75	0.83	-0.22	0.92
	Kalnins	1.63	1.19	0.78	-0.43	1.33
WN-6BR	Test Data	2.05	1.13	-0.54	1.50	--
	Seal-Shell-2	1.99	1.13	(2)	1.46	0.97

(1)  $\sigma_m$  = maximum measured stress,  $\sigma_c$  = maximum calculated stress

(2) Calculated stress incorrect, possibly due to inaccurate boundary conditions.

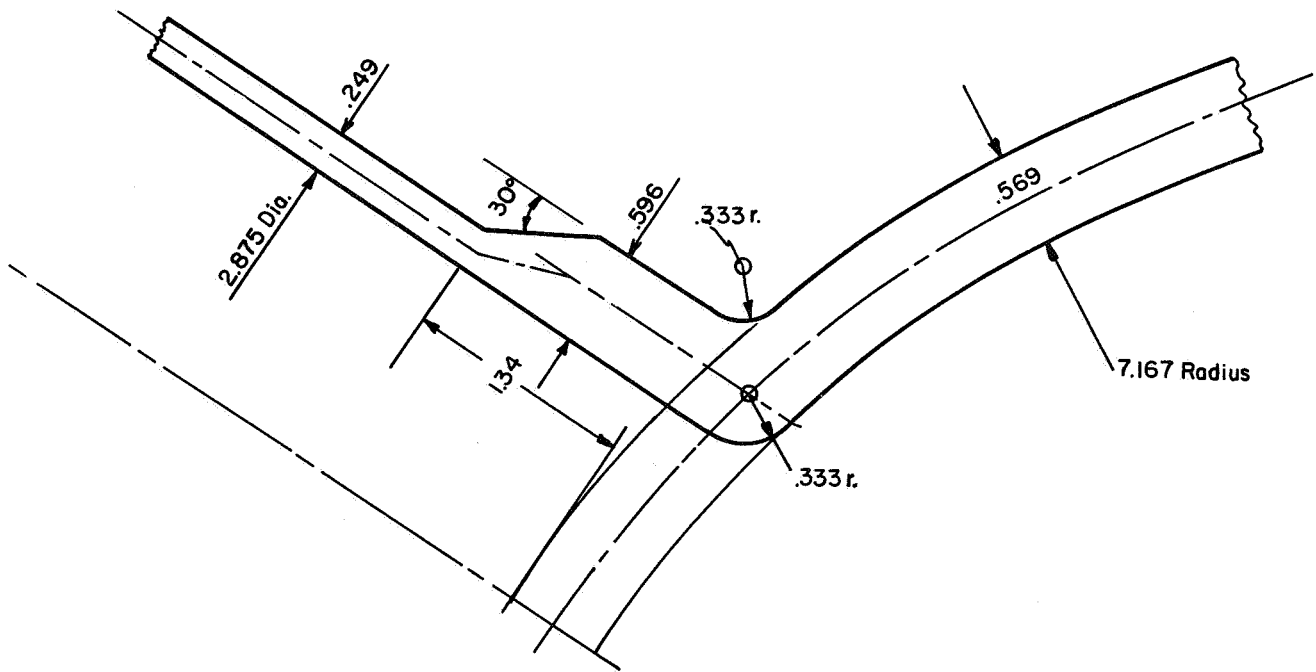
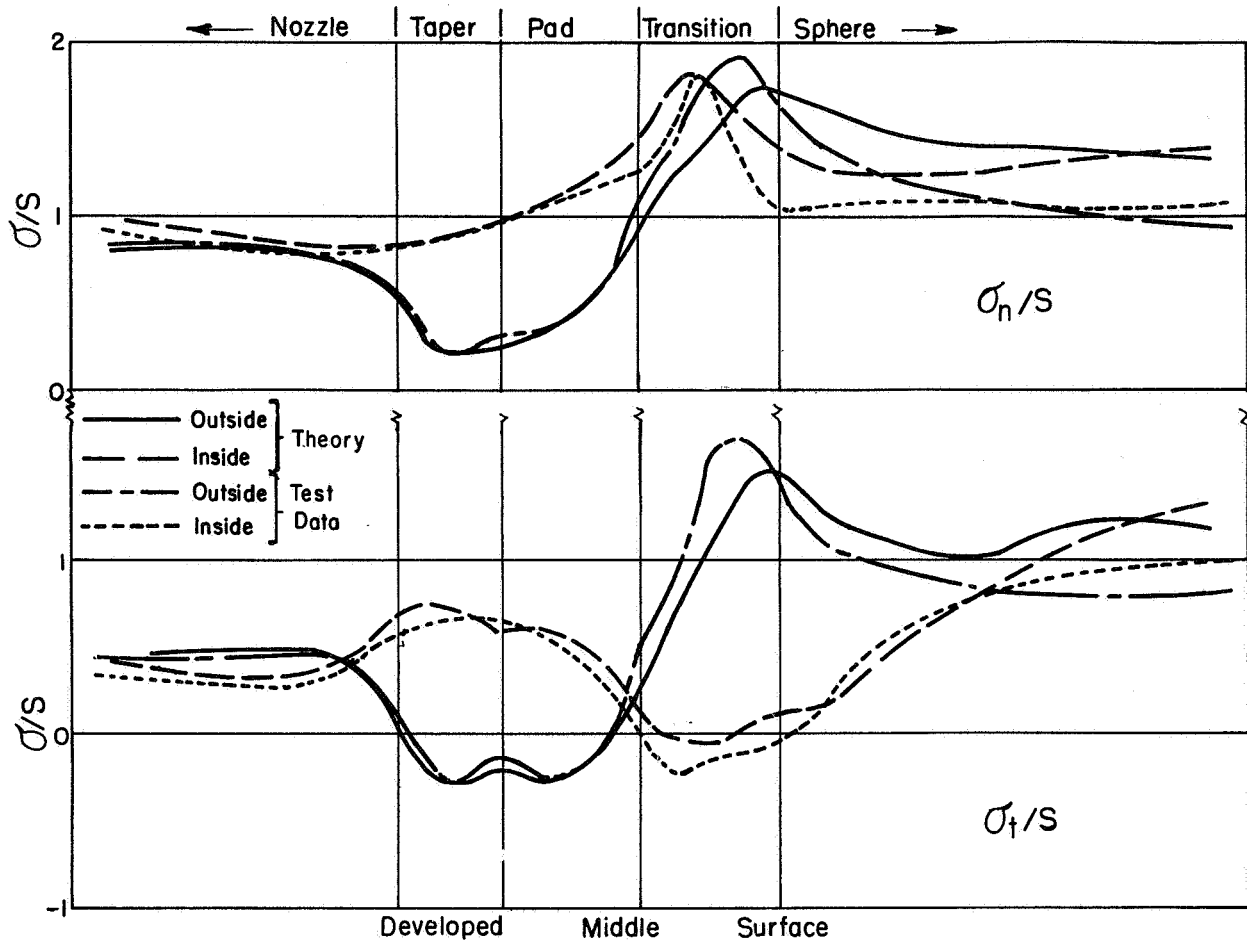


FIGURE 19. TEST DATA AND SEAL-SHELL-2 CALCULATED RESULTS, MODEL N-1B

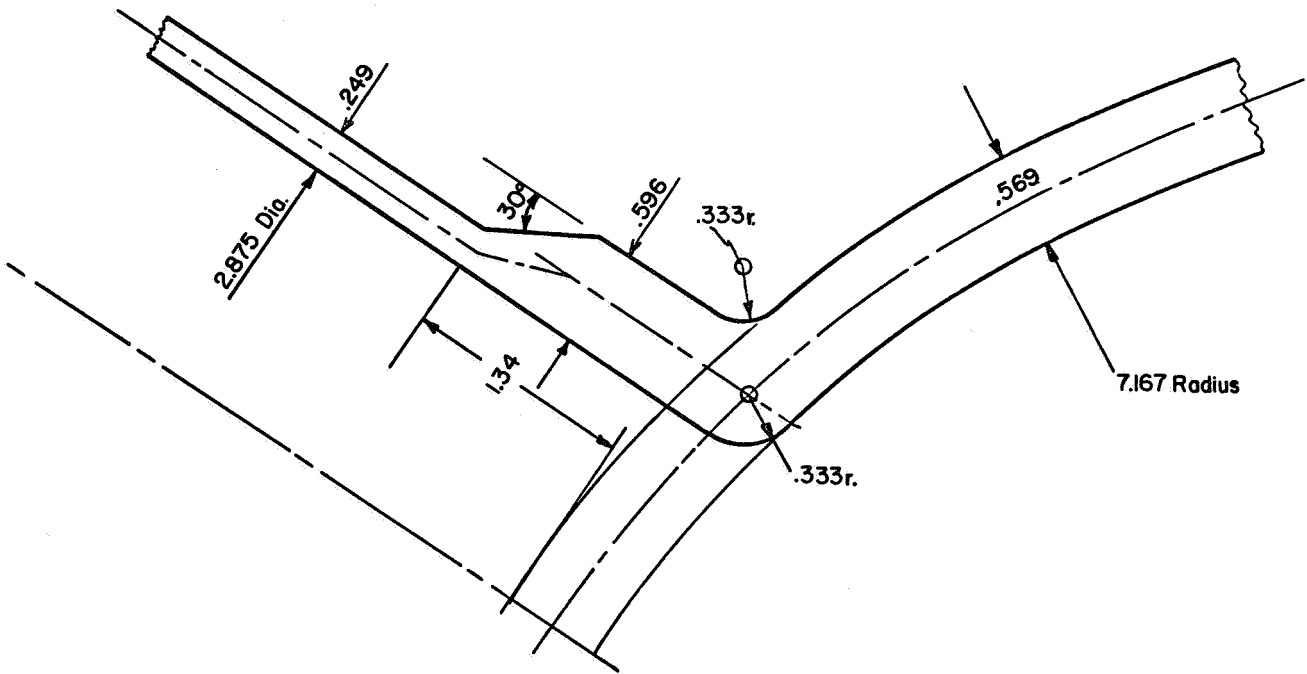
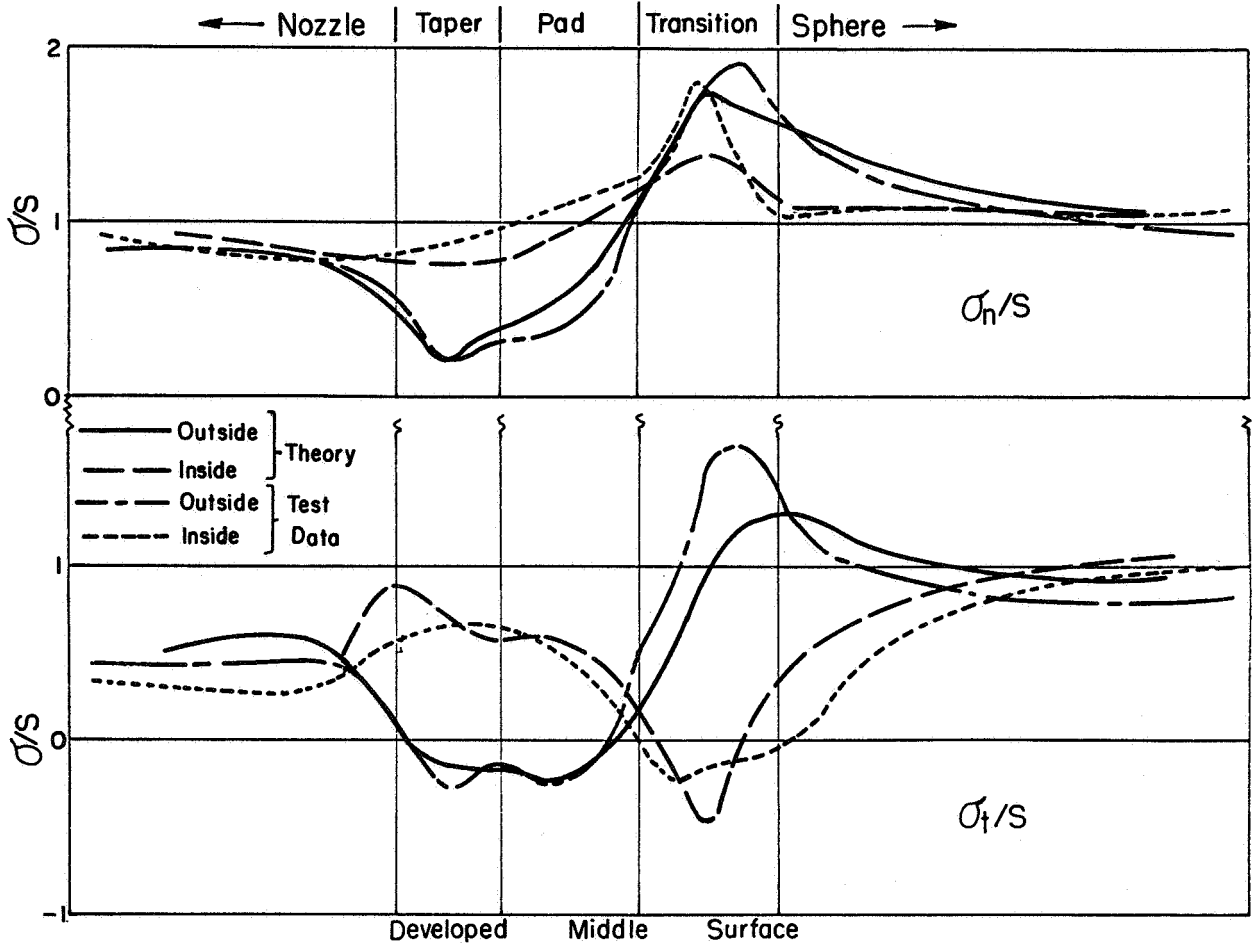


FIGURE 20. TEST DATA AND KALNINS CALCULATED RESULTS, MODEL N-1B

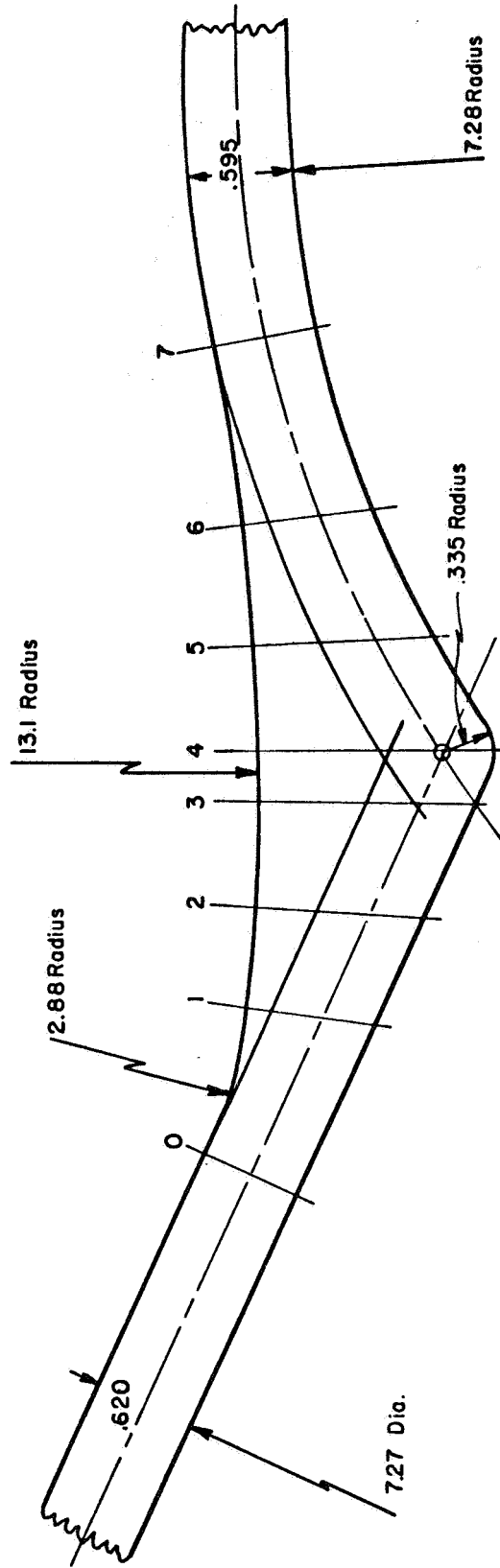
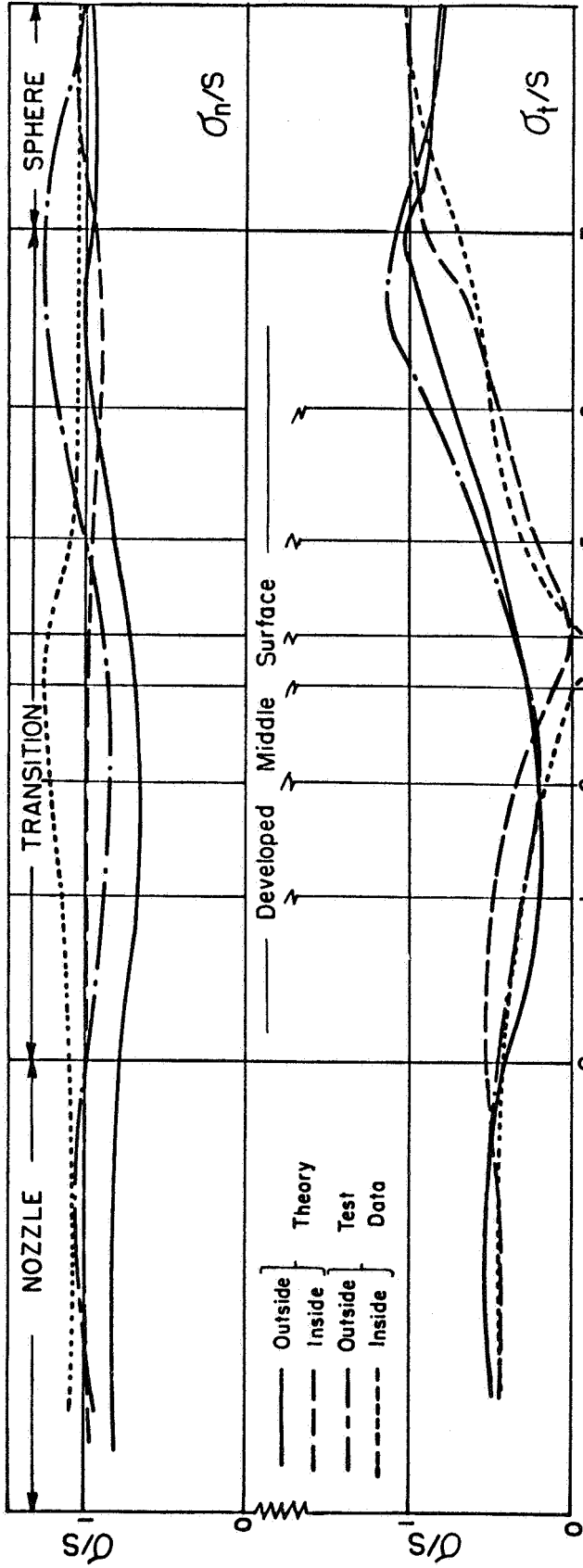


FIGURE 21. TEST DATA AND SEAL-SHELL-2 CALCULATED RESULTS, MODEL WS-51B

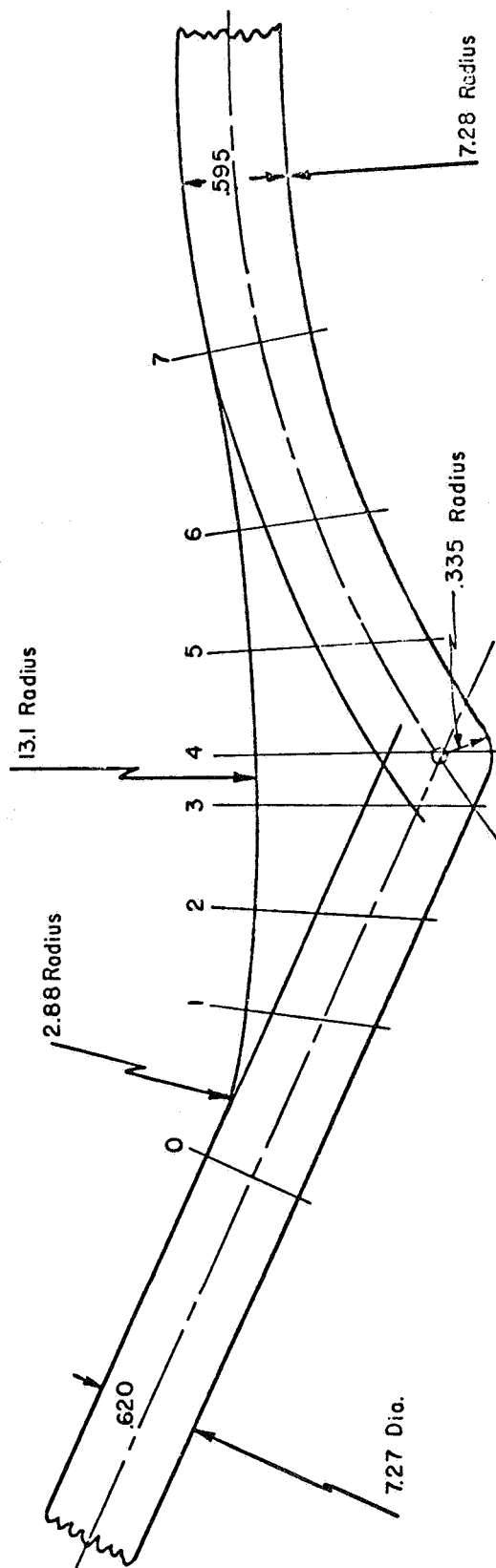
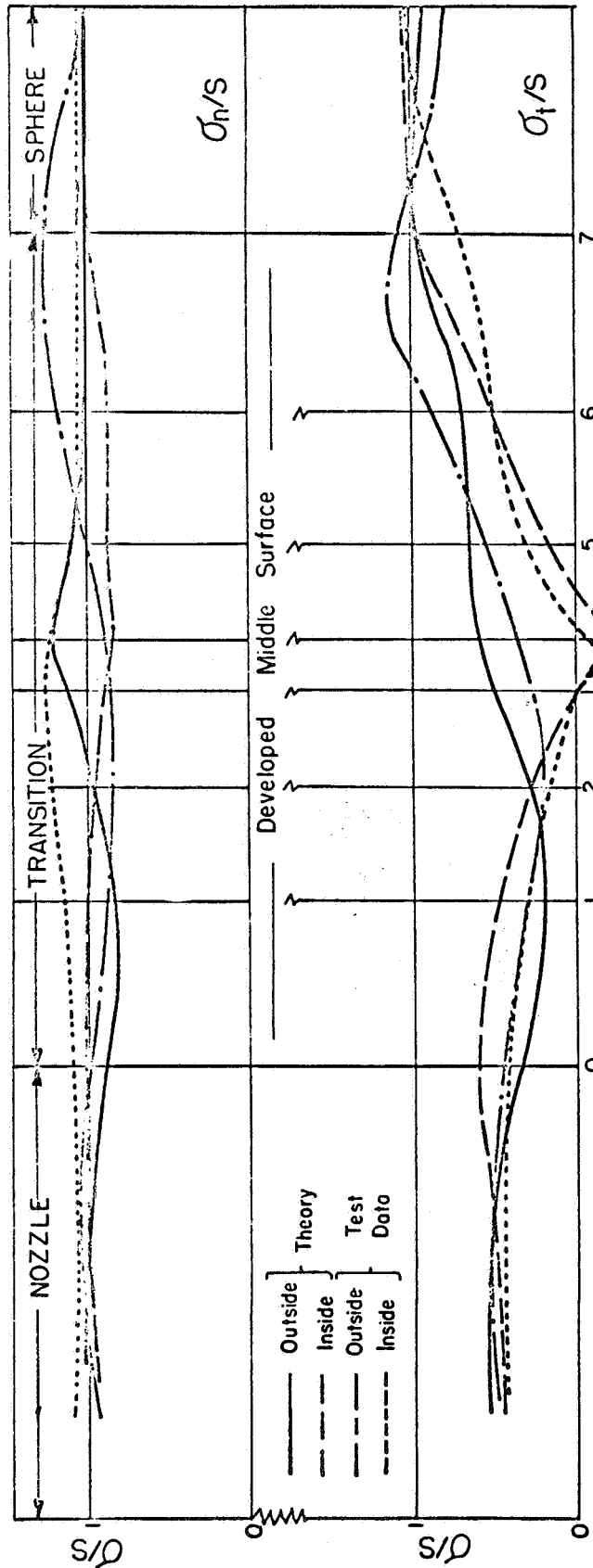


FIGURE 22. TEST DATA AND KALVINS CALCULATED RESULTS  
MODEL WS-51B



Stresses at Reinforcing Edges. Table 13 indicates that many of the maximum stresses are associated with the way that the reinforcing blends in with the nozzle or sphere walls. These stresses can be minimized by the use of very gradual transitions in wall thickness. For example (see Figure 23), Model WN-6B with 65% reinforcing and gradual transitions has a maximum stress index of 1.30 (not at the reinforcing edge) whereas Model WN-6C with 65% reinforcing has a maximum stress index of 2.24. Model N-4G (which is quite realistic in representing a typical fillet-welded, reinforced nozzle) has 75% reinforcing and a maximum stress index of 2.24. It seems unlikely that further increase in the nozzle thickness of model N-4G would significantly reduce the maximum stress and might increase it.

In some models (e.g., N-1B, N-5A) the maximum stresses are quite clearly associated with the problem of a nozzle in a sphere. For other models (e.g., N-7A at the pad-sphere intersection, WS-5LM, N-4D) the stress may be due primarily to the thickness change and only indirectly connected with the problem of a nozzle in a spherical shell. For example, Model WS-5LB includes results on the intersection of the spherical head with a cylindrical shell of equal diameter with an approximation 3:1 transition taper; stresses at this transition were as high as those in the vicinity of the nozzle.

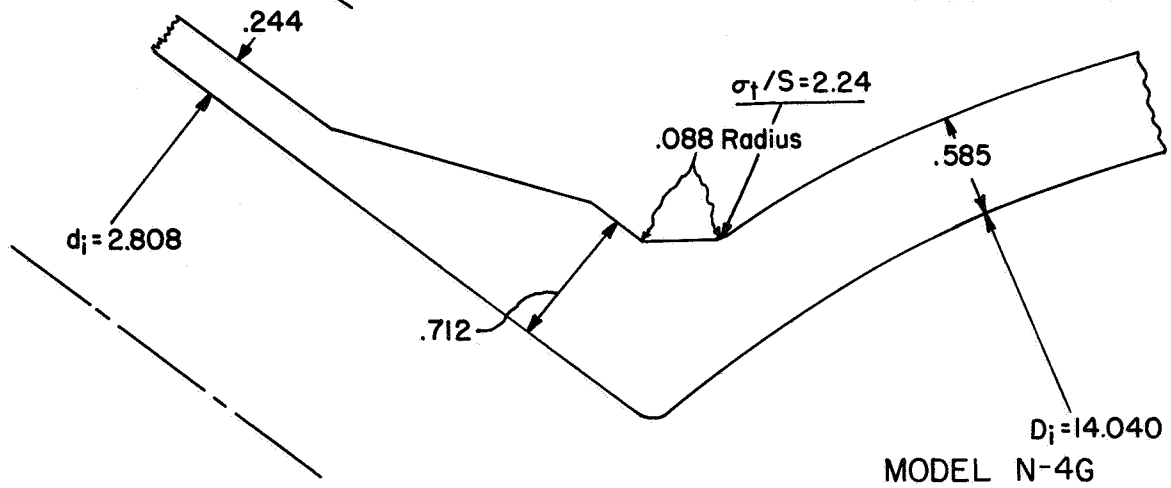
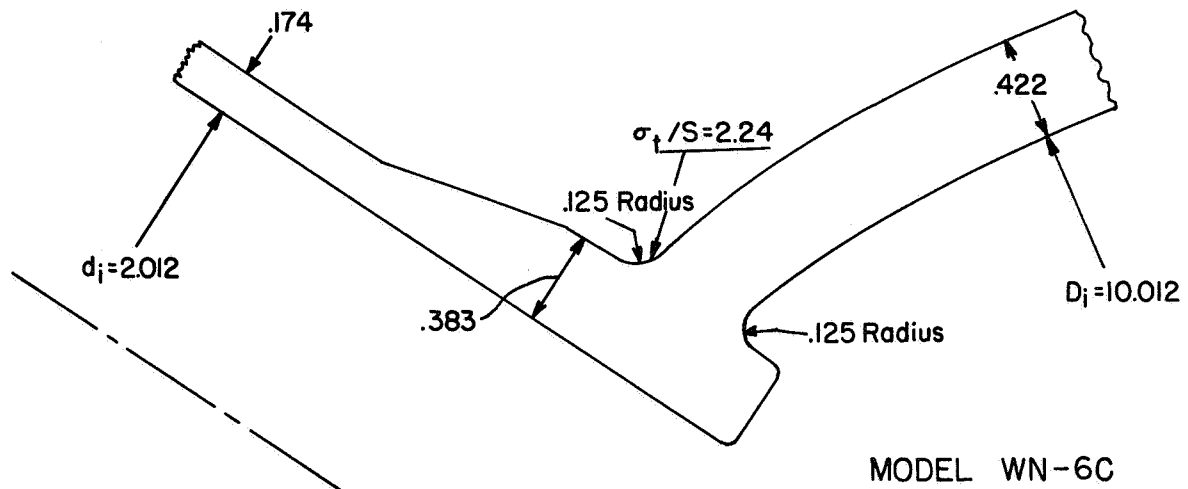
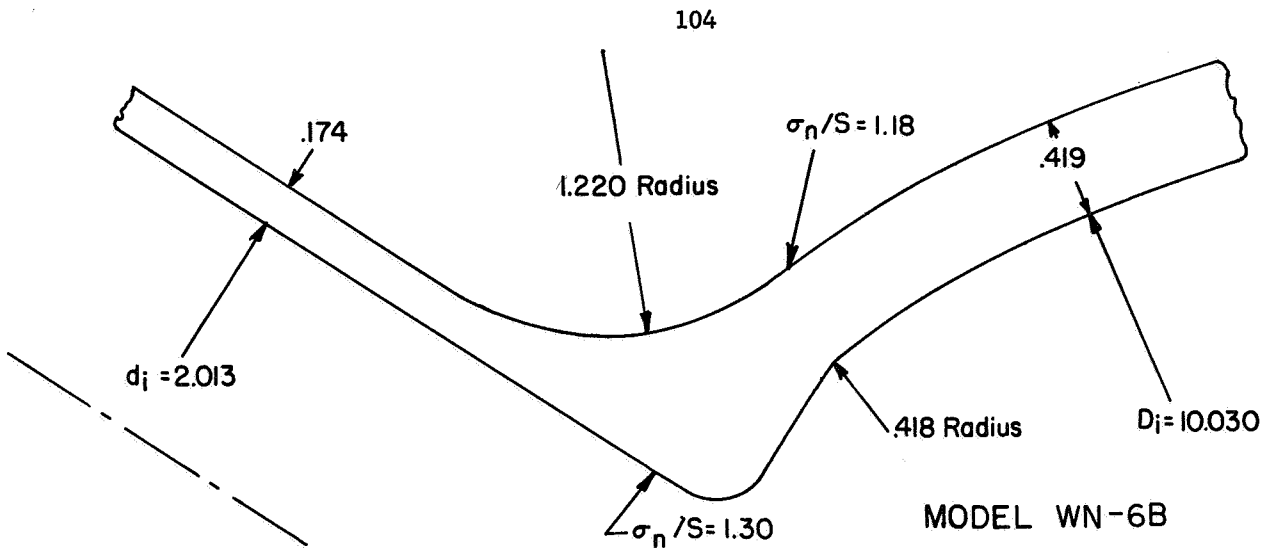


FIGURE 23. SECTIONS ILLUSTRATING STRESSES AT REINFORCING EDGES

Fillet Radius Reinforcing. It is apparent from Table 9 that, in certain dimension ranges, a relatively small amount of reinforcing provided by a fillet radius significantly reduces the elastic stresses, as compared to two-piece shell theory stresses. An example of this is Model WS-5LM, for which Waters' theory gives a maximum elastic stress index of 4.78 as compared to the measured maximum stress index of 1.41. The area of reinforcement provided for the fillet radius is  $0.65 d_i T$ , i.e., 65% of the area of reinforcing required by pressure vessel and piping design codes.

In order to obtain a general indication of the effectiveness of fillet-radii reinforcing, a parametric study\* was made using the Seal-Shell-2 computer program. Results of this parametric study are shown in Table 15.

To generalize this study into terms of area of reinforcing, the following steps were made.

- (1) It was assumed that the maximum stress intensity index,  $K_2^{**}$ , would be limited to 2.0 as a design criteria.
- (2) Values of the stress intensity from Table 15 were plotted as functions of  $r_o/t$  and  $D/T$ . From these graphs, it was found that the value of  $r_o/t$  required to obtain  $K_2 = 2.0$  is approximately given by the equation:

$$\frac{r_o}{t} = 0.336 \left( \frac{D}{T} \right)^{3/4} \quad (17)$$

The parametric study was limited to basic dimensions such that  $s/S = 1.0$ ; accordingly, equation (17) is applicable only for  $s/S = 1.0$ .

- (3) The amount of reinforcing area, as a ratio of  $A'/d_i T$ , provided by the fillet radius  $r_o/t$  was obtained using equation (17) and the geometry of the models. The resulting relationship is:

---

\* This study is somewhat limited in extent because of the relatively high cost of using the Seal-Shell-2 program. Some of the models were also run using Kalnins program (See Table 8).

\*\* Stress intensity at a point is defined as twice the maximum shear stress at that point. The symbol  $K_2$  to define this quantity is the same as that used in References (24) and (25).

TABLE 15. SUMMARY OF SEAL-SHELL-2 STUDY ON FILLET  
RADIUS REINFORCING

$\frac{D}{T}$	$\frac{d}{D}$	$\frac{r_o}{t}$	$\frac{A}{d_i T}$	Maximum Stress, $\sigma/S$		Maximum Stress Intensity, $\bar{\sigma}/S$	
				Surface	Midwall	Surface	Midwall
			(1)	(2)	(2)	(2)	
25	0.05	7.5	0.157	2.83 n,i	1.34 n	2.77 i	1.55
	0.05	10.0	0.272	2.69 n,i	1.25 n	2.63 i	1.46
	0.20	1.875	0.0273	1.90 n,i	1.74 n	2.22 i	1.83
	0.20	3.75	0.101	1.81 n,i	1.50 n	2.14 i	1.69
	0.50	1.875	0.023	2.33 n,o	2.02 n	2.33 o	2.02
	0.50	3.75	0.079	1.71 n,o	1.63 n	1.98 i	1.72
100	0.05	7.5	0.042	1.99 n,i	1.71 n	2.30 i	1.90
	0.05	10.0	0.074	2.02 n,i	1.58 n	2.30 i	1.80
	0.05	15.0	0.164	1.96 n,i	1.42 n	2.17 i	1.63
	0.20	7.5	0.109	2.25 n,o	1.83 n	2.25 o	1.91
	0.20	15.0	0.404	1.49 n,o	1.34 n	1.52 o	1.38
	0.50	7.5	0.099	2.61 n,o	1.99 n	2.61 o	2.04
	0.50	15.0	0.344	1.46 n,o	1.30 n	1.46 o	1.37
400	0.05	30.0	0.168	1.85 n,o	1.55 n	1.85 o	1.55
	0.05	40.0	0.296	1.81 n,i	1.41 n	1.81 i	1.41
	0.20	30.0	0.437	1.89 n,o	1.53 n	1.89 o	1.54
	0.50	30.0	0.406	1.77 n,o	1.53 n	1.77 o	1.57

- (1) A = cross sectional reinforcing area provided by the fillet radius  
(2) n = normal stress direction  
i = maximum stress or stress intensity located at inside surface  
o = maximum stress or stress intensity located at outside surface.

$$\frac{A'}{d_i T} = 0.23 \left( \frac{D}{T} \right)^{1/2} \frac{d/D}{(d/D + 1)^4} \cos \phi \quad (18)$$

where  $A'/d_i T$  is that particular ratio required to obtain  $K_2 = 2.0$

Equation (18) is plotted in Figure 24. Because  $d_i T$  is the ASME Code replacement area, Figure 24 indicates that a fillet radius with area much less than that required by the ASME Code can be used provided: (1)  $K_2 = 2.0$  is considered as an acceptable stress criteria and (2) loadings other than internal pressure are negligible.

Equations (17) and (18) are based on a limited number of theoretical results, hence, it is pertinent to compare these theoretical equations with test data. Equation (18) is compared with test data in Figures 25 thru 29. In general, of course, the test data do not give  $K_2 = 2.0$ , but in some cases this value of  $K_2$  is bracketed by the test data or can be extrapolated from the test data. To the extent that the test data can be interpolated or extrapolated to cross the  $K_2 = 2.0$  line at the same place as given by Equation (18), the theory and test data are in agreement. For example, in Figure 25 a line drawn between Models S-5AZ, WS-5L0, and WS-5LM (all approximately with  $d/D = 0.5$ ,  $D/T = 70$ ,  $s/S = 1$ ) passes almost exactly through the value of  $A'/d_i T$  calculated by Equation (18). Similar agreement exists for the test data shown in Figure 28. This close agreement does not exist for all the test data; for example, in Figure 26 the series of test results (for  $d/D = 0.38$ ,  $D/T = 24$ ,  $s/S = 1$ ) extrapolate to an  $A'/d_i T$  ratio of about 0.05 whereas the value of  $A'/d_i T$  calculated by Equation (18) is about 0.1.

There are two apparent general trends in the combination of test data and calculated results:

- (1) As  $d/D$  decreases, the effect of increasing  $A/d_1T$  becomes smaller (except for the data at  $d/D = 0.38$ ), where  $A$  is now considered as a variable amount of reinforcing area.
- (2) As  $D/T$  increases, the effect of  $A/d_1T$  becomes larger. This trend refers to the slope of the lines shown in Figures 25 through 29. The intercept of the lines with  $K_2 = 2.0$  is roughly given by Equation (18), which indicates that  $A'$  increases in proportion to  $D/T$ .

For  $d/D$  of 0.05 and  $D/T$  of 24 (Figure 29), the above trends combine such that even for  $A = 2d_1T$ , the intended value of  $K_2 = 2.0$  has not been reached. However, for  $D/T = 71.5$  and  $d/D = 0.05$  (Model WS-1LM) a fillet radius with area  $A = 2d_1T$  reduces  $K_2$  to 1.93. Presumably this trend will exist for even smaller  $d/D$  ratios combined with small  $D/T$  ratios, i.e., it will require a large value of  $A/d_1T$  to reduce the maximum shear stress intensity index to 2.0.

Figures 25 through 29 show all the available photoelastic data with  $s/S \cong 1.0$ , along with model Bu.S-A, where  $s/S = 1.92$  but where probably the intersection stress, as distinct from the stress at the juncture of the fillet with the nozzle, would have been about the same for  $s/S = 1.0$ . Several of these models had "balanced reinforcements", i.e., WN-6B, WN-6C, WS-5L0, and Bu.S-A. Three of the models fall reasonably well in line with models with external reinforcing only. The fourth, WN-6C, had a high tangential stress on the outside surface at the fillet. The fillet radius was only  $0.326t'$  (thickness of nozzle at base) or  $0.298T$ . With a fillet radius of  $t'$  instead of  $0.326t'$ , model WN-6C might fall in line with the other test data. These somewhat scant available data do not directly indicate any large difference in the efficiency of compact inside reinforcing as compared with compact outside reinforcing. However, the test models with inside reinforcing had about an equal area of reinforcing inside and outside.

Mershon<sup>(35)</sup> discusses the relative effectiveness of reinforcing entirely inside as compared to entirely outside. It appears that reinforcing entirely inside may be less effective, in reducing maximum stresses, than an equal amount of reinforcing placed entirely on the outside. Accordingly, caution should be used in extrapolating test data for models with reinforcing entirely outside to obtain stresses for designs with reinforcing entirely inside.

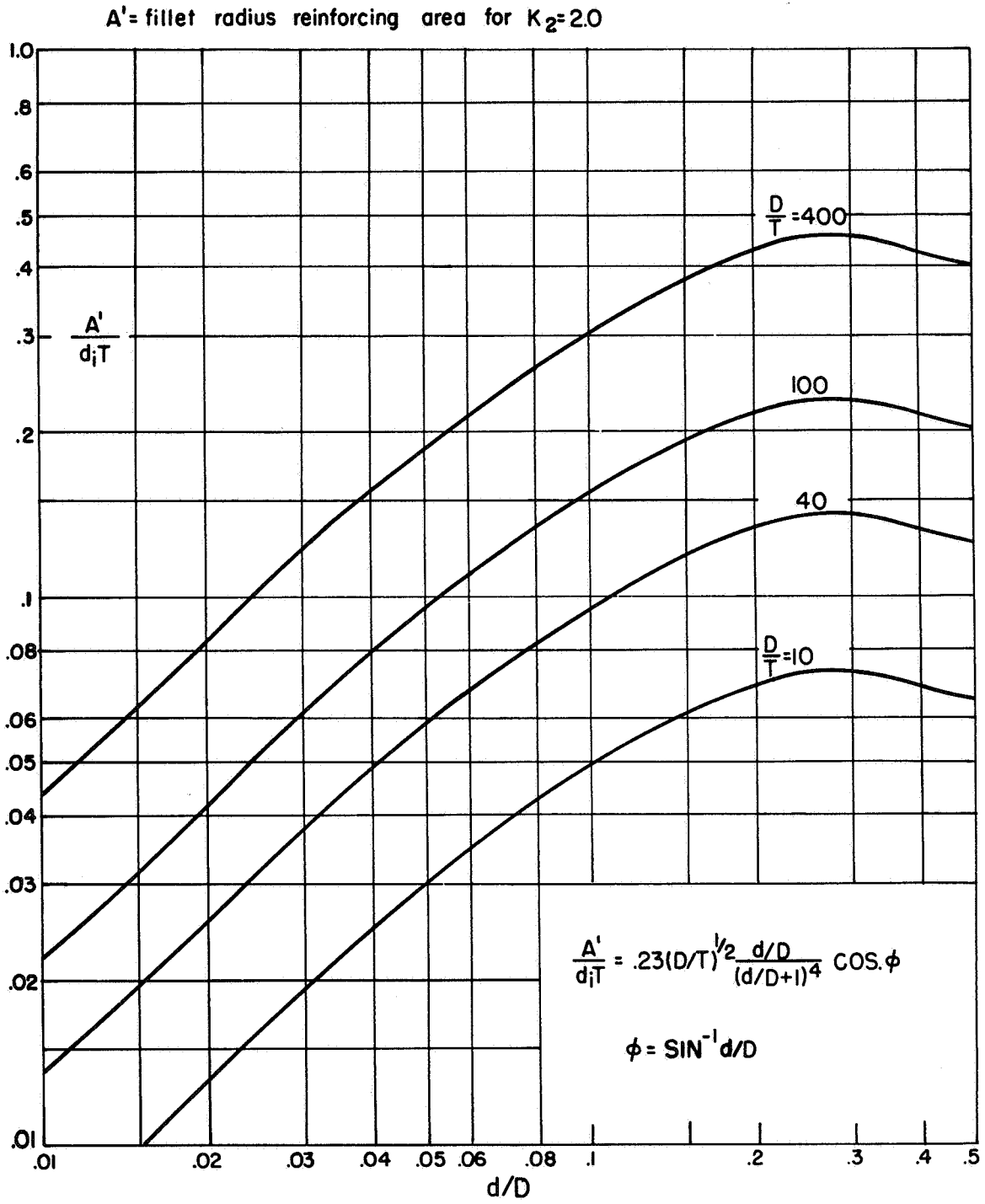


FIGURE 24. REINFORCING AREA REQUIRED FOR REINFORCING PROVIDED BY A FILLET,  $K_2 = 2.0$



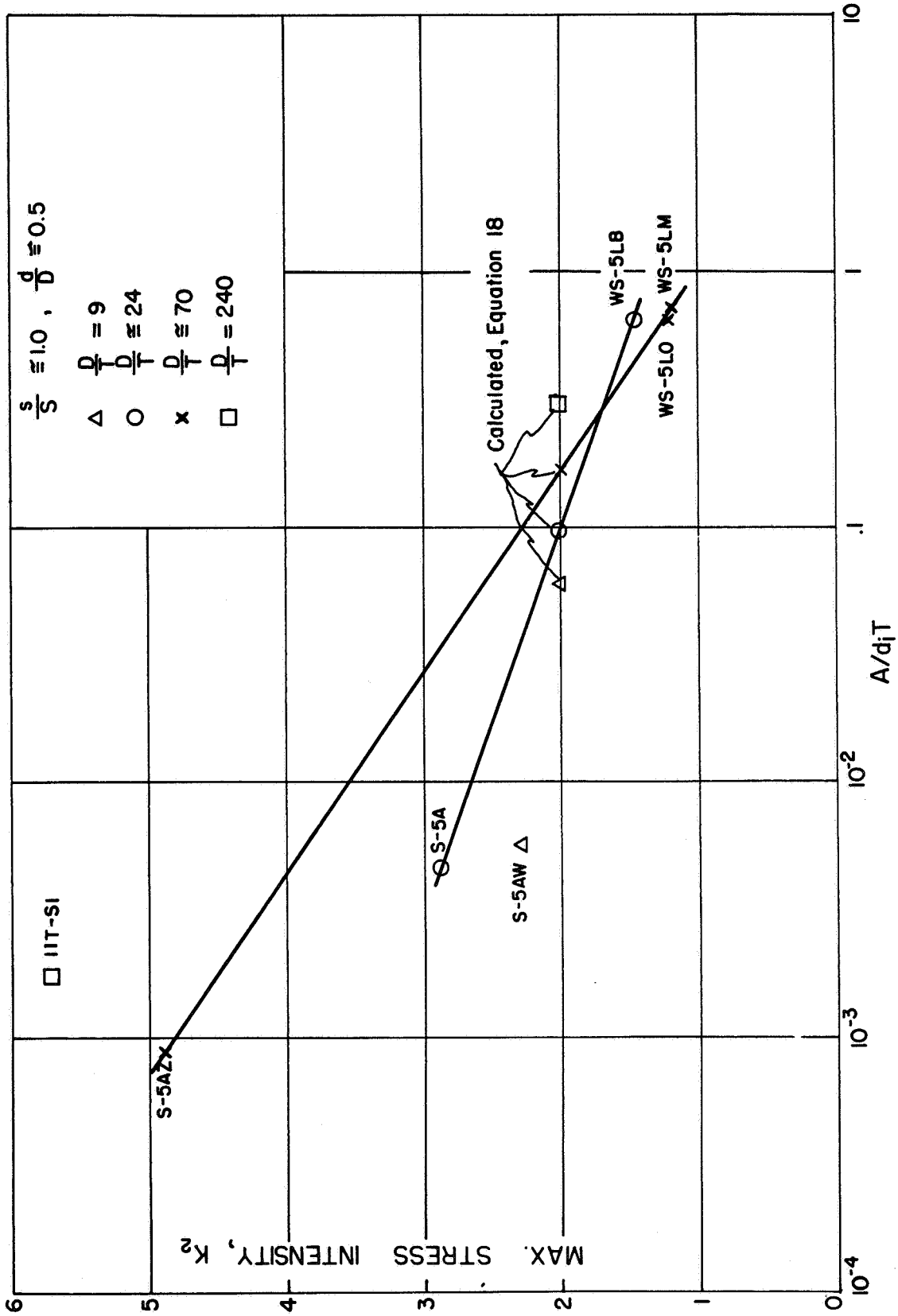


FIGURE 25. COMPARISON OF TEST DATA WITH CALCULATED FILLET REINFORCING,  $d/D = 0.5$

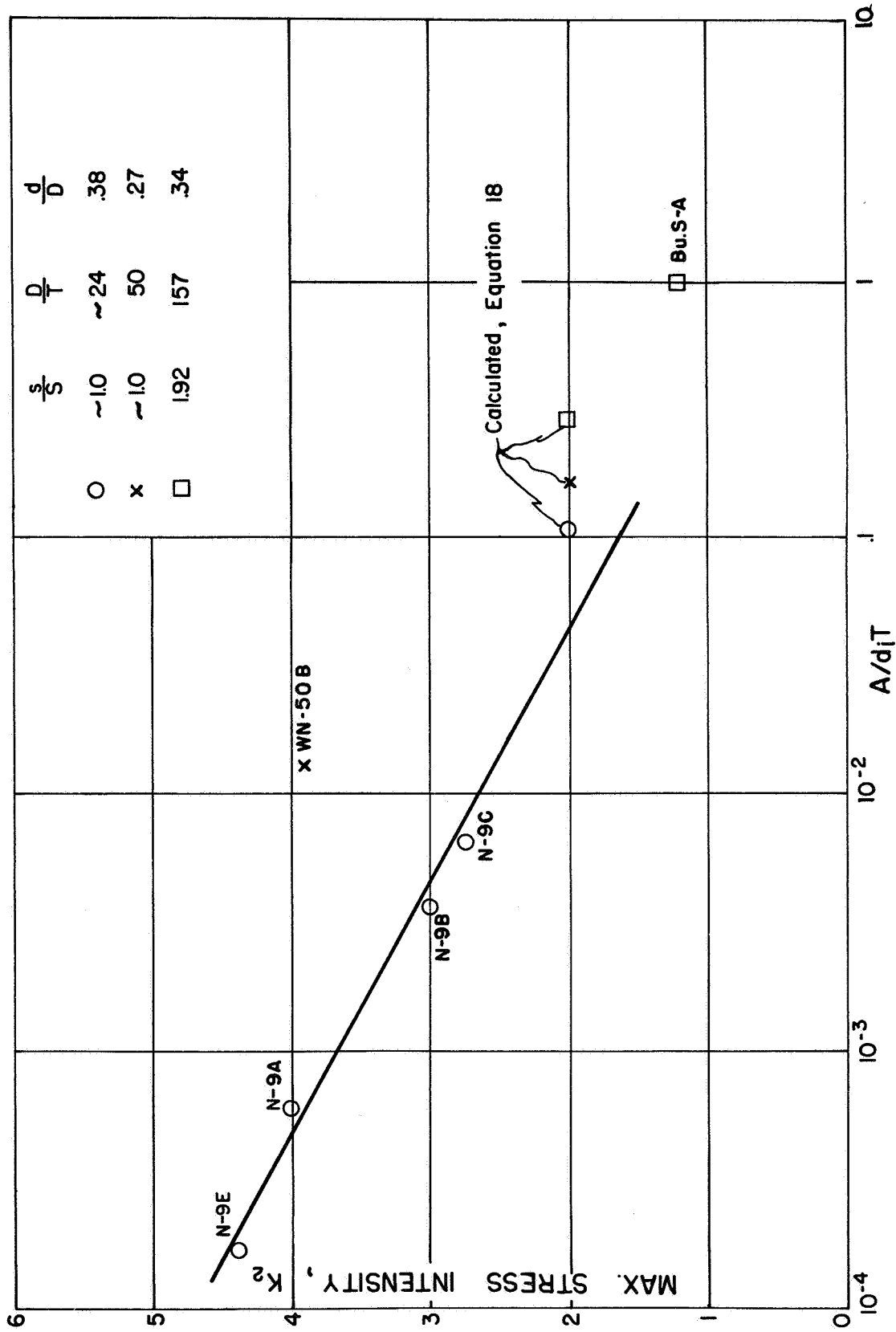


FIGURE 26. COMPARISON OF TEST DATA WITH CALCULATED FILLET REINFORCING,  $d/D = 0.38, 0.34, \text{ and } 0.27$

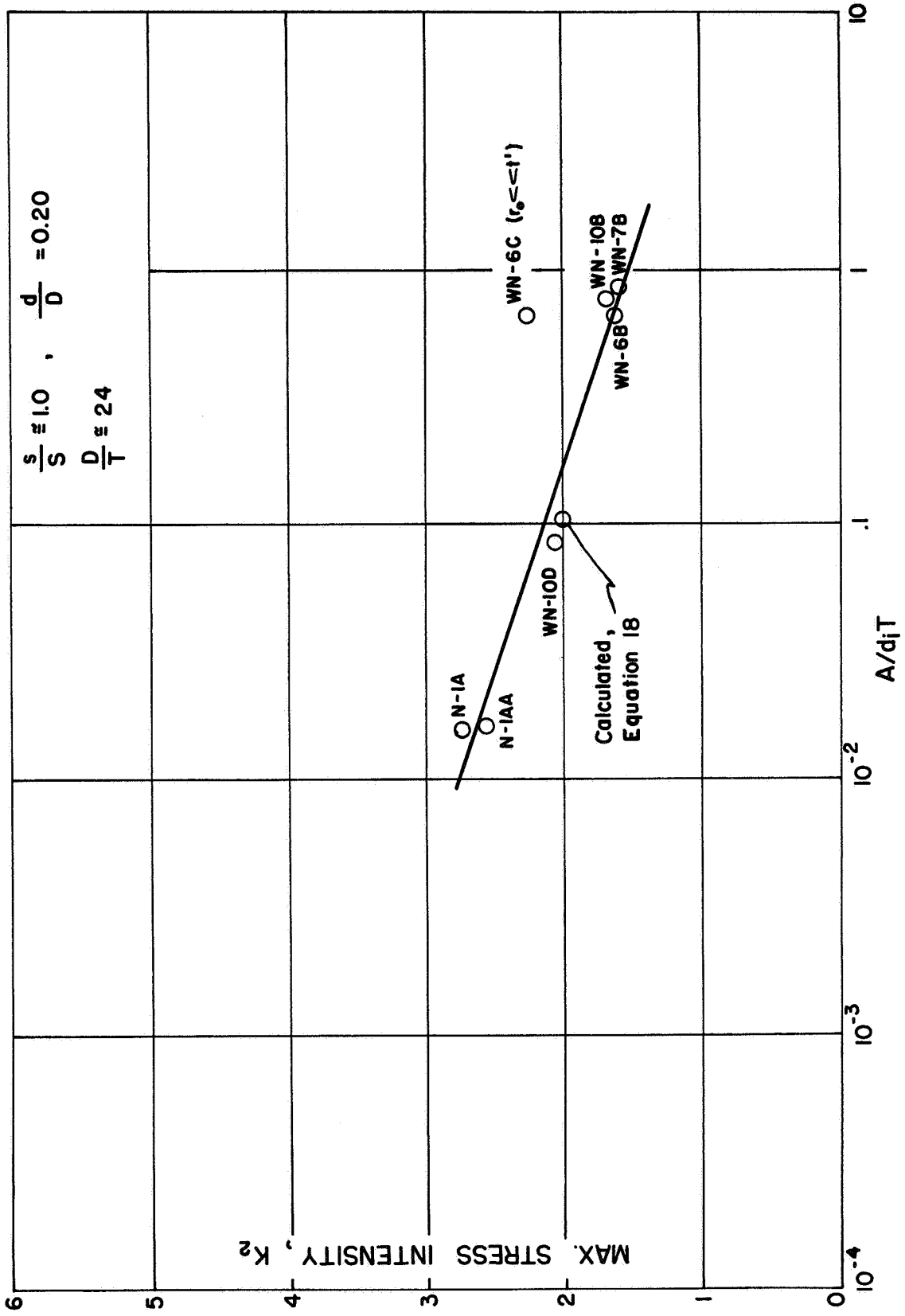


FIGURE 27. COMPARISON OF TEST DATA WITH CALCULATED FILLET REINFORCING,  $d/D = 0.20$

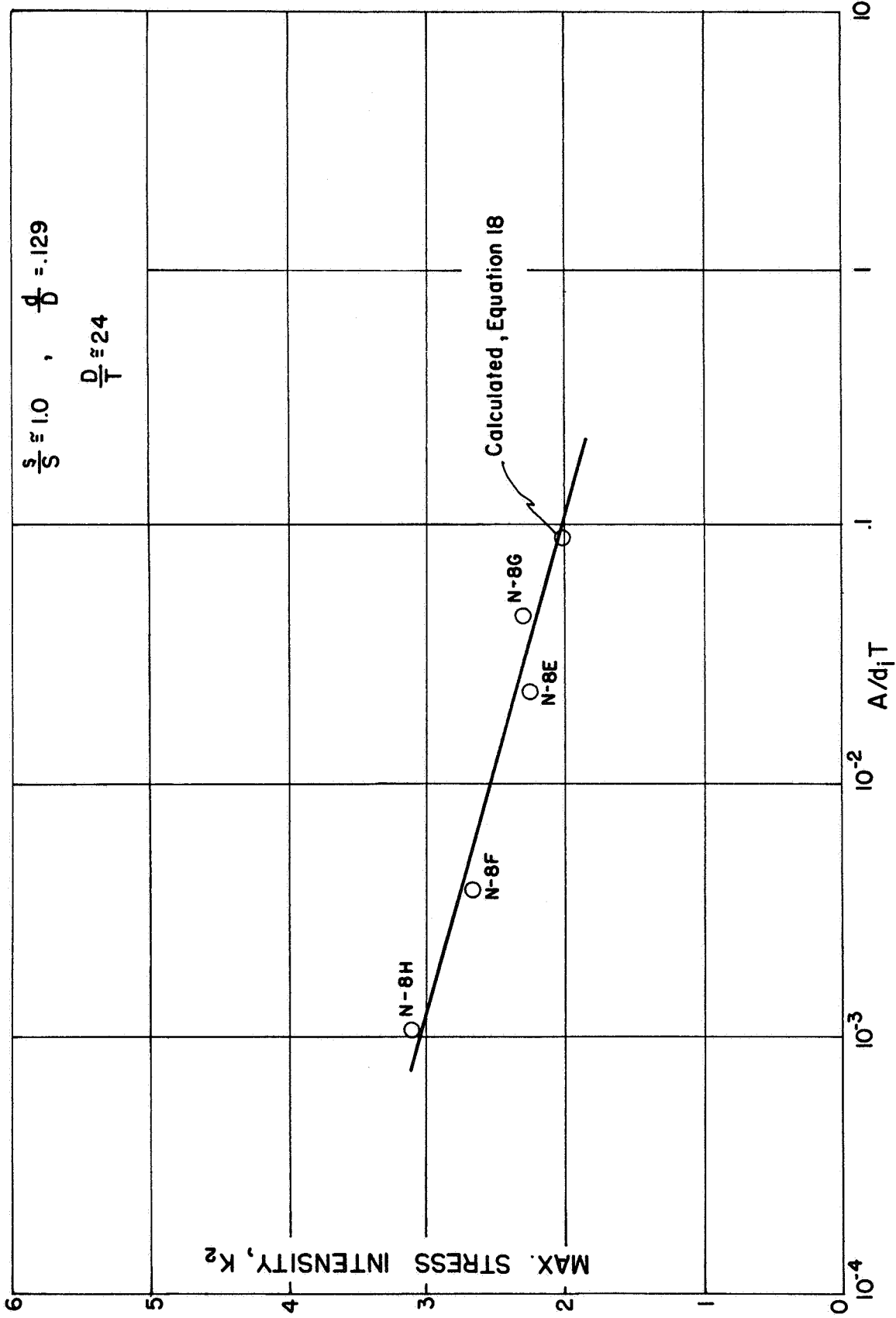


FIGURE 28. COMPARISON OF TEST DATA WITH CALCULATED FILLET REINFORCING,  $d/D = 0.129$

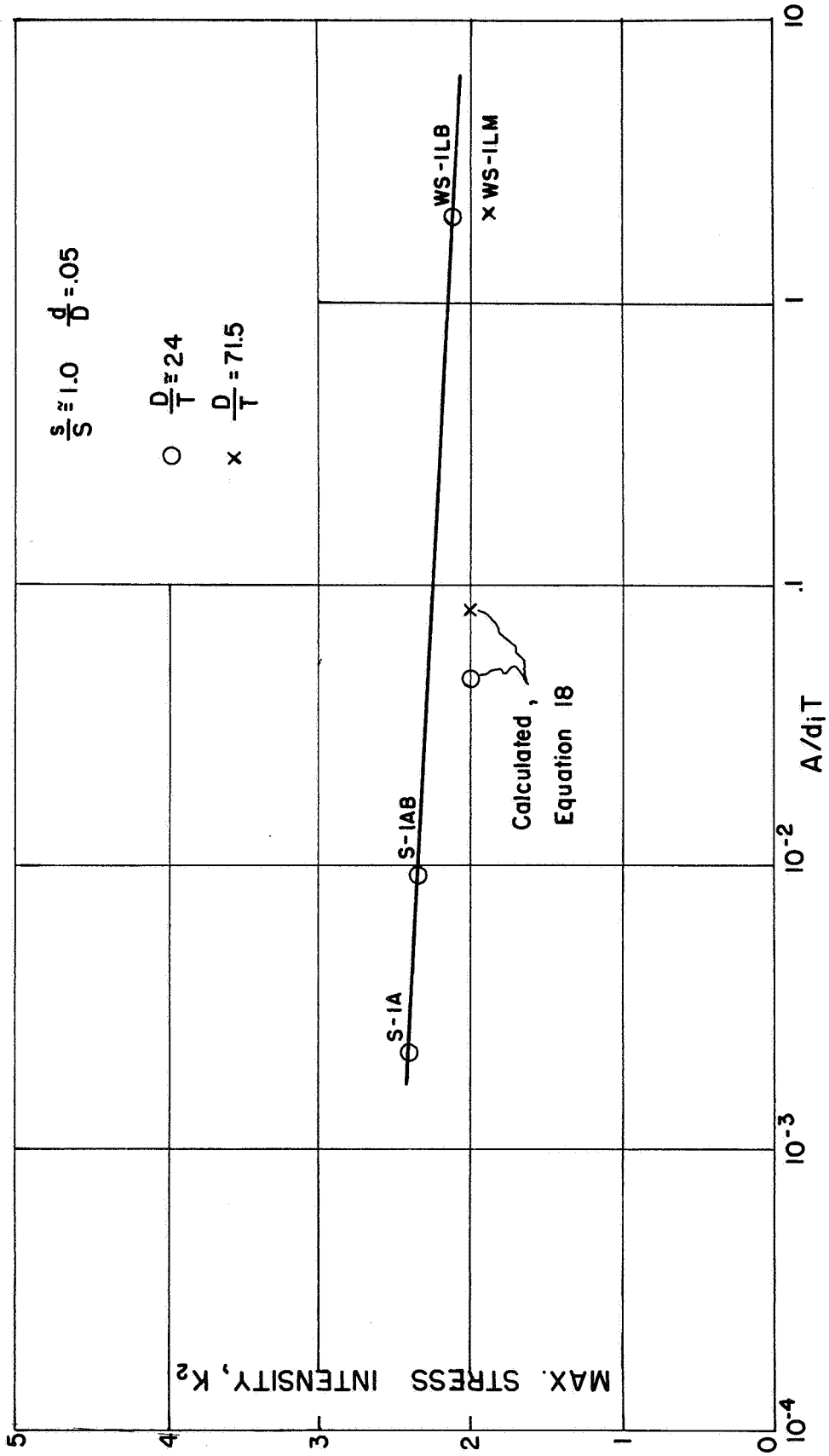


FIGURE 29. COMPARISON OF TEST DATA WITH CALCULATED FILLET REINFORCING,  $d/D = 0.05$

## MOMENT OR THRUST LOADING

Experimental data on nozzles in spheres with moment or thrust loading is relatively limited. Table 16 summarizes the dimensions and test results for 14 tests in which moment loading was applied to the nozzle; 9 tests in which thrust loading was applied to the nozzle. Dimensions are given in the left group of columns of Table 16. The column headed "Load" indicates the type of loading applied to the nozzle. Measured stresses are shown in the next group of five columns,  $\sigma_m$  being the largest measured stress. The next group of five columns shows calculated stresses using either the CERL, Bijlaard or Kalnins analysis;  $\sigma_c$  being the largest calculated stress. The column headed  $\sigma_c/\sigma_m$  gives the ratio of maximum calculated to maximum measured stress. Table 16 is similar to Table 9 (internal pressure loading) and gives the same kind of stress comparisons. For the six models tested by Dally<sup>(28)</sup>, stresses in the sphere and in the nozzle are shown separately since they illustrate certain aspects of the tests discussed later.

The test data is conveniently classified into three groups for discussion:

- (1) The five photoelastic models and IIT-S1, all of which contain a relatively small fillet radius.
- (2) The two ORNL models with essentially no fillet radius.
- (3) The six fabricated test models with significant local reinforcing.

These three groups of tests are discussed separately in the following.

### Models with Small Fillet Radius

Table 16, in the column labeled  $\sigma_c/\sigma_m$ , indicates that calculated stresses are higher than measured stresses. As in the case of pressure loading, this discrepancy appears to be related to the fillet radius reinforcing and the "curved-beam" type of stress intensification. Table 17 shows calculated stresses with adjustments for (1) normal thickness at juncture, indicated by  $\sigma'$ , and (2) normal thickness and curved beam factors, indicated by  $\sigma''$ . These adjustments are identical to those discussed

previously in connection with internal pressure loading. Agreement between test data and adjusted calculated results is fairly good, except for models WN-50C and WN-50D. However, in these two models the maximum stress occurred almost at the start of the fillet radius. Application of the same adjustment to the results of the two-piece shell theory along the nozzle also indicate that the maximum stress occurs at about this location. Figure 30 gives a plot of tangential stresses for model WN-50D along with the test data. It is apparent in Figure 30 that the adjusted theory is in adequate agreement with the test data.

The normal thickness adjustments can be directly introduced into a theoretical model using Kalnins' program. Figures 31 through 35 show the results of such calculations along with the test data. Table 17 includes the maximum stresses obtained from the calculations. Maximum stresses agree quite well. The principal discrepancies between test data and theory apparent in Figures 31 through 35 occur at the inside corners. Kalnins' program is strictly a thin-shell theory, hence it does not reflect stresses analogous to the "curved beam effect". Qualitatively, adjustments to Kalnins' results of this type would produce better agreement, particularly on the inside surface.

TABLE 16. SUMMARY OF DIMENSIONS, MAXIMUM MEASURED STRESSES AND COMPARISON WITH "TWO-PIECE" SHELL THEORY

Model No. (1)	$\frac{d}{D}$	$\frac{D}{T}$	$\frac{s}{S}$	$\frac{t}{T}$	$\frac{d}{t}$	$\frac{r_0}{t}$	$\frac{A_a}{d_1 T}$	$\frac{r_i}{t}$	Load (3)	Measured Stress(4)				Calculated Stress(4)				$\frac{\sigma_c}{\sigma_m}$						
										$\sigma_n/S$		$\sigma_t/S$		$\sigma_n/S$		$\sigma_t/S$			$\sigma_c/S$	$\sigma_m/S$	Inside	Outside	Inside	Outside
										Outside	Inside	Outside	Inside	Outside	Inside	Outside	Inside							
WN-50A1	0.50	51	1.96	0.51	50	1.96	0.0047	0.56	M	4.67	1.34	5.85	-2.85	5.85	4.05	0.82	8.50	8.50	1.45					
WN-50A2	0.50	52	1.95	0.51	50	1.58	0.0030	0.50	M	4.67	1.17	5.92	-3.13	5.92	4.07	0.83	8.55	8.55	1.45					
WN-50B	0.27	51	1.11	0.49	28	1.62	0.013	0.50	M	4.56	1.27	5.72	-3.29	5.72	4.10	1.09	9.66	9.66	1.69					
WN-50C	0.27	52	2.13	0.25	55	3.20	0.014	1.00	M	3.75	1.47	4.36	-2.70	4.36	3.58	0.59	8.01	8.01	1.84					
WN-50D	0.13	50	1.06	0.25	27	3.20	0.072	1.00	M	2.84	1.18	3.11	-1.44	3.11	2.38	0.94	6.27	6.27	2.02					
IIT-S1	0.50	240	1.00	0.99	120	-1.4	0.0018	-1.4	M	8.66	4.17	13.1	-4.69	13.1	9.74	1.85	13.8	13.8	1.05					
IIT-S1	0.50	240	1.00	0.99	120	-1.4	0.0018	-1.4	-L	10.4	-3.80	12.9	3.80	12.9	10.2	2.33	13.9	13.9	1.08					
ORNL-5	0.082	81	0.49	0.33	20	-0	-0	-	M	4.73	-1.25	4.67	-2.85	4.73	2.90	-1.67	7.92	7.92	1.68					
ORNL-5	0.082	81	0.49	0.33	20	-0	-0	-	L	-4.64	-1.84	-6.20	4.37	-6.20	-5.19	1.14	-11.56	9.56	1.87					
ORNL-6	0.084	81	1.01	0.17	41	-0	-0	-	M	2.37	0.96	3.38	-2.18	3.38	1.93	-0.95	5.01	-3.08	1.48					
ORNL-6	0.084	81	1.01	0.17	41	-0	-0	-	L	-3.61	-1.76	-4.55	3.38	-4.55	-3.27	-0.42	-6.99	4.99	1.53					

(1) Model numbers are the same as given in References (25), (26), (27) and (28). The WN- models are from Reference (25), IIT-S1 is from Reference (25), ORNL-5 and -6 and from Reference (27) and models 1 thru 6 and from Reference (28). WN-50B is actually two models; one tested with internal pressure, the other with moment applied to the nozzle.

(2)  $A_a$  = reinforcing area provided by the fillet radius for the WN- and IIT-S1 models.  $A_a$  = reinforcing area provided by fillet welds and inwardly protruding nozzles for models 1 thru 5, plus the excess (over 0.77") thickness in the pad for model 6.

(3) M = moment applied to the nozzle. L = thrust applied to nozzle. For models WN- and IIT-S1, stresses are shown at  $\theta = 180^\circ$  (See Nomenclature, Figure 1). For the other models stresses are at  $\theta = 0$ . References (25), (26) and (27) give stresses as a function of  $\theta$ ; the theoretical relationship  $(\sigma)_\theta = (\cos \theta)$  applies with good accuracy.

(4) For moment loading:  $S = M/\pi r^2 t$ . For thrust loading:  $S = L/2\pi r t$ .

(5)  $\sigma_m$  = maximum measured stress.  $\sigma_c$  = maximum calculated stress.

(6) For Model No. 6, first line is for pad thickness ( $T = 1.63$ " ), second line is for sphere thickness ( $T = 0.77$ " ).



TABLE 16. (CONTINUED)

Model No. (1)	$\frac{d}{D}$	$\frac{D}{T}$	$\frac{s}{S}$	$\frac{t}{T}$	$\frac{d}{t}$	$\frac{A_a}{d_i T}$	Load (3)	Part	Measured Stresses <sup>(4)</sup>				Calculated Stresses <sup>(4)</sup>				$\frac{\sigma_c}{\sigma_m}$	
									$\sigma_n/S$		$\sigma_t/S$		$\sigma_n/S$		$\sigma_t/S$			$\sigma_c/S$ (5)
									Outside	Inside	Outside	Inside	Outside	Inside	Outside	Inside		
1	0.094	80	0.22	0.86	8.7	0.5	M	Head	-1.6	0.8	-2.3	1.8	-3.61	2.44	-6.35	4.72	-6.35	2.76
									-1.3	1.1	-2.0	1.1	-2.70	1.77	-8.45	6.46	-8.45	4.22
							L	Nozzle	-3.0	0.7	-4.1	1.7	-6.21	1.05	-9.45	6.60	-9.45	2.30
									-2.7	-1.7	-3.5	-1.6	-5.65	0.82	-11.80	9.78	-11.80	3.37
2	0.097	91	0.19	1.01	8.7	0.6	M	Head	-2.5	0.7	-4.0	2.7	-4.31	2.68	-8.80	6.78	-8.80	2.19
									-1.3	-0.8	-1.9	-1.2	-2.92	1.65	-8.65	6.61	-8.65	4.55
							L	Nozzle	-3.7	0.8	-5.6	1.8	-7.26	0.97	-12.60	9.10	-12.60	2.25
									-2.1	-2.0	-2.0	-1.8	-6.06	0.29	-11.60	9.60	-11.60	5.50
3	0.10	91	0.28	0.72	12.6	0.45	M	Head	-1.9	0.7	-2.7	1.9	-3.82	2.17	-5.57	4.11	-5.57	2.45
									-0.7	-0.8	-1.6	-1.4	-3.60	2.06	-10.40	8.41	-10.40	6.50
							L	Nozzle	-3.0	0.6	-4.0	1.3	-6.28	0.66	-7.71	5.41	-7.71	1.93
									-2.1	-1.7	-1.8	2.7	-6.57	1.09	-13.8	11.8	-13.8	5.05
4	0.104	91	0.58	0.36	26.4	0.3	M	Head	-1.3	0.5	-1.4	0.6	-3.52	1.46	-1.55	0.97	-3.52	2.52
									-1.3	0.9	-1.3	-1.5	-4.07	1.85	-10.90	8.86	-10.90	7.26
							L	Nozzle	-2.0	0.2	-1.8	-0.3	-4.99	0.21	-1.98	1.20	-4.99	2.50
									-1.7	-0.9	-1.1	-1.7	-6.30	1.19	-13.50	11.50	-13.50	7.94
5	0.113	37	0.48	0.47	8.8	0.3	M	Head	-0.9	0.5	-1.0	0.7	-1.98	1.48	-1.32	0.72	-1.98	1.98
									-1.0	-0.6	-2.0	-1.2	-1.68	1.01	-5.46	3.50	-5.46	4.55
							L	Nozzle	-1.8	0.6	-2.0	-1.2	-3.41	0.94	-2.18	1.12	-3.41	1.71
									-1.7	-1.3	-2.1	-1.5	-3.53	0.83	-8.26	6.30	-8.26	3.93
6	0.104	40	0.44	0.47	8.8	-	M	Head	-1.0	0.3	-1.3	0.9	-2.26	1.59	-1.40	0.80	-2.26	1.74
									-0.9	-0.3	-1.5	-1.1	-2.04	1.01	-5.79	4.17	-5.79	3.86
	0.104	85	0.21	1.00	8.8	1.7	L	Nozzle	-2.6	-1.1	-3.1	1.5	-4.59	1.74	-2.82	1.52	-4.59	1.48
									-1.9	-1.7	-1.9	-1.7	-4.48	1.42	-10.80	8.84	-10.80	5.70

TABLE 17. COMPARISON OF TEST DATA WITH TWO-PIECE, THIN-SHELL THEORY AND MODIFICATIONS THEREOF, MODELS WITH MOMENT OR THRUST LOAD

Model No.	Stress (1)	Stress Indices <sup>(2)</sup>				$\frac{\sigma_c}{\sigma_m}$ (3)
		$\sigma_n/s$		$\sigma_t/s$		
		Outside	Inside	Outside	Inside	
WN-50A1	Test Data	4.67	.90	5.85	-2.85	--
	$\sigma$	4.05	.82	8.50	-6.50	1.45
	$\sigma'$	3.25	.80	6.25	-4.90	1.07
	$\sigma''$	3.65	.97	7.30	-3.77	1.25
	Kalnins	4.46	-.01	5.70	-3.93	.97
WN-50A2	Test Data	4.67	1.17	5.92	-3.13	--
	$\sigma$	4.07	.83	8.55	-6.56	1.45
	$\sigma'$	3.50	.79	6.55	-4.85	1.11
	$\sigma''$	3.91	1.04	6.85	-3.95	1.16
	Kalnins	4.26	-.01	5.32	-3.56	.90
WN-50B	Test Data	4.56	1.27	5.72	-3.29	--
	$\sigma$	4.10	1.09	9.66	-7.66	1.69
	$\sigma'$	3.10	.36	5.40	-4.26	.94
	$\sigma''$	3.46	.24	7.03	-3.42	1.23
	Kalnins	4.06	1.17	5.11	-3.38	.89
WN-50C	Test Data	3.75	1.47	4.36	-2.70	--
	$\sigma$	3.58	.59	8.01	-6.00	1.84
	$\sigma'$	3.47	.06	2.73	-1.01	.79
	$\sigma''$	3.58	.33	3.13	-1.33	.80
	Kalnins	3.71	1.23	4.39	-2.64	1.00
WN-50D	Test Data	2.84	1.18	3.11	-1.44	--
	$\sigma$	2.38	.94	6.27	-4.26	2.02
	$\sigma'$	2.54	1.18	1.82	-.82	.82
	$\sigma''$	2.66	1.14	2.12	-.62	.86
	Kalnins	2.24	.78	2.80	-1.34	.90
IIT-S1 (Moment Load)	Test Data	8.66	4.17	13.1	-4.69	--
	$\sigma$	9.74	1.85	13.8	-11.8	1.05
	$\sigma'$	8.45	2.01	11.7	-9.92	.89
	$\sigma''$	9.23	2.50	14.3	-8.17	1.09

Footnotes on next page

TABLE 17. (contd.)

Model No.	Stress (1)	Stress Indices <sup>(2)</sup>				$\frac{\sigma_c}{\sigma_m}$ (3)
		$\sigma_n/S$		$\sigma_t/S$		
		Outside	Inside	Outside	Inside	
IIT-S1	Test Data	10.4	3.80	12.9	-3.80	--
(Thrust Load)	$\sigma$	10.2	2.33	13.9	-11.9	1.08
	$\sigma'$	8.95	2.45	11.7	-9.91	.91
	$\sigma''$	9.73	2.98	14.3	-8.15	1.11
	Kalnins	10.1	2.31	13.9	-11.8	1.08

(1)  $\sigma$  = two-piece thin-shell theory calculated stress.

$\sigma'$  = theory with modification for normal thickness.

$\sigma''$  = theory with modifications for normal thickness and curved beam effect.

Kalnins = stress calculated using Kalnins computer program as a multi-piece shell theory.

(2)  $S = M/\pi r^2 t$  for moment loading.

$S = L/2\pi r t$  for thrust loading.

(3)  $\sigma_c$  = maximum calculated stress.

$\sigma_m$  = maximum measured stress.

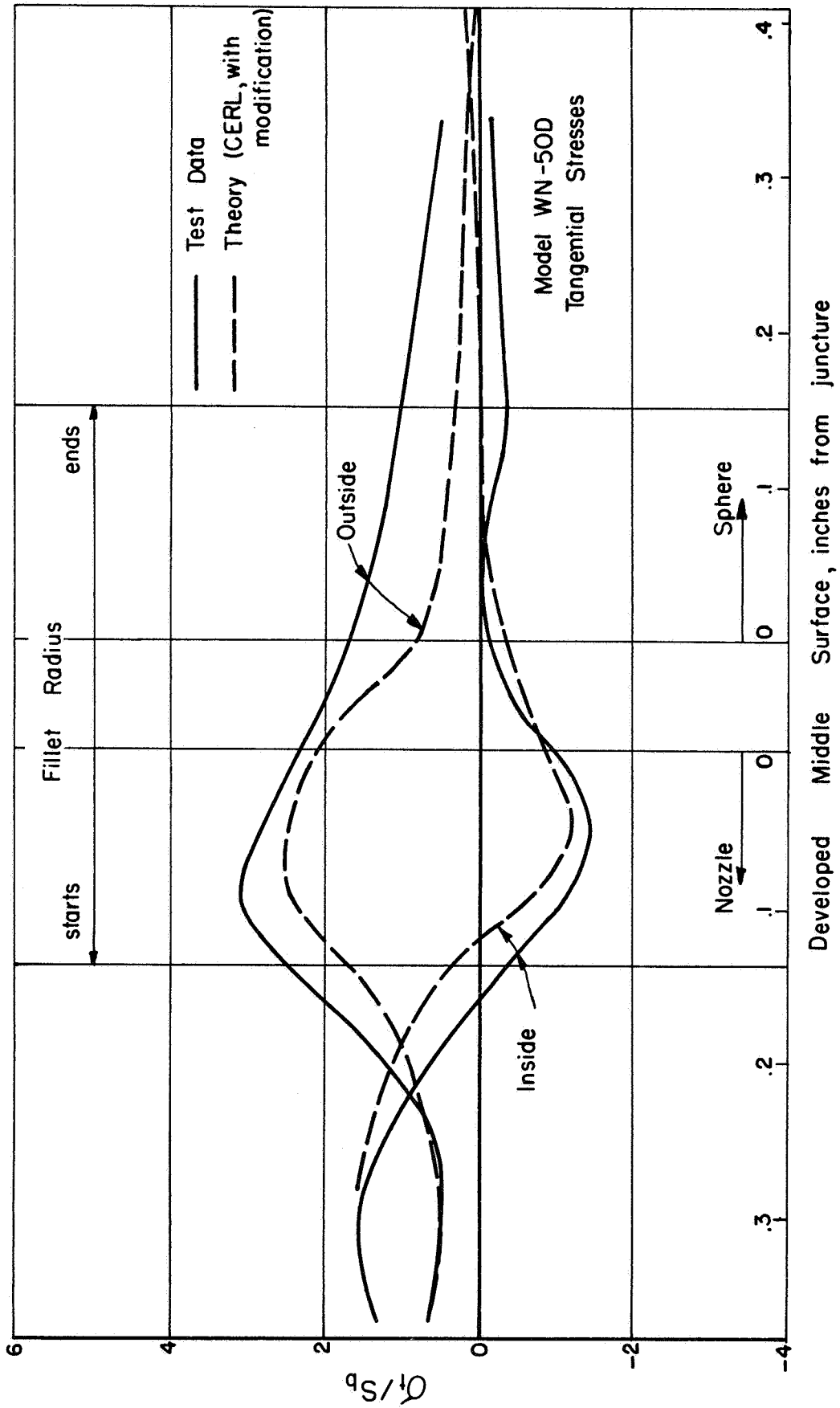


FIGURE 30. TEST DATA AND CALCULATED (CERL WITH MODIFICATIONS) RESULTS FOR MODEL WN-50B, MOMENT LOADING

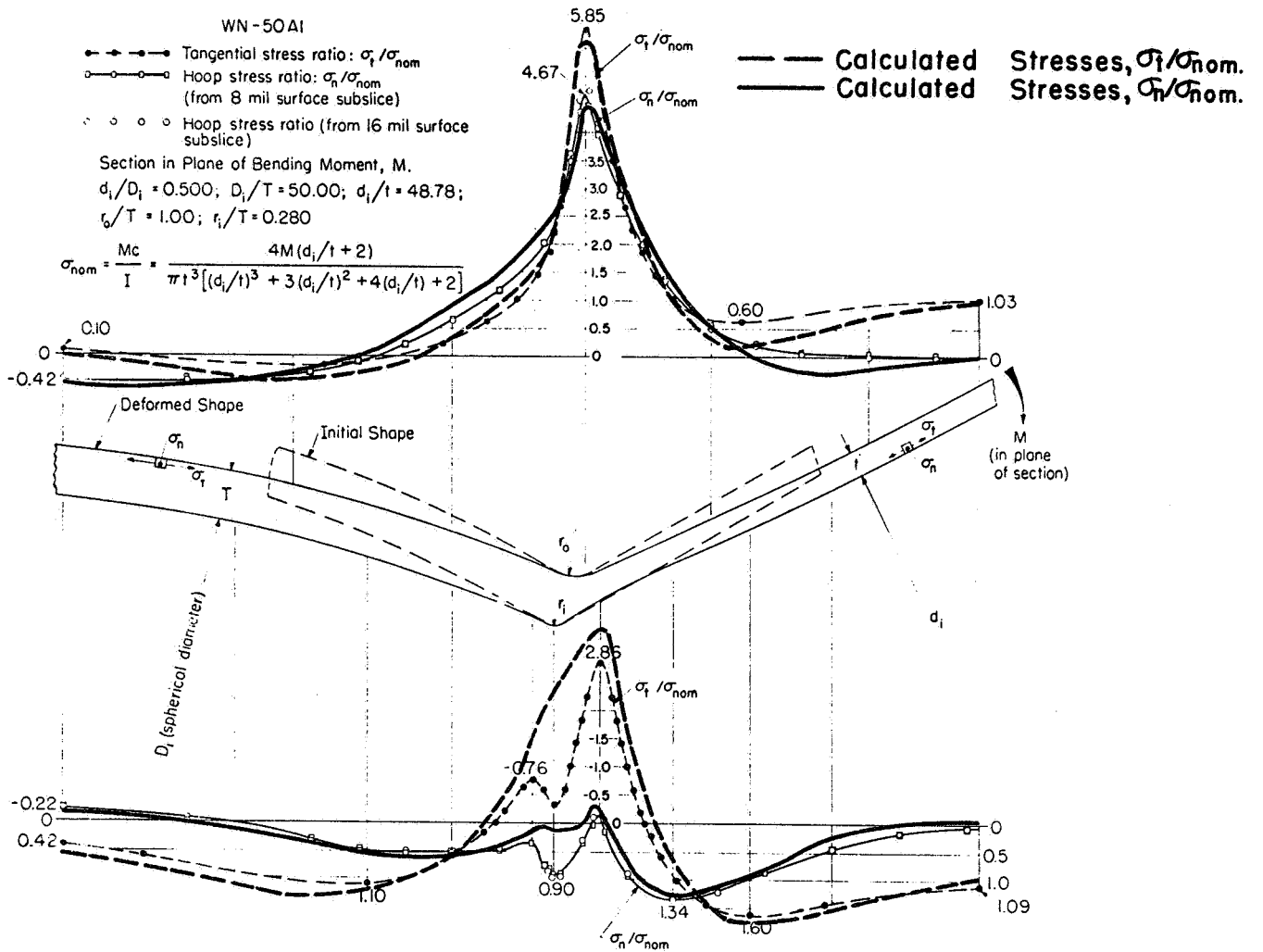


FIGURE 31. TEST DATA AND CALCULATED (KALNINS RESULTS FOR MODEL WN-50A1, MOMENT LOADING

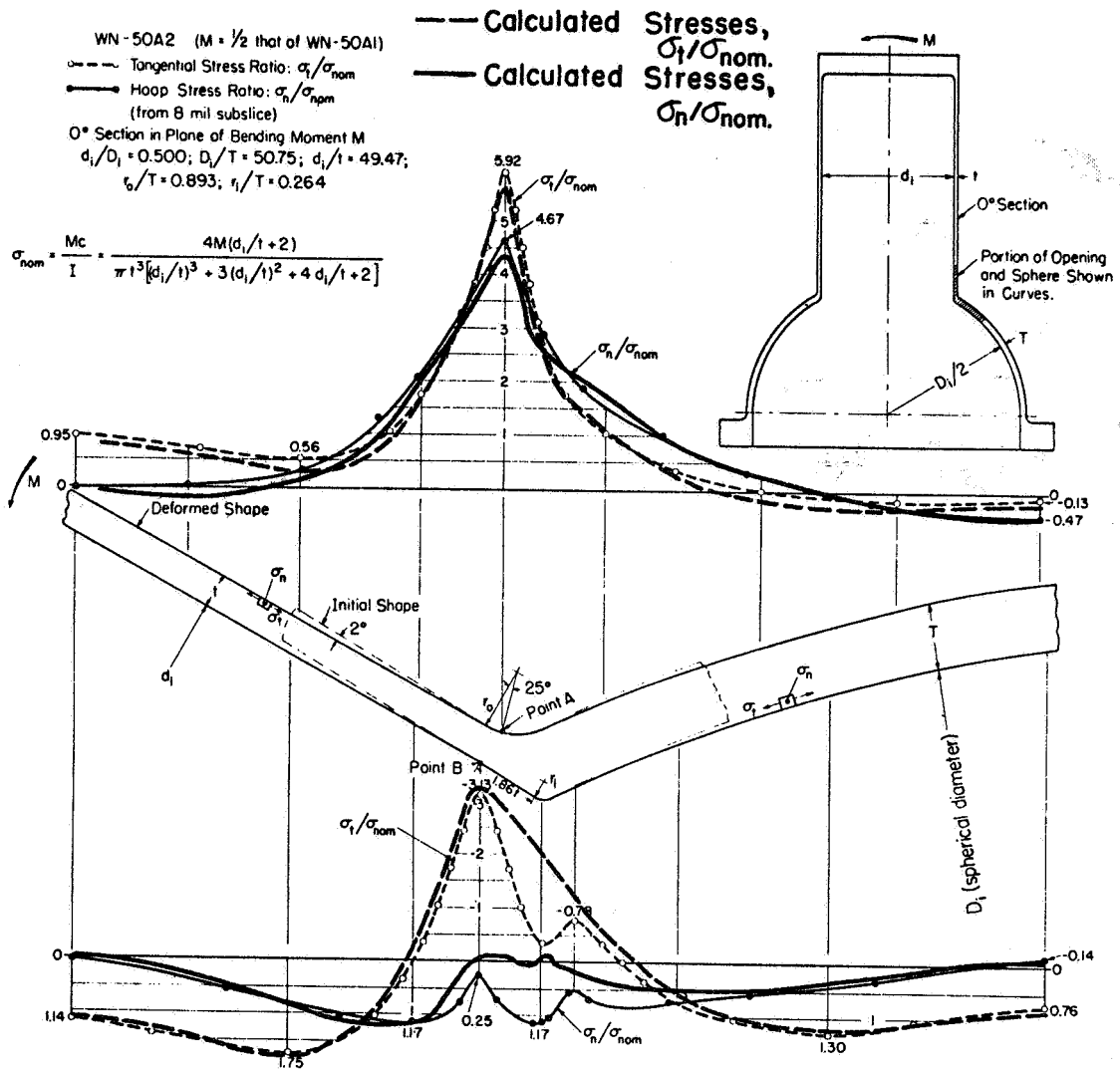


FIGURE 32. TEST DATA AND CALCULATED (KALNINS) RESULTS FOR MODEL WN-50A2

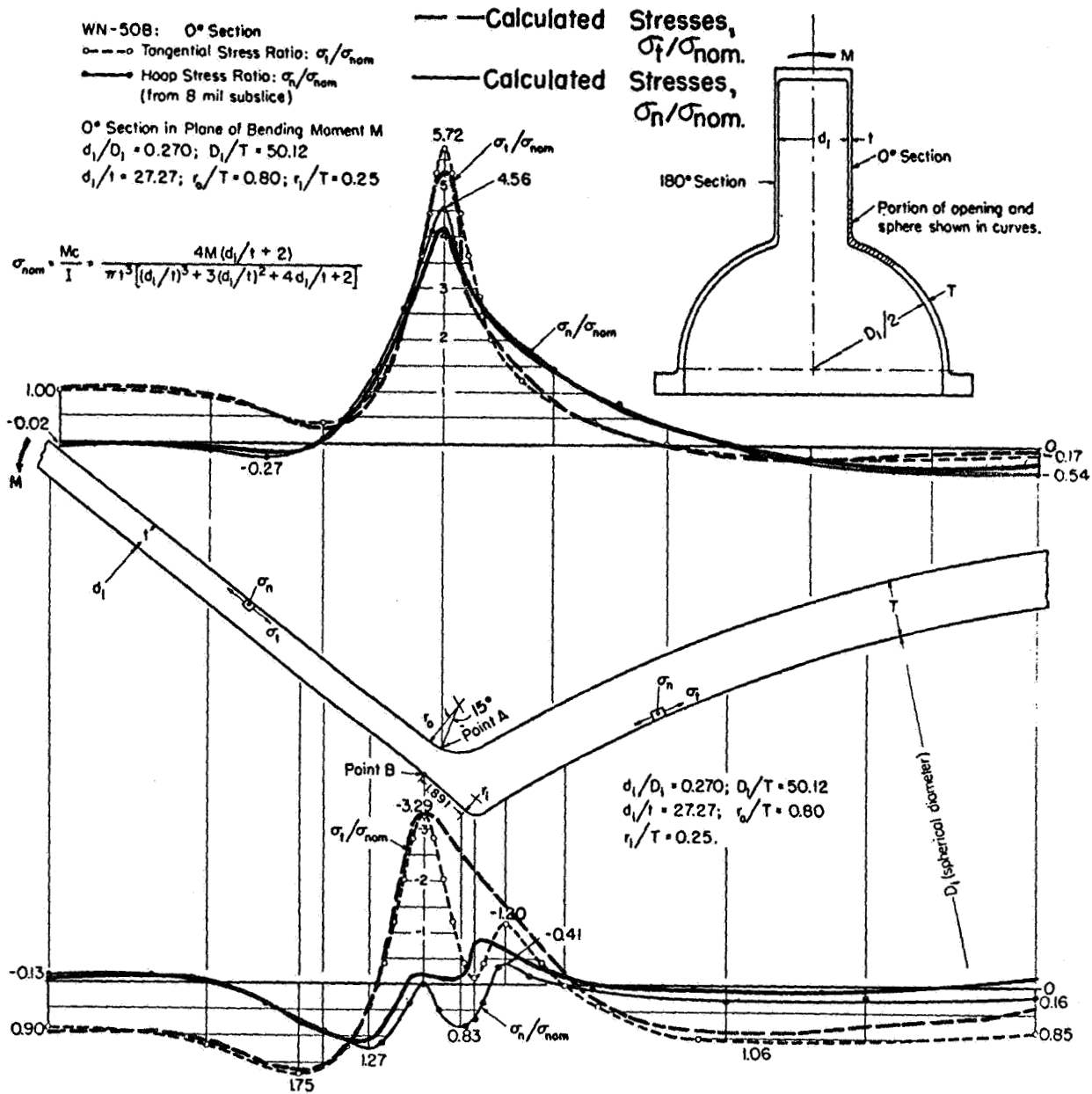


FIGURE 33. TEST DATA AND CALCULATED (KALNINS) RESULTS FOR MODEL WN-50B

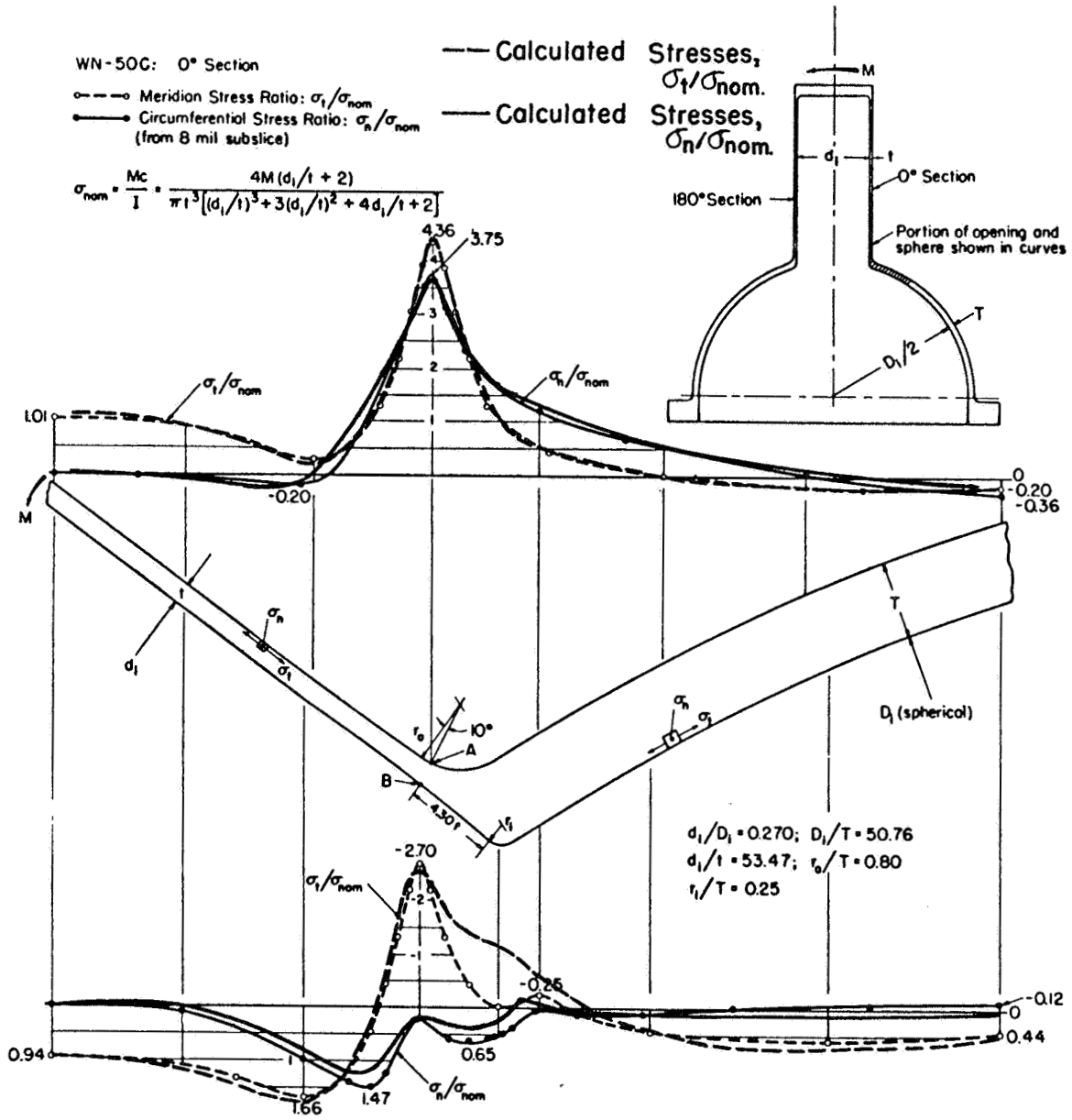


FIGURE 34. TEST DATA AND CALCULATED (KALNINS) RESULTS FOR MODEL WN-50C



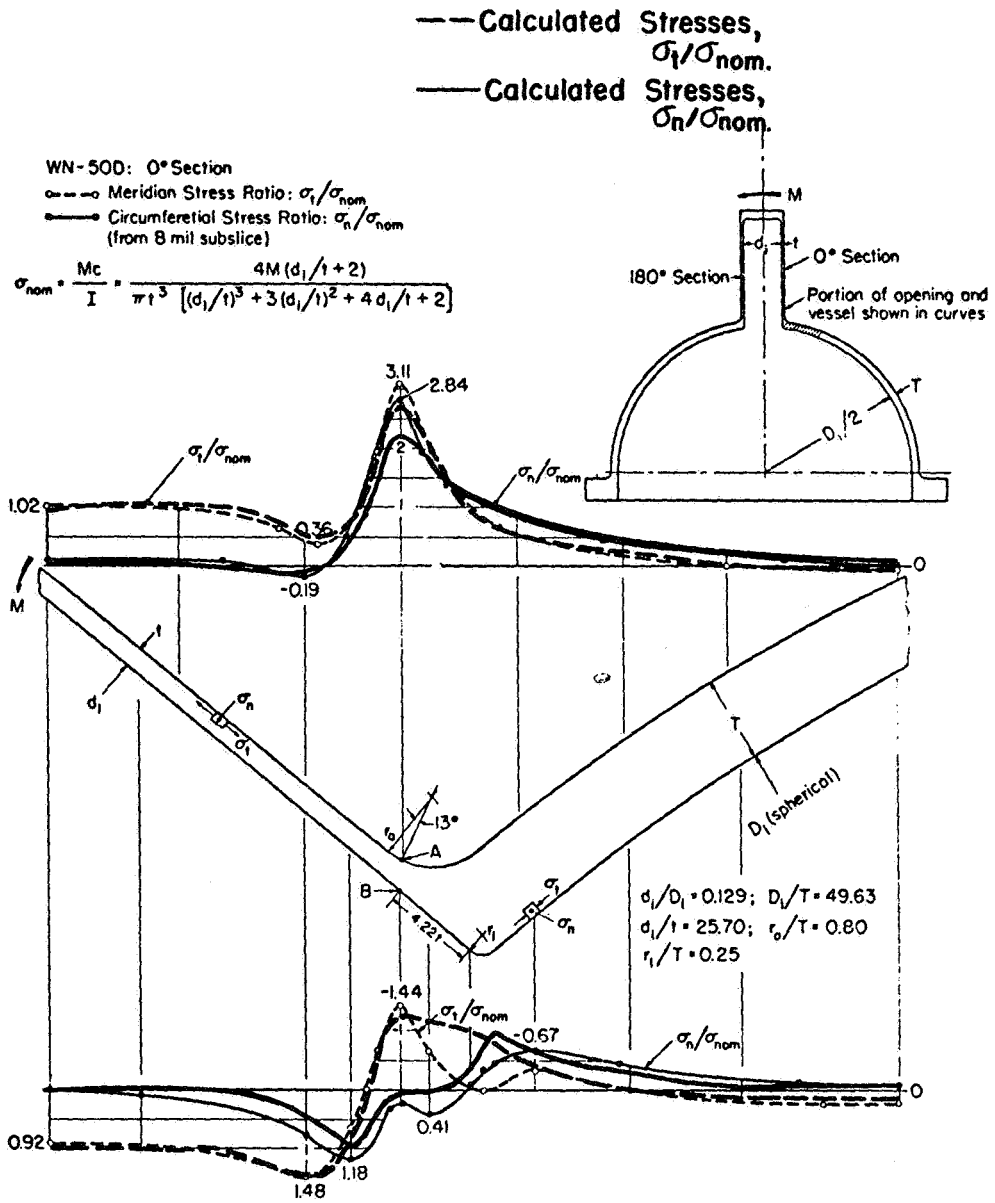


FIGURE 35. TEST DATA AND CALCULATED (KALNINS) RESULTS FOR MODEL WN-50D

Models Without a Fillet Radius

The values of  $\sigma_c/\sigma_m$  shown in Table 16 for the two ORNL models is informative mainly in illustrating that using very small strain gages placed very close to points of maximum theoretical stress still may give measured stresses significantly less than the theoretical (and probably actual) maximum stress.

Stress-location profiles are shown in Figures 36 through 43 for these two models. The theoretical data was computed using Kalnins' program; presumably either Bijlaard's analysis or the CERL program would give essentially the same results. The same assumptions were made in plotting this data as were made and discussed previously in connection with internal pressure loading on these same two models. As in the case of pressure loading, the results from the strain gage placed on the inside of the nozzle at the mid-surface of the sphere agree well with the calculated  $\sigma_n$  at the mid-wall of the sphere. Also, as in the case of pressure loading, all other test results agree quite well with the theory except for the tangential stress on the outside surface of the sphere.

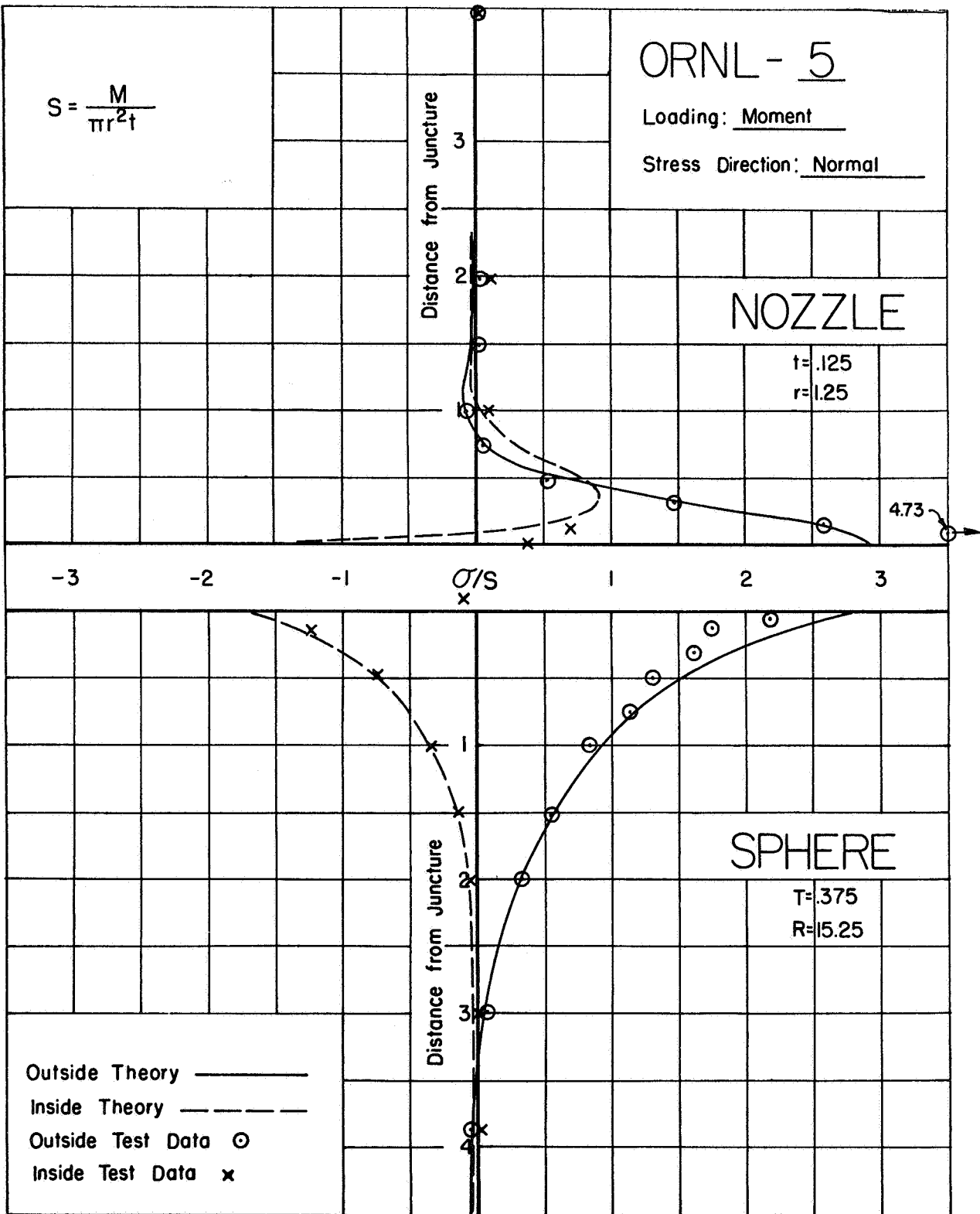


FIGURE 36. NORMAL STRESSES IN MODEL ORNL-5, MOMENT LOADING

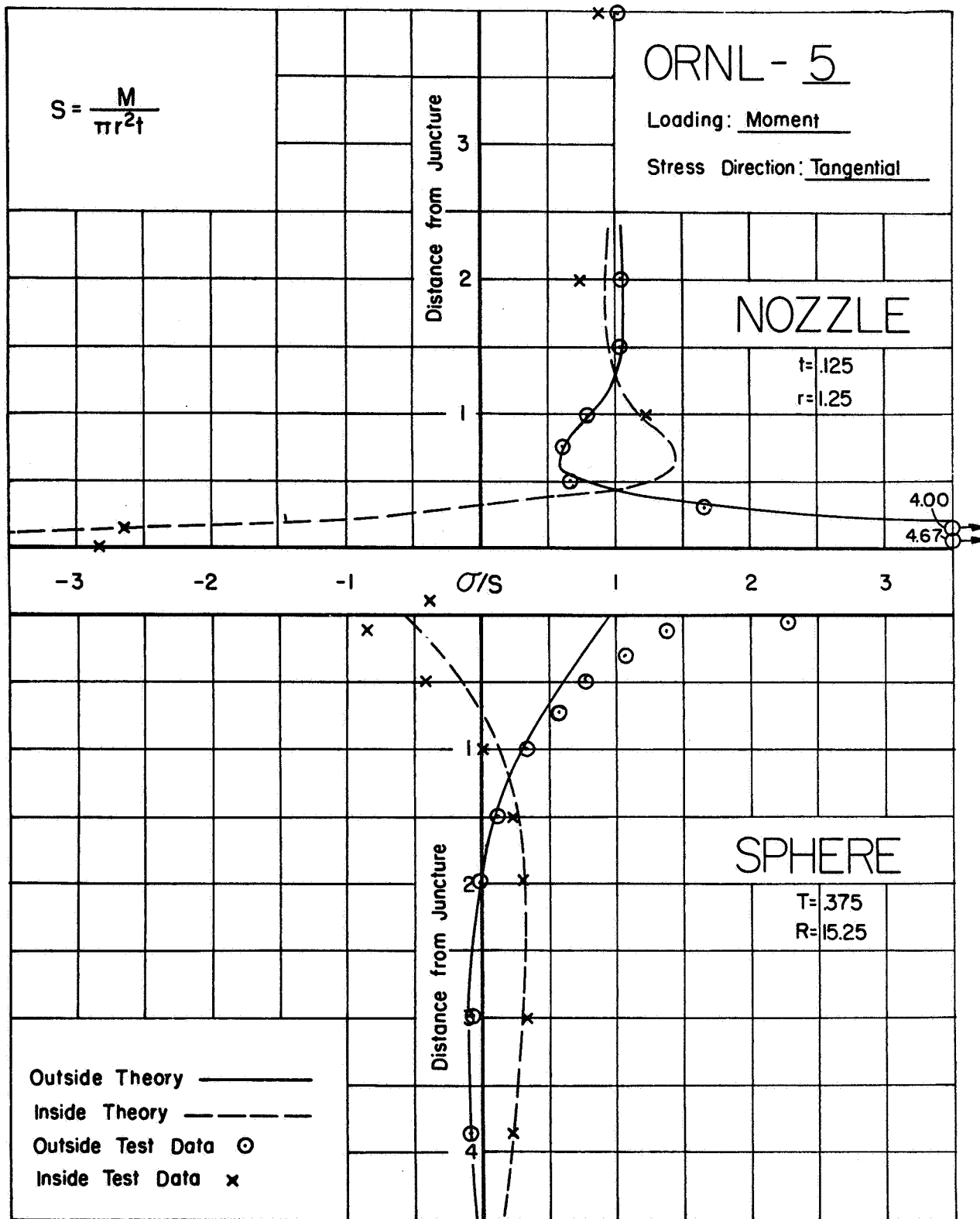


FIGURE 37. TANGENTIAL STRESSES IN MODEL ORNL-5, MOMENT LOADING

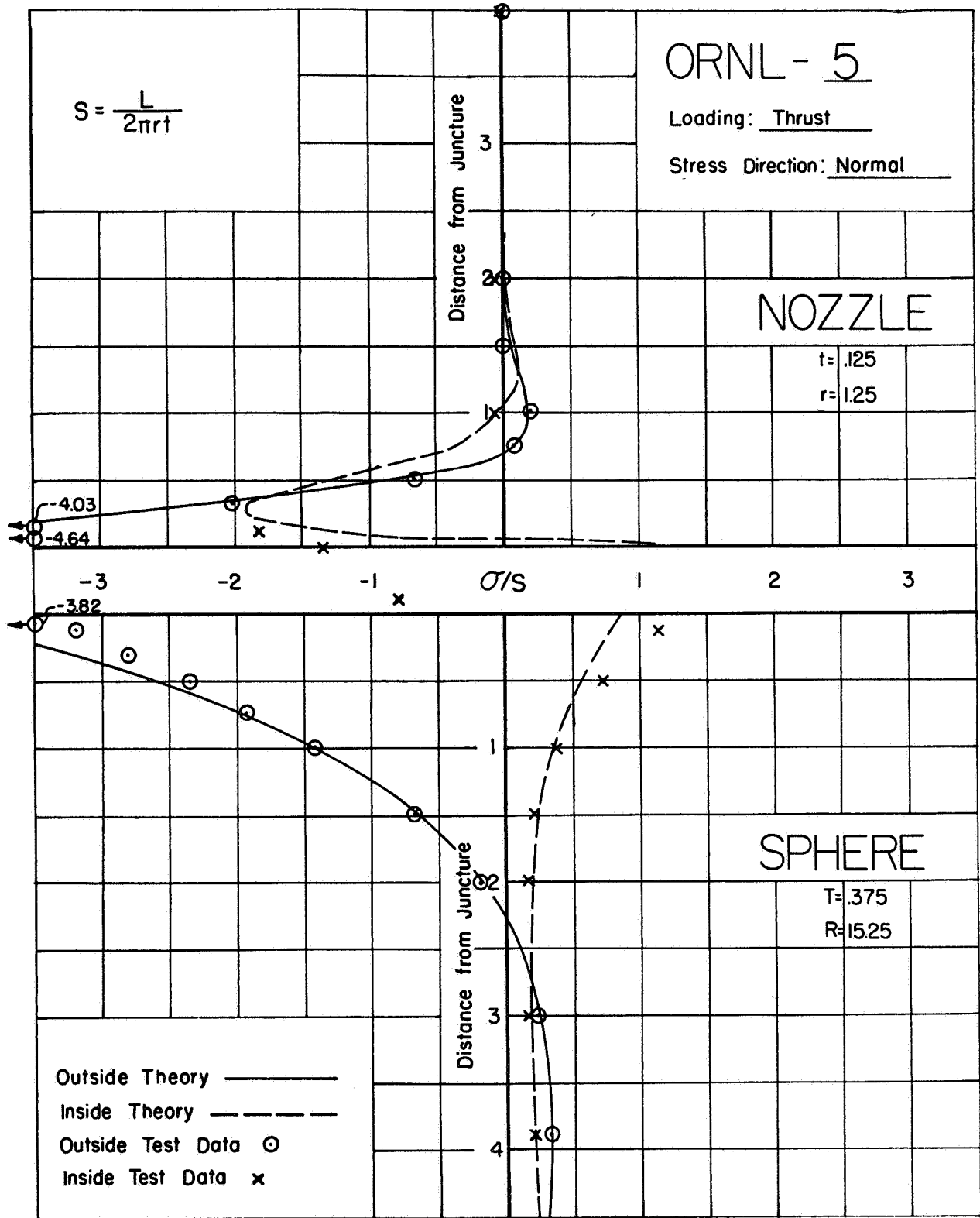


FIGURE 38. NORMAL STRESSES IN MODEL ORNL-5, THRUST LOADING

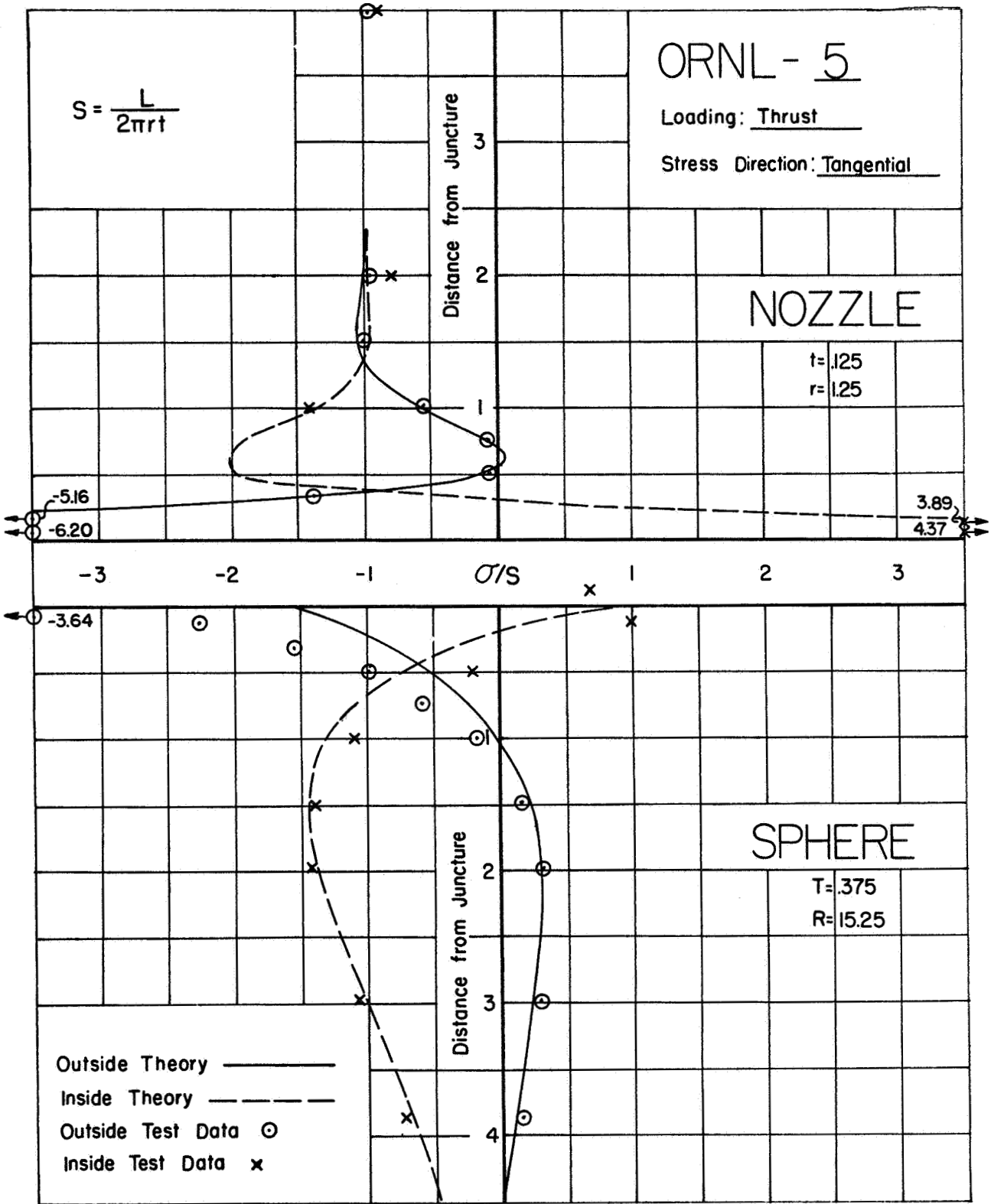


FIGURE 39. TANGENTIAL STRESSES IN MODEL ORNL-5, THRUST LOADING

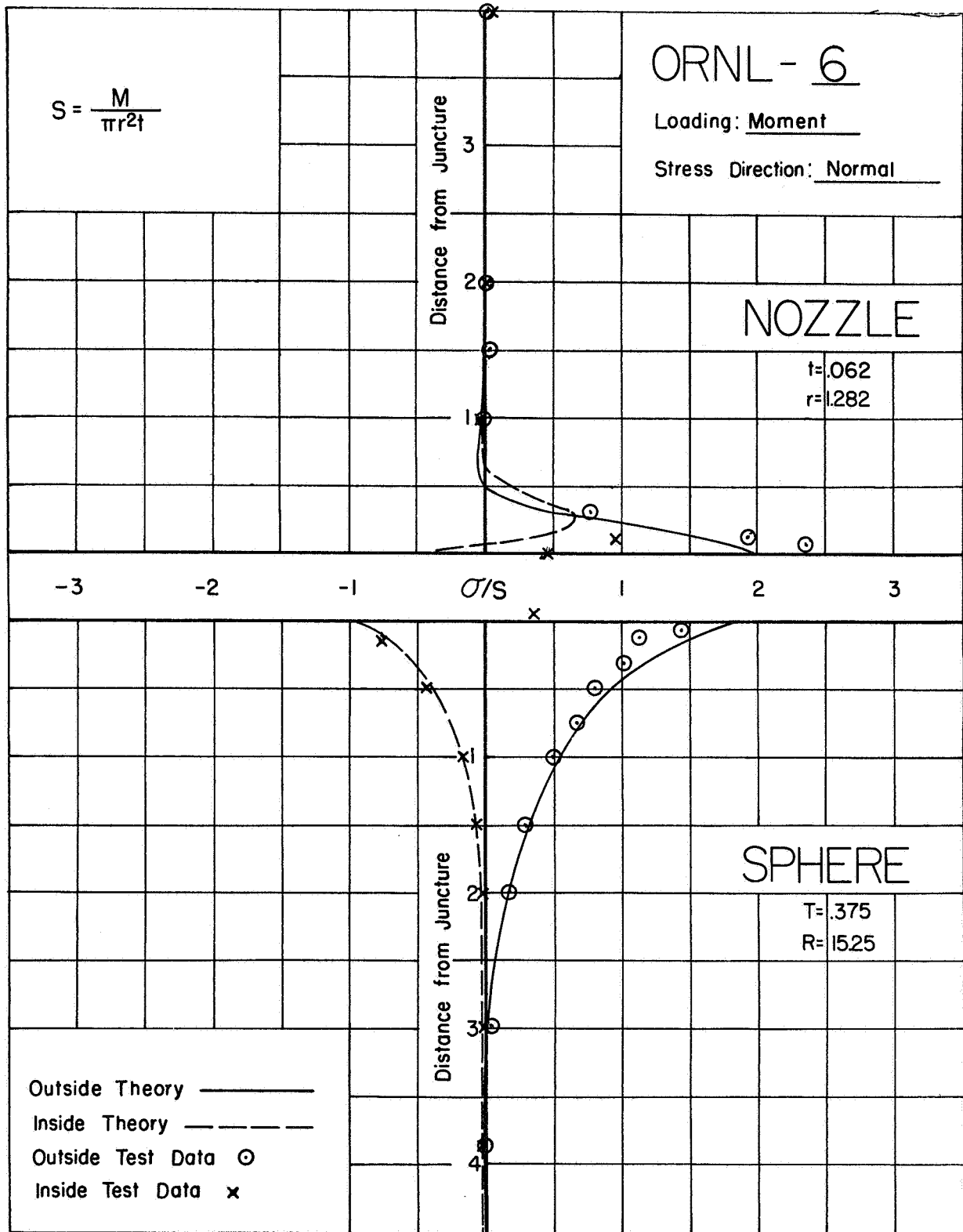


FIGURE 40. NORMAL STRESSES IN MODEL ORNL-6, MOMENT LOADING

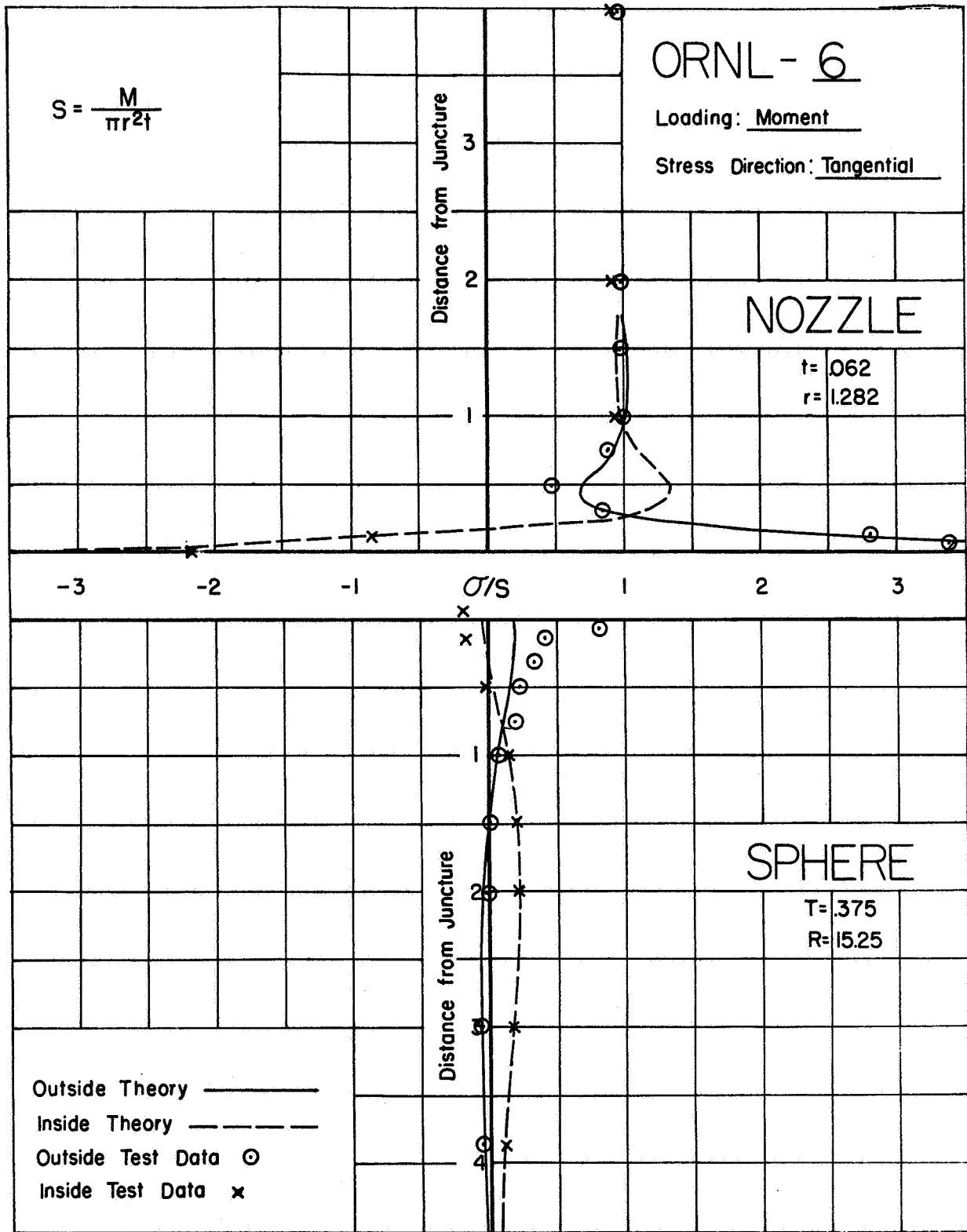


FIGURE 41. TANGENTIAL STRESSES IN MODEL ORNL-6, MOMENT LOADING



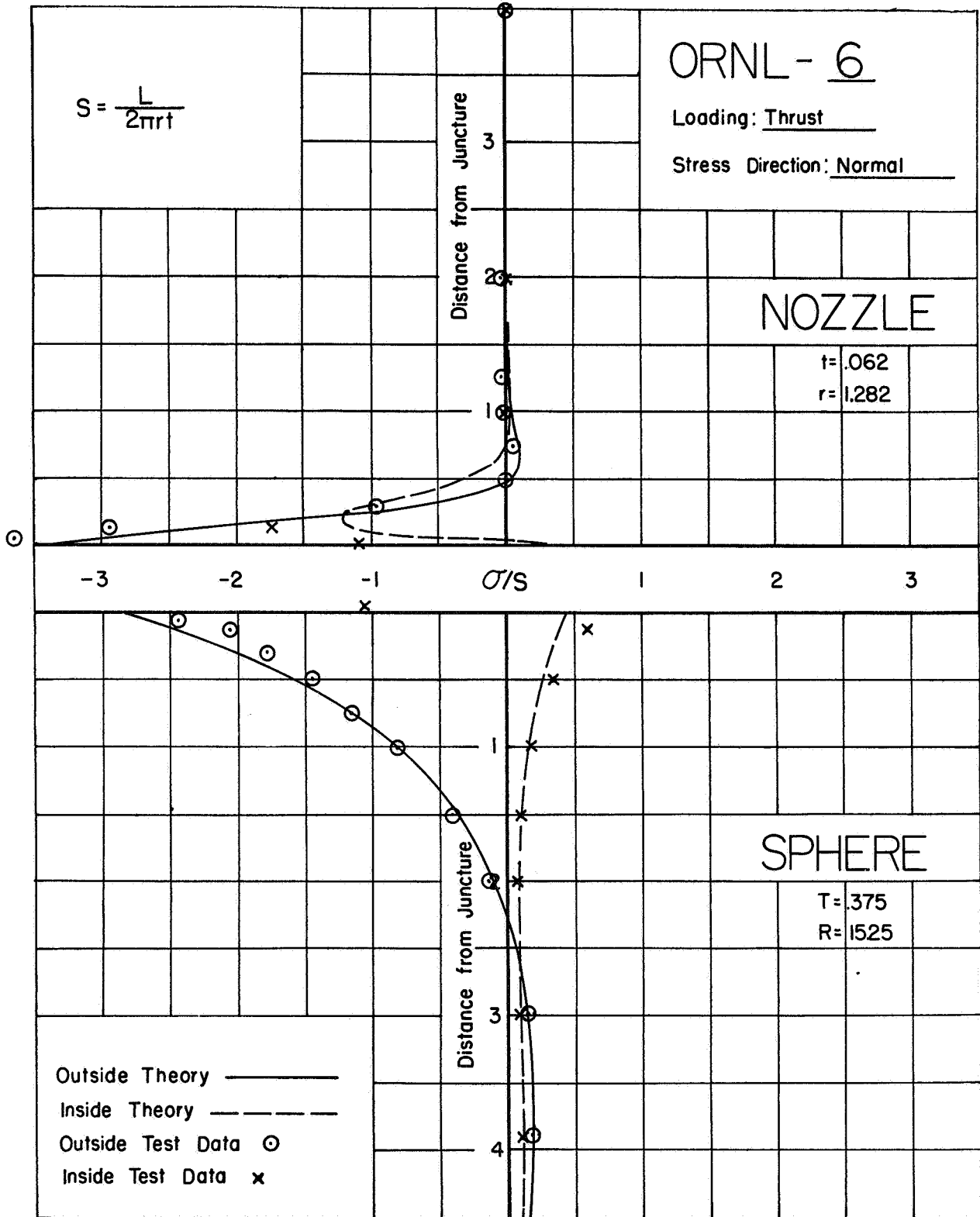


FIGURE 42. NORMAL STRESSES IN MODEL ORNL-6, THRUST LOADING

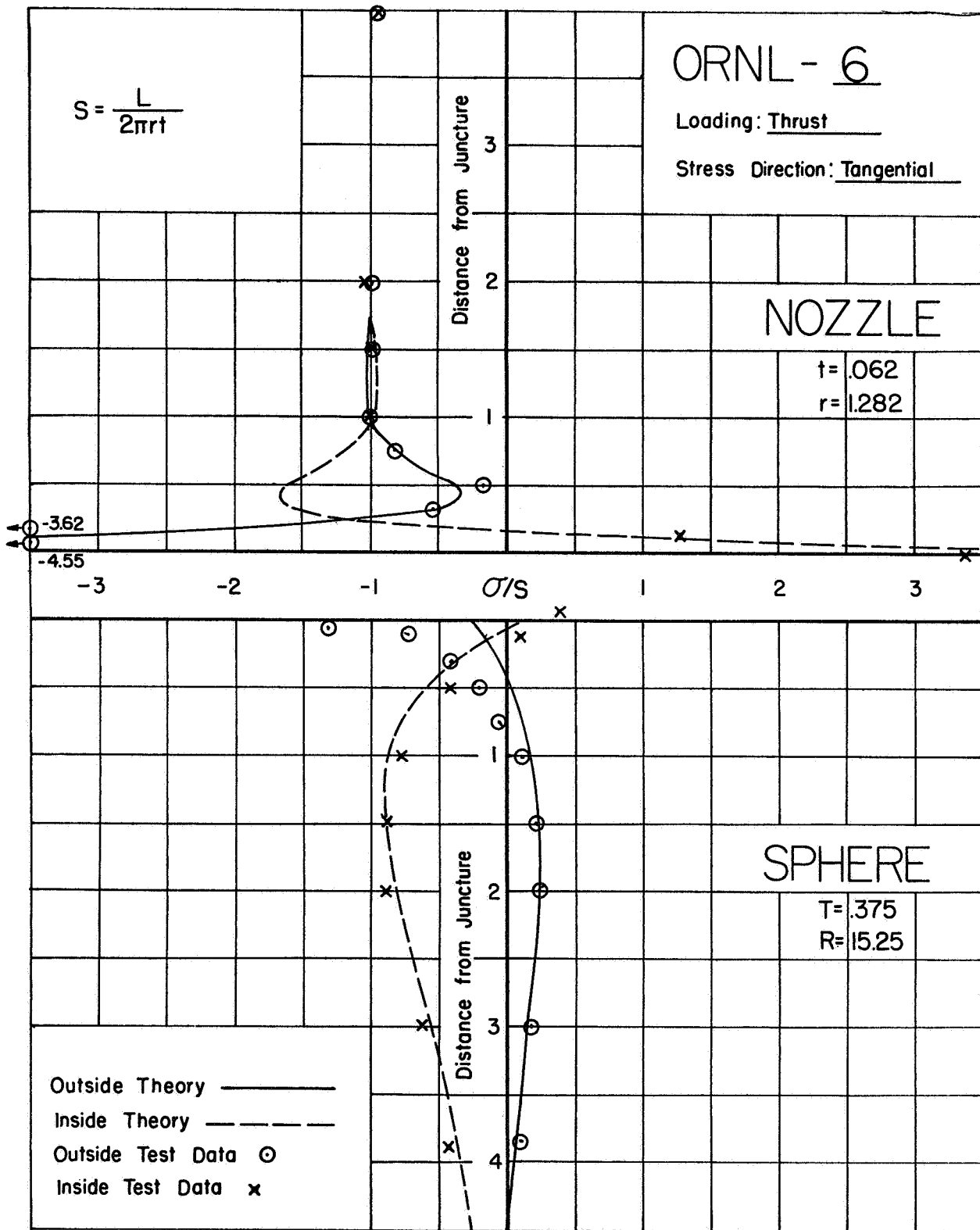


FIGURE 43. TANGENTIAL STRESSES IN MODEL ORNL-6, THRUST LOADING

Fabricated Models with Local Reinforcing

The six models tested are described in detail in Reference (28). The models are generally described in the following tabulation.

<u>Model No.</u>	<u>Type of Model</u>
1	Hemispherical head; 36" radius, 0.90" wall. Nozzle; 3.39" radius, 0.77" wall.
2	Flanged and Dished Head; 35" radius in center, 0.77" wall. Nozzle; 3.39" radius, 0.78" wall.
3	Flanged and Dished Head; 30" radius in center, 0.77" wall. Nozzle; 3.50" radius, 0.55" wall.
4	Flanged and Dished Head; 35" radius in center, 0.77" wall. Nozzle; 3.64" radius, 0.27" wall.
5	Flanged and Dished Head; 30" radius in center; 1.63" wall. Nozzle; 3.38" radius, 0.77" wall.
6	This model was made by cutting out the central part of Model Number 5 at about 15" diameter and inserting it into the outer portion of Model Number 4. The mid-walls of the two pieces were aligned and apparently a linear taper was formed on the outer ~1.4" of periphery of the section from Model Number 5.

A single nozzle was welded to the center of each head with a fillet weld inside and out. Legs of the fillet weld were 3/4". The nozzle protruded inward approximately 1" inside the inside surface of the heads.

These tests are particularly valuable in that they represent the only tests in which nozzle were tested in other than hemispherical heads. It has been assumed that the theory and test data for nozzles in spheres can be applied to nozzles in heads provided only that the local radius of curvature is essentially constant near the nozzle, i.e., for a distance of about  $\sqrt{DT}$  from the nozzle. These tests on flanged and dished heads give some experimental confirmation of this assumption.

Stresses in the Heads. The tests by Dally<sup>(28)</sup> were run, in part, for comparison with Bijlaard's computed results. At that time, interest was directed towards stresses in the heads. Dally shows detailed comparisons of test results with theory for stresses in the heads. As indicated earlier, Bijlaard's analysis, the CERL computer program, and Kalnins' computer program (as a two piece shell theory) all give practically the same results for externally protruding nozzles. Accordingly, detailed comparisons of results for stresses in the heads are not repeated herein, except for Model Number 6. Table 16 shows that the ratios of maximum calculated to measured stresses in the heads range from 1.5 to 2.8. The reasons that these ratios are significantly greater than unity are:

- (1) The fillet welds and inward protruberance of the nozzles provided a substantial amount of reinforcing as shown by the column in Table 16 headed " $A_a/d_i T$ ".
- (2) The strain gage on the head surface closest to the nozzle (at which the maximum measured stress occurred) was 1" away from the nozzle.

Away from the nozzle-head juncture, however, fairly good correlation between theory and test data was obtained, as discussed by Dally.

Model Number 6 includes results for stresses at the transition between the pad and the head. As discussed previously, juncture details between reinforcing and the nozzle or head is important since maximum stresses may occur at the reinforcing juncture. In Model Number 6, maximum measured stresses in the head did occur at the pad-head transition for both moment and thrust loading. Details of the transition are not known, however, apparently it consisted of a linear taper between the pad thickness of 1.63 to the head thickness of 0.77", starting at a radius of about 5.9" and extending to a radius of about 7.3". Calculated stresses for this model, using Kalnins' program, are shown in Figures 44 thru 47, along with measured stresses. Calculated stresses are different than Dally's calculated results in that the tapered transition sections are calculated as such using Kalnins program, rather than as a step change in thickness as assumed by Dally. For moment loading, comparison of test data with theory is about as expected, i.e., a suppression of normal stresses near the juncture because of the local reinforcing and some increase in bending because the local reinforcing constrains

most of the bending to take place in the sphere. The same general trends occur for thrust loading, however, the increased tangential bending is significantly higher than theory; the measured tangential mean stress is about that given by theory. It should be noted that the foundation length of the head ( $\sim \sqrt{RT}$ ) is  $\sim 7.3''$  for the pad section,  $\sim 5''$  for the outer section. Accordingly, the pad and transition section are well within the region influenced by the nozzle-head juncture details. The measured stresses may have been influenced by the head radius change at the transition section; in the pad section the radius was  $30''$ , in the outer section the radius was  $35''$ ;  $32.5''$  radius was used in the calculations. Incidentally, the transition shown in Figure 44 would not be acceptable in ASME pressure vessel designs because the transition length is considerably less than four times the change in thickness.

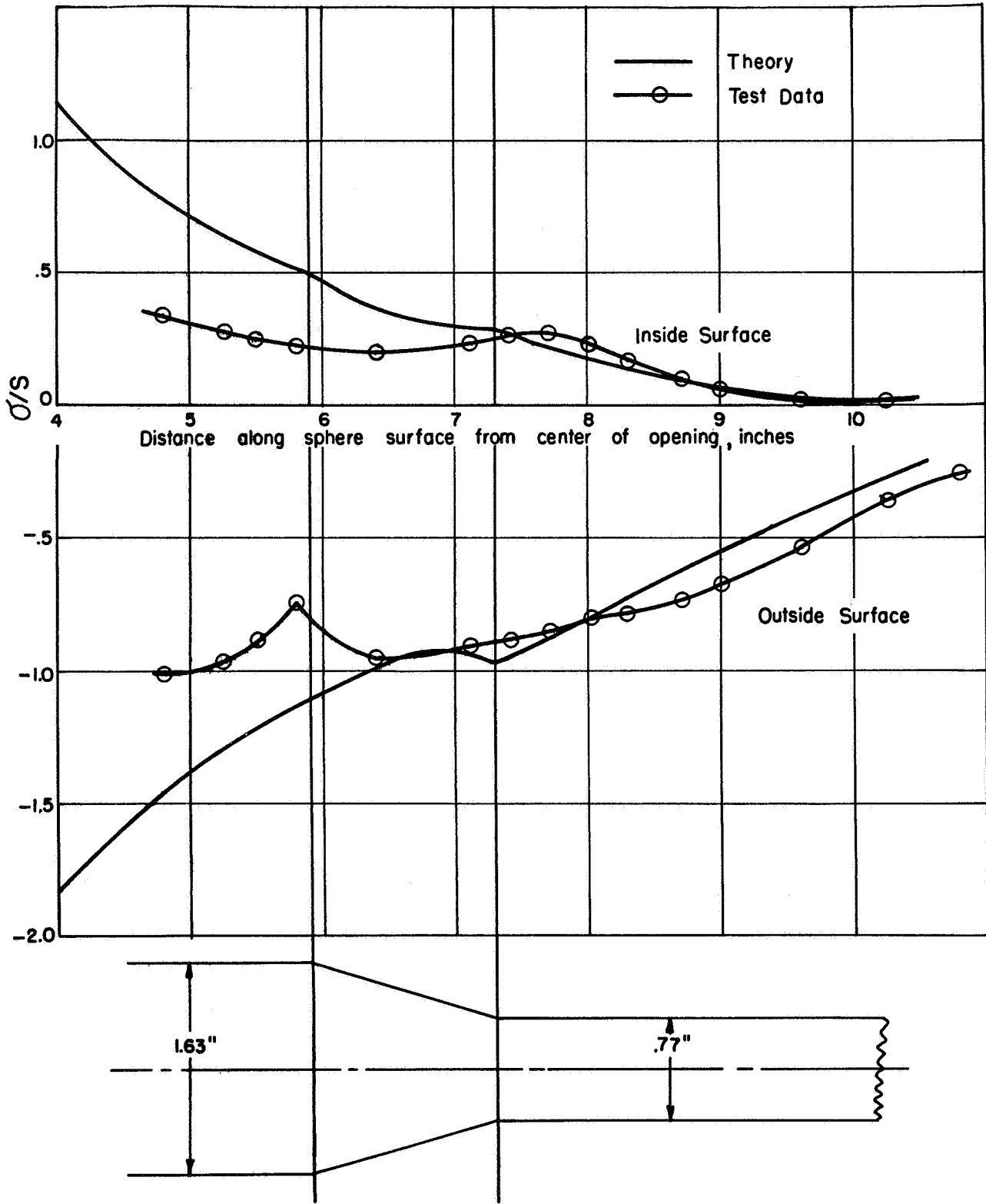


FIGURE 44. NORMAL STRESSES ON HEAD, DALLY MODEL 6, MOMENT LOADING

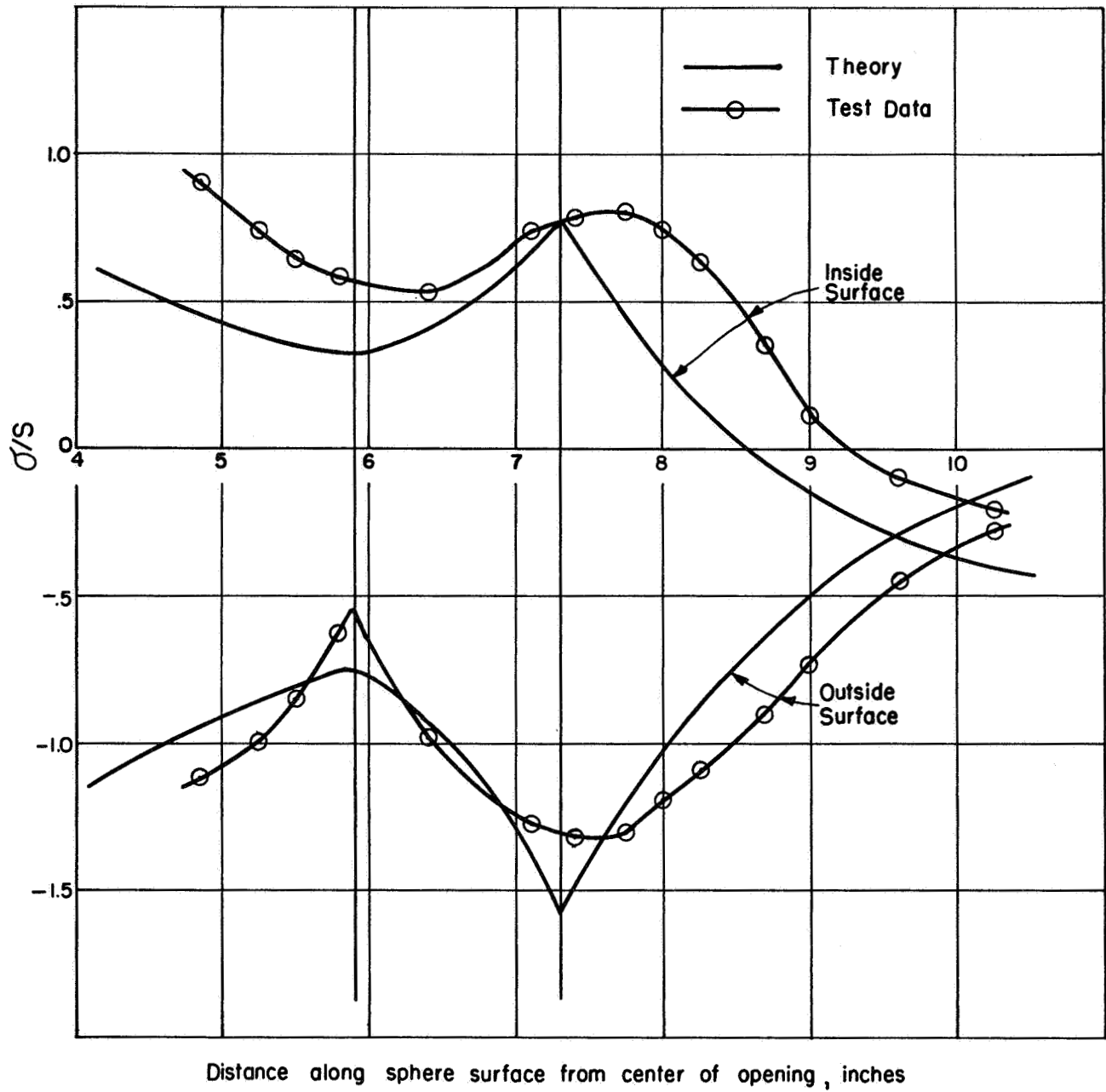


FIGURE 45. TANGENTIAL STRESSES ON HEAD, DALLY MODEL 6, MOMENT LOADING

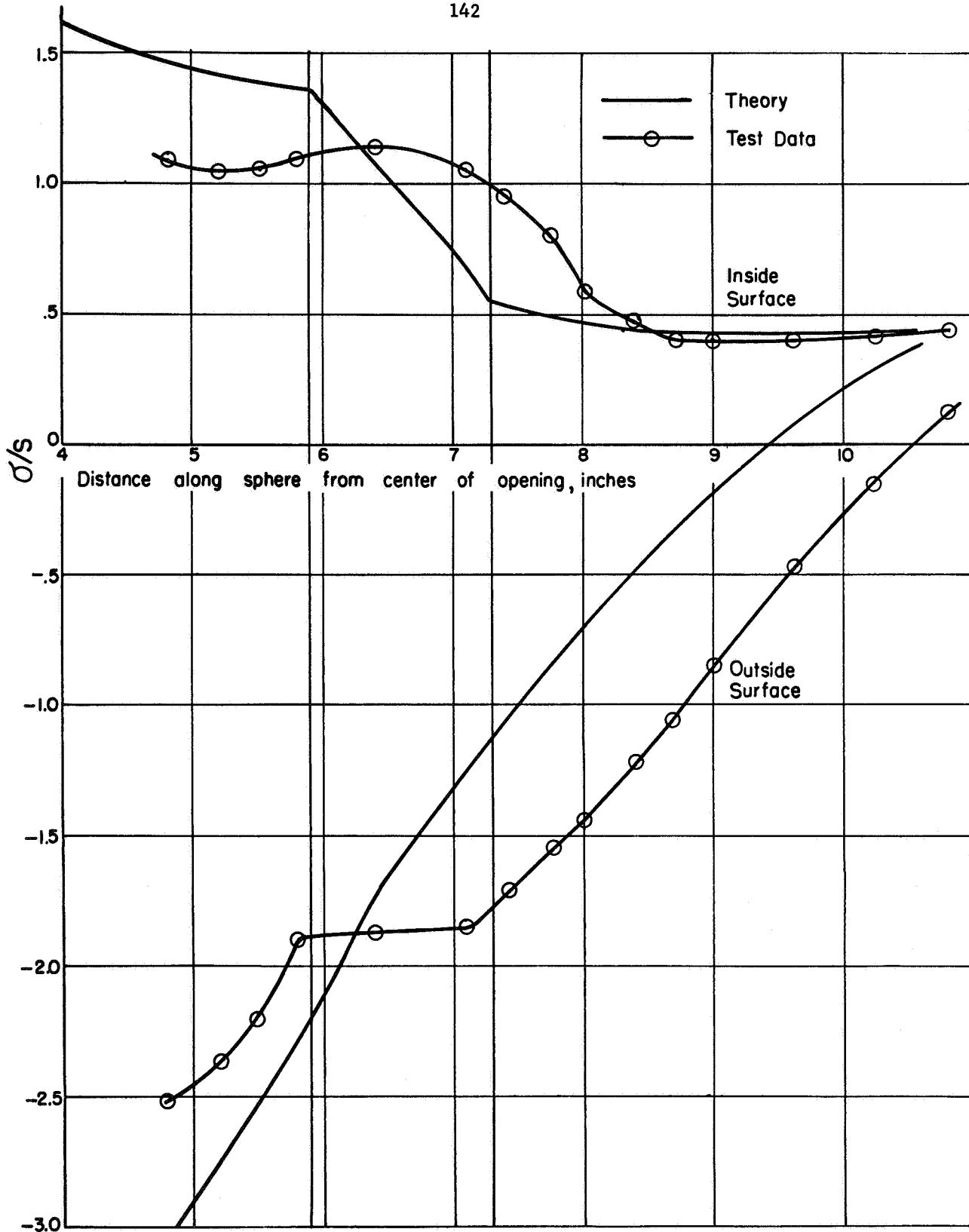


FIGURE 46. NORMAL STRESSES ON HEAD, DALLY MODEL 6, THRUST LOADING



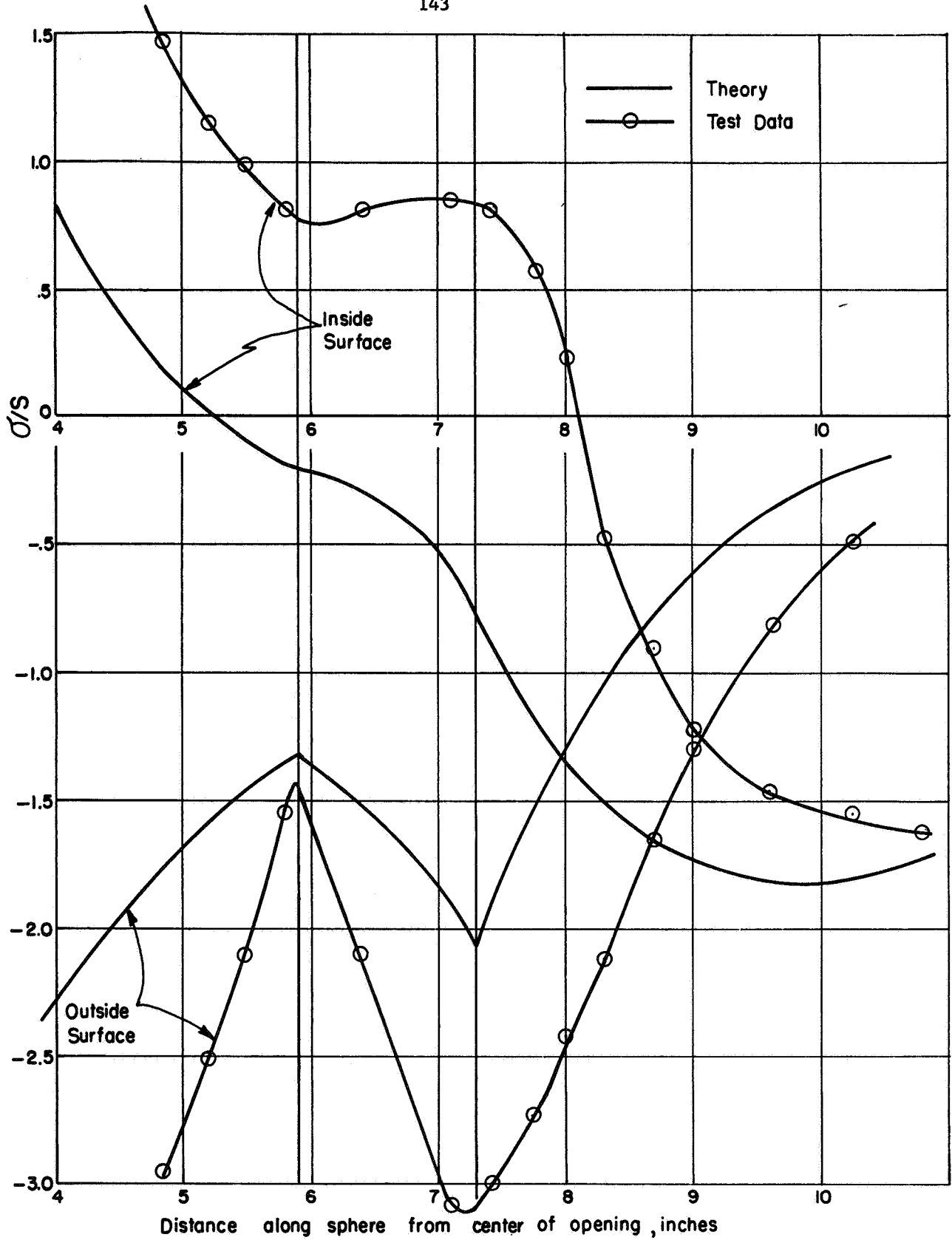


FIGURE 47. TANGENTIAL STRESSES ON HEAD, DALLY MODEL 6,  
\* THRUST LOADING

Stresses in Nozzles. Table 16 shows that the ratio of maximum calculated to measured stresses in the nozzle range from 3.4 to 7.9. Theoretically, maximum stresses occur in the nozzle for all models except Number 2. Measured stresses, however, were larger in the head than in the nozzle for Models 1, 2, and 3 and about the same for Models 4, 5, and 6. The reasons for the calculated-to-measured stress ratio being greater than unity include those discussed previously with regard to stresses in the head. In addition, and more important, the outside fillet weld covers a substantial part of the foundation length of the nozzles. Stresses were measured at the outside fillet weld only on Model Number 1; for which model these stresses were the highest measured stresses on the nozzle. It seems reasonably certain that stresses on the outside fillet weld would have also been the highest stress on the nozzle for all the other models. Also, the nozzles used in these tests were relatively short, the flanges on the nozzles may have reduced the magnitude of the stresses as compared to otherwise equal but longer nozzles.

Figures 48 thru 51 show calculated measured stresses in the nozzles of models 1 and 2 which are typical of all 6 models. Agreement between theory and test data is similar to that obtained in the heads, i.e., the test data roughly confirm the validity of the theory at locations away from the (significantly reinforced) nozzle-to-head intersection.

It is pertinent to note that all six models had nozzles with wall thickness from 2 to 5 times that required for pressure; i.e.,  $s/S \approx 0.5$  to 0.2. Nevertheless, the stresses at the juncture of the nozzle with the fillet weld might be sufficient to cause fatigue failure in the nozzle rather than in the head if these models were subjected to cyclic external loads to produce fatigue failures.

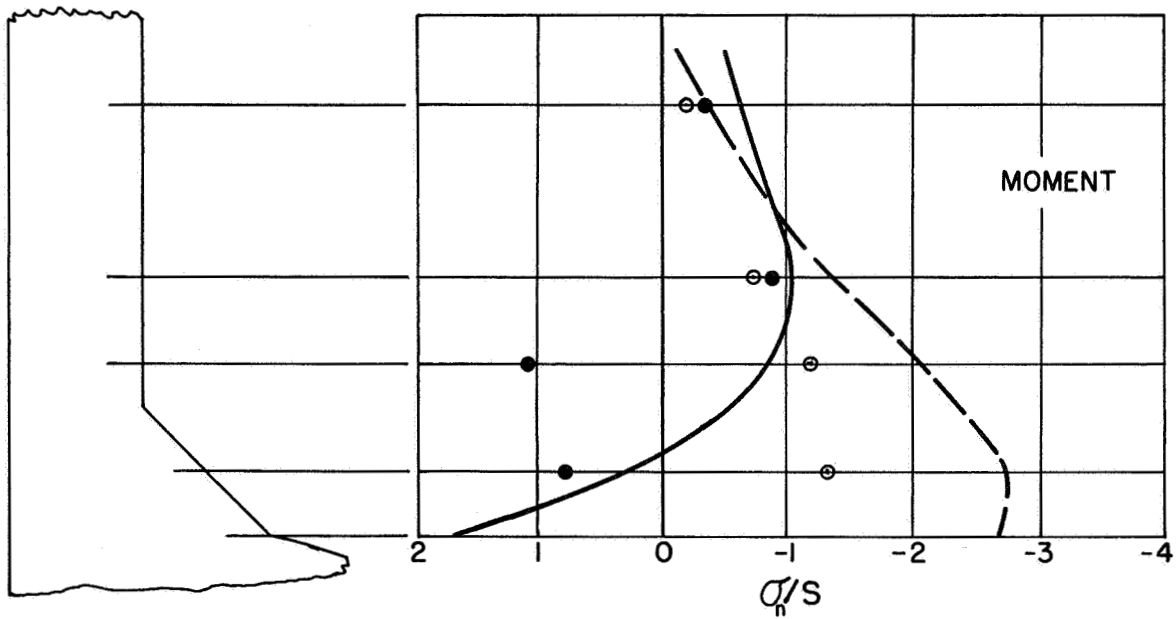
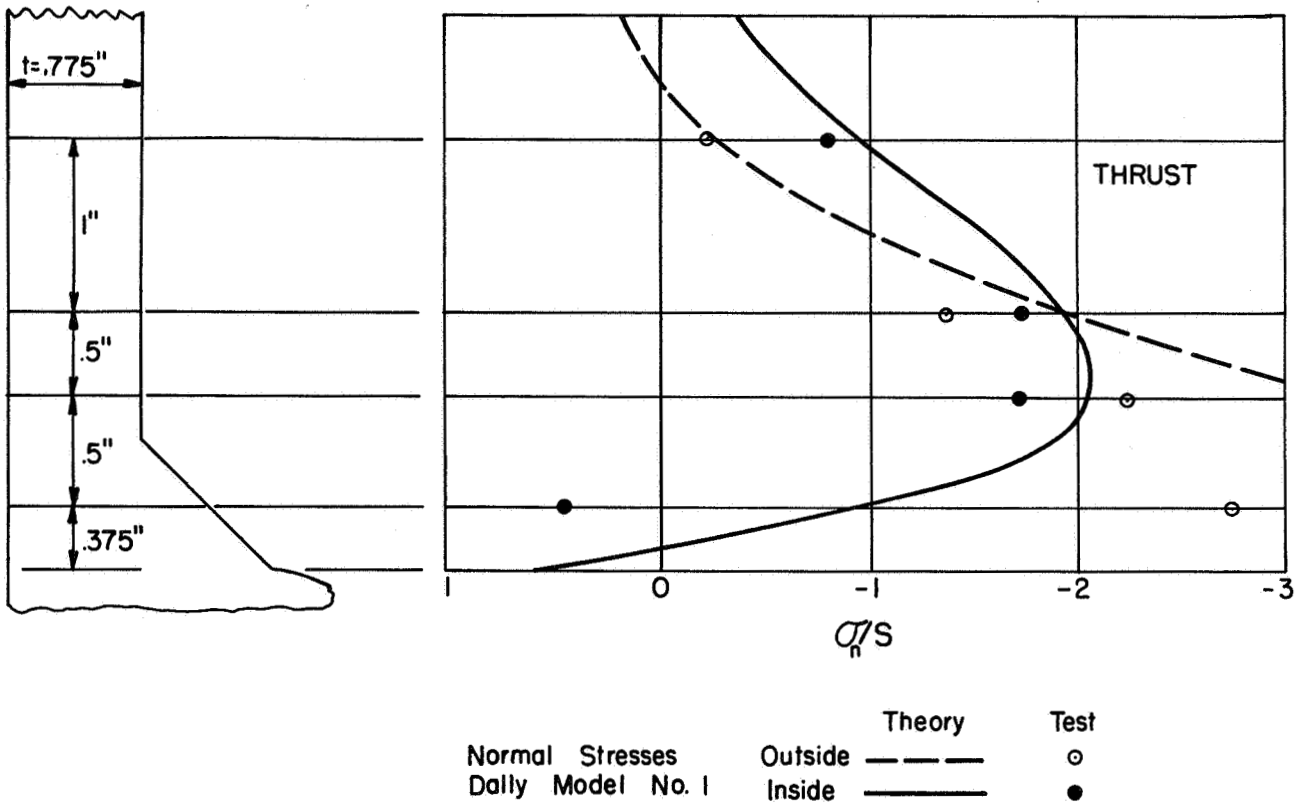
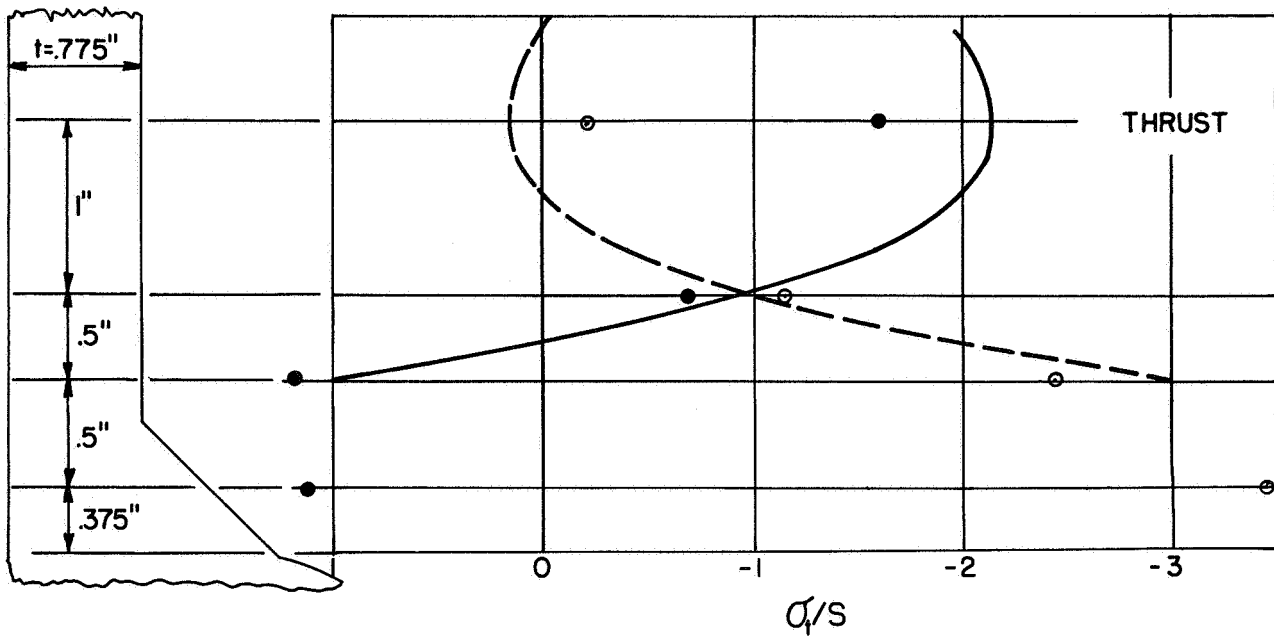


FIGURE 48. NORMAL STRESSES ON NOZZLE, DAILY MODEL 1, MOMENT AND THRUST LOADING



		Theory	Test
Tangential Stresses	Outside	- - - -	○
Dally Model No. 1	Inside	————	●

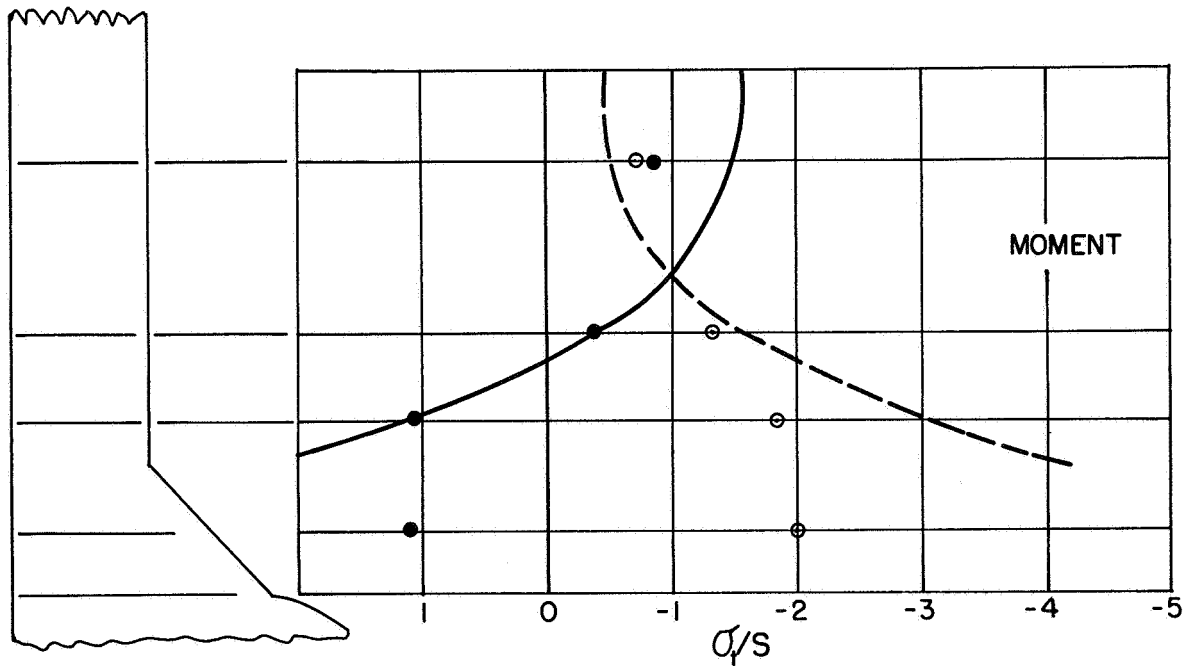
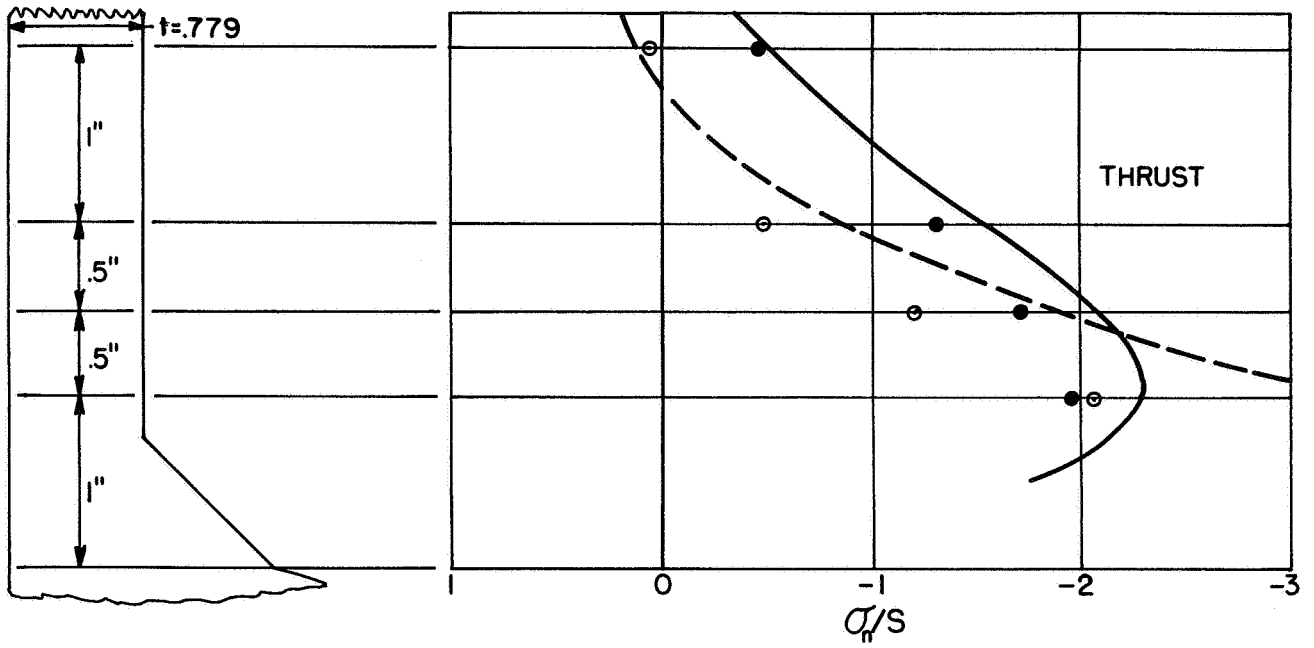


FIGURE 49. TANGENTIAL STRESSES ON NOZZLE, DALLY MODEL 1, MOMENT AND THRUST LOADING



Normal Stresses  
Dally Model No. 2

Outside	---	Theory	○
Inside	—		●

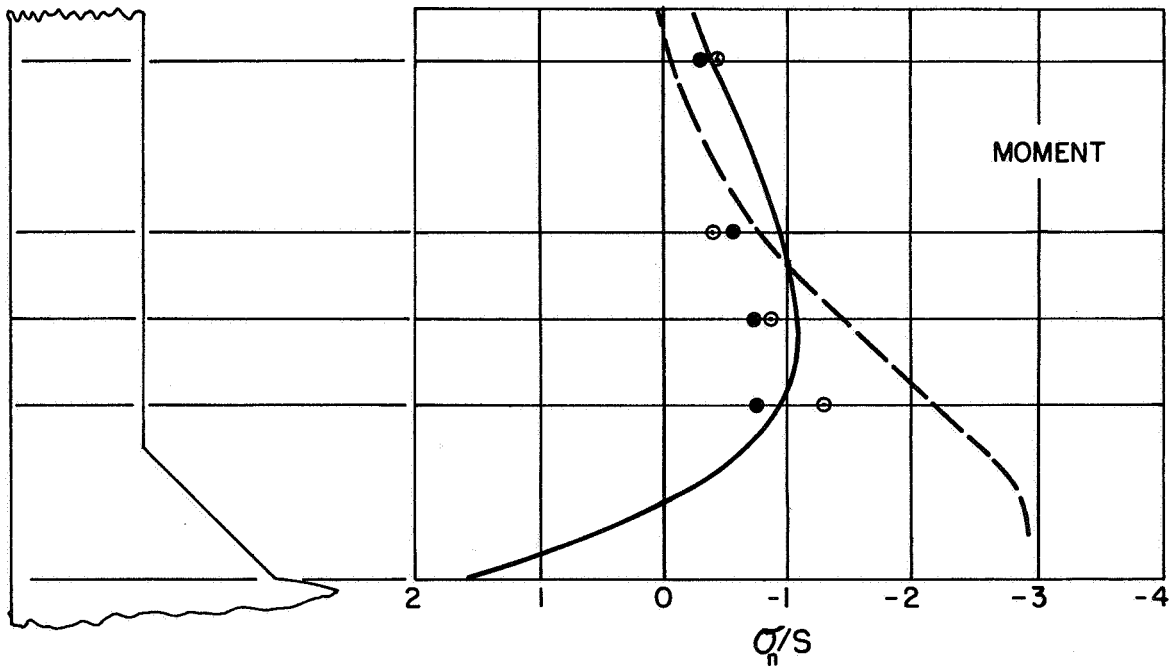
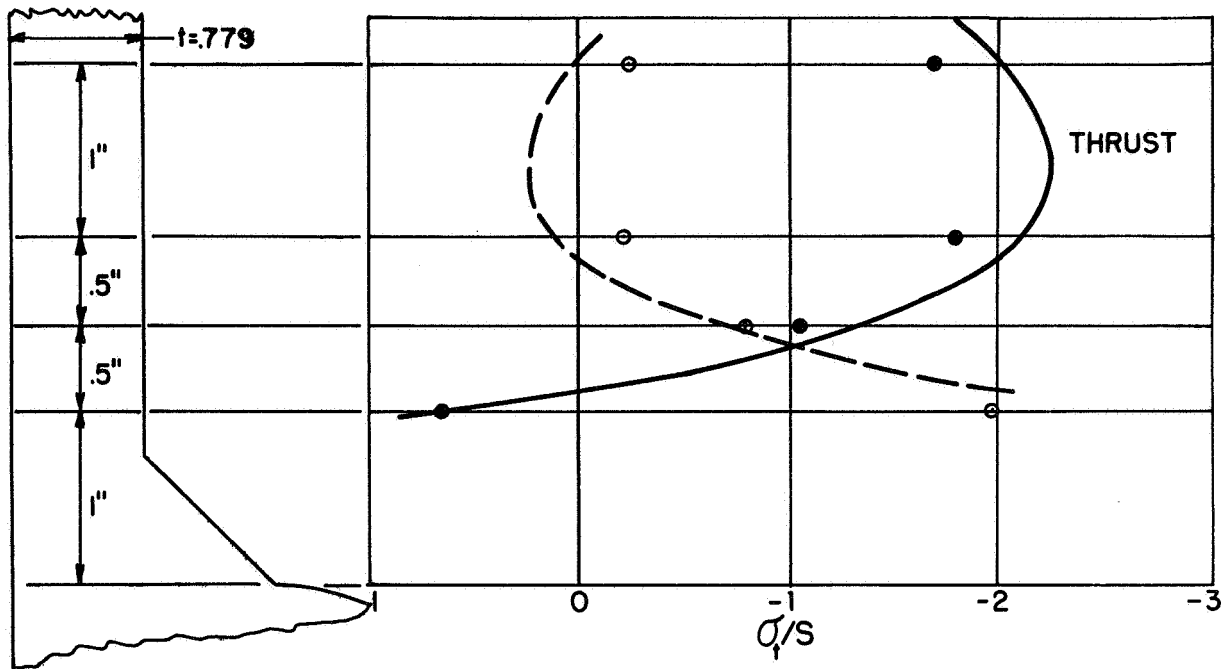


FIGURE 50. NORMAL STRESSES ON NOZZLE, DALLY MODEL 2, MOMENT AND THRUST LOADING



Tangential Stresses	Outside	Theory	Test
Dally Model No. 2	Inside	---	o
		—	•

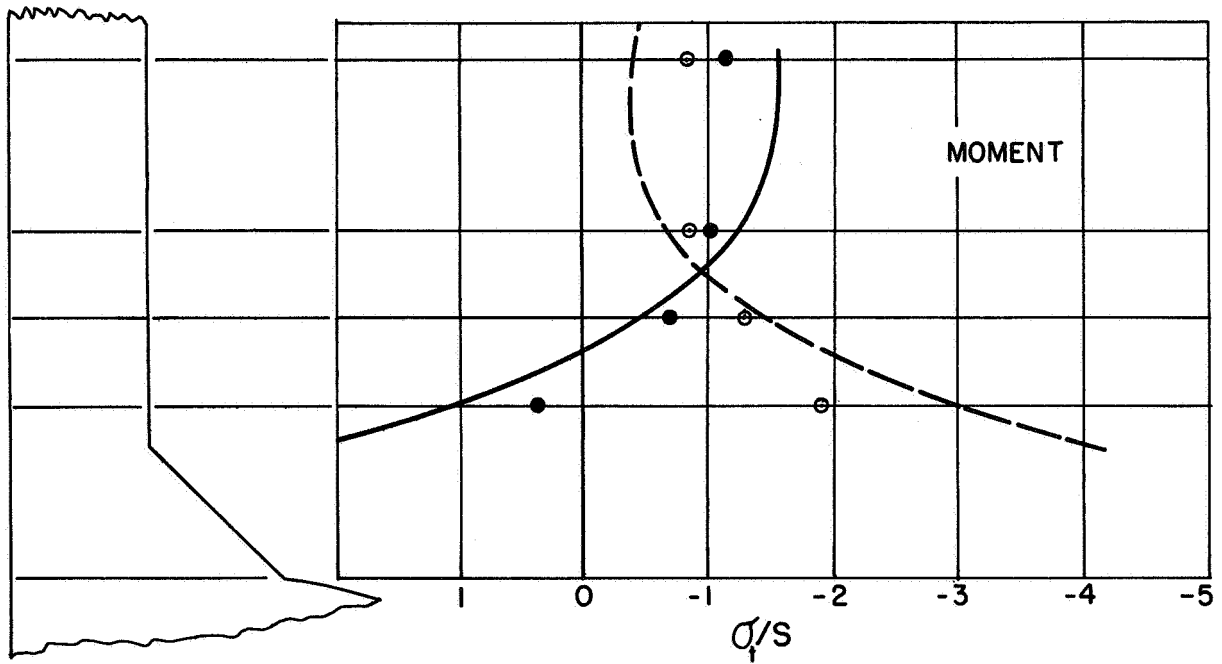


FIGURE 51. TANGENTIAL STRESSES ON NOZZLE, DALLY MODEL 2, MOMENT AND THRUST LOADING

## DISCUSSION OF RESULTS IN RELATIONSHIP TO PRESENT CODES AND PRACTICES

### Pressure Loading

#### Replacement Area, $d_i T$

Present pressure vessel and piping design codes require that the material cut out of the pressure vessel shell or pipe by an opening must be replaced by added material around the opening within a specified zone. Whether these design rules are adequate, from the standpoint of elastic stresses, depends upon the selected design stress limit. Reference (12), using a stress intensity index limit of 3.0, concludes in general that present design rules are conservative for compact reinforcing and for reinforcing placed on the nozzle within the code zone limits; however, for reinforcing placed on the head, the present code rules (except ASME Section III) may be unconservative for large  $d/D$ -ratios combined with large  $D/T$ -values.

#### ASME Section III Stress Indices

The ASME Boiler and Pressure Vessel Code, Section III, Nuclear Vessels, in Paragraph I-612(a) gives stress indices for nozzles in spherical shells and formed heads when subjected to pressure loading. The indices apply if:

- (1) The nozzle is normal to the vessel wall
- (2) The nozzle is isolated from other nozzles
- (3) The dimensional ratios are not greater than  $D/T = 100$ ,  
 $d/D = 0.5$
- (4) The nozzles are designed in accordance with the applicable rules of N-450 to N-467
- (5) The inside corner radii and outside fillet radii meet the requirements of the Nuclear Code, Figure I-613.

The requirements of Par N-450 to N-467 require that the cross sectional area cut out by the nozzle opening be replaced in a zone close to

the opening. This requirement can be met, within the scope of two-piece shell theory, by either a uniform-wall, integral pad on the sphere; by a heavy-wall nozzle, or by a combination thereof. Table 18 shows the stress indices obtained from CERL program results along with the Nuclear Code stress indices for reinforcing entirely on the sphere. This requires an integral pad thickness,  $T'$ , equal to two times the nominal sphere thickness  $T$  with nozzle thickness  $t$  such that  $Pd/2t = PD/4T$ , i.e., there is no excess thickness in the nozzle. Table 19\* shows the stress indices for reinforcing entirely on the nozzle. The nozzle wall thickness  $t'$  was determined by the equation:

$$\frac{d_i T}{2} = (t' - t) \sqrt{\frac{r_m t'}{2}} \quad (19)$$

where  $d_i$  = inside diameter of the nozzle  
 $T$  = sphere wall thickness  
 $r_m$  = mean radius of the nozzle  
 $t$  = nominal wall thickness of nozzle such that  $Pd/2t = PD/4T$   
 $t'$  = required wall thickness of nozzle to provide required area replacement,  $d_i T/2$  on each side.

Tables 18 and 19 indicate that two-piece shell theory agrees with the Nuclear Vessel Code, Par. I-612(a), in that the computed stresses are usually not higher than those given by the Code. Considering the applicable outside fillet radii requirement of the Code, i.e.,  $r_o \geq$  larger of  $t'/2$  or  $T'/2$ , for reinforcing on the nozzle (Table 19) it is probably that the fillet radii will reduce stresses to not more than the Code values throughout the range of parameters covered. For reinforcing on the sphere, however, at large  $D/T$  and  $d/D$ , it appears that stresses will be higher than the Code values. Figure 52 is a sketch of the juncture detail of a nozzle in a sphere with  $D/T = 100$ ,  $D/T' = 50$ ,  $d/D = 0.5$ ,  $r_o = T'/2$ . Also shown in Figure 52 are calculated stress values using Kalnins' program and taking into account the fillet radius. It is apparent that the fillet radius is not sufficient to bring the stresses down to the Code values, i.e., 2.8 from the calculations is somewhat higher than the 2.0 index given by the Code.

---

\* The calculations of Table 19 were limited to  $D/T$  and  $d/D$  combinations such that  $t'/T < 3$ . Larger values of  $t'/T$  are not ordinarily used in designs of nozzles in pressure vessels.



TABLE 18. COMPARISON OF NUCLEAR VESSEL CODE STRESS INDICES WITH CERL CALCULATED STRESSES, REINFORCING ON THE SPHERE

$\frac{D}{T}$ (1)	$\frac{d}{D}$	Part	$\sigma_n/S$ (2)		$\sigma_t/S$ (2)	
			Inside	Outside	Inside	Outside
20	.01	Sphere	1.0	1.0	0	0
		Nozzle	1.1	1.2	.2	.8
	.10	Sphere	.9	1.3	0	0
		Nozzle	1.0	1.3	0	1.0
	.25	Sphere	.8	1.6	0	.1
		Nozzle	.9	1.6	-.8	1.8
.50	Sphere	1.0	1.7	-.2	.6	
	Nozzle	.9	1.8	-1.1	2.1	
50	.01	Sphere	1.0	1.0	0	0
		Nozzle	1.1	1.2	.2	.8
	.10	Sphere	.9	1.5	0	0
		Nozzle	1.0	1.5	-.3	1.3
	.25	Sphere	1.0	2.0	-.1	.2
		Nozzle	.9	2.2	-1.7	2.8
.50	Sphere	1.2	2.2	-.4	.8	
	Nozzle	1.0	2.5	-2.0	3.0	
100	.01	Sphere	1.0	1.0	0	0
		Nozzle	1.0	1.2	.2	.8
	.10	Sphere	.9	1.7	0	0
		Nozzle	1.0	1.8	.9	1.9
	.25	Sphere	1.3	2.4	-.1	.3
		Nozzle	.9	3.0	-3.0	4.0
.50	Sphere	1.6	2.7	-.7	1.2	
	Nozzle	1.0	3.2	-3.2	4.2	

Nuclear Vessel Code

$\frac{D}{T}$	$\frac{d}{D}$	$\sigma_n/S$		$\sigma_t/S$	
		Inside Corner	Outside Corner	Inside Corner	Outside Corner
$\leq 100$	$\leq .5$	2.0	2.0	-0.2	2.0

(1)  $D/T' = 0.5 (D/T)$  where  $T'$  = thickness of integral pad reinforcing on the sphere

(2)  $S = PD/4T$ , not  $PD/4T'$ .

TABLE 19. COMPARISON OF NUCLEAR VESSEL CODE STRESS INDICES WITH CERL CALCULATED STRESSES, REINFORCING ON THE NOZZLE

$\frac{D}{T}$	$\frac{d}{D}$	$\frac{t'}{T}$ (1)	Part	$\sigma_n/S$		$\sigma_t/S$	
				Inside	Outside	Inside	Outside
20	.01	.180	Sphere	1.8	1.8	.2	.3
			Nozzle	.9	2.3	-2.4	2.5
	.1	1.08	Sphere	1.7	1.3	-.2	1.2
			Nozzle	1.1	1.4	-.5	.7
	.25	1.91	Sphere	1.4	1.4	-.2	1.4
			Nozzle	1.0	1.2	-.1	.4
.50	2.88	Sphere	1.3	1.8	-.4	1.9	
		Nozzle	1.1	1.2	0	.3	
50	.01	.385	Sphere	1.9	1.3	.1	.7
			Nozzle	.8	2.0	-2.0	2.1
	.05	1.19	Sphere	1.6	1.1	-.1	1.1
			Nozzle	1.0	1.2	-.5	.5
	.1	1.76	Sphere	1.0	1.2	.2	1.3
			Nozzle	.8	.9	-.1	.2
.25	2.82	Sphere	1.2	1.6	-.2	1.6	
		Nozzle	1.1	1.2	0	.2	
100	.01	.65	Sphere	2.0	1.0	.1	1.1
			Nozzle	.9	1.5	-1.2	1.2
	.025	1.17	Sphere	1.7	1.0	.1	1.1
			Nozzle	.9	1.1	-.4	.4
	.05	1.70	Sphere	1.4	1.1	.2	1.0
			Nozzle	.9	1.1	-.1	.2
.10	2.40	Sphere	1.3	1.3	.2	1.2	
		Nozzle	1.1	1.1	-.1	.2	

Nuclear Vessel Code

$\frac{D}{T}$	$\frac{d}{D}$	$\sigma_n/S$		$\sigma_t/S$	
		Inside Corner	Outside Corner	Inside Corner	Outside Corner
$\leq 100$	$\leq .5$	2.0	2.0	-0.2	2.0

- (1)  $t'$  = wall thickness of nozzle to provide required reinforcing area of  $d.T$ . Calculations are limited to  $D/T$  and  $d/D$  combinations such that  $t'/T < 3^1$ . Larger values of  $t'/T$  are not ordinarily used in designs of nozzles in pressure vessels.

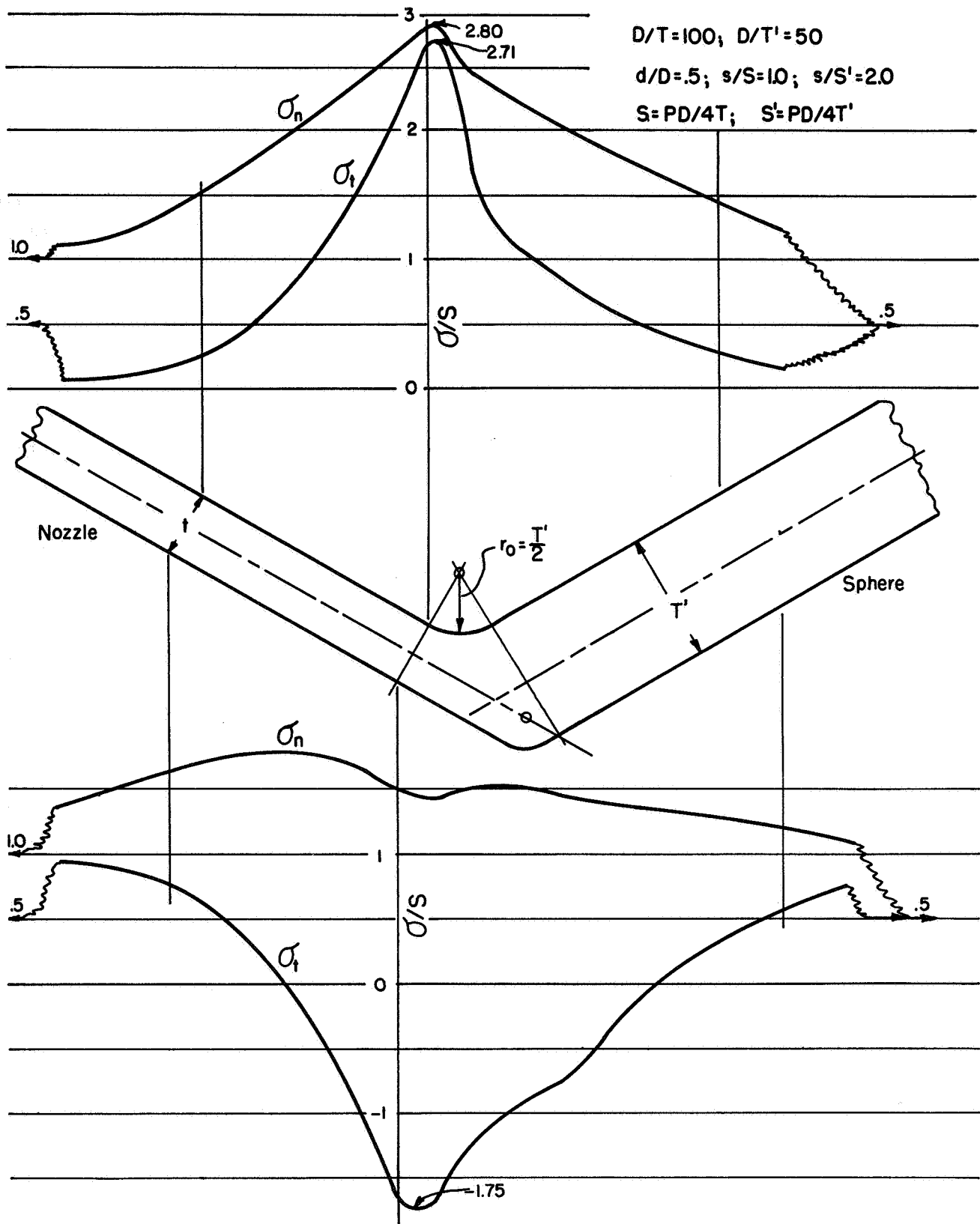


FIGURE 52. CALCULATED (KALNINS) STRESSES IN A CODE-REINFORCED NOZZLE, INCLUDING FILLET RADIUS EFFECT

### Moment Loading, Comparison with ASA B31.1

The computed stress intensification factors for nozzles in spheres due to moment loading become quite high for some combinations of dimensions. It is significant, from a design standpoint, to compare these computed factors with these given in the ASA Code for Pressure Piping<sup>(18)</sup>. The ASA Code does not, of course, include factors for nozzles in heads. However, the factors given for elbows and for tees are pertinent with respect to the general design problem of nozzles in heads. The computed stress intensification factors for nozzle in heads are based on elastic theory and hence are not directly comparable with the "fatigue-test" derived factors given in the ASA Code. However, an indication of the relationship of the elastic stress intensification factors to the fatigue-test factors may be obtained from the factors for elbows. The theoretical elastic stress intensification factor for elbows is approximately twice the fatigue-test factors given in the ASA Code. While the theoretical factor would be reduced somewhat by end effects (i.e., the influence of the pipe welded to the elbows), this would be a relatively small effect for in-plane bending for the elbows used in the fatigue tests. Accordingly, the fatigue-test factors for elbows may be multiplied by a factor of two for comparison with elastic stress factors. While no theory exists for the theoretical elastic stress concentration factor for tees, presumably the relationship of 2:1 for elastic-to-fatigue factors would roughly also hold for tees.

Figure 53 shows the maximum computed stress intensification factors for nozzles in spheres plotted against  $r/t$  for the nozzle, in which  $s/S = 1.0$ ;  $d/D = 0.01, 0.05, 0.25,$  and  $0.50$ . For comparison, Figure 53 also shows the stress concentration factors for ASA B16.9 welding elbows (Bend radius is approximately three times the cross sections radius, in the graph this ratio has been taken as exactly three). The stress concentration factor for the elbows is twice the factor given in ASA B31.1.\* Figures 54 and 55 are

---

\* The theoretical stress concentration factor for in-plane bending of an elbow as given by Rodabaugh and George<sup>(31)</sup> for  $r/t > 10$ , zero internal pressure, is about 4% higher than twice the factor given in ASA B31.1.

similar to Figure 53 except that they are for nozzles in spheres with  $s/S = 2.0$  and  $0.5$ , respectively.

A ratio of  $s/S = 2.0$  could be obtained by local thickening of the sphere around the nozzle to  $2T$ , thereby meeting the usual rules for reinforcing an opening by area replacement. With such reinforcing, the stress factors for nozzles in spheres, for  $d/D$  up to  $0.25$ , are no higher than for ASA B16.9 long radius elbows. In many piping systems, therefore, the controlling component in restricting load magnitudes might be an elbow rather than a nozzle in a head. Also, the calculated maximum stresses for nozzle in spheres with  $d/D \leq 0.25$  are tangential stresses in the nozzle, a fillet radius would serve to substantially reduce the stress levels.

A ratio of  $s/S = 0.5$  represents a nozzle twice as thick as required for internal pressure in the nozzle considered as a pipe. This would not, in general, meet the usual rules for area replacement. However, for small  $d/D$ , doubling the nozzle thickness is quite effective in reducing stress levels. For large  $d/D$ ,  $d/D = 0.5$  in particular, doubling or tripling the nozzle wall thickness does little to reduce the stress levels and in some cases increases them. This is because the maximum stress for large  $d/D$ , occurs in the sphere; increasing the nozzle thickness may increase this stress or decrease it only slightly. It is apparent, therefore, that for moment loading such large nozzles should be reinforced on the sphere rather than on the nozzle.

Figure 56 compares calculated maximum stresses for nozzles in spheres with twice ASA B31.1 Code factors for fabricated tees. For reducing tees, the Code factors are given in ASA B31, Code Case 53, July, 1963. Figure 57 is similar except it shows Code factors for manufactured tees to ASA B16.9. Since ASA B16.9 tees are fully reinforced for pressure loading, the comparison is made with nozzles in spheres with  $s/S = 2.0$ , which may also be considered as fully reinforced by present codes for pressure loading.

In comparing the curves on Figures 56 and 57, the significant difference between nozzles in spheres and nozzles in cylinders (tees) should be kept in mind. Two of these are:

- (1) For tees, available data indicates that maximum elastic stresses may be significantly higher for out-of-plane bending as compared to in-plane bending. Figures 55 and 56 give code factors for out-of-plane bending. For

nozzles in spheres, of course, there is no distinction.

- (2) For nozzles in spheres, with pressure, moment or thrust loading, the maximum stress as a function of  $d/D$  generally reaches a peak somewhere between  $d/D = 0.2$  and  $0.5$ . It is apparent that such a peak must exist since for  $d/D = 1.0$ , a nozzle in a sphere becomes a straight pipe of the nozzle dimensions. For nozzles in cylinders (tees), however, available data indicate that probably the maximum stress increases continuously with increasing  $d/D$  up to  $d/D = 1.0$ .

In a broad sense the kind of agreement between calculated elastic stress factors and fatigue-test derived factors shown by Figure 57 seems reasonably consistent. The general tendency for the slope of the calculated stress factors lines ( $d/D > 0.05$ ) to agree with the fatigue-test data (which slope, in turn, is derivable from elbow theory) is interesting and perhaps basically significant.

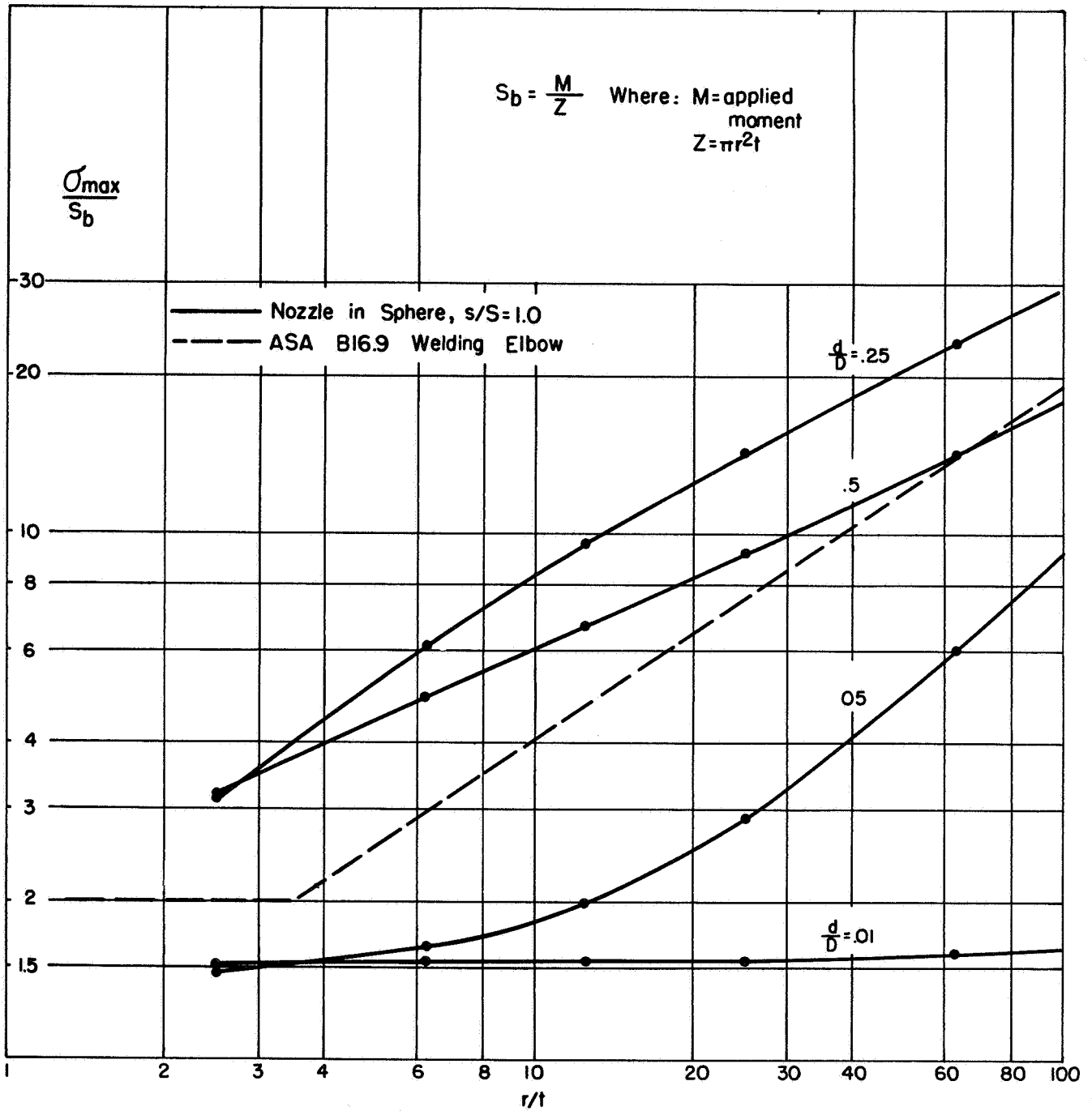


FIGURE 53. STRESS INTENSIFICATION FACTORS (MOMENT LOADING) FOR NOZZLES IN SPHERES WITH  $s/S = 1.0$  AND FOR ASA B16.9 WELDING ELBOWS

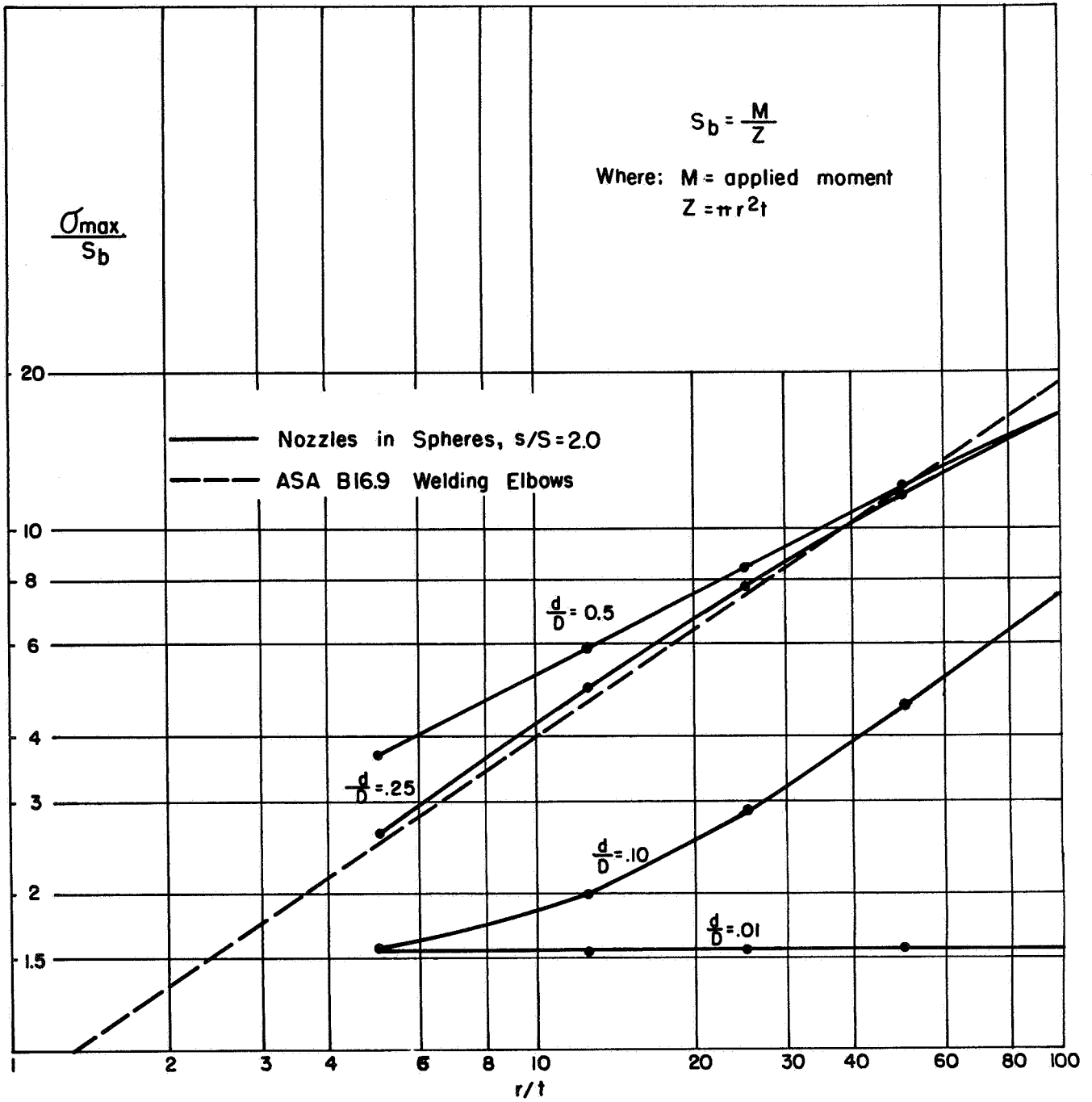


FIGURE 54. STRESS INTENSIFICATION FACTORS (MOMENT LOADING) FOR NOZZLES IN SPHERES WITH  $s/S = 2.0$  AND FOR ASA B16.9 WELDING ELBOWS



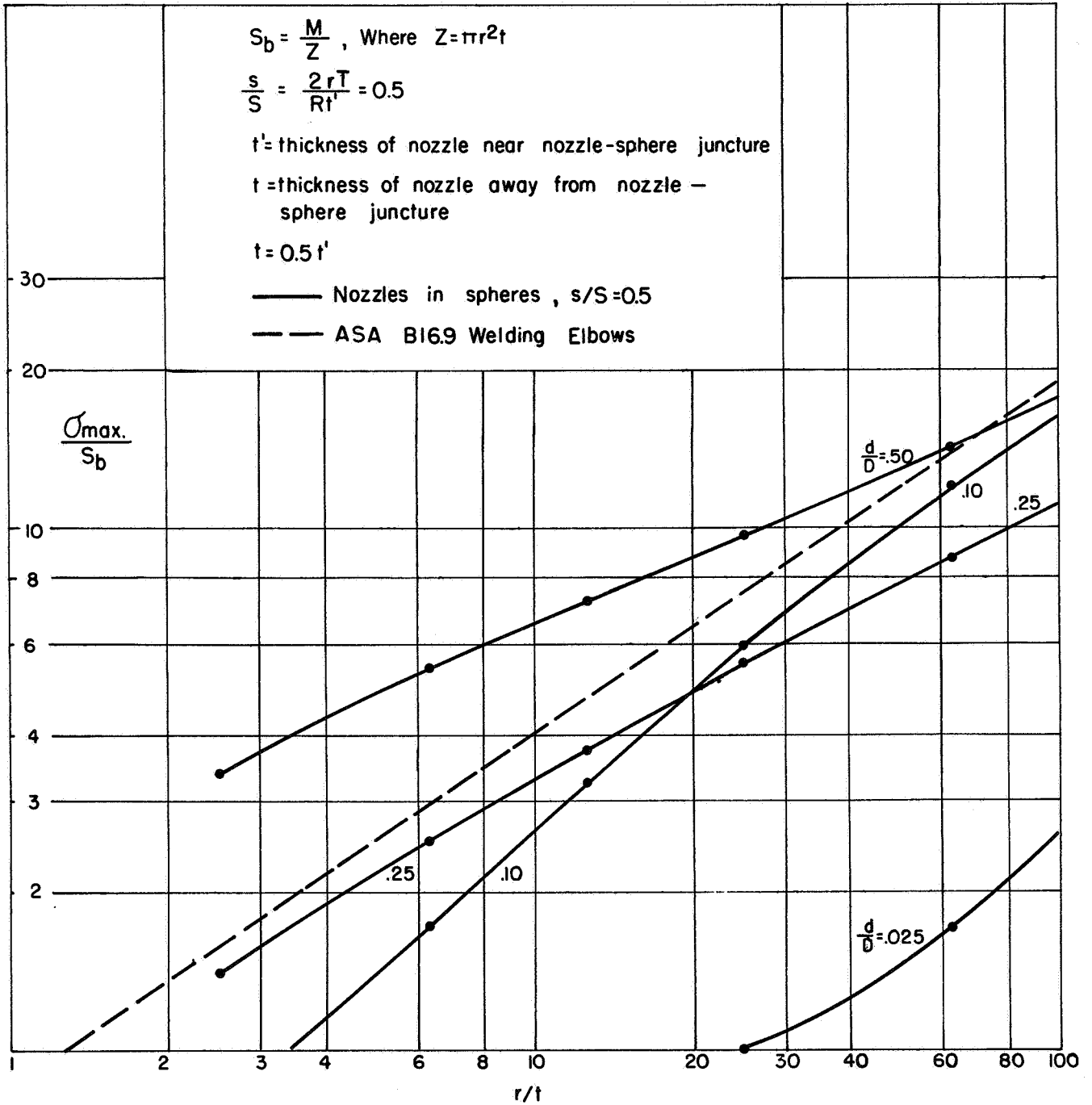


FIGURE 55. STRESS INTENSIFICATION FACTORS (MOMENT LOADING) FOR NOZZLES IN SPHERES WITH  $s/S = 0.5$  AND FOR ASA B16.9 WELDING ELBOWS

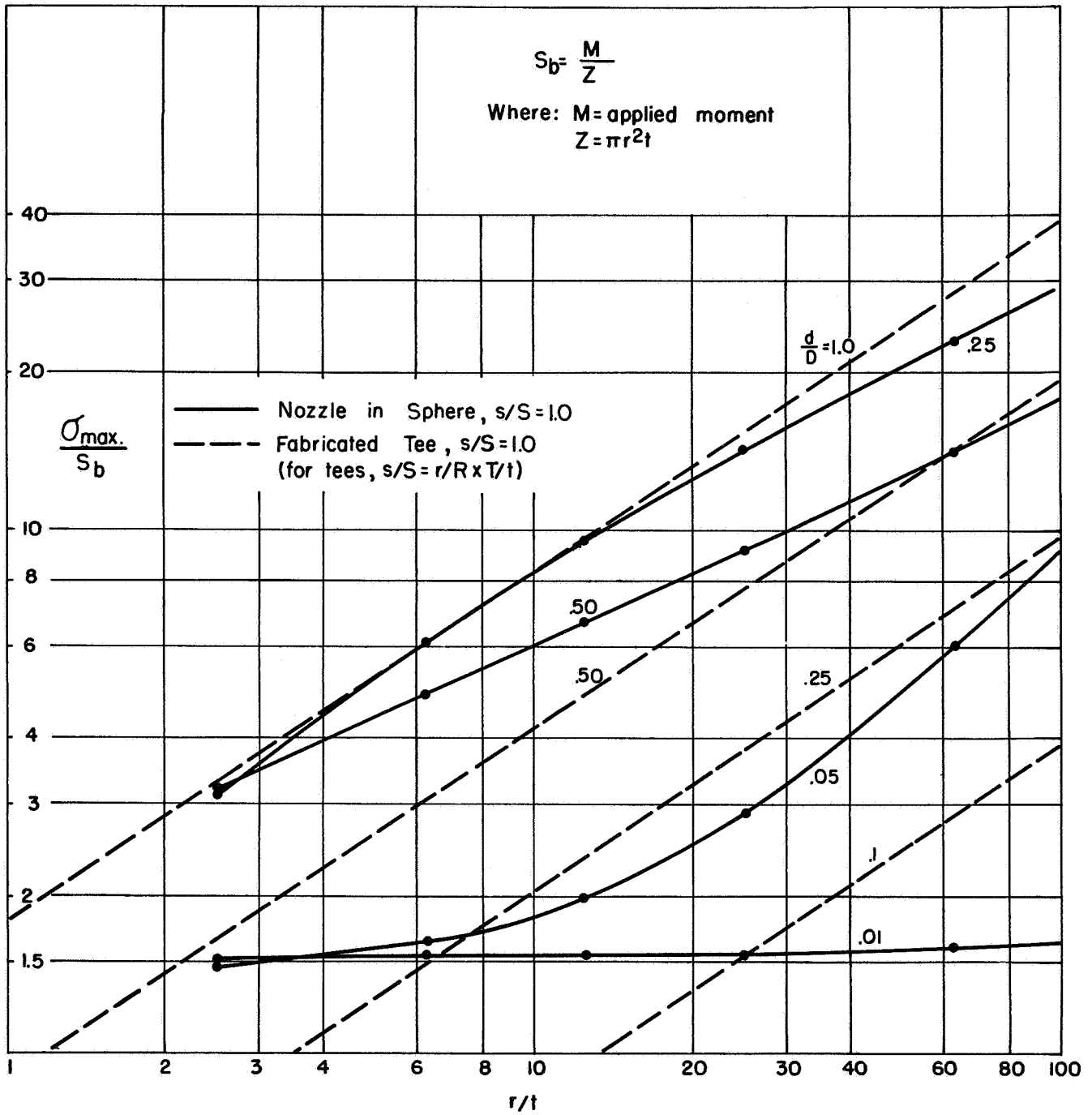


FIGURE 56. STRESS INTENSIFICATION FACTORS (MOMENT LOADING) FOR NOZZLES IN SPHERES WITH  $s/S = 1.0$  AND FOR FABRICATED TEES WITH  $s/S = 1.0$

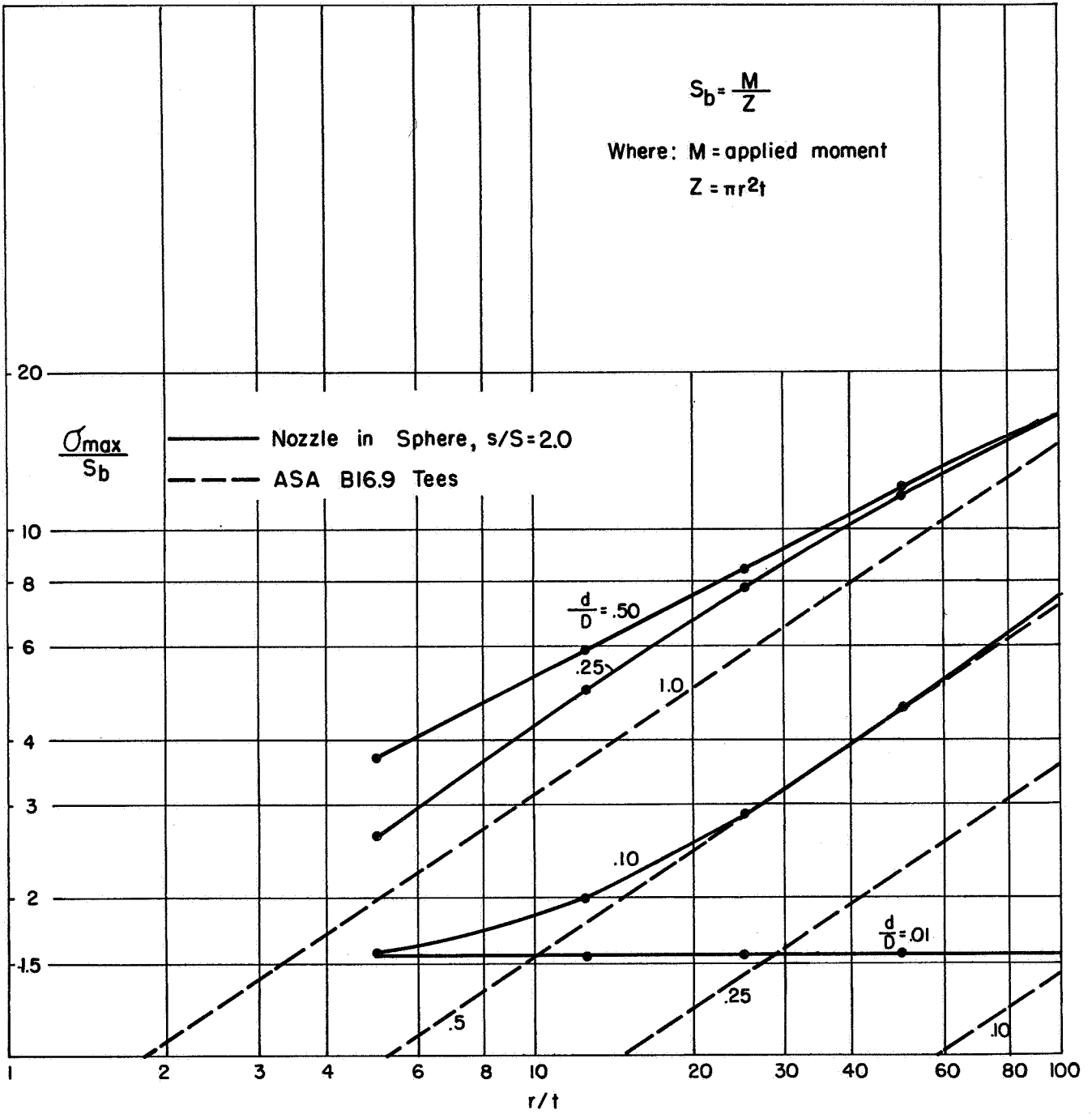


FIGURE 57. STRESS INTENSIFICATION FACTORS (MOMENT LOADING) FOR NOZZLES IN SPHERES WITH  $s/S = 2.0$  AND FOR ASA B16.9 TEES

Combined Pressure and Moment Loading

Nozzles in pressure vessels attached to piping systems will, in general, be subjected to both internal pressure and to loads applied to the nozzle by the attached piping. These two kinds of loads are, of course, independent in magnitude and time history. A fatigue analysis of such a nozzle becomes quite complicated because of the independence of the two loads and the location of critically stressed points for each of the loads. Where the cycles of load is limited to a relatively small number, it may be possible to satisfy design requirements by showing that the maximum stress (or stress intensity) does not exceed a prescribed value when the nozzle is subjected to the combination of maximum design pressure and maximum design loads imposed by the piping on the nozzle. This aspect of design is discussed in the following.

Two questions arise for which positive answers would be desirable for simplification of design work, i.e.,

- (1) Are stresses due to internal pressure and those due to external loads linearly superposable?
- (2) Is the location of the maximum stress (or stress intensity) the same for pressure loading as for external loads?

These questions are briefly discussed in the following two sub-sections.

Linear Superposition of Stresses

The usual assumption of linear superposition of stresses for combinations of loads on thin-wall shells is sometimes invalid (See for example, Reference 31). Bijlaard<sup>(1)</sup> develops the theory and gives an example for combined thrust load and internal pressure applied to a "plug" nozzle in a spherical shell. The example is for a sphere with  $R/T = 100$ , stress in the sphere due to internal pressure = 13,000 psi,  $E = 30,000,000$  psi,  $\nu = 0.3$  and  $U = 1.815 (r/R)(R/T)^{1/2} = 0.1$ . For this example, Bijlaard finds that maximum deflections are reduced 4 to 5% by the internal pressure as compared to zero internal pressure; stresses are reduced by 2%.

Experimental data on Configuration No. 1, Reference 27, ( $D/T = 81$ ,  $d/D = .08$ ) also indicated that superposition of stresses for nozzles in spheres is usually quite accurate. A combined test load was run with  $p = 400$  psi, corresponding to  $S = pD/4T = 8130$  psi, combined with a thrust load on the nozzle of 6000 lb. The average results for 24 strain gages indicated that linear superposition overpredicted actual stresses under combined loading by around 2%.

In view of the somewhat limited data on spheres, a study was made of superposition tests on tees run by Hardenbergh<sup>(37)</sup>, Riley<sup>(26)</sup>, and Cranch<sup>(38)</sup>. All of these tests, as well as the theory for nozzles in the spheres or cylinders, indicates that linear superposition would be conservative. Hardenbergh's tests ( $D/T = 19$ ) indicate linear superposition is not more than 1% conservative; Riley's test ( $\frac{D}{T} = 240$ ), not more than 5%; Cranch's tests ( $D/T = 78$ ), not more than 22% conservative.

The review of the available theoretical and experimental data led to the following conclusions.

- (1) The interaction between pressure and external loads for nozzles in spheres appears to be negligible (less than 5%) for any  $D/T$  up to 50 and for  $d/D$  up to 0.5 and probably is small (less than 25%) for  $D/T$  up to 100 when the nominal stress due to internal pressure is around 15,000 psi or less.
- (2) The interaction effects are probably smaller for moment loading than for thrust loading.
- (3) Use of linear superposition for calculating stresses under combined loads is apparently always conservative.

#### Location of Maximum Stresses

Test data is available on 4 models which were tested under both internal pressure and moment loads. These are models WN-50B\*, IIT-S1

---

\* WN-50B was actually two photoelastic models, one tested with internal pressure, the other with a moment on the nozzle.

ORNL-5 and ORNL-6. In models WN-50B and IIT-S1, the maximum stress occurred in essentially the same place for both pressure and moment loading (and thrust loading for IIT-S1), i.e., a tangential stress on the outside surface in the fillet radius. Also, for both models the maximum stress intensity location is at the same location. The maximum measured stresses in Models ORNL-5 and ORNL-6 were not at the same locations:

<u>Model</u>	<u>Pressure</u>	<u>Moment</u>	<u>Thrust</u>
ORNL-5	n,o, sphere	n,o, nozzle	t,o, nozzle
ORNL-6	n,o, nozzle	t,o, nozzle	t,o, nozzle

where n signifies a normal stress, t tangential stress and o the outside surface. (Actually, in these two models, because of the "zero" fillet radius, the maximum stress probably occurred in the sharp corner for all loadings.)

The maximum stress location is a function of  $d/D$ ,  $D/T$ , and  $s/S$ . The degree of conservatism introduced by assuming the same maximum stress locations for various loads depends upon these dimensional ratios, as well as the relative magnitude of the loads. The graphs given in the Appendix can be used to obtain maximum stresses and locations for any desired combination of pressure, moment or thrust loading for an extensive range of the dimensional ratios:  $d/D$ ,  $D/T$ , and  $s/S$  (or  $t/T$ ).

#### Relative Magnitude of Stresses from Pressure or Moment Loading

The magnitude of the internal pressure, in relationship to the dimensions of a nozzle, is relatively well established in the early design stage. That is, the designer may assume that the design pressure is such that  $S = PD/4T$ , where  $S$  is some established stress limit depending upon the material and operating temperature. The magnitude of the loads applied by a piping system to the nozzle, however, is generally not known at the early design stage. This problem arises because quite often the detailed piping layout is not yet established, hence forces from the piping cannot be calculated.

An ultraconservative approach, in the early design stages, consists of assuming that the nozzle must withstand whatever moment the attached pipe is capable of applying to it. This might be assumed to be the limit load of the pipe in bending, i.e.:

$$M_{\max} = 1.3 S_o Z_p$$

where  $M_{\max}$  = maximum moment applied to nozzle by attached piping  
 $S_o$  = yield strength of the pipe material  
 $Z_p$  = section modulus of pipe.

The significance of this assumption for the maximum moment can be illustrated, for some specific cases, with the additional assumptions:

- (1) The pipe, nozzle, and sphere or head are made of the same material.
- (2) Reinforcing consists of an increase in thickness of the sphere in an area around the nozzle such that  $s/S = 2.0$ , i.e., the local thickness  $T'$  is twice the basic sphere thickness,  $T$ .

Because  $S_b$ , from the maximum moment assumption, is equal to  $1.3 S_o$  and usually  $S_p$  would be limited to  $2/3$  of  $S_o$  or less, the ratio of  $S_b/S_p$  would be 1.95 or greater. It is, therefore, possible that the maximum stress due to moment load will be considerably larger than the maximum stress due to pressure. For example, at  $d/D = 0.25$ ,  $r/t = 50$ , from Figure 58:

$$\frac{(\sigma_{\max})_b}{S_b} = 12. \quad ; \quad \frac{(\sigma_{\max})_p}{S_p} = 5.7$$

$$\frac{(\sigma_{\max})_b}{(\sigma_{\max})_p} = \frac{(\sigma_{\max})_b}{S_b} \cdot \frac{S_p}{(\sigma_{\max})_p} \cdot \frac{S_b}{S_p} = \frac{12.}{5.7} \cdot 1.95 = 4.1$$

Several comments concerning the above comparison are:

- (1) The comparison is purely theoretical, based on the CERL computer program parametric study. A reasonable size fillet radius at the juncture of the nozzle and sphere

Nozzles in spheres with  $s/S = \frac{2r}{R} \cdot \frac{T'}{t} = 2.0$

$$S_b = \frac{M}{\pi r^2 t} \quad , \quad S_p = \frac{PD}{4T} \quad , \quad T' = 2T$$

$(\sigma_{max})_b$  = maximum stress , moment loading

$(\sigma_{max})_p$  = maximum stress , pressure loading

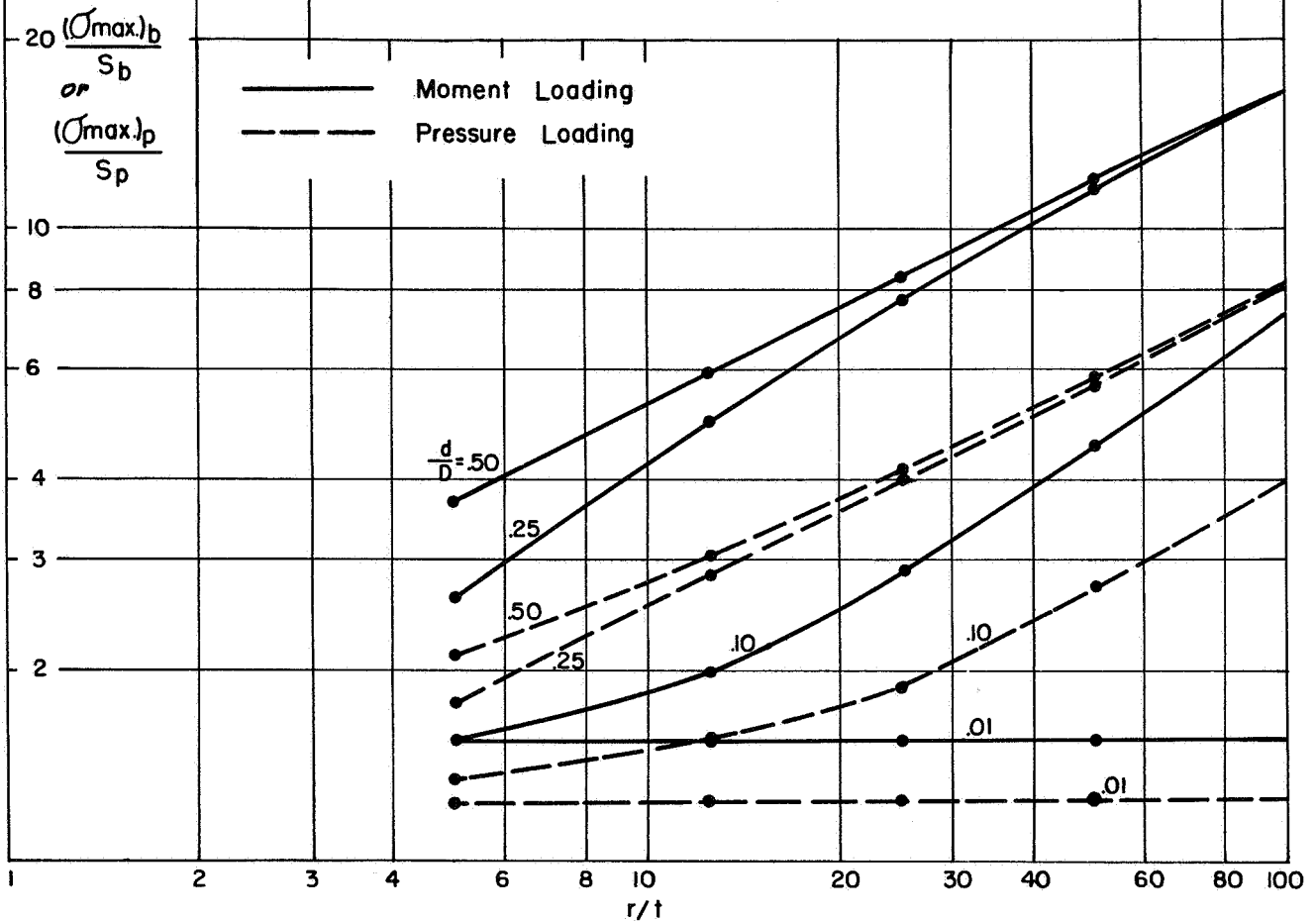


FIGURE 58. MAGNITUDE OF MAXIMUM STRESSES FROM MOMENT LOADING AS COMPARED TO INTERNAL PRESSURE LOADING



would reduce stresses by a significant amount. However, the ratio of stresses  $(\sigma_{\max})_b / (\sigma_{\max})_p$  might not be greatly changed by the fillet radius.

- (2) For small  $d/D$  nozzles, the stress due to the moment could be drastically reduced by using a nozzle with thickness of say 4 to 10 times that required for pressure only, considering the nozzle as a pipe. This would be more or less typical of small  $d/D$  nozzles as customarily designed for pressure vessels. For large  $d/D$  nozzles, similar nozzle thickening might lead to unreasonably heavy forgings and also an inefficient reinforcing for thin-wall spheres, since the maximum stress occurs in the sphere.

It is apparent that the design assumption  $M_{\max} = 1.3 S_o Z_p$  leads, in some cases, to requirements for a large amount of reinforcing to support the assumed moment load. To the extent that the assumption is overconservative, penalties are occurred in unnecessary fabrication costs and, possibly, to increased problems with stresses due to thermal gradients. There are a number of reasons why the assumption that  $M_{\max} = 1.3 S_o Z_p$  is, in most cases, unnecessarily conservative. These are discussed briefly in the following.

- (1) In a critical pipeline it would seem reasonable to restrict the maximum stress (or stress intensity) to the same level as the maximum stress in the nozzle. With this restriction the ratio of  $(\sigma_{\max})_b / (\sigma_{\max})_p$ , for the examples shown in Figure 58, ranges from 1.2 for small  $d/D$ , thin-wall spheres to about 2.1 for large  $d/D$ , thin-wall spheres.
- (2) In most present-day critical piping systems, one or more ASA B16.9 elbows are usually in the system. Assuming that the maximum stress in the elbow is to be restricted to the same maximum stress permitted for the nozzle, these elbows potentially provide a limit to the maximum moment that can be applied to a nozzle in a pressure vessel. Of course, the moment at the elbow or elbows will not, in general, be the

same as at the nozzle. However, in the early design stage, it would seem reasonable to base the nozzle design on the assumption that it will need to carry no more moment than can be transmitted by an elbow in the pipe line. Figures 53, 54, and 55 illustrate the significance of this assumption. Figure 54, in particular, shows that if the assumed moment is restricted by a specified maximum stress in an elbow, nozzles with  $s/S = 2.0$  and  $d/D < 0.25$  would automatically be restricted to the same or lower maximum stress levels insofar as moment loading is concerned.

- (3) Equipment attached to the pipeline may also constitute a limit for moments that can be tolerated in the pipeline and thus provide some early design guide for moments applied on nozzles. NEMA Standard No. SM 20-1958<sup>(32)</sup> gives limits on allowable forces and moments acting on the steam inlet, extraction or exhaust connections of steam turbines. This standard gives several limitations, one of which states:

The total resultant force and total resultant moment imposed on the turbine at any connection must not exceed the following:

$$F = \frac{500 d_e - M}{3} \quad (19)$$

F = resultant force, lbs

M = resultant moment, ft lbs

$d_e$  = pipe size of the connection in sizes up to 8" diameter  
 =  $(16 + \text{I.P.S.})/3$  for sizes larger than 8" diameter.

Assuming that the resultant force is negligible, Equation (19) gives:

$$M_{\max} = 6000 d_e \text{ (in.-lbs)} \quad (20)$$

- (4) Rossheim and Markl<sup>(33)</sup>, from a review of a large number of piping system calculations involving pipeline connections to pumps, gave the following averages for the end reactions:

Vertical thrust (including weight loads)	$3.25 (d + 3)^3$
Lateral thrust	$1.50 (d + 3)^3$
Moment	$60.00 (d + 3)^3$

where  $d$  = outside diameter of pipe.

Figure 59 summarizes all five of the limits to maximum moment discussed above for a particular case where  $P = 600$  psi,  $S = 20,000$  psi =  $0.667 S_o$ , and  $t = Pr/S$ . The equations become:

- (1) Moment limit by limit load of pipe:

$$M_{\max} = 1.3 S_o Z_p = 1.95 S \cdot \pi r^2 t = 1.95 S \pi r^3 \frac{P}{S}$$

- (2) Moment limit by S-limit on pipe:

$$M_{\max} = S \pi r^3 \frac{P}{S}$$

- (3) Moment limit by S-limit on elbows:

$$M_{\max} = \frac{S \pi r^3}{i} \cdot \frac{P}{S}$$

$$i = \frac{1.8}{h^{2/3}} = 1.8 \left(\frac{r}{3t}\right)^{2/3} = 0.866 \left(\frac{S}{P}\right)^{2/3}$$

- (4) Moment limit by NEMA Standard SM 20-1958, permissible moment on steam turbine pipe connections:

$$M_{\max} = 6000 d_e$$

$$d_e = 2r \text{ for } r \leq 4$$

$$d_e = (2r + 16)/3 \text{ for } r \geq 4$$

- (5) Average moment, Rossheim and Markl:

$$M = 60 (2r + 3)^3$$

In the above equations, and Figure 59, it should be noted that while the assumption  $t = Pr/S$  simplifies the comparisons, for small nozzles the thickness is unrealistic. For example, at  $r = 1$ ,  $P = 600$ ,  $S = 20,000$ :  $t = 0.030$ ". A 2" standard weight pipe has a thickness of 0.154". This explains why the Rossheim-Markl average moment is higher than the limit load moment for small nozzles in Figure 59. For large nozzles, the NEMA steam turbine limit is a small fraction of the other limits; at  $r = 10$ ", the NEMA limit is about two percent of the limit load moment; 34 percent of the elbow stress limit.

In summary, the relative significance of stresses from internal pressure as compared to the stresses due to moment loading depends, of course, on the relative magnitude of the pressure and moment loads. The moment load, in the absence of specific information, may be estimated in several ways; the most conservative of these estimates leads to high stresses due to moment as compared to those due to pressure.

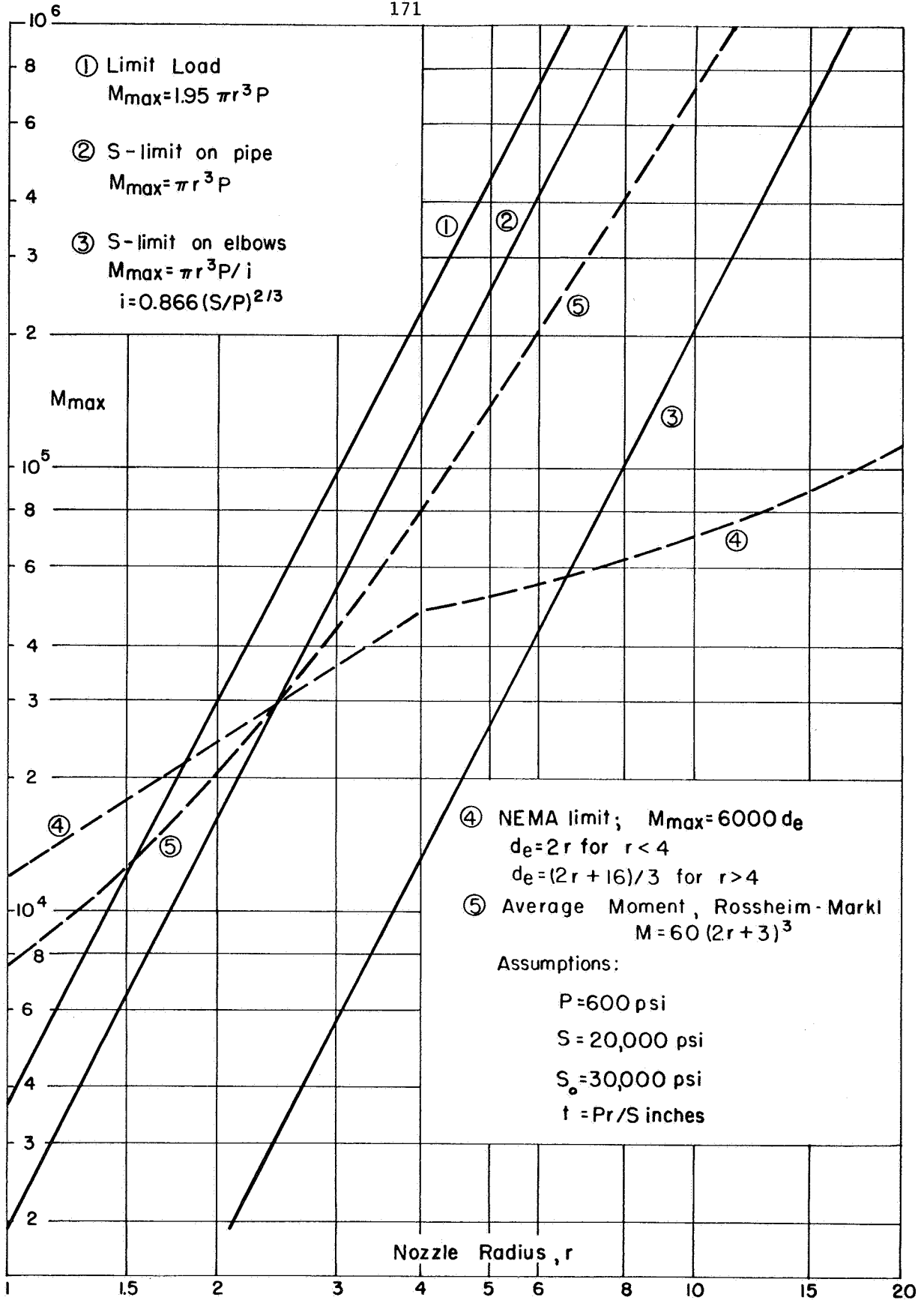


FIGURE 59. COMPARISON OF LIMITATIONS ON BENDING MOMENTS APPLIED TO NOZZLES

Stresses in Phase I Designs

Phase I Report, "Proposed Reinforcement Design Procedures for Radial Nozzles in Spherical Shells with Internal Pressure"<sup>(12)</sup> gives reinforcing dimensions (as a function of  $d/D$  and  $D/T$ ) such that the nozzles with such reinforcing meet two design criteria: (1) the plastic collapse or plastic limit pressure is at least 1.5 times the design pressure, and (2) the maximum stress intensity is not more than 3.0  $S$ , where  $S = PD/4T$ . Because the plastic collapse pressure is the controlling criteria for almost all values of  $d/D$  and  $D/T$ , the maximum stress intensity ( $\bar{\sigma}$ ) is generally less than 3.0  $S$ . If a maximum stress index of 3.0 is used for combined loadings, the Phase I designs have some capacity for other loadings such as moment, thrust or torsional loads on the nozzle, or for thermally induced stresses.

For Phase I nozzles with reinforcing consisting of a uniform increase in wall thickness of nozzle or sphere, for a distance from the juncture such that the increased thickness may be considered as effectively infinite, the stresses can be calculated by Waters' analysis, for internal pressure. Figure 60 shows the Phase I designs, Figure 61 and 62 show the maximum stress intensities due to internal pressure for these designs. As noted in Reference (12), and is apparent in Figures 61 and 62, for small values of  $g = t'/t$  or  $h = T'/T$  at small  $d/D$  ratios, the design criteria of  $\bar{\sigma} \leq 3.0 S$  is slightly exceeded. For other dimensional parameters, however,  $\bar{\sigma}$  is less than 3.0  $S$  by amounts which can be determined from Figures 61 and 62. It should be noted that, for uniform wall nozzle designs to Phase I (Figure 60) requirements, a given value of  $D/T$  and  $d/D$  establishes a value of  $g$  or  $h$ . More general design data is given in the Appendix.

For nozzles attached to piping systems, the major external loading is usually the applied moment. Accordingly, Figures 63 and 64 were prepared using Bijlaard's analysis to compute the maximum stress intensity ( $\bar{\sigma}$ ) due to a moment applied to the nozzle. By making the assumption that stress intensities from these two loads occurs at the same location (which in some dimensional ranges is theoretically correct; in others the

assumption may be appreciably conservative) the moment capacity of any nozzle designed to Figure 60 can be obtained from Figures 61 or 62 along with Figures 63 and 64. The use of these graphs is illustrated by several examples in the following.

Example 1.

Assumed basic dimensions:  $d/D = .13$ ,  $D/T = 100$ .

Nozzle is to be reinforced with an increased wall thickness of the sphere around the opening. From Figure 60b, for such reinforcing:

$$h = T'/T = 2.0, \text{ } T' \text{ is the required local thickness of reinforcing on the sphere for a distance } \sqrt{DhT} \text{ from the nozzle.}$$

From Figure 61 for  $d/D = 0.13$ ,  $h = 2.0$  :  $\bar{\sigma}/S = 2.76$

From Figure 63 for  $d/D = 0.13$ ,  $h = 2.0$  :  $\bar{\sigma}/S_b = 3.90$

With the further assumptions:

(1)  $P$  (internal pressure) is such that  $S = PD/4T = S_a$  where  $S_a$  is the allowable stress for the nozzle material and service conditions.

(2)  $\bar{\sigma} + \bar{\sigma} = 3.0 S_a$  is the design criteria.

The allowable bending stress,  $S_{ba}$ , is then

$$S_{ba} = \frac{3.0 - \bar{\sigma}/S}{\bar{\sigma}/S_b} \times S_a = \frac{0.24}{3.90} \times S_a = 0.0615 S_a$$

The moment capacity of the nozzle is  $S_{ba} = 0.0615 S_a$ , or  $M_a = 0.0615 S_a \cdot Z_n$ , where  $M_a$  is the allowable moment at the nozzle,  $Z_n$  is the section modulus of the nozzle ( $\pi r^2 t$ ). In this example the moment capacity is low. For comparison, an ASA B16.9 elbow in the piping attached to the nozzle would be limited to a moment such that  $S_{ba} = 0.27 S_a$  -- assuming the same design criteria ( $\bar{\sigma} + \bar{\sigma} = 3.0 S_a$ ) for the elbow as for the nozzle and a stress due to pressure of  $\bar{\sigma} = 1.0 S_a$ .

Example 2.

Assumed basic dimensions:  $\frac{d}{D} = 0.03$ ,  $\frac{D}{T} = 30$ .

Nozzle is to be reinforced with an increased wall thickness of the nozzle near the juncture. From Figure 60 a, for such reinforcing:

$$g = t'/t = 4.0, \text{ } t' \text{ is the required local thickness of the reinforced section of the nozzle, for a distance } \sqrt{dgt} \text{ from the juncture.}$$

From Figure 62 for  $d/D = 0.03$ ,  $g = 4.0$  :  $\bar{\sigma}/S = 1.67$

From Figure 64 for  $d/D = 0.03$ ,  $g = 4.0$  :  $\bar{\sigma}/S_b = 0.53$

With the further assumptions:

(1)  $P$  (internal pressure) is such that  $S = PD/4T = S_a$ , where  $S_a$  is the allowable stress for the nozzle material and service conditions.

(2)  $\bar{\sigma} + \bar{\sigma} = 3.0 S_a$  is the design criteria.

The allowable bending stress,  $S_{ba}$ , is then:

$$S_{ba} = \frac{3.0 - \bar{\sigma}/S}{\bar{\sigma}/S_b} \times S_a = \frac{1.33}{0.53} \times S_a = 2.50 S_a$$

It should be noted that the reference stress in Figure 64 is with respect to pipe attached to a locally thickened ( $t' = gt$ ) nozzle, the attached pipe is assumed to be such that  $s/S = 1.0$ . If the piping itself is such that  $s/S = 2dT/Dgt = 0.25$ , then the allowable bending stress for that pipe ( $t_p = gt$ ) is:

$$S'_{ba} = \frac{2.50}{4} S_a = 0.625 S_a$$

In this case, the pipe attached to the nozzle would be definitely "thick-wall",  $d/t$  being 3.75. An ASA B16.9 elbow of this wall thickness ratio would have an allowable bending stress,  $S_{ba} = 2.0 S_a$ ; assuming the same design criteria ( $\bar{\sigma} + \bar{\sigma} = 3.0 S_a$ ) for the elbow as for the nozzle and a stress due to pressure of  $\bar{\sigma} = 1.0 S_a$ .

The above example, along with Figures 60 through 64, indicate that the moment capacity of Phase I designs is highly variable, ranging from none up to the maximum moment capacity of piping attached to the nozzle.

The effect of the assumption that maximum shear stresses due to pressure and moment load are additive can be illustrated by a more detailed consideration of Example 1. The stress indices for this example ( $d/D = .13$ ,  $D/T = 100$ ,  $T'/T = 2.0$ ) are tabulated below.



Part	Outside		Inside	
	$\sigma_n/S$	$\sigma_t/S$	$\sigma_n/S$	$\sigma_t/S$
Pressure Stresses, $S = PD/4T$				
Sphere	1.78	1.10	.96	- .08
Nozzle	2.42	2.33	1.39	-1.37
Moment Stresses, $S = \pm M/\pi r^2 t$				
Sphere	1.32	.09	- .53	- .01
Nozzle	1.56	3.90	- .19	-1.90

In order to obtain the maximum shear stress for pressure and moment loading, it is necessary to examine 32 combinations of the stresses listed above. First, considering the stress normal to the surface as essentially zero, there are 16 combinations of the type  $[(\sigma/S \pm \sigma/S_b) - 0.]$ . Then, considering shear stresses from  $(\sigma_n - \sigma_t)$ , there are an additional 16 combinations of the type:  $[(\sigma_n/S \pm \sigma_n/S_b) - (\sigma_t/S \pm \sigma_t/S_b)]$ . For the present example, where  $S = PD/4T$  is assumed to equal  $S_a$  and  $\bar{\sigma} + \bar{\sigma} = 3.0 S_a$ , the limiting combination is that which arises from the  $(\sigma_n - \sigma_t)$  combination on the inside of the nozzle, i.e.

$$(1.39 S - .19 S_b) - (-1.37 S - 1.90 S_b) = 2.76 S + 1.81 S_b$$

from which

$$S_{ba} = \frac{3.0 - 2.76}{1.81} S_a = .132 S_a$$

Simple addition of the individual maximum shear stresses gave  $S_{ba} = 0.061 S_{ba}$ , hence in this particular example this approach is conservative by a factor of about two.

The graphs in the Appendix give data for evaluation of both maximum stresses and maximum shear stresses for an extensive range of  $d/D$ ,  $D/T$  and  $s/S$  (or  $t/T$ ), with any desired combination of pressure, moment or thrust load, at the midwall as well as at the surfaces.

It should be noted that the particular combination (of the 32 possible combinations) that will give the controlling maximum shear stress depends upon the relative magnitudes of the loads. In the above example, for relatively large stresses due to pressure, the combination given will be controlling. If, however, the stresses due to moment loading were high compared to those due to pressure, then the controlling combination would be the tangential stresses at the inside of the nozzle, i.e.,  $(2.33 S + 3.90 S_b)$ .

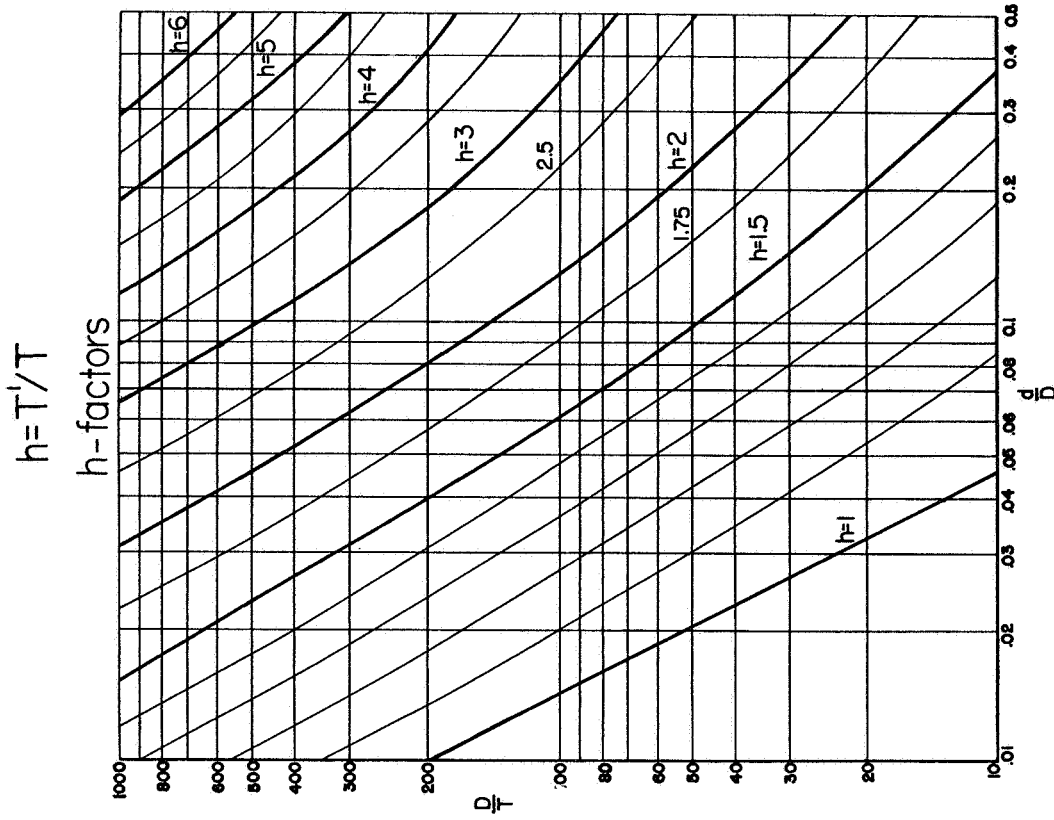


FIGURE 60b: Reinforcing on Sphere

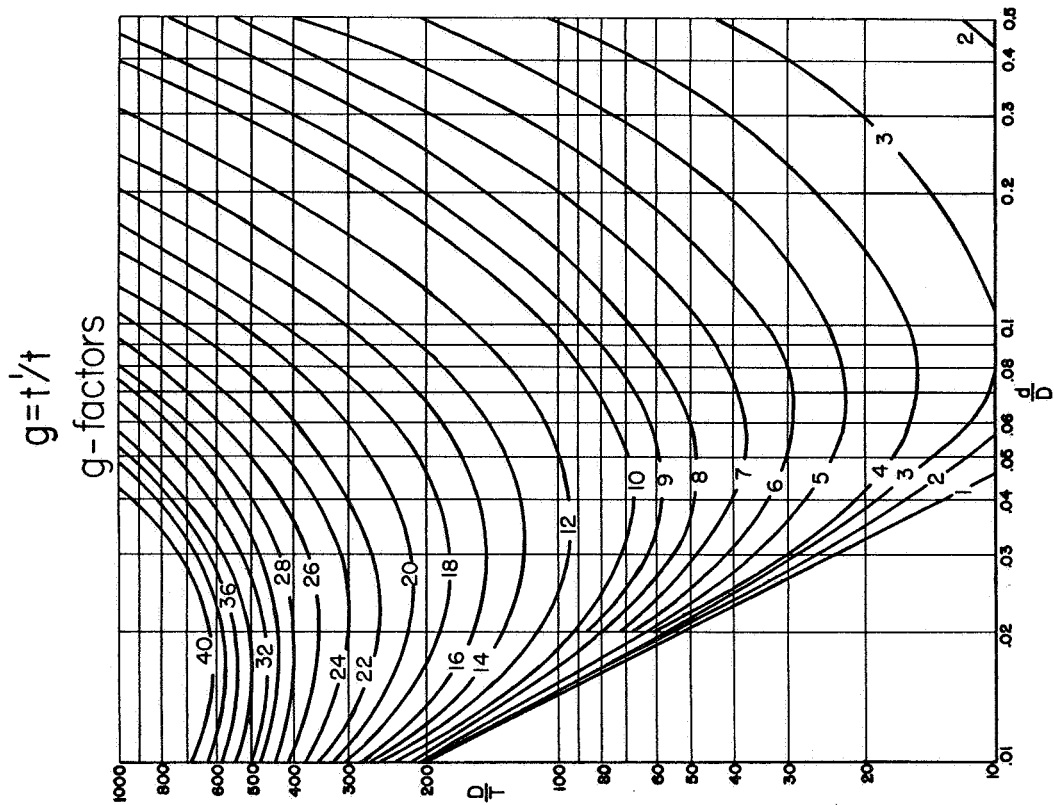


FIGURE 60a: Reinforcing on Nozzle

$$\frac{S}{S} = 1 = \frac{2dI}{Dt}$$

FIGURE 60: GRAPHS FOR OBTAINING g-AND h-FACTORS  
PHASE I DESIGNS

$$\frac{s}{S} = \frac{2dT}{Dt} = 1.0$$

$\bar{\sigma}$  = max. stress intensity,  $S = PD/4T$ ,  $h = T'/T$

( $D/T$  is related to values of  $h$  and  $d/D$  by Figure 60b)

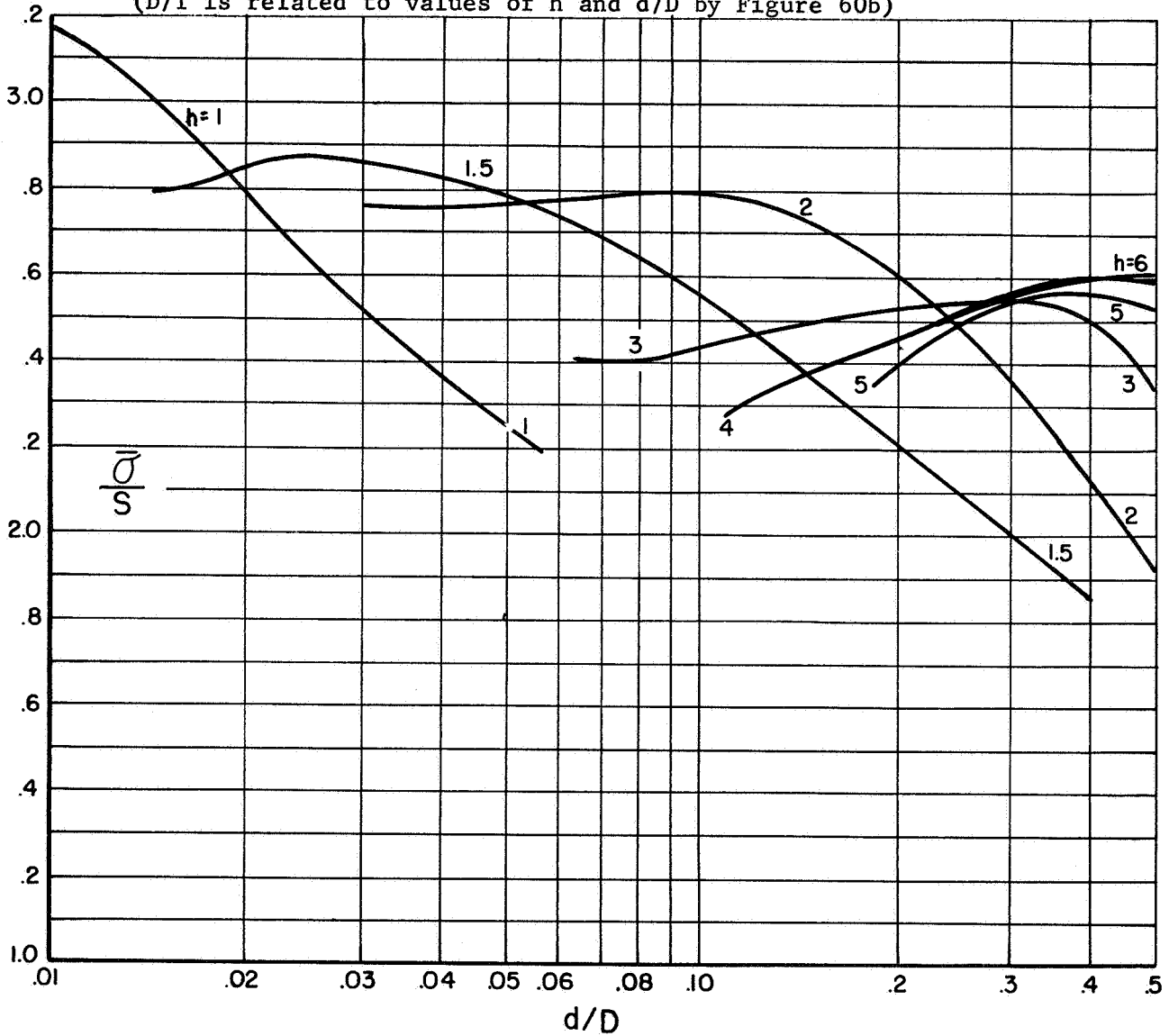


FIGURE 61. PHASE I DESIGNS, INTERNAL PRESSURE REINFORCING ON SPHERE, MAXIMUM STRESS INTENSITY, WATERS ANALYSIS

$$\frac{s}{S} = \frac{2dT}{Dt} = 1.0$$

$\bar{\sigma}$  = max. stress intensity,  $S = PD/4T$ ,  $g = t'/t$   
 ( $D/T$  is related to values of  $g$  and  $d/D$  by Figure 60a)

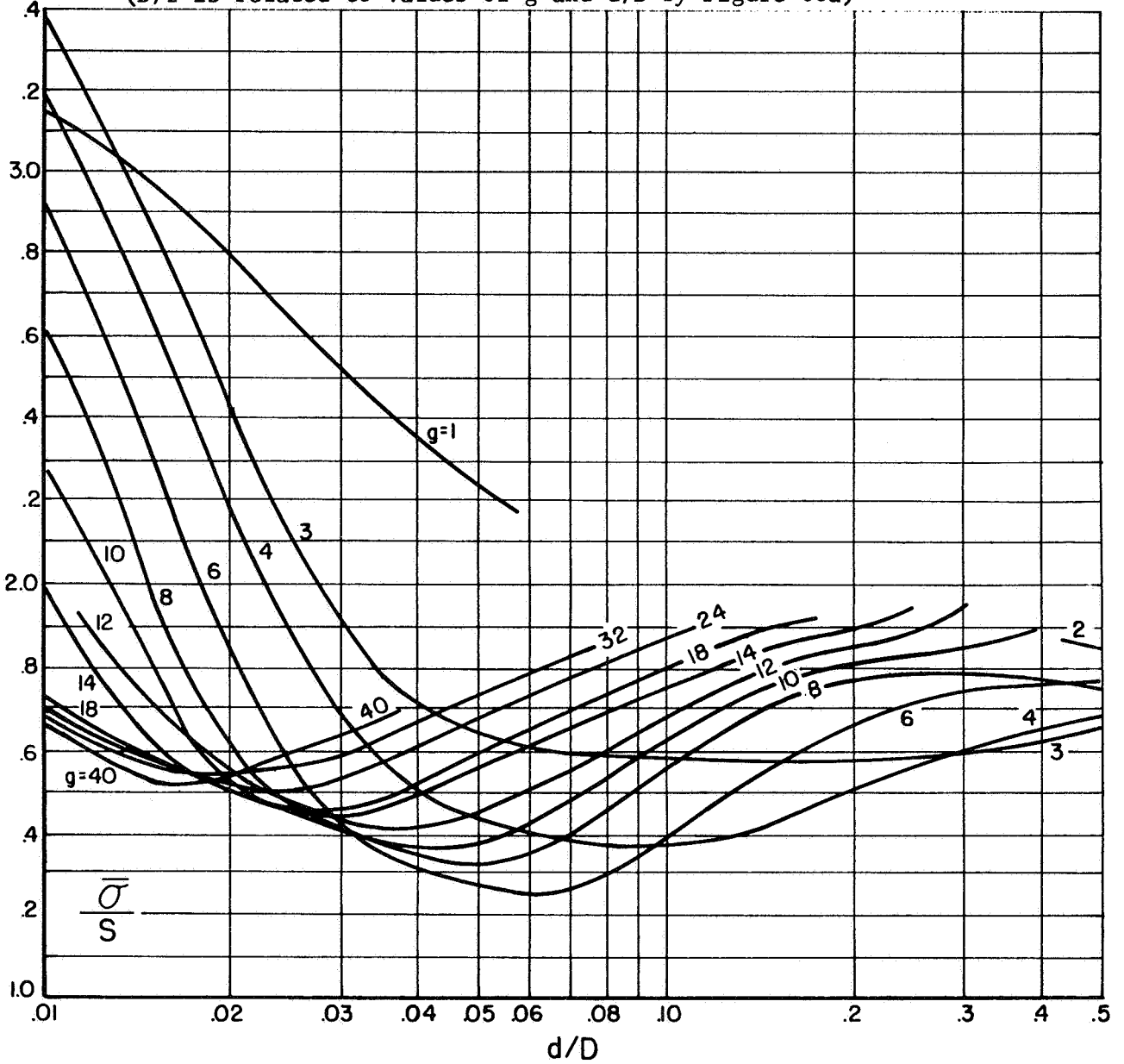


FIGURE 62. PHASE I DESIGNS, INTERNAL PRESSURE, REINFORCING ON NOZZLE, MAXIMUM STRESS INTENSITY, WATERS ANALYSIS

$$\frac{s}{S} = \frac{2dT}{Dt} = 1.0$$

$\bar{\sigma}$  = max. stress intensity,  $S_b = M/\pi r^2 t$ ,  $h = T'/T$

(D/T is related to values of h and d/D by Figure 60b)

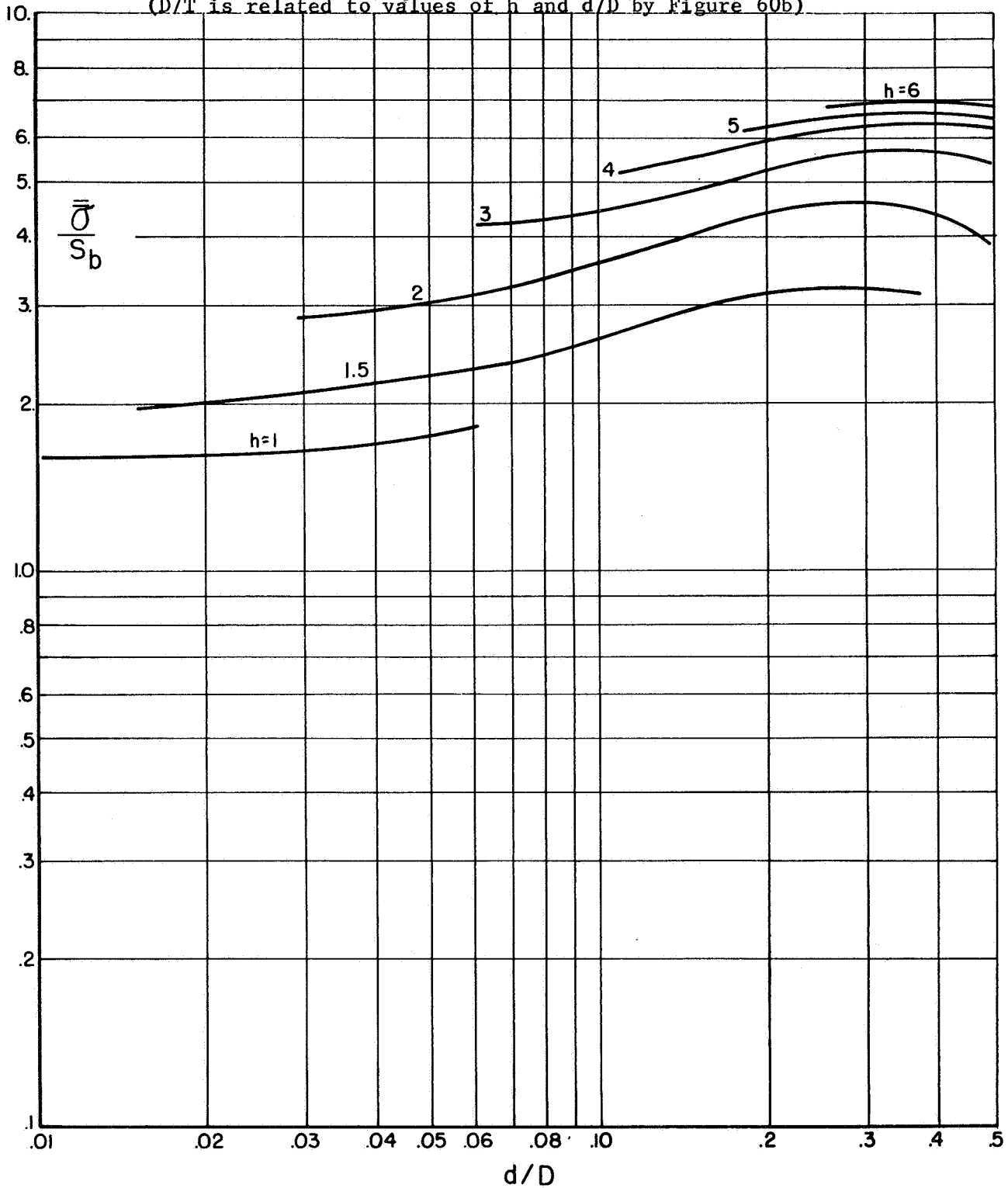


FIGURE 63. PHASE I DESIGNS, MOMENT LOADING, REINFORCING ON SPHERE, MAXIMUM STRESS INTENSITY, BJLAARD ANALYSIS

$$\frac{s}{S} = \frac{2dT}{Dt} = 1.0$$

$\bar{\sigma}$  = max. stress intensity,  $S_b = M/\pi r^2 t, g = t'/t$   
 ( $D/T$  is related to values of  $g$  and  $d/D$  by Figure 60a)

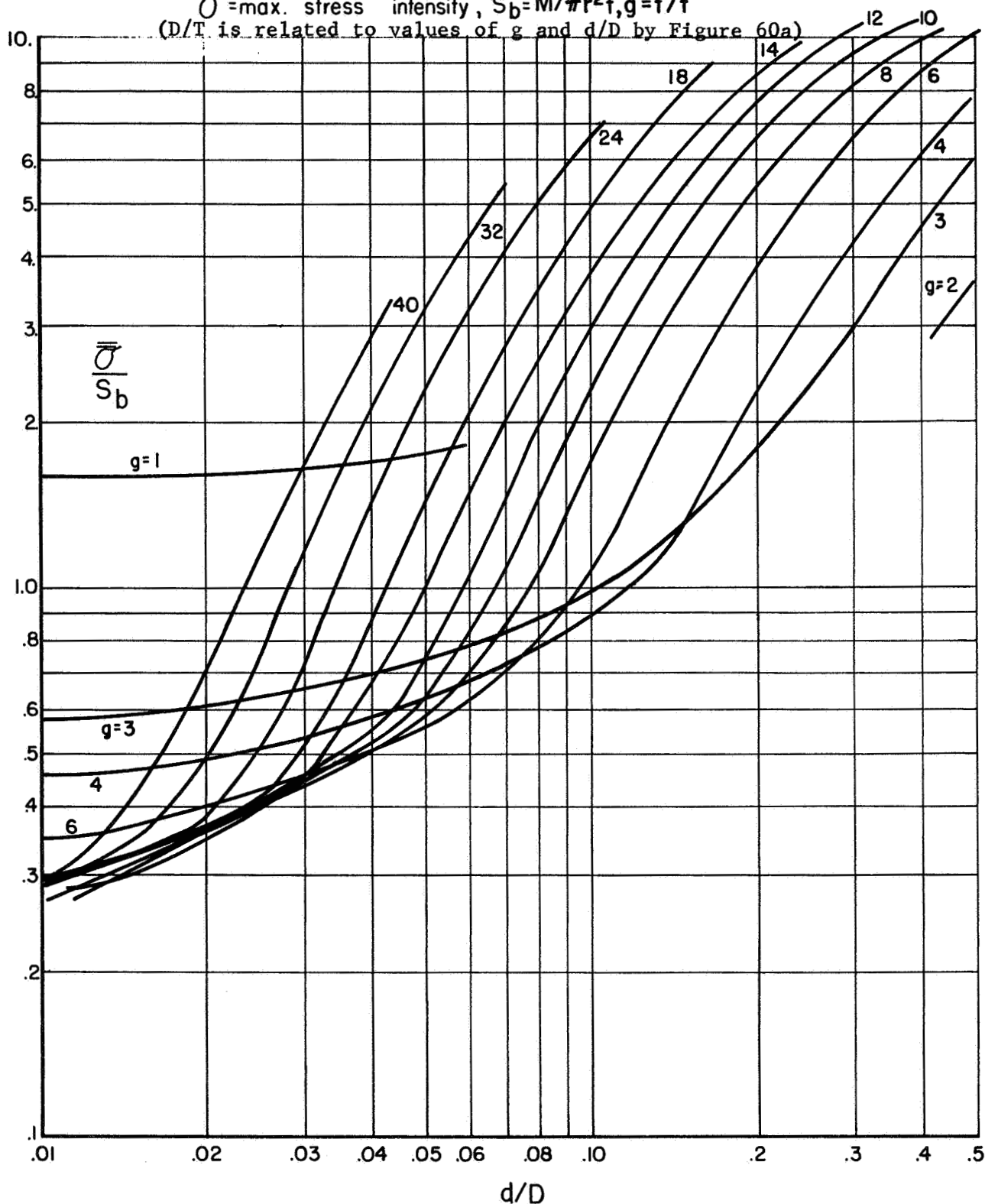


FIGURE 64. PHASE I DESIGNS, MOMENT LOADING, REINFORCING ON NOZZLE, MAXIMUM STRESS INTENSITY, BIJLAARD ANALYSIS

REFERENCES

1. Bijlaard, P. P., "Computation of the Stresses from Local Loads in Spherical Pressure Vessels or Pressure Vessel Heads", Welding Research Council Bulletin No. 34 (March, 1957).
2. Bijlaard, P. P., "Local Stresses in Spherical Shells from Radial or Moment Loadings", The Welding Journal, 36 (5), Research Supplement 240-S to 243-S (1957).
3. Bijlaard, P. P., "Stresses in Spherical Vessels from Radial Loads Acting on a Pipe", Welding Research Council Bulletin No. 49, pages 1 to 30 (April, 1959).
4. Bijlaard, P. P., "Stresses in Spherical Vessels from External Moments Acting on a Pipe", Welding Research Council Bulletin No. 49, pages 31 to 62 (April, 1959).
5. Bijlaard, P. P., "Influence of a Reinforcing Pad on the Stresses in a Spherical Vessel Under Local Loading", Welding Research Council Bulletin No. 49, pages 63 to 73 (April, 1959).
6. Bijlaard, P. P., "Stresses in Spherical Vessels from Local Loads Transferred by a Pipe", Welding Research Council Bulletin No. 50, pages 1 to 9 (May, 1959).
7. Wickman, K. R., Mershon, J. L., and Hopper, A. G., "Local Stresses in Spherical and Cylindrical Shells Due to External Loadings", Welding Research Council Bulletin No. 107 (August, 1965).
8. Leckie, F. A. & Penny, R. K., "A Critical Study of the Solutions for Asymmetric Bending of Spherical Shells", Welding Research Council Bulletin No. 90, pages 1 - 7, (September, 1963).
9. Penny, R. K. & Leckie, F. A., "Solutions for the Stresses at Nozzles in Pressure Vessels", Welding Research Council Bulletin No. 90, pages 8-18 (September, 1963).
10. Leckie, F. A. & Penny, R. K., "Stress Concentration Factors for the Stresses at Nozzle Intersections in Pressure Vessels", Welding Research Council Bulletin No. 90, pages 19-26, (September, 1963).
11. Waters, E. O., "Stresses Near a Cylindrical Outlet in a Spherical Vessel", Welding Research Council Bulletin No. 96, (May, 1964).
12. Cloud, R. L. and Rodabaugh, E. C., "Proposed Reinforcement Design Procedure for Radial Nozzles in Spherical Shells with Internal Pressure", Phase 1 Report on Analysis of Data for Reinforced Openings to the U.S. Atomic Energy Commission, Battelle Memorial Institute (Columbus, Ohio) Contract No. W-7405-3ng-92.
13. Friedrich, C. M., "Seal-Shell-2, A Computer Program for the Stress Analysis of a Thick Shell of Revolution with Axisymmetric Pressures, Temperatures, and Distributed Loads", Bettis Atomic Power Laboratory Report WAPD-TM-398.



14. Kalnins, A., "Analysis of Shells of Revolution Subjected to Symmetrical and Nonsymmetrical Loads", ASME Journal of Applied Mechanics, Sept., 1964.
15. Grieser, D. R., Reider, W. G., Hulbert, L. E., Bell, J. C., Smith, J. C., and Allen, C. M., "A Study of Rotary-Shaft-Sealing Concepts for Pressurized Water-Reactor Applications." Battelle Memorial Institute Report No. BMI-1676, June 30, 1964.
16. Mershon, J. L., "PVRC Research on Reinforcement of Openings in Pressure Vessels", Welding Research Council Bulletin No. 77, (May, 1962).
17. Mershon, J. L., "PVRC Interpretive Report of Pressure Vessel Research, Section I, Design Considerations, Part 1.6, Reinforcement of Openings Under Internal Pressure", Welding Research Council Bulletin No. 95, (April, 1964).
18. American Standard Code for Pressure Piping, ASA B31.8-1956, ASA B31.3-1962, ASA B31.4-1959, ASA B31.8-1963. Published by the American Society of Mechanical Engineers, 345 E. 47th St., New York, N. Y. 10017.
19. Kraus, H., "A Review and Evaluation of Computer Programs for the Analysis of Stresses in Pressure Vessels", Welding Research Council Bulletin No. 108, pages 11-28, (September, 1965).
20. Hoff, N. J., "Boundary Value Problems of the Thin-Walled Circular Cylinder", Journal of Applied Mechanics, 24, 243-250, (1950).
21. Timoshenko & Woinowsky-Krieger, "Theory of Plates and Shells", Second Edition, 1959, p. 466, McGraw-Hill Book Co., New York.
22. Reissner, E., "Stresses and Small Displacements of Shallow Spherical Shells", Part I, Journal of Math. and Phys., 25, 80-85, (1946).
23. Donnell, L. H., "Stability of Thin Walled Tubes Under Torsion", NACA Technical Report No. 479, 1933.
24. Taylor, C. E. and Lind, N. C., "Photoelastic Study of the Stresses Near Openings in Pressure Vessels", University of Illinois, T. & A.M. Report No. 270, (March, 1965). Also, see Reference (35).
25. Leven, M. M., "Photoelastic Determination of the Stresses in Reinforced Openings in Pressure Vessels", Westinghouse Research Laboratories Research Report 64-9D7-514-R1, (October 30, 1964). Also, see Reference (35).
26. Riley, W. F., "Experimental Determination of Stress Distributions in Thin-Walled Cylindrical and Spherical Pressure Vessels with Circular Nozzles", Welding Research Council Bulletin No. 108, pages 1-11, (September, 1965).

27. Maxwell, R. L., Holland, R. W., and Cofer, J. A., "Experimental Stress Analysis of the Attachment Region of Hemispherical Shells with Radially Attached Nozzles", University of Tennessee, Engineering Experiment Station, Knoxville, Tenn., Report ME-7-65-1.
28. Dally, J. W., "An Experimental Investigation of the Stresses Produced in Spherical Vessels by External Loads Transferred by a Nozzle", Welding Research Council Bulletin No. 84 (January, 1963).
29. Atterbury, T. J., Vagins, M., and McClure, G. M., "Branch Connections - Development of Rules for Design", Battelle Memorial Institute Report to the American Gas Association, January 30, 1961.
30. Lind, N. C., Hradek, R. W., and Cook, R. D., "Influence of Fillet Radii on Stresses Near Outlets in Pressure Vessels", University of Illinois, T. & A. M. Report No. 167 (March, 1961).
31. Rodabaugh E. C., and George, H. H., "Effect of Internal Pressure on Flexibility and Stress-Intensification Factors of Curved Pipe or Welding Elbows", ASME Trans., May, 1957.
32. National Electrical Manufacturers Association, "Mechanical Drive Steam Turbines", Pub. No. SM 20-1958 (Revised November, 1959), 155 E. 44th Street, New York 17, N. Y.
33. Rossheim, D. B. and Markl, A.R.C., "The Significance of, and Suggested Limits for, the Stress in Pipe Lines Due to the Combined Effects of Pressure and Expansion", ASME Trans., 1940.
34. Moore, S. E. and Witt, F. J., "CERL-II, A Computer Program for Analyzing Hemisphere-Nozzle Shells of Revolution with Axisymmetric and Unsymmetric Loadings", Oak Ridge National Laboratory, ORNL-3817, October, 1965.
35. Mershon, J. L., "Preliminary Evaluation of PVRC Photoelastic Test Data on Reinforced Openings in Pressure Vessels", Welding Research Council Bulletin No. 113 (April, 1966) pp 53-70. This bulletin also contains References (24) and (25).
36. Witt, F. J. and Greenstreet, B. L., "Analysis of Axisymmetrically Loaded Cylinder-to-Sphere Attachments", Oak Ridge National Laboratory, Oak Ridge, Tennessee, ORNL-3755.
37. Hardenbergh, D. E, Zamrik, S. Y., and Edmondson, A. J., "Experimental Investigation of Stresses in Nozzles in Cylindrical Pressure Vessels", Welding Research Council Bulletin No. 89 (July, 1963).
38. Cranch, E. T., "An Experimental Investigation of Stresses in the Neighborhood of Attachments to a Cylindrical Shell", Welding Research Council Bulletin No. 60 (May, 1960).

# APPENDIX

## TABLE OF CONTENTS

	<u>Page</u>
DEVELOPMENT OF DESIGN GRAPHS . . . . .	A-1
Parametric Study . . . . .	A-1
Stress Indices . . . . .	A-1
Juncture Stresses . . . . .	A-4
Design Graphs for Stress Indices	
at Juncture . . . . .	A-5
Combinations of Variables . . . . .	A-5
Dimensional Limits . . . . .	A-6
APPLICATION OF DESIGN GRAPHS . . . . .	A-9

FIGURES FOR APPENDIX

No.	Titles
A1	Nomenclature and Sign Conventions
A2	$K_{n\theta}$ for Internal Pressure
A3	$K_{b\theta}$ for Internal Pressure
A4	$K_{n\theta}$ for Internal Pressure
A5a	$K_{b\theta}$ for Internal Pressure, $t/T \geq 0.1$
A5b	$K_{b\theta}$ for Internal Pressure, $t/T \leq 0.1$
A6	$K_{ny}$ for Internal Pressure
A7	$K_{n\theta}$ for Moment Loading
A8	$K_{b\theta}$ for Moment Loading
A9	$K_{n\theta}$ for Moment Loading
A10a	$K_{b\theta}$ for Moment Loading, $t/T \geq 0.1$
A10b	$K_{b\theta}$ for Moment Loading, $t/T \leq 0.1$
A11	$K_{ny}$ for Moment Loading
A12	$K_{n\theta}$ for Thrust Loading
A13	$K_{b\theta}$ for Thrust Loading
A14	$K_{n\theta}$ for Thrust Loading
A15a	$K_{b\theta}$ for Thrust Loading, $t/T \geq 0.1$
A15b	$K_{b\theta}$ for Thrust Loading, $t/T \leq 0.1$
A16	$K_{ny}$ for Thrust Loading

DEVELOPMENT OF DESIGN GRAPHSParametric Study

The design information presented herein is based on a parametric study\* conducted at Oak Ridge National Laboratory using the CERL II computer program<sup>(34)</sup>. A Poisson's ratio of 0.3 was used. The nomenclature and sign conventions are shown in Figure A-1, page A-2.

The parametric study covered the following:

1. Sphere diameter to thickness ratio, D/T

$$\frac{D}{T} = 10, 25, 50, 100, 250, 750, 1000.$$

2. Nozzle diameter to sphere diameter ratio, d/D

$$\frac{d}{D} = .01, .025, .05, .1, .25, .3, .4, .5 .$$

3. Nozzle thickness to sphere thickness ratio, t/T

$$\frac{t}{T} = .01, .0133, .02, .04, .10, .25, .3, .4, .5, .6, .8, 1.0, 1.5, 2.0, 3.0.$$

4. Loadings

Internal pressure, moment applied to nozzle, thrust applied to nozzle.

Stress Indices

It is obvious that, in order for the design data to be generally applicable, dimensions must be presented as dimensionless ratios, e. g.,

---

\* The authors wish to acknowledge the efforts of S. E. Moore, who was instrumental in obtaining the results from the CERL Code (see Reference 34).

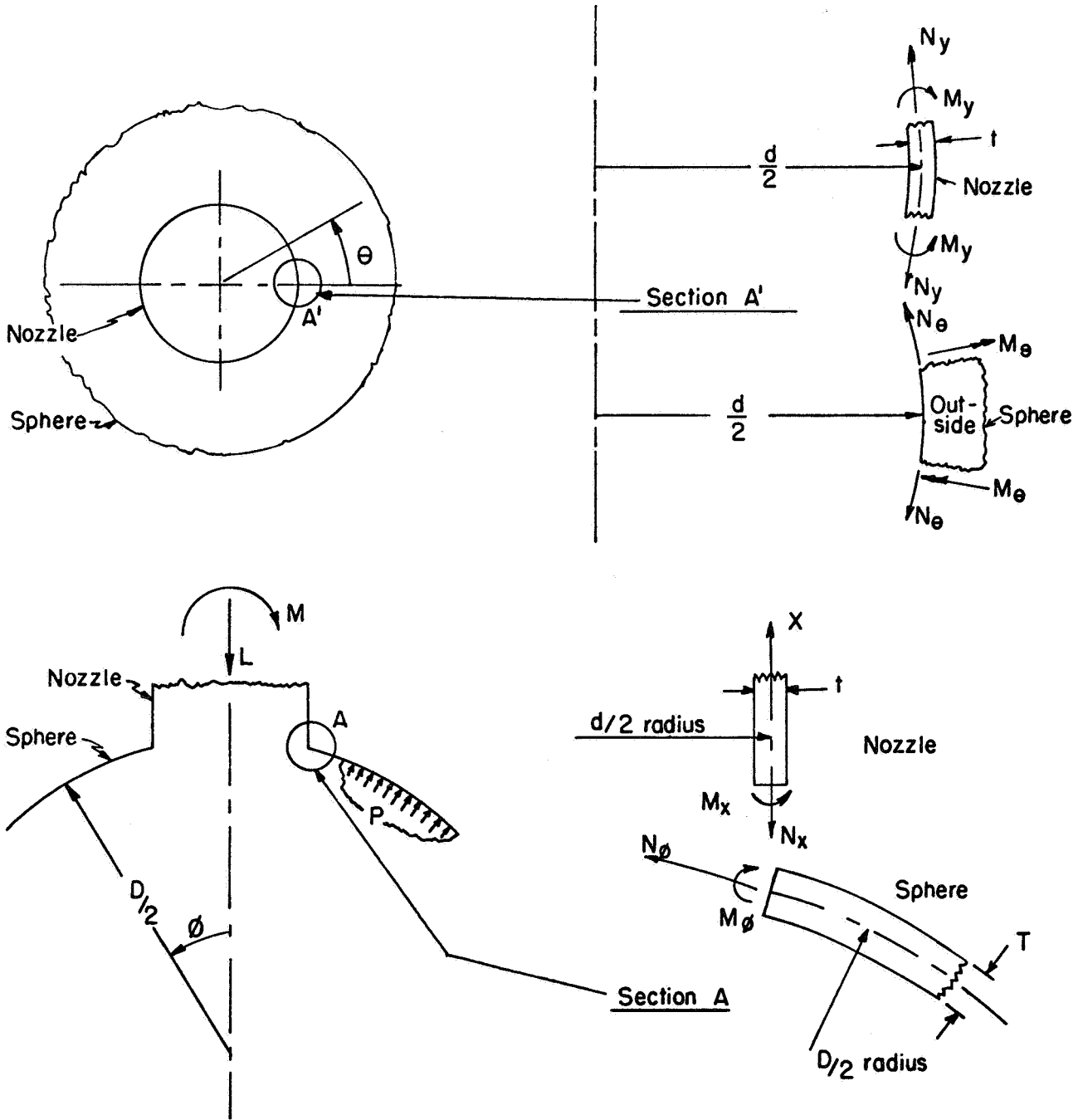


FIGURE A1, NOMENCLATURE ILLUSTRATION

D/T. It is then necessary to also present the stresses as dimensionless ratios, or "stress indices". A question arises as to what stress indices would be most informative to the user of the design data. For pressure loading, the designer will normally know the nominal stress in the sphere or sphere segment and will be interested in the stresses in the vicinity of the nozzle relative to the nominal stress in the sphere. For moment or thrust loading, the designer will generally know the external loads as supplied, for example, by a piping system flexibility analysis\*, and will be interested in the stresses in the vicinity of the nozzle relative to the nominal stress in the nozzle, i.e., stress intensification factors analogous to those presently used for piping system components<sup>(18)</sup>. This reasoning leads to the stress indices:

Pressure Loading

$$K_{ij} = \frac{\sigma_{ij}}{PD/4T} \quad (A1)$$

Moment Loading

$$K_{ij} = \frac{\sigma_{ij}}{4M/\pi d^2 t} \quad (A2)$$

Thrust Loading

$$K_{ij} = \frac{\sigma_{ij}}{L/\pi d t} \quad (A3)$$

where:

- $K_{ij}$  = stress index corresponding to  $\sigma_{ij}$
- P = internal pressure, psi
- M = moment applied to nozzle, in-lb
- L = thrust applied to nozzle, lb
- D = sphere mean diameter, inches
- T = sphere wall thickness, inches
- d = nozzle mean diameter, inches
- t = nozzle thickness, inches

---

\* The flexibility of the nozzle must be known for the piping system analysis. This aspect of nozzles in spheres will be covered in a subsequent report.

Juncture Stresses

The stresses at the nozzle-sphere juncture are given by the equations:

Sphere

$$\sigma_{\theta} = S (K_{n\theta} \pm K_{b\theta}) \quad (A4)$$

$$\sigma_{\phi} = S (K_{n\phi} \pm K_{b\phi}) \quad (A5)$$

Nozzle

$$\sigma_y = S (K_{ny} \pm \nu \left(\frac{T}{t}\right)^2 K_{b\phi}) \quad (A6)$$

$$\sigma_x = S \left(\frac{d}{D} \frac{T}{t} \pm \left(\frac{T}{t}\right)^2 K_{b\phi}\right) \text{ for pressure-loading} \quad (A7a)$$

$$\sigma_x = S \left(-1 \pm \left(\frac{T}{t}\right)^2 K_{b\phi}\right) \text{ for moment or thrust loading} \quad (A7b)$$

where

$S$  = nominal stress, psi

$S$  =  $PD/4T$  for pressure loading

$S$  =  $4M/\pi d^2 t$  for moment loading

$S$  =  $L/\pi dt$  for thrust loading

$\nu$  = Poisson's ratio = .3

For moment loading, equations (A4) through (A7) are multiplied by the factor  $(\cos \theta)$ , where  $\theta$  is the angle from the plane of the applied moment, as shown on Figure A1.

The directions of  $\sigma_{\theta}$ ,  $\sigma_{\phi}$ ,  $\sigma_x$ , and  $\sigma_y$  are shown in Figure A1. The normal stresses are  $\sigma_{\theta}$  and  $\sigma_y$ ; tangential stresses are  $\sigma_{\phi}$  and  $\sigma_x$ .

A tensile stress is defined as positive; a compressive stress as negative. The + part of the  $\pm$  signs applies to the inside surface, the - part of the  $\pm$  signs applies to the outside surface. For the midwall



(average) stress, the bending component ( $K_{b\theta}$ ,  $K_{b\phi}$ ) is taken as zero.

The signs of the stress components are for the loadings applied in the directions shown in Figure A1. For reversed loading directions, all signs are reversed. One may, for such loads, define  $P$  as  $-P$  (in the absence of instability),  $M$  as  $-M$  or  $L$  as  $-L$ . For moment loading, the signs of the stresses are for that section where the moment produces nominal compressive stresses in the nozzle, Section A of Figure A1. These stresses are proportional to  $\cos \theta$  (Figure A1), hence their signs are reversed at  $\theta = 180^\circ$ .

#### Design Graphs for Stress Indices at Juncture

The values of the five stress indices required in Equations A4 through A7 ( $K_{b\theta}$ ,  $K_{n\theta}$ ,  $K_{b\phi}$ , and  $K_{ny}$ ) are presented in:

Pressure Loading	Figures A2 through A6
Moment Loading	Figures A7 through A11
Thrust Loading	Figures A12 through A16.

A discussion of the dimensional variables, dimensional limits and accuracy is given below.

#### Combinations of Variables

It is apparent that the geometric description of a nozzle in a sphere requires four independent dimensions, i.e.,  $D$ ,  $T$ ,  $d$ , and  $t$ . The stress indices are necessarily functions of three dimensional ratios; for the design graphs the ratios  $D/T$ ,  $d/D$ , and  $t/T$  were selected. If these ratios are not in some way interdependent, with respect to the stress indices, then concise graphical presentation of design data becomes difficult since for each stress index and loading, a double family of curves is required. Leckie and Penny<sup>(1)</sup>, however, noted that the maximum stresses in the sphere could be presented as a function of two independent variables;  $(d/D) \sqrt{D/2T}$  and  $t/T$ , with relatively little effect of the  $D/T$  variable by itself. This reduction of independent variables from three to two is, of course, a major advantage in

presentation of the design data since only a single family of curves is required for any particular dependent variable.

Further investigation of the two independent variables  $(d/D)\sqrt{D/2T}$  and  $t/T$  shows that, for pressure loading, the maximum stress index is "practically independent" of  $D/T$ . The term "practically independent" is defined herein as meaning that the stress index plotted against  $(d/D)\sqrt{D/2T}$ , for a given  $t/T$ -value, may be represented by a single line for  $10 < D/T < 250$  with an accuracy, as compared to the computed stress, of  $\pm 20\%$ . For the individual stress indices, except  $K_{b\theta}$  and  $K_{ny}$ , these same two independent variables  $[(d/D)\sqrt{D/2T}, t/T]$  work equally well in reducing the independent variables from three to two. For  $K_{b\theta}$ , elimination of the  $D/T$ -variable occurs only at  $t/T$ -values of 1 and larger; for  $K_{ny}$ , only for midrange (.1 to 1.0) values of  $t/T$ .

In the case of moment or thrust loading (the design graphs are quite similar for these two loadings), the same two independent variables  $[(d/D)\sqrt{D/2T}$  and  $t/T]$  almost eliminate the  $D/T$ -variable ( $\pm 20\%$  accuracy) for  $K_{n\theta}$  and  $K_{b\theta}$ , as well as for  $K_{b\theta}$  with  $t/T \geq .15$ . For  $K_{b\theta}$  with small values of  $t/T$ ,  $D/T$  is a significant variable. Also, for moment or thrust loading, it is necessary to divide the stress index by suitable dimensional ratios in order to eliminate the  $D/T$ -variable. It is unfortunate that this division is necessary, since the significance of the stress index, in relation to nominal stresses, is not directly apparent from the design graphs. For the stress indices  $K_{n\theta}$  and  $K_{ny}$ , the parameter  $(d/D)\sqrt{D/2T}$  does not eliminate the  $D/T$ -variable nor does there appear to be any other combination of dimensions which, over the parameter range covered, is successful in eliminating the  $D/T$ -variable. The independent variables  $d/t$  and  $t/T$  have been used for plotting  $K_{ny}$ . These variables eliminate the  $D/T$ -variable for small values of  $t/T$  ( $\leq .04$ ) and partially eliminates the  $D/T$ -variable for larger values of  $t/T$ .

#### Dimensional Limits

The design graphs encompass the following dimensional ranges

$$10 < D/T < 250$$

$$.01 < d/D < .5$$

$$.01 < t/T < 3$$

Probably a large majority of pressure vessel nozzles will be included in these limits. The lower limit of D/T is based on the applicability of thin-shell theory. The parametric study included values of D/T up to 1,000; however, the method for reducing the design charts to two independent variables does not hold for large D/T and are not included in this report. The upper limit of d/D was established in conformance with the ASME Boiler and Pressure Vessel Code, Section VIII, which suggest that for openings in heads with d/D larger than 0.5, the opening should be designed as a reversed curve section.

There are two areas within the parametric study for which the design graphs are of limited significance. First, for certain combinations of D/T, d/D, and t/T the value of d/t is too small to be within the range of thin-shell theory. For example, the combination of d/D = .01, t/T = 0.1 and D/T = 10 gives d/t = 1.0. The results from models with d/t < 2.5 have been excluded from the design graphs. Secondly, for combinations of small t/T with large d/D, the nozzles are inadequate from the standpoint of nominal stresses due to pressure loading. This area can be examined in terms of the parameter

$$\frac{s}{S} = \frac{2d/D}{t/T}$$

where  $s$  = nominal stress in nozzle due to pressure loading  
 $s = Pd/2t$   
 $S$  = nominal stress in sphere due to pressure loading  
 $S = PD/4T$

For a combination of d/D = .5, t/T = .01, the value of s/S is 100. Models with such large values of s/S are not used in pressure vessels. However, where the sphere wall thickness is increased, locally or generally, as a means of reinforcing the opening, the designer may be

interested in models with  $s/S > 1$ ; reference (12) indicates  $s/S$  values up to around 5 as potentially of interest. Limiting  $s/S$  to a maximum of 5 gives the following limits to  $t/T$  and  $d/D$  combinations.

$t/T$	Maximum $d/D$
.01	.025
.02	.05
.04	.10
.10	.25
.20	.50

As an aid in interpolation, combinations of  $t/T$  and  $d/D$  giving  $s/S$  larger than 5 are shown on the design graphs, except where their presence would detract from the readability of the graphs.

APPLICATION OF DESIGN GRAPHS

The stresses at the juncture between nozzle and sphere are determined by substituting the values of  $K_{n\theta}$ ,  $K_{b\theta}$ ,  $K_{n\phi}$ ,  $K_{b\phi}$ , and  $K_{ny}$  from Figures A2 through A16 into Equations (A4) through (A7). These figures are based on the assumption that Poisson's ratio of the material used is equal to 0.3 and that the nozzle and sphere materials have the same modulus of elasticity; otherwise the properties of the materials do not enter into the stress calculations.

Application of the procedure for obtaining stresses from the design graphs is illustrated in the following by several examples.

Example 1

A 6" standard weight (6.625" O.D. x .280" nominal wall thickness, .245" minimum wall thickness) pipe nozzle is welded to a spherical head with 50" mean diameter, 0.500" nominal (.490" minimum) wall thickness. An internal pressure of 784 psi is the only loading. Stresses at the nozzle-sphere juncture are determined as follows.

Step 1: Calculate the ratios:

$$\frac{D}{T} = \frac{50}{.5} = 100$$

$$\frac{d}{D} = \frac{6.625 - .280}{50} = .127$$

$$\frac{t}{T} = \frac{.245}{.490} = .5$$

$$\frac{d}{D} \sqrt{\frac{D}{2T}} = .127 \times \sqrt{50} = .90$$

Step 2:

Enter Figures A2 through A6 with  $(d/D) \sqrt{D/2T} = .90$  to intersection with  $t/T = 0.5$  and  $D/T = 100$ :

from Figure A2:  $K_{n\theta} = 2.45$   
 from Figure A3:  $K_{b\theta} = -.53$   
 from Figure A4:  $K_{n\phi} = .30$   
 from Figure A5:  $K_{b\phi} = -1.1$   
 from Figure A6:  $K_{ny} = 2.45$

Step 3: Calculate stresses using Equations (A4) through (A7)

Stresses in the sphere:

$$S = \frac{PD}{4T} = \frac{784 \times 50}{4 \times .49} = 20,000 \text{ psi}$$

$$\sigma_{\theta} = 20,000 (2.45 \pm -.53)$$

On inside surface:  $\sigma_{\theta} = 20,000 (1.92) = 38,400 \text{ psi}$

On outside surface:  $\sigma_{\theta} = 20,000 (2.98) = 59,600 \text{ psi}$

At midwall  $\sigma_{\theta} = 20,000 (2.45) = 49,000 \text{ psi}$

$$\sigma_{\phi} = 20,000 (.30 \pm -1.1)$$

On inside surface:  $\sigma_{\phi} = 20,000 (-.80) = -16,000 \text{ psi}$

On outside surface:  $\sigma_{\phi} = 20,000 (1.40) = 28,000 \text{ psi}$

At midwal:  $\sigma_{\phi} = 20,000 (.30) = 6,000 \text{ psi}$

Stresses in the nozzle

$$\begin{aligned} \sigma_y &= 20,000 [2.45 \pm 0.3 \times \left(\frac{1}{.5}\right)^2 \times (-1.1)] \\ &= 20,000 (2.45 \pm -1.32) \end{aligned}$$

On inside surface:  $\sigma_y = 20,000 (1.13) = 22,600 \text{ psi}$

On outside surface:  $\sigma_y = 20,000 (3.77) = 75,400 \text{ psi}$

At midwall:  $\sigma_y = 20,000 (2.45) = 49,000 \text{ psi}$

$$\begin{aligned} \sigma_x &= 20,000 [.127 \times \frac{1}{.5} \pm \left(\frac{1}{.5}\right)^2 \times (-1.1)] \\ &= 20,000 (.25 \pm -4.40) \end{aligned}$$

On inside surface:  $\sigma_x = 20,000 (-4.15) = -83,000$  psi

On outside surface:  $\sigma_x = 20,000 (4.65) = 93,000$  psi

At midwall:  $\sigma_x = 20,000 (.25) = 5,000$  psi

### Example 2

The same nozzle and head as in Example 1, but the loading consists of a moment applied to the nozzle such that the nominal stress in the nozzle is 20,000 psi, i.e.,  $4M/\pi d^2 t = 20,000$ .

Step 1: Calculate the dimensional ratios as in Step 1 of Example 1 and, in addition;

$$\frac{d}{t} = \frac{6.345}{.245} = 25.9$$

Step 2: Enter Figures A7, A8, and A10 with  $(d/D) \sqrt{D/2T} = .90$ , Figures A9 and A11 with  $d/t = 25.9$ . Proceed to intersection with  $t/T = 0.5$ ,  $D/T = 100$ .

from Figure A7:  $K_{n\theta} = -.06 (D/T)^{1/2} (D/d)^{1/4}$

Figure A8:  $K_{b\theta} = .28 (D/T)^{1/2}$

Figure A9:  $K_{n\emptyset} = -.51$

Figure A10:  $K_{b\emptyset} = .17 (D/T)^{1/2} (D/d)^{1/4}$

Figure A11:  $K_{ny} = -1.45$

Step 3: Calculate values of  $K_{n\theta}$ ,  $K_{b\theta}$ ,  $K_{n\emptyset}$ ,  $K_{b\emptyset}$ ,  $K_{ny}$ :

$$K_{n\theta} = .06 \times (100)^{1/2} \times \left(\frac{1}{.127}\right)^{1/4} = .06 \times 10 \times 1.67 = -1.0$$

$$K_{b\theta} = .28 \times 10 \qquad \qquad \qquad 2.80$$

$$K_{n\emptyset} = \qquad \qquad \qquad -0.51$$

$$K_{b\phi} = .17 \times 10 \times 1.67 = 2.84$$

$$K_{ny} = -1.45$$

Step 4: Calculate stresses using Equations (A4) through (A7).

Stresses in sphere at  $\theta = 0$

It was assumed that  $S = 4M/\pi d^2 t = 20,000$ , hence

$$\sigma_{\theta} = 20,000 (-1.0 \pm 2.80)$$

On inside surface :  $\sigma_{\theta} = 20,000 (1.80) = 36,000$  psi

On outside surface:  $\sigma_{\theta} = 20,000 (-3.80) = -76,000$

At midwall:  $\sigma_{\theta} = 20,000 (-1.0) = -20,000$

$$\sigma_{\phi} = 20,000 (-.51 \pm 2.84)$$

On inside surface :  $\sigma_{\phi} = 20,000 (2.33) = 46,600$  psi

On outside surface :  $\sigma_{\phi} = 20,000 (-3.35) = -67,000$

At midwall:  $\sigma_{\phi} = 20,000 (-.51) = -10,200$

Stresses in nozzle at  $\theta = 0$

$$\sigma_y = 20,000 [-1.45 \pm 0.3 \times \left(\frac{1}{.5}\right)^2 \times (2.84)]$$

$$= 20,000 [-1.45 \pm 3.41]$$

On inside surface :  $\sigma_y = 20,000 (1.96) = 39,200$  psi

On outside surface :  $\sigma_y = 20,000 (-4.86) = -97,200$

At midwall:  $\sigma_y = 20,000 (-1.45) = -29,000$

$$\sigma_x = 20,000 [(-1) \pm \left(\frac{1}{.5}\right)^2 \times (2.84)]$$

$$= 20,000 \pm [(-1) \pm 11.36]$$



On inside surface :  $\sigma_x = 20,000 (10.36) = +207,000$  psi  
 On outside surface :  $\sigma_x = 20,000 (-12.36) = -247,000$   
 At midwall:  $\sigma_x = 20,000 (-.1) = -20,000$

Step 5: Stresses at  $\theta \neq 0$ .

Multiply stresses obtained in Step 4 by  $\cos \theta$ .

### Example 3

The same nozzle and head as in Example 1, except that an integral, uniform wall thickness pad around the opening is used to reinforce the opening. The thickness of this pad is  $T'$  and is equal to  $2T$ . The length of the pad is assumed to be greater than  $\sqrt{DT'}$  hence, the design graphs are applicable. With an internal pressure of 784 psi, the question is what moment can be applied to the nozzle as limited by a maximum midwall stress intensity of 30,000 psi; maximum surface stress intensity of 60,000 psi.

Step 1: Calculate the ratios

$$\frac{D}{T'} = \frac{50}{1} = 50$$

$$\frac{d}{D} = .127$$

$$\frac{t}{T'} = .25$$

$$\frac{d}{D} \sqrt{\frac{D}{2T'}} = .127 \times \sqrt{25} = .64$$

$$\frac{d}{t} = 25.9$$

Step 2: Calculate the stresses due to pressure as in Example 1.

$$S = \frac{PD}{4T} = \frac{784 \times 50}{4 \times .98} = 10,000 \text{ psi}$$

$$\begin{aligned} \sigma_{\theta} &= 10,000 (2.5 \pm -.78) = 17,200 \text{ psi inside} \\ &= 32,800 \text{ psi outside} \\ &= 25,000 \text{ psi midwall} \\ \sigma_{\phi} &= 10,000 (.13 \pm -.30) = -1,700 \text{ psi inside} \\ &= 4,300 \text{ psi outside} \\ &= 1,300 \text{ psi midwall} \\ \sigma_y &= 10,000 [2.6 \pm (.3) \left(\frac{1}{.25}\right)^2 (-.30)] = 11,600 \text{ psi inside} \\ &= 40,400 \text{ psi outside} \\ &= 26,000 \text{ psi midwall} \\ \sigma_x &= 10,000 [.51 \pm \left(\frac{1}{.25}\right)^2 (-.30)] = -42,900 \text{ psi inside} \\ &= 53,000 \text{ psi outside} \\ &= 5,100 \text{ psi midwall} \end{aligned}$$

Step 3: Calculate stresses due to moment as in Example 3, except that  $S = 4M/\pi d^2 t$  is retained as a factor.

$$\begin{aligned} \sigma_{\theta} &= S(-.32 \pm 1.56) = 1.24 S \text{ inside at } \theta = 0 \\ &= -1.88 S \text{ outside} \\ &= -.32 S \text{ midwall} \\ \sigma_{\phi} &= S (-.14 \pm .33) = .19 S \text{ inside} \\ &= -.47 S \text{ outside} \\ &= -.14 S \text{ midwall} \\ \sigma_y &= S(-.62 \pm 1.58) = .96 S \text{ inside} \\ &= -2.20 S \text{ outside} \\ &= -.62 S \text{ midwall} \\ \sigma_x &= S (-1. \pm 5.28) = 4.28 S \text{ inside} \\ &= -6.28 S \text{ outside} \\ &+ -1.0 S \text{ midwall} \end{aligned}$$

Step 4: Determine stress intensities due to pressure plus moment

Stress intensities are defined by the quantities:

$$(\sigma_{\theta} - \sigma_{\phi}), (\sigma_{\theta} - \sigma_r), (\sigma_{\phi} - \sigma_r)$$

$$(\sigma_y - \sigma_x), (\sigma_y - \sigma_r), (\sigma_x - \sigma_r) .$$

The radial stress is equal to  $-P$  on the inside surface, zero on the outside surface and, as an approximation,  $-P/2$  at the midwall. Since the stresses due to the moment vary with  $\theta$ , this variation must be considered. However, only the values at  $\theta = 0$  and  $\theta = 180$  are significant in this example; intermediate values of  $\theta$  will give intermediate values of the stress intensities.

From Steps 2 and 3:

	Inside	Outside	Midwall
$\sigma_{\theta} - \sigma_r$	18,000 + 1.24 S /	32,800 + 1.88 S *	25,400 + .32 S *
$\sigma_{\phi} - \sigma_r$	- 900 - .19 S *	4,300 + .47 S *	1,700 + .14 S *
$\sigma_{\theta} - \sigma_{\phi}$	+18,900 + 1.05 S /	+28,500 + 1.41 S *	+23,700 + .18 S *
$\sigma_y - \sigma_r$	12,400 + .96 S /	40,400 + 2.20 S *	26,400 + .62 S *
$\sigma_x - \sigma_r$	-42,100 - 4.28 S *	53,000 + 6.28 S *	5,500 + 1.0 S *
$\sigma_y - \sigma_x$	+54,500 + 3.32 S *	-12,600 - 4.08 S *	+20,900 + .38 S /

/ at  $\theta = 0^{\circ}$

\* at  $\theta = 180^{\circ}$

In the above tabulation, the stresses due to the moment have been taken at  $\theta = 0$  or  $\theta = 180$  so that they add to the stress intensity due to pressure and hence indicate the maximum absolute value of the stress intensity around the nozzle.

Step 5: Determine maximum value of  $S$  ( $=4M/\pi d^2 t$ ).

(a) Midwall stress intensity limited to 30,000 psi.

Each of the six stress intensity values listed under "Midwall" are equated to 30,000 and solved for  $S$ ; the smallest value of  $S$  must be used. The controlling stress intensity is  $\sigma_y - \sigma_r$ , giving:

$$26,400 + .62 S = 30,000$$

$$S = \frac{30,000 - 26,400}{.62} = 5,800 \text{ psi}$$

(b) Surface stress intensity limited to 60,000 psi.

Each of the twelve stress intensity listed under "Inside" and "Outside" are equated to 60,000 psi and solved for  $S$ ; the smallest value of  $S$  must be used. The controlling stress intensity is  $\sigma_x$  on the outside surface (actually  $\sigma_x - \sigma_r$ , where  $\sigma_r = 0$ ), giving:

$$53,000 + 6.28 S = 60,000$$

$$S = \frac{60,000 - 53,000}{6.28} = 1,110 \text{ psi}$$

Step 6: Determine maximum permissible moment.

The value of  $S$  must be limited to 1,110 psi in order to limit the maximum stress intensity on the surface to 60,000 psi. This value of  $S$  will also insure that the maximum midwall stress intensity is less than 30,000 psi.

$$S = \frac{4M}{\pi d^2 t} = 1,110$$

$$M = \frac{1.110 \pi d^2 t}{4} = \frac{1.110 \times \pi \times (6.345)^2 \times .280}{4} = 9,800 \text{ in-lb.}$$

Accordingly, the maximum moment that can be applied to the nozzle, within the prescribed stress limits, is 9,800 in-lb. If higher moment load capacity is desired, an obvious next step would be to make the nozzle of heavier pipe, e.g., 6" Sch 80, at least for a distance of  $\sqrt{dt}$  from the juncture.

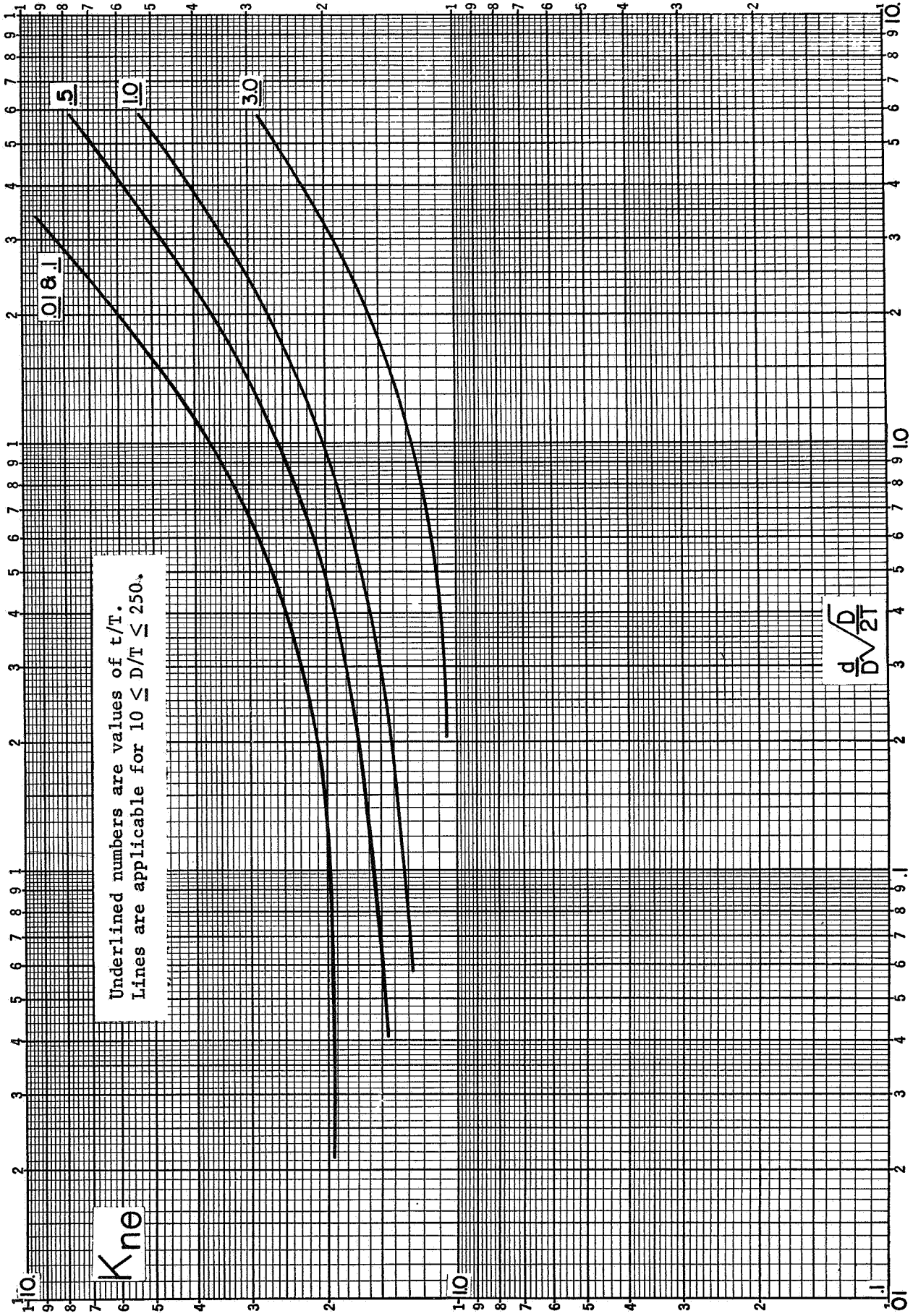


FIGURE A-2.  $K_{n\theta}$  FOR INTERNAL PRESSURE

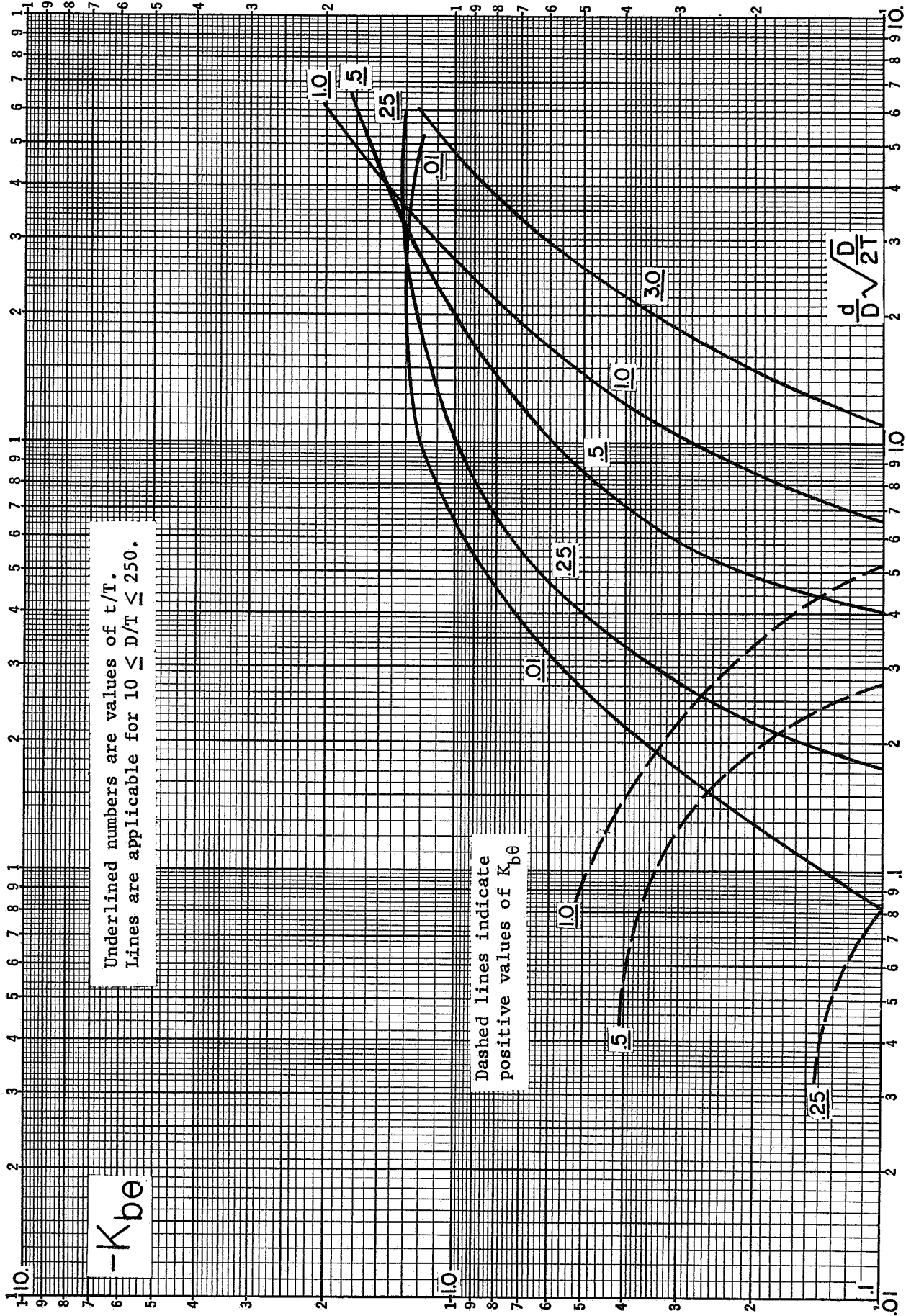


FIGURE A-3.  $K_{b\theta}$  FOR INTERNAL PRESSURE

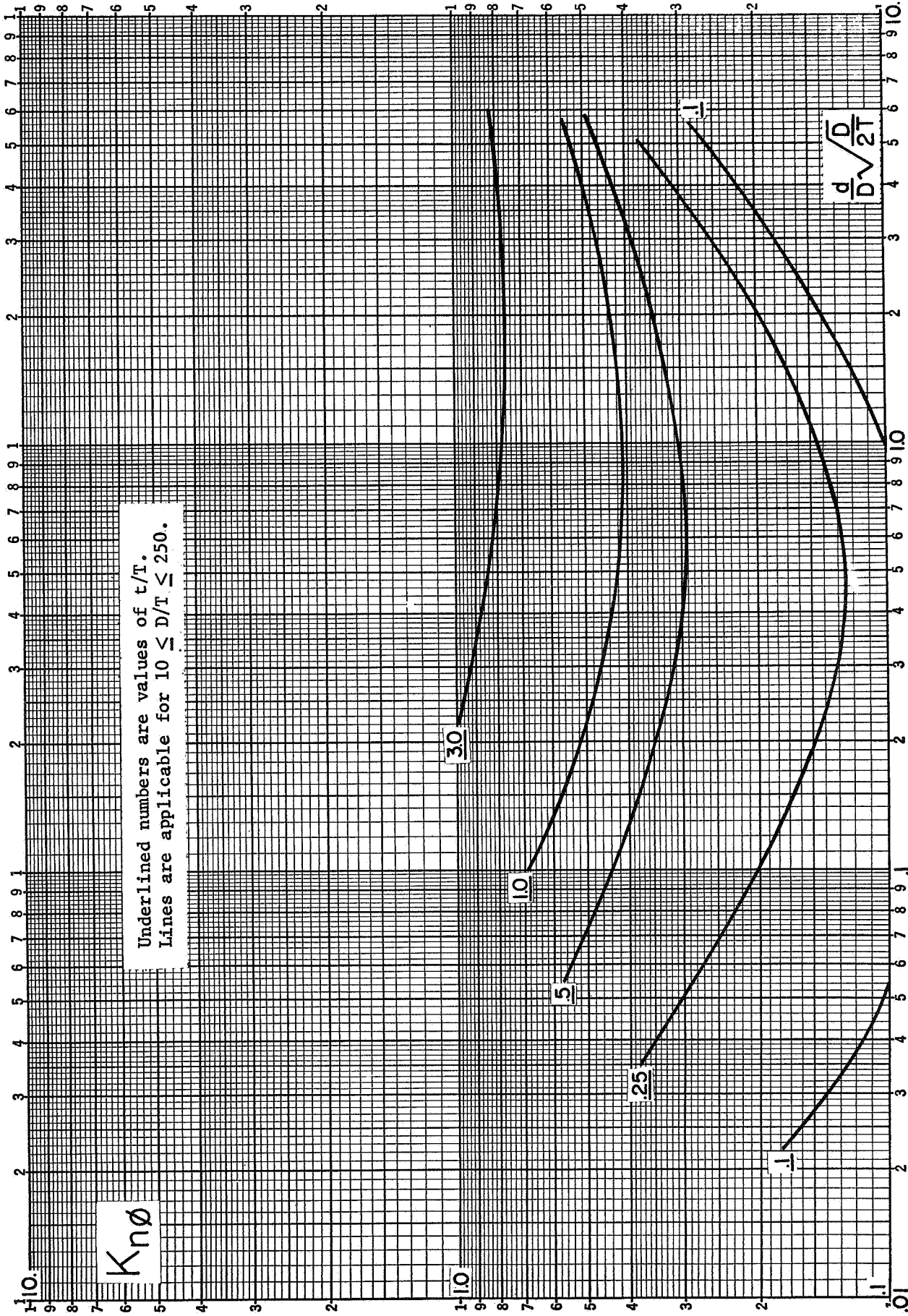


FIGURE A-4.  $Kn\phi$  FOR INTERNAL PRESSURE



(Max values of  $-K_{b\phi}$  are at  $\frac{t}{T} = 1.0$ )

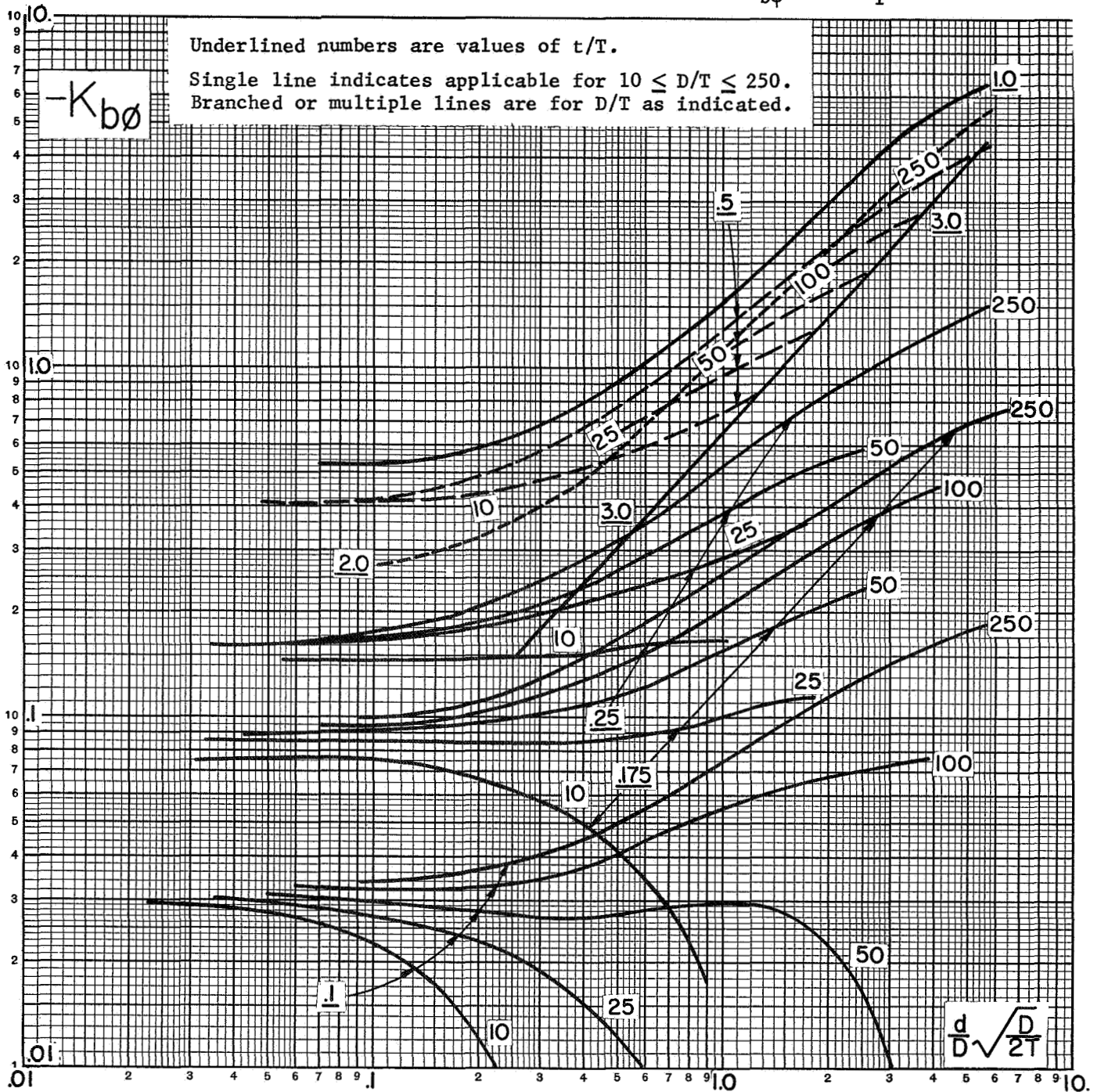


FIGURE A-5a.  $K_{b\phi}$  FOR INTERNAL PRESSURE (continued)

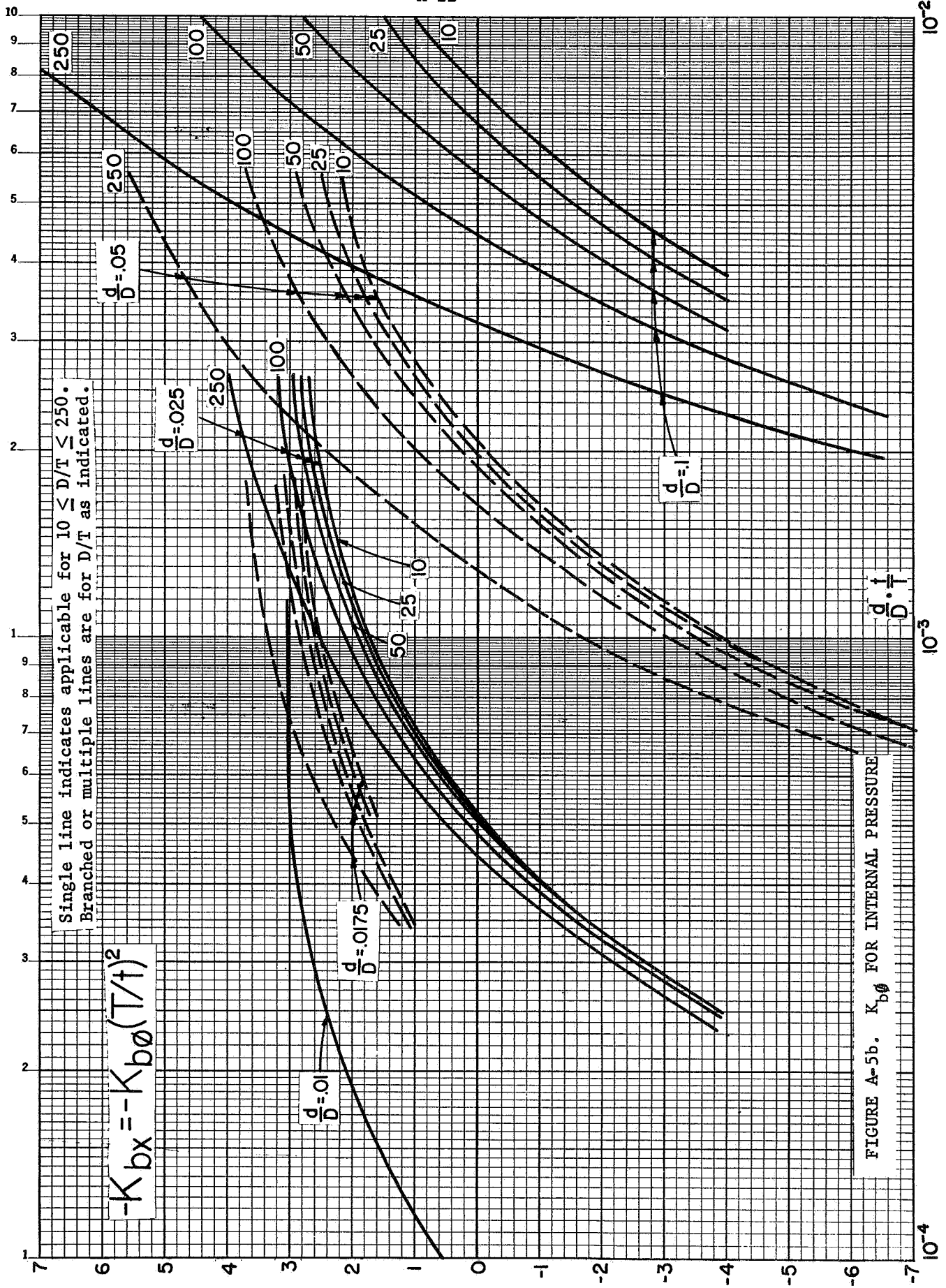


FIGURE A-5b.  $K_{b\phi}$  FOR INTERNAL PRESSURE

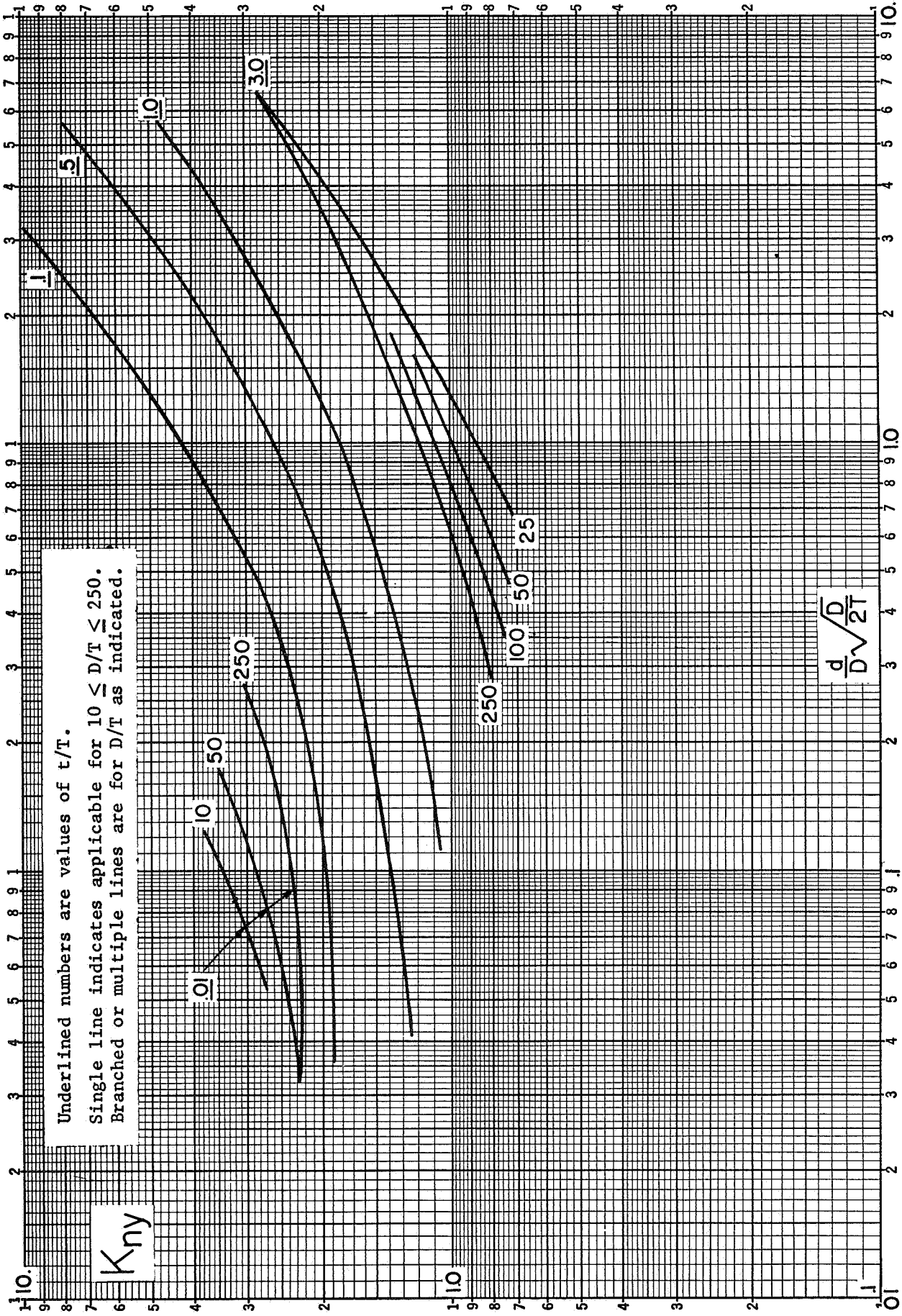


FIGURE A-6.  $K_{ny}$  FOR INTERNAL PRESSURE

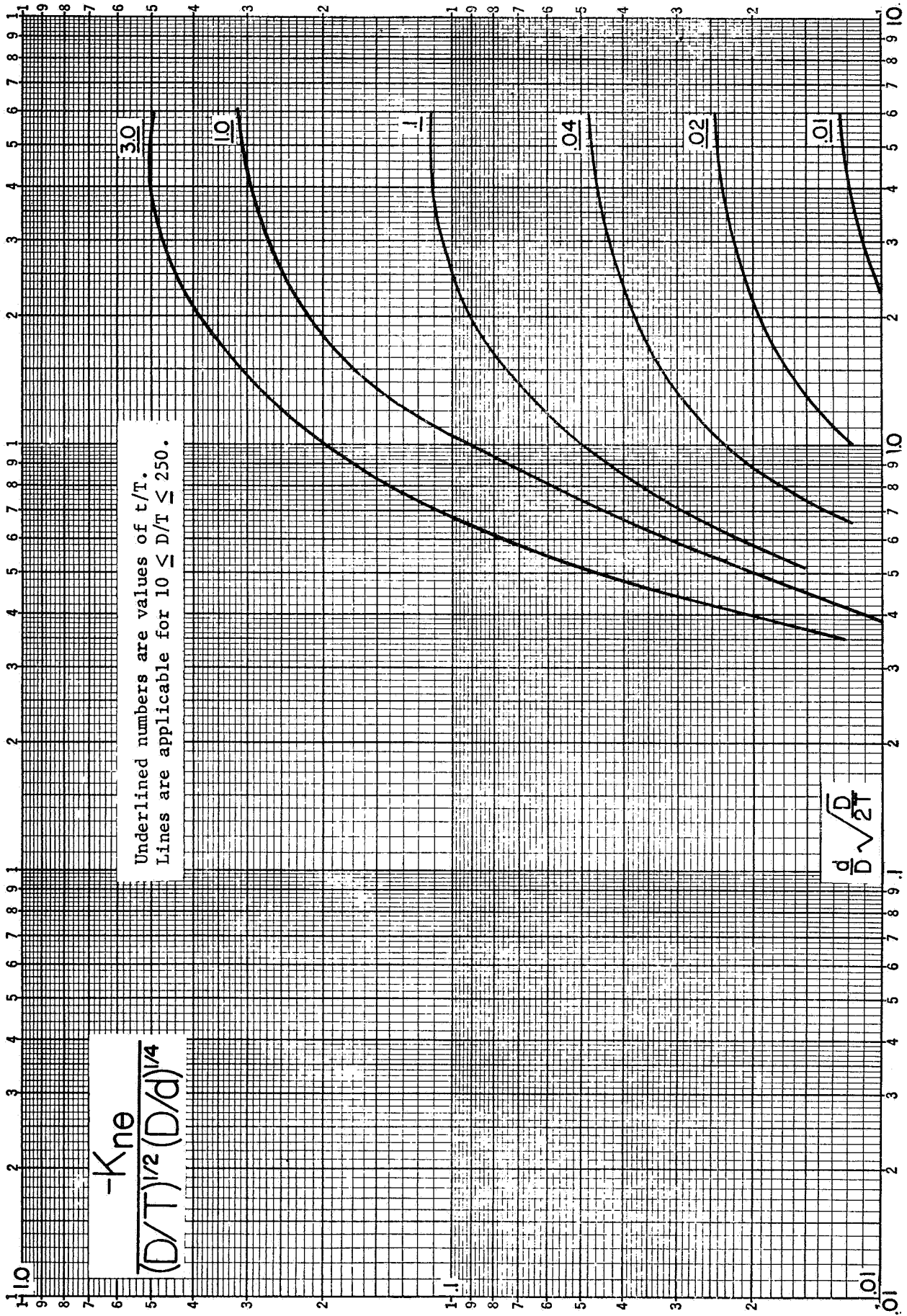


FIGURE A-7.  $K_{ne}$  FOR MOMENT LOADING

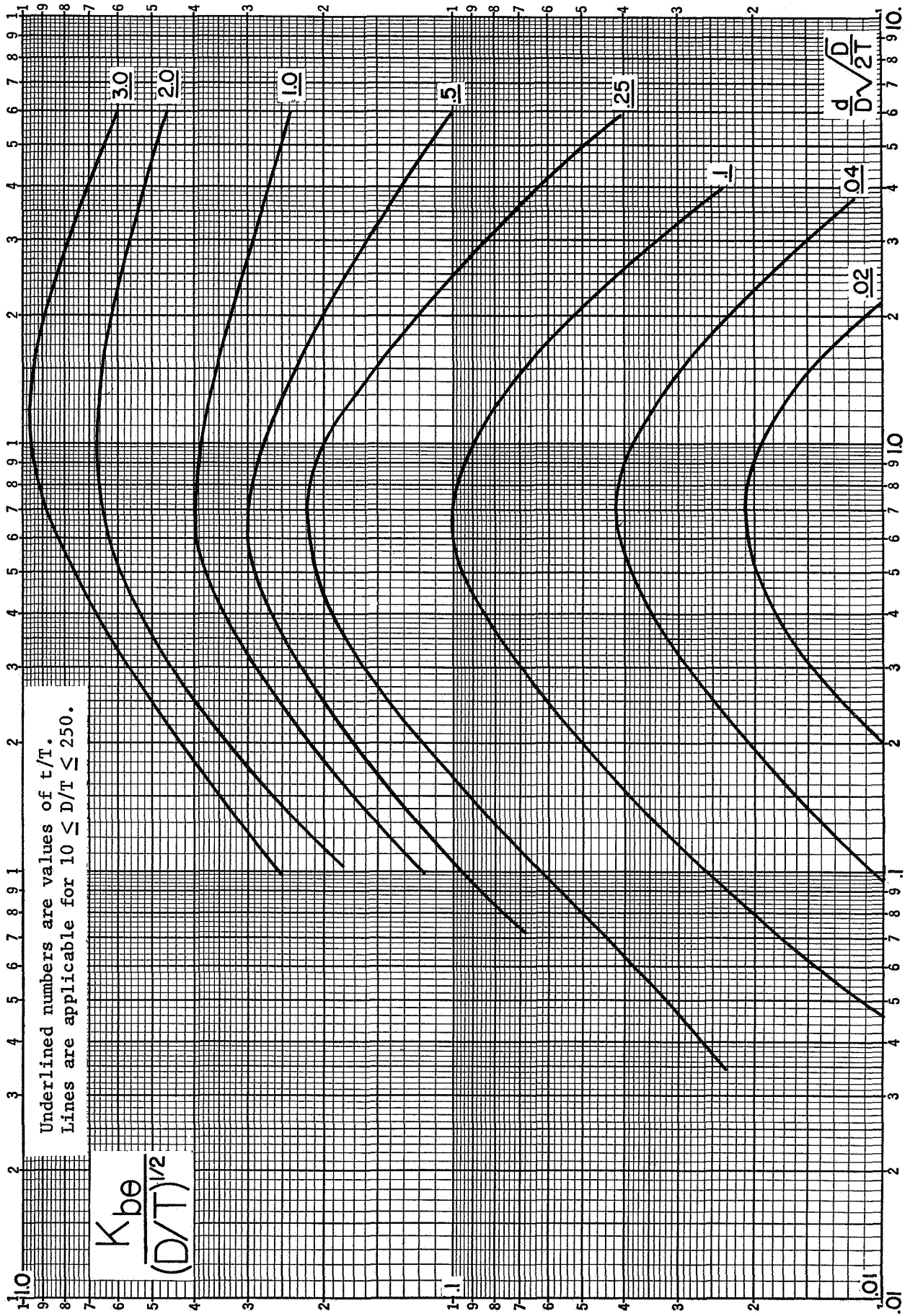


FIGURE A-8.  $K_{b\theta}$  FOR MOMENT LOADING

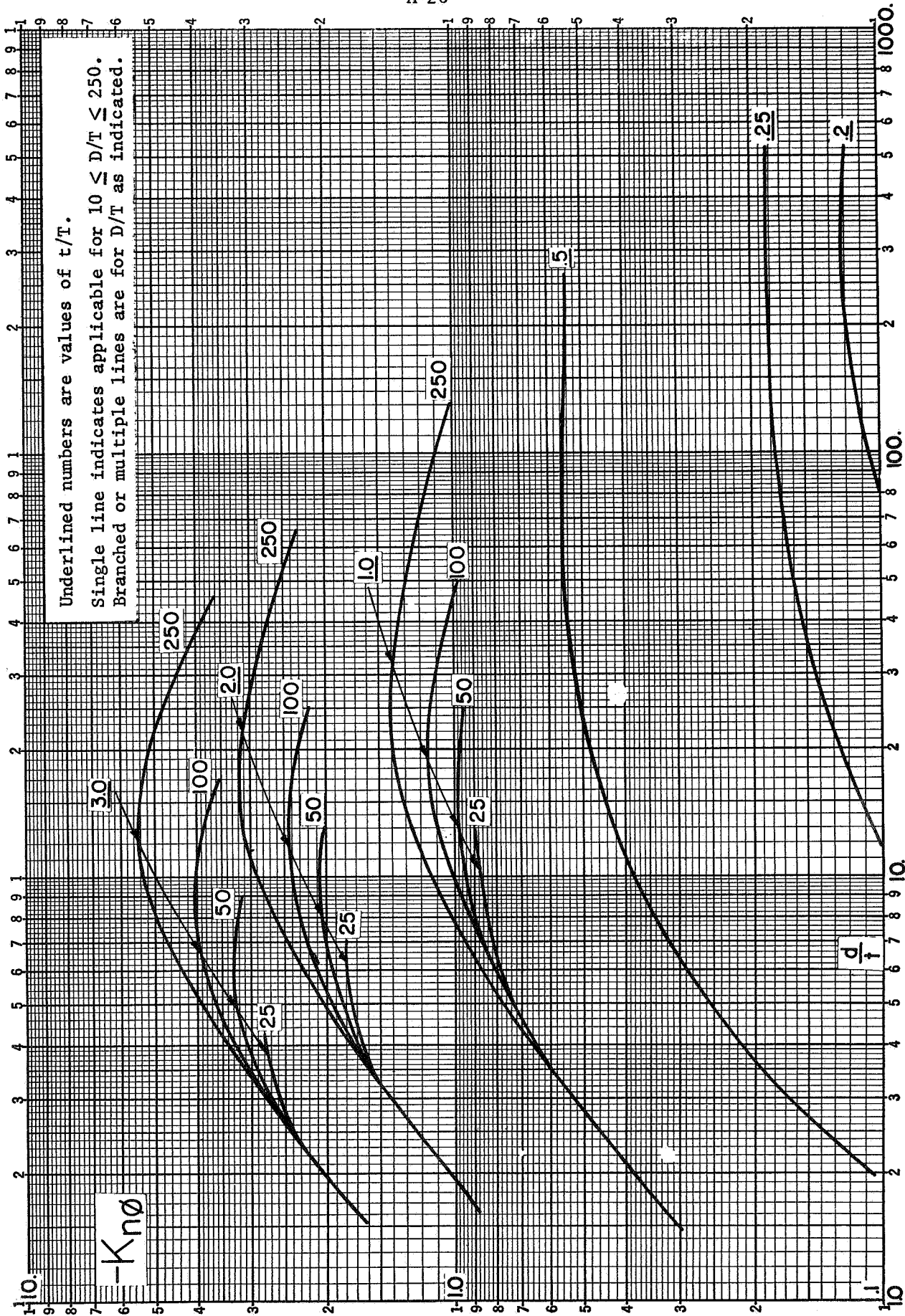


FIGURE A-9.  $K_n\phi$  FOR MOMENT LOADING

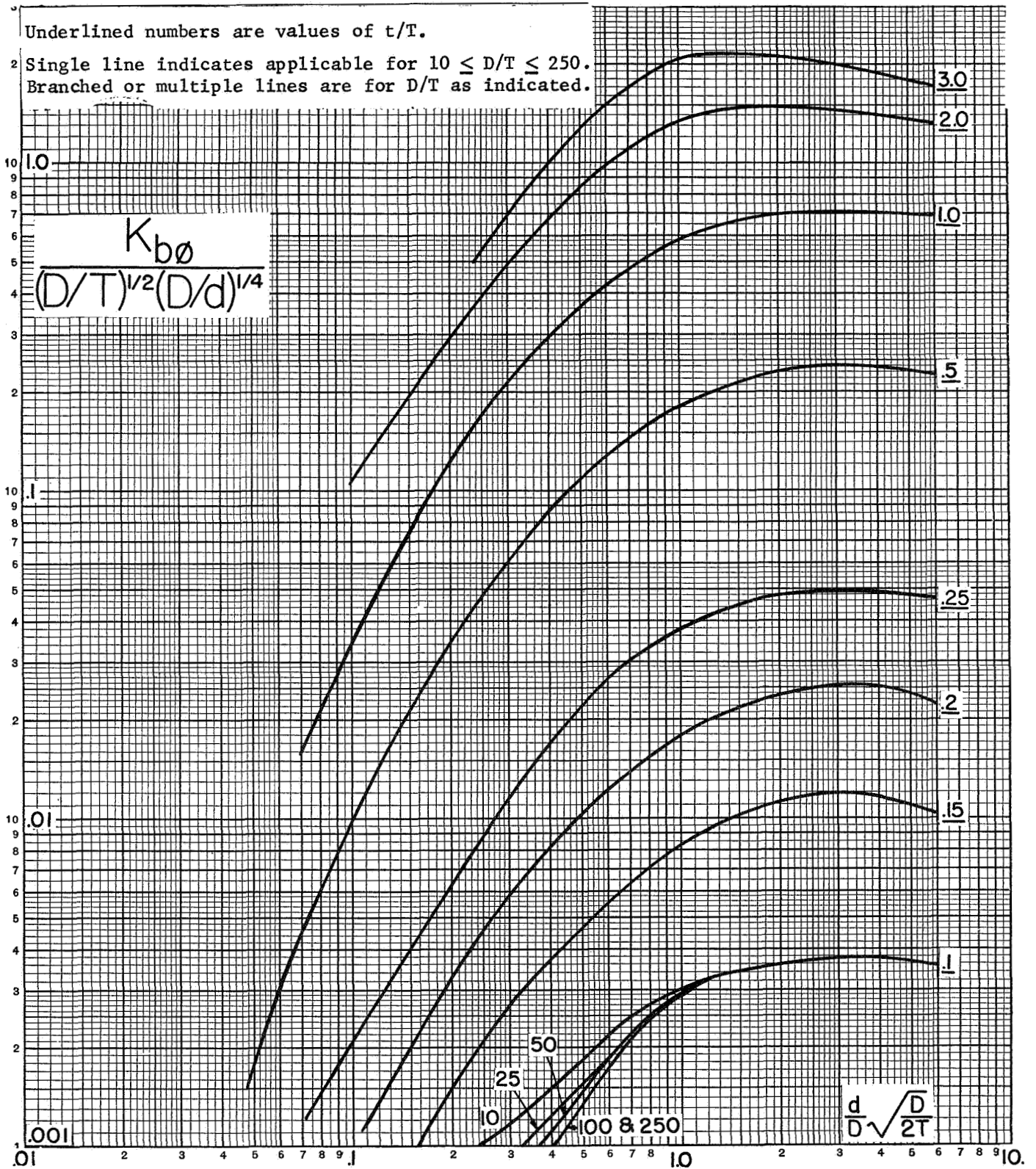


FIGURE A-10a.  $K_{b0}$  FOR MOMENT LOADING (continued)

Underlined numbers are values of  $t/T$ .

Single line indicates applicable for  $10 \leq D/T \leq 250$ .  
 Branched or multiple lines are for  $D/T$  as indicated.

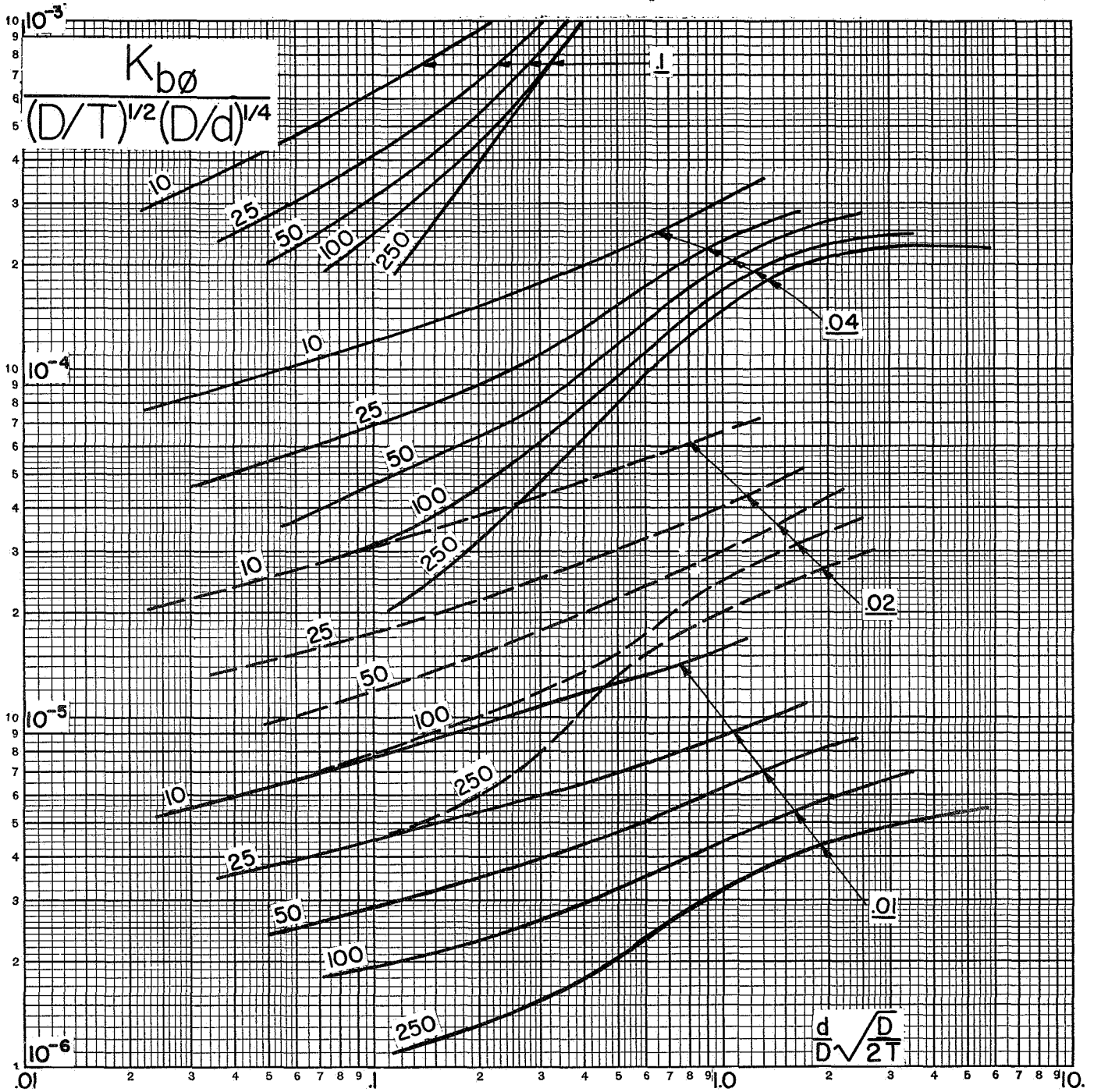


FIGURE A-10b.  $K_{b0}$  FOR MOMENT LOADING



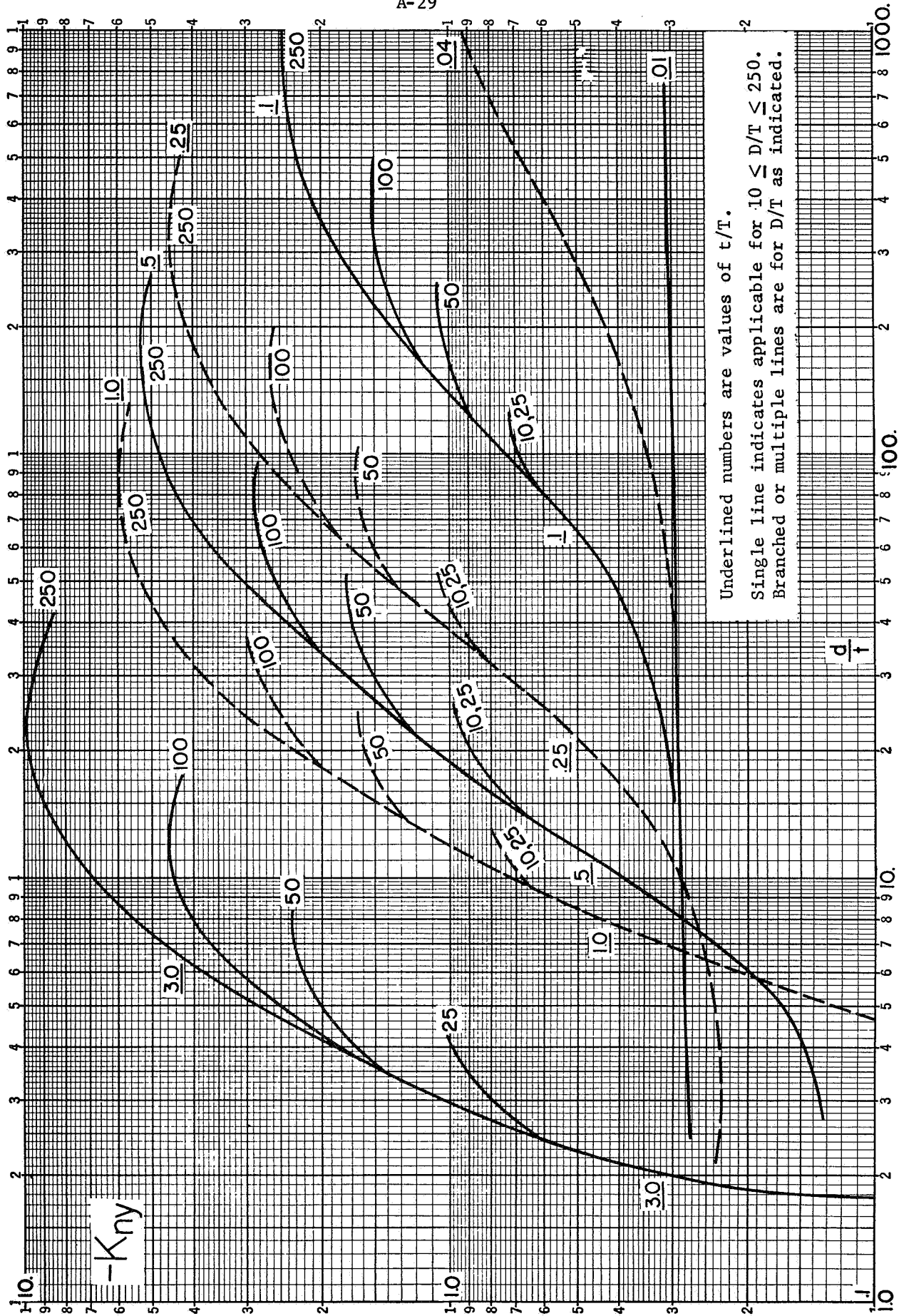


FIGURE A-11.  $K_{ny}$  FOR MOMENT LOADING

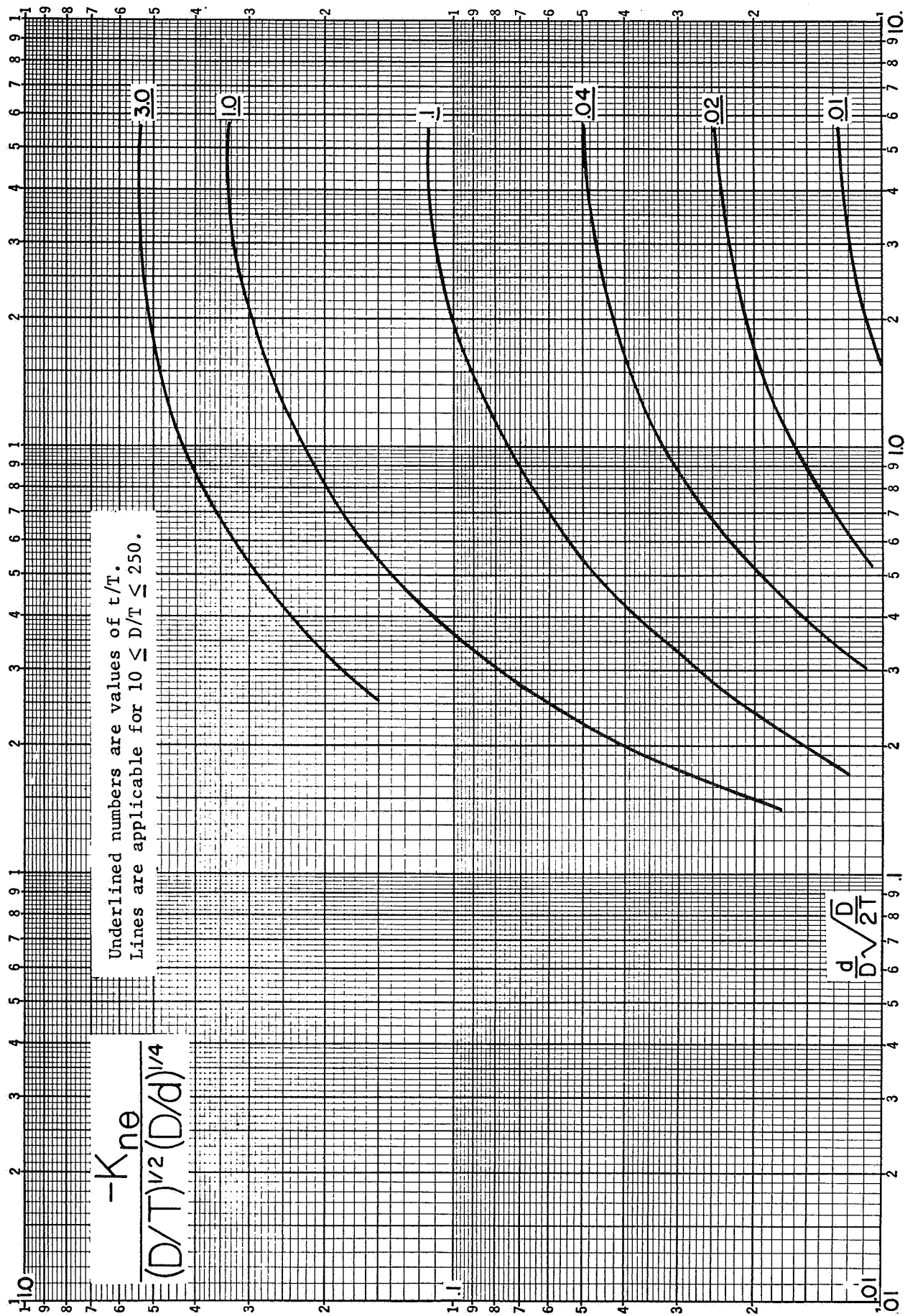


FIGURE A-12.  $K_{n\theta}$  FOR THRUST LOADING

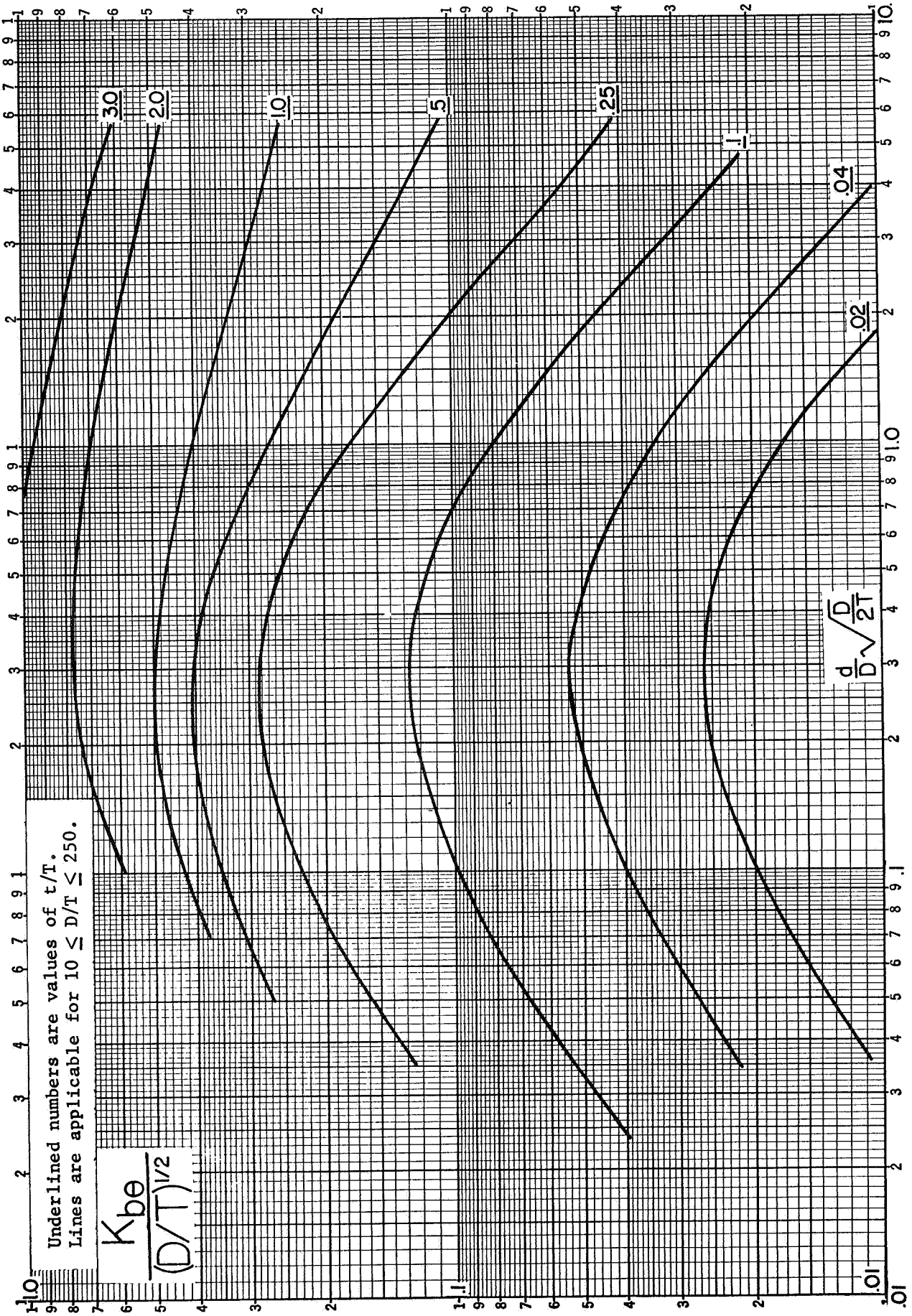


FIGURE A-13.  $K_{b\theta}$  FOR THRUST LOADING

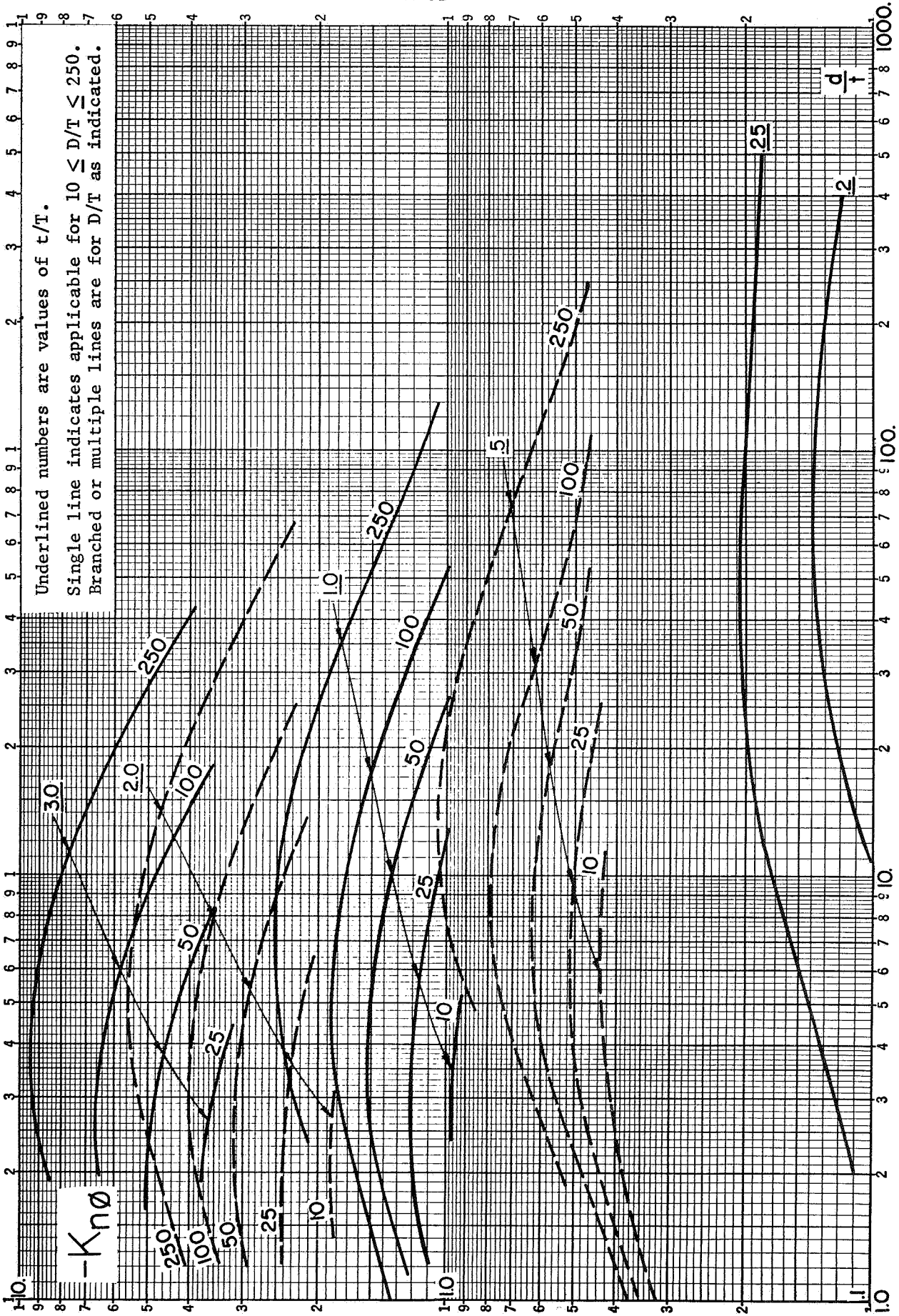


FIGURE A-14.  $K_{n0}$  FOR THRUST LOADING

Underlined numbers are values of  $t/T$ . A-33

Single line indicates applicable for  $10 \leq D/T \leq 250$ .

Branched or multiple lines are for  $D/T$  as indicated.

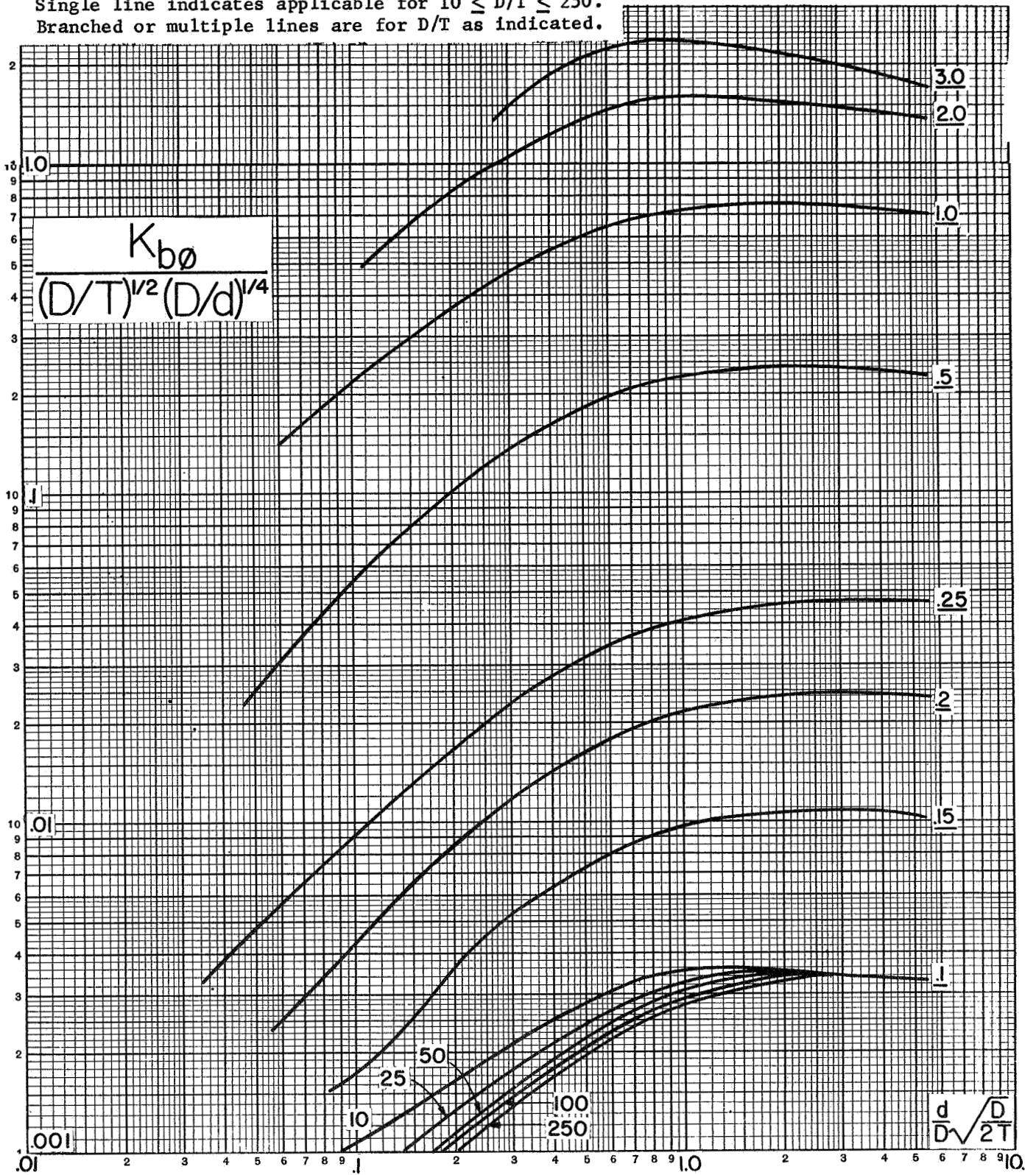


FIGURE A-15a.  $K_{b0}$  FOR THRUST LOADING (continued)

Underlined numbers are values of  $t/T$ .

Single line indicates applicable for  $10 \leq D/T \leq 250$ .

Branched or multiple lines are for  $D/T$  as indicated.

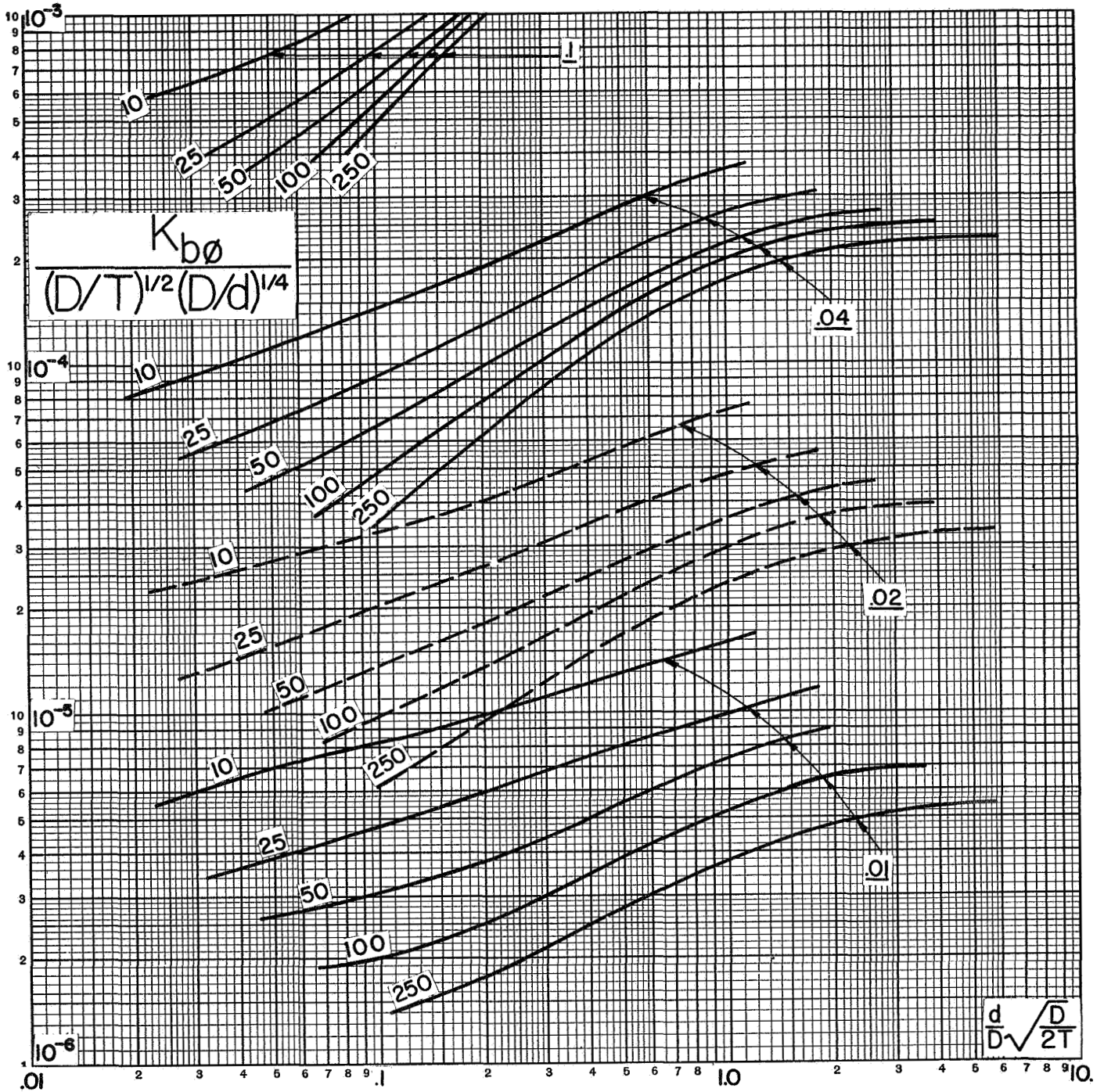


FIGURE A-15b.  $K_{b0}$  FOR THRUST LOADING

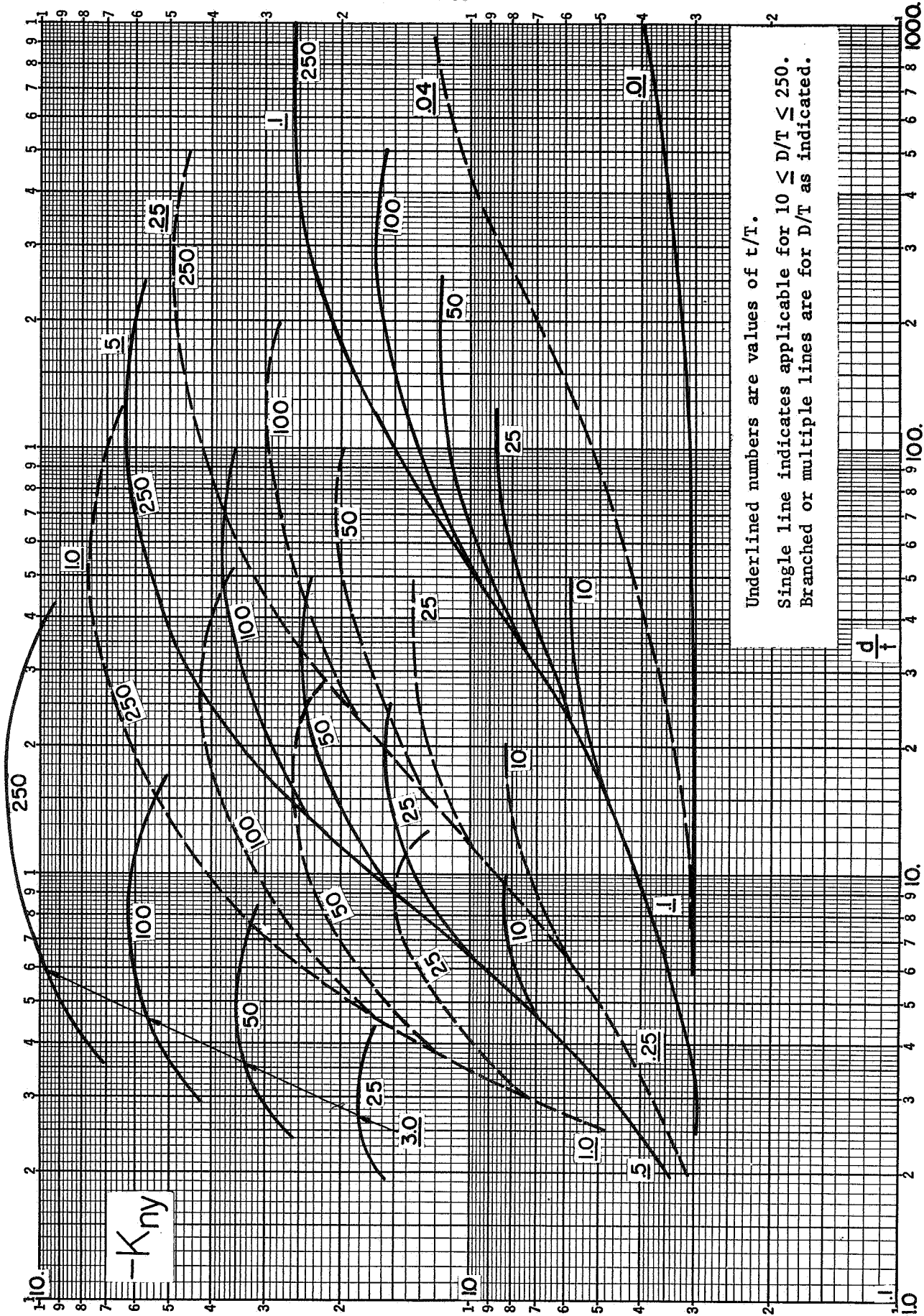


FIGURE A-16.  $K_{ny}$  FOR THRUST LOADING

PHASE REPORT No. 3

on

FLEXIBILITY OF NOZZLES IN SPHERICAL SHELLS

June 28, 1966

to

UNITED STATES ATOMIC ENERGY COMMISSION

by

E. C. Rodabaugh and T. J. Atterbury

Contract No. W-7405-eng-92

BATTELLE MEMORIAL INSTITUTE  
Columbus Laboratories  
505 King Avenue  
Columbus, Ohio 43201

Section 3



TABLE OF CONTENTS

	<u>Page</u>
INTRODUCTION . . . . .	1
SUMMARY . . . . .	2
NOMENCLATURE . . . . .	3
THEORY . . . . .	5
COMPARISON OF TEST DATA WITH THEORY. . . . .	9
FLEXIBILITY OF PHASE 1 DESIGNS . . . . .	15
SIGNIFICANCE OF FLEXIBILITY OF NOZZLES . . . . .	18
DESIGN GRAPHS FOR FLEXIBILITY FACTORS. . . . .	21
REFERENCES . . . . .	32

## INTRODUCTION

In many critical piping systems, one of the design problems consists of the determination of the forces and moments in the system when the piping undergoes thermal expansion or contraction or, in some cases, due to weight, wind load, shock, or vibration. The solution of the general problem of a three-dimensional piping system with two or more anchor points, while basically simple, involves a large amount of computations. Prior to about 1950, considerable effort was devoted to approximate and thereby simplified solutions. With such approximate methods, accurate characteristics of the piping components were not particularly useful since the methods were approximate. The advent of high-speed digital computers, however, has made it possible to quickly and economically obtain "exact" solutions for moments and forces acting on piping systems.

The adjective "exact" in the above paragraph is used to distinguish between the approximate methods and the computer methods. The computer solutions are, of course, limited in accuracy by the available knowledge of the characteristics of components used in the actual piping systems. One such source of inaccuracy is the local deformation of a nozzle in a pressure vessel head. In most present analyses of piping systems attached at one end to such a nozzle, it is assumed that the nozzle constitutes a rigid anchor. The "anchor" assumption is usually\* conservative since forces will be overestimated. The degree of conservatism in some piping systems may be excessive and lead to unnecessary expense in construction of the piping system.

---

\* The "anchor" assumption may be unconservative for shock or other dynamic loading.

SUMMARY

Design graphs are presented by means of which the flexibility can be determined for nozzles in spherical heads, or in heads which are locally spherical in the vicinity of the nozzle. Graphs are applicable for  $10 \leq D/T \leq 250$ ,  $d/D \leq 0.5$ , and  $t/T \leq 3.0$ . Both the nozzle and sphere are assumed to have constant wall thickness in the vicinity of the nozzle and the nozzle protrudes externally only. Graphs for flexibility are given for both moment and thrust loadings applied to the nozzles.

The design graphs are based on the theoretical development by Bijlaard<sup>(1)\*</sup>. Numerical comparisons of Bijlaard's "shallow shell" theory with "non-shallow shell" theories show that Bijlaard's relatively simple theory gives sufficiently accurate results for the dimensional ranges covered herein. Comparisons between Dally's<sup>(2)</sup> test results and Bijlaard's theory are given.

Flexibility factors for moment loading are given for the designs of the report, "Proposed Reinforcement Design Procedure for Radial Nozzles in Spherical Shells with Internal Pressure". This report<sup>(3)</sup> constitutes the first phase report on nozzles in pressure vessels and gives specific reinforcing dimensions for nozzles in spheres such that the reinforced nozzles meet specified design criteria. The flexibility factors of Phase 1 designs do not exceed a value of 10 and usually are in the range of 1 to 8.

The significance of the flexibility of nozzles in heads, as a part of a piping system, is illustrated by calculation of forces and moments in a number of simple piping systems with (a) the usual assumption of the nozzle as an anchor and (b) with the nozzle flexibility included. For this particular set of examples, the ratio  $(M_n)_o / (M_n)_K$  ranges from 2.5 to 6, i.e., the moment at the nozzle is overestimated by factors of 2.5 to 6 by using the "anchor" assumption. These examples were selected to show where the nozzle flexibility factor can be significant; in many piping systems the effect of the nozzle flexibility will be insignificant.

---

\* References on page 32

NOMENCLATURE

(See Figure 1)

Dimensions

D = mean diameter of sphere, inches

d = mean diameter of nozzle, inches

R = mean radius of sphere, inches

r = mean radius of nozzle, inches

T = wall thickness of sphere, inches

t = wall thickness of nozzle, inches

T', t' are used for locally increased thickness near the nozzle-sphere juncture

 $Z_n = \pi r^2 t$  (section modulus of nozzle), in.<sup>3</sup> $I_n = \pi r^3 t$  (moment of inertia of nozzle), in.<sup>4</sup> $A_n = 2\pi r t$  (cross-sectional metal area of nozzle), in.<sup>2</sup>Coordinates $\varphi$  = meridional angle on sphere $\theta$  = latitude angle on sphere $\rho = R \sin \varphi$ , inchesLoads

P = internal pressure, psi

M = moment applied to nozzle, in.-lb

L = thrust load applied to nozzle, lb

Displacementsw = radial displacement at  $\rho = r$  ( $\theta = 0$  for moment loading) $\alpha = w/r$  (rotation of axis of nozzle, moment loading)Flexibility Factors $K_\alpha = \alpha / (Md/EI_n)$  - moment loading $K_w = w / (Ld/EA_n)$  - thrust loadingMaterial Properties

E = modulus of elasticity, psi

 $\nu$  = Poisson's ratio

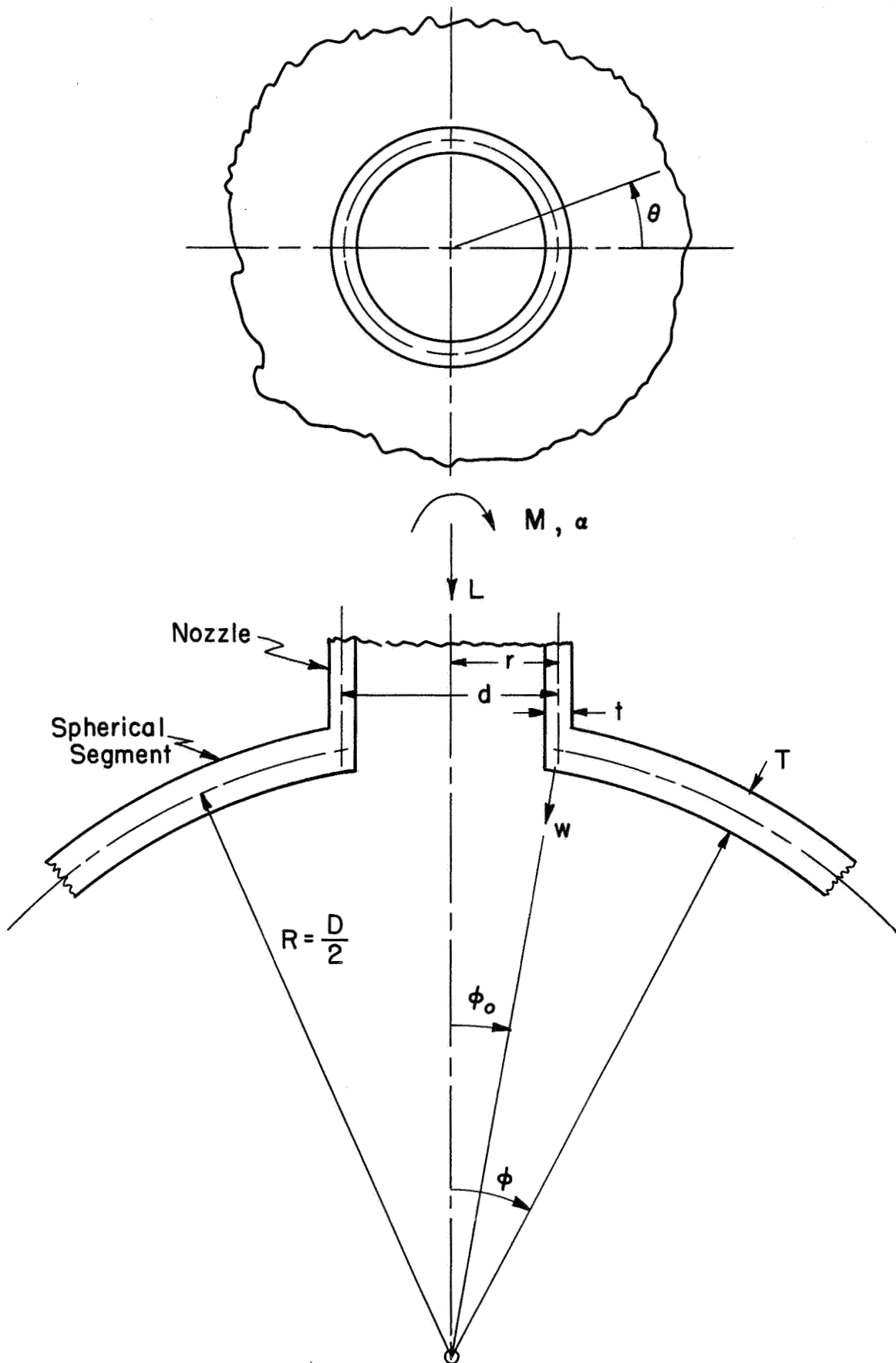


FIGURE 1. NOMENCLATURE ILLUSTRATION

THEORY

There are several theoretical developments, available in the form of digital computer programs, which can be used to determine local deformations of nozzles in spherical shells or in heads which are spherical in the neighborhood of the nozzle. Three of these developments (1, 4, & 5) were compared with each other in Reference (7) with respect to stresses due to thrust or moment loading applied to the nozzle. References (4) and (5) are based on "non-shallow" shell theory whereas the first reference, by Bijlaard, is based on "shallow" shell theory. It was found that the differences in stresses for  $d/D$  up to 0.5,  $D/T$  up to 250 were small.

Radial displacements calculated using Bijlaard's analysis are compared with those calculated by Kalnins' computer program<sup>(5)</sup> in Table 1. Kalnins' analysis does not use the "shallow-shell" assumption. For moment loading, Bijlaard and Kalnins' analysis give almost the same results except for a  $\cos \varphi$  factor. That is, for  $d/D = 0.1$ , ( $\cos \varphi_0 \cong 1.00$ ) the two methods give the same deflections within 1 percent. For  $d/D = 0.5$  ( $\cos \varphi_0 = 0.866$ ), Kalnins gives a displacement of 0.866 times that given by Bijlaard, within a few percent. For thrust loading, at small  $D/T$  values, there is a small additional discrepancy between Kalnins and Bijlaard results. This apparently arises because, for thrust loading, the displacements of the spherical shell remote from the nozzle can be significant; the shallow-shell theory is not accurate at large values of  $\varphi$ , e.g.,  $\varphi = \pi/2$ . The comparisons shown in Table 1, with respect to Kalnins' computer program, were made for a hemispherical head with the edges of the hemisphere at  $\varphi = \pi/2$  assumed fixed. Other types of heads or spherical shells (e.g., a tori-spherical head) would lead to slightly different displacements.

While there are some discrepancies between Bijlaard's "shallow-shell" analysis and the theoretically more accurate "non-shallow-shell" analysis, these differences are small in an engineering sense and, since Bijlaard's analysis is much simpler and more economical to use than

TABLE 1. COMPARISON OF CALCULATED RADIAL DISPLACEMENTS, BIJLAARD AND KALNINS

$\frac{D}{T}$	$\frac{d}{D}$	$\frac{t}{T}$	$w/(2r^2M/EI_n) - \text{Moment Loading}$		
			Bijlaard	Bijlaard <sup>(a)</sup>	Kalnins
				$\times \cos \phi_o$	
25	0.10	0.04	0.148	0.147	0.147
25	0.10	0.25	0.828	0.825	0.825
25	0.50	0.25	0.996	0.865	0.840
25	0.50	1.00	1.76	1.52	1.53
250	0.10	0.10	7.37	7.35	7.30
250	0.10	1.00	25.28	25.2	25.1
250	0.50	0.25	3.97	3.44	3.28
250	0.50	3.00	12.63	10.97	10.40
			$w/(2rL/EA) - \text{Thrust Loading}$		
$\frac{D}{T}$	$\frac{d}{D}$	$\frac{t}{T}$	Bijlaard	Bijlaard <sup>(a)</sup>	Kalnins
				$\times \cos \phi_o$	
10	0.01	0.01	0.066	0.066	0.077
10	0.01	0.04	0.263	0.263	0.302
10	0.5	0.25	0.654	0.575	0.645
10	0.5	1.00	1.425	1.23	1.72
250	0.01	0.01	1.79	1.78	1.81
250	0.01	1.00	145.7	145.7	148.
250	0.5	0.25	4.075	3.53	3.46
250	0.5	3.00	13.47	11.65	12.20

(a) Bijlaard analysis results multiplied by  $\cos \phi_o$ .

Kalnins' computer program, design information given herein was developed using Bijlaard's analysis. Theoretically, increased accuracy is obtained by multiplying the results from Bijlaard's analysis by  $\cos \phi_0$ , however, in this report the maximum value of  $d/D$  is limited to 0.5, hence the correction factor of  $\cos \phi_0$  is not greater than 0.866.

For thrust loading, the significant displacement is given by the radial displacement,  $w$ . For moment loading, the significant displacement is the rotation of the nozzle given by

$$\alpha = \frac{(w)_{\rho=r, \theta=0}}{r} \quad . \quad (1)$$

The value of  $\alpha$  could, of course, be used directly in a piping system analysis to account for the flexibility of a nozzle in a spherical shell. However, a more informative parameter is obtained by defining a flexibility factor,  $K$ , by the equation:

$$K_\alpha = \frac{\alpha}{(Md/EI_n)} \quad . \quad (2)$$

The quantity  $(Md/EI_n)$  in Equation (2) is simply the rotation in a nozzle of one-diameter length, subjected to a moment,  $M$ . The utility of a flexibility factor as defined by Equation (2) arises from two considerations:

- (1) The  $K_\alpha$ , for a given nozzle and piping system, immediately indicates whether the flexibility of the nozzle is significant. For example, if  $K_\alpha = 2$  and the length of the pipe attached to the nozzle is  $50d$ , then the local flexibility of the nozzle will have only a small effect on the flexibility of the piping system. If, on the other hand,  $K_\alpha = 10$  and the length of the pipe attached to the nozzle is  $2d$ , then the local flexibility of the nozzle may have a very significant effect on the flexibility of the piping system.
- (2) The use of a flexibility factor as defined by Equation (2) is analogous to the flexibility factor for elbows or curved pipe presently given in the ASA Code for Pressure



Piping<sup>(6)</sup> and generally used in piping flexibility analyses\*.

The flexibility of a nozzle under thrust loading is usually not significant in piping systems; in most piping flexibility analyses the axial displacements due to axial loads are not included. In unusual piping systems, in which a pipe extends from a nozzle to an anchor with little or no offset, the flexibility of a nozzle due to thrust load could be significant. Also, in applications such as nozzles for control-rod insertion in nuclear pressure vessels, the displacement for thrust loading may be significant. In analogy to the flexibility factor for moment loading, a flexibility factor for thrust loading has been defined as:

$$K_w = \frac{w}{(Ld/EA_n)} \quad (3)$$

The quantity  $(Ld/EA_n)$  is the axial displacement in the nozzle of one-diameter length, subjected to the axial load, L.

---

\* The analogy, however, is imposed by definition rather than inherent. The flexibility of a nozzle in a sphere is inherently a lumped parameter where as the flexibility of an elbow or curved pipe is inherently a distributed parameter associated with a unit length and, for an exact solution, an integration over the elbow length must be carried out.

COMPARISON OF TEST DATA WITH THEORY

Test data on the flexibility of nozzles in heads is quite limited. The only data known to the authors is that given by Dally<sup>(2)</sup>, who reports tests on six fabricated steel test models briefly described in the following tabulation:

Model No.	Type of Model*
1	Hemispherical head, 36-inch radius, 0.90-inch wall. Nozzle; 3.39-inch radius, 0.77-inch wall.
2	ASME Flanged and Dished Head, 35-inch crown radius, 0.77-inch wall. Nozzle; 3.39-inch radius, 0.78-inch wall.
3	ASME Flanged and Dished Head, 35-inch crown radius, 0.77-inch wall. Nozzle; 3.50-inch radius, 0.55-inch wall.
4	ASME Flanged and Dished Head, 35-inch crown radius, 0.77-inch wall. Nozzle; 3.64-inch radius, 0.27-inch wall.
5	ASME Flanged and Dished Head, 30-inch crown radius, 1.63-inch wall. Nozzle; 3.39-inch radius, 0.77-inch wall.
6	See Figure 2.

---

\* Radii are average of midwall radii; wall thicknesses are average of measured thicknesses.

A single nozzle was welded into the center of each head, with a fillet weld inside and out. Legs of the fillet welds were 3/4 inch. The nozzles protruded inward approximately 1 inch inside the inside surface of the heads.

Tests consisted of applying either a thrust load or a moment to the nozzle. Stresses were measured by means of resistance strain gages, radial displacements of the head were measured (presumably with dial gages). The radial displacements of the head are significant with respect to the flexibility of a nozzle in a head. Measurements were taken at various radial distances from the center of the nozzle, starting at a radius,  $\rho$ ,

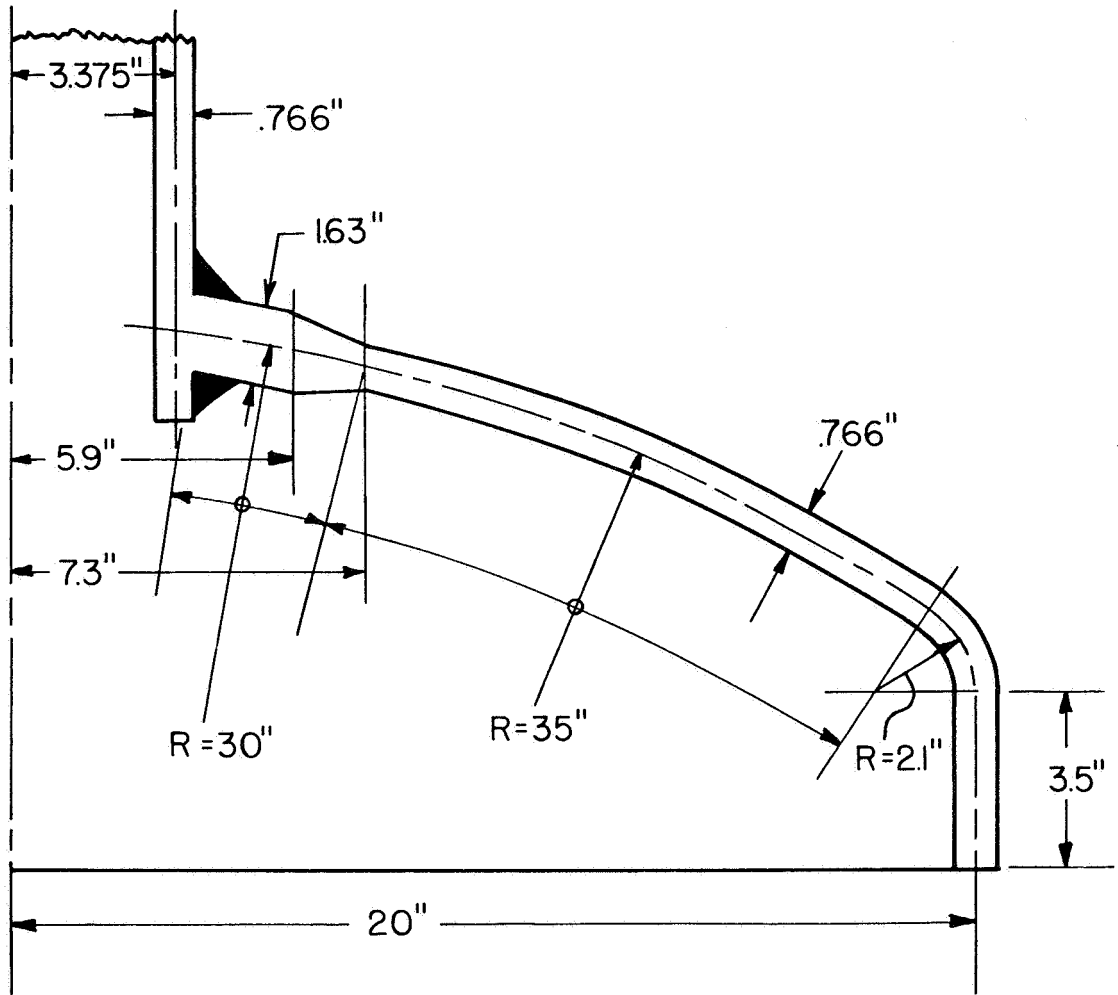


FIGURE 2. CROSS-SECTION OF DALLY<sup>(2)</sup> MODEL NO. 6

of 5 inches. These measured radial displacements are then compared with Bijlaard's<sup>(1)</sup> theoretical radial displacements. In all tests the largest displacement occurred at the radial location closest to the nozzle. A summary of the ratios of theoretical to measured displacements at  $\rho = 5$  inches is given in Table 2.

Model No. 6 is basically different than Models 1 through 5; the results for it are discussed separately later herein. For Models 1 through 5, Table 2 shows the ratios of theoretical to experimental radial deflections,  $w_t/w_x$ , consistently larger than unity. The theory slightly over-predicts radial displacements for thrust loading, and significantly over-predicts radial displacements for moment loading. Considering the significant reinforcing provided by the fillet welds and inwardly protruding portion of the nozzles, which as shown in Table 2 gives an area reinforcement of 30 to 60 percent of the cut-out area ( $d_i T$ ), that the theory over-predicts radial displacements for moment loading is not unexpected. The relatively good agreement between test and theory for thrust loading is somewhat unexpected.

For moment loading, Table 2 indicates a rough parallel between reinforcing (as measured by  $A_a/d_i T$ ) and agreement with theory; i.e., as ( $A_a/d_i T$ ) decreases,  $w_t/w_x$  becomes closer to 1.0; therefore, results from Models 1 through 5 indicate that Bijlaard's theory is sufficiently accurate, in an engineering sense, for calculating flexibility factors for nozzles in heads in the absence of a large amount of local reinforcing at the nozzle-head juncture.

As shown in Figure 2, test Model No. 6 is different than Models 1 through 5 in that the thickness of the head is not constant. Bijlaard's analysis, as used by Dally for comparison with experimental results, is not applicable to the test model in that:

- (a) The theory used by Dally for Model 6 assumes that the nozzle is a solid plug of 7.5-inch outside diameter.
- (b) The theory assumed a step change in thickness from 1.63 to 0.77 inches at  $\rho = 7.5$  inches whereas the actual model had a linear taper starting at about  $\rho = 5.9$  inches and ending at about  $\rho = 7.3$  inches (see Figure 2).

TABLE 2. SUMMARY OF COMPARISONS, DALLY TEST DATA WITH BIJLAARD THEORY

Model No.	$\frac{d}{D}$	$\frac{D}{T}$	$\frac{t}{T}$	$\frac{A_a}{d_i T}$ (1)	Loading	$\frac{w_t}{w_x}$ (2)
1	0.094	80	0.86	0.5	Thrust	1.09
					Moment	1.48
2	0.097	91	1.01	0.6	Thrust	1.05
					Moment	1.54
3	0.10	91	0.72	0.45	Thrust	1.09
					Moment	1.40
4	0.104	91	0.36	0.3	Thrust	1.08
					Moment	1.31
5	0.113	91	0.47	0.3	Thrust	1.05
					Moment	1.22
6	0.104	40	0.47	---	Thrust	0.61
		85(3)	1.00(3)	1.7	Moment	0.71

(1)  $A_a$  = reinforcing provided by fillet welds and inwardly protruding nozzle.

(2)  $w_t$  = theoretical (Bijlaard) radial displacement at  $\rho = 5$  in.

$w_x$  = measured (Dally) radial displacement at  $\rho = 5$  in.

(The outside radius of the nozzles in these tests was 3.75 in.)

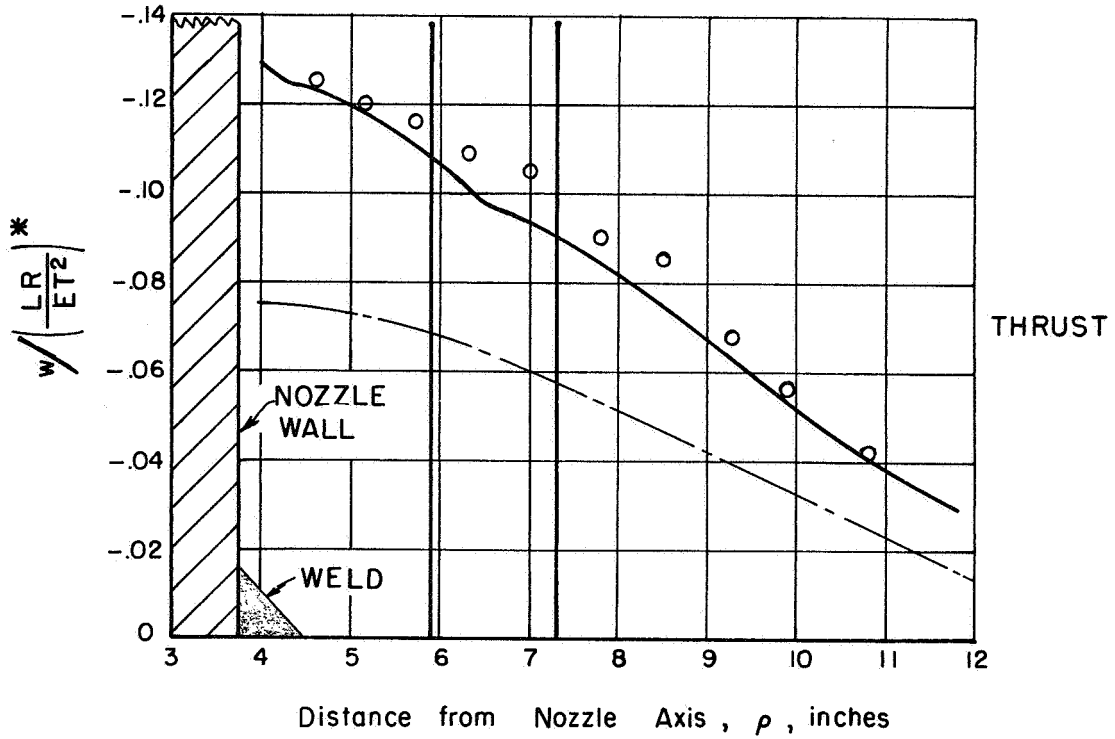
(3) First line is for pad thickness ( $T' = 1.63''$ ); second line is for sphere thickness ( $T = .77''$ ).

- (c) The spherical radius of the pad section was 30 inches; the spherical radius of the outer section (near the pad) was 35 inches. The calculated results given by Dally are based on  $R = 32.5$  inches.
- (d) In common with Models 1 through 5, significant local reinforcing was provided by fillet welds and in inwardly protruding nozzle stub.

Figure 3 gives test results for Model No. 6, along with displacements calculated using Kalnins' computer program. In this analysis:

- (a) The theoretical model has a nozzle with  $r = 3.385$  inches,  $t = 0.766$  inch.
- (b) The linear taper is included in the theoretical model.
- (c) The theoretical model uses  $R = 30$  inches to the OD of the taper,  $R = 35$  inches to the beginning of the knuckle; a toroidal segment representing the flanged and dished-head knuckle, and a cylindrical section representing the flange on the head.
- (d) The local reinforcing is included in the theoretical model as an increased head thickness near the nozzle.

It is apparent from Figure 3 that the more complete analysis described above agrees much better with the test data than does Bijlaard's analysis. This better agreement arises primarily from inclusion of construction details not in Bijlaard's analysis and not from inaccuracies in Bijlaard's analysis for construction details for which it is directly applicable.



\* In these parameters ,  $R=32.5$ ,  $T=.77$ ,  $E=3 \times 10^7$

Theory , Kalnins  
 Theory , Dally - Bijlaard      ○ Test Data

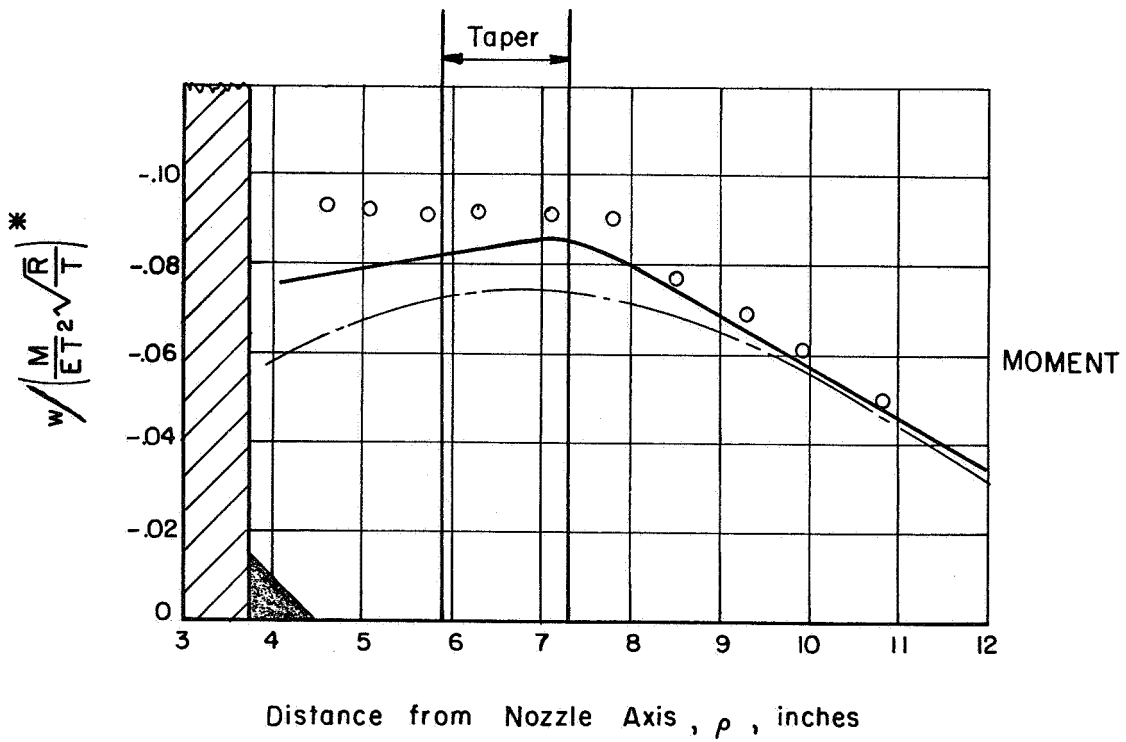


FIGURE 3. COMPARISON OF MEASURED AND THEORETICAL DISPLACEMENTS, DALLY MODEL NO. 6

FLEXIBILITY OF PHASE 1 DESIGNS

Phase 1 report, "Proposed Reinforcement Design Procedures for Radial Nozzles in Spherical Shells with Internal Pressure"<sup>(3)</sup> gives reinforcing dimensions (as a function of  $d/D$  and  $D/T$ ) such that the nozzles with such reinforcing meet two design criteria: (1) the plastic collapse or limit pressure is at least 1.5 times the design pressure, and (2) the maximum stress intensity is not more than  $3.0S$ , where  $S = PD/4T$ . Phase Report No. 2, "Stresses at Nozzles in Spherical Shells Loaded with Pressure, Moment or Thrust"<sup>(7)</sup> gives the stress intensities, with internal pressure or moment loading, for Phase 1 designs in which reinforcing consists of a uniform increase in wall thickness of nozzle or sphere. Figure 4 gives the required reinforcing dimensions of Phase 1 designs. Figure 5 gives the calculated flexibility factors for Phase 1 designs. It should be noted that, for uniform wall reinforced nozzles to Phase 1 design requirements, a given value of  $D/T$  and  $d/D$  establishes a value of  $g = t'/t$  or  $h = T'/T$ . More general data on flexibility factors is given in the subsequent section, "Design Graphs for Flexibility Factors".

In Figure 5,  $K_\alpha$  is defined as  $\alpha/(Md/EI_n)$ . For reinforcing on the nozzle ( $g = t'/t$ ), it is assumed that the nozzle is of increased thickness  $t'$  near the nozzle-sphere juncture, but the pipe thickness is  $t$ . If the entire pipe is of thickness  $t'$ , the flexibility factor with respect to that pipe is  $(t'/t)$  times the value of  $K_\alpha$  obtained from Figure 5.



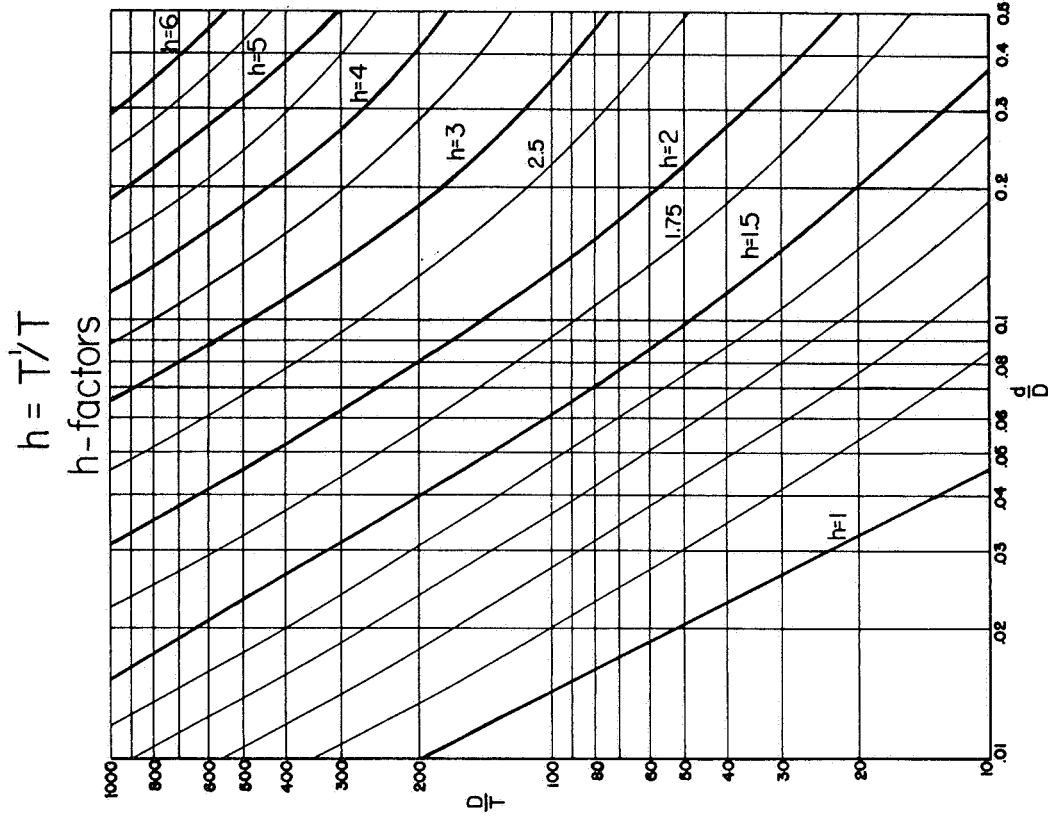


FIGURE 4a: Reinforcing on Nozzle

$$\frac{S}{S} = 1 = \frac{2dT}{Dt}$$

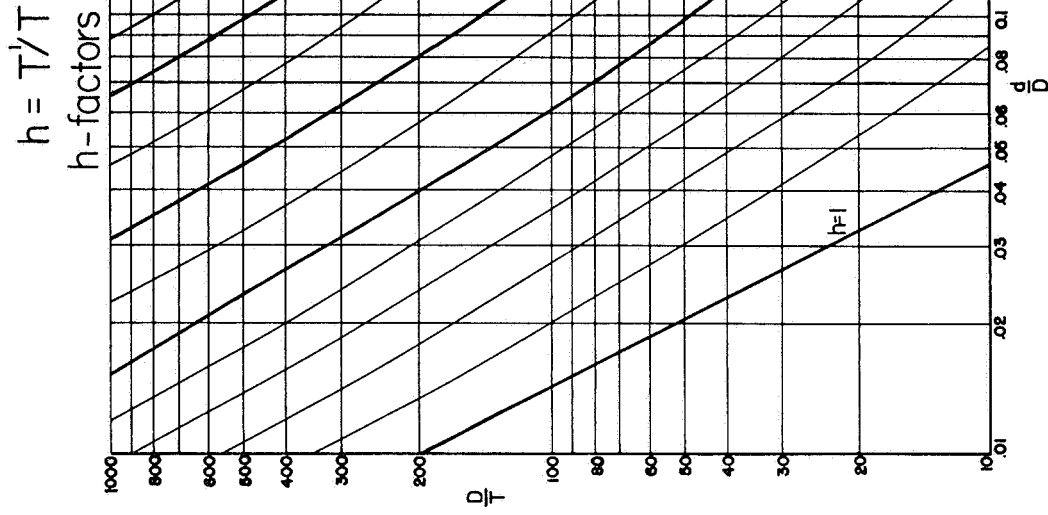


FIGURE 4b: Reinforcing on Sphere

FIGURE 4: GRAPHS FOR OBTAINING g-AND h-FACTORS  
PHASE I DESIGNS

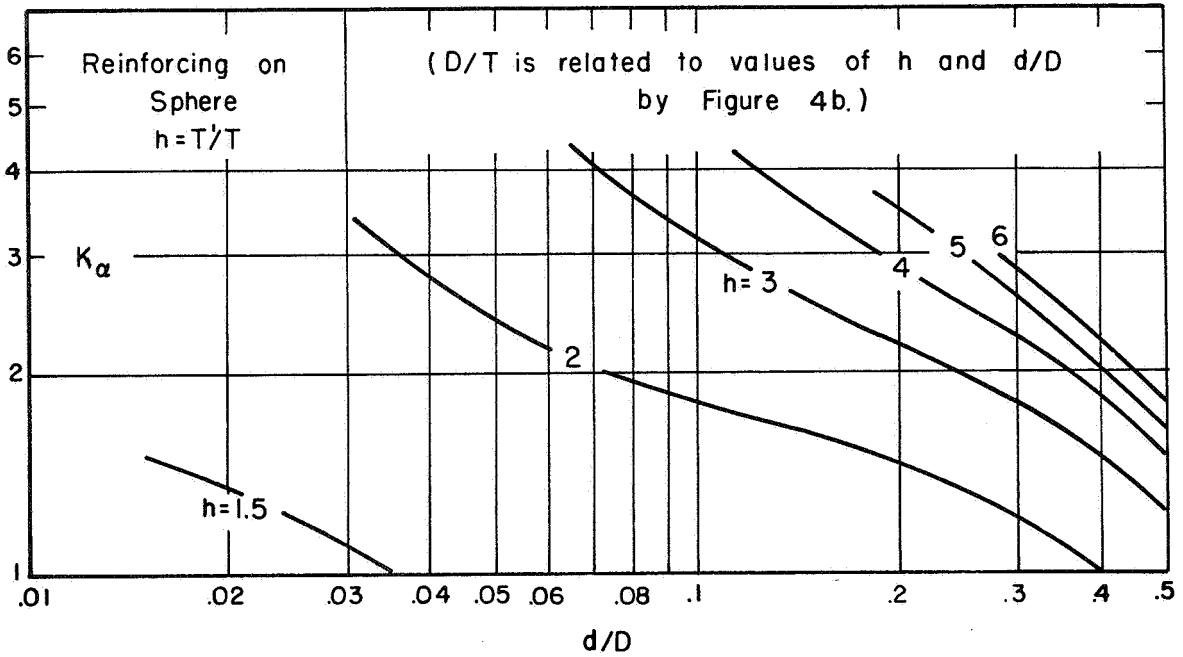
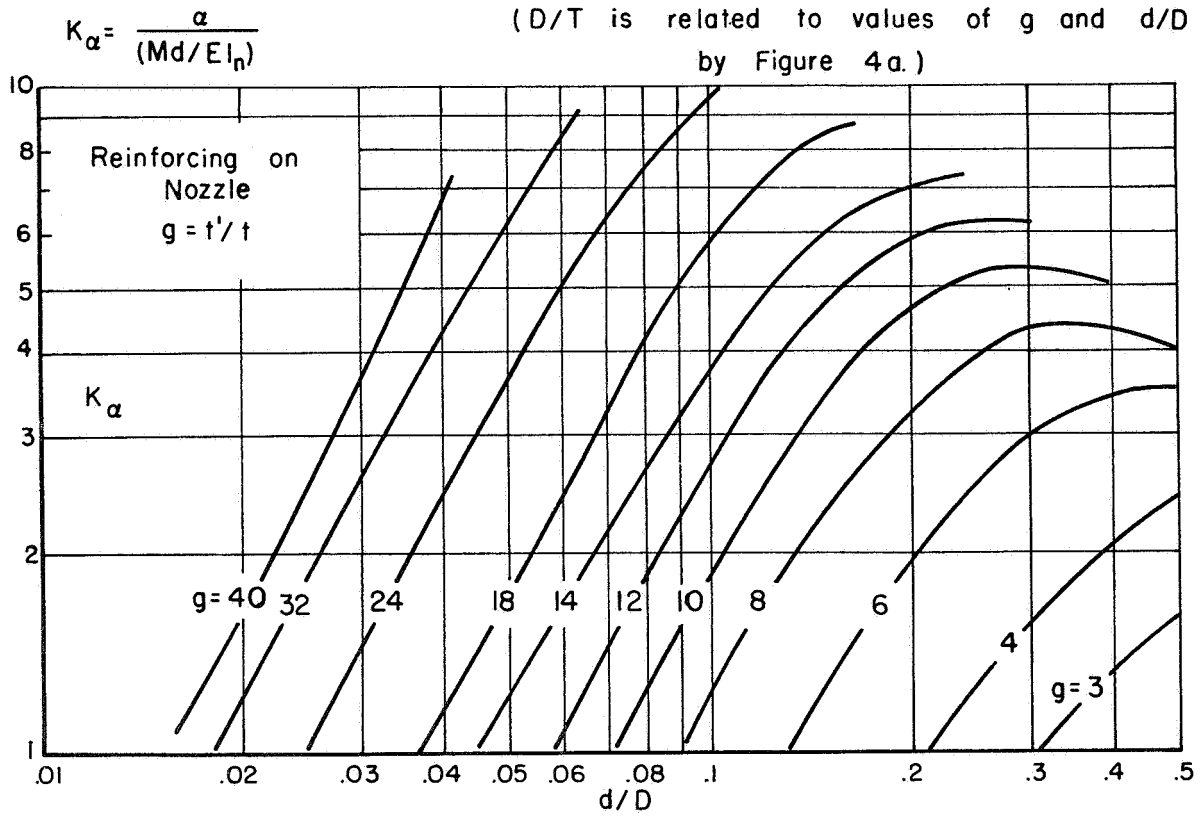
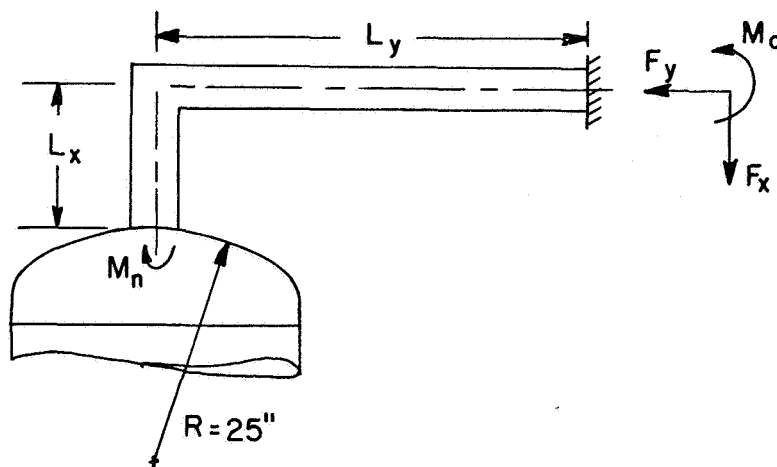


FIGURE 5. FLEXIBILITY FACTORS OF PHASE 1 DESIGN NOZZLES IN SPHERICAL SHELLS, MOMENT LOADING

SIGNIFICANCE OF FLEXIBILITY OF NOZZLES

Forces and moments in a piping system will be decreased by the flexibility of a nozzle attached to the piping system. It is conservative to ignore the flexibility of the nozzle under static loading conditions; whether ignoring the flexibility of a nozzle (or nozzles) results in excessive conservatism depends upon the particular piping system. Obviously, if the lengths of the straight pipe sections are many times that of the nozzle flexibility factor times the pipe diameter ( $l \gg K_d$ ), then the nozzle flexibility will have little effect on the forces and moments. For "tight" systems, however, where the pipe lengths and total piping system length is not large compared to  $K_d$ , ignoring the nozzle flexibility factor can result in gross over-estimates of forces and moments.

To illustrate how the nozzle flexibility factor influences end reactions, calculations were made for the simple piping system shown in Figure 6. The assumed lengths of straight pipe have been varied as shown in Table 3, along with the resulting forces and moments. From the standpoint of design of the nozzle, the moment at the nozzle is of particular significance. As shown by the last column in Table 3, the moment at the nozzle may be overestimated by factors of 2.5 to 6.5 if the flexibility of the nozzle is ignored; i.e.,  $K_\alpha$  taken as zero.



### Assumptions for Calculations Shown in Table 3

- (1) Vessel Head is tori-spherical, with a crown mean-radius of 25", wall thickness of 0.500".
- (2) Pipe is 4" std. wt. (4.5" O.D. x .237" wall)
- (3) Pipe increases in length due to temperature increase, the increase in length is  $(\epsilon\Delta T)L$ , where  $\epsilon\Delta T$  was taken as  $10^{-4}$  in/in  
 $\epsilon$  = unit expansion of pipe material. (The ratio of  $(F, M)_{k=0} / (F, M)_{k \neq 0}$  is not dependent upon the value of  $\epsilon\Delta T$ .)

### Flexibility Factor of Nozzle in Head

For this example:  $D/T = 50/.5 = 100$

$$t/T = .237/.5 = .474$$

$$d/D = 4.263/50 = .085$$

From Figure 10, for these ratios,  $K_{\alpha} \cong 7$ .

FIGURE 6. SIMPLE PIPE SYSTEM USED TO ILLUSTRATE THE EFFECT OF INCLUSION OF THE FLEXIBILITY OF A NOZZLE ON THE CALCULATED FORCES IN THE SYSTEM

TABLE 3. FORCES AND MOMENTS FOR THE PIPING SYSTEM SHOWN IN FIGURE 6

Figure 6		$K_\alpha$	$F_x,$ lbs	$F_y,$ lbs	$M_o,$ in.-lb	$M_n,$ in.-lb	$(M_n)_{K_\alpha=0}$
$L_x,$ inches	$L_y,$ inches						$(M_n)_{K_\alpha=7}$
20	80	7.	75	324	2146	2612	6.05
		0	106	1065	2969	15779	
20	60	7.	101	293	2270	2038	6.13
		0	142	895	3073	12472	
20	40	7.	166	267	2750	1475	6.25
		0	224	732	3525	9218	
20	20	7.	533	297	5720	999	6.51
		0	651	651	6507	6507	
40	20	7.	661	134	8740	907	3.89
		0	732	224	9218	3525	
60	20	7.	833	94	12064	1035	2.97
		0	895	142	12472	3073	
80	20	7.	1009	75	15405	1189	2.50
		0	1065	106	15779	2969	

DESIGN GRAPHS FOR FLEXIBILITY FACTORS

Based upon the reasoning and assumptions presented earlier, flexibility factors for design purposes can be obtained from Bijlaard's<sup>(1)</sup> analysis. A series of design graphs have been prepared and are presented in this section of the report.

Calculations are based on a Poisson's ratio of 0.3 and it was assumed that the materials in the nozzle and sphere have the same modulus of elasticity; otherwise the properties of the materials do not enter into the flexibility factors. Figures 7 through 11 give flexibility factors for moment loading. Figures 12 through 16 give flexibility factors for thrust loading. The graphs are applicable to nozzles in spherical shells or shells which are spherical in the region of the nozzle, e.g., a tori-spherical head with the nozzle in the center. The graphs are applicable to nozzles with local reinforcing as provided by a heavy-wall nozzle, and/or an integral pad on the spherical shell, provided the reinforcing lengths, measured from the nozzle-sphere juncture, less than  $\sqrt{dt'}$  along the nozzle axis;  $.7 \sqrt{DT'}$  along the sphere surface.

$$K_{\alpha} = \frac{\alpha}{Md/EI_n}$$

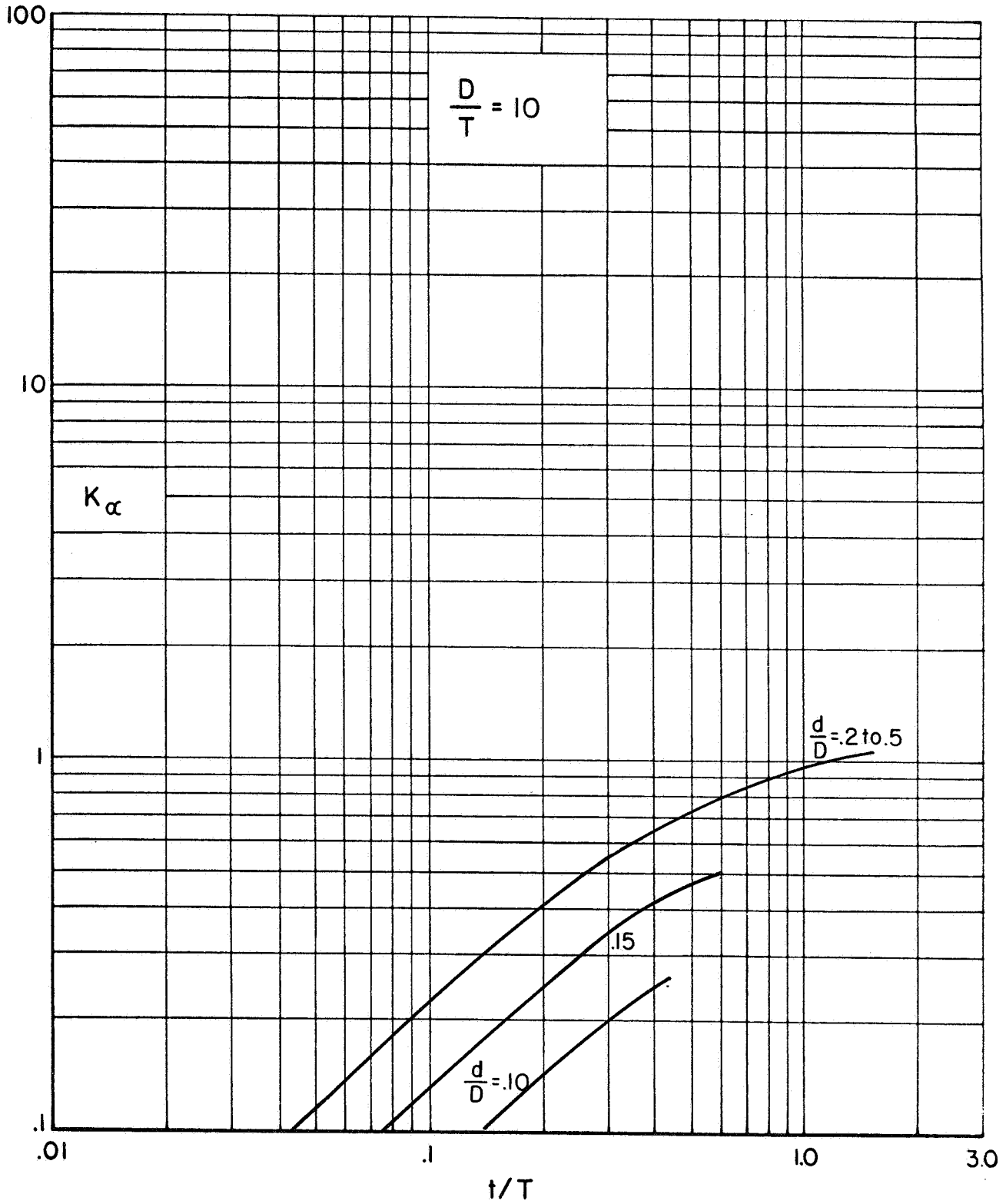


FIGURE 7. FLEXIBILITY FACTORS, MOMENT LOAD,  $D/T = 10$

$$K_{\alpha} = \frac{\alpha}{Md/EI_n}$$

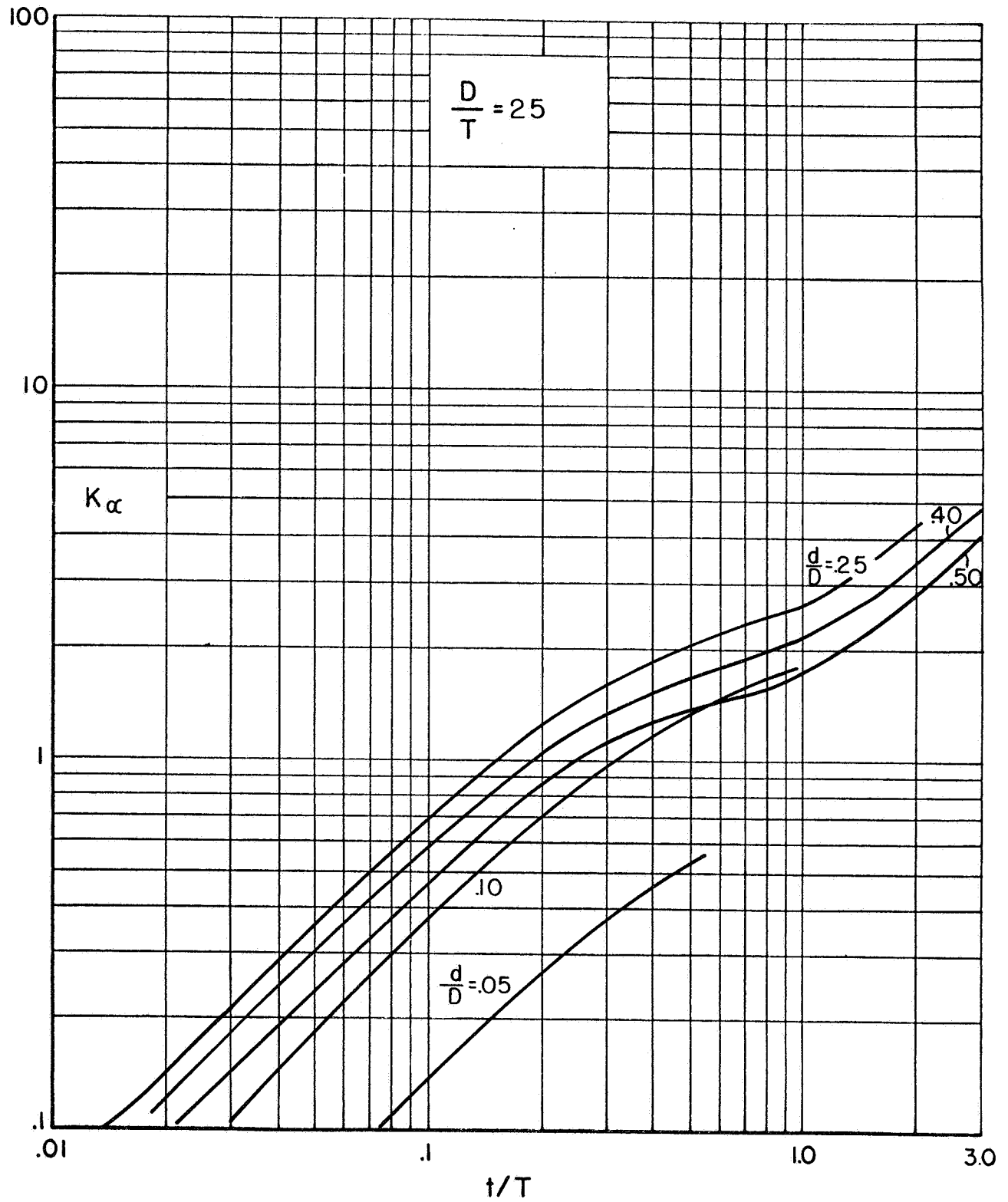


FIGURE 8. FLEXIBILITY FACTORS, MOMENT LOAD,  $D/T = 25$



$$K_{\alpha} = \frac{\alpha}{Md/EI_n}$$

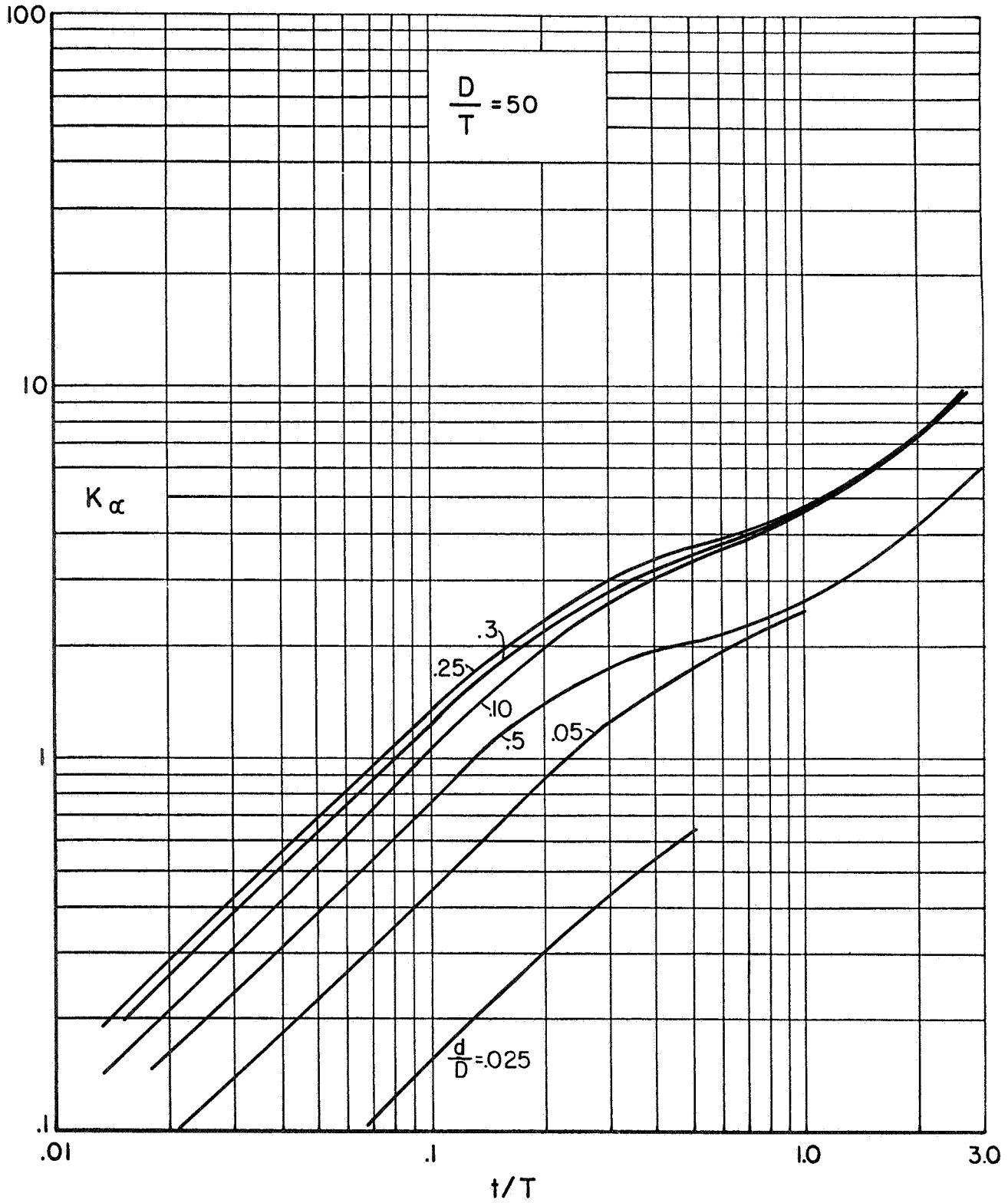


FIGURE 9. FLEXIBILITY FACTORS, MOMENT LOAD,  $D/T = 50$

$$K_{\alpha} = \frac{\alpha}{Md/EI_n}$$

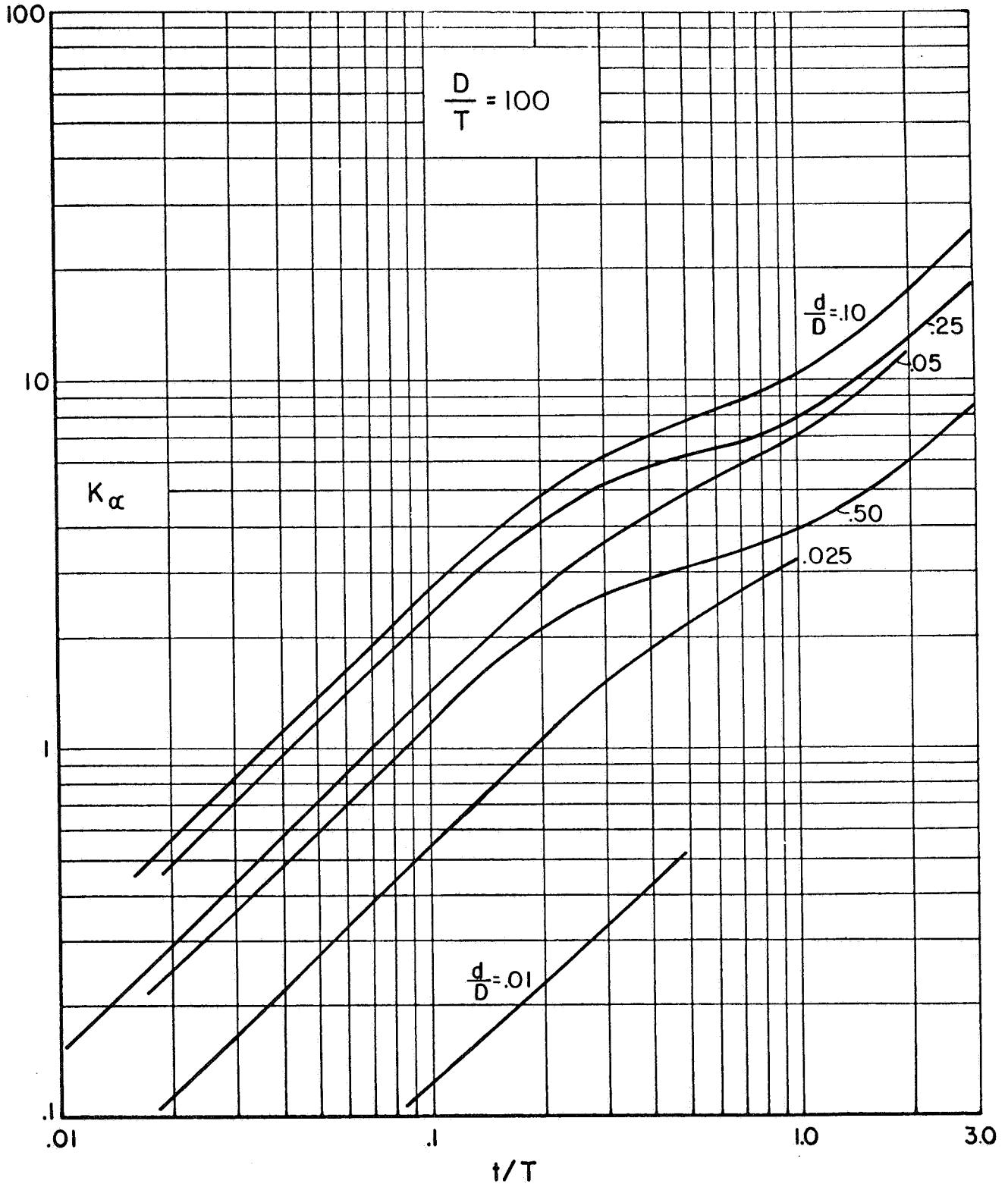


FIGURE 10. FLEXIBILITY FACTORS, MOMENT LOAD,  $D/T = 100$

$$K_{\alpha} = \frac{\alpha}{Md/EI_n}$$

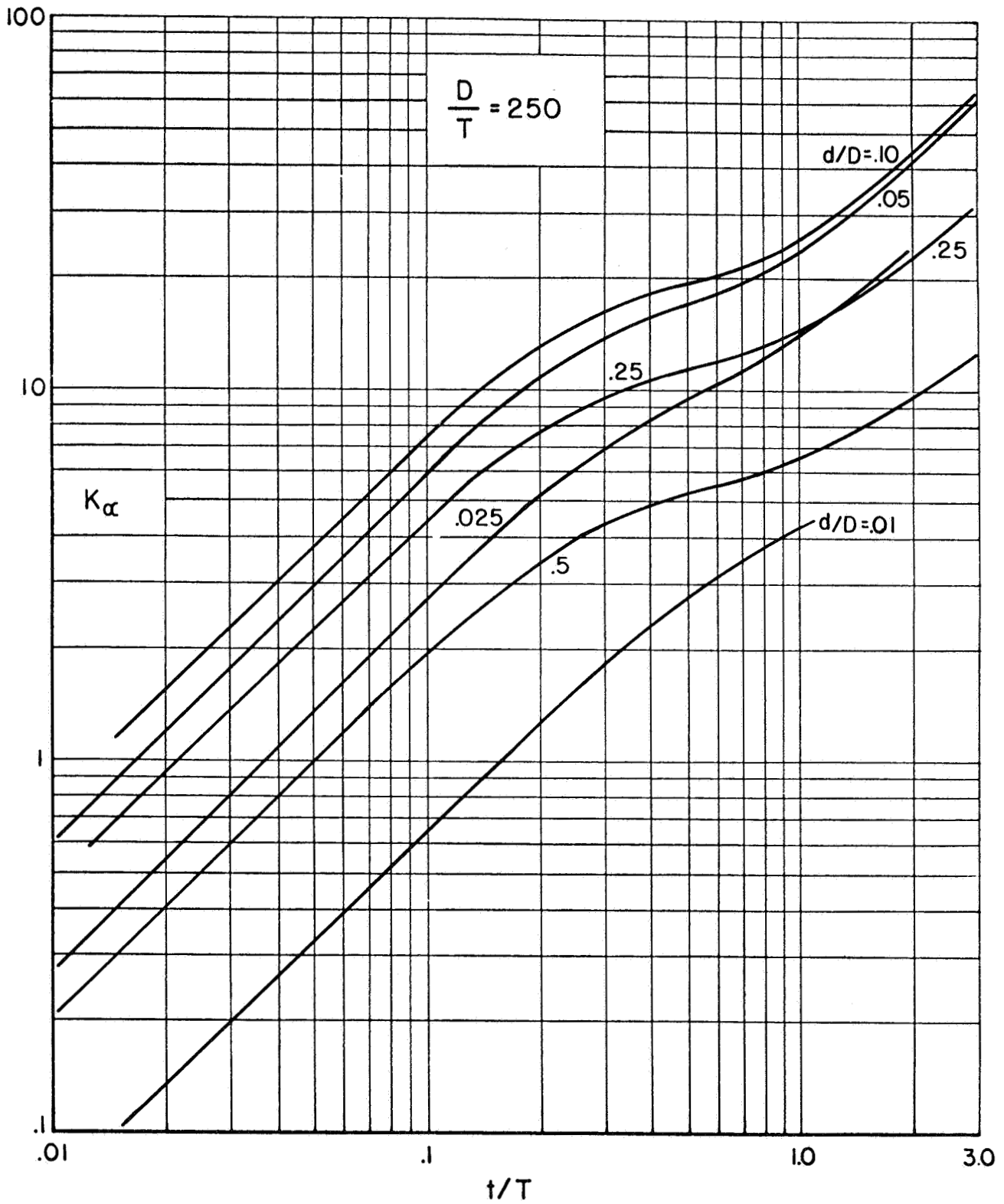


FIGURE 11. FLEXIBILITY FACTORS, MOMENT LOAD,  $D/T = 250$

$$K_w = \frac{w}{Ld/EA_n}$$

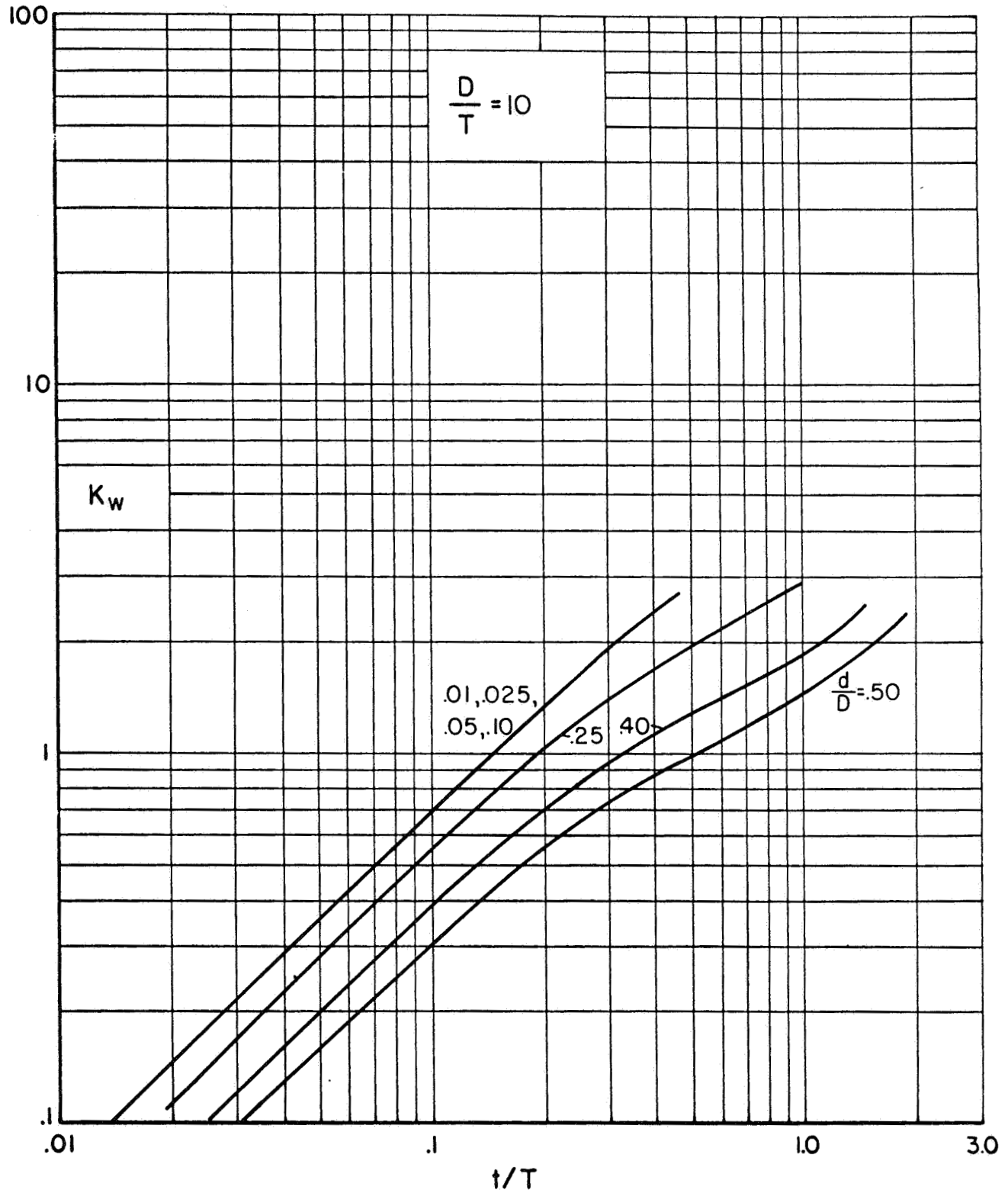


FIGURE 12. FLEXIBILITY FACTORS, THRUST LOAD,  $D/T = 10$

$$K_w = \frac{w}{Ld/EA_n}$$

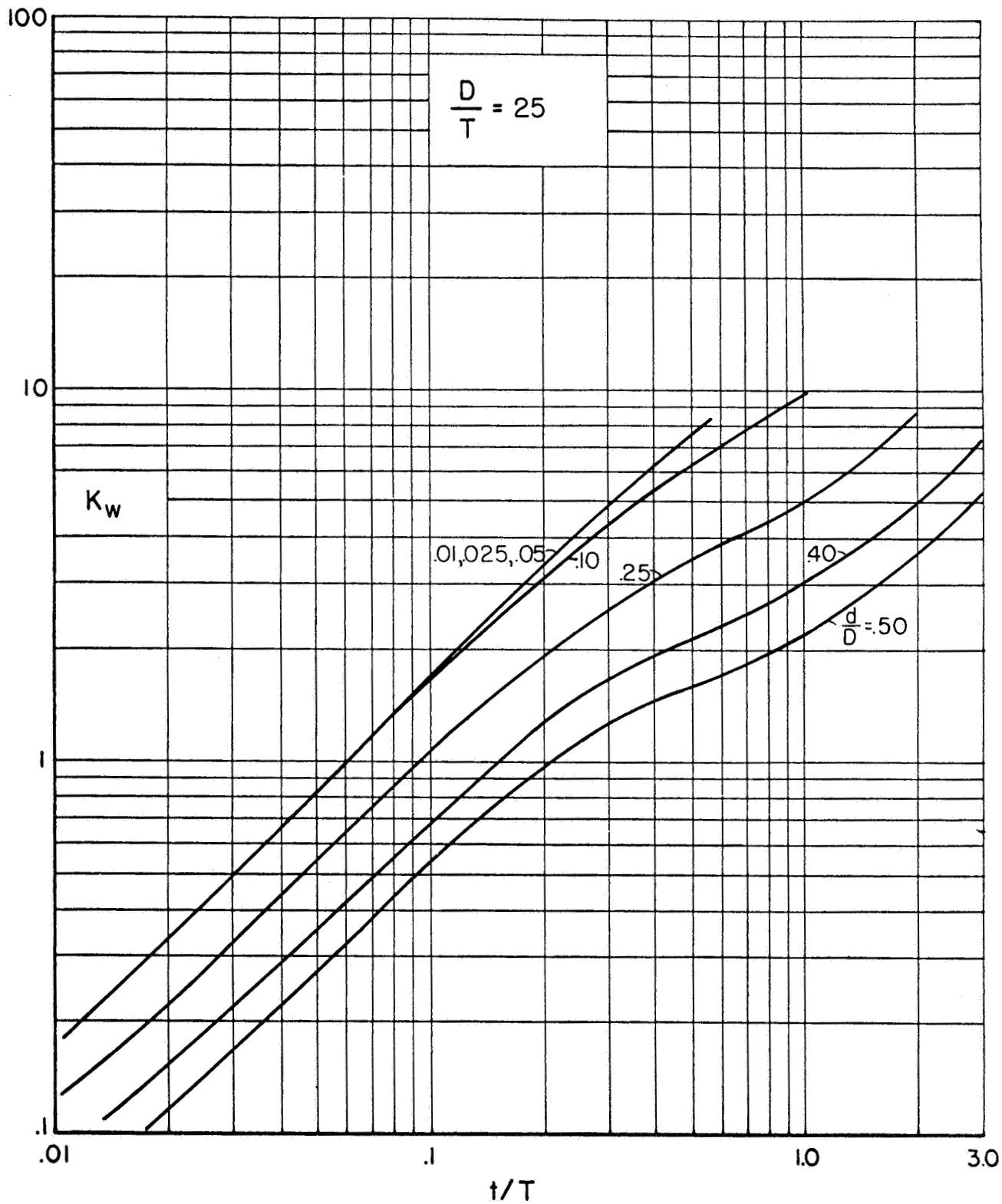


FIGURE 13. FLEXIBILITY FACTORS, THRUST LOAD,  $D/T = 25$

$$K_w = \frac{w}{Ld/EA_n}$$

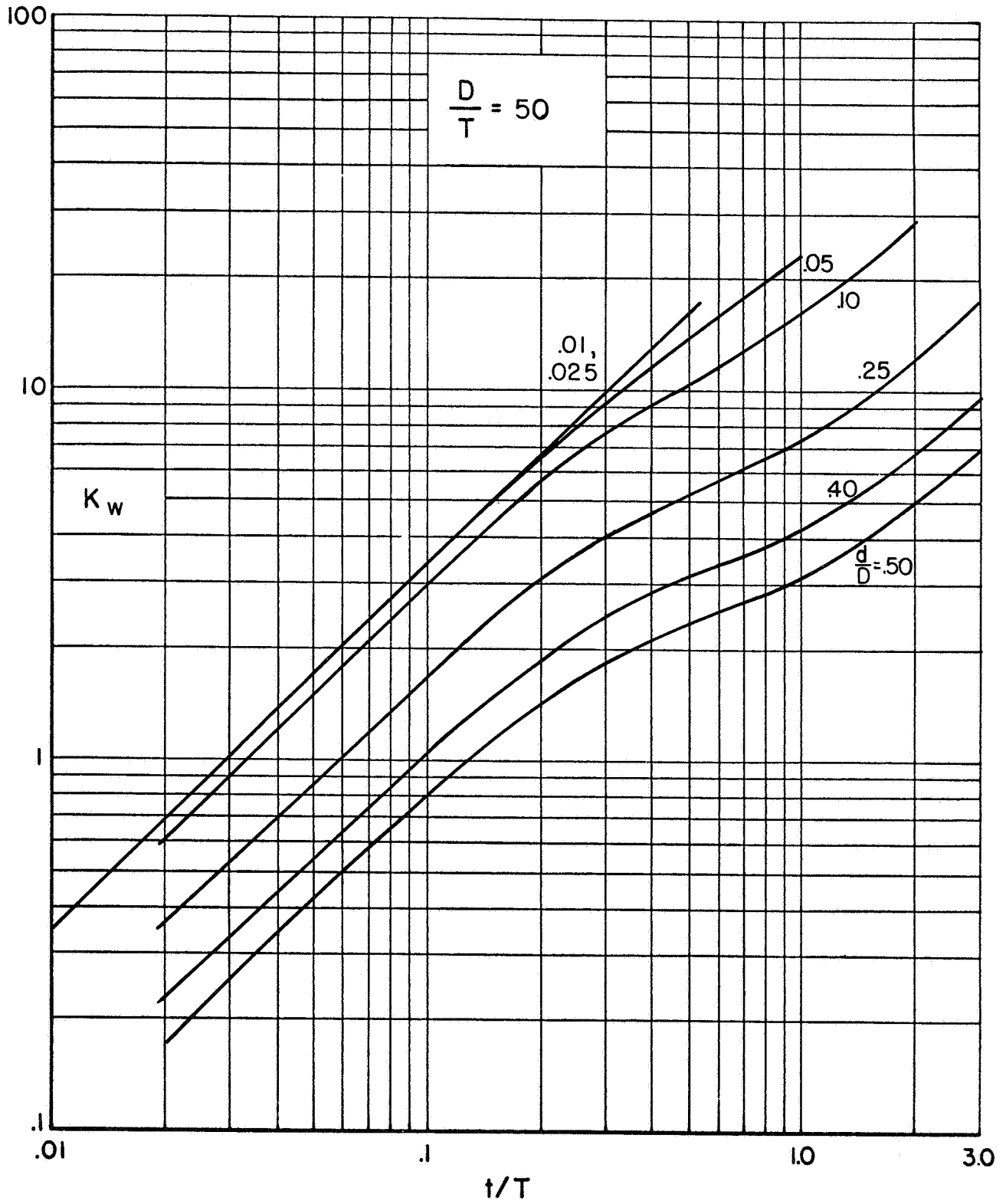


FIGURE 14. FLEXIBILITY FACTORS, THRUST LOAD,  $D/T = 50$

$$K_w = \frac{w}{Ld/EA_n}$$

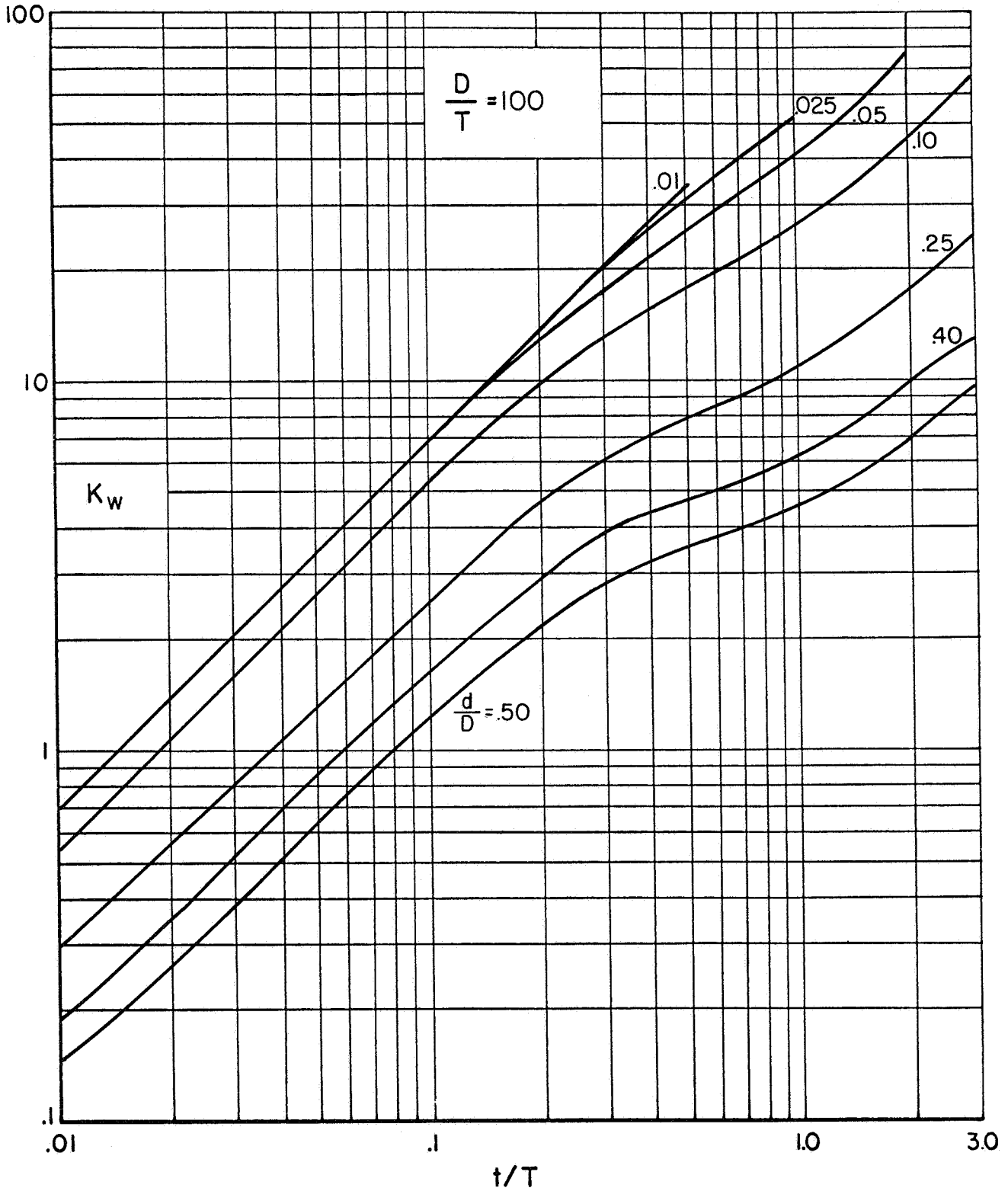


FIGURE 15. FLEXIBILITY FACTORS, THRUST LOAD,  $D/T = 100$

$$K_w = \frac{w}{Ld/EA_n}$$

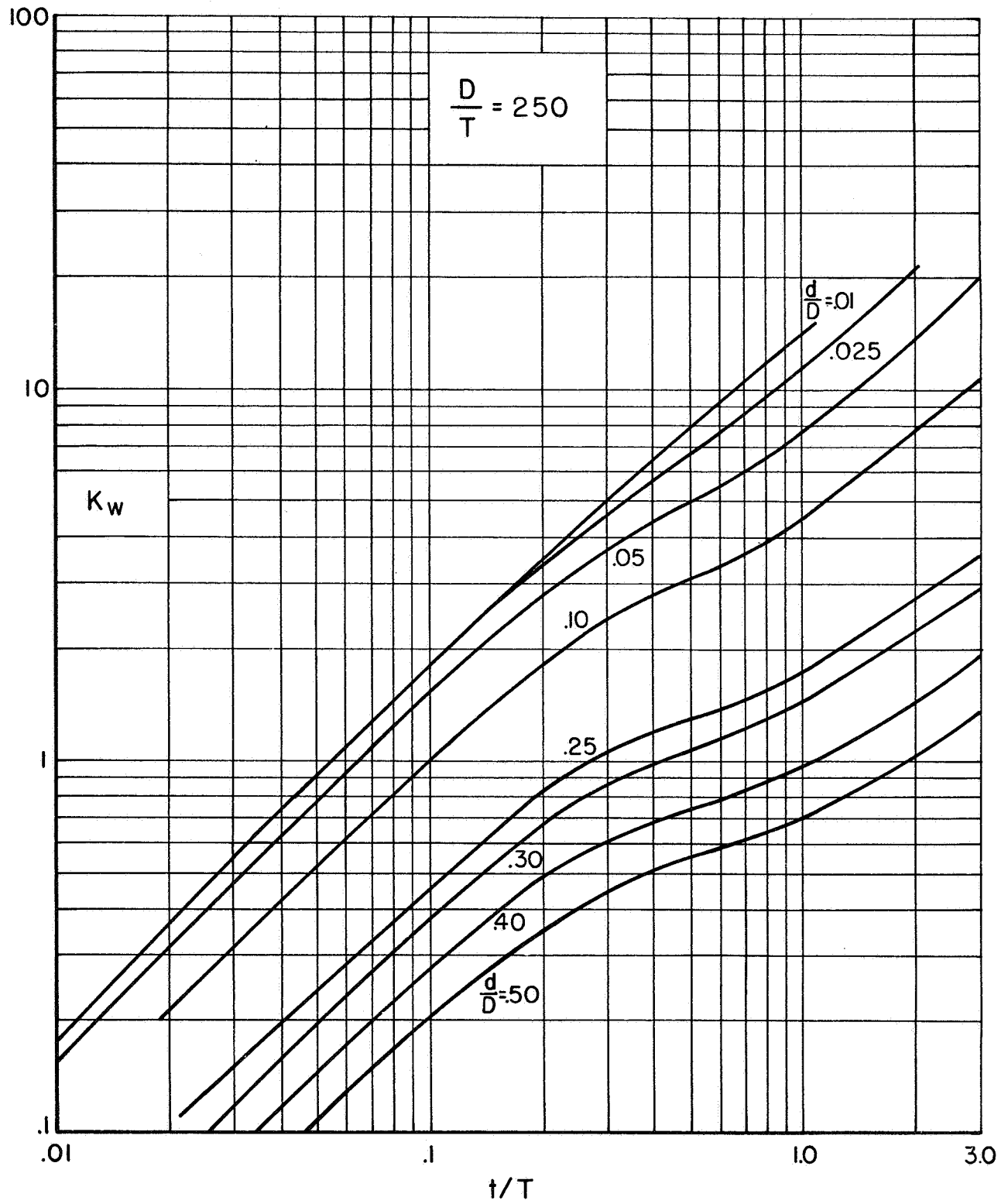


FIGURE 16. FLEXIBILITY FACTORS, THRUST LOAD,  $D/T = 250$



REFERENCES

- (1) Bijlaard, P. P., "Stresses in a Spherical Vessel from Radial Loads Acting on a Pipe" and "Stresses in a Spherical Vessel from External Moments Acting on a Pipe", Welding Research Council Bulletin No. 49 (April, 1959).
- (2) Dally, J. W., "An Experimental Investigation of the Stresses Produced in Spherical Vessels by External Loads Transferred by a Nozzle", Welding Research Council Bulletin No. 84 (January, 1963).
- (3) Cloud, R. L. and Rodabaugh, E. C., "Proposed Reinforcement Design Procedure for Radial Nozzles in Spherical Shells with Internal Pressure", Phase Report No. 1 to U.S. Atomic Energy Commission (Contract No. W-7405-eng-92) (March 31, 1966).
- (4) Penny, R. K. and Leckie, F. A., "Solutions for the Stresses at Nozzles in Pressure Vessels", Welding Research Council Bulletin No. 90 (September, 1963).
- (5) Kalnins, A., "Analysis of Shells of Revolution Subjected to Symmetrical and Nonsymmetrical Loads", ASME Journal of Applied Mechanics (September, 1964).
- (6) American Standards Association, "Code for Pressure Piping, ASA B31. 1-1955", published by the American Society of Mechanical Engineers, 345 E. 47th St., New York, New York 10017.
- (7) Rodabaugh, Witt, and Cloud, "Stresses at Nozzles in Spherical Shells Loaded with Pressure, Moment or Thrust", Phase Report No. 2 to U.S. Atomic Energy Commission (Contract No. W-7405-eng-92) (July, 1966).

PHASE REPORT NO. 4

on

PROPOSED REINFORCEMENT DESIGN PROCEDURE  
FOR RADIAL NOZZLES IN CYLINDRICAL  
SHELLS WITH INTERNAL PRESSURE

(Battelle Contract No. W-7405-eng-92)

Task 16

to

UNITED STATES ATOMIC ENERGY COMMISSION

December 22, 1967

by

E. C. Rodabaugh  
Battelle Memorial Institute  
Columbus, Ohio

and

R. L. Cloud  
Westinghouse Electric Corporation  
Bettis Atomic Power Laboratory  
Pittsburgh, Pennsylvania

**Section 4**

## DISCLAIMER

The work covered by this report was sponsored under contract with the Atomic Energy Commission in cooperation with the Pressure Vessel Research Committee. Although this report is one of a series of reports summarizing the results of PVRC research on reinforced openings, it is issued at this time primarily for informational purposes, indicating current thinking concerning development of design procedures for reinforced openings. It has not yet been approved for publication by PVRC, nor has it been submitted for review and consideration by ASME Code Groups. Therefore, it should be understood that it has no status whatever insofar as the ASME Code is concerned.

TABLE OF CONTENTS

	<u>Page</u>
INTRODUCTION . . . . .	1
NOMENCLATURE . . . . .	3
LIMITATIONS . . . . .	5
DESIGN PROCEDURE FOR RADIAL NOZZLES IN CYLINDRICAL SHELLS UNDER INTERNAL PRESSURE . . . . .	6
DESIGN CRITERIA . . . . .	9
DEVELOPMENT OF DESIGN PROCEDURE . . . . .	11
Reinforcing on Nozzle or Shell . . . . .	11
Reinforcing on Nozzle and Shell . . . . .	18
Length of Uniform Thickness . . . . .	20
Compact Reinforcing . . . . .	21
Distribution of Reinforcing . . . . .	30
Fillet Radii . . . . .	30
Transition Sections . . . . .	30
COMPARISON WITH OTHER DESIGN PROCEDURES . . . . .	32
Current American Practice . . . . .	32
Required Thicknesses . . . . .	32
Required Areas . . . . .	35
United Kingdom to ISO Proposal . . . . .	38
German Rules, AD-Merkblatt B9 . . . . .	47
Nozzles in Spheres vs Nozzles in Cylinders . . . . .	52
REFERENCES . . . . .	55

PROPOSED REINFORCEMENT DESIGN PROCEDURE  
FOR RADIAL NOZZLES IN CYLINDRICAL  
SHELLS WITH INTERNAL PRESSURE

INTRODUCTION

Phase Report No. 1, "Proposed Reinforcement Design Procedure for Radial Nozzles in Spherical Shells With Internal Pressure" covers one aspect of the general subject of reinforced openings in pressure vessels. This Phase Report No. 4 gives analogous information for nozzles in cylindrical pressure vessels. The design procedure is intended to define acceptable reinforcing details for radial nozzles in cylindrical shells based on the criteria:

- (1) The maximum calculated stress intensity in the cylindrical shell is limited to  $3S$ , where  $S$  is the nominal stress due to pressure in the unperforated cylinder
- (2) The calculated limit pressure of the nozzle-cylinder is essentially equal to the yield pressure of the unperforated cylinder.

The "Design Procedure", in a brief form suitable for use in design work, is presented in the section following the "Nomenclature". The remainder of the report provides the background and basis of the design procedure along with comparisons with other design procedures.

It is emphasized that this design procedure covers internal pressure loading only, and that modifications may be necessary to accommodate other superimposed loadings; particularly external loadings from the attached piping system and thermally induced stresses. The elastic stress criterion chosen (maximum stress intensity  $\cong 3S$ ) is the limit which, under the rules of the ASME Nuclear Vessel Code<sup>(1)</sup>, applies to the sum of the primary and secondary

stresses, including pressure, thermal and external loading effects. Since the limit analysis criterion controls almost throughout the dimensional range covered herein, the design procedure inherently contains at least a small margin to accommodate stresses from additional sources\*.

---

\*For nozzles in spherical shells, Phase Report No. 2 gives graphical data from which the stresses due to moment or thrust loading can be obtained. For nozzles in cylindrical shells, Phase Report No. 5 gives empirical data and Bijlaard's theory from which estimates of stresses due to moment or thrust loads can be obtained. Work is under way to extend the theory of radial nozzles in cylindrical shells to include moment and thrust loadings on the nozzle.

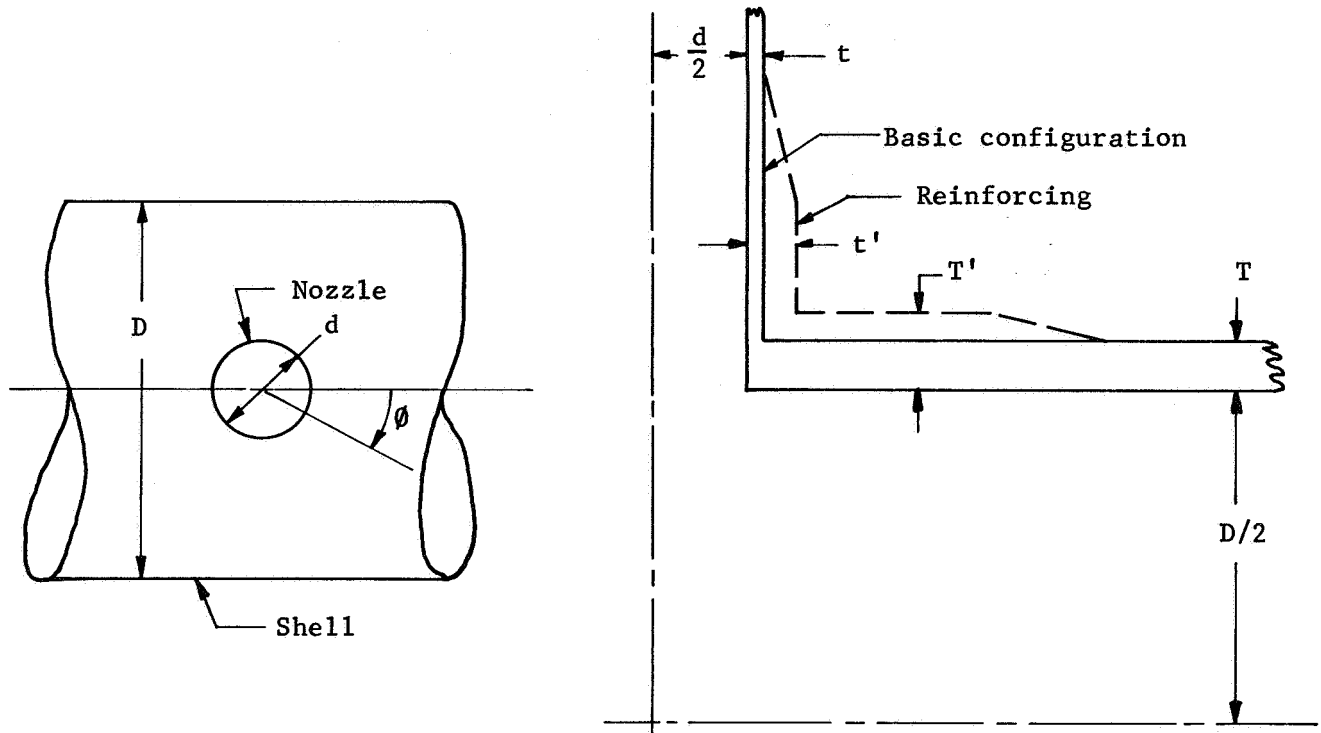
NOMENCLATURE

FIGURE 1. NOMENCLATURE ILLUSTRATION

$D$  = inside diameter of shell, inches

$d$  = inside diameter of nozzle, inches

$T$  = basic thickness of shell, inches

$T'$  = required thickness of the shell, as an unperforated cylinder,  
for the design pressure

$t$  = basic thickness of the nozzle, inches

(It is assumed that  $D$ ,  $T$ ,  $d$ , and  $t$  are related by the equation

$$D/T = d/t$$

$T'$  = reinforced thickness of the shell, inches

$t'$  = reinforced thickness of the nozzle, inches

$$h = T'/T$$

$$g = t'/t$$

S = nominal stress in shell, psi

$$= PD/2T$$

s = nominal stress in nozzle, psi

$$= Pd/2t$$

P = internal pressure, psi

$\bar{\sigma}$  = maximum stress intensity, psi

Stress intensity = 2x(shear stress)

$\varphi$  = location angle, see sketch above.

A = reinforcing area (in excess of basic configuration) on each side of nozzle centerline, sq in.



LIMITATIONS

The design procedure is limited, as indicated by the title, to internal pressure loading only. Other limitations are listed below.

- (1) Small nozzles as defined by:

$$\frac{d}{D} \leq \frac{1}{3} \text{ and } \frac{d}{D} \sqrt{\frac{D}{T}} \leq 1.1.$$

These limitations are on the elastic analysis used as a basis herein. The limit pressure analysis does not have any inherent  $(d/D) \sqrt{D/T}$  limitation and is considered valid (as judged by comparison with test data) up to a  $d/D$  of 0.5.

- (2) Nozzles are cylindrical, mounted radially to the shell cylinder surface and isolated from other nozzles or from any other significant local stress discontinuity.
- (3) Any reinforcement must be integral with the shells, as contrasted to "welded-on" pads or saddles.
- (4) Since limit analysis is used to establish the design procedure, an implied assumption is that the material of the shells and the weld metal is ductile; e.g., is capable of withstanding several percent of local strain in a complex stress field at all temperatures at which the vessel may be loaded.

DESIGN PROCEDURE FOR RADIAL NOZZLES IN  
CYLINDRICAL SHELLS UNDER INTERNAL PRESSURE

1. Nozzles may be reinforced by increasing the thickness of the nozzle and/or shell near the nozzle-to-shell juncture according to Par. 3, or by applying extra material around the nozzle-to-shell juncture according to Par. 4. The reinforcing requirements apply to all planes passing through the axis of the nozzle. These rules apply to isolated nozzles in which the edge of the opening is at least a distance equal to  $2.5 \sqrt{DT/2}$  from the nearest edge of any other local stress discontinuity.
2. Dimension T is the required\* thickness of the unperforated shell for the design pressure; t is the required\* thickness of the nozzle (as a cylindrical shell) for the design pressure. Other dimensions and symbols are defined in the following text and Figure 2. All dimensions shall be taken in the "corroded" condition. It is assumed that the materials used in the shell, nozzle, weld metal and reinforcement section (if any) are of equal strength.

3. (a) Uniformly thickened nozzle wall, Figure 2a

$$t' \geq gt, \quad \ell \geq \sqrt{dgt}, \quad g \text{ obtained from Figure 3a.}$$

- (b) Uniformly thickened shell wall, Figure 2b

$$T' \geq hT, \quad L \geq \sqrt{DhT}, \quad h \text{ obtained from Figure 3b.}$$

- (c) Uniformly thickened nozzle and shell wall, Figure 2c

$$\text{Determine } g' \text{ and } h' \text{ according to } \frac{g' - 1}{g - 1} + \frac{h' - 1}{h - 1} = 1$$

g and h obtained from Figures 3a and 3b, respectively.

$$t' \geq g't, \quad \ell \geq \sqrt{dg't}$$

$$T' \geq h'T, \quad L \geq \sqrt{Dh'T}$$

4. Compact reinforcements, Figures 2d, 2e, 2f

$A_r$  = required cross sectional area of reinforcement in any plane containing the nozzle axis.

A = actual reinforcing cross sectional area on each side of the nozzle centerline. Only the area within the circle defined by the radius  $L_c$  may be taken as contributing to  $A_r$ .

$$\text{For: } d/D \leq 0.1414\sqrt{T/D}; \quad A_r = 0$$

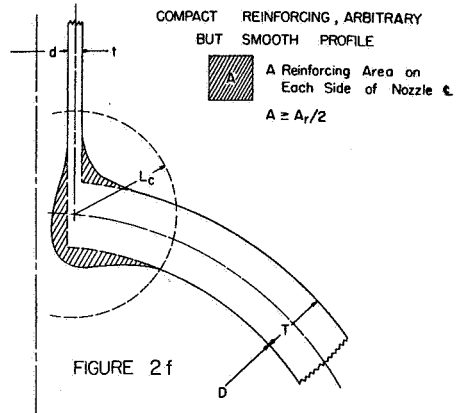
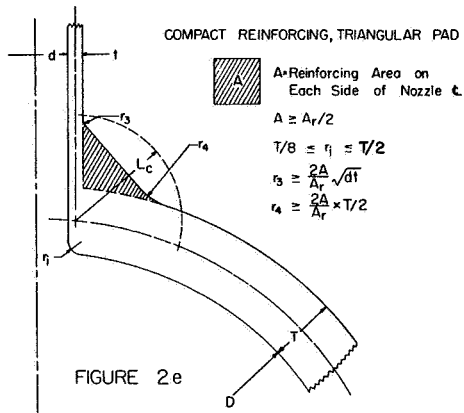
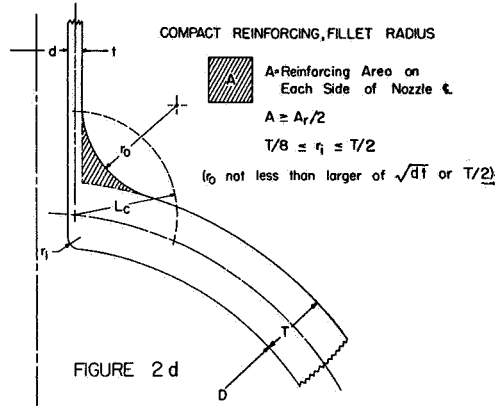
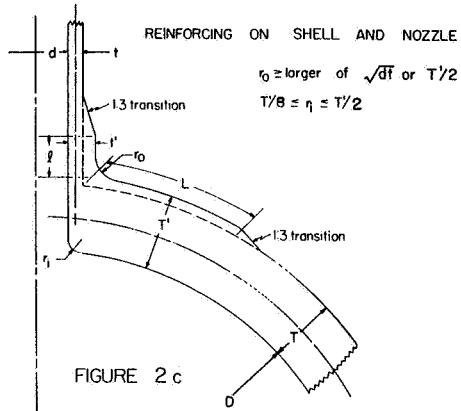
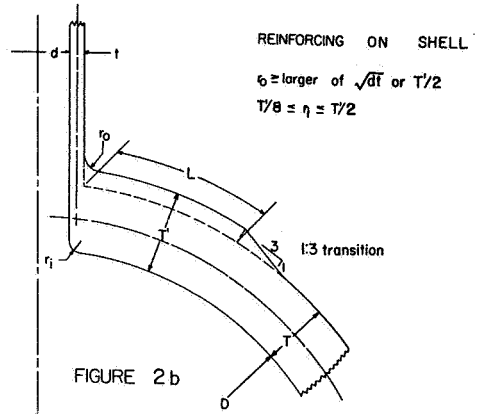
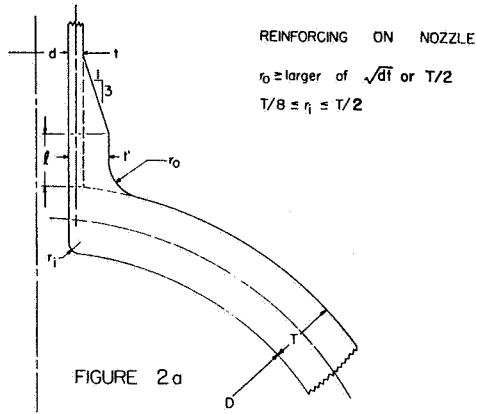
$$\text{For: } 0.1414\sqrt{T/D} \leq d/D \leq 0.425\sqrt{T/D}; \quad A_r = [2.65(d/D)\sqrt{D/T} - .375]dT$$

$$\text{For: } 0.425\sqrt{T/D} \leq d/D \quad A_r = .75 dT$$

$$L_c = 0.75 (T/D)^{2/3} D$$

---

\* Required thickness according to the appropriate design code; e.g., for the ASME Boiler Code, Section VIII:  $T = PD/(2S_a E - 1.2P)$ , where P = internal pressure, D = shell inside diameter,  $S_a$  = allowable stress, E = joint efficiency of welded joint in shell.



Transitions to shell walls shall be equivalent to not more than 20° (included angle) transition sections or by radii not less than  $\frac{2A}{A_r}t$  at nozzle wall;  $\frac{2A}{A_r}T$  at shell wall. Outside fillet radii shall in no case be less than the larger of  $\frac{2A}{A_r}\sqrt{dt}$  or  $\frac{2A}{A_r} \times T/2$ .

Sections are shown in plane transverse to shell axis.  
Requirements apply to all planes containing the nozzle axis.

FIGURE 2: REINFORCED NOZZLE DETAILS

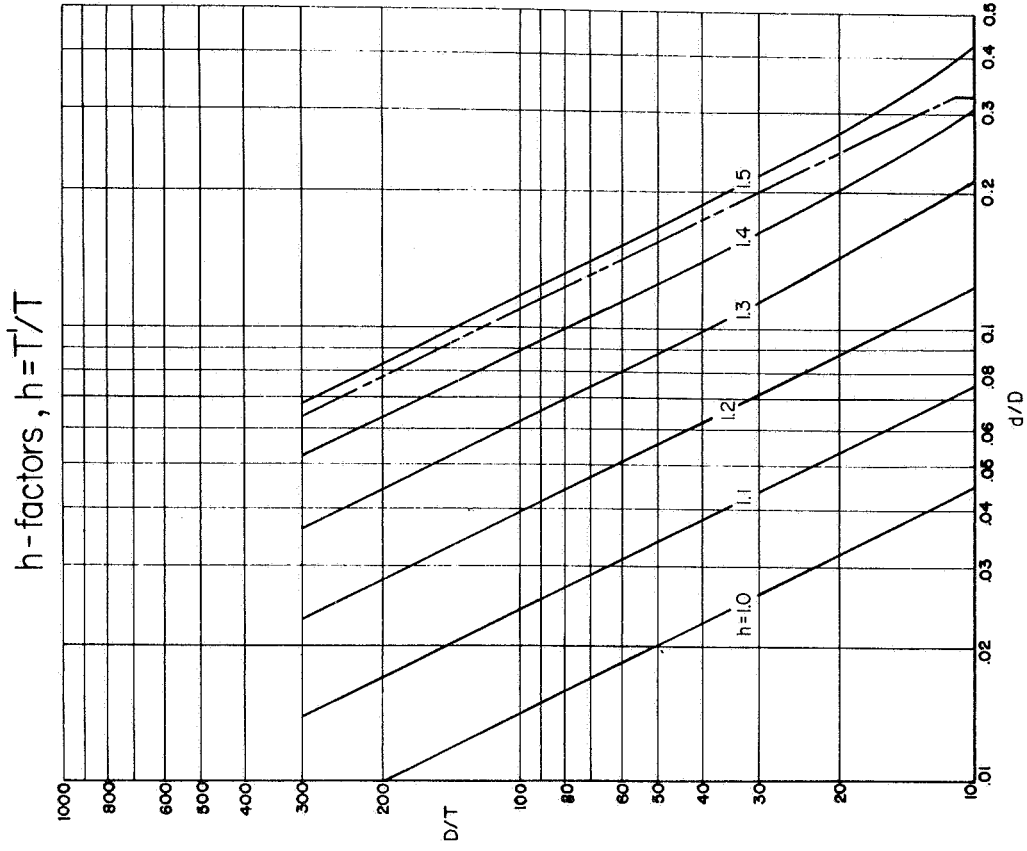


FIGURE 3b

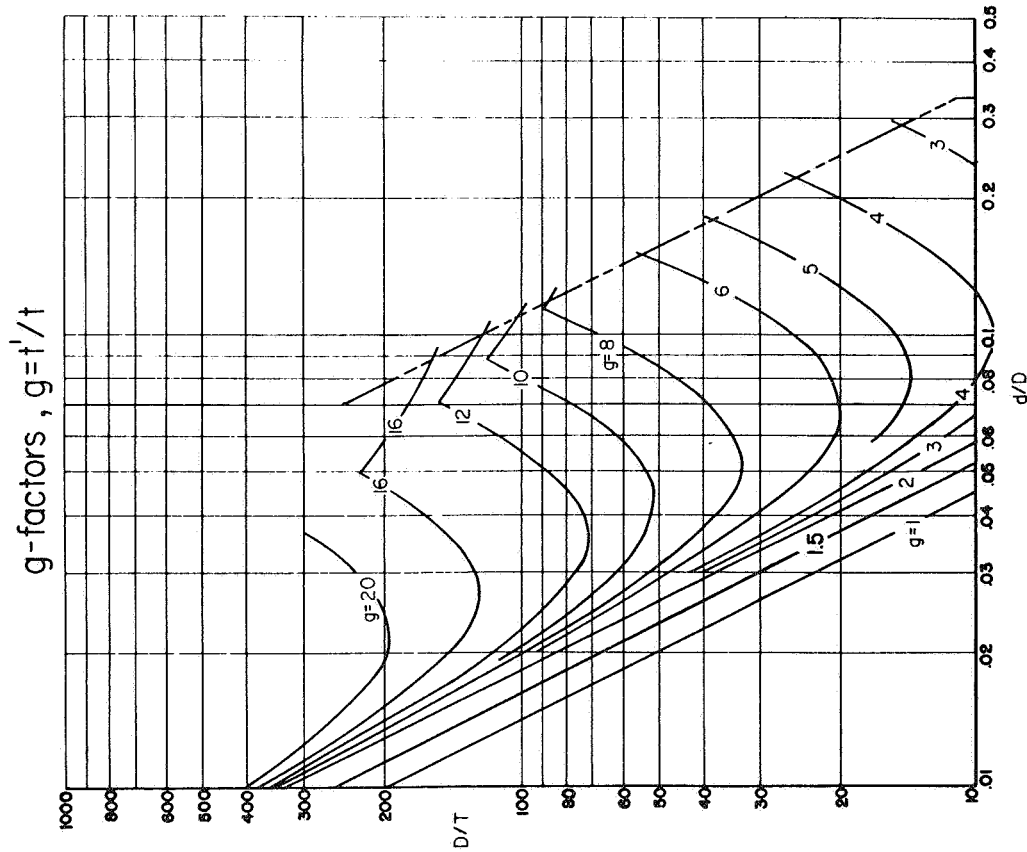


FIGURE 3a

FIGURE 3. GRAPHS FOR OBTAINING g-AND h-FACTORS

DESIGN CRITERIA

Static failure of a ductile material is a plastic process, and a rational basis for determining allowable stresses will necessarily involve plasticity considerations. The principles of plastic limit design were used to set allowable stresses in Section III of the ASME Boiler and Pressure Vessel Code, Nuclear Vessels<sup>(1,2)</sup>. Conservative simplifications and generalizations were made to achieve complete stress limits for all parts of a nuclear vessel. In particular, the  $1.5 S_m$  limit on local membrane stress was set to insure against local plastic collapse. A satisfactory, consistent nozzle design procedure cannot be constructed with this limit as a basis because it is too restrictive. This can be readily seen by considering very small nozzles, which should require no reinforcement, yet produce local membrane stresses of  $2.5 S$  in the shell. Therefore, the  $1.5 S_m$  limit of Section III is replaced in the proposed procedure by an actual limit analysis.

The design procedure presented herein results from a direct application of limit design principles to a specific geometry when subjected to internal pressure. The design philosophy is therefore the same as that of the ASME Nuclear Vessels Code.

It is the intent of the Nuclear Vessels Code to (1) provide a safety margin of 1.5 against plastic collapse when strain-hardening is neglected and (2) to insure shakedown to elastic action. In accordance with this intent, the proposed reinforcements were proportioned so that (1) the collapse pressure is at least 1.5 times the design pressure and (2) so that the most highly stressed regions of the nozzle will shakedown to elastic action. The collapse limit was established using the results of the plastic-limit analysis described in Reference 3. The shakedown criteria used was that of limiting the maximum

elastic stress intensity\* to three times the nominal stress in the unperforated shell; for materials with design stress intensity values established by the limit of two-thirds of the yield strength, this is the equivalent of limiting the maximum stress intensity,  $\bar{\sigma}$ , to twice\*\* the yield strength of the material. Elastic stresses were calculated according to Reference 4. The graphs are based on the maximum calculated stress intensity in the shell. Calculated stress intensities in the nozzle are higher; however, as discussed in Phase Report No. 5, test data indicate that with fillet radii as specified herein the calculated nozzle stresses do not occur and can be safely disregarded.

---

\*Stress intensity at a point is defined as twice the maximum shear stress at that point.

\*\*For vessel materials in which the ratio of ultimate strength to yield strength is less than two, the design stress intensity is one-third of the ultimate strength. For such materials the margins against plastic collapse or continued nonelastic straining are greater than indicated.

DEVELOPMENT OF DESIGN PROCEDURE

The design of a cylindrical nozzle in a cylindrical shell may be considered as consisting of a basic configuration plus reinforcement. The basic configuration is defined as an outwardly protruding nozzle and cylindrical shell segment, as shown in Figure 1, in which the nozzle and shell have the same nominal stress for a given pressure. Specifically:

$$\text{For the nozzle: } s = Pd/2t$$

$$\text{For the shell: } S = PD/2T$$

where    P = internal pressure  
           d = inside diameter of nozzle  
           t = wall thickness of nozzle  
           D = inside diameter of shell  
           T = wall thickness of shell.

For the basic configuration, by definition,  $s = S =$  allowable design stress intensity for the material used in the nozzle and shell--assumed to be made of equal strength materials.

The design procedure consists of specifications of the dimensions of reinforcing required, if any, in order to meet the design criteria described above.

Reinforcing on Nozzle or Shell

Within the scope of available analysis, the basic configuration may be reinforced either by increasing the wall thickness of the nozzle or by increasing the wall thickness of the shell, as shown in Figures 2a and 2b.

As a first step in developing the design procedure, an extensive dimensional parametric study was made using the analysis and computer program by Eringen<sup>(4)</sup>. The range\* of  $d/D$  and  $D/T$  included is shown in Figure 3. The slant line is the limit:  $(d/D) \sqrt{D/T} = 1.1$ . The parametric study included values of  $s/S$  from 1/64 to 4.0. The stresses obtained in this parametric study indicated which basic configurations required reinforcing in order to meet the elastic stress criteria  $\bar{\sigma} = 3S$  and how much reinforcing would be required if:

- (1) Reinforcing consisted only of an increase in wall thickness of the shell, or
- (2) Reinforcing consisted only of an increase in wall thickness of the nozzle.

Figure 4 shows the reinforcement required on the shell only, in terms of the parameters  $d/D$ ,  $D/T$ , and  $h = T'/T$ . The line marked  $h = 1$  indicates those combinations of  $D/T$  and  $d/D$  for which the maximum calculated stress intensity in the basic configuration (with an adequate fillet radius,  $r_0$ ) does not exceed  $3S$ . The lines marked  $h > 1$  indicate the thickness required in the shell so that  $\bar{\sigma} = 3S$ . Note that  $S = PD/2T$ , not  $PD/2T'$ ; i.e., the index stress is that of the unreinforced cylindrical shell.

Figure 5 shows the reinforcement required on the nozzle only, in terms of the parameters  $d/D$ ,  $D/T$ , and  $g = t'/t$ . The line marked  $g = 1$  is the same as on Figure 4 for  $h = 1$ ; higher values of  $g$  indicate the nozzle thickness required so that  $\bar{\sigma} = 3S$ .

Using the limit pressure analysis for nozzles in cylindrical shells developed by Cloud and Rodabaugh<sup>(3)</sup>, the reinforcing required to make the limit

---

\* The parametric study and resulting design curves cover up to  $D/T = 250$ . This is not an upper limit to the applicability of Eringen's analysis and computer program.



$$h = T'/T$$

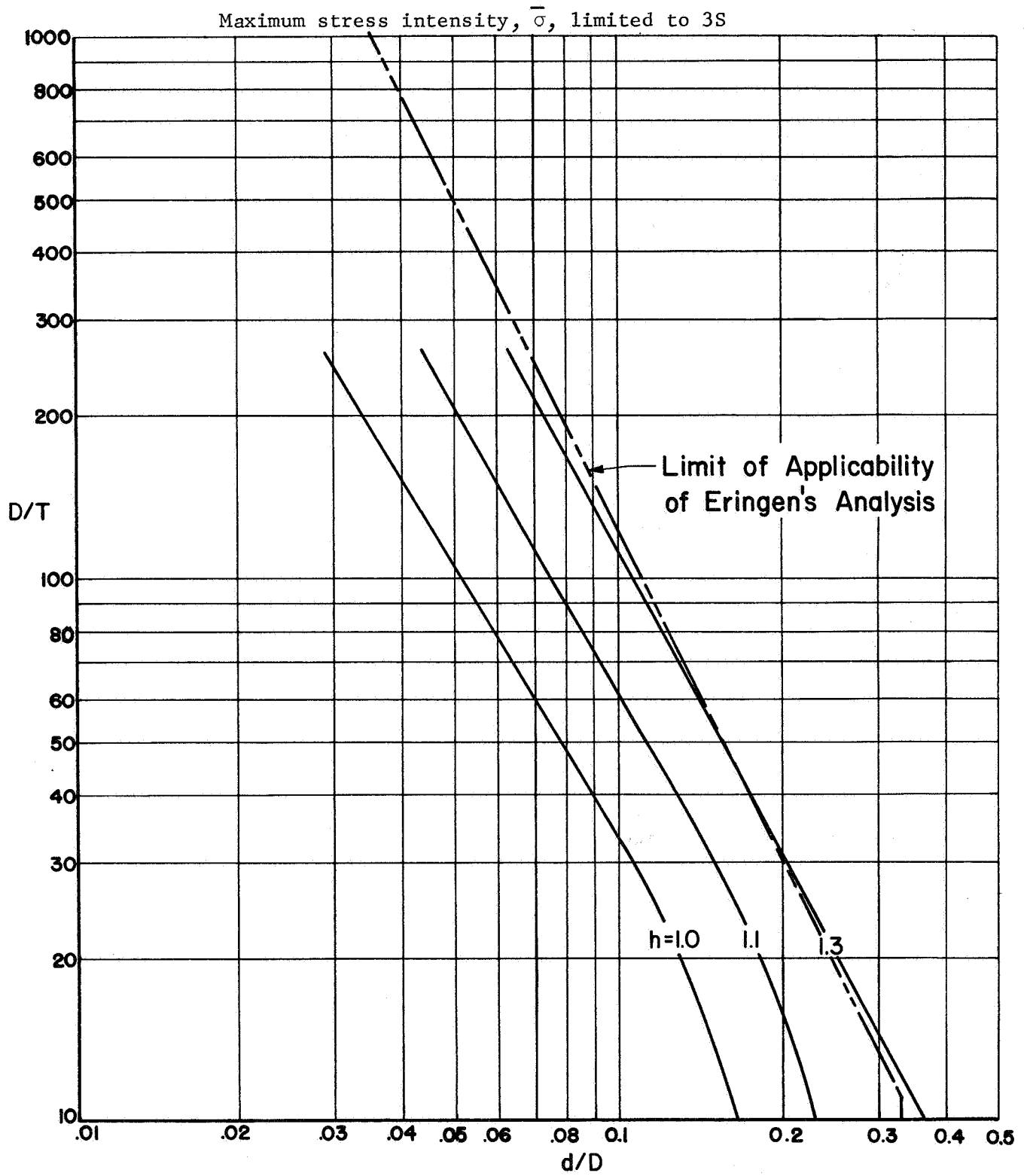


FIGURE 4. REQUIRED REINFORCING ON SHELL FOR  $\bar{\sigma} = 3S$ , ERINGEN'S ANALYSIS

$$g = t'/t$$

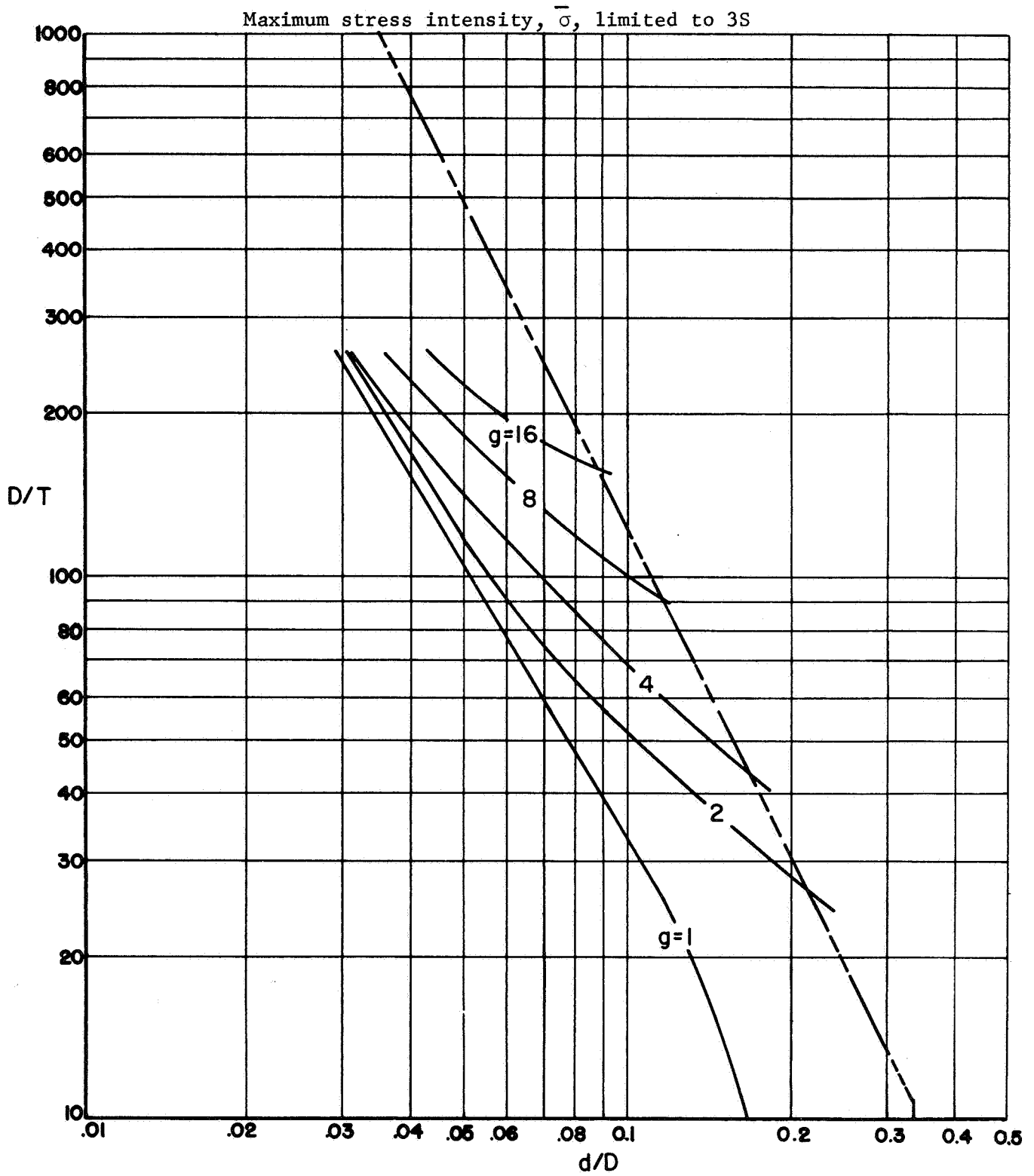


FIGURE 5. REQUIRED REINFORCING ON NOZZLE FOR  $\bar{\sigma} = 3S$ , ERINGEN'S ANALYSIS

pressure essentially equal to the yield pressure of the unperforated cylinder was calculated.

The method of calculation gives a conservative margin on the reinforcing thickness by a factor of 8/7, except for  $h$  or  $g$  close to unity. In addition, test data<sup>(5)</sup> indicate that the fillets required by the design procedure will provide an additional strengthening effect not considered in the theory.

The curves resulting from the limit pressure analysis shown as dashed lines in Figures 6 and 7 and are superimposed over the analogous curves based on the elastic analysis. The limit pressure criterion is more restrictive than the elastic criterion ( $\bar{\sigma} = 3S$ ) except for a small area in Figure 7; e.g.,  $d/D = 0.06$ ,  $D/T = 200$ . The design graphs, Figure 2, are based on the more conservative of the elastic or limit pressure criteria.

In constructing the design graphs shown in Figure 2, one modification was made\*: the line for  $h = g = 1$  was obtained by the equation

$$d = 0.1414 \sqrt{DT} \quad (1)$$

This results in shifting the limit pressure lines for  $h = 1$  or  $g = 1$  on Figures 6 and 7 down and to the left. This was done for two reasons:

- (a) A degree of conservatism is introduced in the limit pressure analysis results near  $h = g = 1.0$
- (b) Equation (1) agrees with the limitation given in the ASME Nuclear Vessel Code, Para. N-452(a)(1), below which reinforcing of openings is not required.

---

\*This modification was also made in Phase Report No. 1, nozzles in spheres.

$h = T'/T$

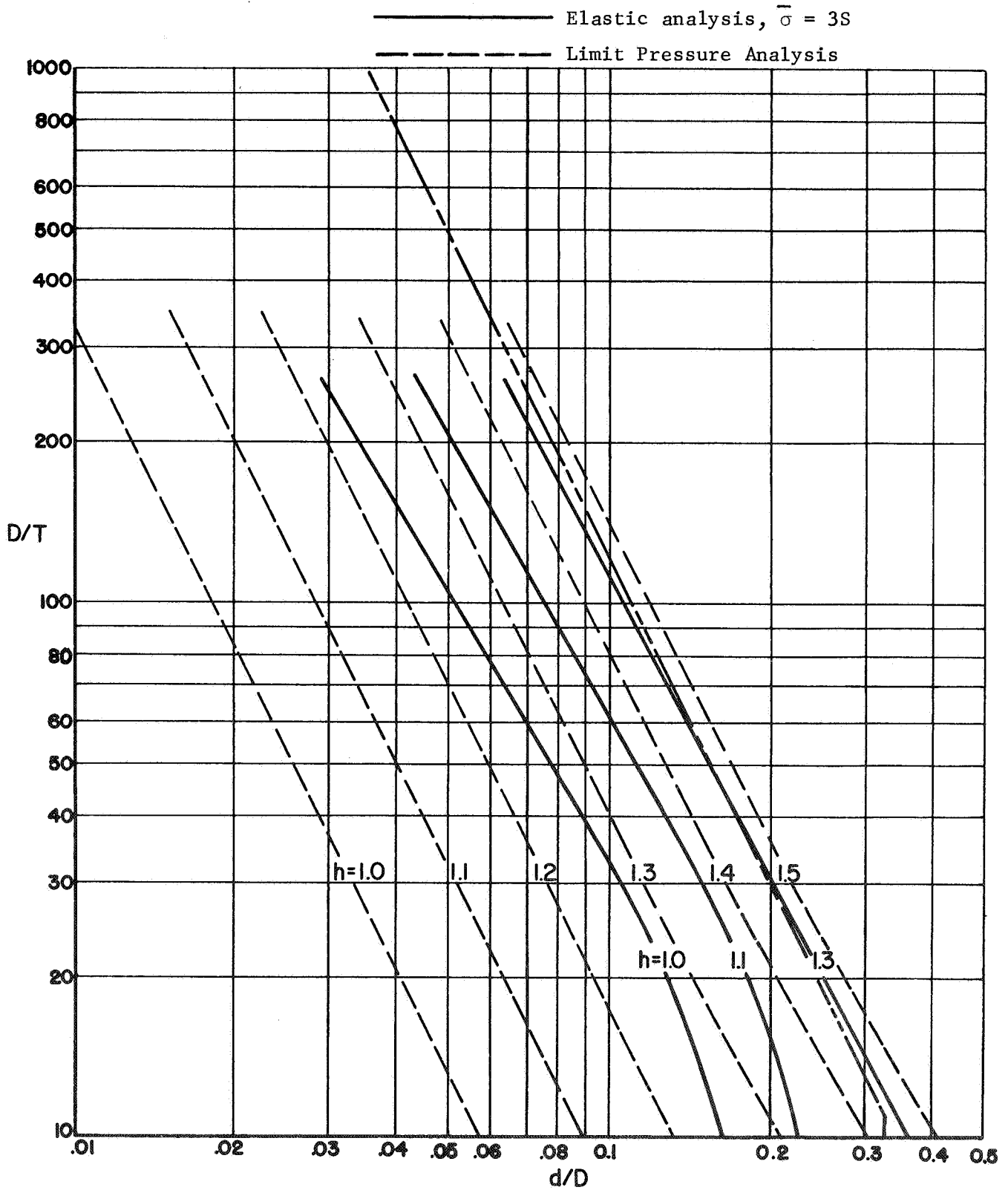


FIGURE 6. REQUIRED REINFORCING ON SHELL BY LIMIT ANALYSIS

$$g = \frac{t'}{t}$$

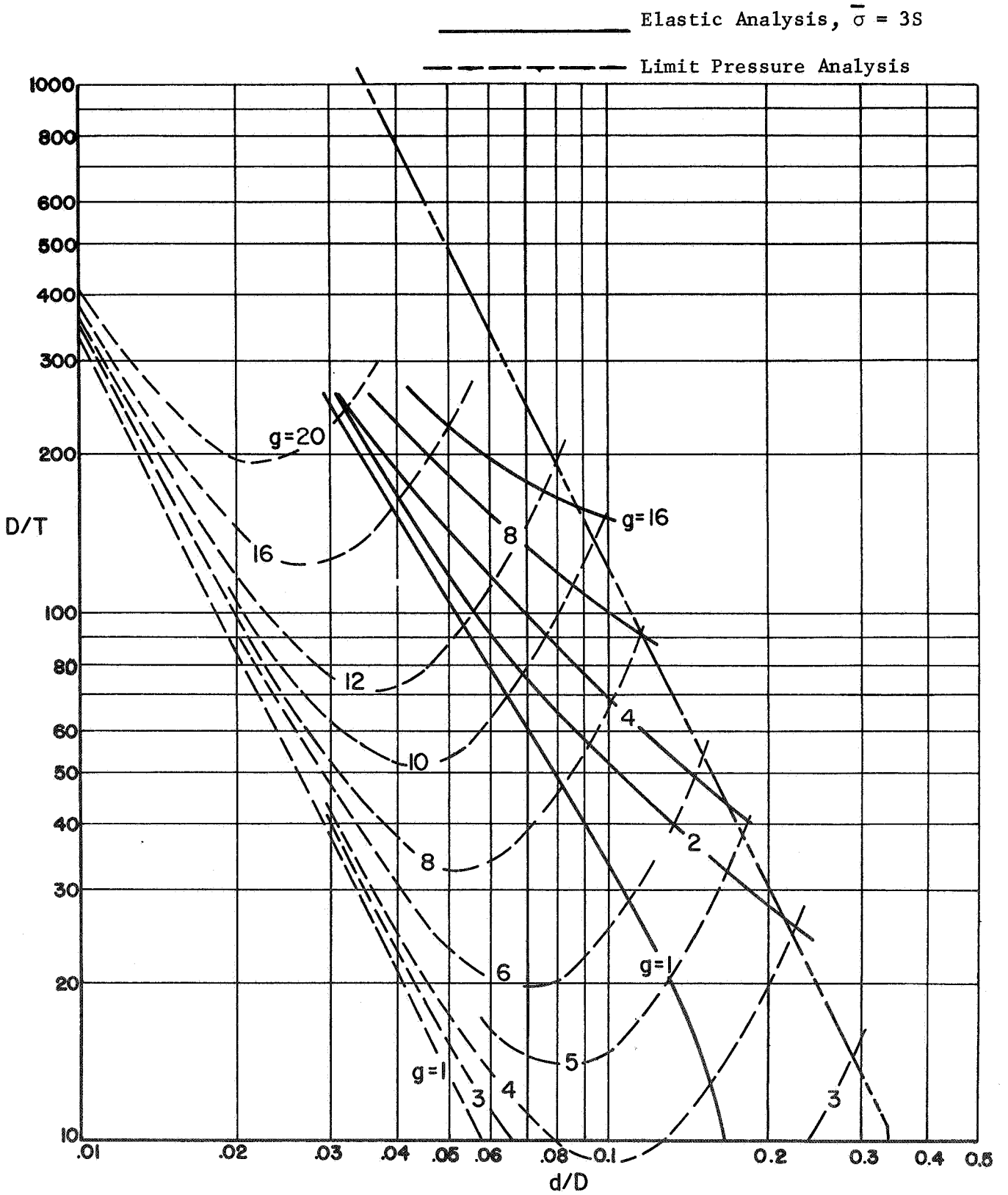


FIGURE 7. REQUIRED REINFORCING ON NOZZLE BY LIMIT ANALYSIS

The lines on Figure 2b for  $h = 1.1$  and  $1.2$  are interpolated between  $h = 1.0$  and  $h = 1.3$  (limit analysis) of Figure 6. The line on Figure 2a for  $g = 1.0$  (limit analysis) has been changed to  $g = 2.0$ ; the lines for higher values of  $g$  are the lower of the limit analysis or elastic stress criteria shown in Figure 7.

### Reinforcing on Nozzle and Shell

The requirements given above relate to either a reinforced cylindrical shell or a reinforced nozzle. In many practical designs, it may be desirable to use a combination of reinforcing on the shell and nozzle, as shown in Figure 2c, while it is possible to construct a number of graphs similar to Figures 3a and 3b which, with interpolation, would cover these designs, in the interest of simplicity the following linear relationship was developed:

$$\frac{g' - 1}{g - 1} + \frac{h' - 1}{h - 1} = 1 \quad (2)$$

where  $g = t'/t$  from Figure 3a

$g' =$  partial nozzle reinforcement,  $1 < g' < g$ .

$h = T'/T$  from Figure 3b

$h' =$  partial shell reinforcement,  $1 < h' < h$ .

This rule is, of course, in agreement with the general analysis at either end of its range; i.e., for either  $g' = g$ ,  $h' = 1$ , or  $h' = h$ ,  $g' = 1$ . Table 1 shows calculated maximum stress intensities for reinforcements at the mid-range of Equation (1). The maximum stress intensities are shown in the next to last column of Table 1. The calculated values of  $\bar{\sigma}/S$  are all less than 3.0, indicating that the linear approximation is conservative insofar as the elastic

TABLE 1. MAXIMUM STRESS INTENSITIES AND LIMIT PRESSURE RATIOS FOR NOZZLES DESIGNED BY THE LINEAR INTERPOLATION EQUATION<sup>(1)</sup>, DESIGN PROCEDURE PARAGRAPH 3(c)

d/D	D/T	h	g	h'	g'	$\bar{\sigma}/S$	$P_L/P_{yc}$ <sup>(2)</sup>
0.10	10	1.16	4.2	1.08	2.6	2.4	1.04
0.25	10	1.35	3.1	1.17	2.05	2.7	1.07
0.05	25	1.12	6.2	1.06	3.6	2.4	1.03
0.25	25	1.53	3.8	1.26	2.4	2.5	1.04
0.05	50	1.18	9.6	1.09	5.3	2.4	1.04
0.15	50	1.47	5.9	1.23	3.45	2.6	1.03
0.025	100	1.10	13.	1.05	7.0	2.5	1.02
0.10	100	1.44	9.	1.22	5.0	2.7	1.03
0.01	250	1.03	1.5	1.01	1.25	2.6	1.00
0.05	250	1.37	18.	1.18	9.5	2.7	1.04

(1) Linear interpolation equation:

$$\frac{g' - 1}{g - 1} + \frac{h' - 1}{h - 1} = 1$$

g and h obtained from Figures 3a and 3b, respectively. Examples are at midrange of equation.

(2)  $P_L$  = calculated limit pressure, Reference (3)

$P_{yc}$  = nominal yield pressure of unperforated, unreinforced cylindrical shell

$$= 2\sigma_{oc} T/D$$

$\sigma_{oc}$  = yield strength of material (assumed to be the same for shell, nozzle, and weld material).

stress criteria is concerned. The last column of Table 1 shows calculated limit pressure ratios for the same configurations. The ratios of  $P_L/P_{yc}$  are equal to or greater than unity, indicating the linear interpolation formula is adequate or conservative from the limit pressure aspect.

#### Length of Uniform Thickness Reinforcing

The length of uniformly increased wall thickness necessary so that the local stresses at the nozzle-shell juncture will be the same as if that length were infinite may be estimated in two ways:

- (1) The results of an elastic analysis (e.g., Eringen's) can be examined to determine that distance from the nozzle-shell juncture at and beyond which the calculated elastic stresses are essentially those for an unperforated cylinder.
- (2) The results of test data can be examined to determine the length as described in (1) above.

Investigation of the results of a parametric study using Eringen's analysis, as well as examination of available test data, indicate that reinforcement lengths equal to  $\sqrt{dt'}$  on the nozzle;  $\sqrt{DT'}$  on the shell should be sufficient. This reinforcement length for the nozzle is the same as used in Phase Report No. 1 for nozzles in spheres. For the shell reinforcing length, the value of  $\sqrt{DT'}$  is larger than the  $0.7 \sqrt{DT'}$  suggested in Phase Report No. 1 for the length of reinforcement on the sphere.



Compact Reinforcing

Nozzles in pressure vessels are quite often designed with a local reinforcing such as the triangular-shape of Figure 2e. For nozzles in spheres, as discussed in Phase Reports 1 and 2, there are analytical methods for both limit pressure and elastic stresses which were used to guide the design rules for compact reinforcing of nozzles in spheres. For nozzles in cylinders, such analytical methods are not available; the approach used is guided to a large extent by the procedure developed for nozzles in spheres.

Figures 8 and 9 show the area of reinforcing required for uniform-wall reinforcing on the shell and reinforcing on the nozzle, respectively. For compact reinforcing, which may be considered as reinforcing on both the shell and nozzle, it appears appropriate to specify an area equal to about the average of that required in Figures 8 and 9. Figure 10 shows the data from both Figures 8 and 9, along with curves which represent the average thereof. The equations of these average curves are:

For:

$$(d/D) < 0.1414 \sqrt{T/D} \qquad 2 A/dT = 0 \qquad (3a)$$

$$0.1414 \sqrt{T/D} < (d/D) < 0.425 \sqrt{T/D} \qquad 2 A/dT = 2.65(d/D) \sqrt{D/T} - .375 \qquad (3b)$$

$$(d/D) > 0.425 \sqrt{T/D} \qquad 2 A/dT = .75 \qquad (3c)$$

Equation 3a permits zero reinforcing for the same  $d/D$  and  $D/T$  ratios as shown in Figure 3. Equation 3b gives the transition between where no reinforcing is required and where  $0.75 dT$  reinforcing is required, Equation 3c. Reinforcement area of  $0.75 dT$ , within the reinforcing zone

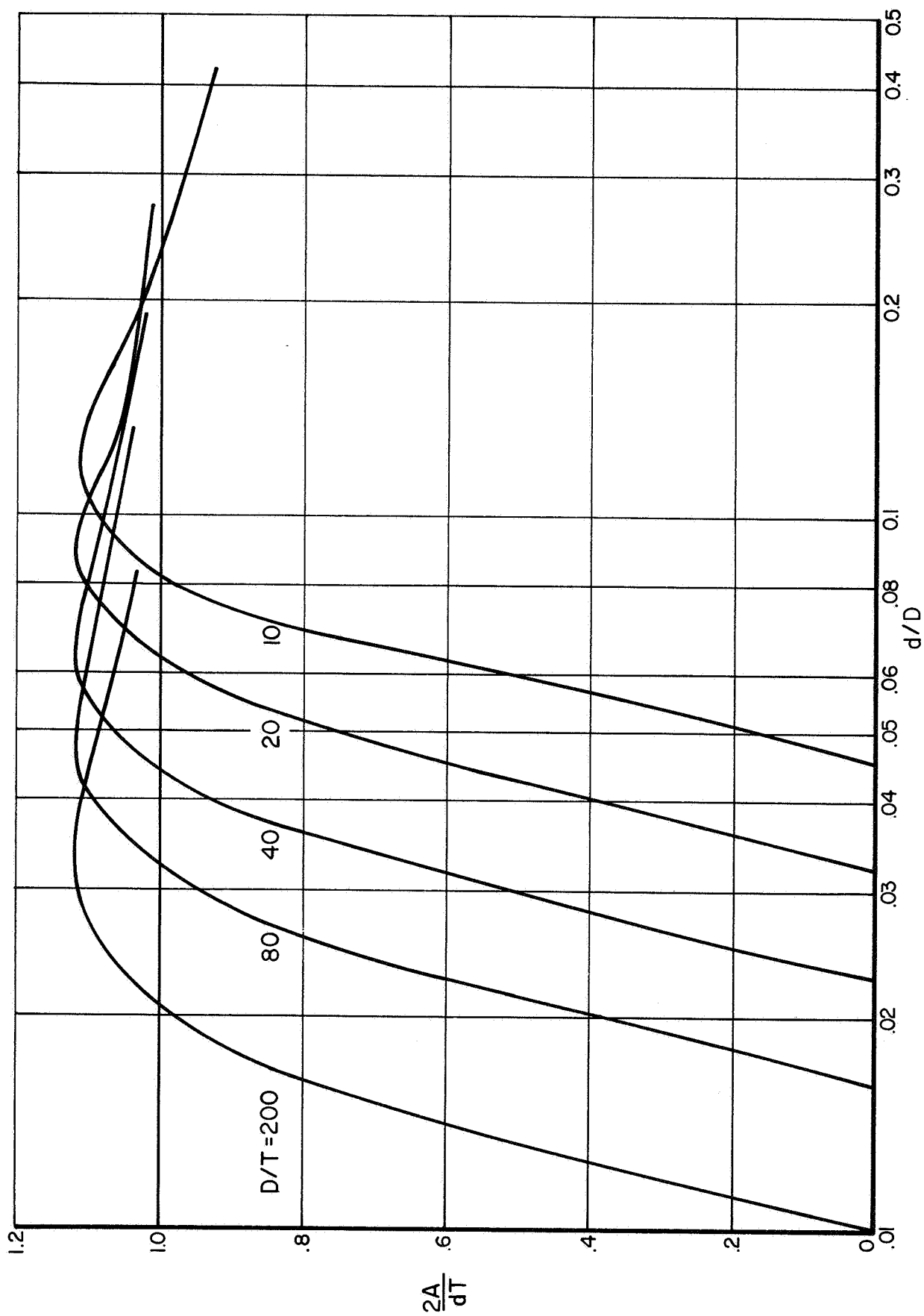


FIGURE 8 . AREA OF REINFORCING REQUIRED BY PROPOSED RULES FOR REINFORCING ON THE SHELL (A = area on one side of section)

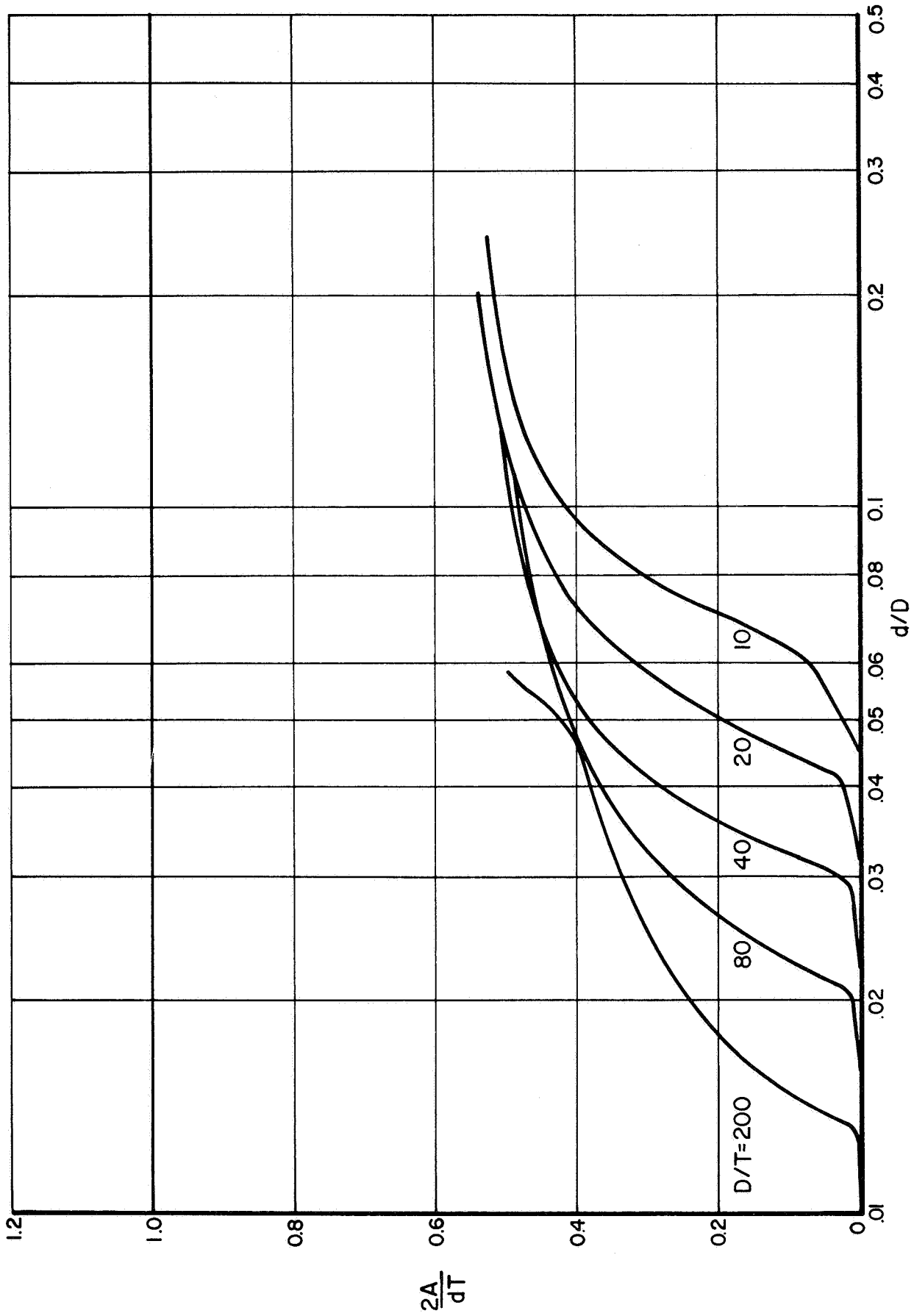


FIGURE 9 . AREA OF REINFORCING REQUIRED BY PROPOSED RULES FOR REINFORCING ON THE NOZZLE (A = area on one side of section)

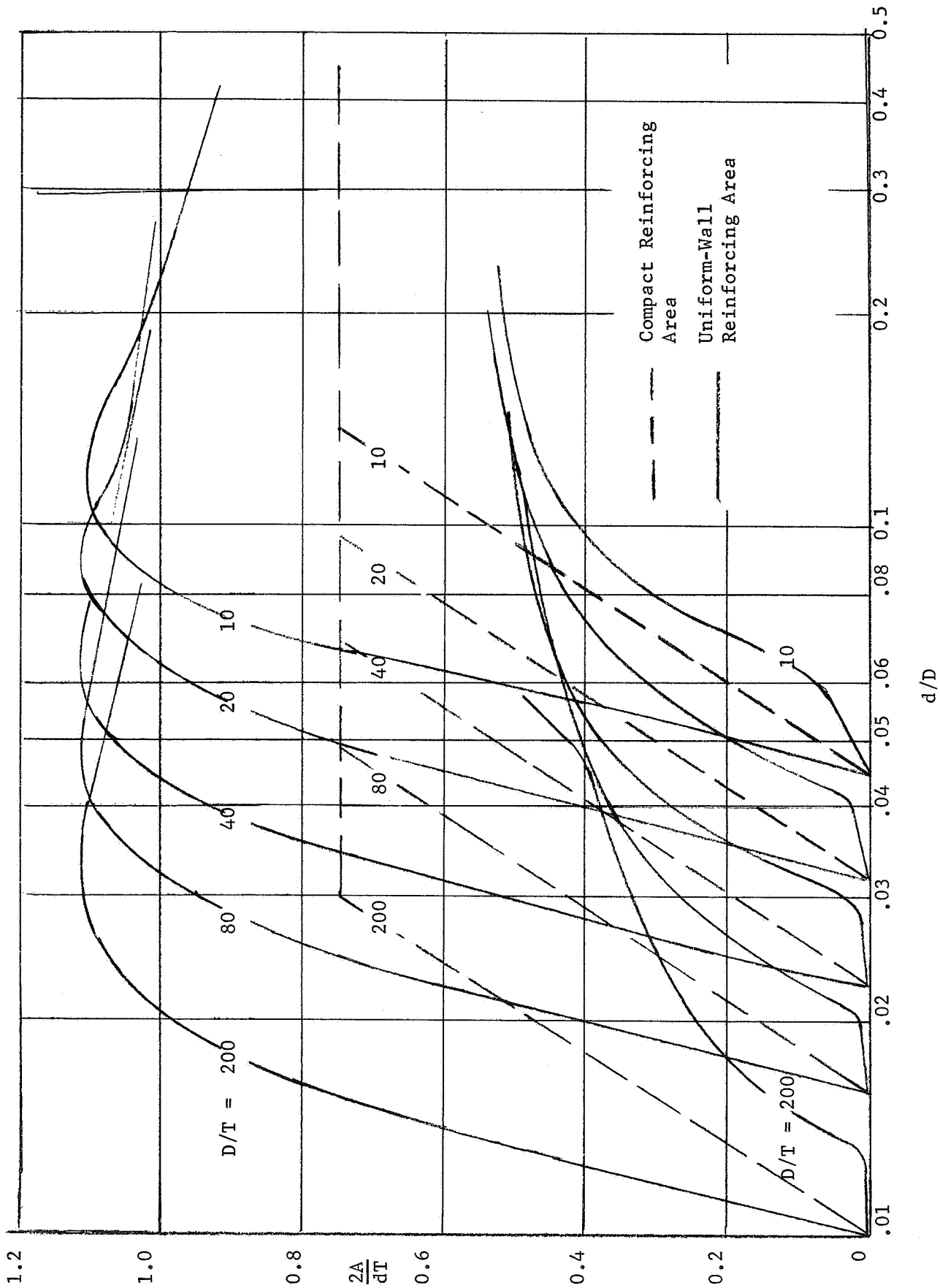


FIGURE 10: COMPARISON OF COMPACT AND UNIFORM -WALL REINFORCING AREAS

discussed below, appears\* to give adequate reinforcing insofar as limiting elastic stresses to  $3S$  is concerned.

In connection with compact reinforcing, a reinforcing zone consistent with the areas and lengths of uniform-wall reinforcing is desired. In Phase Report No. 1, a zone radius  $L_c$  as shown in Figure 2f was established, where

$$L_c = 1.5 (T/D)^{2/3} D$$

For nozzles in cylinders, in order to suitably limit the zone parallel to the nozzle wall, it is necessary to use the zone radius limit:

$$L_c = 0.75 (T/D)^{2/3} D \quad (4)$$

This change from nozzles in spheres comes about, in part, because of the relations:

$$\text{For nozzles in spheres:} \quad \frac{d}{t} = (1/2) \frac{D}{T}$$

$$\text{For nozzles in cylinders:} \quad \frac{d}{t} = \frac{D}{T}$$

Table 2 gives some comparisons of  $L_c$  with reinforcing zone limits of  $\sqrt{DT}$ ,  $\sqrt{dt}$ , and  $2.5T^{**}$ . The ratios of  $L_c/\sqrt{DT}$  of from 0.51 to 0.30 may be compared with the ASME Section III rule that two-thirds of the reinforcing must be placed within a zone along the shell of  $0.5 \sqrt{RT} = 0.353 \sqrt{DT}$ . Table 2 indicates that  $L_c$  can be a large multiple of  $\sqrt{dt}$ . However, as illustrated by Table 3, if the rules of Figures 2f are used to compute the  $g_a$ -value † for the design shown in Figure 2a, the  $g_a$ -values are in

---

\* See Phase Report No. 5.

\*\* Used in present ASME Code, Section VIII.

† The identification  $g_a$  is used to distinguish these values from those given in Figure 3a.

reasonable accord with those given in Figure 2f. Both  $g_a$  and  $g$  converge to 1.0 for  $d/D \leq .1414 \sqrt{D/T}$ ; for  $d/D \geq 0.425 \sqrt{D/T}$ ,  $g_a$  is greater than  $g$ .

Table 3 also shows values of  $h_a$  obtained by applying the rules of Figure 2f to the design shown in Figure 2b. Except for  $d/D$  close to  $0.1414 \sqrt{D/T}$  (for and below which both  $h_a$  and  $h$  converge to 1.0),  $h_a$  is greater than  $h$  as obtained from Figure 3b.

As indicated by Figure 11, it is possible to place the required area of reinforcing on the outside of the shell within the zone limit shown in Figure 2f for values of  $(d/D) \sqrt{D/T} < 1.1$  and  $D/T > 10$ . For  $D/T$  less than 15,  $d/D$  is limited to about 0.28 if all reinforcing is placed on the outside as shown in Figure 11.

TABLE 2. COMPARISONS OF ZONE OF REINFORCEMENT FOR  
 COMPACT REINFORCING WITH  $\sqrt{DT}$ ,  $\sqrt{dt}$ ,  
 AND  $2.5T$

$\frac{D}{T}$	$\frac{L_c}{\sqrt{DT}}$	$\frac{L_c - .5T}{2.5T}$	$(L_c - T/2)/\sqrt{dt}$ for d/D of:					
			.01	.025	.05	.10	.25	.35
10	.51	.45	--	--	7.04	3.52	1.41	1.01
25	.44	.67	--	--	6.75	3.37	1.35	--
50	.39	.81	--	12.7	6.38	3.19	--	--
100	.35	1.19	--	11.9	5.97	2.98	--	--
250	.30	1.69	19.7	7.85	3.93	1.97	--	--

$$L_c = 0.75 (T/D)^{2/3} D$$

TABLE 3. VALUES OF  $g_a$  AND  $h_a$  OBTAINED FROM THE RULES OF FIGURE 2f FOR DESIGNS OF FIGURES 2a AND 2b

$\frac{D}{T}$	$g_a$ for $d/D$ of:					
	.01	.025	.05	.10	.25	.35
10	1.00	1.00	1.19	3.08	4.38	4.38
25	1.00	1.00	3.17	6.66	6.66	--
50	1.00	2.05	7.22	9.30	--	--
100	1.00	5.90	13.7	13.7	--	--
250	2.30	20.9	23.1	23.1	--	--

$\frac{D}{T}$	$h_a$ for $d/D$ of:					
	.01	.025	.05	.10	.25	.35
10	1.00	1.00	1.02	1.21	1.84	2.18
25	1.00	1.00	1.11	1.57	2.42	--
50	1.00	1.05	1.31	1.83	--	--
100	1.00	1.22	1.63	2.27	--	--
250	1.13	1.50	2.11	3.21	--	--

$g_a$  obtained by:

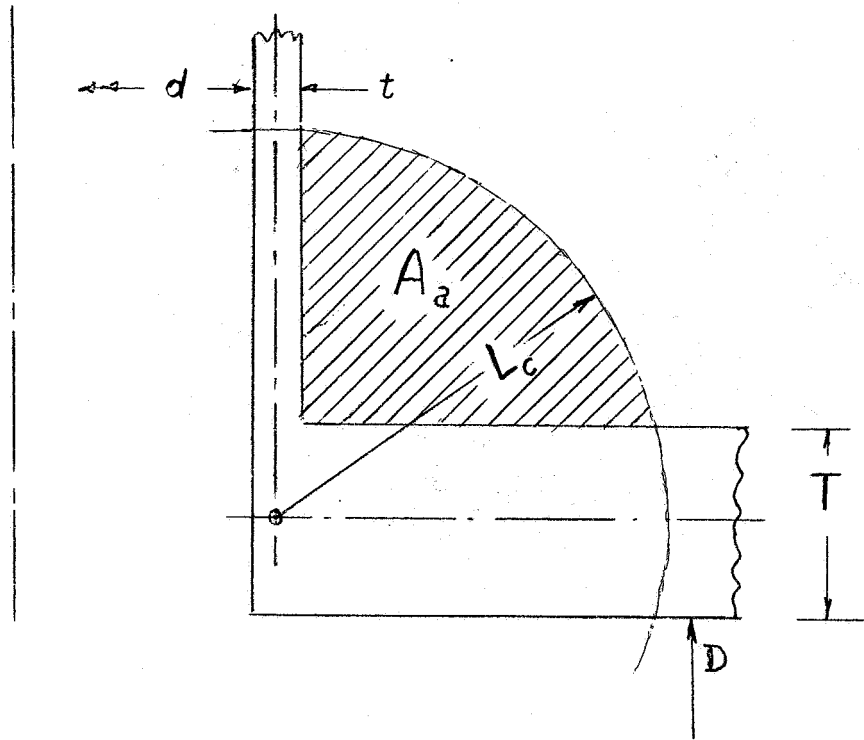
$$2t(g_a - 1)[.75 (T/D)^{2/3} D - .5T] = (A/dT) dT$$

$h_a$  obtained by:

$$2T(h_a - 1)[.75 (T/D)^{2/3} D - .5T] = (A/dT) dT$$

$A/dT$  from Equation (3).





$$L_c = .75 (T/D)^{2/3} D$$

$$A_a = .785L_c^2 - \frac{1}{2} (t + T)L_c + tT/4$$

$$\frac{2A_a}{dT} = \frac{.88}{Y} \left(\frac{D}{T}\right)^{1/6} - \frac{.75}{(D/T)^{2/3}} \left(\frac{\sqrt{D/T}}{Y} + 1\right) + \frac{T}{2D}$$

where:  $Y = (d/D)\sqrt{D/T}$

For  $Y < 1.1$  and  $D/T \geq 10$

$\frac{2A_a}{dT}$  is greater than 0.75,

except for  $D/T$  less than 15, for which  $d/D$  is limited to about 0.28.

FIGURE 11. SPACE AVAILABLE FOR COMPACT REINFORCING

### Distribution of Reinforcing

Within the scope of the analysis used as a basis herein, reinforcing, if any is required, must be placed in all planes containing the axis of the nozzle. In some current design codes\*, the reinforcing in the  $\varphi = 0$  plane (see Figure 1) must have an area of  $dT$ ; the area is permitted to diminish to 0.5  $dT$  in the  $\varphi = 90$ -degree plane. While maximum stresses usually occur in the  $\varphi = 0$  plane, it is not apparent whether reduction in reinforcing as  $\varphi$  goes from 0 to 90 degrees can be justified.

### Fillet Radii

As mentioned on page 10, the design procedure given herein is based on the maximum calculated elastic stress intensity in the shell; the usually higher calculated elastic stress intensity in the nozzle is ignored. The investigation of this aspect given in Phase Report No. 5 leads to the conclusion that the calculated stresses in the nozzle may be disregarded for configurations as shown in Figures 2a, 2b, and 2c herein, provided that the fillet radius is not less than  $\sqrt{dt}$ . A further limitation, in order to insure a reasonable fillet radius even for small, thin-wall nozzles, is that the fillet radius must not be less than  $T'/2$ .

### Transition Sections

Transitions between different wall thicknesses in a shell, such as at the outer edges of the reinforcements prescribed herein, can give high local

---

\*For example, ASME Nuclear Pressure Vessels, Figure N-452; ASME Power Boilers, Figure PG-33. ASME Unfired Pressure Vessels does not contain any provision for varying reinforcing around the opening.

stresses unless a suitable transition is used. Based on current code practice, and studies of tapered-wall transition joints in cylindrical shells, a transition slope of 1:3 is specified.

COMPARISON WITH OTHER DESIGN PROCEDURES

Current American Practice

Reinforcement of openings is specified in several American design codes (1,6,7,8,9). These codes all require that the material cut out by the opening,  $dT$ , be replaced around the opening within a specified zone. For all except the ASME Nuclear Vessel Code, the zone of reinforcement is defined as shown in Figure 12. The Nuclear Vessel Code specifies a reinforcing zone in terms of the foundation modulus of the nozzle or shell, as shown in Figure 13. In this respect, the Nuclear Vessel Code is similar to the proposed design procedure.

In the following, comparisons between the proposed procedure and current American practice are made in two ways:

- (1) On the basis of required thickness of the shell or nozzle
- (2) On the basis of required reinforcing area.

Required Thicknesses

Required thickness comparisons are made on the assumption that (a) reinforcing consists of the uniform-wall increase of the shell thickness, or (b) reinforcing consists of a uniform-wall increase of the nozzle thickness. For reinforcing on the shell, the requirement for  $T'$  where the reinforcing zone is prescribed as  $L = d$  is that  $T'/T = 2.0$ . As can be noted in Figure 3b,  $T'/T = 2.0$  is conservative for all combinations of  $D/T$  and  $d/D$  covered by the proposed rules.

For reinforcing on the nozzle, the requirement of  $t'$  (where, in Figures 13 and 13d,  $l = 0.5 \sqrt{r_m t'} + 0.5 r_2$  and  $r_2 = \text{larger of } T/2 \text{ or } t'/2$ ) is

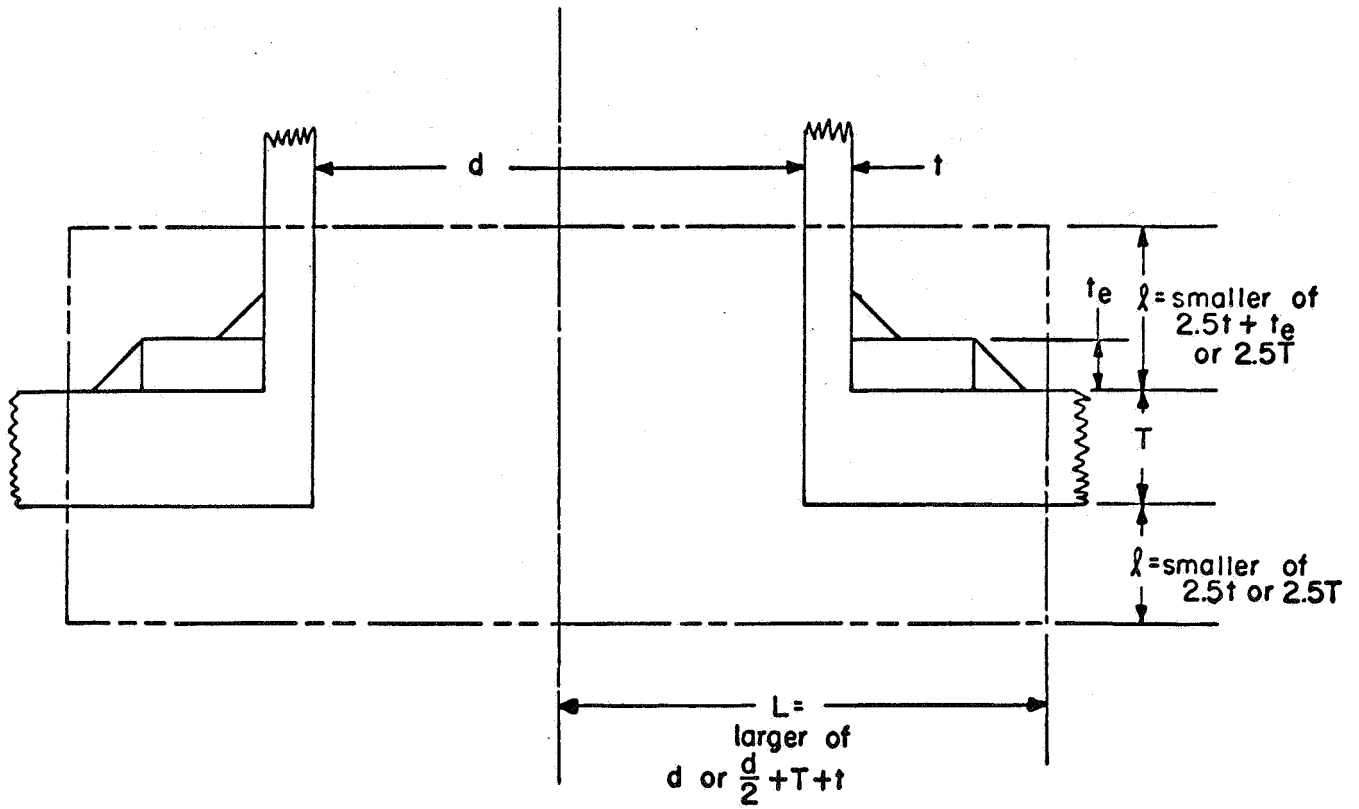
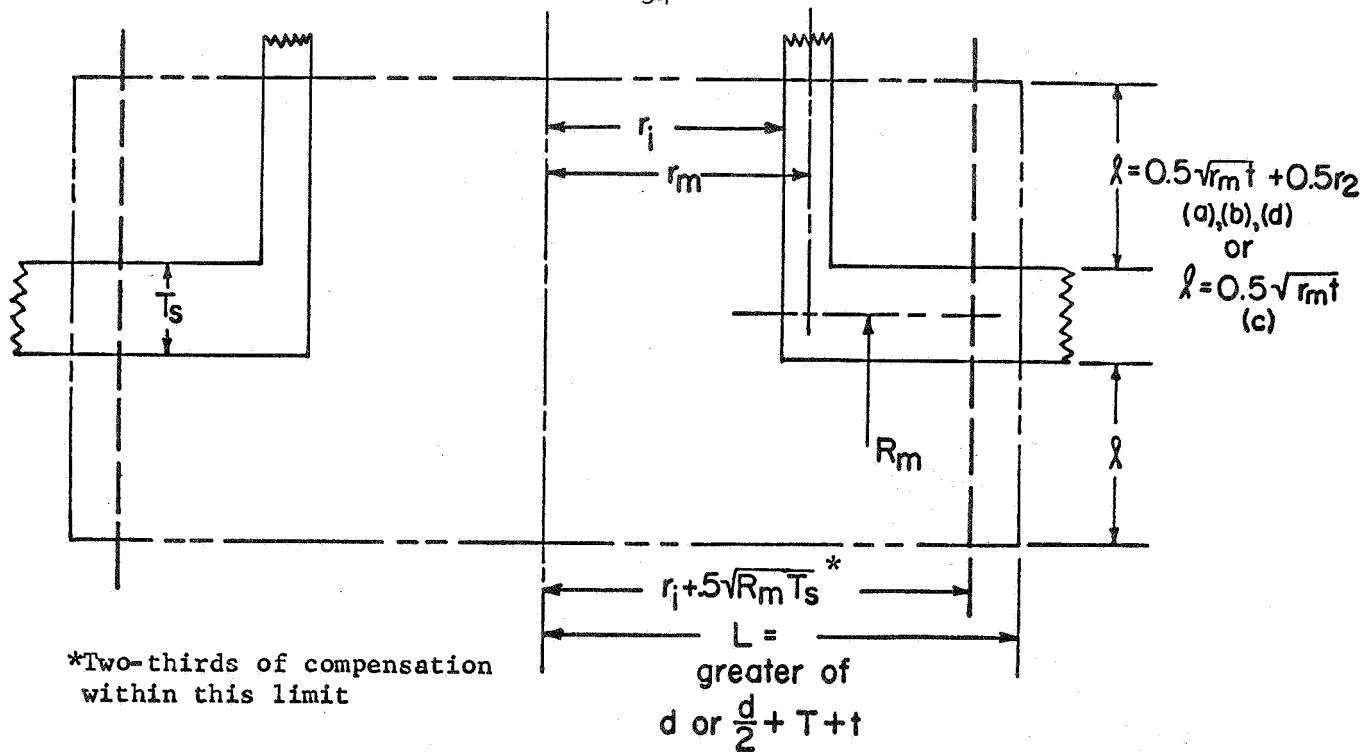
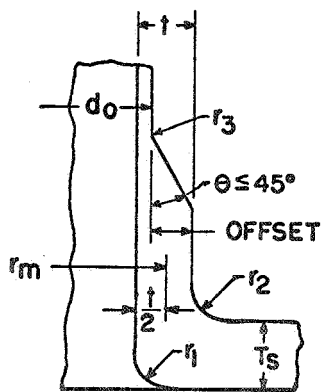


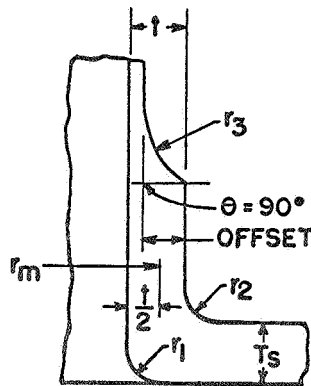
FIGURE 12. REINFORCEMENT ZONE, CURRENT AMERICAN PRACTICE EXCEPT THE ASME NUCLEAR VESSEL CODE



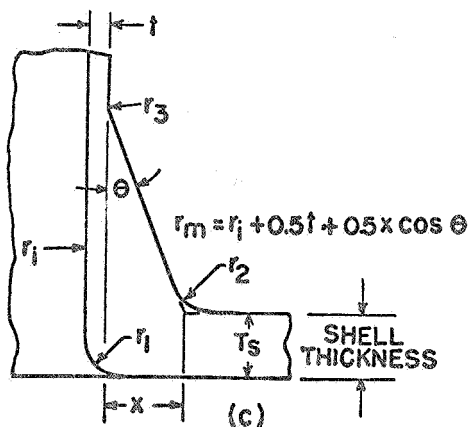
\*Two-thirds of compensation within this limit



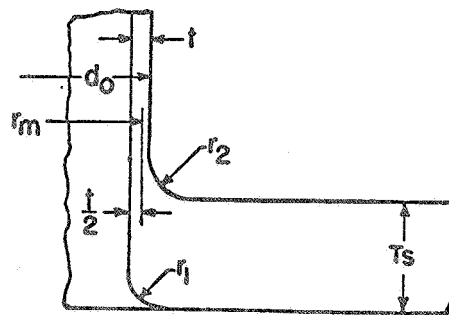
(a)



(b)



(c)



(d)

FIGURE 13. REINFORCEMENT ZONE, ASME NUCLEAR VESSEL CODE

shown in Figure 14, superimposed on the proposed rules for values of  $g = t'/t$ . This comparison represents the ASME Nuclear Vessel Code rules, Figure 13d herein. It is apparent that the Code rules are conservative with respect to the proposed rules. Another comparison of reinforcing requirements on the nozzle can be made by using  $l = 2.5 T$ , Figure 15 herein. The resulting values of  $t'/t$  are shown in Figure 15, superimposed on the proposed rules. For large values of  $D/T$ , this Code rule is also conservative with respect to the proposed rules.

#### Required Areas\*

Required area comparisons for reinforcing consisting of a uniform-wall increase of the shell thickness are shown in Figure 8. For shell reinforcing, even though the reinforcing thickness requirement is less than  $h = T'/T = 2.0$ , the area required is generally equal to  $dT$ , as in present codes, except close to those combinations of  $d/D$  and  $D/T$  for which no reinforcing is required. This is because the proposed rules herein require a reinforcing length of  $\sqrt{DT'}$  compared to most present rules length of  $d/2$  or less. In the range covered by the proposed rules,  $\sqrt{DT'}$  is always greater than  $d/2$ .

Required area comparison for reinforcing consisting of a uniform increase in the nozzle thickness are shown in Figure 9. The area required by the proposed rules is less than about  $0.5dT$ ,  $dT$  being the area required by present rules.

It should again be emphasized that the proposed rules are for internal pressure loading only, whereas current rules presumably contain some margin for loads other than internal pressure.

---

\*In these comparisons, the area provided by transitions and fillet radii of the proposed rules are not included.

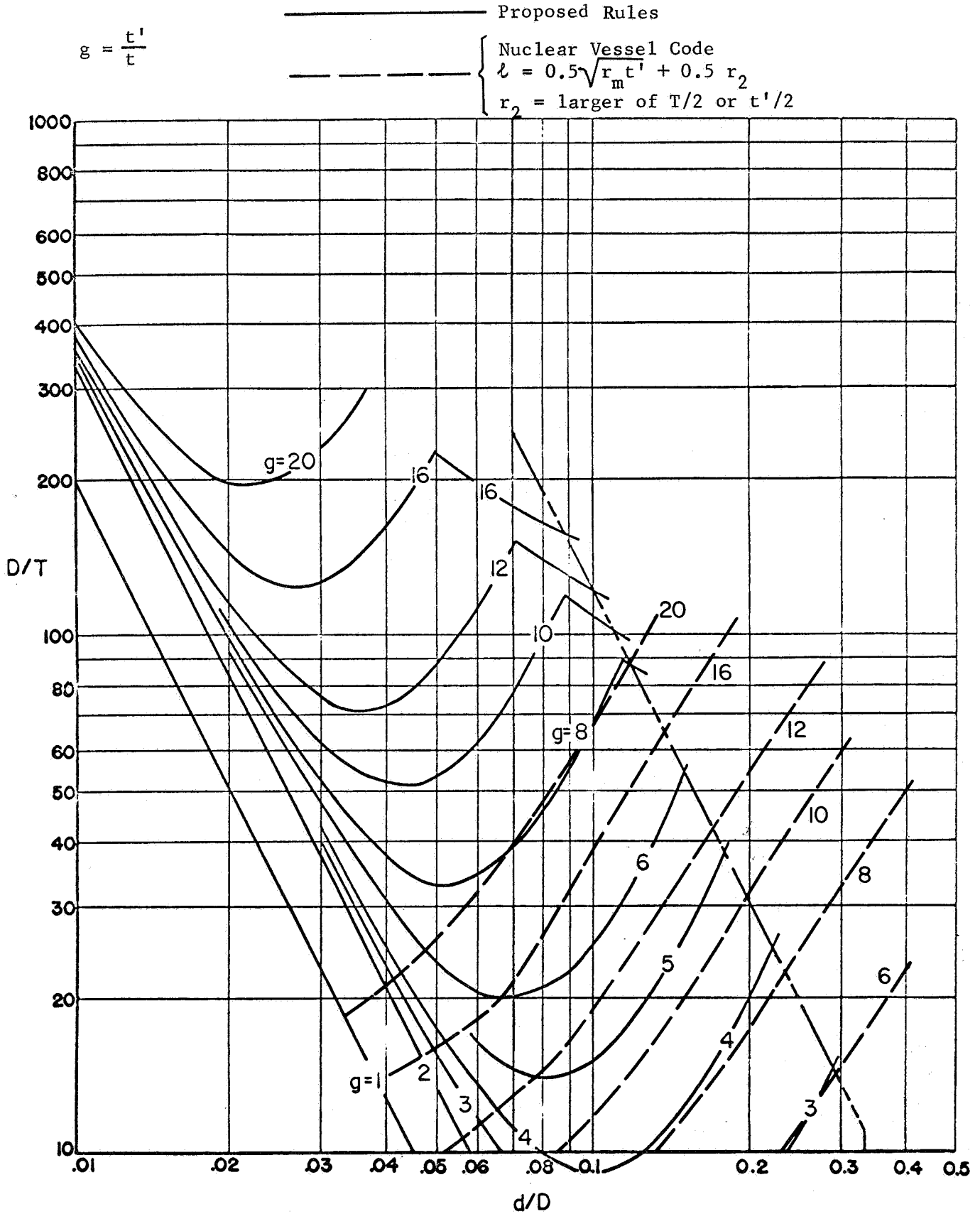


FIGURE 14. COMPARISON OF NOZZLE THICKNESS REQUIREMENTS, PROPOSED RULES WITH ASME NUCLEAR VESSEL CODE,  $l = 0.5\sqrt{r_m t'} + 0.5 r_2$



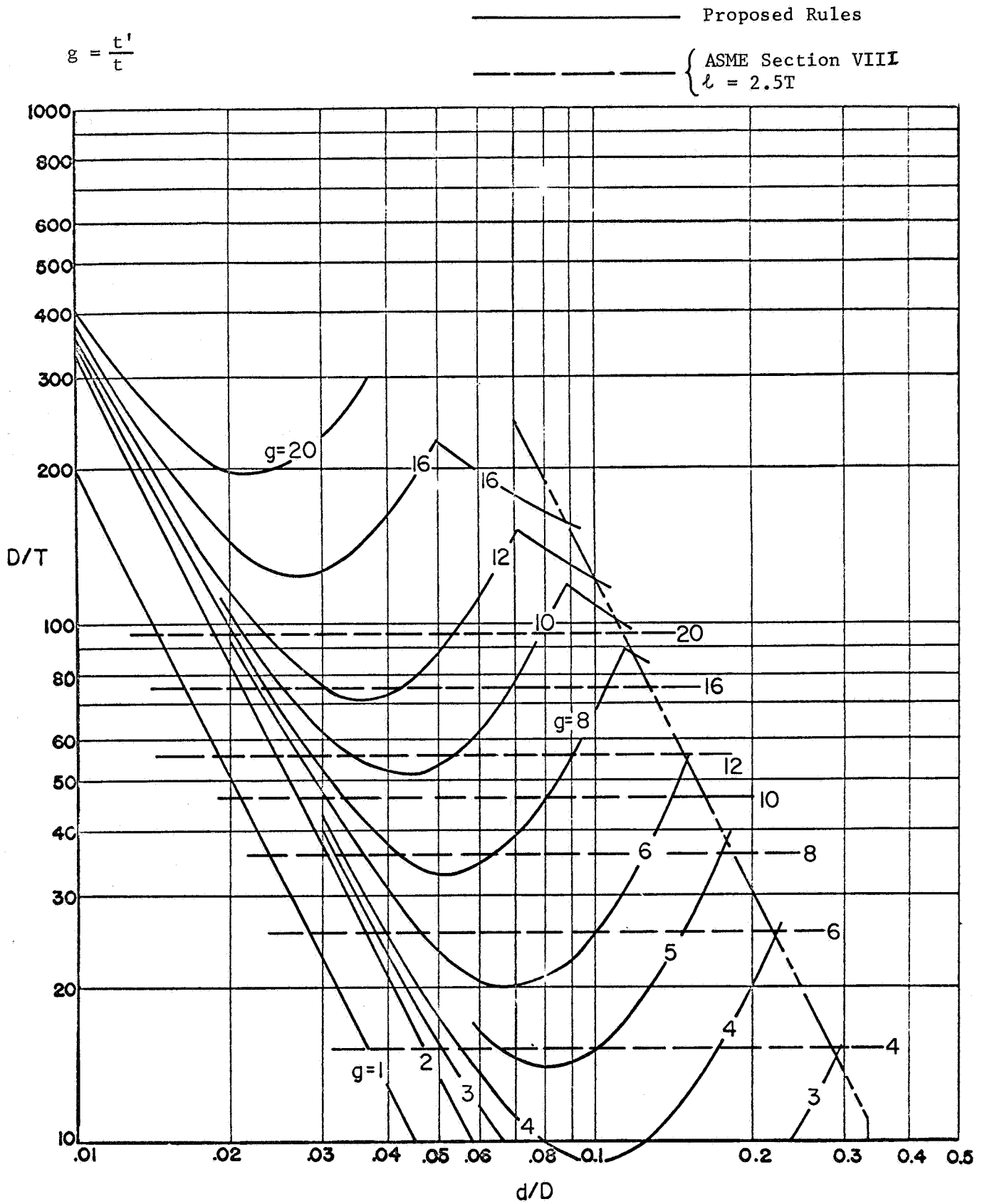


FIGURE 15. COMPARISON OF NOZZLE THICKNESS REQUIREMENTS, PROPOSED RULES WITH ASME SECTION VIII,  $l = 2.5T$

United Kingdom to ISO Proposal

The proposal by the United Kingdom to the International Organization for Standards (ISO) for the "Design of Openings and Branch Connections for inclusion in the ISO Boiler and Pressure Vessel Codes" is extracted\* from British Standard 3915. The design rules contained therein are based on the analysis of a radial nozzle in a spherical shell; specifically that developed by Leckie and Penny<sup>(10)</sup>. The design rules are based on the criteria that the calculated maximum stress in the spherical shell is limited to  $2.25 S_1$ , where  $S_1$  = nominal stress in the unperforated sphere. The reinforcement requirement curves, derived from the nozzle-in-sphere theory, are assumed to be applicable to nozzles in cylindrical shells. Table 4 gives a summary comparison of the basis of the UK-ISO proposal with both Phase Report No. 1 and the present Phase Report No. 4. The UK-ISO proposal is limited to  $d/D = 0.5$  for nozzles in spherical shells;  $d/D = 0.333$  for nozzles in cylindrical shells. The UK-ISO proposal is for internal pressure loading only and states that "the effect of any other loads shall be taken into account".

The design curve from the UK-ISO proposal for flush nozzles is shown herein as Figure 16. This set of curves is predicated upon the approximation that the calculated stresses for a nozzle in a sphere (Leckie-Penny analysis) can be expressed as functions of two-dimensional parameters:  $(d/D)\sqrt{D/T}$  and  $t'/T$ . As discussed in Phase Report No. 2, this approximation is reasonably accurate for the calculated stresses in the sphere but not for the stresses in the nozzle. As discussed in Phase Report No. 5, the approximation is not good for either stresses in the shell or nozzles for nozzles in cylinders\*\*. However,

\* With editorial amendments and a few minor changes.

\*\* Except where the thickness of the nozzle is negligible, in which case the theory reduces to a function of  $(d/D)\sqrt{D/T}$  alone.

TABLE 4. SUMMARY COMPARISON OF THE BASIS OF PHASE REPORT 1  
AND PHASE REPORT 4 WITH UK-ISO PROPOSAL

<u>Nozzles in Spheres</u>		
	<u>Phase Report No. 1</u>	<u>UK-ISO</u>
Elastic Stress Limit	Maximum stress intensity  = $3S_1$  (where $S_1$ = nominal stress in unperforated sphere)	Maximum stress in spherical shell  = $2.25S_1$
Elastic Theory	Waters	Leckie-Penny
Limit Pressure	Cloud, nozzles in spherical shells	None
<u>Nozzles in Cylinders</u>		
	<u>Phase Report No. 4</u>	<u>UK-ISO</u>
Elastic Stress Limit	Maximum stress intensity  = $3S$	Unknown
Elastic Theory	Eringen	Uses theory for nozzles in spherical shells
Limit Pressure	Cloud and Rodabaugh nozzles in cylindrical shells	None

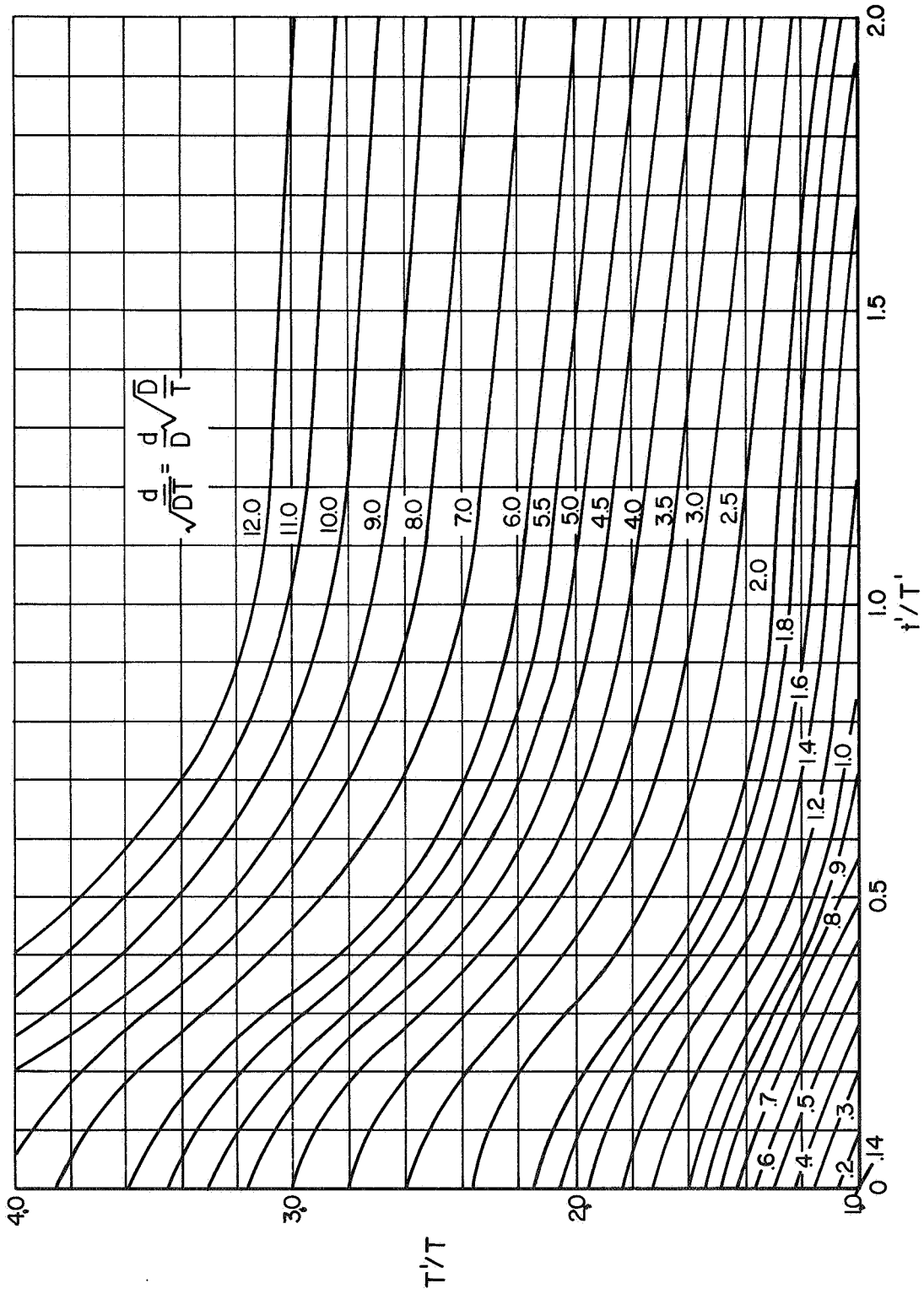


FIGURE 16. UNITED KINGDOM TO ISO PROPOSAL GRAPH FOR REINFORCING OF FLUSH NOZZLES IN SPHERES OR CYLINDERS

the use of  $(d/D) \sqrt{D/T'}$  and  $t'/T'$  is a good approximation for the limit pressure analysis for both nozzles in spheres and nozzles in cylinders. Since the rules of both Phase Report Nos. 1 and 4 are essentially based on limit analysis, a presentation like that of Figure 14 could be used, if deemed easier to use than the rules as given.

The UK-ISO reinforcement requirements are compared with Phase Report No. 1 requirements for nozzles in spheres in Figures 17 and 18. Analogous comparisons for nozzles in (cylindrical) shells are shown in Figures 19 and 20. It will be noted that, while using the same graph from the UK-ISO proposal (i.e., Figure 16 herein), the resulting reinforcement curves are not the same for nozzles in spheres as for nozzles in cylinders. The reason for this, as shown in Table 5, is that:

For nozzles in spheres	$t/T = 2 d/D$
For nozzles in cylinders	$t/T = d/D$

Figure 19, for reinforcing on the cylinder for nozzles in cylinders, indicates that the UK-ISO proposal and the rules proposed herein are quite close to each other. Figures 17, 18\*, and 20 indicate that the UK-ISO proposal rules are unconservative, with respect to Phase Report No. 1 and Phase Report No. 4 proposed rules, except near  $h = g = 1$ . It is pertinent to note that the UK-ISO proposal incorporates the same limit for "openings not requiring reinforcing" as is given in the ASME Nuclear Vessel Code, Para. N-452(a)(1); i.e.,  $d \leq 0.14 \sqrt{DT}$ . This limit is also used in Phase Report No. 1 and in the present report, with the slightly different interpretation that the basic configuration of Figure 1 need not be reinforced.

---

\*The somewhat irregular curves of Figure 18 are similar to the elastic criteria curves shown in Figure 5 of Phase Report No. 1.

$$h = \frac{T'}{T}$$

————— Phase Report No. 1  
 - - - - - United Kingdom to ISO Proposal

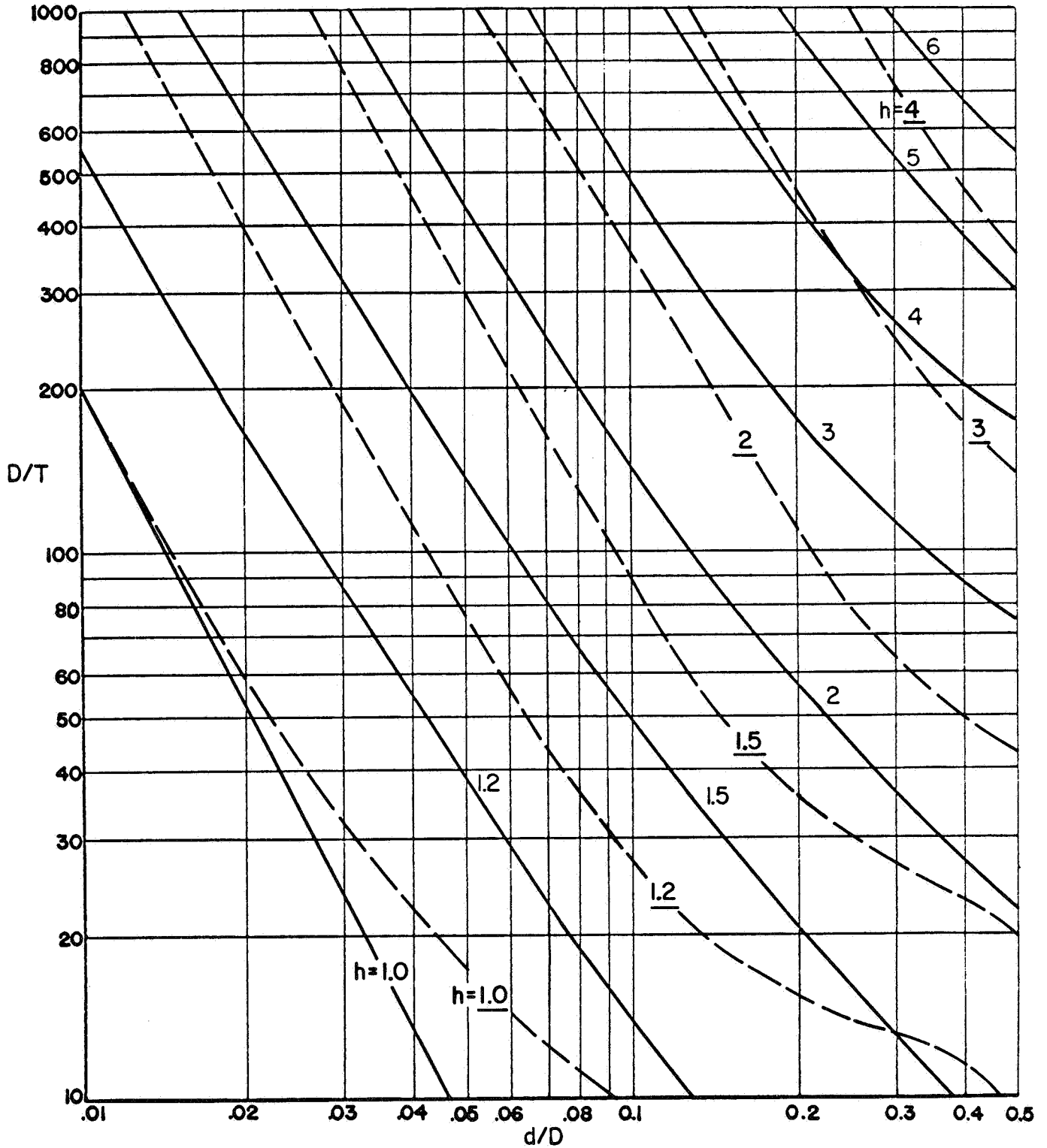


FIGURE 17. COMPARISON OF SHELL THICKNESS REQUIREMENTS, NOZZLES IN SPHERES, UNITED KINGDOM TO ISO PROPOSAL WITH PHASE REPORT NO. 1

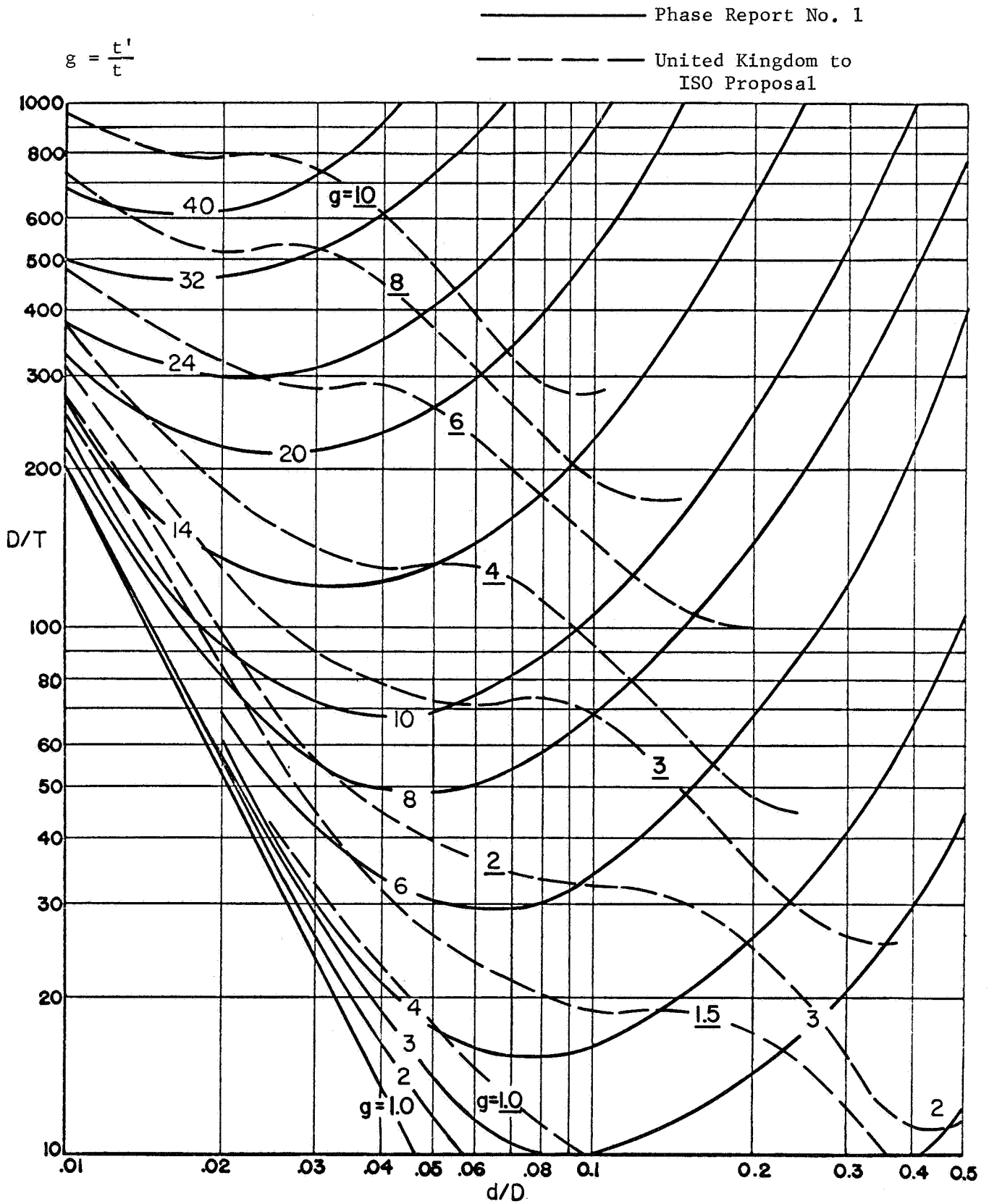


FIGURE 18. COMPARISON OF NOZZLE THICKNESS REQUIREMENTS, NOZZLES IN SPHERES, UNITED KINGDOM TO ISO PROPOSAL WITH PHASE REPORT NO. 1

$$h = \frac{T'}{T}$$

———— Phase Report No. 4  
 - - - - - United Kingdom to ISO Proposal

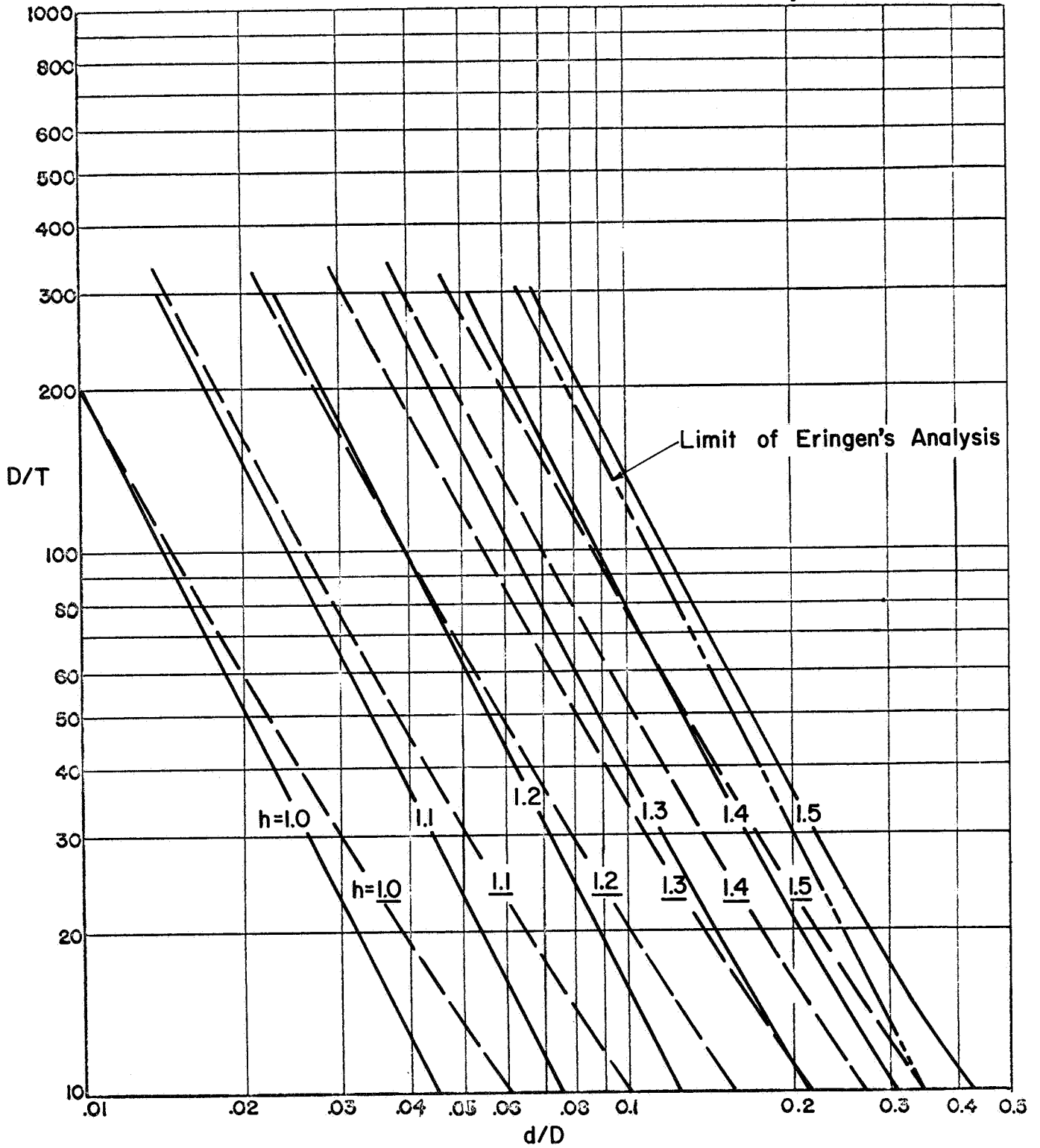


FIGURE 19. COMPARISON OF SHELL THICKNESS REQUIREMENTS, NOZZLES IN CYLINDERS, UNITED KINGDOM TO ISO PROPOSAL WITH PHASE REPORT NO. 4



$$g = \frac{t'}{t}$$

————— Phase Report No. 4  
 - - - - - United Kingdom to ISO Proposal

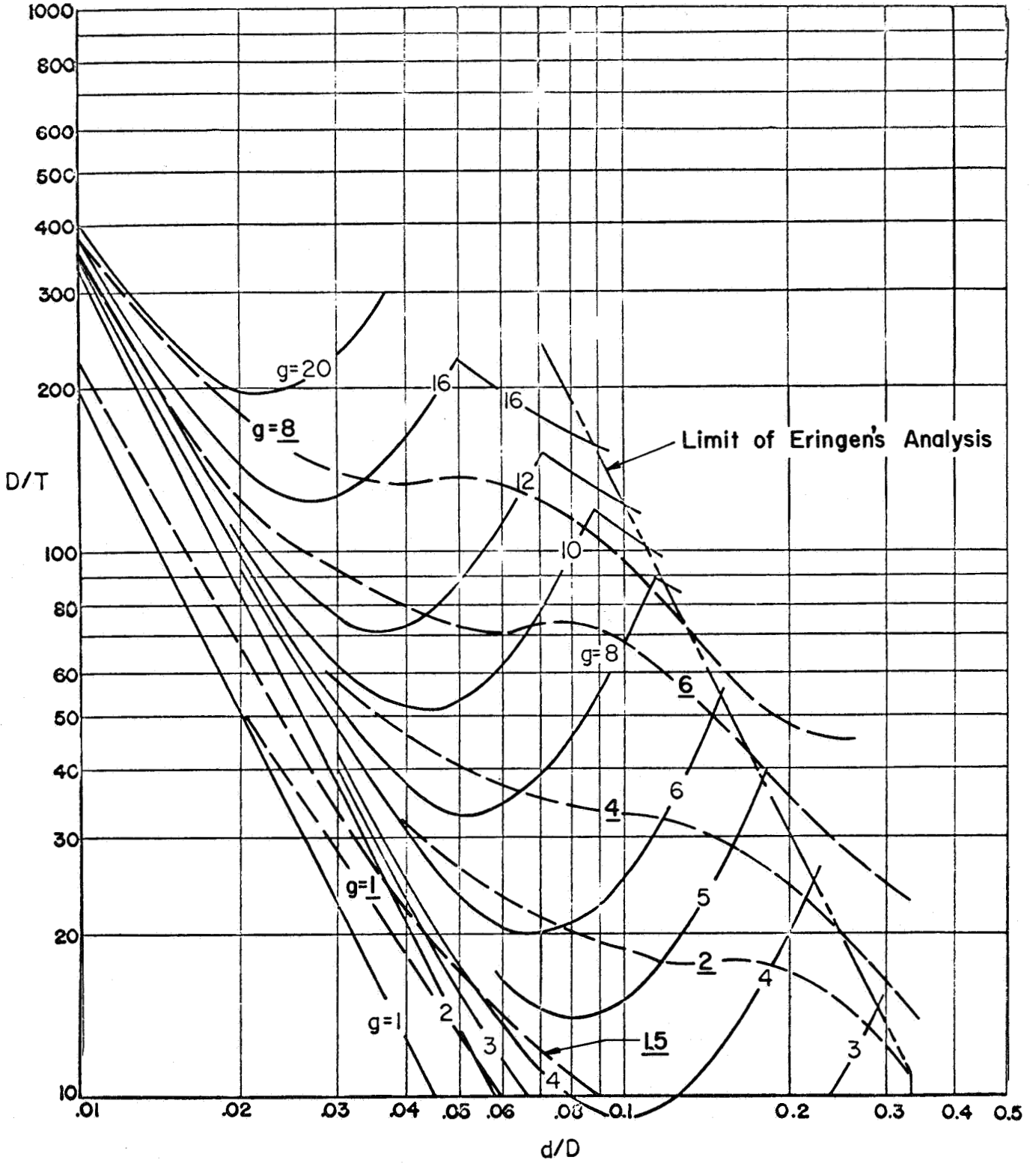


FIGURE 20. COMPARISON OF NOZZLE THICKNESS REQUIREMENTS, NOZZLES IN CYLINDERS, UNITED KINGDOM TO ISO PROPOSAL WITH PHASE REPORT NO. 4

TABLE 5. PROCEDURE USED FOR CONVERTING UK-ISO RULES TO  
FORM OF PHASE REPORT NO. 1 AND NO. 4 RULES

Flush Nozzles in Spheres, $t/T = 2d/D$	Flush Nozzles in Cylinders, $t/T = d/D$
(a) Shell reinforcement ( $t = t'$ )	Same procedure as for nozzles in spheres except
(1) Select values of $h = T'/T$ and $d/D$	
(2) Calculate corresponding value of $T'/T' = t/T'$ by:	
$\frac{t'}{T'} = \frac{2d/D}{h}$	$\frac{t'}{T'} = \frac{d/D}{h}$
(3) Enter Figure 16 with $h = T'/T$ and find corresponding value of $d/\sqrt{DT} \equiv \rho$	
(4) Calculate:	
$\frac{D}{T} = \left[ \frac{\rho}{d/D} \right]^2$ , for selected $h$ and $\frac{d}{D}$	
(b) Nozzle reinforcement ( $T = T'$ )	
(1) Select values of $g = t'/t$ and $d/D$	
(2) Calculate corresponding value of $t'/T'$ $= t'/T$ by:	
$\frac{t'}{T'} = g \times 2 \frac{d}{D}$	$\frac{t'}{T'} = g \times \frac{d}{D}$
(3) Enter Figure 16 with $T'/T = 1.0$ and $t'/T'$ from Step 2 and find correspond- ing value of $d/\sqrt{DT} \equiv \rho$	
(4) Calculate:	
$\frac{D}{T} = \left[ \frac{\rho}{d/D} \right]^2$ , for selected $g$ and $\frac{d}{D}$ .	

Another significant comparison is that of the required length of reinforcing. The reinforcing lengths compare as follows:

	<u>Phase Report No. 1</u> <u>Nozzles in Spheres</u>	<u>Phase Report No. 2</u> <u>Nozzles in Cylinders</u>	<u>UK-ISO</u> <u>Proposal</u>
On nozzle	$\sqrt{dt'}$	$\sqrt{dt'}$	$\sqrt{dt'}$
On shell	$0.7 \sqrt{DT'}$	$\sqrt{DT'}$	Smaller of $d/2$ or $\sqrt{DT'}$

The principal discrepancy in the above is the "d/2" length permitted for reinforcing on the shell by the UK-ISO proposal. For small values of d/D, this can lead to quite small areas of reinforcing. For example, in Figure 19 at D/T = 100, d/D = 0.04, both the UK-ISO proposal and the rules given herein require  $h = T'/T$  of 1.2. However, the area of reinforcing required by the rules given herein is essentially 100 percent of the cut out area  $dT$ , whereas the UK-ISO proposal, using the reinforcement length of  $d/2$ , requires an area of only 20 percent of  $dT$ . Available theory and test data indicate that  $\sqrt{DT}$  is a more realistic dimension for reinforcing length if uniform wall shell theory is used as the basis of design; as is the case with both the UK-ISO proposal and Phase Report Nos. 1 and 4.

#### German Rules, AD-Merkblatt B9

The design rules established in AD-Merkblatt<sup>(11)</sup> are based, in a general sense, upon a limit design concept. The rules are based on a fairly large number of tests in which strain gages were used to determine that pressure which produced a permanent strain of 0.2 percent. The AD-Merkblatt B9 graph is reproduced herein as Figure 21. The German rules, like the UK-ISO proposal, use the dimensional parameters  $(d/D)\sqrt{D/T'}$  and  $t'/T'$ .

$V_a$  = weakening factor =  $P_L/P_{yc}$

$P_L$  = pressure to produce 0.2% strain

$P_{yc}$  = yield pressure of unperforated sphere or cylinder

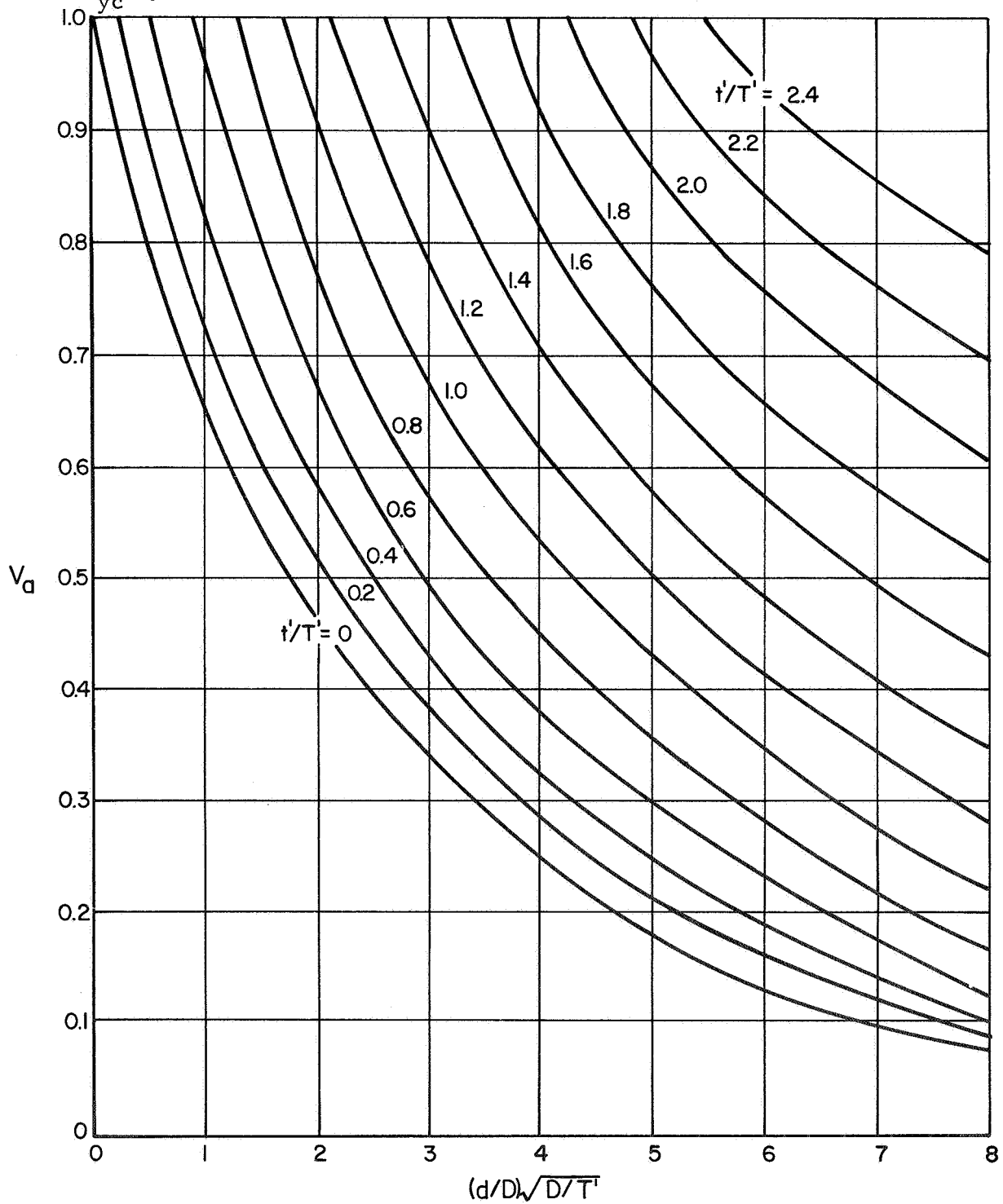


FIGURE 21. AD-MERKBLATT B9 GRAPH FOR REINFORCING OF FLUSH NOZZLES IN SPHERES OR CYLINDERS

Comparisons of the German rules with those given herein are shown in Figures 22 and 23 for reinforcing on the shell and nozzle, respectively. It should be noted that the graph representing the German rules (Figure 21 herein) is difficult to read accurately for the range of variables covered herein. It was assumed that the line for  $t'/T' = 0$  intersects the coordinates  $V_a = 0$ ,  $(d/D)\sqrt{D/T'} = 0$ . With this assumption, there is no line obtainable from Figure 21 which corresponds to the  $h = g = 1$  lines. However, as shown by Figure 22, the German rules and those given herein are quite close to each other for  $h = 1.1$  to  $1.5$ . This is also the case when comparing the German rules with the UK-ISO proposal.

Similar comparisons were made between the German rules and the rules given in Phase Report No. 1 for nozzles in spherical shells; these are contained in Figures 25 and 26 of Phase Report No. 1. It may be noted that, for the German rules as for the UK-ISO proposal rules, the reinforcement requirements (in terms of  $T'/T$  or  $t'/t$ ) are different for nozzles in spheres than for nozzles in cylinders.

The length of reinforcing required by the German rules is the same as that in the proposed rules; i.e.,  $\sqrt{dt'}$  on the nozzle;  $\sqrt{DT'}$  on the shell. Both the German rules and the UK-ISO proposal rules permit the use of welded-on pads for reinforcing on the shell, whereas the proposed rules do not include this kind of reinforcement.

The proposed design procedure is essentially based on a limit pressure analysis. The generally good agreement between these rules and the German rules, which are based on a limiting plastic strain from test data, makes these comparisons highly significant because it further confirms the validity of the limit pressure analysis.

$$h = \frac{T'}{T}$$

————— Proposed Rules  
 - - - - - German Rules,  
 AD-Merkblatt B9

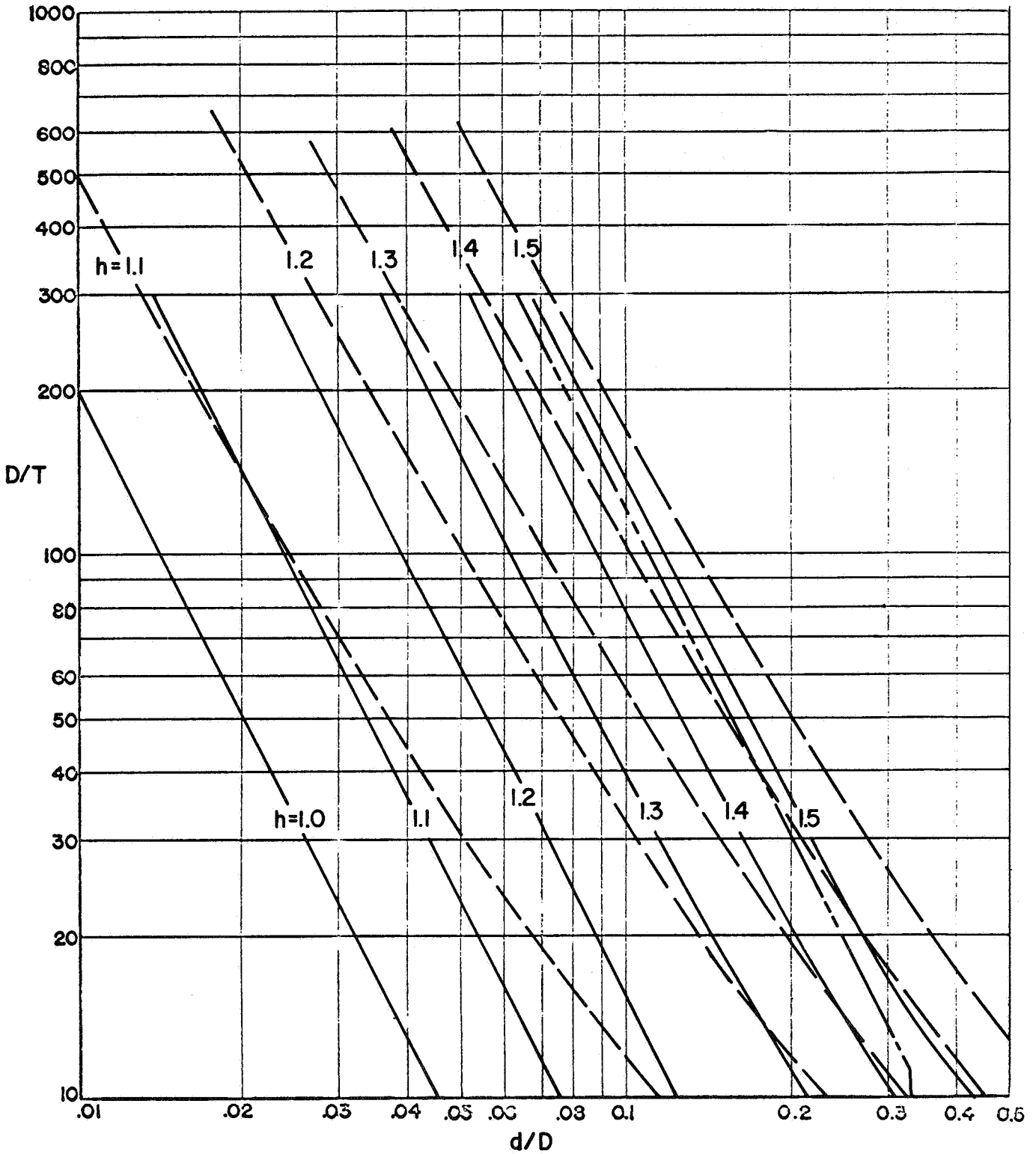


FIGURE 22. COMPARISON OF SHELL THICKNESS REQUIREMENTS, PROPOSED RULES WITH GERMAN RULES, AD-MERKBLATT B9

$$g = \frac{t'}{t}$$

————— Proposed Rules  
 - - - - - German Rules, AD-Merkblatt B9

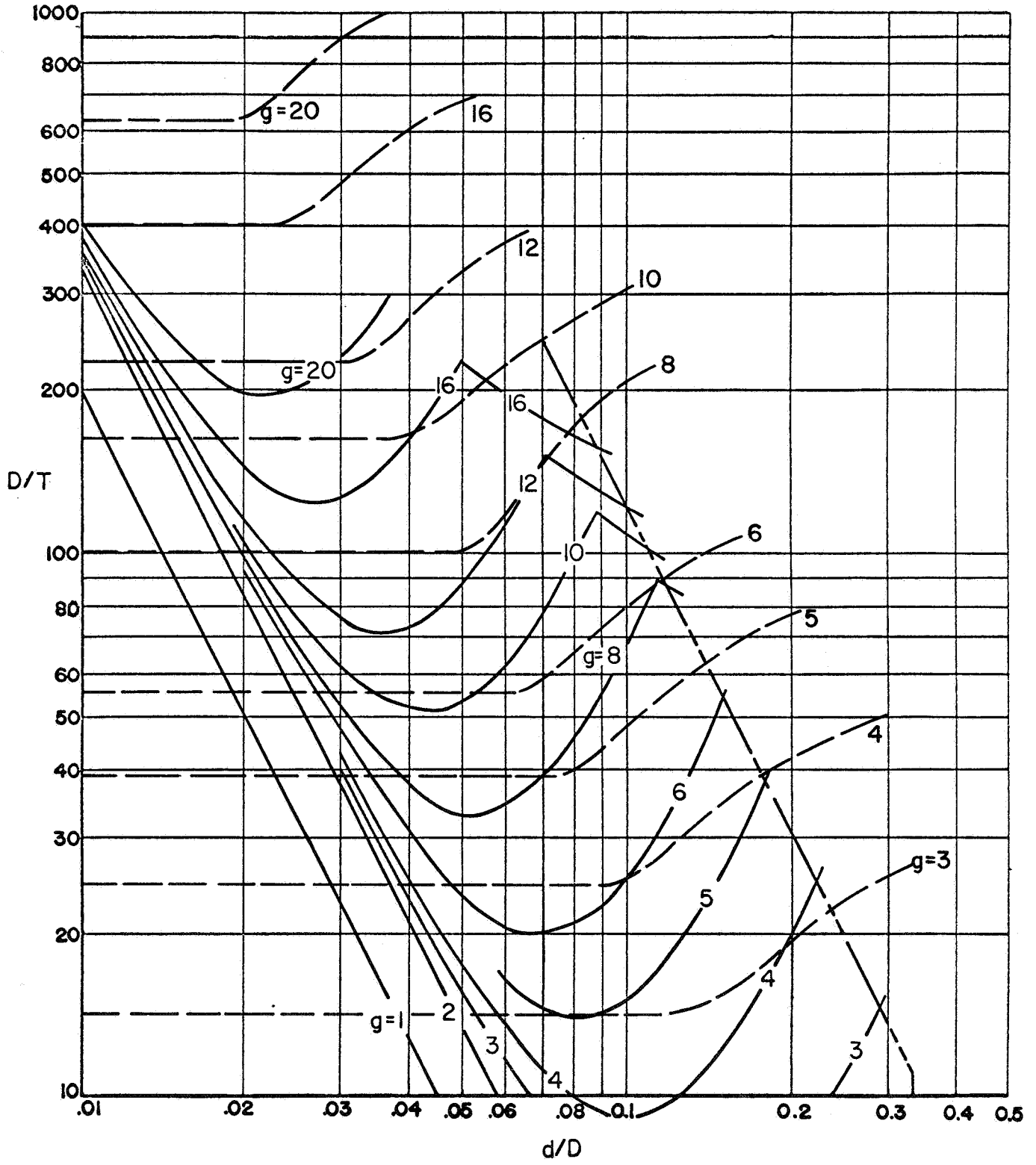


FIGURE 23. COMPARISON OF NOZZLE THICKNESS REQUIREMENTS, PROPOSED RULES WITH GERMAN RULES, AD-MERKBLATT B9

Nozzles in Spheres vs Nozzles in Cylinders

Phase Report No. 1 (Figure 2 therein) gives graphs for h- and g-factors for nozzles in spheres. These are shown as dashed lines on Figures 24 (reinforcing on shell) and Figure 25 (reinforcing on nozzle).

In both Phase Report Nos. 1 and 4, the line for  $h = g = 1$  has been adjusted downward from the limit pressure analysis so that it is given by the equation:  $d = 0.1414 \sqrt{DT}$ . Accordingly these lines on Figures 24 and 25 coincide with each other. For values of h or g greater than unity, the curves for nozzles in spheres are quite similar, both qualitatively and quantitatively, to the corresponding curves for nozzles in cylinders. In view of this fairly close agreement, it may be desirable to use a single set of curves applicable to both nozzles in cylinders and nozzles in spheres.



$$h = \frac{T'}{T}$$

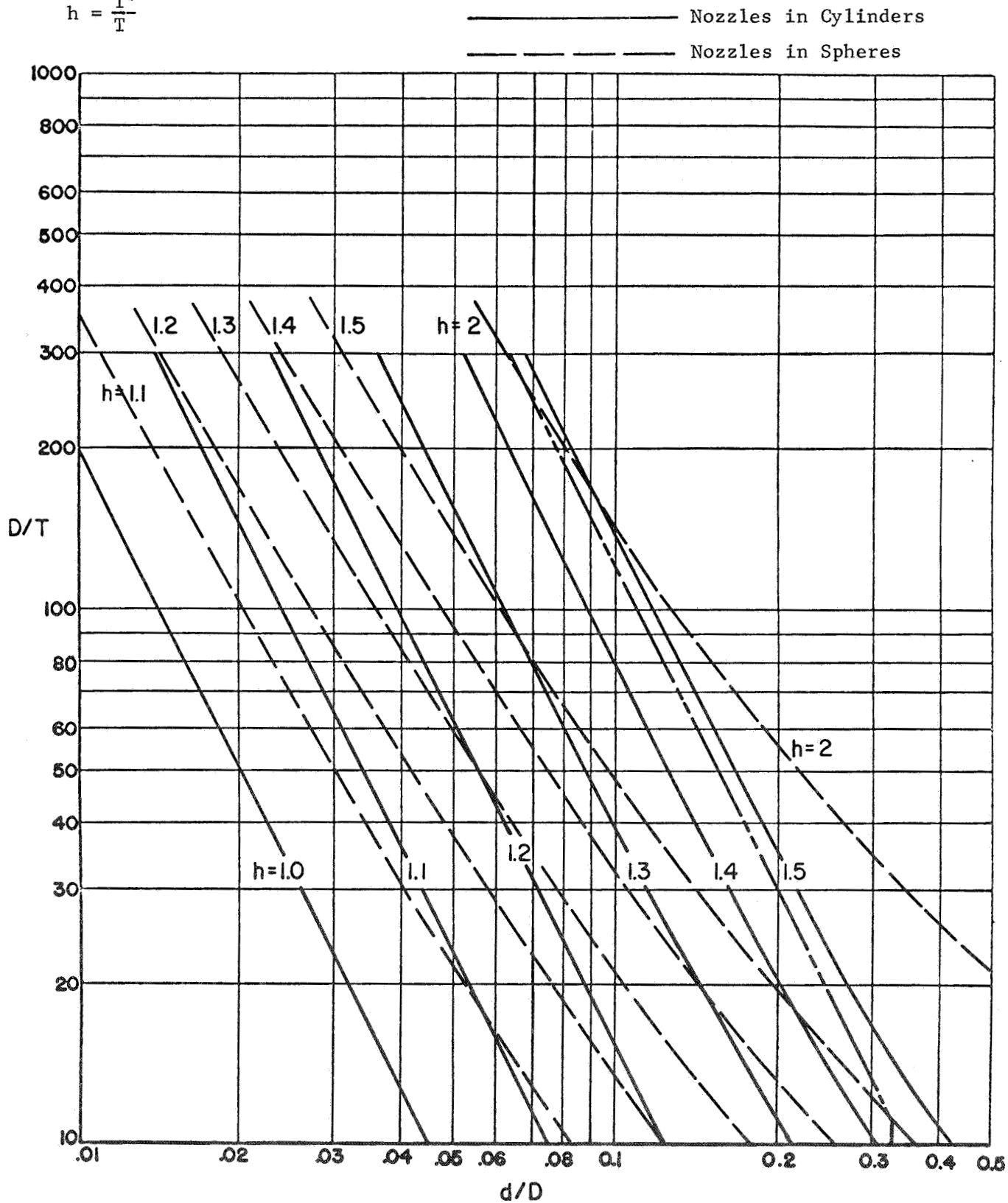


FIGURE 24. COMPARISON OF SHELL THICKNESS REQUIREMENTS, NOZZLES IN CYLINDERS (PHASE REPORT NO. 4) WITH NOZZLES-IN-SPHERES (PHASE REPORT NO. 1)

$$g = \frac{t'}{t}$$

————— Nozzles in Cylinders  
 - - - - - Nozzles in Spheres

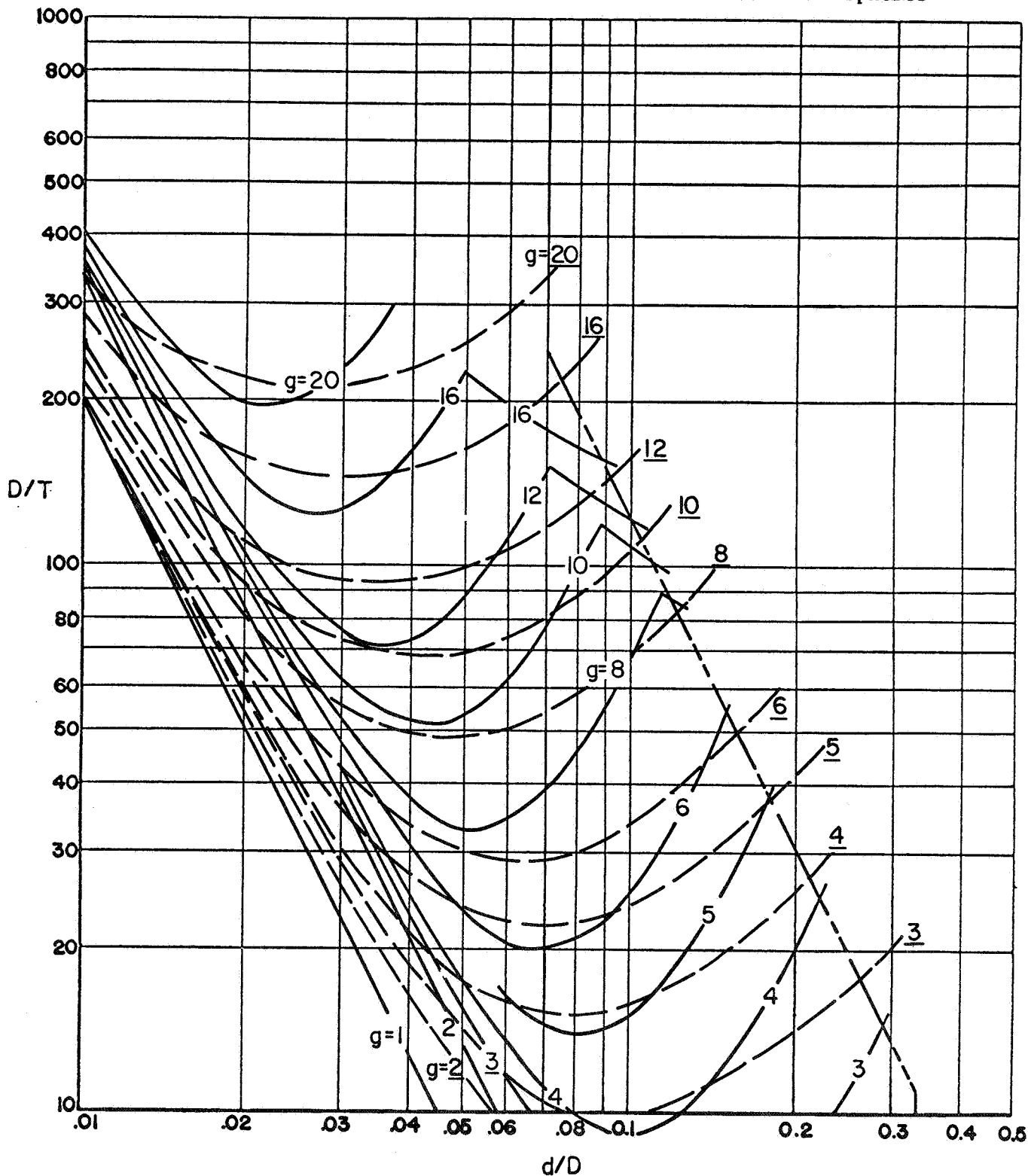


FIGURE 25. COMPARISON OF NOZZLE THICKNESS REQUIREMENTS, NOZZLES-IN-CYLINDERS (PHASE REPORT NO. 4) WITH NOZZLES-IN-SPHERES (PHASE REPORT NO. 1)

REFERENCES

- (1) ASME Boiler and Pressure Vessel Code, Section III, Rules for Construction of Nuclear Vessels, published by the American Society of Mechanical Engineers, 345 East 47th Street, New York, N. Y.
- (2) Criteria of Section III of the ASME Boiler and Pressure Vessel Code for Nuclear Vessels, published by the American Society of Mechanical Engineers, 345 East 47th Street, New York, N. Y.
- (3) Cloud, R. L. and Rodabaugh, E. C., "Approximate Analysis of the Plastic Limit Pressures of Nozzles in Cylindrical Shells", ASME Paper No. 67-WA/PVP-4.
- (4) Eringen, A. C., et. al., "Analysis of Stress and Deformation in Two Normally Intersecting Cylindrical Shells Subject to Internal Pressure", General Technology Corporation, Technical Report No. 3-8.
- (5) Rodabaugh, E. C. and Cloud, R. L., "Comparison of Experimental and Analytical Limit Pressures of Nozzles in Cylindrical Shells", Bettis Atomic Power Laboratory Report WAPD-T-2050.
- (6) ASME Boiler and Pressure Vessel Code, Section I, Power Boilers, published by the American Society of Mechanical Engineers, 345 E. 47th Street, New York, N. Y.
- (7) ASME Boiler and Pressure Vessel Code, Section VIII, Unfired Pressure Vessels, published by the American Society of Mechanical Engineers, 345 East 47th Street, New York, N. Y.
- (8) Code for Pressure Piping, ASA B31.1, American Standards Association, 10 East 40th Street, New York, N. Y.
- (9) API Recommended Rules for Design and Construction of Large, Welded, Low Pressure Storage Tanks, API Standard 620, American Petroleum Institute, 111 West 50th Street, New York, N. Y.
- (10) Leckie, F. A. and Penny, R. K., "Stress Concentration Factors for the Stresses at Nozzle Intersections in Pressure Vessels", Welding Research Council Bulletin No. 90 (September, 1963).
- (11) AD-Merkblatt, B9, Openings in Cylinders, Cones, and Spheres Under Internal Pressure, DK621.642.02.001.24, Design of Pressure Vessels (January, 1960).

PHASE REPORT NO. 5

on

STRESSES AT NOZZLES IN CYLINDRICAL SHELLS  
LOADED WITH PRESSURE, MOMENT OR THRUST

December 22, 1967

to

UNITED STATES ATOMIC ENERGY COMMISSION

by

E. C. Rodabaugh AND T. J. Atterbury

Contract No. W-7045-eng-92

Task 16

BATTELLE MEMORIAL INSTITUTE  
Columbus Laboratories  
505 King Avenue  
Columbus, Ohio 43212

**Section 5**

TABLE OF CONTENTS

	<u>Page</u>
INTRODUCTION . . . . .	1
SUMMARY. . . . .	2
Comparison of Theories for Internal Pressure Loading. . . . .	2
Comparison of Eringen's Theory with Test Data . . . . .	2
Test Models with Local Reinforcing. . . . .	3
Inside Corner Radii . . . . .	4
Outside Fillet Radius . . . . .	5
Stresses at Reinforcing Edges . . . . .	5
Comparison of Lind's Analysis with Test Data. . . . .	5
Stresses Due to External Loads Applied to Nozzles . . . . .	6
Stresses Due to External Loads on Nozzles Designed in Accordance with Phase Report No. 4 . . . . .	6
Stresses Due to Combined Internal Pressure and External Loads Applied to the Nozzle. . . . .	7
Appendix on Stresses from Eringen's Analysis. . . . .	8
NOMENCLATURE . . . . .	9-12
COMPARISON OF THEORIES FOR INTERNAL PRESSURE LOADING . . . . .	13
General Comments. . . . .	13
Hole-in-Plate Analysis. . . . .	14
Hole-in-Cylinder Analysis . . . . .	15
Reidelbach Analysis . . . . .	17
Lind Area Method Analysis . . . . .	19
Flat Plate with a Nozzle. . . . .	26
Nozzles in Spherical Shells . . . . .	29
COMPARISON OF ERINGEN'S THEORY WITH TEST DATA. . . . .	36
General Comments. . . . .	36
Steel Test Models . . . . .	38
Cranch Test Data, Attachment No. 2 . . . . .	38
Pickett & Grigory Test Data, Nozzle No. 11 . . . . .	44
Mehringer & Cooper, Appendage E. . . . .	47
Berman & Pai, Nozzles 7 and 8. . . . .	49
Berman & Pai, Nozzle 15. . . . .	51
Wells, et al, Nozzles K and M. . . . .	53
Photoelastic Test Models. . . . .	56
Stresses in the Cylinder . . . . .	56
Stresses in the Nozzles. . . . .	61
Fillet Radius Requirement. . . . .	78

TABLE OF CONTENTS (contd)

	<u>Page</u>
TEST MODELS WITH LOCAL REINFORCING . . . . .	79
Test Data . . . . .	79
Reinforcing Area. . . . .	85
Comparisons of Semi-Uniform Wall Nozzles with Eringen's Theory. . . . .	91
Effect of Inside Corner Radius . . . . .	91
Stresses at Reinforcing Edge . . . . .	98
COMPARISON OF LIND'S ANALYSIS WITH TEST DATA . . . . .	100
STRESSES DUE TO EXTERNAL LOADS APPLIED TO NOZZLE . . . . .	102
Test Data--Elastic Stresses . . . . .	102
Test Data--Fatigue. . . . .	111
Correlation of Elastic Stress Indices with Fatigue	
Stress Intensification Factors. . . . .	117
In-Plane vs Out-of-Plane Moments, $M_i$ vs $M_o$ . . . . .	129
Torsional Moment, $M_t$ . . . . .	130
Force Loads. . . . .	130
B16.9 Tee. . . . .	131
B31.1-1955 Factors . . . . .	131
B31.1 Case 53. . . . .	131
Comparisons of Measured Stresses with	
Calculated Stresses . . . . .	133
Bijlaard and Bijlaard-Wichman Comparisons. . . . .	133
Nozzle-in-Sphere Comparisons . . . . .	139
Nonuniform-Wall Models . . . . .	140
STRESSES DUE TO EXTERNAL LOADS ON NOZZLES DESIGNED IN ACCORDANCE WITH PHASE REPORT NO. 4 . . . . .	142
Uniform-Wall Models . . . . .	142
Nonuniform-Wall Models. . . . .	146
Summary . . . . .	152
STRESSES DUE TO COMBINED INTERNAL PRESSURE AND EXTERNAL LOADS APPLIED TO THE NOZZLE. . . . .	153
LIST OF REFERENCES . . . . .	155-158

APPENDIX A

STRESSES FROM ERINGEN'S ANALYSIS

## INTRODUCTION

Phase Report No. 2, "Stresses at Nozzles in Spherical Shells Loaded With Pressure, Moment or Thrust", gives background data on theories used for computation of stresses, comparison of test data with those theories and a discussion of the theories and test results in relationship to current codes and practices. An Appendix gives graphs of calculated stresses for a large range of dimensions; the loadings consisting of internal pressure, moment or thrust applied to the nozzle.

The present Phase Report No. 5 is intended to give analogous data for nozzles in cylindrical shells, to the extent feasible with available theory and test data. The elastic theory used as a basis in this report is that developed by Eringen.<sup>(1)</sup> This theory is at present limited to internal pressure loading only; and dimensionally to uniform-wall, normally intersecting cylindrical shells limited to  $d/D < 1/3$  and  $(d/D)\sqrt{D/T} < 1.1^*$ . The area method developed by Lind<sup>(2)</sup> is discussed as a method of extrapolating Eringen's theory for internal pressure to larger values of  $d/D$ .

At present, an adequate theory for stresses due to moments or thrust applied to the nozzle is not available. The theory developed by Bijlaard<sup>(3,4,5)</sup> for distributed loads on the surface of a cylinder is used as a guide herein for empirical correlations of test data giving stresses due to moment or thrust loads. The results obtained by Bijlaard are modified on the basis of test results and replotted in a more readable form as a part of a design manual by Wickman, Mershon, and Hopper<sup>(6)</sup>. The theory for nozzles in spherical shells is also used as a guide for correlation of test data giving stresses due to moment or thrust load.

---

\* See Nomenclature section of report for definition of  $d$ ,  $D$ , and  $T$ .

SUMMARYComparison of Theories for  
Internal Pressure Loading

Numerical comparisons are made between Eringen's analysis for a nozzle in a cylindrical shell with:

- (a) Hole-in-plate analysis
- (b) Hole-in cylinder analysis
- (c) Reidelbach's analysis
- (d) Lind's area method analysis
- (e) Flat-plate with a nozzle.

Eringen's analysis, as reduced to special limits in some of the comparisons, is in satisfactory agreement with the other analyses listed.

Numerical comparisons are also made between Eringen's analysis for a nozzle in a cylindrical shell with the (thin-shell) analysis for a nozzle in a sphere. These comparisons show similarities in trends but significant differences in qualitative magnitudes of the stresses.

Comparison of Eringen's Theory With Test Data

No entirely suitable test models are available for comparison with Eringen's analysis. However, 7 steel test models and 8 photoelastic test models were selected as representing the best available test data for comparison with the theory.

The calculated  $\sigma_{\theta}$ -stresses\* at  $\theta = 0$ ,  $\rho = \rho_0$  are in satisfactory agreement with the measured stresses at the inside corner of the nozzle at  $\theta = 0$ . Ratios of  $K_t/K_e$  ranged from .88 to 1.06 with an average of 0.97.

\* See Nomenclature section of report.



Comparisons were also made with "semi-uniform" wall nozzles in which the uniform-wall length of the nozzle was at least equal to  $\sqrt{dt}$ . One photoelastic and 6 steel test models were included in this comparison;  $K_t/K_e$  ranged from .83 to 0.99 with an average of 0.91.

For the 7 steel test models and 8 photoelastic test models, stresses were calculated at  $\phi = 0$  and  $\phi = \pi/2$  and for appropriate values of  $\rho$  and  $x$ . These calculated stresses were compared with corresponding measured stresses, leading to the conclusions that:

- (a) Agreement between theory and test results are reasonably good for stresses on the shell,
- (b) Agreement between theory and test results are poor for stresses in nozzle, particularly at the nozzle-shell junction ( $x = 0$ ).

The photoelastic test models used for comparison all had significant fillet radii as compared to the nozzle parameter  $\sqrt{rt}$ . Ratios of  $r_o/\sqrt{rt}$  ranged from .46 to 4.47. A detailed analysis of the nozzle stresses was made for two test models. By adjusting the calculated stresses for a "normal" nozzle thickness (similar to the comparisons made in Phase Report No. 2 for nozzles in spheres), reasonable agreement was obtained between theory and test data. This analysis indicates that maximum stresses will not necessarily always occur at the inside corner.

#### Test Models With Local Reinforcing

Test data for 10 photoelastic test models and 17 steel test models are summarized. The results from these test models are compared with results

for analogous models without reinforcing. Some trends observed from this comparison are:

- (1) In test models where  $d/D$  is small ( $d/D < 0.084$ ), the addition of reinforcement on the outside surface produced only small changes in maximum stress ( $\sigma_{\theta}$  at inside corner) as compared to an unreinforced model.
- (2) For larger  $d/D$  ratios, addition of the same reinforcement, in terms of the area ratio ( $A/d_i T$ ), produced a greater reduction in maximum stress as compared to an unreinforced nozzle.
- (3) A relatively small amount of reinforcing placed on the inside of the shell near the opening was more effective in reducing maximum stresses than an equal reinforcing area placed on the outside surface. Also, this inwardly protruding reinforcement changed the location of the maximum measured stress from the inner corner to about the middle of the shell wall.

Comparisons were made between the area of reinforcing used in test models and the area of reinforcing required by the rules given in Phase Report No. 4. While the direct comparisons are limited, such comparisons as can be made indicate that the maximum elastic stress will be less than  $3S$  for nozzles reinforced in accordance with Phase Report No. 4 rules.

#### Inside Corner Radii

The available test data indicate that Eringen's analysis is reasonably accurate for inside corner radii in the range of  $r_i/T$  between about  $1/8$  and  $1/2$ .

### Outside Fillet Radius

In connection with comparisons between Eringen's theory and test data, the background for the rule in Phase Report No. 4 is discussed; i.e.,  $r_o = \text{larger of } \sqrt{dt} \text{ or } T/2$ .

### Stresses at Reinforcing Edges

Values of the  $\sigma_{\rho_0}$  stress at  $\emptyset = \pi/2$  are tabulated. In many models, this stress approaches the value of the stress of the inside corner and, in two test models, it is the highest measured stress. It is noted that fatigue tests and field failures have shown this area to be a potential location of failure. The rules given in Phase Report No. 4 are considered in relationship to possible high stresses at the edge of the reinforcing with the conclusion that Phase Report No. 4 rules are sufficient to prevent stresses greater than 3S at the reinforcing edges.

### Comparison of Lind's Analysis With Test Data

Eringen's theory is limited to  $d/D < 1/3$  and  $(d/D)\sqrt{D/T}$  less than 1.1. For larger values of  $d/D$ , Lind's analysis appears to be a useful means of estimating the  $\sigma_{\emptyset}$  stress at  $\emptyset = 0$ . Numerical comparisons are given between Lind's analysis and 44 test models. The ranges of the parameters  $d/D$ ,  $D/T$ , and  $s/S$  included in the comparisons are quite extensive; in particular  $d/D$  ratios up to 1.0 are included. The ratio of  $K/K_e$  ranges from 0.79 to 1.45 with an average of 0.96.

Stresses Due to External Loads Applied to Nozzles

Test data on external loads applied to nozzles in cylindrical shells are summarized. Test data consists of two types: (1) measured (strain gages) stresses and (2) cyclic loading of nozzles to produce fatigue failure. A correlation is established between stress indices (measured stresses) and fatigue stress intensification factors as defined in the ASA Code for Pressure Piping, B31.1. Comparisons are made between measured stress indices and those determined by (a) Bijlaard-Wichman Graphs, (b) Bijlaard Theory, and (c) Nozzle-in-Sphere analogy. For test models within the range  $(d/D) \sqrt{D/T} < 1.1$ , Bijlaard's results (and Bijlaard-Wichman graphs, since there is no difference in this dimensional range) are in reasonably good agreement with measured stresses on cylindrical shells. Measured stresses on nozzles are not available in this dimensional range.

Stresses Due to External Loads on Nozzles Designed in  
Accordance with Phase Report No. 4

An attempt was made to establish stress indices for nozzle loads  $M_i$  and  $M_o$  on those nozzles covered in Phase Report No. 4 for internal pressure, i.e., with  $(d/D) \sqrt{D/T} \leq 1.1$ . The available test data includes only two models with  $(d/D) \sqrt{D/T}$  within the range of Phase Report No. 4, those being close to the upper limit. A few other models not far beyond the limit are also available. Using these test data, along with guidance from all other available test data and theory, the following suggested stress indices for either  $M_i$  or  $M_o$  loading were obtained.

(1) Uniform Wall Reinforcing

For Nozzle-to-cylinder juncture, use larger of:

- (a) Stress indices calculated by Bijlaard's analysis, or
- (b) Stress indices calculated by nozzle-in-sphere analogy.

For Transition from  $t'$  to  $t$  on nozzle

$$\text{Stress index} = 1.5.$$

For transition from  $T'$  to  $T$  on cylinder

$$\text{Stress index} = I_1 \left[ \frac{0.75}{h^{1/2} (D/T)^{1/6}} \right]$$

$$h = T'/T, \text{ given in Phase Report No. 4}$$

$$I_1 = 1.8/h_e^{2/3}$$

$$h_e = 3.3 T/R$$

(2) For compact reinforcing

Stress index =  $I_1$ , defined above

The stress indices are not accurate but are believed to be conservative.

Stresses Due to Combined Internal Pressure  
and External Loads Applied to the Nozzle

It is noted that linear superposition is apparently always conservative, but not much conservative for thick-wall shells.

Consideration of external loads on the nozzle poses a complex problem because of the independence of these loads from each other and from the internal pressure. It is noted that, in test models with  $(d/D) \sqrt{D/T} < \sim 1.6$ , the stress due to external loads is relatively small at the point of maximum stress due to internal pressure, i.e., at  $\theta = 0$ ,  $\rho = \rho_o$ , inside surface. However, presently available test data is completely inadequate to define the stress fields due to the external loads, even for uniform-wall models with  $(d/D) \sqrt{D/T} < 1.1$ . Accordingly, it appears necessary for conservative design to assume that maximum stresses due to pressure are coincident in location and direction with maximum stresses due to external loads.

Appendix on Stresses from Eringen's Analysis

Tables of membrane, bending and surface stresses are given for the parameters:

D/T from 10 to 250

d/D from .01 to  $(d/D)\sqrt{D/T} \approx 1.1$

s/S from 1/64 to 4.0

Tables of maximum stress intensities in the shell and in the nozzle are also included.

A brief discussion is presented concerning the location of maximum stresses with respect to  $\emptyset$  and distance from the nozzle-shell juncture.

The use of Eringen's computer program and limitations thereof are briefly discussed.

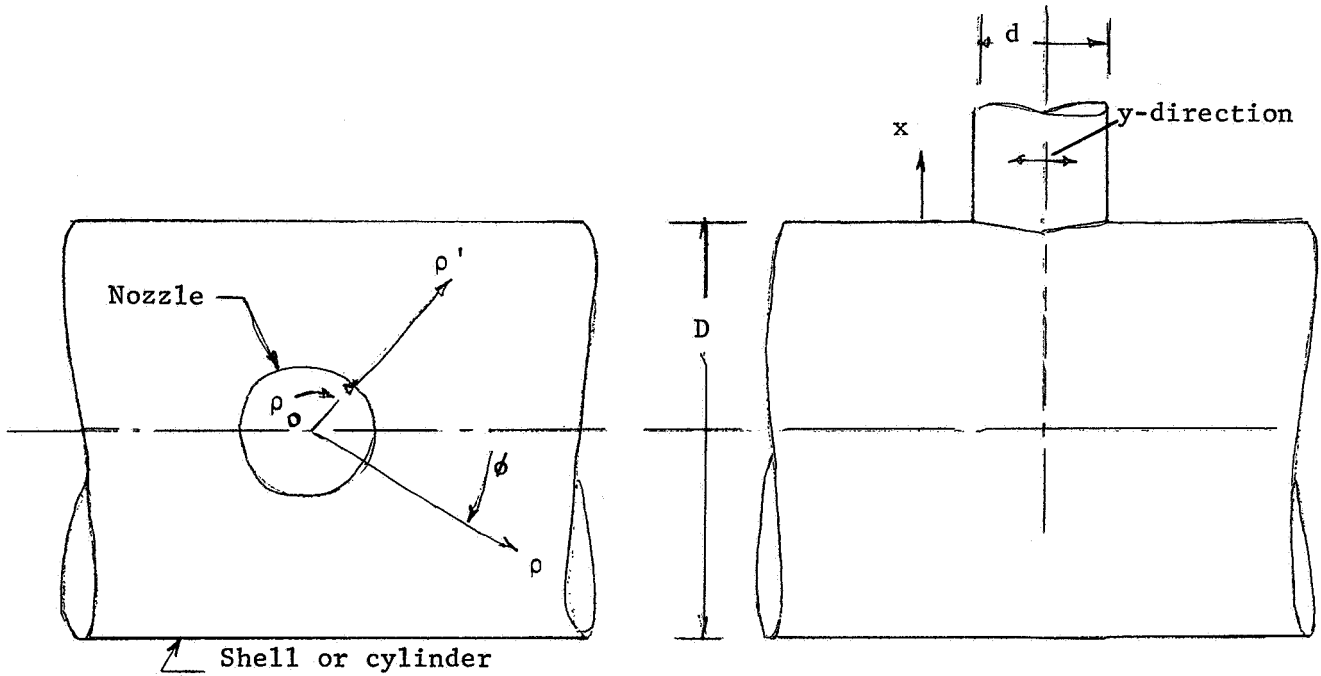
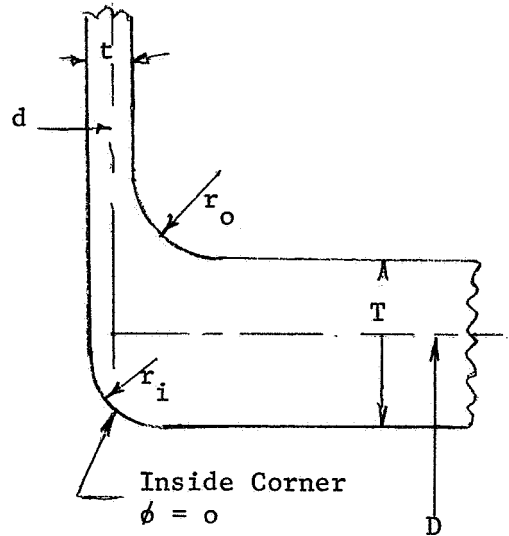
NOMENCLATURE

FIGURE 1. NOMENCLATURE ILLUSTRATION

Dimensions

- D = mean diameter of shell, inches  
 d = mean diameter of nozzle, inches  
 $d_i$  = inside diameter of nozzle, inches  
 T = wall thickness of shell, inches  
 t = wall thickness of nozzle, inches  
 R = mean radius of shell, inches  
 $\left. \begin{matrix} \rho_o \\ r \end{matrix} \right\}$  = mean radius of nozzle, inches  
 $\beta \rho_o = 0.454 (d/D) \sqrt{D/T} *$   
 $r_i$  = inside corner radius, inches  
 $r_o$  = fillet radius, inches  
 A = reinforcement area on both sides  
 of nozzle, sq.in.

$$\beta = \frac{[3(1 - \nu^2)]^{1/4}}{2} \frac{1}{\sqrt{RT}}$$



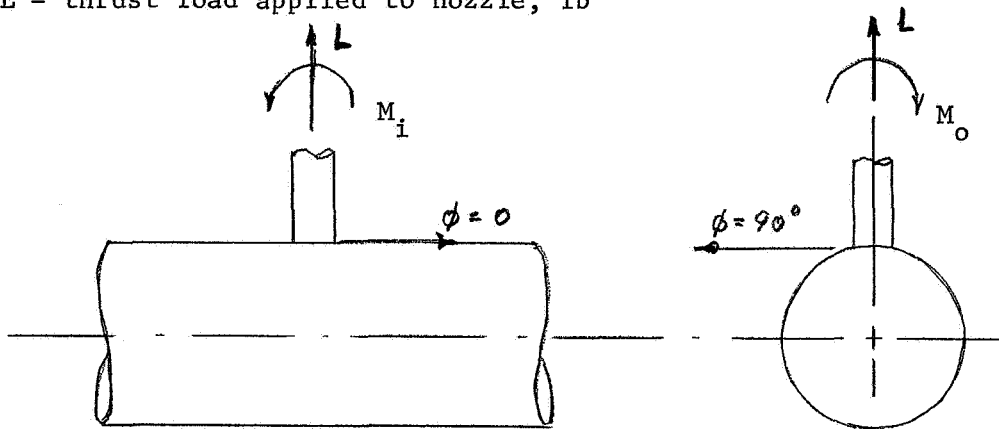
\* For Poisson's ratio = 0.3 .

NOMENCLATURE (Continued)Co-ordinates

- $\phi$  = angle around nozzle, see Figure 1  
 $\rho$  = distance from center of nozzle on shell  
 $\rho'$  = distance from edge of nozzle on shell  
 $x$  = distance along nozzle axis measured from nozzle-shell juncture  
 $y$  = circumferential direction on nozzle

Loads

- $P$  = internal pressure, psi  
 $M_i$  = in-plane moment applied to nozzle, in.-lb  
 $M_o$  = out-of-plane moment applied to nozzle, in.-lb  
 $L$  = thrust load applied to nozzle, lb

Stresses

Nominal stresses are designated by  $S$  or  $s$ ; measured or calculated stresses by  $\sigma$ ; with appropriate subscripts.



NOMENCLATURE (contd.)

For pressure loading:

$$S = PD/2T, \text{ psi}$$

$$s = Pd/2t, \text{ psi}$$

The ratio  $s/S$  is also used as a dimensional parameter,

$$s/S = (d/t)/(D/T)$$

For external loads:	$M_i$	$M_o$	(Torsion) $M_t$	L
S =	M / Z	M / Z	M / 2Z	L / A
	$Z = \pi r^2 t$			$A = 2\pi r t$

$\sigma_{\phi o}$  = stress in shell,  $\phi$  - direction, outside surface, psi

$\sigma_{\phi i}$  = " " " ,  $\phi$  - " , inside " , "

$\sigma_{\rho o}$  = " " " ,  $\rho$  - " , outside " , "

$\sigma_{\rho i}$  = " " " ,  $\rho$  - " , inside " , "

$\sigma_{x o}$  = " " nozzle, x - " , outside " , "

$\sigma_{x i}$  = " " " , x - " , inside " , "

$\sigma_{y o}$  = " " " , y - " , outside " , "

$\sigma_{y i}$  = " " " , y - " , inside " , "

$\sigma_{n\phi}$  = membrane stress in shell,  $\phi$  - direction, psi

$\sigma_{b\phi}$  = bending " " " ,  $\phi$  - " , psi

$\sigma_{n\rho}$  = membrane " " " ,  $\rho$  - " , psi

$\sigma_{b\rho}$  = bending " " " ,  $\rho$  - " , psi

$\sigma_{nx}$  = membrane " " nozzle, x - " , psi

$\sigma_{bx}$  = bending " " " , x - " , psi

$\sigma_{ny}$  = membrane " " " , y - " , psi

$\sigma_{by}$  = bending " " " , y - " , psi

Most of the data cited herein give surface stresses using the nomenclature:

## NOMENCLATURE (contd.)

$\sigma_n$  = stress normal to section

$\sigma_t$  = stress tangential to section

The correlations are:

$\sigma_n = \sigma_\theta$  on shell

$\sigma_n = \sigma_y$  on nozzle

$\sigma_t = \sigma_\rho$  on shell

$\sigma_t = \sigma_x$  on nozzle.

Stress Indices

$K_t = \sigma_\theta/S$  at  $\theta = 0$ ,  $\rho = \rho_0$ , Eringen's theory

$K$  = stress index from Lind's Analysis

$K_e$  = experimentally determined stress index

Material Properties

$E$  = modulus of elasticity, psi

$\nu$  = Poisson's ratio, taken to be 0.3 for all calculations herein.

COMPARISON OF THEORIES FOR  
INTERNAL PRESSURE LOADING

General Comments

The analysis of shells of revolution, which include nozzles in spherical shells as a special case, is well advanced and provides a good basis for design of nozzles in spheres. The problem of nozzles in cylindrical shells, however, presents formidable analytical difficulties. Until a few years ago, analytical estimates of stresses in small nozzles ( $d/D \ll 1$ ) in cylindrical shells were often obtained by reducing the problem to that of an opening or nozzle in a flat plate with edge loads. Papers by Beskin<sup>(7)</sup> and Waters<sup>(8)</sup> are examples of this kind of approximation. A further step towards the analysis of nozzles in cylindrical shells consisted of the solution of a cylindrical shell with a circular opening. Papers by Lourye<sup>(9)</sup>, Withum<sup>(10)</sup>, Eringen, et al<sup>(11)</sup>, Lekkerkerker<sup>(12)</sup>, Savin<sup>(13)</sup>, and Van Dyke<sup>(14)</sup> give solutions to this problem. The next step consisted of solution of two normally intersecting cylindrical shells. Solutions to this problem are given by Reidelbach<sup>(15)</sup> and Eringen, et al<sup>(16)</sup>.

The analysis and computer program developed by Eringen<sup>(16)</sup> is used in this report as the basis for calculated elastic stresses with internal pressure loading. One purpose of the following discussion is to indicate how Eringen's analysis, as reduced to special limits, agrees with related analyses.

The analysis methods listed above are mostly limited to small values of  $d/D$ . An accurate analysis for large nozzles in cylinders is not available. The approximate analysis by Lind<sup>(2)</sup>, applicable to nozzles with  $d/D$  up to unity, is also compared with Eringen's analysis in the following discussion.

#### Hole-in-Plate Analysis

The problem of an opening in a cylinder with internal pressure loading approaches a plane-stress problem as the  $d/D$  ratio becomes very small. The stresses around a circular hole, normal to a flat plate surface, subjected to tension stresses equal to  $S$  in one direction,  $S/2$  in a direction 90 degrees thereto, are well known. In particular, at points corresponding to  $\phi = 0$ ,  $\rho = \rho_0$  and  $\phi = \pi/2$ ,  $\rho = \rho_0$  (See Figure 1), the stresses tangential to the hole are  $2.5S$  and  $0.5S$ , respectively. For small  $d/D$ -ratios combined with small  $t/T$  ratios, Eringen's<sup>(16)</sup> analysis for a nozzle in a cylinder would be expected to give these stresses. As can be seen in Table A-1 of the Appendix, the analysis does converge to these membrane stresses in the cylinder for small  $d/D$  and  $t/T$ . Further, as shown in Table A-3, the bending stresses at these limits are small. Accordingly, agreement between the "hole-in-plate" analysis and Eringen's stresses on the cylinder are good.

The membrane stress in the nozzle,  $\sigma_{ny}$ , should also approach the values of  $2.5S$  at  $\phi = 0$ ,  $0.5S$  at  $\phi = \pi/2$  for small  $d/D$  and  $t/T$ . As shown in Table A-2, the limit values are approximately met, however,  $\sigma_{ny}$  appears to be larger than expected for a small opening. The reason for this discrepancy is not known.

Hole-in-Cylinder Analysis

The analyses of a circular hole in a cylindrical shell by Lourye<sup>(9)</sup>, Withum<sup>(10)</sup>, Eringen<sup>(11)</sup>, Lekkerkerker<sup>(12)</sup>, and Van Dyke<sup>(14)</sup> all lead to results expressible in terms of the parameter  $(d/D)\sqrt{D/T}$ . Figure 2 shows the membrane stress  $\sigma_{n\phi}$  at  $\rho = \rho_0$ ,  $\phi = 0$  plotted against  $(d/D)\sqrt{D/T}$ . The relationship shown in Figure 2 is obtainable from References (9), (11), and (14)\* although the theoretical approaches are not identical.

It would be anticipated that the membrane stress in the cylinder ( $\sigma_{n\phi}$  at  $\rho = \rho_0$ ,  $\phi = 0$ ) obtained from Eringen's analysis of a nozzle in a cylinder would approach the values shown in Figure 2 for very thin-wall nozzles; i.e., where  $s/S$  is large. As can be seen in Table A-1 of the Appendix, for  $s/S = 4$  the values of  $\sigma_{n\phi}$  at  $\phi = 0$  are essentially identical to the values given in Figure 2. For example, for  $D/T = 100$ ,  $d/D = 0.10$ ,  $s/S = 4.0$  Table A-1 gives  $\sigma_{n\phi} = 3.73S$ . The corresponding value from Figure 2 for  $(d/D)\sqrt{D/T} = 1.0$  is  $3.7S$ .

---

\* Except Lourye<sup>(9)</sup> wherein, according to Lekkerkerker<sup>(12)</sup>, the curvature influence was overestimated by a factor of 2. Making this correction to Lourye's analysis brings it into agreement with the data of Figure 2, to the degree of approximation included in Lourye's analysis.

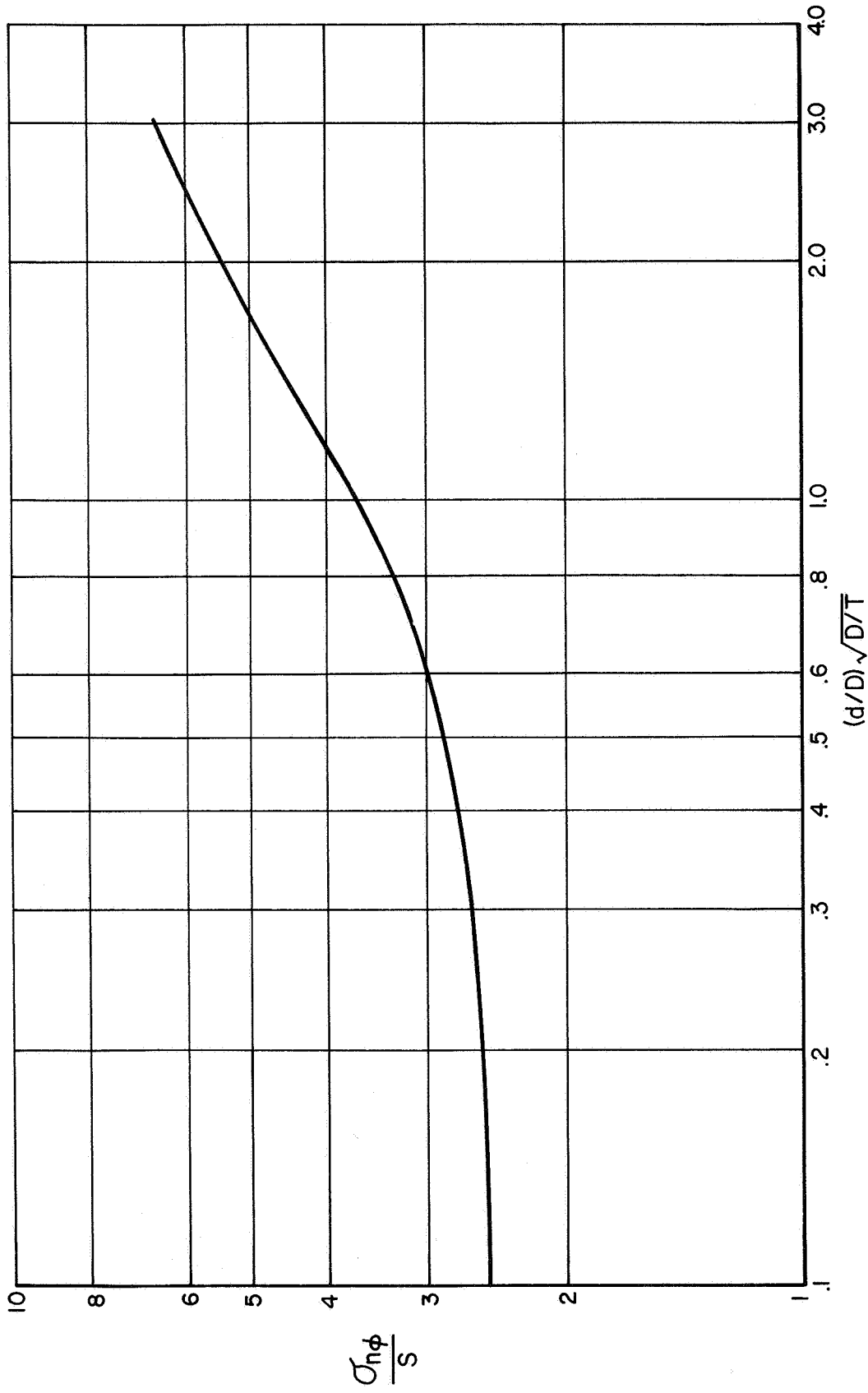


FIGURE 2. MEMBRANE STRESS AT  $\rho = \rho_0$ ,  $\theta = 0$  FROM ANALYSIS OF A HOLE IN A CYLINDER

Reidelbach Analysis

Reidelbach<sup>(15)</sup> gives an example\* of the application of his analysis. The example is for the parameters:

$$\frac{D}{T} = 19.38, \quad \frac{d}{D} = 0.2, \quad \frac{s}{S} = 0.563$$

These parameters were used in Eringen's computer program to obtain directly comparable results. Comparisons are shown in Table 1. General qualitative agreement exists for this particular example and, for the larger stresses, fairly good quantitative agreement exists.

The largest discrepancy between the two analyses is in the values of  $\sigma_{ny}/S$  and  $\sigma_{n\emptyset}/S$  at  $\emptyset = \pi/2$ . Reidelbach's values of  $\sigma_{ny}$  and  $\sigma_{n\emptyset}$  are about the same whereas Eringen's values of  $\sigma_{ny}$  is about 3 times his value of  $\sigma_{n\emptyset}$ . In this aspect, Reidelbach's analyses appears to be more self-consistent.

---

\* For Reidelbach's "3-terms assumption", a system of 22 simultaneous equations must be set up and solved. A computer program would be required to economically make additional comparisons between Eringen's and Reidelbach's analyses.

TABLE 1. COMPARISON OF REIDELBACH<sup>(15)</sup> AND ERINGEN<sup>(16)</sup> RESULTS FOR EXAMPLE CASE WITH  $D/T = 19.38$ ,  $d/D = 0.2$ ,  $s/S = 0.563$ ,  $\rho = \rho_0$ ,  $x = 0$ .

Stress	$\phi = 0$		$\phi = \pi/4$		$\phi = \pi/2$	
	Reid.	Erin.	Reid.	Erin.	Reid.	Erin.
$\sigma_{nx}/S$	.166	.307	.288	.290	.381	.238
$\sigma_{bx}/S$	-2.78	-2.69	-2.66	-2.29	-2.34	-2.72
$\sigma_{ny}/S$	2.75	2.63	1.64	1.58	.600	1.10
$\sigma_{by}/S$	- .326	- .301	- .761	- .634	-1.24	-1.43
$\sigma_{n\rho}/S$	.212	.201	.160	.144	.115	.150
$\sigma_{b\rho}/S$	.354	.343	.322	.291	.298	.343
$\sigma_{n\phi}/S$	2.56	2.82	1.56	1.69	.712	.367
$\sigma_{b\phi}/S$	- .132	- .242	.255	.285	.920	.876
$\sigma_{xo}/S$	2.95	3.00	2.95	2.58	2.72	2.96
$\sigma_{xi}/S$	-2.61	-2.38	-2.37	-2.00	-1.96	-2.48
$\sigma_{yo}/S$	3.08	2.93	2.40	2.21	1.84	2.53
$\sigma_{yi}/S$	2.42	2.33	.88	.95	- .64	- .33
$\sigma_{\rho o}/S$	.566	.544	.482	.435	.413	.493
$\sigma_{\rho i}/S$	- .142	- .142	- .162	- .147	- .183	- .193
$\sigma_{\phi o}/S$	2.43	2.58	1.82	1.98	1.63	1.24
$\sigma_{\phi i}/S$	2.69	3.06	1.30	1.40	- .208	.509
$\bar{\sigma}_n/S^*$	5.03	4.71	3.25	2.95	1.96	2.48
$\bar{\sigma}_c/S^*$	2.83	3.20	1.82	1.98	1.63	1.24

\*  $\bar{\sigma}_n$  = maximum stress intensity in nozzle.

$\bar{\sigma}_c$  = maximum stress intensity in cylinder.



Lind Area Method Analysis

The concept of the "area method" for design of tees and complex branch connections has been used for many years<sup>(17)</sup>. Recently, however, Professor N. C. Lind<sup>(2)</sup> has placed this approach on a quantitative basis. The approach assumes that the "effective" length along the nozzle axis is equal to  $0.4\sqrt{rt}$  and that the effective length along the cylinder axis is equal to the smaller of  $0.4\sqrt{RT}$  or  $2r/3$ . These lengths are measured from the nozzle-cylinder junction in the  $\phi = 0$  plane. Two equations are developed for computing the stress concentration factor:

$$K = \text{larger of } K_a \text{ or } K_b$$

$$K_a = \frac{[1 + 1.77(d/D)\sqrt{D/T} + (d/D)^2/(s/S)] [1 + (T/D)/(s/S)]}{1 + (d/D)^2/(s/S)\sqrt{s/S}} \quad (1)$$

$K_a$  is based on effective length along cylinder of  $0.4\sqrt{RT}$

$$K_b = \frac{[1.67\sqrt{s/S}\sqrt{D/T} + 0.565(d/D)] [1 + (T/D)/(s/S)]}{0.67\sqrt{s/S}\sqrt{D/T} + 0.565(d/D)/(s/S)} \quad (2)$$

$K_b$  is based on effective length along cylinder of  $2r/3$ .

As  $(d/D) \rightarrow 0$ ;  $K_a \rightarrow 1.0 [1 + (T/D)/(s/S)]$  while  $K_b \rightarrow 2.5 [1 + T/D/(s/S)]$ .

The factor  $[1 + (T/D)/(s/S)]$ , called a "bending factor" by Lind, generally ranges from 1.0 to 1.10; accordingly  $K_b$  converges roughly to 2.5 for small  $d/D$ .

Figures 3 through 7 give comparisons of Lind's  $K$  with Eringen's  $\sigma_{n\phi}$  at  $\rho = \rho_0$ ,  $\phi = 0$ . Comparisons are made for  $s/S = .25, .5, 1.0, 2.0$ , and  $\infty$ ; and for  $D/T = 10$  and  $100$ . In general, the qualitative trends

and magnitudes are quite similar. However, there are areas where significant quantitative differences exist. For example, for  $s/S = 1.0$  (Figure 5),  $\frac{D}{T} = 100$ ,  $d/D = .085$ ; Lind's  $K = 2.5$  whereas  $\sigma_{n\phi}/S = 3.4$ .

Lind's analysis is applicable to large values of  $d/D$ , as contrasted to Eringen's limit of  $(d/D) \sqrt{D/T} = 1.1$ . Lind has made comparisons\* of his analysis with test data for large  $d/D$  models and has found good agreement but cautions against routine application of the analysis for branch connections with parameters beyond the range of test results. Nevertheless, in the absence of a theoretical analysis for large  $d/D$ -ratios, Lind's analysis appears as perhaps the best guide to estimating stresses in such branch connections.

---

\* See page 100.

———— Eringen,  $K = \frac{\sigma_n \theta}{s}$  at  $\rho = \rho_0, \theta = 0$

- - - - - Lind

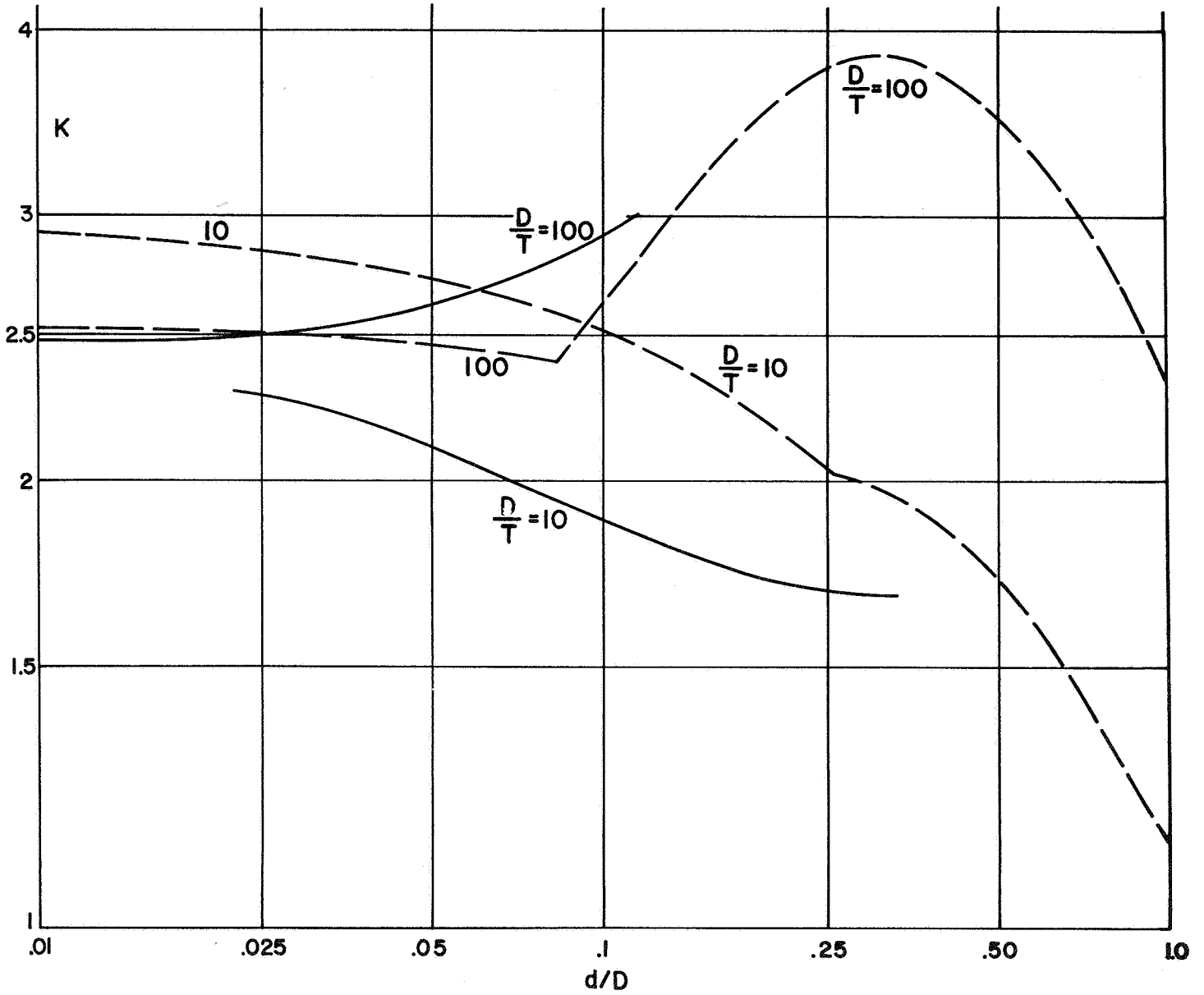


FIGURE 3. COMPARISON OF ERINGEN AND LIND ANALYSES FOR  $s/S = .25$

————— Eringen,  $K = \frac{\sigma_n \theta}{S}$  at  $\rho = \rho_0$ ,  $\theta = 0$   
 - - - - - Lind

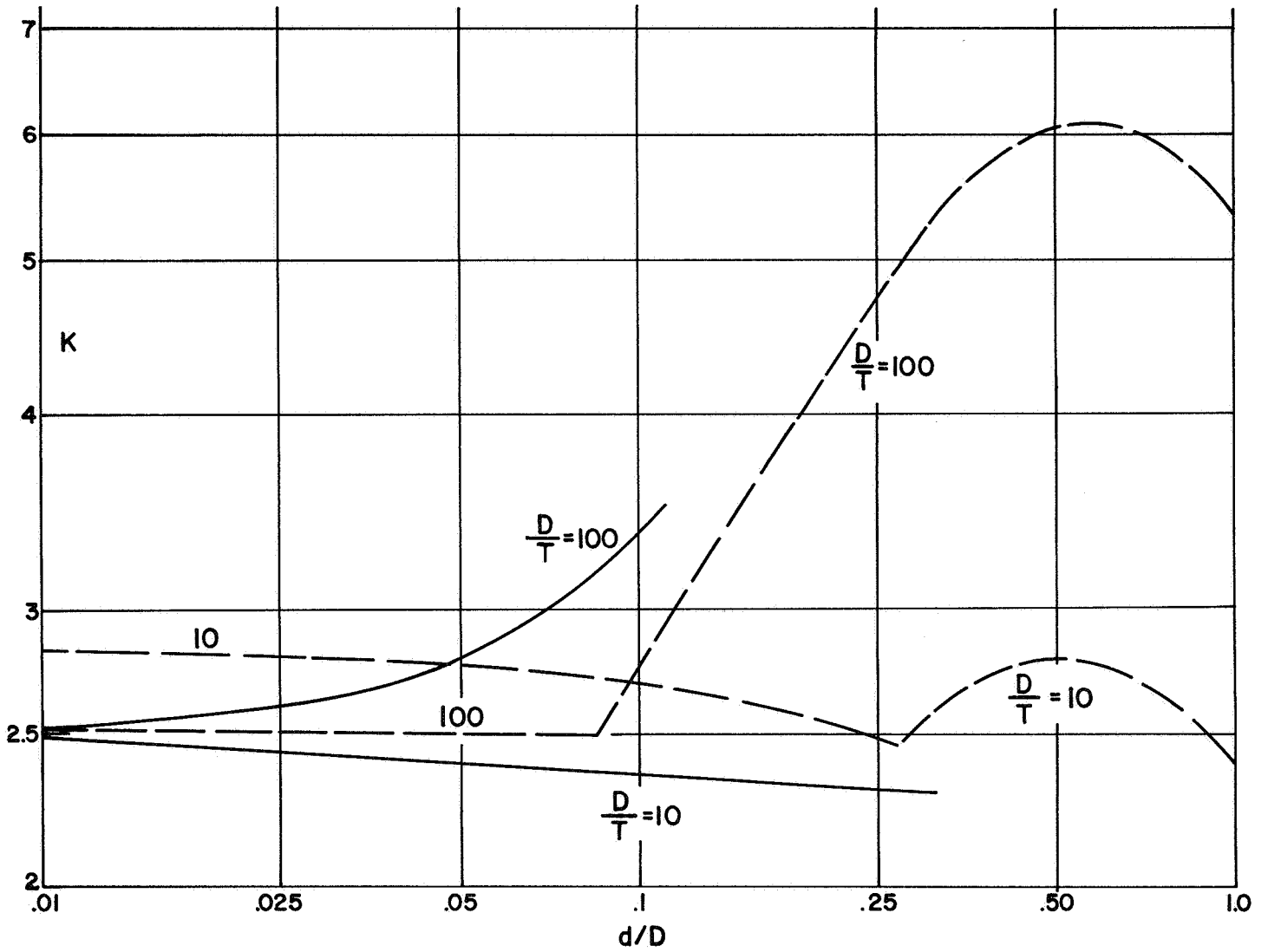


FIGURE 4. COMPARISON OF ERINGEN AND LIND ANALYSES FOR  $s/S = .5$

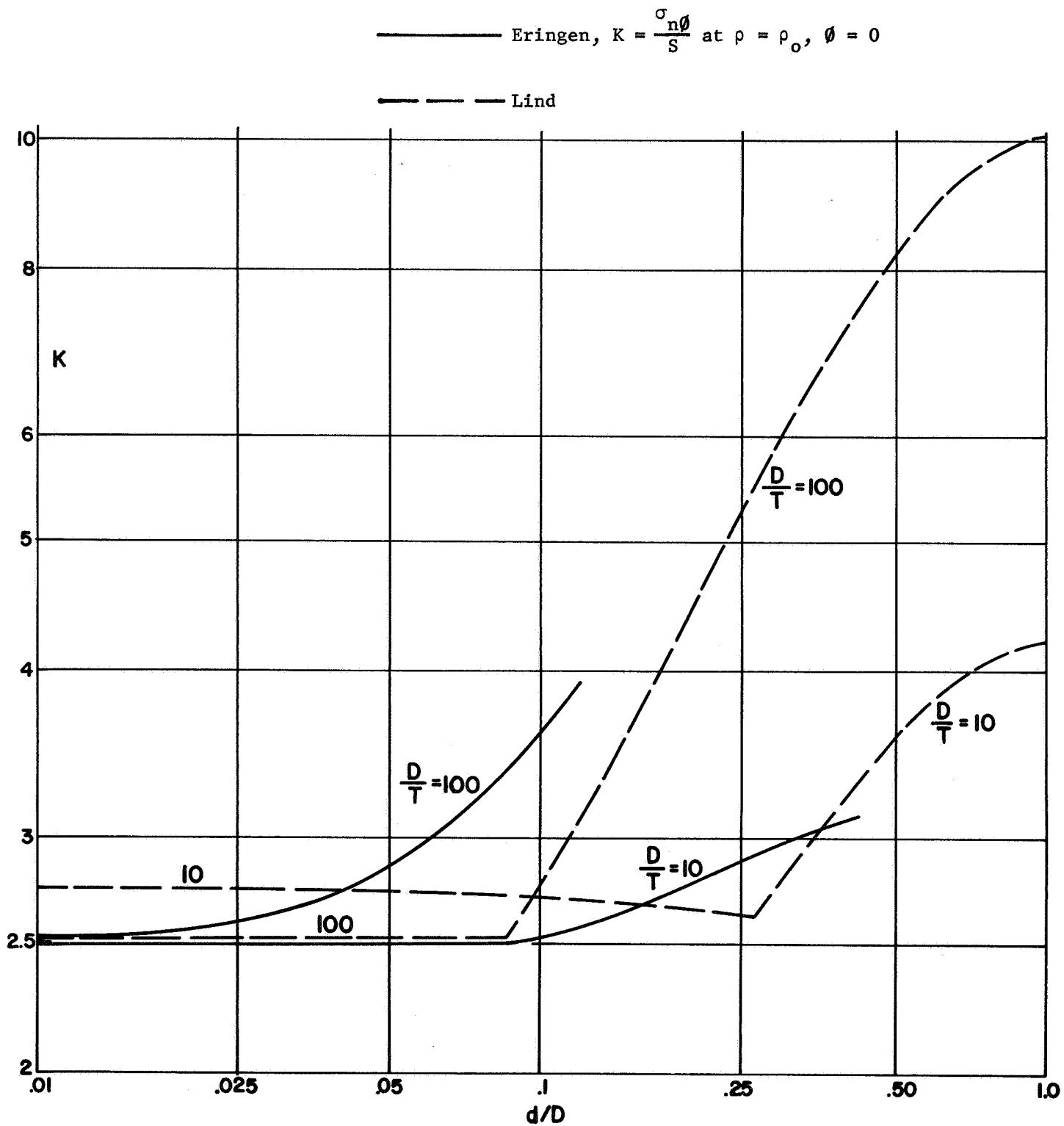


FIGURE 5. COMPARISON OF ERINGEN AND LIND ANALYSES FOR  $s/S = 1$ .

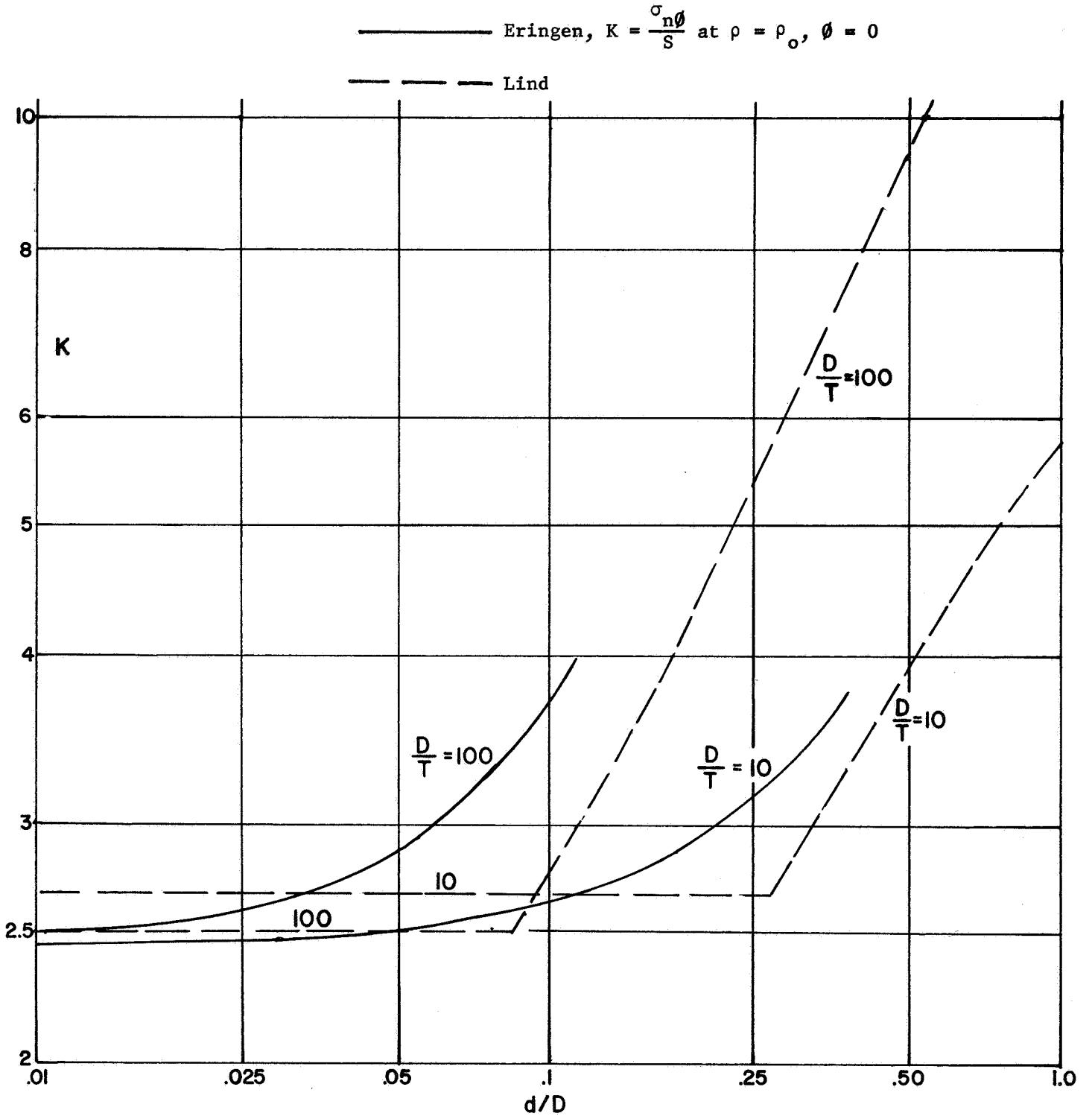


FIGURE 6. COMPARISON OF ERINGEN AND LIND ANALYSES FOR  $s/S = 2$ .

(25)

————— Eringen,  $K = \frac{\sigma_n \theta}{S}$  at  $\rho = \rho_o, \theta = 0$   
- - - - - Lind

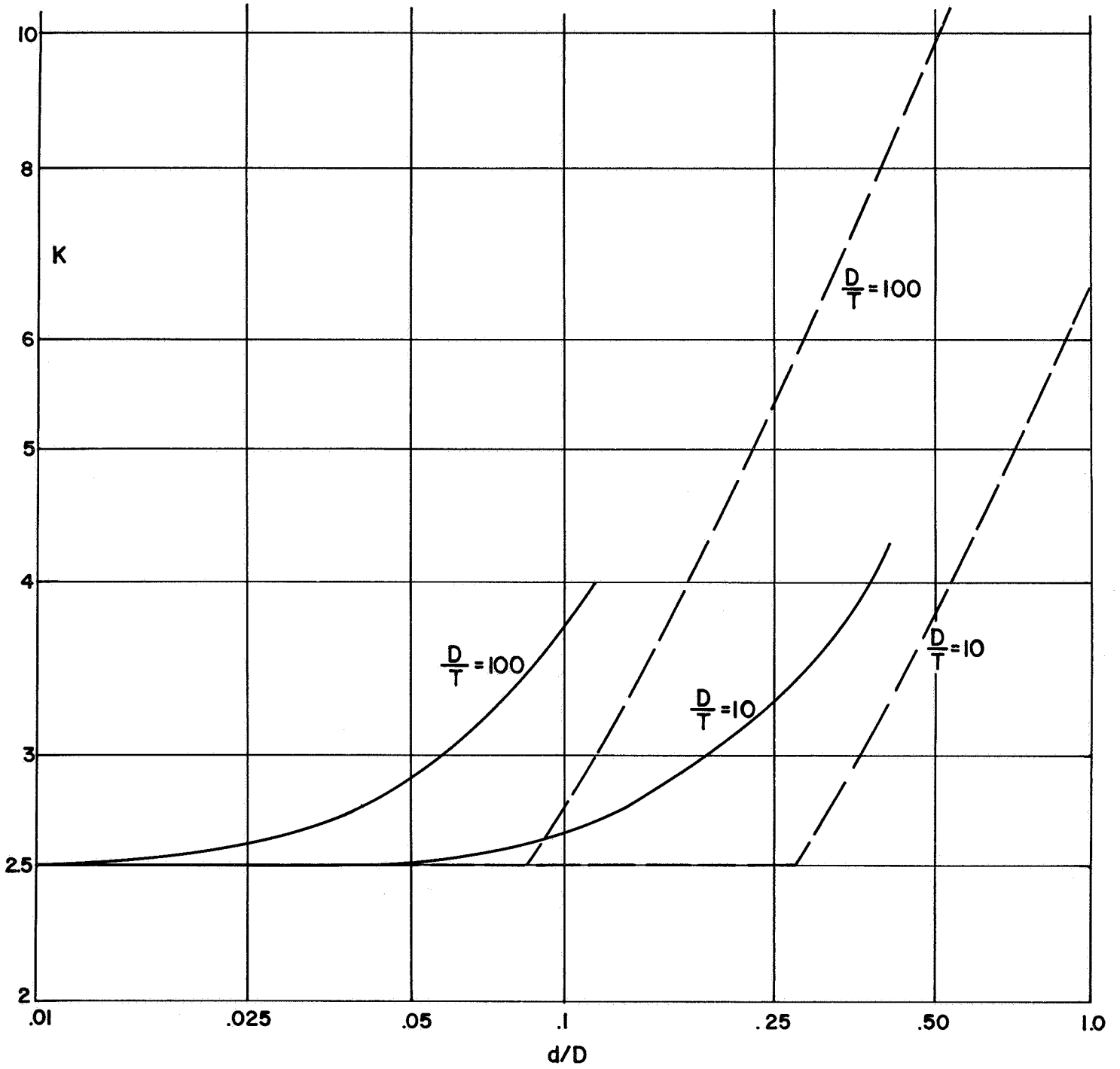


FIGURE 7. COMPARISON OF ERINGEN AND LIND ANALYSES FOR  $s/S = \infty$

Flat Plate with a Nozzle

Eringen's analysis is limited to internal pressure loading of two normally intersecting uniform wall cylinders. The limits on  $d/D$  and  $(d/D) \sqrt{D/T}$  are such that most nozzles in pressure vessels are included. However, many such nozzles (and perhaps optimum-design nozzles) involve tapered-wall reinforcing and/or significant fillet radii for which the theory for uniform wall cylinders is not applicable. Test data given later herein indicate that such local reinforcing can be quite effective in reducing stresses. Further, most pressure vessel nozzles are subjected to some bending moments and/or axial thrust for which theory is not available. For very small nozzles ( $d/D < 0.10$ ), some guidance in these areas may be obtained by using the theory for axisymmetric structures. Waters<sup>(2)</sup> gives a development involving this approach; since then axisymmetric computer programs have become available which permit investigation of the approach for tapered-wall reinforcing and with either "pressure" or a bending load applied to the nozzle.

To investigate this approach for "pressure" loading, Battelle's MOLSA\* computer program was used to calculate stresses in a circular flat plate with a nozzle; comparable to an actual nozzle in a cylindrical shell with  $D/T = 250$ ,  $d/D = .01$ ,  $s/S = 1.0$ . The edge loadings applied to the circular plate were:

$$N_{\phi} = \left( \frac{3}{4} - \frac{1}{4} \cos 2\phi \right) PR \quad (3)$$

---

\* MOLSA is a multi-layer orthotropic shell analysis computer program for axisymmetric structures with arbitrary loadings.



where  $N_{\theta}$  = stress resultant in the plane of the flat plate  
 $\theta$  = location angle as shown in Figure 1  
 $P$  = internal pressure  
 $R$  = radius of cylinder.

Equation (3) gives the in-plane loading imposed by the internal pressure on an actual nozzle in the cylinder. In addition, an axial force was applied to the end of the nozzle, representing the end thrust of the pressure in the nozzle. Table 2 gives a comparison of the results from the MOLSA computer program with those obtained from Eringen's computer program for nozzles in cylindrical shells. In general, the agreement is satisfactory for the results in both the cylinder and the nozzle.

This approach requires the selection of an outside diameter of the circular plate. For the example shown this diameter was selected as 4 times the diameter of nozzle, based on the attenuation of stresses given by Eringen's results for the model. However, some preliminary calculations indicate the results are not overly sensitive to the selection of the plate diameter.

For bending moments applied to the nozzle, the flat plate analogy will not distinguish between in-plane and out-of-plane moments. According to available test data given later herein, this is not correct for  $d/D$  of around 0.2 or larger. No test data is available for very small nozzles, however, the trend of the test data indicates that for  $d/D < 0.1$ , the difference between in-plane and out-of-plane bending may be small.

TABLE 2. COMPARISON OF MOLSA AXISYMMETRIC STRUCTURE AND ERINGEN RESULTS FOR EXAMPLE CASE WITH  $D/T = 250$ ,  $d/D = .01$ ,  $s/S = 1.0$

	Stress Resultants, $\rho = \rho_0$				Stress Index, $\rho = \rho_0$ *			
	$\phi = 0$		$\phi = \pi/2$		$\phi = 0$		$\phi = \pi/2$	
	Erin.	MOLSA	Erin.	MOLSA	Erin.	MOLSA	Erin.	MOLSA
$N_\phi$	254.	269.	49.8	43.6	2.54	2.69	.50	.44
$N_\rho$	.116	.127	-.0274	-.0270	.00	.00	.00	.00
$M_\phi$	.775	1.26	1.62	1.27	.06	.09	.12	.10
$M_\rho$	.00403	.00440	-.00073	-.00088	.00	.00	.00	.00
$n_y$	2.68	2.83	.653	.590	2.68	2.83	.65	.59
$n_x$	.483	.489	.517	.511	.48	.49	.52	.51
$m_y$	.00118	.00131	-.00019	-.00025	.88	.98	-.14	-.19
$m_x$	.00403	.00440	-.00073	-.00088	3.02	3.30	-.55	-.66

\* Stress index =  $\sigma/S$ .

### Nozzles in Spherical Shells

Current practice in reinforcing of openings in pressure vessels requires that the cut out area be replaced in a prescribed zone around the opening, regardless of whether the shell is spherical or cylindrical. One set of proposed design rules\* is based on an analysis of nozzles in spherical shells only. It is of interest, therefore, to compare calculated stresses at nozzles in cylindrical shells with the calculated stresses in corresponding nozzles in spherical shells.

The membrane stress tangential to the opening is perhaps the most significant stress. For nozzles in cylinders\*\*, this stress ( $\sigma_{n\theta}$ ) is a maximum at  $\rho = \rho_o$ ,  $\theta = 0$ . For nozzles in spheres\*\*, the corresponding stress is a maximum at  $\rho = \rho_o$ , but is independent of  $\theta$ . Figure 8 (a) gives a comparison of the stress for  $t/T = 0$ , i.e., a hole in the shell. For both cylinders and spheres, the stress is a function of  $(d/D) \sqrt{D/T}$ . For the range of dimensions covered, Figure 8(a) indicates that the value of  $\sigma_{n\theta}/S$  for nozzles in cylinders is about 0.5 higher than for the corresponding nozzles in spheres.

Figures 8 (b) and 8 (c) give comparisons for  $t/T = 0.5$  and  $t/T = 1.0$ . For nozzles in spheres,  $\sigma_{n\theta}$ , is essentially a function of  $(d/D) \sqrt{D/T}$  and  $t/T$  only. However, for nozzles in cylinders, as indicated on Figures 8 (b) and 8 (c), as  $t/T$  increases the value of  $\sigma_{n\theta}$  depends upon  $d/D$ . In a rough qualitative sense, however, Figure 8 indicates that the  $\sigma_{n\theta}$  stress for nozzles in spheres is about the same as for

---

\* Proposal by United Kingdom to the International Organization for Standards.

\*\* Here and subsequently in this report, the terminology "nozzles in cylinders" is used to define a structure consisting of a cylindrical nozzle in and with its axis normal to the surface of a cylindrical shell. Stresses described for the structure may occur either in the nozzle or in the cylinder shell as indicated by the subscripts for the stress under consideration. Analogous terminology is used for the structure consisting of a cylindrical nozzle in a spherical shell.

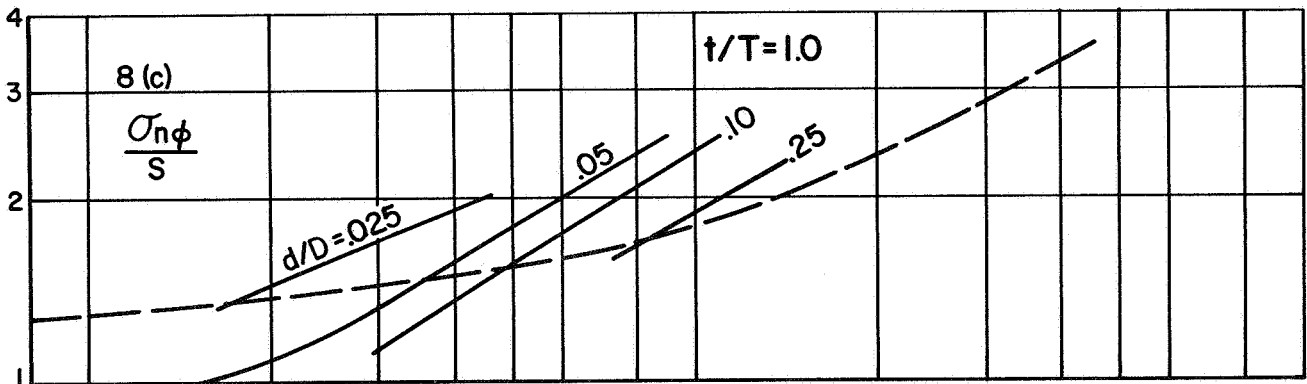
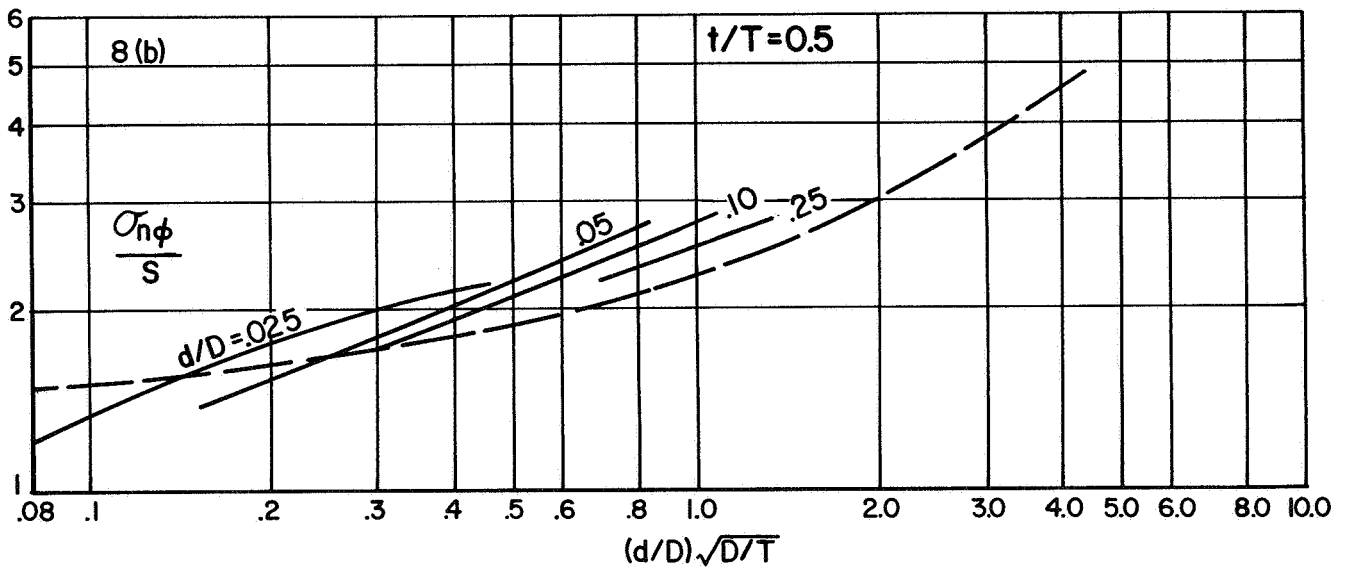
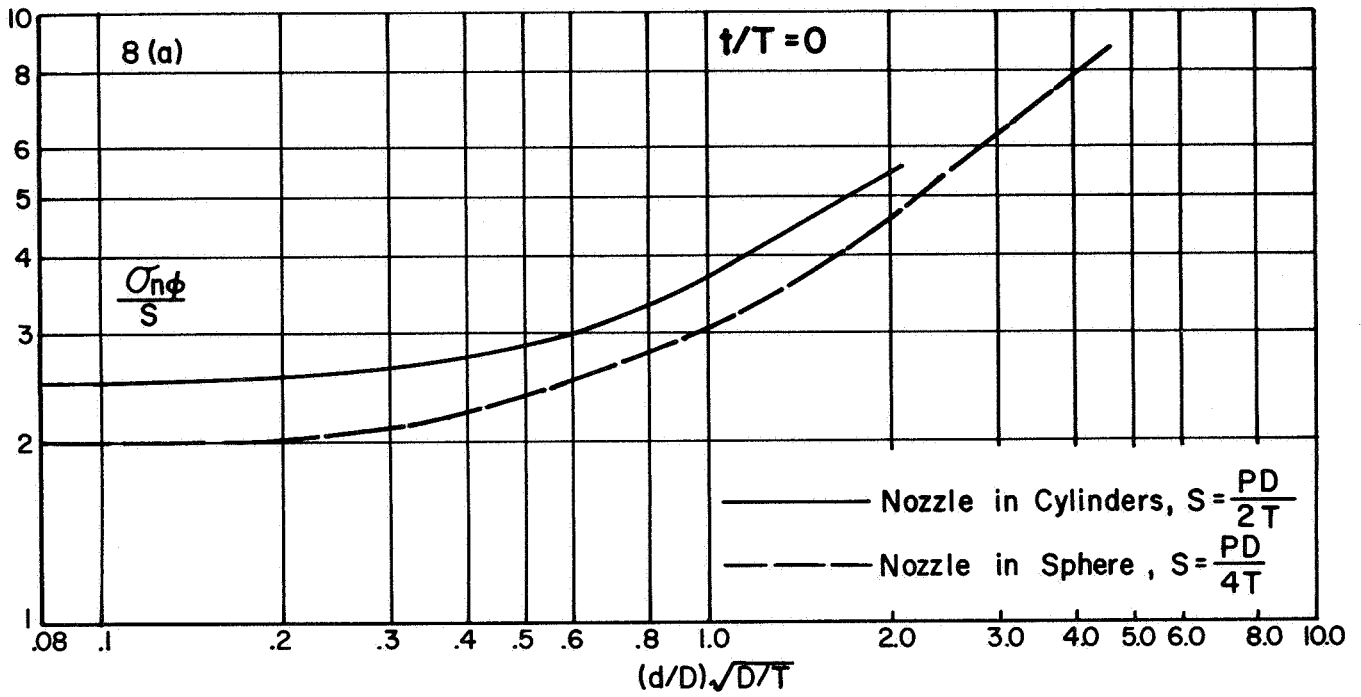


FIGURE 8. COMPARISON OF NOZZLE IN CYLINDERS WITH NOZZLE IN SPHERES,  $\sigma_{n\phi}$  STRESSES

nozzles in cylinders. This comparison is valid only within the range of Eringen's analysis; i.e.,  $(d/D)\sqrt{D/T} < 1.1$ ,  $d/D < 1/3$ .

According to Eringen's analysis, the maximum stress for nozzles in cylinders almost always occurs in the nozzle, not in the cylinder\* . For nozzles in spheres, the maximum stress occurs in the nozzle if  $t/T$  is less than about 0.5. These high stresses arise, in large part, from local bending stresses. Table 3 gives a comparison of the bending stresses for nozzles in cylinders and nozzles in spheres. For nozzles in spheres, the  $\sigma_{by}$  stress is simply Poisson's ratio times the  $\sigma_{bx}$  stress. While there are similarities in the trends, it is apparent from Table 3 that there can be large differences in the nozzle bending stresses of nozzles in spheres as compared to nozzles in cylinders.

---

\* Comparisons are shown in Table A-7 of the Appendix.

TABLE 3. COMPARISONS OF NOZZLES IN CYLINDER WITH NOZZLE  
IN SPHERE, BENDING STRESSES\* IN THE NOZZLE

( 1 of 4)

$\frac{D}{T}$	$\frac{d}{D}$	$\frac{s}{S}$	Nozzles in Cylinder				Nozzles in Sphere	
			$\phi = 0$		$\phi = \pi/2$		$\sigma_{bx}$	$\sigma_{by}$
			$\sigma_{bx}$	$\sigma_{by}$	$\sigma_{bx}$	$\sigma_{by}$		
10 ↓	.025	.25	.47	-1.24	3.87	2.52	2.55	.77
		.5	1.33	-.38	2.51	1.53	2.64	.79
		1.0	1.53	.06	.84	.65	2.05	.61
	.05	.25	.53	-1.06	3.46	2.23	1.93	.58
		.5	1.33	-.37	2.49	1.51	2.46	.74
		1.	1.57	.07	.87	.66	2.07	.62
		2.	.74	.02	-1.36	-.20	.64	.19
		4.	-1.94	-.68	-4.86	-1.35	-2.42	-.73
	.10	.25	.50	-.89	2.67	1.76	.91	.27
		.5	1.37	-.36	2.50	1.51	2.05	.61
		1.	2.04	-.20	1.03	.73	2.24	.67
		2.	.98	-.08	-1.23	-.16	.98	.30
		4.	-1.67	-.61	-4.79	-1.33	-2.07	-.62
	.25	.25	.14	-.97	1.04	1.30	.13	.04
		.5	1.12	-.55	2.51	1.67	.87	.26
		1.	2.42	.18	2.19	1.27	2.30	.69
		2.	2.16	.36	-.11	.30	2.44	.73
		4.	-.37	-.26	-3.94	-1.02	-.24	-.07
	.35	.25	.18	-1.02	.60	1.49	.06	.02
		.5	1.02	-.66	2.35	1.93	.53	.16
	1.	2.89	.26	3.36	1.88	1.90	.57	
	1.5	3.51	.62	2.58	1.41	--	--	
	2.	3.46	.70	1.44	.93	2.91	.87	

\* All stresses are divided by S.  $S = PD/2T$  for nozzles in cylinders,  
 $S = PD/4T$  for nozzles in spheres.

TABLE 3. (Continued)

(2 of 4)

$\frac{D}{T}$	$\frac{d}{D}$	$\frac{s}{S}$	Nozzles in Cylinder				Nozzles in Sphere		
			$\phi = 0$		$\phi = \pi/2$		$\sigma_{bx}$	$\sigma_{by}$	
			$\sigma_{bx}$	$\sigma_{by}$	$\sigma_{bx}$	$\sigma_{by}$			
25	.025	.25	1.98	.03	2.53	1.38	2.78	.84	
		.5	2.54	.44	1.38	.73	2.77	.83	
		1.	2.39	.55	.03	.17	2.12	.64	
	.05	.25	1.93	-.04	2.50	1.36	2.22	.67	
		.5	2.62	.46	1.48	.77	2.80	.84	
		1.	2.54	.59	.12	.20	2.34	.70	
		2.	1.35	.32	-1.79	-.46	.84	.25	
		4.	-1.57	-.51	-5.07	-1.48	-2.26	-.68	
		.10	.25	1.65	-.15	2.30	1.33	1.13	.34
			.5	2.91	.51	1.90	.96	2.66	.80
	1.		3.07	.73	.55	.36	3.03	.91	
	2.		1.94	.49	-1.47	-.34	1.72	.52	
	4.		-1.00	-.35	-4.87	-1.41	-1.44	-.43	
	.25	.25	1.08	-.44	1.21	1.55	.23	.07	
		.5	3.35	.53	3.00	1.60	1.33	.40	
		1.	5.82	1.48	3.28	1.38	3.61	1.08	
		2.	5.75	1.59	.66	.41	4.51	1.35	
		4.	2.47	.64	-3.17	-.88	1.94	.58	
	50	.01	.25	2.89	.55	1.75	.84	3.12	.94
			.5	3.12	.77	.79	.40	2.84	.85
1.			2.69	.73	-.31	-.01	2.10	.63	
.025		.25	2.65	.54	1.80	.86	2.98	.89	
		.5	3.18	.79	.85	.42	2.92	.88	
		1.	2.78	.75	-.26	.00	2.73	.67	
		2.	1.40	.38	-1.98	-.56	.69	.21	
		4.	-1.61	-.52	-5.12	-1.54	-2.41	-.72	

TABLE 3. (Continued)

(3 of 4)

$\frac{D}{T}$	$\frac{d}{D}$	$\frac{s}{S}$	Nozzles in Cylinder				Nozzles in Sphere	
			$\phi = 0$		$\phi = \pi/2$		$\sigma_{bx}$	$\sigma_{by}$
			$\sigma_{bx}$	$\sigma_{by}$	$\sigma_{bx}$	$\sigma_{by}$		
50	.05	.25	2.93	.54	1.99	.93	2.54	.76
		.5	3.45	.86	1.11	.51	3.75	.97
		1.	3.10	.84	-.08	.06	2.74	.82
		2.	.73	.47	-1.86	-.52	1.18	.35
	.10	4.	-1.30	-.41	-5.12	-1.51	-1.98	-.59
		.25	1.74	.42	2.18	1.09	1.44	.43
		.5	4.21	1.05	1.96	.82	3.47	1.04
		1.	4.13	1.13	.74	.35	4.13	1.24
	.15	2.	2.75	.77	-1.24	-.31	2.76	.83
		4.	-.33	-.12	-4.65	-1.36	-.53	-.16
		.25	2.46	.29	2.11	1.23	.84	.25
		.5	5.08	1.28	3.12	1.25	2.98	.89
100	.01	1.	6.13	1.71	1.85	.72	5.05	1.52
		.25	3.49	.89	1.20	.52	3.20	.96
		.5	3.47	.96	.48	.22	2.88	.86
	.025	1.	2.87	.82	.47	.10	2.13	.64
		.250	3.61	.91	1.36	.58	3.28	.98
		.5	3.65	1.01	.61	.27	3.18	.95
	.05	1.	3.07	.88	-.38	-.07	2.44	.73
		2.	1.60	.46	-2.04	-.59	.86	.26
		4.	-1.47	-.44	-5.13	-1.56	-2.26	-.68
	.05	.25	4.00	1.02	1.83	.74	3.10	.93
		.5	4.29	1.19	1.12	.43	4.03	1.21
		1.	3.68	1.06	.02	.05	3.47	1.04
2.		2.20	.63	-1.76	-.50	1.80	.54	
4.		-.91	-.28	-4.01	-1.49	-1.45	-.43	



TABLE 3. (Continued)

(4 of 4)

$\frac{D}{T}$	$\frac{d}{D}$	$\frac{s}{S}$	Nozzles in Cylinder				Nozzles in Sphere		
			$\phi = 0$		$\phi = \pi/2$		$\sigma_{bx}$	$\sigma_{by}$	
			$\sigma_{bx}$	$\sigma_{by}$	$\sigma_{bx}$	$\sigma_{by}$			
100 ↓ ↓ ↓ ↓ ↓ ↓ ↓ ↓ ↓ ↓ ↓ ↓ ↓ ↓ ↓	.10 ↓ ↓ ↓ ↓	.25	4.31	1.05	2.73	1.11	1.94	.58	
		.5	6.55	1.84	2.57	.93	4.72	1.42	
		1.	6.38	1.85	1.15	.43	5.85	1.76	
		2.	4.40	1.28	-.69	-.18	4.42	1.33	
		4.	1.10	.26	-3.96	-1.22	.93	.28	
	250 ↓ ↓ ↓ ↓ ↓ ↓ ↓ ↓ ↓ ↓ ↓ ↓ ↓ ↓ ↓	.01 ↓ ↓ ↓ ↓	.25	3.97	1.13	.86	.32	3.36	1.01
			.5	3.73	1.09	.30	.12	3.00	.90
			1.	3.02	.89	-.55	-.15	2.22	.67
			2.	1.49	.44	-2.18	-.62	.66	.20
			4.	-1.60	-.44	-5.24	-1.60	-2.44	-.73
		.025 ↓ ↓ ↓ ↓	.25	4.50	1.28	1.27	.46	4.06	1.22
			.5	4.26	1.24	.66	.24	3.91	1.17
			1.	3.50	1.04	-.29	-.07	3.04	.91
			2.	1.96	.51	-1.98	-.57	1.36	.41
			4.	-1.14	-.35	-5.13	-1.53	-1.84	-.55
.05 ↓ ↓ ↓ ↓ ↓ ↓ ↓ ↓ ↓	.0625 ↓ ↓ ↓ ↓	.25	1.27	.03	.92	.69	—	—	
		.125	3.61	.90	2.31	.90	—	—	
		.25	5.71	1.62	2.54	.86	4.43	1.33	
		.5	5.94	1.73	1.76	.56	5.94	1.78	
		1.	4.95	1.46	.58	.20	5.29	1.59	
	.07 ↓ ↓ ↓ ↓	.25 ↓ ↓ ↓ ↓	2.	3.17	.94	-1.24	-.36	3.36	1.01
			4.	-.03	-.02	-4.60	-1.38	-.12	-.03
			.25	7.52	2.16	3.22	1.08	3.75	1.12
			.5	9.57	2.82	1.55	.52	7.13	2.14
			1.	8.19	2.43	.23	.10	7.61	2.28
2.	5.31	1.58	-1.03	-.29	5.68	1.70			

COMPARISON OF ERINGEN'S THEORY  
WITH TEST DATA

General Comments

The number of test models suitable for comparison with Eringen's theory is quite limited. For valid comparisons, the value of  $B\rho_0$  of the test model should be less than one-half and the test model should consist of a uniform wall cylindrical nozzle with axis normal to the surface of a uniform wall cylindrical shell. There should be no inward protuberance of the nozzle and the fillet weld or other local reinforcement should be very small. The values of  $D/T$  and  $d/t$  should be larger than 10. Finally, in order to eliminate stresses due to out-of-roundness and to have uniform wall thicknesses, ideally the model should be machined to close tolerances all over.

There are no test models known to the writers which meet all these requirements, however, 7 steel test models and 8 photoelastic test models have been selected as representing the best available test data for comparison with the theory. The dimensional parameters of these models are listed in Table 4 along with the maximum measured stress and maximum theoretical stress. Comparisons are discussed in detail in the following.

Stresses were calculated at the nozzle-cylinder juncture and away from the juncture on the cylinder at  $\rho' = 0.3, 0.6, 1.0,$  and  $2.0$  times  $\sqrt{RT}$ ; away from the juncture on the nozzle at  $x = .3, .6, 1.0,$  and  $2.0$  times  $\sqrt{rt}$ . Stresses were calculated at  $\emptyset = 0, \pi/8, \pi/4, 3\pi/8,$  and  $\pi/2$ , however, the test data gives stresses only at  $\emptyset = 0$  and  $\emptyset = \pi/2$  or at  $\emptyset = 0$  only. Comparisons of test data with theory are given as functions of  $\rho'/\sqrt{RT}$  or  $x/\sqrt{rt}$  and  $\emptyset$  ( $\rho' \equiv \rho - \rho_0$ ).

TABLE 4. SUMMARY OF TEST MODELS USED IN COMPARISONS  
WITH ERINGEN'S THEORY

Model Iden.	Ref.	$\frac{D}{T}$	$\frac{d}{D}$	$\frac{s}{S}$	$\frac{d}{t}$	$\frac{t}{T}$	$\beta \rho_0$	Inside Corner Stress		$\frac{K_t}{K_e}$
								Test $\frac{K_e}{K_e}$	Theory $\frac{K_t}{K_t}$	
E	(18)	93.	.12	.30	27.8	.41	.544	---	---	---
Att.2	(19)	78.	.13	.29	22.6	.45	.521	---	---	---
7 & 8	(20, 21)	29.5	.043	.34	9.90	.13	.107	2.64	2.45	.93
11	(22)	19.	.058	.62	11.7	.094	.114	2.57**	2.47	.96
15	(20, 21)	11.9	.16	1.13	13.5	.14	.252	2.70	2.87	1.06
K	(23)	9.35	.203	1.05	9.80	.19	.282	3.3	2.98	.90
M	(23)	9.35	.294	.99	9.26	.30	.408	3.3	3.42	1.04
C-1A	(24)	13.0	.05	1.04	13.5	.048	.0815	2.45	2.45	1.00
C-2A		13.1	.13	.97	12.6	.13	.213	2.80	2.72	.97
C-3A		13.0	.20	1.01	13.0	.20	.326	3.0	3.15	1.05
E1		13.1	.29	.58	7.53	.50	.473	3.32	2.94	.89
E2		13.1	.29	.58	7.53	.50	.473	2.90	2.94	1.01
E3		13.1	.29	.58	7.53	.50	.473	3.28	2.94	.90
E7		13.1	.29	.58	7.53	.50	.473	3.36	2.94	.88
C-3C		6.50	.18	2.01	13.1	.091	.213	3.09	2.72	.88

\* Stresses were not measured at the nozzle-shell juncture nor at the inside corner, however, stresses were measured away from the juncture. Test data are compared herein with Eringen's results at corresponding distances from the nozzle-shell juncture. These two models were included because they give some test data check with Eringen's analysis for large values of  $D/T$ .

\*\* Average of four tests.

It is well known that shell theory gives anomalous results when applied to structures with discontinuities in wall thickness or curvature. The theory involves both of these kinds of discontinuities at the nozzle-cylinder juncture. Figure 9 illustrates the force transfers assumed in shell theory in the  $\rho$ -direction on the cylinder, x-direction on the nozzle. If it is assumed that the cylinder extends to the hole, the theory gives  $\sigma_{\rho}$ -stresses on the face of the hole; an obviously fictitious stress since  $\sigma_{\rho}$  can only be -P on this surface. If it is assumed that the nozzle extends to the inside of the cylinder, the thickness of the nozzle from  $x = 0$  to  $x = T$  becomes indeterminate. In the following comparisons, it is assumed that nozzle extends to the outside surface of the cylinder and the cylinder extends to the hole. This is analogous to the assumption made in comparing test data with theory for nozzles in spherical shells, Phase Report No. 2. However, for two of the photoelastic test models, a more detailed and realistic comparison of theory and test data in the neighborhood of the nozzle-cylinder juncture is presented.

#### Steel Test Models

Cranch<sup>(19)</sup> Test Data, Attachment No. 2

The model consisted of a 48-inch-ID cylinder with 0.625-inch wall thickness into which was welded a 6-inch standard weight pipe, 6.625-inch-OD x 0.280-inch wall. The nozzle was flush with the ID of the cylinder and the external fillet weld appears to have a leg length of around 1/4 inch to 3/8 inch.

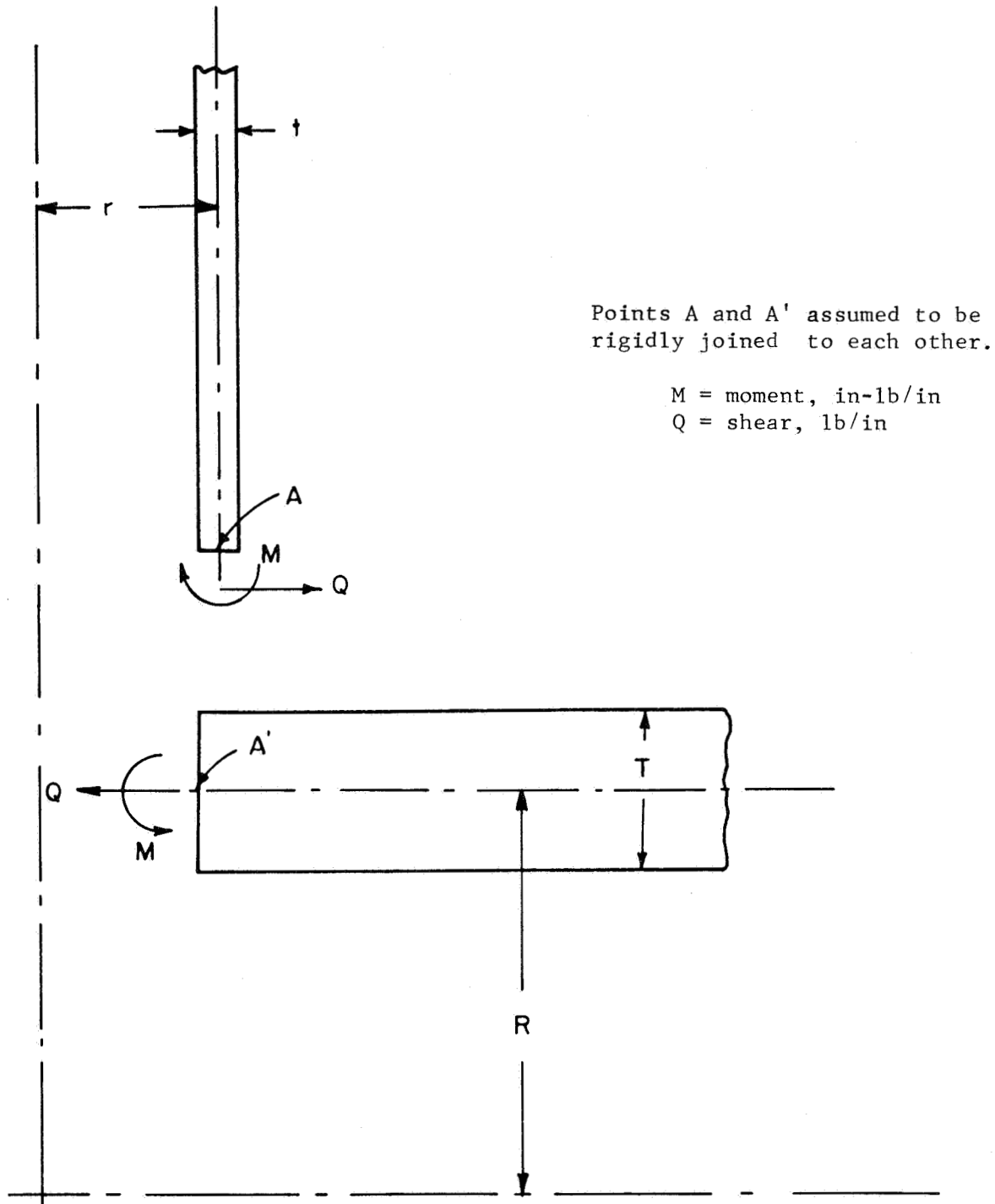


FIGURE 9. ILLUSTRATION OF FORCE TRANSFERS ASSUMED IN SHELL THEORY AT  $\phi = 0$

Table 5 shows stresses calculated from Eringen's analysis, along with the stresses determined by use of strain gages. Cranch measured stresses only at  $\varphi = 0$  and  $\varphi = \pi/2$ . In general, the agreement between theory and test data is good. In comparing theory and test data in Table 5, the following points should be considered:

- (1) The presence of the fillet weld might be expected to reduce stresses at the juncture. The maximum experimental stress of 2.2 versus 2.86 theoretical may be due to this effect.
- (2) The stresses given by Cranch at the juncture,  $\rho = \rho_0$ , were extrapolated from strain gage data along the cylinder. The extrapolation may involve significant errors.
- (3) The stresses away from the juncture were picked off of Cranch's Figures 2.013 and 2.014 by the writers. They are, at best, accurate only to  $\pm 30$  percent.
- (4) The test model possibly had thickness variations in the nozzle wall of  $\pm 10$  percent and was possibly out-of-round to some extent.
- (5) Considering the maximum stress readings given by Cranch, along with typical strain gage random errors, one could assume that Cranch's maximum stress values in Table 5 should be accurate to within  $\pm 10$  percent, or an error range of  $\sim \pm 0.2 \sigma/S$ . However, the low stress readings could have about the same errors so that a measured stress  $\sigma/S = 0.2$  should also have a  $\pm 0.2$  to indicate its order of accuracy.

TABLE 5. COMPARISON OF ERINGEN THEORY WITH CRANCH TEST DATA, ATTACHMENT 2, STRESSES IN CYLINDER

$\frac{\rho'}{RT}$	$\varphi$	Data Source	Membrane	Bending	Membrane	Bending
			$\frac{\sigma_{\varphi}}{S}$	$\frac{\sigma_{\varphi}}{S}$	$\frac{\sigma_{\rho}}{S}$	$\frac{\sigma_{\rho}}{S}$
0.0	0	Test*	2.2	0.2	0.6	0.9
	0	Theory	2.859	0.507	0.218	0.865
	$\pi/2$	↓	2.570	0.477	0.197	0.795
	$\pi/4$		1.763	0.428	0.157	0.655
	$3\pi/8$		0.715	0.411	0.140	0.574
	$\pi/2$		0.184	0.402	0.144	0.560
	$\pi/2$		Test*	0.8	0.6	0.2
0.3	0	Test	1.6	0.2	0.6	0.3
	0	Theory	1.811	0.267	0.482	0.339
	$\pi/8$	↓	1.657	0.262	0.480	0.343
	$\pi/4$		1.244	0.288	0.472	0.358
	$3\pi/8$		0.754	0.367	0.448	0.380
	$\pi/2$		0.526	0.413	0.432	0.392
	$\pi/2$		Test	0.8	0.5	0.5
0.6	0	Test	1.2	0.0	0.6	0.0
	0	Theory	1.388	0.164	0.534	0.168
	$\pi/8$	↓	1.289	0.167	0.550	0.186
	$\pi/4$		1.024	0.214	0.586	0.230
	$3\pi/8$		0.720	0.317	0.615	0.276
	$\pi/2$		0.581	0.375	0.623	0.297
	$\pi/2$		Test	0.7	0.4	0.8
1.0	0	Test	1.1	0.0	0.6	-0.2
	0	Theory	1.124	0.103	0.539	0.088
	$\pi/8$	↓	1.058	0.110	0.570	0.109
	$\pi/4$		0.880	0.162	0.648	0.156
	$3\pi/8$		0.673	0.266	0.731	0.203
	$\pi/2$		0.578	0.324	0.766	0.224
	$\pi/2$		Test	0.7	0.3	0.9
2.0	0	Test	0.9	0.0	0.6	0.0
	0	Theory	0.875	0.0545	0.514	0.033
	$\pi/8$	↓	0.839	0.0635	0.562	0.059
	$\pi/4$		0.736	0.112	0.689	0.107
	$3\pi/8$		0.605	0.197	0.835	0.138
	$\pi/2$		0.542	0.243	0.902	0.148
	$\pi/2$		Test	0.5	0.0	1.0
$\infty$	0	{ Membrane }	1.000	0.0	0.500	0.0
	$\pi/2$	{ Theory }	0.500	0.0	1.000	0.0

\* Extrapolated data.

Table 6 shows theoretical stresses in the nozzle of Cranch's "Attachment 2". The theory predicts that maximum stresses occur in the nozzle; specifically,  $\sigma_{x_0}/S = 4.604$  as compared to  $\sigma_{\phi_i}/S = 3.365$ . However, the only significant strain gage on the nozzle was placed about 5/8 inch to 3/4 inch from the juncture with the cylinder. The stress determined from this gage is not given in Cranch's paper. For this model,  $\sqrt{rt} = .945$ ; hence, the nearest gage was about 0.6 to 0.8 times  $\sqrt{rt}$  away from the juncture. As can be seen in Table 6 for  $x/\sqrt{rt} = 0.6$ , the stresses measured at this gage would not be expected to be as high as on the cylinder. If a series of strain gages had been placed along the nozzle and the results extrapolated to the juncture, possibly the highest stress area would have been found to be in the nozzle.



TABLE 6. CALCULATED STRESS INDICES (ERINGEN THEORY)  
IN THE NOZZLE; CRANCH ATTACHMENT 2

$\frac{x}{\sqrt{rt}}$	$\varphi$	$\frac{\sigma_{nx}}{S}$	$\frac{\sigma_{bx}}{S}$	$\frac{\sigma_{ny}}{S}$	$\frac{\sigma_{by}}{S}$	$\frac{\sigma_x}{S}$		$\frac{\sigma_y}{S}$	
						Outside	Inside	Outside	Inside
0	0	0.288	-4.316	2.208	-1.249	4.604	-4.028	0.959	3.457
	$\pi/8$	0.264	-3.959	1.904	-1.151	4.223	-3.696	0.752	3.055
	$\pi/4$	0.151	-3.260	1.393	-0.971	3.411	-3.108	0.422	2.364
	$3\pi/8$	0.0269	-2.860	1.366	-0.894	2.887	-2.883	0.471	2.260
	$\pi/2$	-0.0097	-2.804	1.545	-0.901	2.794	-2.814	0.644	2.446
0.3	0	0.350	-1.034	1.996	-0.269	1.384	-0.683	1.726	2.265
	$\pi/8$	0.285	-0.997	1.769	-0.267	1.282	-0.711	1.502	2.036
	$\pi/4$	0.114	-0.881	1.373	-0.258	0.995	-0.766	1.116	1.631
	$3\pi/8$	0.0055	-0.715	1.249	-0.246	0.720	-0.709	1.003	1.495
	$\pi/2$	0.0020	-0.628	1.293	-0.242	0.630	-0.626	1.051	1.535
0.6	0	0.380	0.477	1.317	0.184	-0.097	0.857	1.502	1.133
	$\pi/8$	0.295	0.375	1.188	0.144	-0.080	0.670	1.331	1.045
	$\pi/4$	0.102	0.216	0.954	0.0683	-0.114	0.317	1.022	0.886
	$3\pi/8$	-0.0046	0.197	0.833	0.0282	-0.202	0.193	0.861	0.805
	$\pi/2$	-0.0020	0.236	0.817	0.0221	-0.239	0.234	0.839	0.795
1.0	0	0.384	0.814	0.573	0.288	-0.432	1.199	0.862	0.285
	$\pi/8$	0.295	0.694	0.539	0.239	-0.399	0.989	0.778	0.300
	$\pi/4$	0.104	0.472	0.473	0.142	-0.369	0.576	0.615	0.330
	$3\pi/8$	-0.0045	0.351	0.412	0.075	-0.356	0.347	0.489	0.338
	$\pi/2$	-0.0011	0.332	0.383	0.054	-0.343	0.322	0.438	0.329
2.0	0	0.345	0.0600	0.212	0.056	0.056	0.285	0.405	0.269
	$\pi/8$	0.275	0.051	0.226	0.042	0.042	0.224	0.326	0.268
	$\pi/4$	0.125	0.022	0.252	0.0068	0.007	0.104	0.147	0.259
	$3\pi/8$	0.0156	-0.022	0.258	-0.033	-0.033	0.038	-0.007	0.225
	$\pi/2$	-0.0145	-0.047	0.253	-0.052	-0.052	0.032	-0.061	0.201
$\infty$	any	0.145	0	0.290	0	0.145	0.145	0.290	0.290

Pickett & Grigory<sup>(22)</sup> Test Data, Nozzle No. 11

The model consisted of a 36-inch-ID cylinder with 2-inch wall thickness into which was welded a 2-inch-ID x 0.188-inch wall nozzle. The external fillet weld appeared to have a leg length of about 0.3-inch.

Table 7 shows stresses calculated from Eringen's analysis, along with stresses determined by use of strain gages. In this model,\* the maximum stress occurred at the inside corner;  $\sigma_{\phi_i}/S = 2.76$  as compared to  $\sigma_{\phi_i}/S = 2.47$  theoretical.

This model included a pair of strain gages on the nozzle placed about 1/2 inch from the outer surface of the cylinder. In terms of the shell length parameter  $\sqrt{rt}$ , the gages were fairly remote from the nozzle-cylinder juncture. The highest measured stress in the nozzle was  $\sigma_{yc}/S = 1.79$ ; the theoretical stress at about this point and surface is  $\sigma_{yi}/S = 1.44$ . In general, it appears that the fillet weld does two things:

- (1) It provides a relatively flexible transition between nozzle and cylinder, thus reducing maximum stresses significantly.
- (2) It tends to shift the moments and forces up along the x-axis.

On the other hand, there is probably a fairly high stress concentration at the toe of the fillet weld where it joins the branch pipe.

Nozzle No. 11 was incorporated in 7 different pressure vessels subjected to cyclic pressure tests at Southwest Research Institute. Fatigue cracks initiated in the nozzle-to-vessel weld on vessels 1 and 2; the location, direction or initiating surface are not reported. Fatigue cracks initiated at the inside corner (point of maximum measured stress)

---

\* Nozzle No. 11 in Vessel No. 1. The average value of  $\sigma_{\phi_i}/S$  was 2.57, See Table 16.

TABLE 7. COMPARISON OF ERINGEN THEORY WITH PICKETT & GRIGORY TEST DATA, NOZZLE NO. 11

$\frac{\rho'}{\sqrt{RT}}$	$\emptyset$	Source	$\frac{\sigma_{\emptyset o}}{S}$	$\frac{\sigma_{\emptyset i}}{S}$	$\frac{\sigma_{\rho o}}{S}$	$\frac{\sigma_{\rho i}}{S}$
Cylinder						
0.0	0	Theory	2.50	2.47	.068	.026
0.0	↓	Test	--	2.76	--	.27
0.083	↓	Test	.89	1.51	.48	.53
0.25	↓	Test	--	1.38	--	.60
0.3	↓	Theory	1.15	1.14	.50	.50
0.0	$\pi/2$	Theory	.82	.25	.03	.00
0.0	↓	Test	--	-.14	--	.39
0.083	↓	Test	.70	.46	.76	.70
0.25	↓	Test	--	.53	--	.70
0.3	↓	Theory	.63	.51	.82	.80
$\frac{x}{\sqrt{rt}}$	Nozzle		$\frac{\sigma_{x o}}{S}$	$\frac{\sigma_{x i}}{S}$	$\frac{\sigma_{y o}}{S}$	$\frac{\sigma_{y i}}{S}$
0	0	Theory	2.41	-2.36	2.84	2.12
.3	↓	↓	.23	.05	1.69	2.32
.6	↓	↓	-.57	1.00	.76	1.98
1.0	↓	↓	-.55	1.05	.15	1.44
1.1	↓	Test	.31	.02	.70	1.79
0	$\pi/2$	Theory	1.96	-.78	1.48	-.05
.3	↓	↓	1.05	-.11	1.31	.26
.6	↓	↓	.63	.18	1.16	.26
1.0	↓	↓	.48	.25	1.06	.17
1.1	↓	Test	.20	-.16	.70	.38

on vessels 4, 6 and 7. No cracks were observed at nozzle No. 11 in vessels 3 and 5. Leak type failures (cracks penetrated through wall) occurred at nozzle No. 11 in vessels 1, 4 and 7. The other observed cracks did not penetrate through the wall prior to termination of the fatigue test for other causes. The failures of nozzle 11 in vessels 1 and 2 presumably were caused by high stresses in the nozzles, however, no explanation is given as to why weld failures occurred in vessels 1 and 2 but not in subsequent vessels. Possibly, the welding technique and/or weld contour details were improved in the later vessels.

From a fatigue standpoint, it might be noted that the theoretical stresses in the nozzle at the juncture in the x-direction are almost pure bending. A fatigue crack started by the  $\sigma_x$ -stresses would encounter a rapidly decreasing stress as it propagated into the nozzle wall, hence might not propagate very much. In the cylinder, however, the  $\sigma_\phi$ -stress is almost pure membrane and is high over a large area of metal, hence a fatigue crack would be expected to propagate through the wall relatively easily.

Mehring & Cooper<sup>(18)</sup>, Appendage E

The model consisted of 34.47-inch-ID cylinder with 3/8 inch wall thickness into which was welded a 4.5-inch-OD x .156-inch wall thickness nozzle. The external fillet weld is not clearly indicated but may have had leg lengths of about 3/8 inch.

Table 8 shows stresses calculated from Eringen's analysis, along with stresses determined by strain gages. Gages were not placed at the inside corner; the nearest gage to the bore was about 1.3-inch from the bore, corresponding to about  $0.5 \sqrt{RT}$ . No stresses are given for the nozzle.

The maximum stress in the cylinder given by the theory is  $\sigma_{\theta o}/S = 3.55$ . The (apparently) relatively large fillet weld might have reduced the maximum stresses significantly. As shown in Table 8, the maximum measured stress  $\sigma_{\theta o}/S = 1.4$ , is in reasonable agreement with the theoretical stress  $\sigma_{\theta o}$  in the region of the strain gage. The principal discrepancy between test and theory appears to be  $\sigma_{\theta i}$  at  $\theta = 0$ , where  $\sigma_{\theta i}/S$  would theoretically be around 1.2 whereas the test data gives  $\sigma_{\theta i}/S \cong 0$ ; and at  $\sigma_{\rho i}$  at  $\theta = \pi/2$ , where  $\sigma_{\rho i}/S$  would theoretically be around 0.3 whereas the test data gives  $\sigma_{\rho i}/S \cong 1.3$ . Otherwise the theory and test are in reasonable agreement.

No measurements of stresses in the nozzle are given. The theoretical stresses in the nozzle of this model are quite high;  $\sigma_{x o}/S = 5.41$  at  $\theta = 0$ ,  $x = 0$ . As in other models, the fillet might have significantly reduced the actual stress since the fillet leg length apparently is around 0.5 to 0.7 times  $\sqrt{rt}$ .

TABLE 8. COMPARISON OF ERINGEN THEORY WITH MEHRINGER & COOPER  
APPENDAGE E EXPERIMENTAL DATA, STRESSES IN CYLINDER

$\frac{\rho'}{RT}$	$\theta$	Data Source	$\frac{\sigma_{\theta o}}{S}$	$\frac{\sigma_{\theta i}}{S}$	$\frac{\sigma_{\rho o}}{S}$	$\frac{\sigma_{\rho i}}{S}$
0.0	0	Theory	3.55	2.28	1.08	- .67
0.3	↓	Theory	1.68	1.49	.82	.12
0.5		Test	~1.4	~ 0	~1.0	~ .25
0.6		Theory	1.61	1.17	.71	.35
0.0		$\pi/2$	Theory	.68	- .20	.63
0.3	↓	Theory	1.00	.10	.80	.03
0.5		Test	~1.0	~ .3	~1.3	~1.3
0.6		Theory	1.01	.18	.91	.31

Berman & Pai (20, 21), Nozzles 7 and 8

The model consisted of a 48-inch-ID cylinder with 1.687-inch wall thickness into which were welded 2-inch Sch 80 pipes, 2.375-inch-OD x 0.218-inch wall. Nozzles 7 and 8 were identical in-so-far as the theory is concerned; nozzle 7 was "set-in" for welding whereas nozzle 8 was "set-on" for welding. The fillet weld leg lengths were about 3/8 inch. The nozzles were first tested and results reported in Reference (20); later additional tests were run and results reported on Reference (21).

Table 9 shows stresses calculated from Eringen's analysis, along with stresses determined by use of strain gages. Measurements were made only at  $\theta = 0$ . Maximum measured stress occurred at the inside corner of the opening,  $\sigma_{\theta_i}/S = 2.64$  as compared to  $\sigma_{\theta_i}/S = 2.45$  by theory.

In the second test series, gages were placed on the nozzle about 1-inch from the surface of the cylinder or roughly 2 times the  $\sqrt{rt}$  from the surface. Considering the possible influence of the fillet weld, the theory and test data are in reasonable agreement.

TABLE 9. COMPARISON OF ERINGEN THEORY WITH BERMAN & PAI  
TEST DATA (at  $\theta = 0$ ), NOZZLES 7 AND 8

$\frac{p'}{\gamma RT}$	Source	Gage No.	Model No.	$\frac{\sigma_{\theta o}}{S}$	$\frac{\sigma_{\theta i}}{S}$	$\frac{\sigma_{\rho o}}{S}$	$\frac{\sigma_{\rho i}}{S}$
0.0	Theory	--	--		2.45		.03
↓	Test	1	7		2.64		.28
		1	8		2.64		.30
		2	7		2.42		-.06
		2	8		2.34		.13
		3a	7		2.30		-.17
		3a	8		2.25		.12
		3	7		2.27		.63
		3	8		2.03		.59
		4	7		1.32		.50
		4	8		1.32		.59
0.15							
0.15							
0.31							
0.31	Test	5	8		1.13		.54
0.3	Theory	--	--		1.13		.50
0.0	Theory	--	--	2.38		.12	
↓	Test	2a	7	1.93		.10*	
		2a	8	2.08		.19*	
		5a	7	.65		.26	
0.12							
0.3	Theory	--	--	1.13		.51	
$\frac{x}{\sqrt{rt}}$	(Nozzle)			$\frac{\sigma_{x o}}{S}$	$\frac{\sigma_{x i}}{S}$	$\frac{\sigma_{y o}}{S}$	$\frac{\sigma_{y i}}{S}$
0	Theory	--	--	2.46	-2.61	2.72	2.02
2	Theory	--	--	.09	.25	-.06	.68
2	Test	4a, 1a	7	.13	.41	.23	.79
2	Test	4a, 1a	8	.09	.51	.11	.82
$\infty$	Theory	--	--	.14	.14	.29	.29

\* Tangential, inside of bore; shell theory does not give this stress.



Berman & Pai<sup>(20, 21)</sup>, Nozzle 15

The model consisted of a 45.5-inch-ID cylinder with 4.187-inch wall thickness with an 8-inch Sch 100 pipe as a nozzle, 8.625-inch-OD x 0.593-inch wall. The fillet weld leg lengths were about 0.8-inch.

Table 10 shows stresses calculated from Eringen's analysis, along with stresses determined by use of strain gages. Measurements were made only at  $\theta = 0$ . Maximum measured stress occurred at the inside corner of the opening,  $\sigma_{\theta i}/S = 2.70$  as compared to  $\sigma_{\theta i}/S = 2.87$  by theory ( $\sigma_{\theta o}/S = 2.68$  by theory.)

No measurements of stresses in the nozzle are given. The theoretical maximum stress in the nozzle is  $\sigma_{yi}/S = 3.20$ . The fillet weld leg length is about  $0.5 \sqrt{rt}$  hence the actual maximum stress in the nozzle presumably was significantly less than  $3.20S$ .

TABLE 10. COMPARISON OF ERINGEN THEORY WITH BERMAN & PAI TEST DATA (at  $\theta = 0$ ), NOZZLE 15

$\frac{\rho'}{RT}$	Source	Gage No.	$\frac{\sigma_{\theta i}}{S}$	$\frac{\sigma_{\rho i}}{S}$
0.0	Theory	--	2.87	.015
0.0	Test	1	2.70	.05 *
0.0	Test	2	2.67	-.46 *
0.0	Test	2a	2.48	-.53 *
0.0	Test	3	2.62	.38
0.3	Theory	--	1.49	.53
0.4	Test	4	1.60	.68
0.6	Theory	--	1.23	.56

\* Tangential, inside of bore, shell theory does not give this stress.

Wells, et al, (23) Nozzles K and M

The models consisted of a 40.5" inside diameter cylinder with 4.845" wall thickness. The branch of model K consisted of an 8.25" inside diameter cylinder with 0.938" wall thickness. The branch of model M consisted of a 11.875" inside diameter cylinder with 1.438" wall thickness.

The top portions of Tables 11 and 12 give comparisons of calculated and measured stresses in the cylinder. Agreement between theory and test are generally fairly good. The largest discrepancy appears to be in  $\sigma_{\theta i}$  at  $\rho' = 0$ ,  $\theta = \pi/2$ , where a negative stress is predicted by theory.

The bottom portions of Tables 11 and 12 give comparisons of calculated and measured stresses in the nozzle. The fillet weld leg lengths were about  $0.75 \sqrt{rt}$ , hence the high calculated stresses would not be expected to occur, except where the high calculated stress persists for some distance from the juncture; e.g.,  $\sigma_{yi}$  at  $\theta = 0$ . The strain gages used in the tests were large compared to the length  $\sqrt{rt}$ , hence only average stresses would be measured. About all that can be said is that the measured stresses in the nozzle follow the trends predicted by the theory.

TABLE 11. COMPARISON OF ERINGEN THEORY WITH WELLS, LANE AND ROSE TEST DATA, NOZZLE K

$\frac{\rho'}{\sqrt{rt}}$	$\phi$	Source	$\sigma_{\phi o}/S$	$\sigma_{\phi i}/S$	$\sigma_{\rho o}/S$	$\sigma_{\rho i}/S$
<u>Cylinder</u>						
0.0	0	Theory	2.54	2.98	.18	.02
		Test	--	3.3	--	~0
0.3		Theory	1.44	1.59	.43	.53
		Test	1.2	2.1	.6	.8
0.6		Theory	1.20	1.27	.48	.56
		Test	.8	1.7	.4	1.
0.0	$\pi/2$	Theory	1.55	-.45	.12	.00
		Test	--	.4	--	--
0.3		Theory	1.05	.23	.63	.53
		Test	1.0	.9	.8	.8
0.6		Theory	.84	.36	.85	.74
		Test	.7	.7	.6	1.0
<u>Nozzle</u>						
$\frac{x}{\sqrt{rt}}$	$\phi$	Source	$\sigma_{x o}/S$	$\sigma_{x i}/S$	$\sigma_{y o}/S$	$\sigma_{y i}/S$
0	0	Theory	2.36	-1.90	2.93	2.65
		Test	--	.5	--	2.6
.3		Theory	.43	.33	1.90	2.81
		Test	--	.5	--	2.5
.6		Theory	-.30	1.22	1.04	2.49
		Test	.8	.6	1.1	2.4
1.0		Theory	-.26	1.26	.48	1.96
		Test	.4	1.3	.8	2.2
0	$\pi/2$	Theory	2.46	-.81	1.93	-.10
		Test	--	.3	--	1.0
.3		Theory	1.53	-.15	1.92	.33
		Test	--	.2	--	1.1
.6		Theory	1.00	.22	1.81	.44
		Test	1.0	.2	1.2	1.2
1.0		Theory	.73	.40	1.67	.44
		Test	.65	.3	1.0	1.1

TABLE 12. COMPARISON OF ERINGEN THEORY WITH WELLS, LANE AND ROSE TEST DATA, NOZZLE M

$\frac{\rho'}{\sqrt{RT}}$	$\phi$	Source	$\sigma_{\phi o}/S$	$\sigma_{\phi i}/S$	$\sigma_{\rho o}/S$	$\sigma_{\rho i}/S$	
<u>Cylinder</u>							
0.0	0	Theory	2.44	3.42	.36	-.04	
		Test	--	3.3	--	~0	
0.3	↓	Theory	1.55	1.93	.51	.46	
		Test	--	2.2	--	.9	
0.6		Theory	1.26	1.47	.51	.55	
		Test	.9	1.8	.5	1.3	
0.0	$\pi/2$	Theory	1.76	-.86	.39	-.06	
		Test	--	.4	--	.0	
0.3	↓	Theory	1.36	-.09	.74	.35	
		Test	1.2	.5	1.3	.3	
0.6		Theory	1.09	.16	.88	.59	
		Test	1.0	.5	1.0	.6	
<u>Nozzle</u>							
$\frac{x}{\sqrt{rt}}$	$\phi$	Source	$\sigma_{x o}/S$	$\sigma_{x i}/S$	$\sigma_{y o}/S$	$\sigma_{y i}/S$	
0	0	Theory	2.61	-1.93	2.97	2.81	
		Test	--	.5	--	2.5	
.3	↓	Theory	.51	.46	1.82	2.93	
		Test	--	.6	--	2.5	
.6		Theory	-.27	1.37	.90	2.54	
		Test	--	.7	--	2.3	
1.0		Theory	-.21	1.35	.33	1.95	
		Test	.5	1.1	.8	2.2	
0		$\pi/2$	Theory	3.28	-1.96	2.76	-.30
			Test	--	.3	--	1.0
.3	↓	Theory	1.72	-.56	2.51	.28	
		Test	--	.2	--	1.0	
.6		Theory	.88	.16	2.13	.39	
		Test	--	.0	--	.9	
1.0		Theory	.51	.46	1.76	.33	
		Test	.5	.2	1.3	1.1	

Photoelastic Test Models

Test data for the photoelastic test models are presented by Taylor and Lind<sup>(24)</sup>. In this reference, stresses in the normal and tangential directions are given at  $\phi = 0$  and  $\phi = \pi/2$ . The  $\sigma_n$ -stresses correspond to  $\sigma_\phi$  (cylinder) or  $\sigma_y$  (nozzle) stresses of the theory. Except on the inner face of the opening of the cylinder,  $\sigma_t$ -stresses correspond to  $\sigma_\rho$  (cylinder) or  $\sigma_x$  (nozzle) stresses.

Stresses in the Cylinder

Table 13 gives comparisons of calculated\* and measured stresses on the cylinder. The maximum measured stress for all models was  $\sigma_n$  at the inside corner radius at  $\phi = 0$ . This is compared, in Table 13, with  $\sigma_{\phi i}$  at  $\rho'/\sqrt{RT} = 0.0$ ,  $\phi = 0$ . There are no comparable  $\sigma_{\phi o}$ ,  $\sigma_{\rho o}$ , or  $\sigma_{\rho i}$ -stresses from the test data. At  $\phi = \pi/2$ , the  $\sigma_t$  stress at the center of the inside corner radius is shown for comparison with the theoretical  $\sigma_{\phi i}$  at  $\rho'/\sqrt{RT} = 0.0$ ,  $\phi = \pi/2$ .

In general, the theoretical value of  $\sigma_{\phi i}$  at  $\rho'/\sqrt{RT} = 0$ ,  $\phi = 0$  is reasonably close to the maximum measured stress. The ratio of  $\sigma_{\phi i}$  at  $\rho = \rho_o$ ,  $\phi = 0$  to the maximum measured stress ranges from .88 to 1.05 with an average of 0.95. The stresses away from the juncture are generally in adequate agreement with the theory. The largest disagreement appears to be the normal stress at the inside corner at  $\phi = \pi/2$ . For all models

---

\* At present, Eringen's computer program is based on a Poisson's ratio of 0.3. All calculated results are based on this value, even though the Poisson's ratio of the photoelastic test models was probably about 0.5. It is believed that the Poisson's ratio effect is small for membrane stresses but may be significant for bending stresses.

except C-1A, the theory predicts a negative stress at this point. The test data, while trending toward a low stress at this point in the normal direction, does not give negative stresses.

TABLE 13. COMPARISON OF ERINGEN THEORY WITH TAYLOR AND LIND  
PHOTOELASTIC TEST DATA, STRESS IN CYLINDER  
(1 of 3)

Model No.	$\frac{\rho'}{\sqrt{RT}}$	$\phi$	Source	$\sigma_{\phi o}/S$	$\sigma_{\phi i}/S$	$\sigma_{\rho o}/S$	$\sigma_{\rho i}/S$	
C-1A ↓	0.0	0	Theory	2.55	2.45	.02	.01	
	0.0	↓	Test	--	2.45	--	--	
	0.3	↓	Theory	1.10	1.08	.51	.50	
	0.3	↓	Test	0.9	1.0	.5	.4	
	0.0	$\pi/2$	Theory	.36	.69	.00	.00	
	0.0	↓	Test	--	.7	--	--	
	0.3	↓	Theory	.57	.52	.88	.86	
	0.3	↓	Test	.5	.4	.9	.8	
	C-2A ↓	0.0	0	Theory	2.62	2.72	.10	.02
		0.0	↓	Test	--	2.80	--	--
		0.3	↓	Theory	1.36	1.38	.46	.51
		0.3	↓	Test	.9	1.4	.6	.5
0.6		↓	Theory	1.15	1.16	.48	.54	
0.6		↓	Test	.8	1.2	.6	.5	
0.0		$\pi/2$	Theory	1.23	-.16	.04	.00	
0.0		↓	Test	--	.4	--	--	
0.3		↓	Theory	.86	.38	.70	.62	
0.3		↓	Test	1.	.3	.8	.3	
0.6		↓	Theory	.70	.44	.86	.81	
0.6		↓	Test	.8	.3	.9	.7	
C-3A ↓	0.0	0	Theory	2.66	3.15	.21	-.01	
	0.0	↓	Test	--	3.0	--	--	
	0.3	↓	Theory	1.53	1.73	.41	.56	
	0.3	↓	Test	1.2	1.7	.6	.6	
	0.6	↓	Theory	1.25	1.34	.48	.57	
	0.6	↓	Test	.9	1.3	.4	.7	
	0.0	$\pi/2$	Theory	1.65	-.64	.12	-.01	
	0.0	↓	Test	--	.2	--	--	
	0.3	↓	Theory	1.16	.13	.64	.47	
	0.3	↓	Test	1.2	.3	.8	.3	
	0.6	↓	Theory	.94	.29	.83	.69	
	0.6	↓	Test	1.0	.4	.9	.7	
C-3C ↓	0.0	0	Theory	2.74	2.72	.03	.01	
	0.0	↓	Test	--	3.09	--	--	
	0.3	↓	Theory	1.38	1.39	.44	.51	
	0.3	↓	Test	.9	1.3	.5	.0	
	0.6	↓	Theory	1.16	1.16	.48	.54	
	0.6	↓	Test	.9	1.0	.6	.2	
	1.0	↓	Theory	1.08	1.07	.48	.54	
	1.0	↓	Test	.9	.9	.6	.3	



TABLE 13. (Continued)  
 (2 of 3)

Model No.	$\frac{\rho'}{\sqrt{RT}}$	$\phi$	Source	$\sigma_{\phi_0}/S$	$\sigma_{\phi_1}/S$	$\sigma_{\rho_0}/S$	$\sigma_{\rho_1}/S$
C-3C ↓	0.0	$\pi/2$ ↓	Theory	1.26	-.15	.00	.01
	0.0		Test	--	.3	--	--
	0.3		Theory	.87	.38	.68	.62
	0.3		Test	1.	.1	.7	-.2
	0.6		Theory	.71	.44	.86	.81
	0.6		Test	.8	.0	.9	.2
	1.0		Theory	.62	.47	.94	.91
	1.0		Test	.7	.0	1.	.5
E-1 ↓	0.0	0 ↓	Theory	2.37	2.94	.77	-.24
	0.0		Test	--	3.32	--	~.0
	0.3		Theory	1.55	1.84	.65	.35
	0.3		Test	1.1	1.6	.7	.7
	0.6		Theory	1.26	1.43	.61	.48
	0.6		Test	1.0	1.4	.4	.8
	1.0		Theory	1.09	1.18	.58	.50
	1.0		Test	.8	--	.3	--
	0.0	$\pi/2$ ↓	Theory	.97	-.64	1.07	-.39
	0.0		Test	--	.0	--	~.2
	0.3		Theory	1.10	-.05	.98	.15
	0.3		Test	1.4	.2	1.0	.0
	0.6		Theory	1.00	.14	1.00	.44
	0.6		Test	1.3	.2	.8	.3
	1.0		Theory	.89	.25	1.03	.64
	1.0		Test	1.	.2	.7	.6
E-2 ↓	0.0	0 ↓	Theory	2.37	2.94	.77	-.24
	0.0		Test	--	2.90	--	--
	0.3		Theory	1.55	1.84	.65	.35
	0.3		Test	1.0	2.3	.7	.4
	0.6		Theory	1.26	1.43	.61	.48
	0.6		Test	.9	1.9	.5	.7
	1.0		Theory	1.09	1.18	.58	.50
	1.0		Test	.8	1.7	.3	.9
	0.0	$\pi/2$ ↓	Theory	.97	-.64	1.07	-.39
	0.0		Test	--	.0	--	--
	0.3		Theory	1.10	-.05	.98	.15
	0.3		Test	1.3	.0	1.0	-.3
	0.6		Theory	1.00	.14	1.00	.44
	0.6		Test	1.0	.1	1.0	.1
	1.0		Theory	.89	.25	1.03	.64
	1.0		Test	.9	.3	.9	.6

TABLE 13. (Continued)  
 (3 of 3)

Model No.	$\frac{\rho'}{\sqrt{RT}}$	$\phi$	Source	$\sigma_{\phi o}/S$	$\sigma_{\phi i}/S$	$\sigma_{\rho o}/S$	$\sigma_{\rho i}/S$
E-3	0.0	0	Theory	2.39	2.94	.77	-.24
	0.0		Test	--	3.28	--	--
	0.3		Theory	1.55	1.84	.65	.35
	0.3		Test	1.2	2.3	.6	.3
	0.6		Theory	1.26	1.43	.61	.48
	0.6		Test	1.0	1.9	.4	.7
	1.0		Theory	1.09	1.18	.58	.50
	1.0		Test	.9	1.7	.4	.9
	0.0	$\pi/2$	Theory	.97	-.64	1.07	-.39
	0.0		Test	--	.0	--	--
	0.3		Theory	1.10	-.05	.98	.15
	0.3		Test	1.3	.0	1.0	-.3
	0.6		Theory	1.00	.14	1.00	.44
	0.6		Test	1.0	.2	1.0	.2
	1.0		Theory	.89	.25	1.03	.64
	1.0		Test	.8	.4	1.0	.7
E-7	0.0	0	Theory	2.37	2.94	.77	-.24
	0.0		Test	--	3.36	--	--
	0.3		Theory	1.55	1.84	.65	.35
	0.3		Test	1.5	1.8	.9	.3
	0.6		Theory	1.26	1.43	.61	.48
	0.6		Test	1.0	1.4	.5	.7
	1.0		Theory	1.09	1.18	.58	.50
	1.0		Test	.8	1.2	.4	.6
	0.0	$\pi/2$	Theory	.97	-.64	1.07	-.39
	0.0		Test	--	.1	--	--
	0.3		Theory	1.10	-.05	.98	.15
	0.3		Test	1.3	.1	1.0	-.2
	0.6		Theory	1.00	.14	1.00	.44
	0.6		Test	1.9	.2	1.0	.3
	1.0		Theory	.89	.25	1.03	.64
	1.0		Test	.9	.2	1.0	.7

Stresses in the Nozzle

In the preceding comparisons, it is shown that the maximum measured stress agrees reasonably well with the maximum theoretical stress in the cylinder. However, as shown in Table 14, the maximum theoretical stresses occur in the nozzle. The question arises as to why the test data does not agree with this aspect of the theory. A partial answer to the question is indicated in Table 14, in which the ratio of the outside fillet radius to the nozzle foundation length,  $\sqrt{rt}$ , is shown in the last column. The fillet radius forms a significant reinforcement of the branch because it extends over about 0.5 to 4.5 times the nozzle foundation length.

The purpose of the following detailed discussion of stresses in the nozzles in two test models (E7 and C-3C) is to illustrate that the calculated stresses are qualitative correct (insofar as shell theory is applicable) and, more important, to indicate conditions under which the calculated nozzle stresses can safely be disregarded.

Phase Report No. 2 discusses the analogous problem of nozzles in spheres. It was found there that the principal effect of the fillet radius on stresses appears to be accountable by its alteration of the thickness of the nozzle. If it is assumed, for relatively small amount of reinforcing added by the fillet, that Eringen's theory gives a good estimate of the stress-resultants at and near the nozzle shell juncture, then the stresses are given by the equations:

TABLE 14. MAXIMUM THEORETICAL STRESSES IN CYLINDER AND NOZZLE  
AND RATIOS OF  $r_o/\sqrt{rt}$ ,  $r_o$  = FILLET RADIUS

Model No.	Maximum Theoretical Stresses				Outside Fillet Radius, $r_o$	$\sqrt{rt}$	$\frac{r_o}{\sqrt{rt}}$
	Cylinder		Nozzle				
	$\sigma/S$	Identification*	$\sigma/S$	Identification*			
C-1A	2.55	$\phi, o, o$	2.82	y, o, o	.3125	.070	4.47
C-2A	2.72	$\phi, i, o$	3.05	y, o, o	.3125	.189	1.65
C-3A	3.15	$\phi, i, o$	3.38	y, o, o	.3125	.285	1.10
C-3C	2.74	$\phi, o, o$	2.99	y, i, o	.5625	.235	2.39
E1, E2, E3, E7	2.94	$\phi, i, o$	3.42	y, o, $\pi/2$	.250	.542	.46

\* Identification of direction and location of maximum stress,

First symbol: stress direction

Second symbol: surface, o = outside, i = inside

Third symbol:  $\phi$  = angle location.

$$\sigma_n = \frac{n}{h} \quad (4)$$

$$\sigma_b = \frac{6m}{h^2} \quad (5)$$

where

$\sigma_n$  = membrane stress

$\sigma_b$  = bending stress

$n$  = membrane stress resultant, Eringen theory

$m$  = bending stress resultant, Eringen theory

$h$  = normal thickness of section.

The thickness  $h$  in the transition zone has been somewhat arbitrarily defined as shown in Figure 10. For test models under consideration, planes radiating from the fillet radius center appear to be suitable for use as "normal planes" in the transition zone between cylinder and nozzle. In particular, the plane from the center of the fillet radius through the intersection of the outside surfaces of nozzle and cylinder (point  $P_o$  in Figure 10) is used to determine the starting point of the nozzle ( $x/\sqrt{rt} = 0$  on Figure 10).

Stresses in the nozzle of test model E7 were calculated using Equations (4) and (5) with  $h$  as shown in Figure 10 ( $\theta = 0$  section) and Figure 12 ( $\theta = \pi/2$  section). Calculated and test results are shown on Figures 10 through 13. It can be seen that the adjusted theory stresses qualitatively agree with the test results; which are shown in Figure 14. In particular, the second highest peak stress of  $\sigma_{y0}$  at  $\theta = \pi/2$  ( $\sigma_{y0}/S = 1.86$ ) is reasonably well predicted by the adjusted theory, as well as the peak in the  $\sigma_{x0}$  stress at the same location.

The largest discrepancy occurs for  $\sigma_{yi}$  at  $\theta = 0, x = 0$  (Figure 11).

The calculated  $\sigma_{n\theta}$ -stress in this region, however, is 2.94 S which is about the same as the measured stress in the region.

Model C-3C was selected for detailed analysis because its value of  $s/S = 2.01$  represents the opposite end of the  $s/S$  range from Model E7 (for which  $s/S = .58$ ) and also because the second highest peak stress,  $\sigma_{y0}$  at  $\theta = \pi/2$ , is approaching the maximum measured stress at the inside corner. Calculations of the stresses, adjusted for the normal thickness  $h$ , were made in the same way as described above for model E7. Figure 15 shows the stresses for model C-3C as obtained from the theory. Figures 16 through 19 show the calculated stresses, adjusted for the normal thickness  $h$ , and the test results. The  $\sigma_y$ -stresses are also plotted as a function of  $x/\sqrt{rt}$  in Figures 20 and 21. The original test data is shown in Figure 22\*.

It may be noted, in Figure 19 or Figure 21, that the peak stress at  $\theta = \pi/2, \sigma_{y0}/S = 2.52$  measured in the test, is accurately predicted by the adjusted theory. As in model E7, some calculated stresses on the nozzle for  $x/\sqrt{rt} = 0$  are lower than test results and are better represented by the calculated stress in the cylinder in that region.

In general, these comparisons indicate that the Eringen's calculated stresses in the nozzle are probably reasonably accurate as applied to a nozzle with no fillet radius\*\* - as assumed in the development of the theory.

---

\* The test data, at points remote from the juncture, is seemingly inconsistent (for some stresses) as compared with Lamé' stresses. The Lamé' stresses are shown in parenthesis in Figure 22.

\*\* Except, of course, that the shell theory would not give the stress concentration due to the notch-effect if the fillet radius were zero.

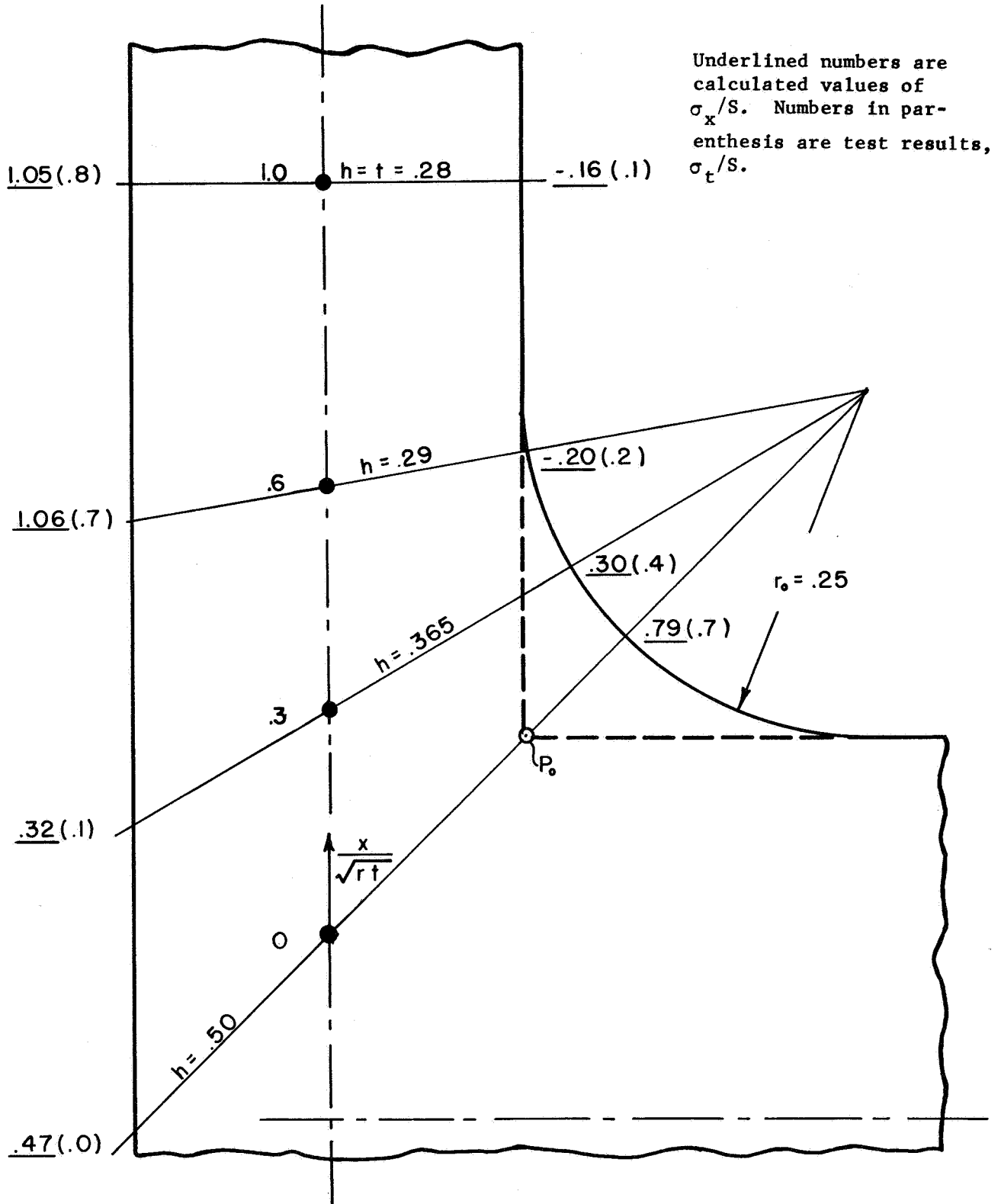


FIGURE 10. NOZZLE STRESSES ADJUSTED FOR NORMAL THICKNESS,  $h$ , TEST MODEL E7,  $\sigma_x$  OR  $\sigma_t$  STRESSES AT  $\theta = 0$

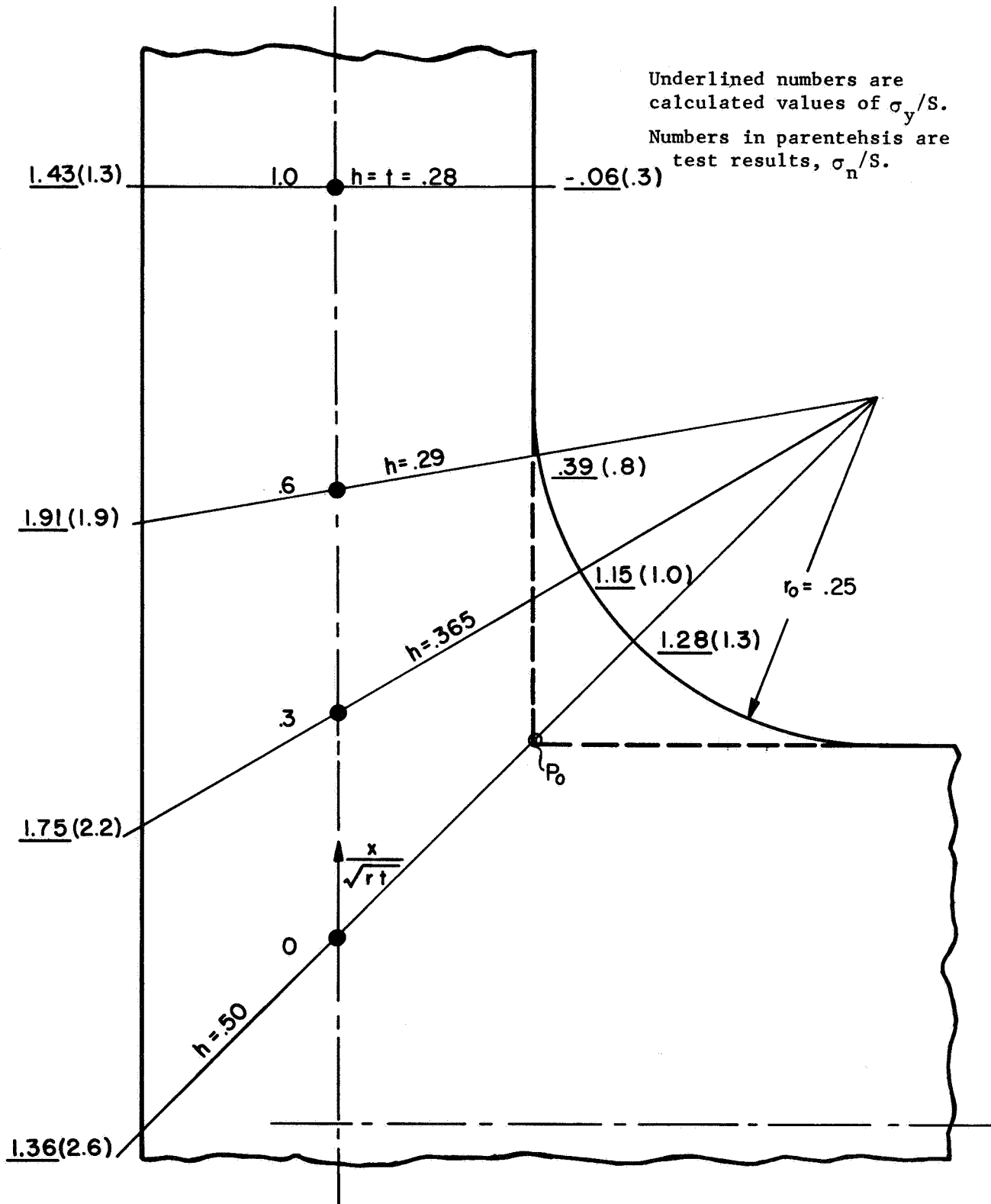


FIGURE 11. NOZZLE STRESSES ADJUSTED FOR NORMAL THICKNESS,  $h$ , TEST MODEL E7,  $\sigma_y$  OR  $\sigma_n$  STRESS AT  $\phi = 0$ .



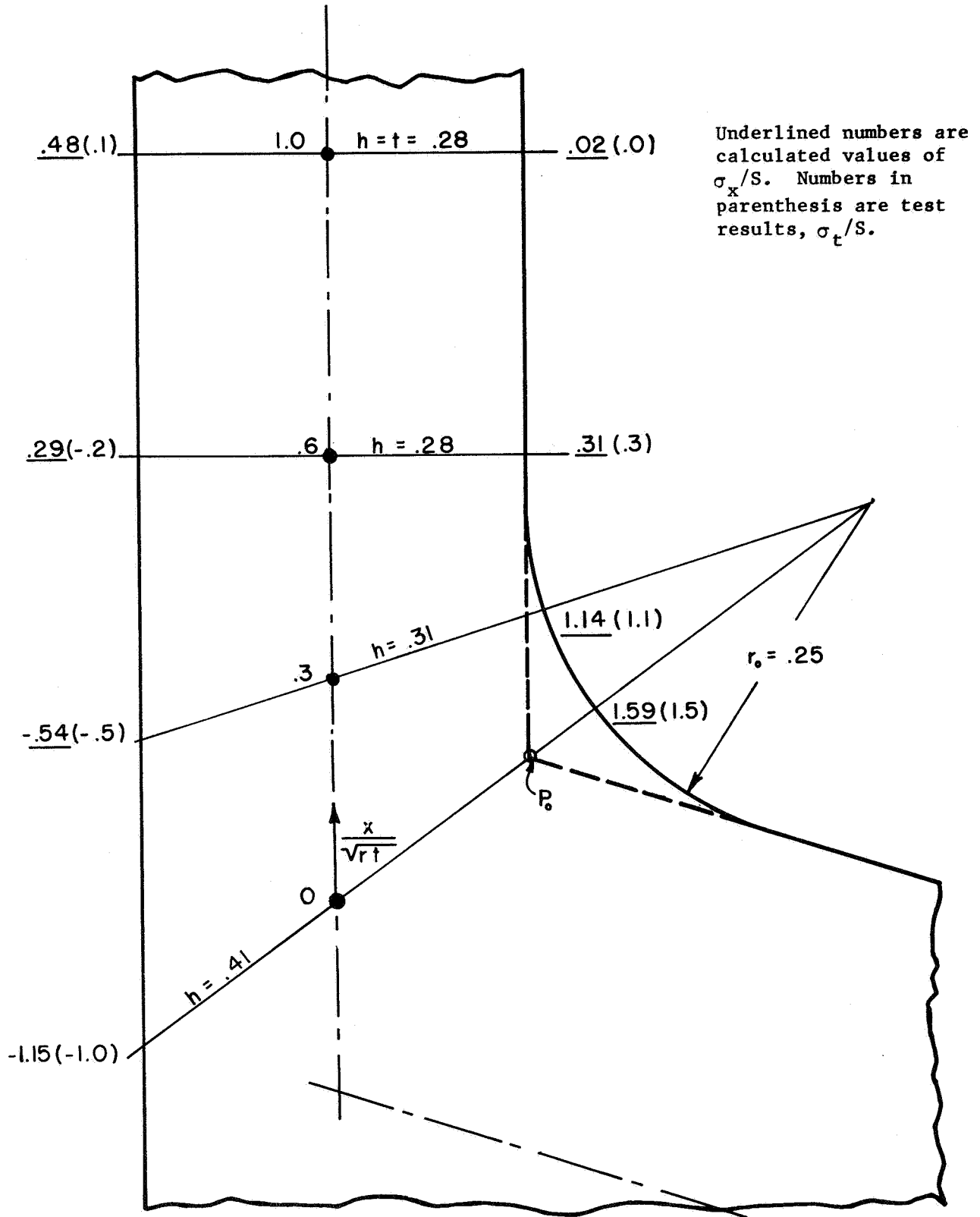


FIGURE 12. NOZZLE STRESSES ADJUSTED FOR NORMAL THICKNESS,  $h$ , TEST MODEL E7,  $\sigma_x$  OR  $\sigma_t$  STRESS AT  $\phi = \pi/2$

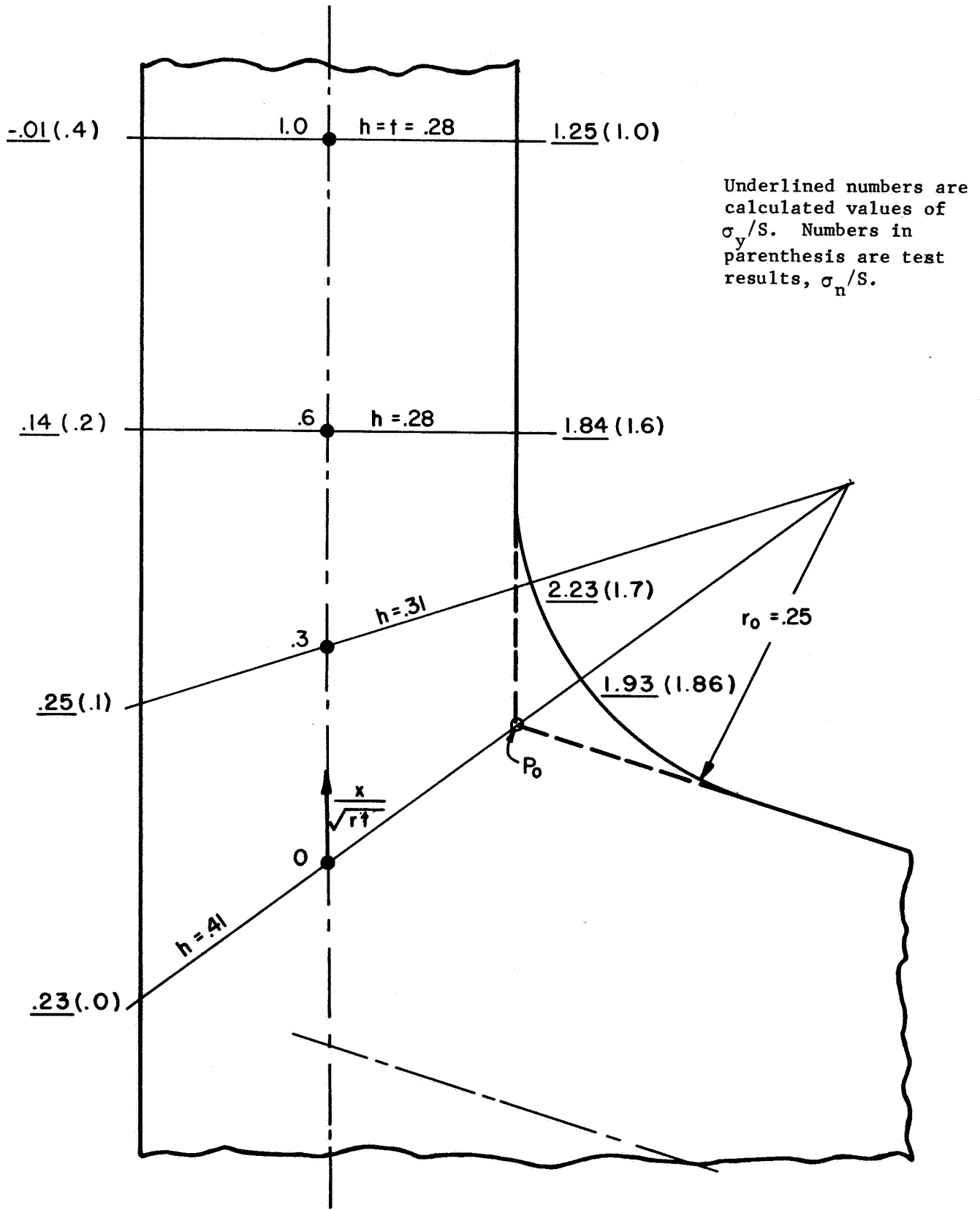


FIGURE 13. NOZZLE STRESSES ADJUSTED FOR NORMAL THICKNESS, h, TEST MODEL E7,  $\sigma_y$  OR  $\sigma_n$  STRESS AT  $\phi = \pi/2$

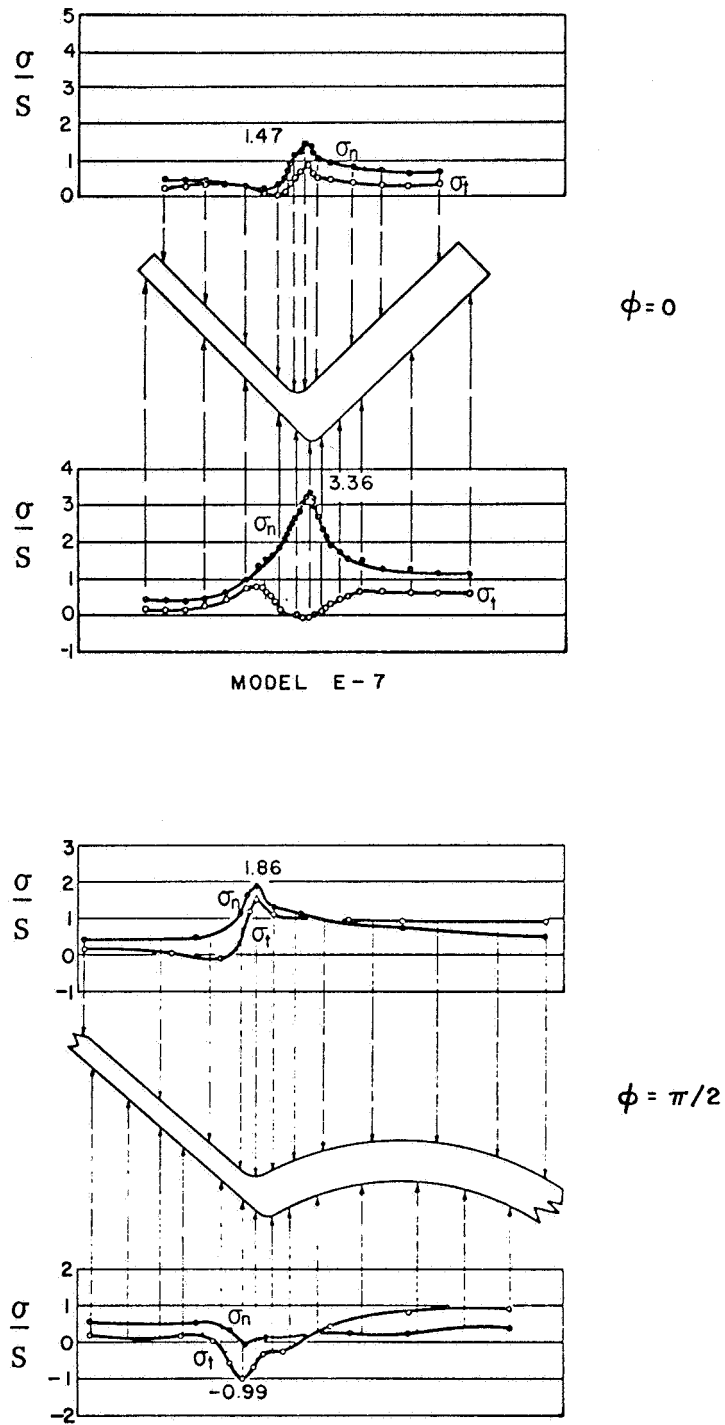


FIGURE 14: TEST RESULTS FOR MODEL E7 FROM REFERENCE (24)

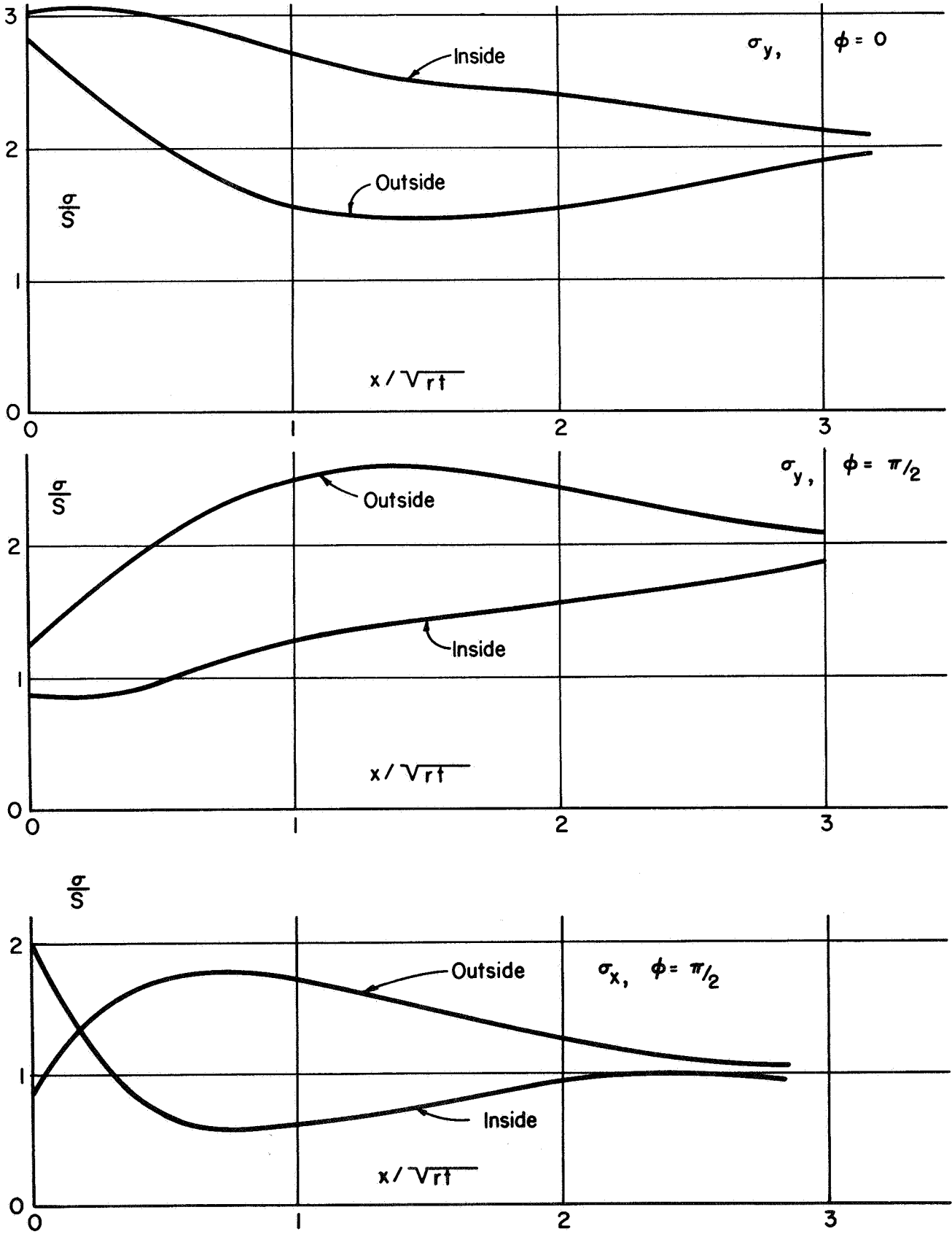


FIGURE 15: ERINGEN THEORY STRESSES IN THE NOZZLE OF MODEL C-3C

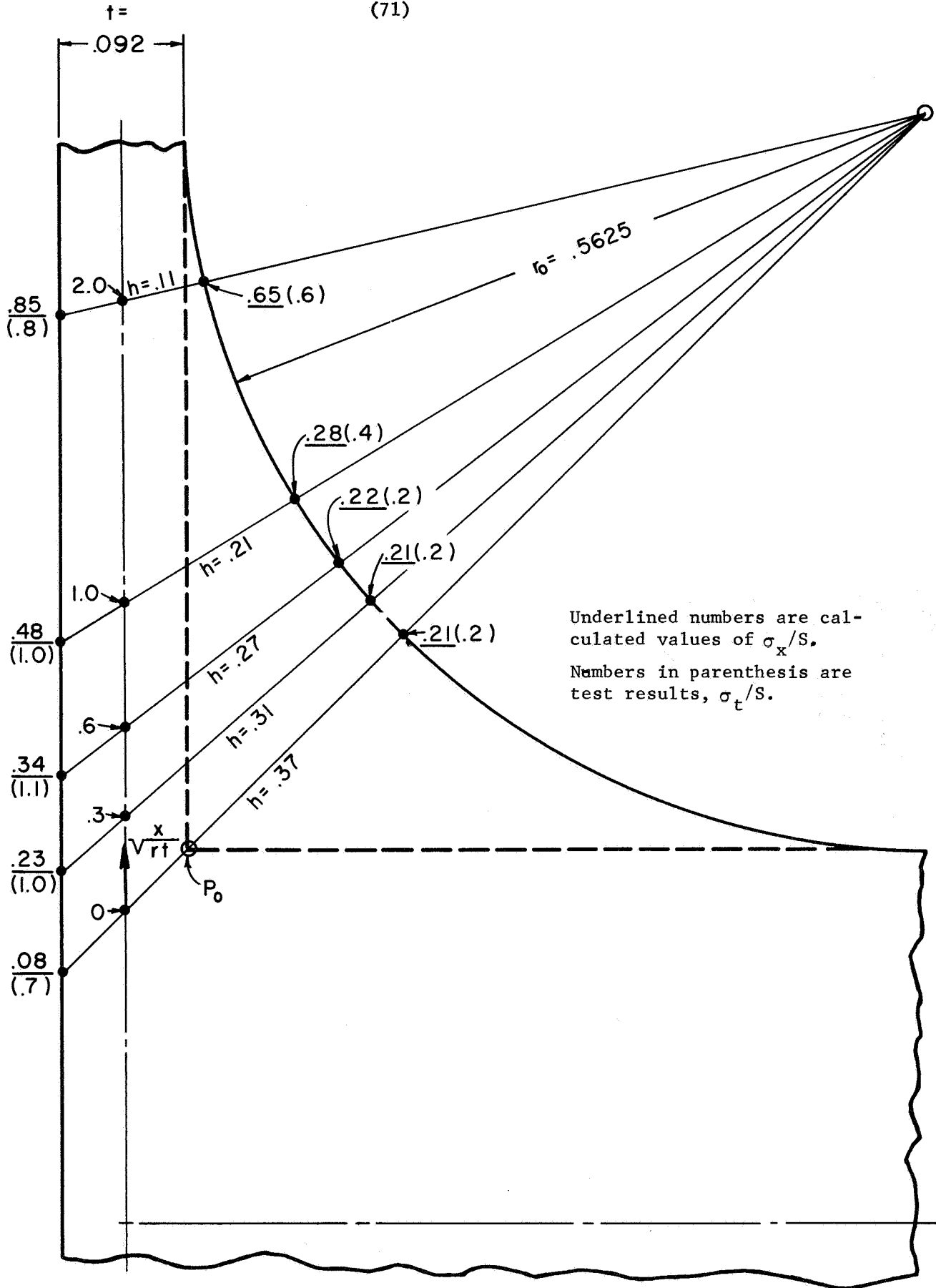


FIGURE 16. NOZZLE STRESSES ADJUSTED FOR NORMAL THICKNESS,  $h$ , TEST MODEL C-3C,  $\sigma_x$  OR  $\sigma_t$  AT  $\phi = 0$ .

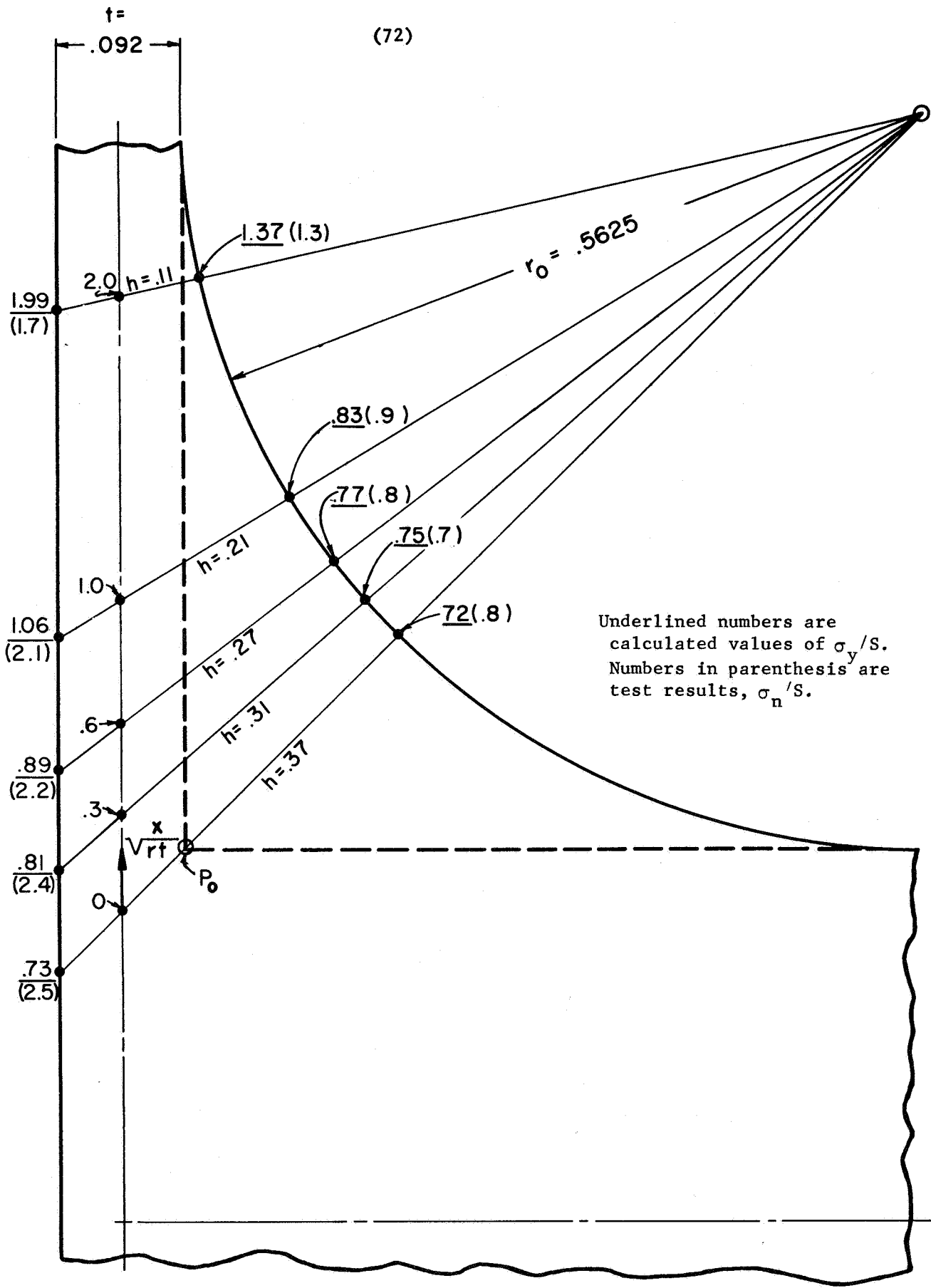


FIGURE 17. NOZZLE STRESSES ADJUSTED FOR NORMAL THICKNESS,  $h$ , TEST MODEL C-3C,  $\sigma_y$  OR  $\sigma_n$  AT  $\theta = 0$ .

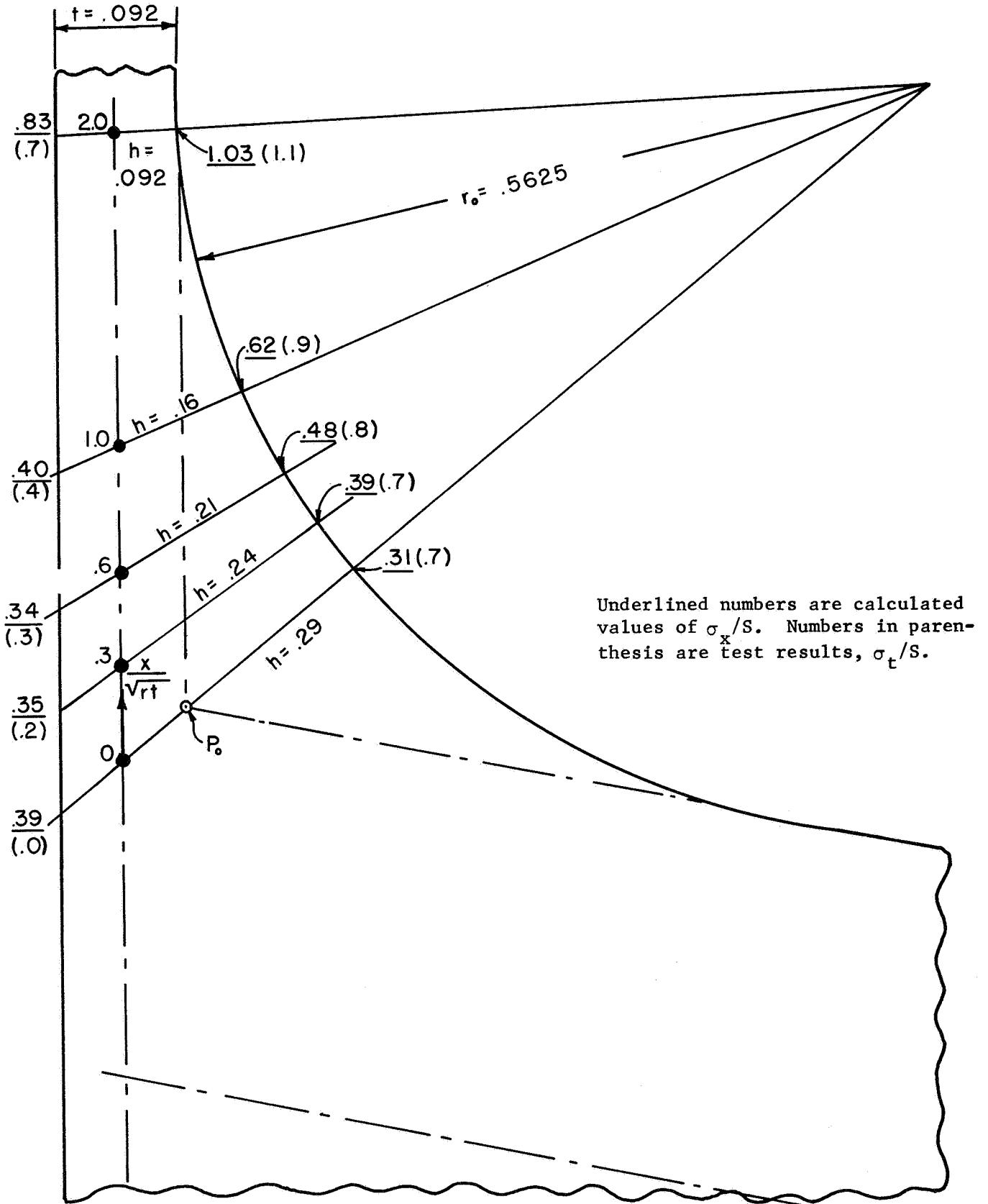


FIGURE 18. NOZZLE STRESSES ADJUSTED FOR NORMAL THICKNESS,  $h$ , TEST MODEL C-3C,  $\sigma_x$  OR  $\sigma_t$  AT  $\phi = \pi/2$

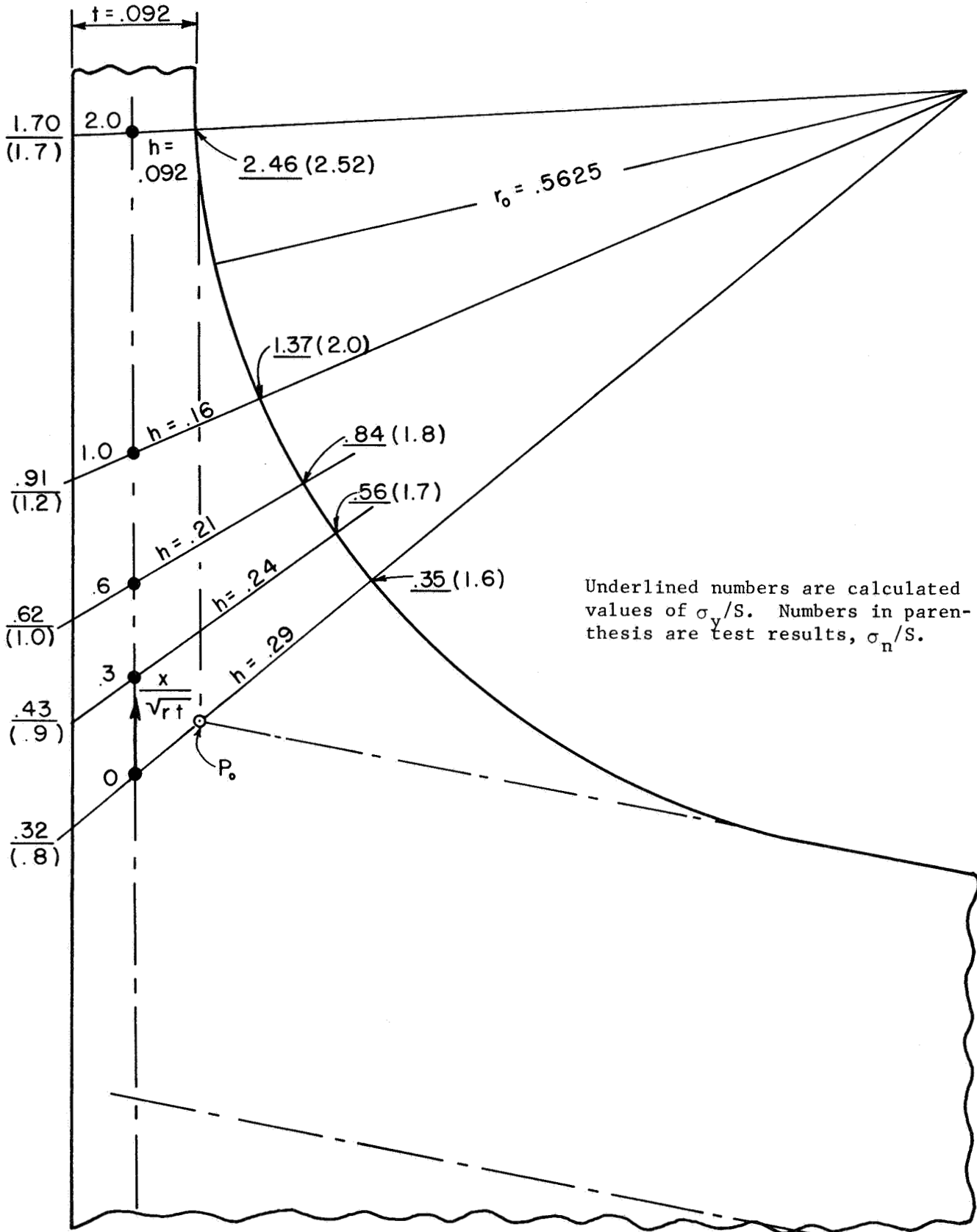


FIGURE 19. NOZZLE STRESSES ADJUSTED FOR NORMAL THICKNESS,  $h$ , TEST MODEL C-3C,  $\sigma_y$  OR  $\sigma_n$  AT  $\phi = \pi/2$



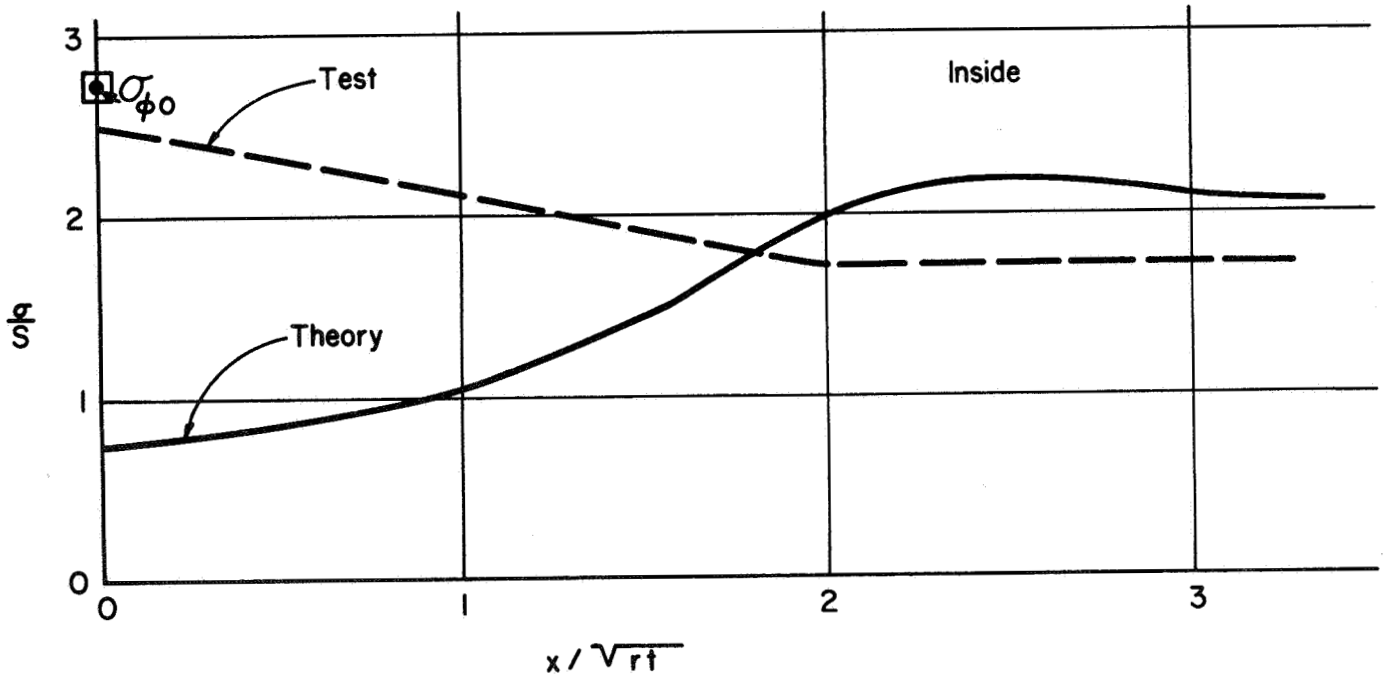
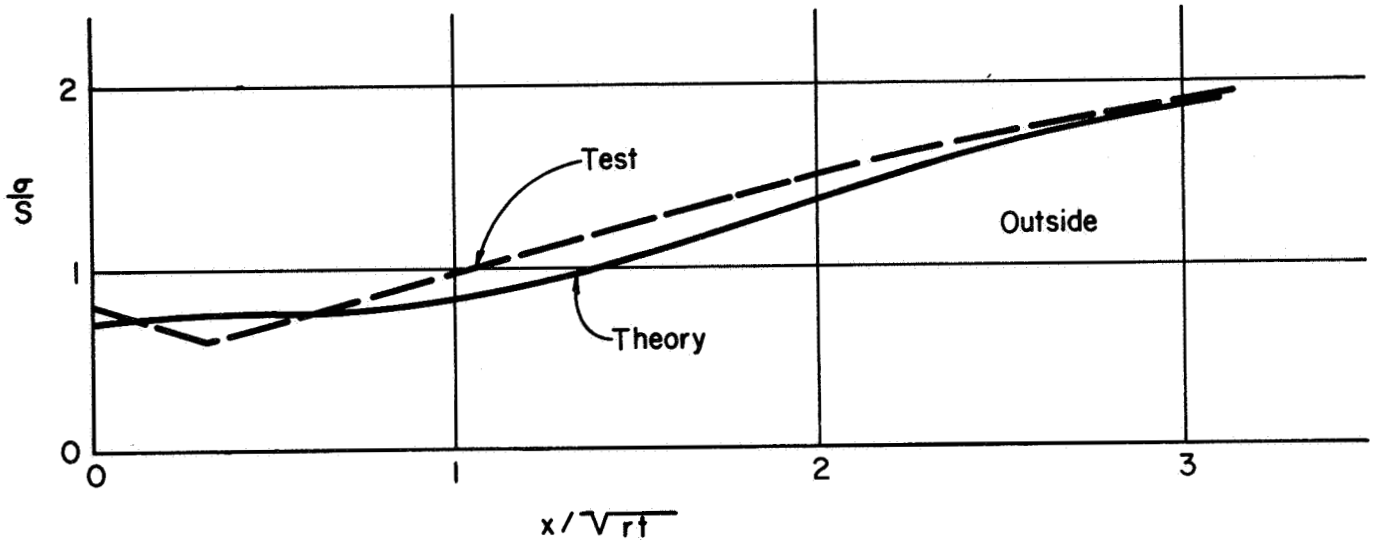


FIGURE 20. NOZZLE STRESSES ADJUSTED FOR NORMAL THICKNESS,  $h$ , TEST MODEL C-3C,  $\sigma_y$  - STRESS AT  $\phi = 0$

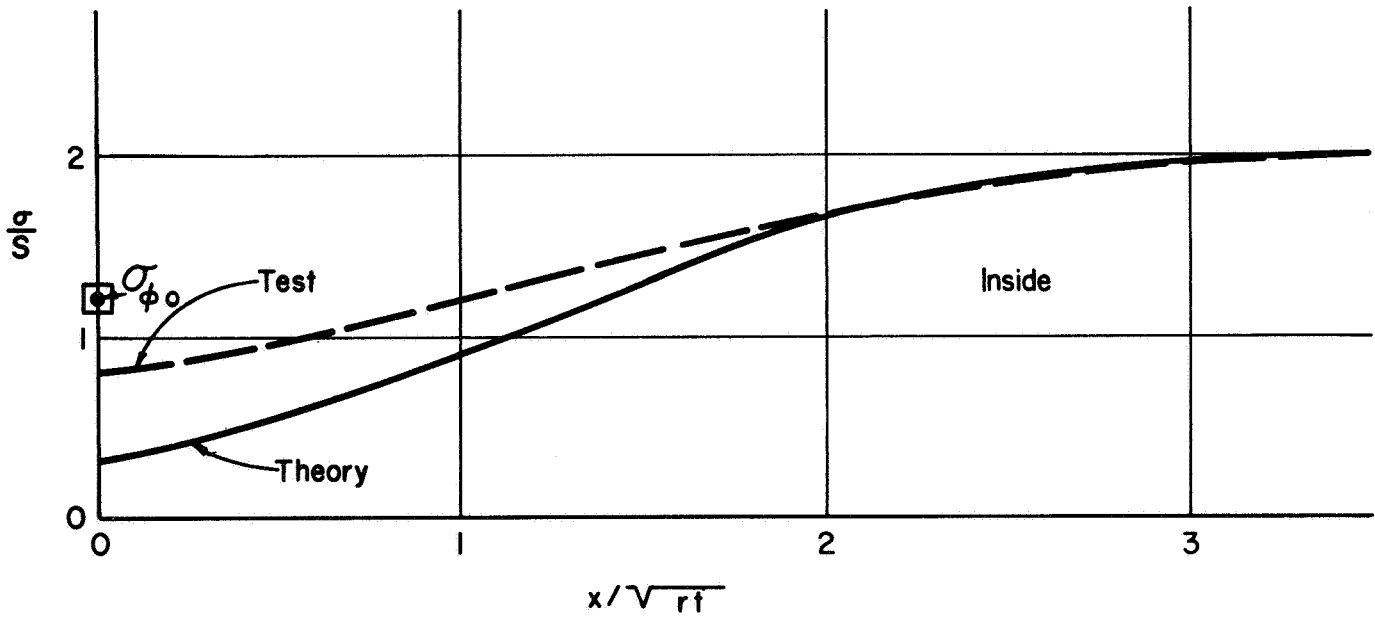
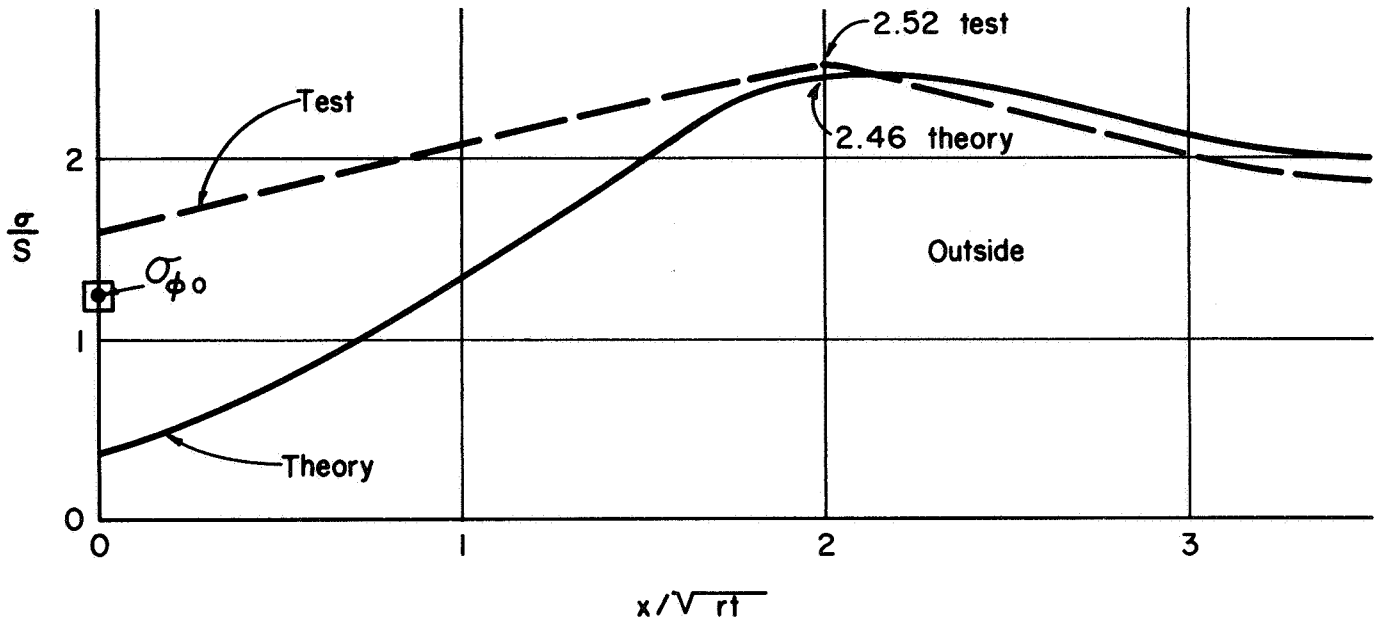
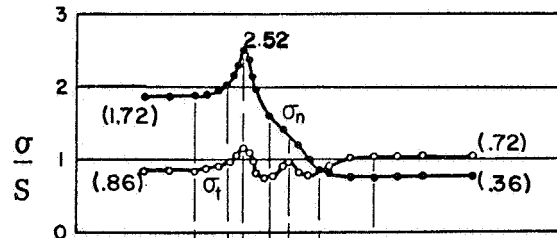
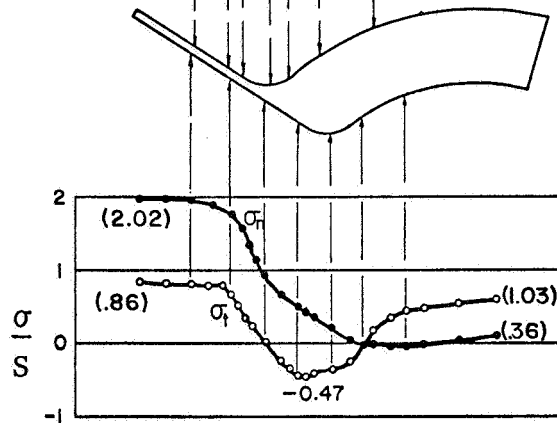


FIGURE 21. NOZZLE STRESS ADJUSTED FOR NORMAL THICKNESS,  $h$ , TEST MODEL C-3C,  $\sigma_y$  - stress at  $\phi = \pi/2$

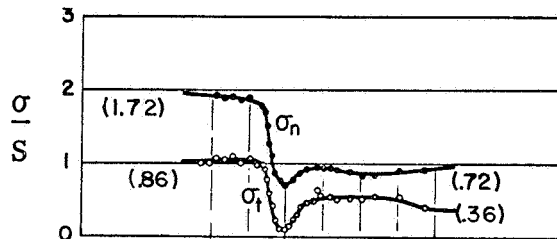


$\phi = \pi/2$



Numbers in parenthesis are Lamé stresses

MODEL C-3C



$\phi = 0$

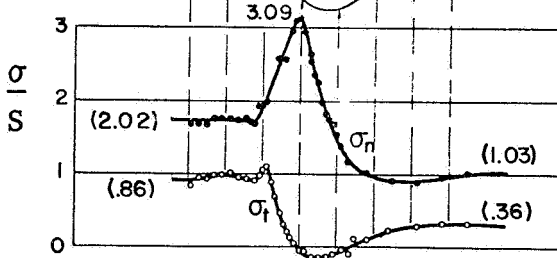


FIGURE 22: TEST RESULTS FOR MODEL C-3C FROM REFERENCE (24)

Fillet Radius Requirement

The summary shown in Table 4 indicates that the maximum stresses measured in test models is reasonably well predicted by the maximum stress in the cylinder given by Eringen's theory. The question arises as to whether the maximum measured stress in nozzles in cylinders (within the range at Eringen's analysis) always occurs at the inside corner. The theory suggests that the maximum stress may occur in the nozzle and that the test results of the models listed in Table 4 do not show this because:

- (1) For some steel models, insufficient strain gages were placed on the nozzle to detect a high stress, if such existed.
- (2) For photoelastic models, test models included a sufficiently large fillet radius to reinforce the nozzle at the critical juncture location.

Examination of the test data and calculated stresses indicates that the maximum stress will not occur in the nozzle if:

- (1)  $r_o/\sqrt{dt} \geq 1.0$  for  $s/S$  from 1.0 to 2.0.
- (2)  $r_o/\sqrt{dt} \geq s/S$  for  $s/S$  less than 1.0.
- (3)  $r_o$  in no case less than  $T/2$ .

The second requirement for  $r_o$  permits a smaller fillet radius to be used as  $t/T$  becomes larger. Calculations given in Table A7 show that as  $s/S$  decreases, the maximum calculated stress in the nozzle approaches that in the cylinder. Accordingly, a smaller fillet radius can be used. The third requirement for  $r_o$  is to insure the absence of high stresses due to a notch; such stresses would not be given by Eringen's theory.

TEST MODELS WITH LOCAL REINFORCINGTest Data

The preceding comparisons of theory and test data were restricted to test models which consisted of a uniform wall nozzle in a uniform wall cylinder with a fillet radius or fillet weld as the only reinforcing. Additional test data are available in which the test models included various types of local reinforcing, as shown by Figure 23. A summary of this data, for nozzles with small  $d/D$ -ratios, is given in Table 15. The test models and test data are briefly discussed in the following.

References (24) and (25) give test data from photoelastic test models. Reference (24) gives data at  $\phi = 0$  and  $\phi = \pi/2$  while Reference (25) gives data at those two  $\phi$ -planes plus other  $\phi$ -planes. Models FIW and AIW were actually one model; E6. This model consisted of a cylinder with a tapered wall transition from 0.490" to 0.350". The nozzle was placed in the 0.490" wall section but near the tapered transition such that one part of the model (AIW) can be considered as a nozzle in a 0.490" wall cylinder with reinforcing in the nozzle, the other part of the model (FIW) can be considered as a nozzle in a 0.350" wall cylinder with reinforcing in the run and in the nozzle.

References (20), (21), and (22) give test results on steel test models. References (20) and (21) give data at  $\phi = 0$  only. Reference (22) gives data at  $\phi = 0$ ,  $\phi = 90^\circ$  and other  $\phi$ -planes.

TABLE 15. TEST MODELS WITH LOCAL REINFORCING

Model Iden.	Ref. No.	$\frac{D}{T}$	$\frac{d}{D}$	$\frac{s}{S}$	$\frac{r_i}{T}$	$\frac{r_o}{T}$	Rein. Type (2)	$\frac{A}{d_i T}$ (3)	Measured Stresses		
									$\sigma_n$ Corner (4)	$\sigma_n$ Inside Reinforcing Edge (5)	
F	(24)	19.0	.33	.76	.38	.66	A	1.40	2.28	1.85	
P-4A		12.5	.42	1.00	.53	.53	B	.45	2.84	2.10	
P-4D		12.5	.42	1.00	.53	.53	A	.65	3.07	2.58	
FIW		20.2	.16	.68	---	---	---	1.90	1.80	---	
AIW		14.8	.15	.92	.31	.31	C	.85	2.22	.82	
WC-5LB	(25)	13.2	.50	1.00	.56	.80	D	.65	2.49	2.18	
WC-5LA		13.1	.50	1.00	.56	.80	E	.65	2.81	1.60	
WCN-6C		13.1	.20	1.00	.30	.30	A	.64	(2.18)	1.94	
WC-11B		13.2	.20	1.00	.56	.80	D	.63	2.64	1.70	
WC-5LM		73.4	.50	.99	.56	.80	D	.65	2.23	2.71	
9	(20,21)	29.5	.043	.34	---	a	F	.25	(2.08)	---	
10a			.043	.34	.074		C	.60	(2.18)	---	
10b	See Text		.084	.42	.500		C	.70	2.77*	---	
11a					.074				2.53	---	
11a'					.074				2.44	---	
11b			.043	.34	.500				2.41	---	
12a			.043	.34	.074		C	.75	2.72	---	
12b					.500				2.67	---	

\* 2.64 appears to be the correct value,  
based on the reported strains.

Continued on next page.

TABLE 15. (contd)

Model Iden.	Ref. No.	$\frac{D}{T}$	$\frac{d}{D}$	$\frac{s}{S}$	$\frac{r_i}{T}$	$\frac{r_o}{T}$	Rein. Type (2)	$\frac{A}{d_i T}$ (3)	Measured Stresses		
									$\sigma_n$ Corner (4)	$\sigma_n$ Inside (5)	Reinforcing Edge (5)
13	(20,21)	29.5	.084	.42	---	a	F	.65	(2.04)	---	---
14a			.084	.42	.074		C	1.00	(2.53)	---	---
14a'					.074				(2.53)	---	---
14b					.500				2.44	---	---
16a			.161	.46	.074		C	.80	2.54	---	---
16a'					.074				2.57	---	---
16b					.500				2.67	---	---
2	(22)	19.0	.27	.90	.25	a	C	1.30	2.91	2.91	1.29
6			.27	.90	.25	.75	A	.75	2.96	2.96	1.83
6A			.27	.90	.75	.75	A	.75	2.78	2.78	---
8			.084	.56	.25	a	C	.75	2.60	2.60	1.25
9			.083	1.01	.25	.15	B	1.10	2.61	2.61	1.53

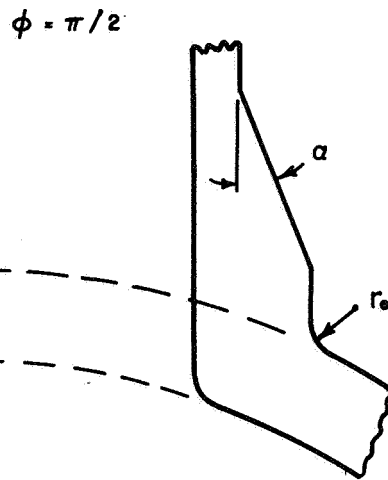
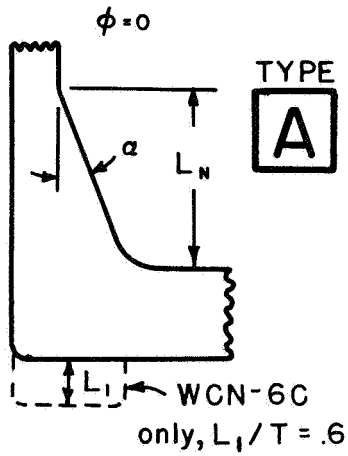
(1) Radius between nozzle or reinforcing edge and shell at  $\phi = \pi/2$ . a  $\equiv$  fillet weld.

(2) See Figure 23.

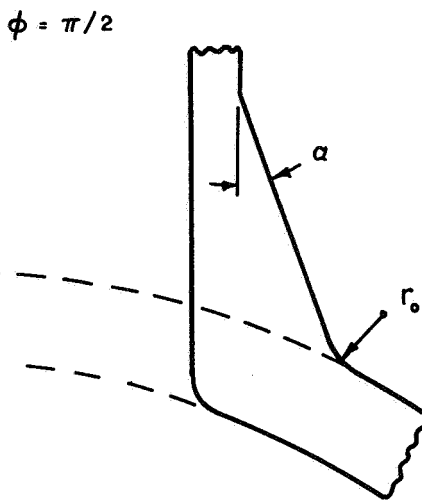
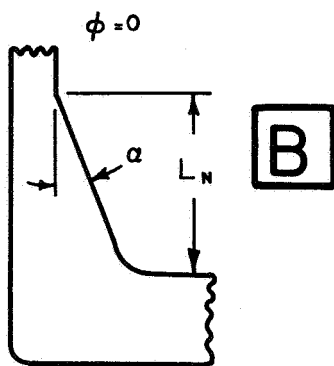
(3) Reinforcing area, including excess thickness in nozzle, within a zone  $\sqrt{dt}$  or  $\sqrt{d_a t}$  measured along nozzle axis from outside surface of shell. For tapered nozzles,  $d_a \equiv d_i + t_a$ ,  $t_a \equiv$  average thickness of tapered nozzle in  $\sqrt{d_a t}$  zone. Area is given for  $\phi = 0$  plane; area at  $\phi = \pi/2$  is significantly larger for most models.

(4) Values in parenthesis are not at inside corner, but are approximately at the middle of the shell wall. Maximum stress may be significantly higher.

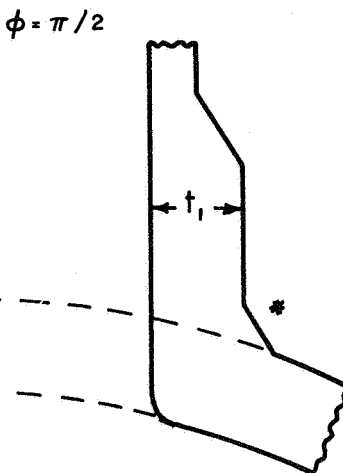
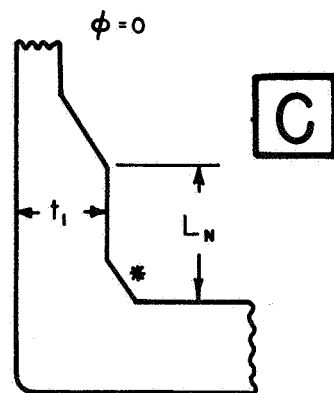
(5) These are  $(\sigma_{to}/S)$ -stresses at the edge of the reinforcing or nozzle at  $\phi = \pi/2$ .



Model Iden.	$\alpha$ degrees	$\frac{L_n}{T}$
F	30	3.61
P-4D	30	2.37
WCN-6C	15	1.84
6, 6A	30	2.50



Model Iden.	$\alpha$ degrees	$\frac{L_n}{T}$
P-4A	13.6	3.23
9	30	2.50



Model Iden.	$\frac{t_1}{T}$	$\frac{L_n}{T}$
AIW	0.753	1.48
10	0.434	2.22
11	0.650	2.82
12	0.434	0.96
14	0.650	1.48
16	0.940	3.71
2	1.200	2.00
8	0.572	1.44

\*Fillet weld on all except AIW

FIGURE 23a. TYPES OF REINFORCING FOR MODELS LISTED IN TABLE 15.



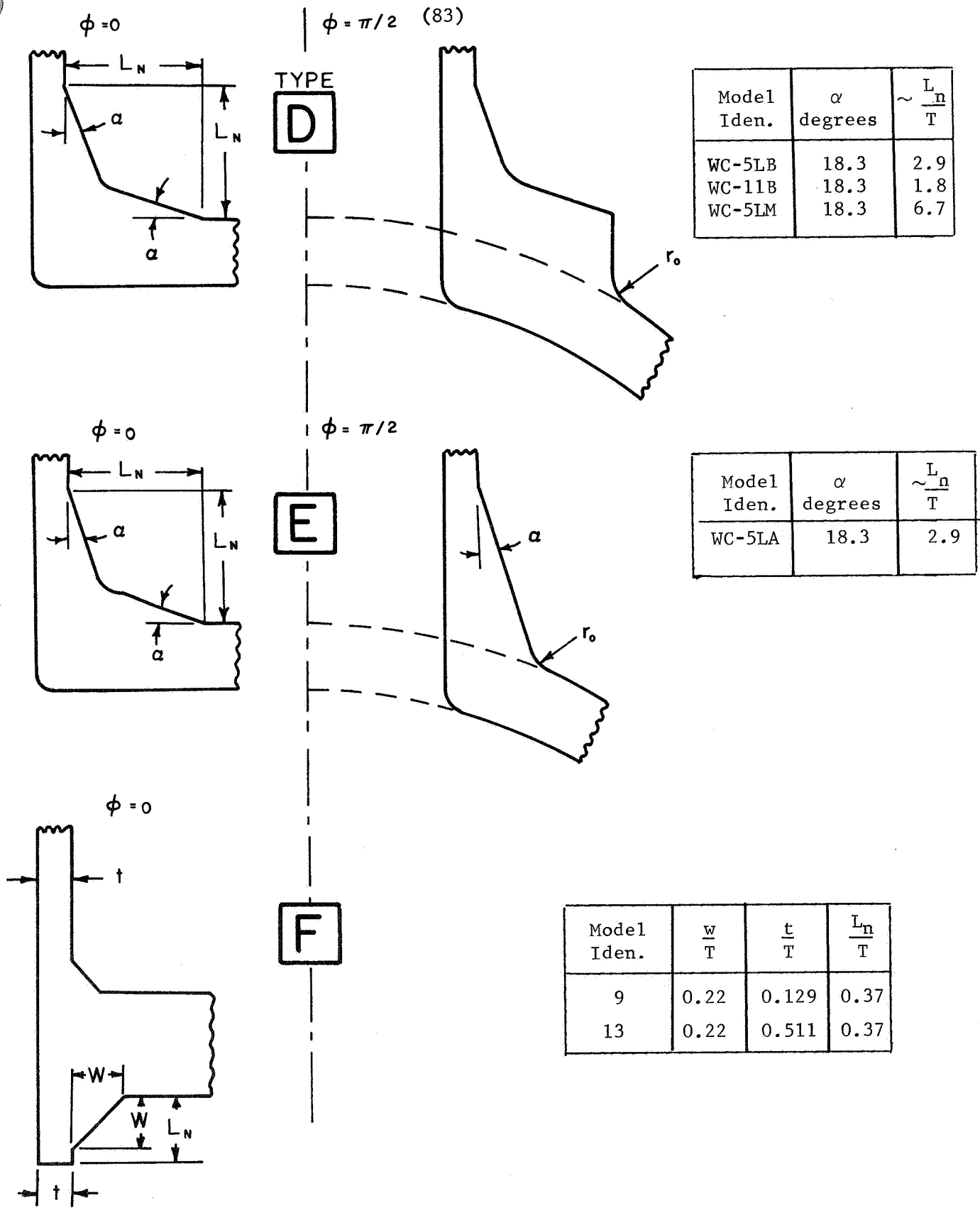


FIGURE 23b. TYPES OF REINFORCING FOR MODELS LISTED IN TABLE 15

The test data of Reference (20) and (21) require additional comment. Reference (20) gives the results of tests on several nozzles in a pressure vessel. Subsequently, some modifications were made to part of the nozzles and additional tests were run; the results are given in Reference (21). The modifications consisted of:

- (1) The inner corner radii of Nozzles 10 and 12 were ground from the original  $1/8''$  to  $27/32''$ .
- (2) The inner corner radii of Nozzles 11, 14, and 16 were ground from the original  $1/8''$  to  $27/32''$  for  $\phi$  from  $-90^\circ$  to  $+90^\circ$ ; the remaining portion,  $\phi$  from  $90^\circ$  to  $270^\circ$ , was left with the original  $1/8''$  radius.
- (3) Nozzle 9 and 13 originally included an inward protuberance of the nozzles of  $1-1/8''$ . This protuberance was reduced to  $5/8''$  for the second test series.

Accordingly, in table 15 herein:

- (1) Nozzles 10 and 12 show results for the  $1/8''$  inside corner radius (Ref. 20) and  $27/32''$  radius (Ref. 21).
- (2) Nozzles 11, 14, and 16 show results for the  $1/8''$  inside corner radius (Ref. 20); the results at  $\phi = 180''$ ,  $1/8''$  inside corner radius and at  $\phi = 0$ ,  $27/32''$  inside corner radius (Ref. 21).
- (3) Nozzles 9 and 13 (nozzles protruding inwardly) in Reference (20) did not have strain gages on the inside of the nozzle bore, midway in the shell thickness. Tests by Leven<sup>(25)</sup> indicate that the maximum stress occurs at about this point. In Reference (21), strain gages were placed at this point

and did give maximum measured stresses. Accordingly, only the results of Reference (21) are shown for these nozzles.

In Reference (22), the nozzles were used in a series of eight different pressure vessels; in each of these models some data were obtained on stresses in the nozzles. The individual results are shown in Table 16. The data shown in Table 15 are the averages of the test data shown in Table 16. The scatter of test data shown in Table 16 may be indicative of variations in the nozzle-vessel construction and/or variations in strain gage placement and accuracy of strain gage results.

#### Reinforcing Area

The ratio of reinforcing area to the cut-out area ( $d_1 T$ ) is shown in Table 15. It is pertinent to compare the measured stresses in these models with the stresses that would have been expected if no reinforcing had been used. Table 17 shows calculated stresses for analogous test models without reinforcing and, where available, measured stresses from analogous models without reinforcing.

In all but three of the test models in Table 17, reinforcing was placed on the outside of the shells only. For Model WC-5LM, reinforcing produced a large decrease in stress as compared to the calculated stress of an analogous unreinforced model. For other models, reinforcement on the outside surface produced relatively small decreases in stress. This is most apparent for very small  $d/D$ -ratios. For models with  $d/D < 0.084$ , the addition of reinforcement on the outside surface seems to have very little effect in reducing the stress on the inside corner.

TABLE 16. MAXIMUM MEASURED  $\sigma_{\pi}/S$  ON THE INSIDE CORNERS OF NOZZLES, PICKETT & GRIGORY, REFERENCE (22) (1)

Nozzle No.	$\theta$	Vessel Number							2-1/4 Cr-Mo	AVG.	
		1	2	3	4	5	6	7 (2)			
2	{ 0	3.14	2.98	2.74 (3)	---	2.94	---	2.70	2.96	}	2.91
	{ 180°	---	2.87	---	---	---	---	2.75	---		
6	{ 0	2.71 (4)	2.85 (5)	3.11	---	2.73	2.80	---	3.23	}	2.96
	{ 180°	---	2.84 (5)	3.14	---	---	---	---	---		
6A	{ 0	---	---	---	2.85	---	2.66	---	---	}	2.78
	{ 180°	---	---	---	2.93	---	2.69	---	---		
8	---	2.63	---	2.53	---	---	2.57	---	2.66		2.60
9	---	2.59	---	2.50	---	---	2.67	---	2.70		2.61
11	---	2.76	---	---	2.78	---	2.52	---	2.24		2.57

88

(1) With additions and corrections as given in private communications from J. L. Merzhon (9/28/67) and S. C. Grigory (11/2/67).

(2) Vessel No. 7 also contained Nozzles 2A, 2M, 2G, and 2B.

Stress indices and  $r_i/T$  are shown at right.

Nozzle 2A:  $r_i/T = 0.375$ , 304 stainless cladding with austenitic defects

Nozzle 2B:  $r_i/T = 0.0$ , square inside corner

Nozzle 2G:  $r_i/T = 0.375$ , 304 stainless cladding

Nozzle 2M:  $r_i/T = 0.375$ , 304 stainless cladding with martensitic defects

(Nozzle 2N same as Nozzle 2,  $r_i/T = 0.25$ )

\* Based on an estimated longitudinal strain

Nozzle No.	$\frac{r_i}{T}$	$\theta$	$\sigma_{\pi}/S$
2A	.375	0	2.62
		180°	2.78
2M	.375	0	2.74
		180°	2.75
2G	.375	0	2.46
		180°	2.71
2B	0	0	3.09*

AVG. of 2A, 2M, 2G = 2.68

Footnotes continued on next page

## Continuation of footnotes to Table 16

- (3) Not "on the corner". This value is not included in the average. The corresponding stress for nozzle 2 in Vessel 1 at this location was 2.80 S as compared to 3.14 S on the corner.
- (4) Not "on the corner". This value is not included in the average.
- (5) Nozzle 6 in vessel 2 was retested with the inside corner radius on the 180° side increased by grinding from 0.5" to 1.0" ( $r_i/T$  from 0.25 to 0.50). New strain gages were installed on both the 0° and 180° sides. The results were:

$$\begin{array}{ll} \text{at } \phi = 0^\circ & \sigma_n/S = 2.81 \\ \text{at } \phi = 180^\circ & \sigma_n/S = 2.60 \end{array}$$

The value of  $\sigma_n/S$  for  $\phi = 180^\circ$  is shown in Figure 24 as Nozzle 6',  $r_i/T = 0.5$ .

TABLE 17. COMPARISON OF REINFORCED NOZZLES WITH UNREINFORCED NOZZLES

Model Iden.	Ref.	$\frac{A}{d_i T}$	Measured Stress		Calculated Stress Without Reinforcing		Comparable Models Without Reinforcing	
			(1)	(2)	Eringen	Lind	Model Iden.	Stress(2)
F	(24)	1.40		2.28	---	3.34		
P-4A	↓	.45		2.84	---	3.49	E-4	3.50
P-4D		.65		3.07	---	3.49	E-4B	3.50
FIW		1.90		1.80	2.9	2.54		
AIW		.85		2.22	2.9	2.61		
WC-5LB		(25)	.65		2.49	---	3.84	E-4
WC-5LA	↓	.65		2.81	---	3.83	E-4B	3.50
WCN-6C		.64	(2.18)	3.1	2.61	C-3A	3.0	
WC-11B		.63	2.64	3.1	2.61	C-3A	3.0	
WC-5LM		.65	2.23	---	7.14			
9		(20,21)	.25	(2.08)	2.45	2.56	7, 8	2.64
10	↓	.60		2.77	2.45	2.56	7, 8	2.64
11		.70		2.53	2.65	2.52		
12		.75		2.72	2.45	2.56	7, 8	2.64
13		.65	(2.04)	2.65	2.52			
14		1.00	2.53	2.65	2.52			
16		.80	2.67	3.0	2.51			
2		(22)	1.30		2.91	3.7	3.05	
6	↓	.75		2.96	3.7	3.05		
8		.75		2.60	2.6	2.59		
9		1.10		2.61	2.7	2.60		

(1) Except for values in parenthesis, stresses are  $\sigma_n$  at the inside corner.

(2) Stresses are shown as stress indices,  $\sigma/S$ .

In three models (WCN-6C of Ref. 25; 9 and 13 of Ref. 20 and 21), part of the reinforcing was placed on the inside. This shifted the maximum stress point from the inside corner to about the mid-wall of the shell. Also, the inside reinforcing was more effective in reducing the maximum stress than an equal amount of outside reinforcing.

The reinforcing area requirements of Phase Report 4, based on plastic collapse pressure considerations, are:

d/D Range	A/(d <sub>i</sub> T)
$d/D < 0.1414 \sqrt{T/D}$	0
$0.1414 \sqrt{T/D} < d/D < 0.425 \sqrt{T/D}$	$2.65 (d/D) \sqrt{D/T} - .375$
$d/D > 0.425 \sqrt{T/D}$	.75

Within the limitations:  $\frac{d}{D} < \frac{1}{3}$  and  $\frac{d}{D} \sqrt{\frac{D}{T}} < 1.1$

Table 18 gives comparisons of reinforcing areas used in test models with those required by Phase Report No. 4. Phase Report No. 4 does not specify whether the reinforcing must be placed on the inside or the outside. While the direct comparisons available in Table 18 are limited, such comparisons as can be made indicate that the maximum elastic stress\* will be less than 3S for nozzles reinforced in accordance with Phase Report No. 4 rules, even if all of the reinforcing is placed on the outside.

It may be noted that no test data giving stresses at the inside corner are available within the range of Eringen's analysis for either a reinforced or unreinforced model with large D/T; i.e., greater than 29.5.

---

\* The elastic stress limit of 3S is one of two criteria used in establishing Phase Report No. 4 rules.

TABLE 18. COMPARISON OF REINFORCING AREA USED IN TEST MODELS WITH THE REINFORCING AREA REQUIRED BY PHASE REPORT NO. 4

Model Iden.	$\frac{D}{T}$	$\frac{d}{D}$	$A/d_1 T$		Measured Stress $\sigma/S$ (1)
			Required P.R. 4	Used in Model	
FIW	20.2	.16	.75	1.90	1.80
AIW	14.8	.15	.75	.85	2.22
WCN-6C	13.1	.20	.75	.64	(2.18)
WC-11B	13.2	.20	.75	.63	2.64
9	29.5	.043	.24	.25	(2.08)
10	↓	.043	.24	.60	2.77
11		.084	.75	.70	2.53
12		.043	.24	.75	2.72
13		.084	.75	.65	(2.04)
14		.084	.75	1.00	2.53
16		.161	.75	.80	2.67
2		19.0	.27	.75	1.30
6	↓	.27	.75	.75	2.96
8		.084	.59	.75	2.60
9		.083	.58	1.10	2.61

(1)  $\sigma_n$  at inside corner, except values in parenthesis were at approximately the middle of the shell wall.



Comparisons of Semi-Uniform Wall  
Nozzles with Eringen's Theory

If it is assumed that the effective length of a uniform-wall nozzle is equal to  $\sqrt{dt}$ , then a number of the test models\*listed in Table 15 can be considered to be effectively uniform-wall models and hence directly comparable with Eringen's theory. Table 19 shows such comparisons. The values of  $s/S$  and  $d/D$  are different than those shown in Table 15 because they are based on the nozzle thickness near the juncture with the shell.

As shown in the last column of Table 19, on the average the theory gives somewhat lower stresses than measured. It is not apparent that this is entirely due to the nozzle-thickness reduction since in some models the uniform-wall nozzles length was considerable greater than  $\sqrt{dt}$ . (e.g., Model 10, in which  $L_n = 2.7 \sqrt{dt}$ .)

Effect of Inside Corner Radius,  $r_i$

Eringen's analysis does not give any direct guidance as to the effect of variations in  $r_i$ . This report, in so far as internal pressure loading is concerned, is directed principally to comparisons of Eringen's analysis with test data. It has been shown (see p.61) that the analysis can be highly conservative with respect to stresses in the nozzle of test models with a large (compared to  $\sqrt{rt}$ ) fillet radius or, perhaps, a large fillet weld. A very small (compared to  $\sqrt{rt}$ ) fillet radius might

---

\* Type C reinforcing as shown in Figure 23.

TABLE 19. COMPARISON OF SEMI-UNIFORM WALL NOZZLES WITH ERINGEN'S THEORY

Model Iden.	Ref. No.	$\frac{D}{T}$	$\frac{d}{D}$	$\frac{s}{S}$	$\sqrt{dt}$	$L_n(1)$	Test $K_e$	Calculated $K_t(2)$	$\frac{K_t}{K_e}$
AIW	(24)	14.8	.19	.25	.72	.73	2.22	2.2	.99
10	(20,21)	29.5	.054	.12	1.39	3.75	2.77	2.3	.83
11			.099	.15	2.32	4.75	2.53	2.4	.95
12			.054	.12	1.39	1.62	2.72	2.3	.85
14			.099	.15	2.32	2.50	2.53	2.4	.95
16			.18	.19	3.76	6.25	2.67	2.5	.94
8	(22)	19.0	.11	.19	2.14	2.88	2.62	2.2	.84
								Average	.91

(1) See Figure 23.

(2) Eringen's analysis,  $\sigma_{\theta_1}$  at  $\rho = \rho_0$ ,  $\theta = 0$ . Obtained by interpolation using Tables A1 and A3 of the Appendix.

increase stresses so that Eringen's analysis would be unconservative. The question also arises; within what range of inside corner radius will Eringen's analysis be reasonably accurate.

Experimental data on the effect of inside corner radius on maximum stresses (which occur on the inside corner) were reviewed by Mershon<sup>(26)</sup>. Since the publication of Reference (26), some additional test data has become available. These additional data, along with part of the data given by Mershon<sup>(26)</sup> are summarized in Figure 24 and will be discussed in the following.

(1) Photoelastic Test Models, Reference (24)

Results are given for four models\* essentially identical to each other except for  $r_i$ . The results are:

<u>Model Iden.</u>	<u>E-1</u>	<u>E-7</u>	<u>E-2</u>	<u>E-3</u>
$r_i/T$	0.11	0.34	0.55	1.00
$\sigma_n/S$ (original)	3.32	2.92	2.80	3.04
$\sigma_n/S$ (revised)	--	3.36	2.90	3.28
$\sigma_{\phi_i}/S$ (Eringen)	2.94	2.94	2.94	2.94

Because of inconsistencies in some of the original test data, slices from Models E-7, E-2, and E-3 were re-examined in the light of additional experience and practice in the photoelastic "frozen stress" technique. On the average, the revised stresses are 9% higher than the original stresses. Unfortunately, slices from the model with the sharpest corner (E-1) could not be found; in Figure 24 it is assumed that the comparative stress for Model E-1 is 1.09 times the original reported stress.

---

\* See Table 4 for dimensional parameters of these models.

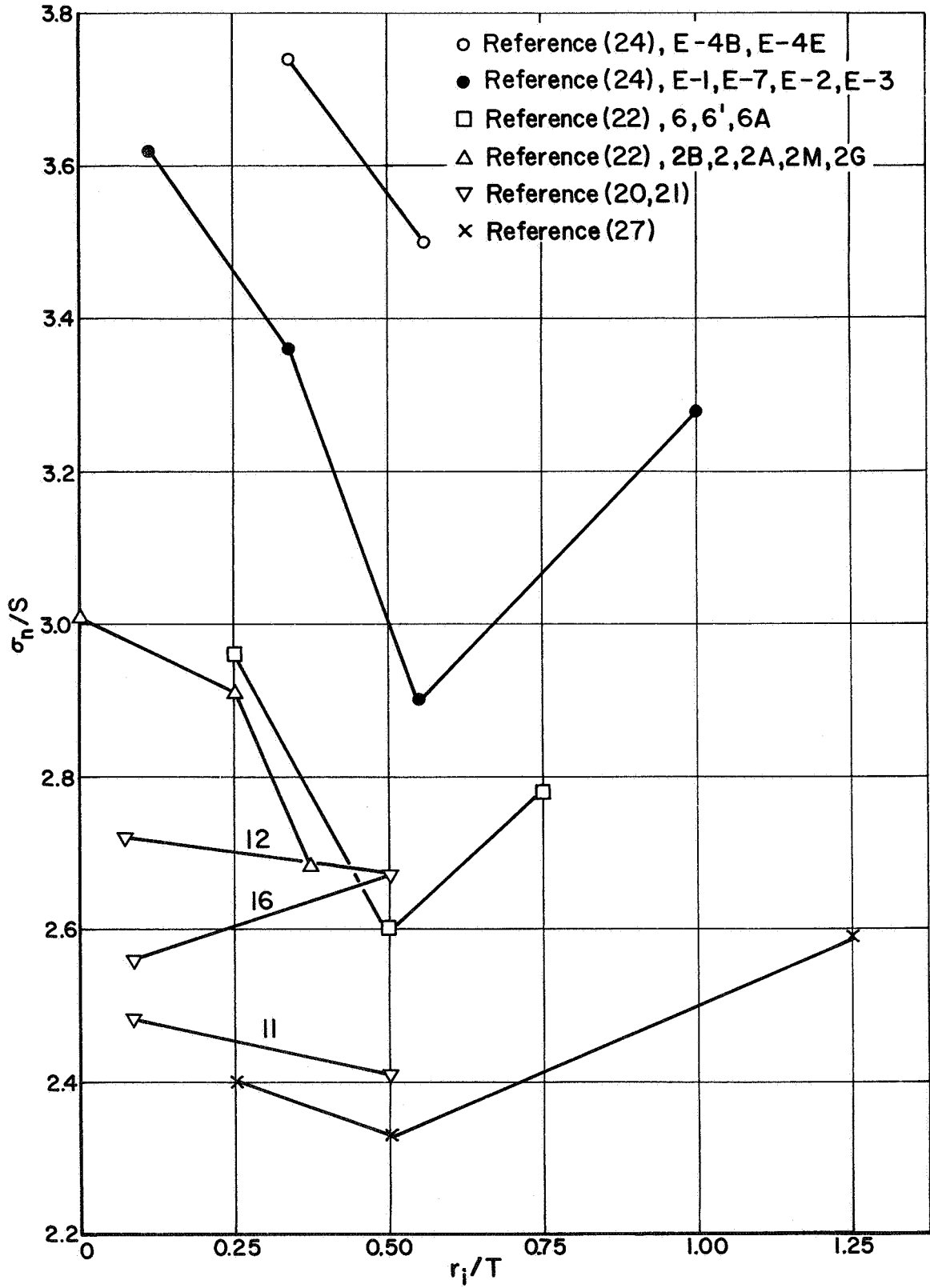


FIGURE 24. EFFECT OF INSIDE CORNER RADIUS  $r_i$  ON MAXIMUM MEASURED STRESSES

Models E-4B and E-4E ( $D/T = 13$ ,  $d/D = 0.5$ ,  $s/S = .99$ ,  $r_o/T = .67$ ) are beyond the range of Eringen's analysis, but they give additional information of the effect of  $r_i$ . The results are:

<u>Model Iden.</u>	<u>E-4B</u>	<u>E-4E</u>
$r_i/T$	0.56	0.34
$\sigma_n/S$	3.50	3.74

(2) Steel Test Models, Reference (22)\*

There are two sets of data on nozzles with  $r_i/T$  as the only variable. Results are:

Nozzle	6	6' **	6A	2B	2	2A, 2M, 2G †
$r_i/T$	.25	.50	.75	0	.25	.375
$\sigma_n/S$	2.96	2.60	2.78	3.09	2.91	2.68
No. of Tests	7	1	4	1	7	3

The value of  $\sigma_n/S$  is the average of the test data (see Table 16). The single result for the square corner (2B) is based on an estimated longitudinal strain as measured on the corner 180° opposite.

(3) Steel Models, Reference (20, 21)\*\*\*.

There are three sets of data with  $r_i/T$  variable; i.e.,

- 
- \* See Table 15 for dimensional parameters of these models.
  - \*\* See Footnote (5) of Table 16.
  - † See Footnote (2) of Table 16.
  - \*\*\* See Table 15 for dimensional parameters of these models.

Nozzle	11a, 11a'	11b	12a	12b	16a, 16a'	16b
$r_i/T$	.074	.50	.074	.50	.074	.50
$\sigma_n/S$	2.48	2.41	2.72	2.67	2.56	2.67
$\sigma_{\phi_i}/S^*$	2.4	2.4	2.3	2.3	2.5	2.5

These sets of data do not indicate a large influence of  $r_i$  on maximum stresses. Models 11 and 12 agree with the general trend of test data shown in Figure 24 in that stresses are reduced by increasing  $r_i/T$  in the range from 0 to 0.50. Models 16 give an opposite indication.

#### (4) Steel Models, Reference (27)

Tests were run on three nozzles with dimensional parameters as follows:

Model No.	$\frac{D}{T}$	$\frac{d}{D}$	$\frac{r_i}{T}$	Reinf. Type	$\frac{A}{d_i T}$	$\sigma_n/S$ at Inside Corner
R25-1	23.7	.055	.25	B	1.52	2.40
R25-2	↓	↓	.50	↓	1.46	2.33
R25-3	↓	↓	1.25	↓	1.01	2.59

The only dimensional variable is the inside corner radius,  $r_i$ . The reinforcing type is shown in Figure 23, type B, with  $\alpha = 18^\circ$ ,  $L_n = 2.25 T$ . The reinforcing area A was calculated as indicated in footnote (3) of Table 15. These nozzles are three of a set of 12 nozzles placed around the circumference of the cylindrical shell. The space between openings is  $0.93 \sqrt{RT}$  (on outside surface), hence some interaction between adjacent nozzles probably occurred. Also, it appears that the nozzles were directly welded to flanges or plugs; possibly these closures also influenced the results. Neither of these conditions would be expected to significantly change the relative values of  $\sigma_n/S$  at the inside corner.

\* Eringen analysis, see Table 19.

As can be noted in Figure 24, the photoelastic model tests and most of the steel model tests indicate a reasonably consistent trend of  $\sigma_n/S$  with  $r_i/T$ ; a high stress for a sharp corner, decreasing as  $r_i/T$  increases to about 0.5, then increasing as  $r_i/T$  is increased further.

Additional evidence of the effect of a square inside corner is available from the fatigue tests of Reference (22). Vessel 7 contained nozzles 2B and 2N, which differ only in the inside corner radius:

Nozzle	$r_i/T$	Cycles-to-Failure*
2B	0	147,665
2N	.25	375,357

The ratio of cycles for 2N to 2B is 2.54. Assuming that  $N \propto \sigma^{-5}$ , where  $\sigma$  is the fatigue effective stress, the ratio of cycles-to-failure implies a stress ratio of  $(2.54)^{.2} = 1.205$ . The measured stress ratios for these nozzles on Vessel 7 is  $3.09/2.725 = 1.14$ .

The only other comparison\*\* in the fatigue tests of Reference (22) is in Vessel 4, Nozzles 6 and 6A. Nozzle 6 leaked at 40,041 cycles at which time both Nozzles 6 and 6A were removed from the vessel. This indicates some qualitative superiority of Nozzle 6A ( $r_i/T = 0.75$ ) over Nozzle 6 ( $r_i/T = 0.25$ ).

---

\* Nozzle 2B did not leak at 147,665 but was removed at that number of cycles to avoid a large fracture. Nozzle 2N leaked at 375,357 cycles. A crack was detected (ultrasonic examination) in Nozzle 2B at 135,233 cycles. No crack was detected in Nozzle 2N prior to the leak at 375,357 cycles. In both nozzles 2B and 2N, at the cycles listed, a smaller crack had also developed at the 180° location, giving some statistical weight to the relative fatigue resistance of these two nozzles.

\*\* In Vessel 6, containing both nozzles 6 and 6A, a failure occurred first at Nozzle 6A, however the crack initiated from an arc strike on the outside surface.

It might be remarked that accurate measurement of strains on an inside corner with small  $r_i$  is quite difficult, hence the confirming evidence of the fatigue tests is significant.

The increase in stress with large values of  $r_i/T$  may be the result of removing a substantial amount of reinforcing material in comparison to the total effective reinforcing area. If so, the optimum value of  $r_i/T \approx 0.5$  indicated by Figure 24 may not be correct for larger values of  $D/T$  (test data covers  $D/T$  from 13 to 30) or for different types of reinforcing.

It appears from the test data cited above that Eringen's analysis is reasonably accurate for inside corner radii in the range  $r_i/T$  from about 1/8 to 1/2. As pointed out by Mershon<sup>(26)</sup>, for nozzles subjected to rapid temperature variation the sharp inside corner should be removed to reduce thermal stresses. Also, some radius on the inside corner appears desirable to remove any machining tears left at the sharp corner which might be fatigue crack initiation points.

#### Stresses at Reinforcing Edge

In the section, "Comparison of Eringen's Theory with Test Data", it was noted that the maximum measured stress always occurred at the inside corner\*. The hypothesis was advanced that with a sufficiently small fillet radius the maximum stress might appear in the nozzle at its juncture with the outside surface of the shell wall. The last column of Table 15 shows the maximum measured stresses at the reinforcing edge. These all occurred on the outside surface, tangential to the shell wall at  $\theta = \pi/2$ .

---

\* Models with no inwardly protruding reinforcement. Table 15 shows three test models with inside reinforcing in which the maximum measured stress was not at the inside corner.



It will be noted that in some models this stress is approaching the value of the maximum measured stress and in Model WC-5LM the maximum measured stress was at the reinforcing edge, not at the inside corner. In the following section, "Comparison of Lind's Analysis with Test Data", nozzles with large  $d/D$ -ratios are included. In Table 20, Model C-7C is another example of the maximum stress occurring at  $\phi = \pi/2$ . It should be noted that fatigue tests of welded-on-pad reinforced nozzles<sup>(28)</sup> have shown that the  $\phi = \pi/2$  location may be a critical location. Field failures<sup>(28, 29, 30)</sup> of welded-on-pad reinforced branch connections also indicate that stresses at the fillet weld between pad and shell may be the critical location\*. Accordingly, stresses at the edges of reinforcing should not be ignored.

In the rules of Phase Report No. 4, requirements for transitions between reinforcing and the nozzle and/or shell are included. It might be noted that for reinforcing to area requirements (Figures 2e and 2f of Phase Report No. 4), the transition radii are proportioned to the amount of reinforcing area actually used. That is, if the section is heavily over-reinforced (such as at  $\phi = \pi/2$  on Model WC-5LM), a correspondingly greater transition fillet radius is required. The data presented herein indicates that the rules of Phase Report No. 4 should be sufficient to prevent the development of high stresses at the reinforcing edges. In this respect, it might be noted that the rules of Phase Report No. 4 are limited to the range covered by Eringen's theory. Both of the test models cited herein which had maximum stresses at  $\phi = \pi/2$  also had  $d/D$ -ratios well above the range covered by Phase Report No. 4; i.e., WC-5LM,  $d/D = 0.50$ ; C-7C,  $d/D = .73$ .

---

\* However, welded-on pad reinforcing is not permitted in the design rules of Phase Report No. 4.

COMPARISON OF LIND'S ANALYSIS  
WITH TEST DATA

Lind<sup>(2)</sup> gives a comparison of the K-factors\* obtained by his analysis with test data for a number of uniform-wall nozzles in cylinders. Table 20 herein includes those comparisons along with comparisons with additional test data. Included in the comparisons are several "semi-uniform" wall nozzles as shown in Figure 23, Type C, with  $L_n > \sqrt{dt}$ . These are: Ref. (24), Model AIW; Ref (20, 21), Models 10, 11, 12, 14, and 16 and Ref. (24), Models 2 and 8. Also included are five "drawn outlet" nozzles; Models G, H, D, E, and L from Reference (31).

The 44 models listed in Table 20 represent a fairly wide range of the parameters  $d/D$ ,  $D/T$ , and  $s/S$ . The ratio of  $K/K_e$  ranges from 0.79 to 1.45, with an average for the 44 models of 0.96. It appears, therefore, that Lind's analysis provides a good method of calculating the normal stress on the inside corner of nozzles similar to those listed in Table 20.

The maximum stress in Model C-7C occurred at the outside surface at  $\theta = \pi/2$ . Lind's analysis does not give stresses other than the  $\sigma_n$ -stress at the inside corner,  $\theta = 0$ .

---

\* See page 19.

TABLE 20. COMPARISON OF TEST DATA,  $\sigma_{\phi i}$  at  $\rho = \rho_o$ ,  $\phi = 0$ ,  
WITH LIND K-FACTOR

Model Iden.	Ref.	$\frac{D}{T}$	$\frac{d}{D}$	$\frac{s}{S}$	Test $K_e$	Lind $K$	$\frac{K}{K_e}$	Eringen Theory
C-1A	(24)	13.0	.05	1.04	2.45	2.66	1.09	2.45
C-2A		13.1	.13	.97	2.80	2.64	.94	2.62
C-3A		13.0	.20	1.01	3.0	2.61	.87	3.15
E-4		13.4	.50	.98	3.50	3.84	1.10	
E-4B		13.2	.50	.99	3.50	3.83	1.09	
E-4E		13.3	.50	.98	3.8	3.83	1.01	
C-7A		13.1	.80	.99	4.10	4.42	1.08	
C-8A		13.0	1.00	1.00	4.11	4.51	1.10	
C-3C		6.50	.18	2.02	3.09	2.75	.89	2.72
C-5C		6.58	.46	1.96	4.1	3.33	.81	
C-7C		6.50	.73	1.98	4.16*	4.35	1.04	
C-5H		13.1	.57	.42	2.70	2.63	.98	
C-7H		13.0	.91	.41	2.73	2.18	.80	
E-1		13.1	.29	.56	3.32	2.73	.82	2.94
E-2		12.9	.29	.59	2.90	2.74	.95	2.94
E-3		13.0	.29	.58	3.28	2.74	.84	2.94
E-7		13.3	.29	.56	3.36	2.74	.82	2.94
AIW		14.8	.19	.26	2.22	2.00	.99	2.2
7	(20,21)	29.5	.043	.34	2.64	2.56	.97	2.45
8		29.5	.043	.34	2.64	2.56	.97	2.45
10		29.5	.054	.12	2.77	2.30	.83	2.3
11		29.5	.099	.15	2.53	2.18	.86	2.4
12		29.5	.054	.12	2.72	2.30	.85	2.3
14		29.5	.099	.15	2.53	2.18	.86	2.4
15		11.9	.16	1.13	2.70	2.64	.98	2.87
16		29.5	.18	.19	2.67	2.17	.81	2.5
2	(22)	19.0	.32	.26	2.91	2.28	.79	
8		19.0	.11	.19	2.60	2.27	.87	2.2
11		19.0	.058	.62	2.57	2.61	1.01	2.47
G	(29)	19.0	.63	.92	3.70	4.57	1.24	
H		19.0	.65	1.74	3.84	5.56	1.45	
D		19.0	.63	.92	4.93	4.57	.93	
E		19.0	.65	1.74	5.08	5.56	1.10	
L		19.0	.33	.76	3.78	3.34	.89	
R		19.0	.63	.92	5.00	4.57	.92	
S		19.0	1.00	1.00	5.42	5.11	.95	
A	(23)	26.9	.31	.31	2.6	2.75	1.06	
B		26.9	.30	.48	3.0	3.22	1.07	
C		26.9	.28	1.23	4.0	3.56	.89	
K		9.35	.20	1.04	3.3	2.67	.81	2.98
M		9.35	.29	.99	3.3	2.71	.82	3.42
R1	(30)	98.	.34	1.02	5.7	6.42	1.13	
R2		98.	.35	.15	2.5	2.46	.98	
--	(31)	240.	.50	.50	8.33	8.88	1.07	
Average							.96	

\* Stress at inside corner; maximum stress was 4.72 S,  $\sigma_{to}$  at  $\phi = \pi/2$

STRESSES DUE TO EXTERNAL LOADS APPLIED TO NOZZLE

A complete set of external loadings on a branch connection is shown in Figure 25. There are twelve independent forces\*, each of which produce a complex field of stresses in the vicinity of the nozzle-to-cylinder juncture. By linear elastic theory, the stress due to any combination of these twelve forces can be obtained if the stress field due to each of the twelve forces is known.

For small nozzles in cylindrical shells, major simplification is possible, because the stresses in the vicinity of the nozzle due to forces applied at (2) are not significantly altered by the relative-magnitude of the reactant forces at (A) and (1). For example,  $M_{2x}$  could be equilibrated entirely by  $-M_{1x}$ ; or by  $M_{1x} = -.5 M_{2x}$  plus  $M_{Ax} = -.5 M_{2x}$ , without significant change in the stress field in the vicinity of the nozzle. The same assumption could not be made where the nozzle is about the same size as the cylindrical shell.

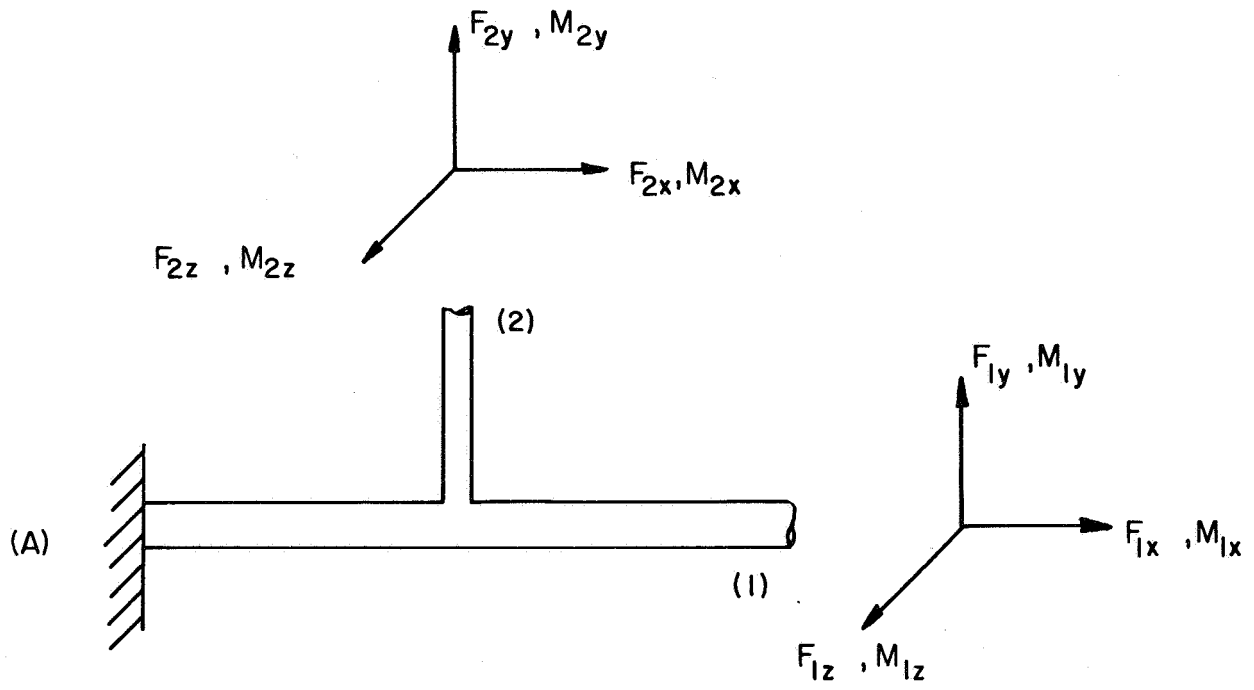
Test Data--Elastic Stresses

Available test data on stresses produced by external loadings of uniform wall cylindrical nozzles in uniform wall cylindrical shells are summarized in Table 21\*\*. Available test data for models with local reinforcing are summarized in Table 22. All test data are for forces or moments applied to the nozzle.

---

\* The set of forces at the anchor (A) and the stresses induced thereby are obtainable from the applied forces at (1) and (2) and their stress fields.

\*\* Table 21 includes three "drawn-outlet" tees which are not "uniform-wall" but appear to be best classified as such.



$F_{ij}$  = force , lb.

$M_{ij}$  = moment , in.-lb.

FIGURE 25 . GENERAL SET OF EXTERNAL LOADS ON A BRANCH CONNECTION

TABLE 21. SUMMARY OF TEST DATA FOR EXTERNAL LOADS APPLIED TO  
A UNIFORM WALL NOZZLE IN A UNIFORM WALL CYLINDER

Ref. No.	Nominal Size (1)	$\frac{D}{T}$	$\frac{d}{D}$	$\frac{s}{S}$	Load	(2)		Location & Direction of		$\frac{\sigma'}{S}$	
						$\frac{\sigma_{max}}{S}$	$\phi$	Surface	$\alpha$		
(34)	56x12 (T=1.3")	43	.19	.29	Mi	2.49	0	Out	0	4.1(a)	
					Mo	4.11	90	Out	0	6.2(a)	
					L	7.05	90	Out	0	9.8(a)	
(35)	56x12 (T=2.08")	27	.19	.46	Mi	1.42	0	Out	90	2.1(a)	
					Mo	2.54	45	Out	-	3.8(a)	
					L	3.10	45	Out	-	4.6(a)	
(36)	24x4	76	.18	.24	Mi	3.75	0	Out(b)	0	4.5	
					Mo	7.18	90		0	10.	
(37)	24x12	76	.53	.66	Mi	2.43	30		130	5.1	
					Mo	6.22	90		0	12.	
(38)	24x24	76	1.00	1.00	Mi	5.15	90		45	8.4	
					Mo	11.2	90		90	14.	
(39)	36x4 (E)	93	.12	.30	Mi	1.4	0(d)	Out	0	2.1(a)	
					Mo	2.7	90	Out	0	3.5	
					L	6.0	90	Out	0	8.1	
(40)	36x6 (C)	93	.18	.25	Mi	4.25	0	Out	0	4.7	
					Mo	8.5	90	Out	0	10.5	
					L	14.0	90	Out	0	16.7	
(41)	10x10	16	1.00	1.00	Mi	2.2	45	Out	-	(e)	
					Mo	3.4	67.5	Out	-	(e)	
(42)	48x6(f)	78	.13	.29	Mi	3.0	0	Out	0	3.1(a)	
					Mo	4.4	90	Out	90	4.4(a)	
					L	9.3	90	Out	90	9.9(a)	
(43)	20x6(f)	19	.32	.76	Mi	1.73	0	Out	90	-	
					Mo	2.19	90	Out	90	-	

TABLE 21. (Continued)

Ref. No.	Nominal Size (1)	$\frac{D}{T}$	$\frac{d}{D}$	$\frac{s}{S}$	Load	(2)		(3)		$\frac{\sigma'}{S}$	(4)
						$\frac{\sigma_{max}}{S}$	Location & Direction of $\sigma_{max}$ Surface	$\alpha$	$\varphi$		
(31)	20x12(f) (D)	19	.63	.92	Mi	2.70	Trans.	Out	168	30	-
					Mo	4.36	Trans.	Out	90	-	
					L	8.70	Nozzle	In	90	-	
					$M_t$	-3.18	Trans.	In	31	-	
(32)	20x12(f) (E)	19	.65	1.74	Mi	2.03	Nozzle	Out	172	15	-
					Mo	2.33	Nozzle	Out	175	-	
					L	5.25	Nozzle	Out	24	-	
					$M_t$	3.41	Trans.	Out	42	-	
(33)	20x12(f) (R)	19	.64	.92	Mi	3.53	Flillet	Out	90	0	-
					Mo	8.55	Nozzle	Out	90	-	
					L	12.5	Nozzle	Out	90	-	
(34)	20x20 (S)	19	1.00	1.00	Mi	5.2	Flillet	Out	90	0	-
					Mo	5.25	Cyl	Out	24	-	
					L	23.6	Cyl	Out	46	-	
(35)	24x12 (C-1)	230	.50	.50	Mi	18.5	Flillet	Out	0	60	-
					Mo	90.	Flillet	Out	0	-	
					L	100.	Flillet	Out	0	-	

(1) Symbols in parentheses under the nominal size give further identification of the test models in accordance with the references cited.

(2) S = nominal stress in nozzle  
 $S = M/Z$   
 $Z = \pi r^2 t$   
 $M_t$   
 $S = M_t/2Z$   
 $S = L/A$   
 $A = 2\pi r t$   
 $\sigma_{max}$  = maximum measured stress

TABLE 21. (Continued)

Footnotes to Table 21 (Continued)

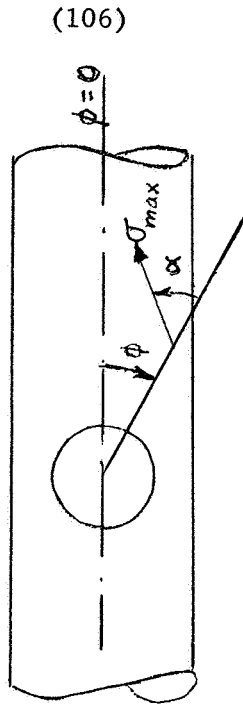
(3) Location and Direction of Maximum Measured Stress

Column Shell identifies whether  $\sigma_{max}$  occurred on nozzle, cylinder or the juncture between cylinder and nozzle. For Reference (31) models L, D and E (drawn-outlet tees), trans. means  $\sigma_{max}$  occurred in the radius between cylinder and nozzle. For References (31) and (33) fillet means  $\sigma_{max}$  occurred in the (ground-off) fillet weld between cylinder and nozzle.

Column  $\varphi$  identifies location around nozzle; see Nomenclature, page 9.

Column Surface, Out means  $\sigma_{max}$  occurred on outside surface; In means  $\sigma_{max}$  occurred on the inside surface.

Column  $\alpha$  identifies direction of  $\sigma_{max}$  as shown in sketch.



(4)  $\sigma'/S$  is an approximate extrapolated value of test data to the toe of the fillet weld between cylinder and nozzle. It does not include stress concentrations at the toe of the fillet weld.

(a) Extrapolated stress in cylinder. Test data is not sufficient to estimate maximum stress in branch pipe; in some models, the maximum stress in the nozzle is probably higher than the stress shown.

(b) Strain gages on the outside only.

(c) No data for stresses in nozzle.

(d) Test data at  $\varphi = 0$  and  $\varphi = 90$  only.

(e) Data insufficient to extrapolate to maximum stress on either cylinder or nozzle.

(f) These test models are "drawn-outlet" tees. Contours of Models L and D are shown in Figures 30 and 31.



TABLE 22. SUMMARY OF TEST DATA FOR EXTERNAL LOADS, APPLIED TO NOZZLE, MODELS WITH LOCAL REINFORCING

Ref. No.	Nominal Size (1)	D T	d D	s S	Load	$\sigma_{max}$ S	(2)		(3)		$\sigma$ S	(4)																								
							$\sigma_{max}$ S	Location & Direction of $\sigma_{max}$ Surface $\alpha$	Shell	$\alpha$																										
(38)	24x4(a) (Saddle)	76	.18	.24	Mo	2.6	Cyl	90°	Out	0	4.	(g)																								
													24x8(a) (Saddle)	76	.35	.44	Mo	4.8	Cyl	90°	Out	0	7.	(g)												
																									24x12(a) (Saddle)	76	.53	.66	Mo	4.9	Cyl	90°	Out	0	7.	(g)
24x8(b) (Pad)	76	.35	.44	Mo	3.7	Cyl	90°	Out	0	6.	(g)																									
												24x12(b) (Pad)	76	.53	.66	Mo	5.7	Cyl	90°	Out	0	8.	(g)													
(36)	10x10(c) (Pad)	16	1.00	1.00	Mi Mo	1.7 2.0	Nozzle Nozzle	22.5 61.5	Out Out	-	-	(h) (h)																								
													8x8(d) (Tee)	16	1.00	1.00	Mi	1.4(i)	Cyl	~80	In	-	-	-												
(37)	48x6(e)	78	.13	.29	Mi Mo L	1.2 4.3 8.5	Nozzle Nozzle Nozzle	0 90 90	Out Out Out	0 0 90	1.4 4.3 8.4	(g) (g) (g)																								
													20x6(f) (F)	19	.32	.75	Mi Mo L	1.41 1.49 3.28	Nozzle Nozzle Juncture	22.5 67.5 45	Out Out Out	0 2 9	-	-	-											
																										20x6(f) (I)	19	.32	.75	Mi Mo	1.15 1.14	Nozzle Juncture	22.5 90	Out Out	5 90	-
20x6(f) (J)	19	.32	.75	Mi Mo	1.42 1.18	Nozzle Nozzle	22.5 67.5	Out Out	7 4	-	-	-																								

## FOOTNOTES FOR TABLE 22.

(1) Symbols in parentheses under the nominal size give further identification of the test models in accordance with the references cited.

(a) Saddle Dimensions:	24x4	24x8	24x12
$T_s$	0.375"	0.468"	0.468"
$D_s$	9.625"	17.25"	23.75"
$H_s$	2.0"	3.0"	3.5"

$T_s$  = Saddle thickness (average),  $D_s$  = saddle outside diameter,  $H_s$  = height of saddle above cylinder surface.

(b) Pad Dimensions:	24x4	24x8	24x12
$T_p$	0.375"	0.375"	0.375"
$D_p$	7.75"	15.75"	24.5"

$T_p$  = pad thickness,  $D_p$  = pad outside diameter.

(c) Pad Dimensions:  $T_p = 0.625"$ ,  $D_p = 19.875"$ .

(d) This specimen is described as an 8" Sch.80 welding tee. Presumably, it met the dimensional and strength requirement of ASA B16.9 and was typical of tees sold under this standard.

(e) Pad Dimensions:  $T_p = 0.625"$ ,  $D_p = 10.5"$

(f) Dimensions of these specimens are shown in Figure 26.

(2) S = nominal stress in nozzle

$M_i$ or $M_o$	$M_t$	L	$\sigma_{max}$ = maximum measured stress
$S = M/Z$	$S = M_t/Z$	$S = L/A$	
$Z = \pi r^2 t$		$A = 2\pi r t$	

(3) Location and Direction of maximum measured stress

Column Shell identifies whether  $\sigma_{max}$  occurred on nozzle, cylinder or the juncture between cylinder and nozzle. For Reference (31), models F, I, & J, juncture means  $\sigma_{max}$  occurred in the radius between cylinder and nozzle.

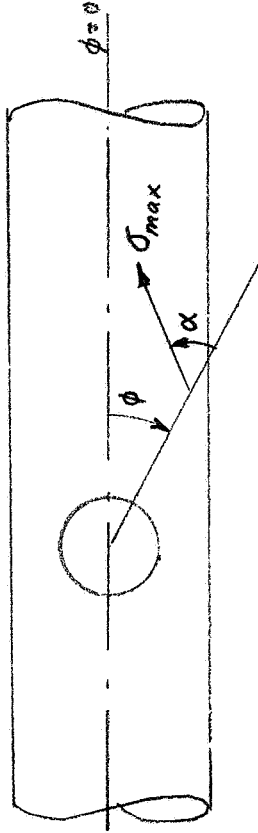
Column  $\varphi$  identifies location around nozzle; see Nomenclature, page 9.

Column Surface, Out means  $\sigma_{max}$  occurred on outside surface; In means  $\sigma_{max}$  occurred on the inside surface.

Footnotes for Table 22. (Continued)

(3) (Continued)

Column  $\alpha$  identifies direction of  $\sigma_{max}$  as shown in sketch

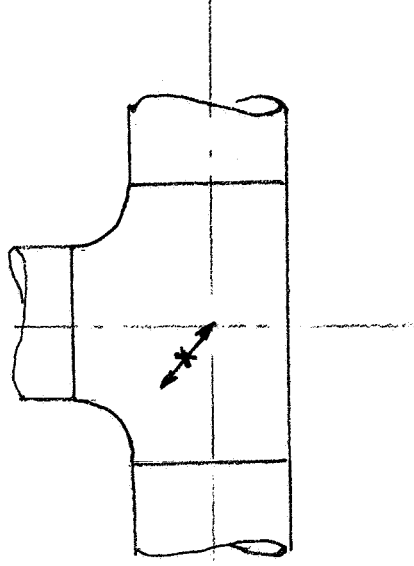


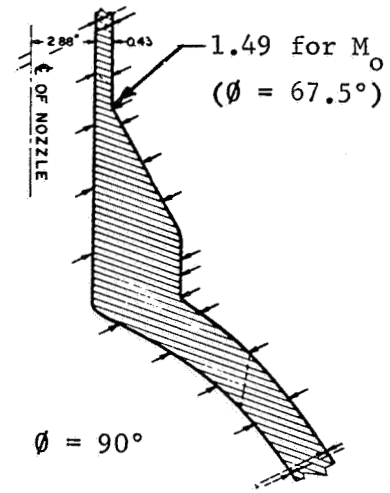
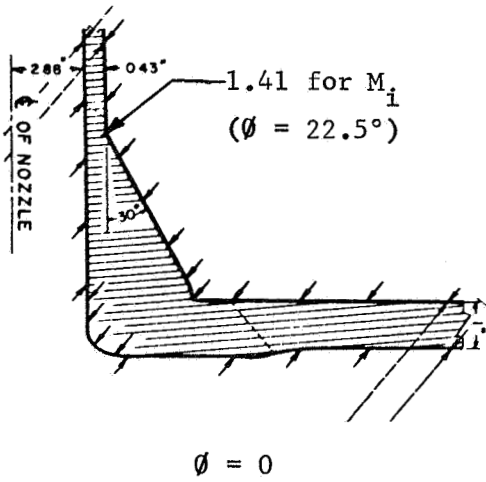
(4)  $\sigma' / S$  is an extrapolated value of test data to the toe of the fillet weld between cylinder and pad or saddle. It does not include stress concentrations at the toe of the fillet weld.

(g) Extrapolated stress in cylinder. Test data is not sufficient to estimate maximum stress in nozzle; in some models, the maximum stress in the nozzle is probably higher than the stress shown.

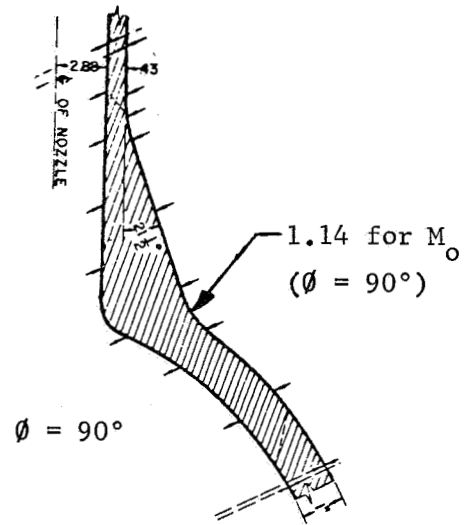
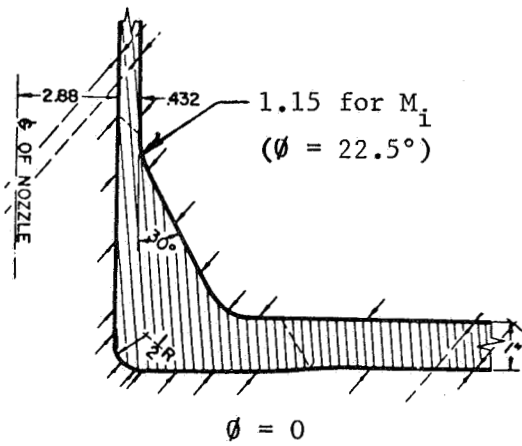
(h) Data insufficient to extrapolate to maximum stress in either cylinder or nozzle.

(i) Location and direction of  $\sigma_{max} / S$  shown in sketch at right.

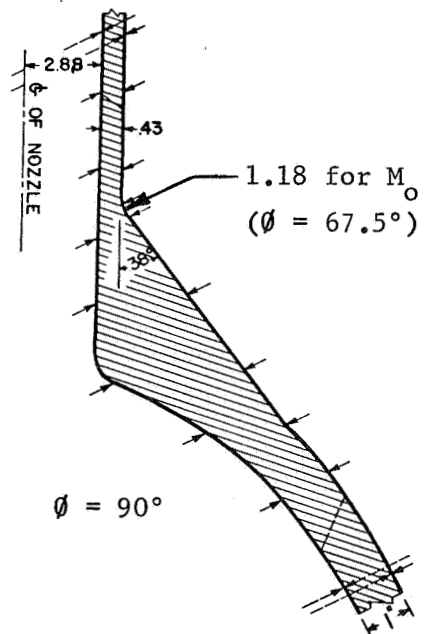
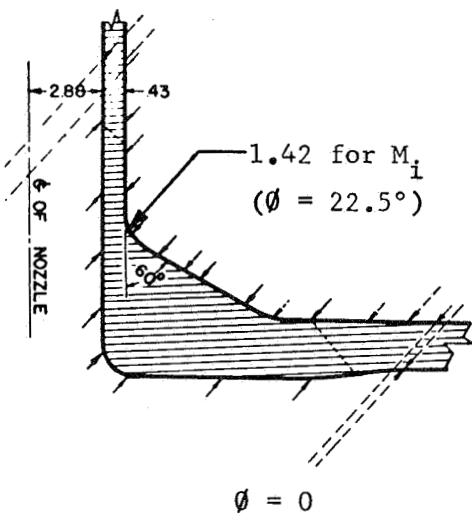




MODEL F



MODEL I



MODEL J

FIGURE 26. CONTOURS OF MODELS F, I, AND J, REFERENCE (31) AND MAGNITUDES AND LOCATIONS OF MAXIMUM STRESS INDICES

The location and type of reactant forces are not clearly indicated in most of the references cited. In most of the references, moment loads  $M_i$  and  $M_o$  were actually obtained by forces applied to the nozzle at a distance from the surface of the cylinder. To the extent that this distance was large, the moment at the nozzle-cylinder juncture would be large compared to the shear force and, presumably, the stresses arise almost entirely from the moment.

The signs of the stresses are for the force directions and  $\phi$ -locations as defined in the nomenclature, page 10. In-so-far as the behavior of the test models is linear and elastic, all stress signs change with a change in force direction.

Some of the test data is based on strain gage results in only one quadrant. For small nozzles, and large nozzles with symmetric reactant forces, the stresses in the other three quadrants would be the same magnitude as those measured; with appropriate sign changes. This assumes, of course, that the test model itself is symmetrical.

Elastic stresses in Tables 21 and 22 are shown as stress indices, the nominal stress being that in the nozzle when the nozzle is subjected to the indicated load. The stress indices are defined in the same manner as those for nozzles in spherical shells, Phase Report No. 2.

#### Test Data--Fatigue

Stress intensification factors for branch connections have been given in the ASA Code for Pressure Piping, ASA B31.1<sup>(39)</sup> since 1955. In July, 1963, ASA Code Case 53 was published with deals specifically with branch connections in which the branch is smaller than the run pipe.

The stress intensification factors given in the ASA Code are for the types of loadings shown in Figure 27. The data given in ASA B31.1-1955 are based upon bending fatigue tests reported by Markl<sup>(40, 41)</sup> and the equations he developed for the generalization of the test results. The stress intensification factors are related to a basic stress intensification factor of unity for a "typical" girth butt weld in straight pipe.

Three types of tees were tested:

- (1) Forged welding tees meeting the dimensional and strength requirements of ASA B16.9<sup>(42)</sup>
- (2) Fabricated (welded intersection) tees, without reinforcing
- (3) Fabricated tees, with a saddle or pad reinforcing.

All test specimens were made of carbon steel (ASTM A106 Gr B or equivalent). All of Markl's test were on 4-inch nominal size. A few tests by Blair<sup>(43)</sup> are included in Markl's evaluation of his tests; these were 6.5-inch outside diameter by 0.26-inch wall, fabricated reinforced and unreinforced tees. For fabricated tees, tests were made to investigate the effect of diameter-to-wall thickness ratio; i.e., wall thicknesses of 0.237-inch, 0.203-inch, and 0.053-inch.

The loading conditions are shown in Figure 27. For any one kind of tee, the first and second loading positions of Figure 27 gave practically identical results. The third loading position of Figure 27 gave higher fatigue cycles; data from it were disregarded in arriving at average stress intensification factors.

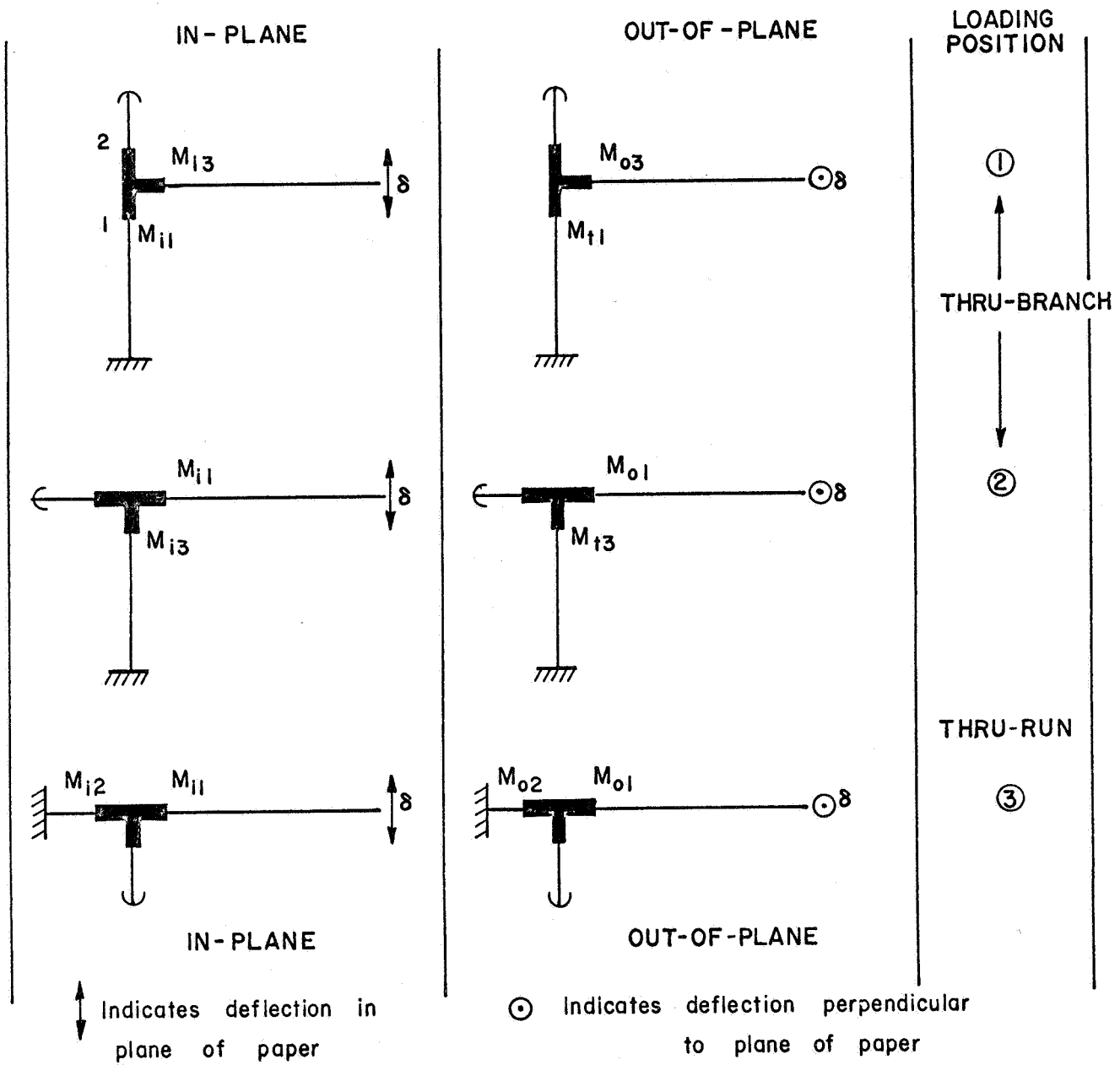


FIGURE 27 . TYPES OF LOADINGS, REFERENCE (40), FATIGUE TESTS ON TEES

Analysis of the fatigue tests of tees by Markl indicated that the general equation for fatigue life developed for girth butt welds in pipe and for welding elbows could also be applied to tees; i.e.:

$$i_f SN^2 = 245,000 \quad (6)$$

where

$i_f$  = fatigue stress intensification factor

( $i_f = 1.0$  for typical girth butt weld in pipe)

$S$  = nominal stress =  $M/Z$

$M$  = applied moment

$Z$  = section modulus of pipe

(for these tests nozzle size and run pipe size were equal)

$N$  = number of cycles to failure.

Because of the similarity of location and direction of fatigue failures in elbows, miter bends and tees, Markl based his empirical correlation equation for tees on an analogy with elbows. For elbows, the elastic stress intensification factor is known from theory; an asymptotic solution is of the form:

$$i_e = \text{constant}/h^{2/3} \quad (7)$$

where

$i_e$  = elastic stress intensification factor

$h = t R/r^2$

$t$  = elbow wall thickness

$R$  = elbow bend radius

$r$  = elbow cross-section radius



Markl's equation for the stress intensification factor for tees is:

$$i_f = \frac{0.9}{h_e^{2/3}}; \geq 1 \quad (8)$$

$$h_e = c t_e R_e / R^2 \quad (9)$$

where

$$c = (t_e / T)^{1.5}$$

$t_e$  = average of crotch and side-wall thickness, for welding tees

$t_e$  = pipe-wall thickness increased by one-half of the excess thickness provided in either run or branch, by use of thicker piping or pad or saddle, for reinforced fabricated tees.

$t_e$  = T for unreinforced fabricated tees, of a thickness equal to that of the matching pipe

T = thickness of matching pipe

R = mean radius of matching pipe (test data and equation are for "straight" tees, only, i.e., run and branch pipe are same size)

$R_e$  =  $R + r_c$  for welding tees, where  $r_c$  designates the crotch radius

$R_e$  = R for fabricated tees.

In a foot note in Reference (41), Markl stated: "For welding tees conforming to ASA Standard B16.9, assumption of  $R_e = 1.35 R$  and  $t_e = 1.60 T$  usually will produce conservative estimates of  $i$  on the basis of representative

measurements". This assumption was used to derive the equation for  $h$  given in the ASA Code, i.e.,

$$h_e = \left(\frac{t_e}{T}\right)^{1.5} \left(\frac{t_e R_e}{R^2}\right) = (1.6)^{1.5} \left(\frac{1.6 T \times 1.35 R}{R^2}\right) = 4.4 \frac{T}{R} \quad (10)$$

For unreinforced fabricated tees, Equation (9) with the definitions given reduces to:

$$h_e = \frac{T}{R} \quad (11)$$

and similarly for reinforced (pad or saddle) fabricated tees:

$$h_e = \left[\frac{T + T_p/2}{T}\right]^{1.5} \left[\frac{(T + T_p/2)R}{R^2}\right] = \frac{(T + T_p/2)^{5/2}}{T^{3/2}R} \quad (12)$$

where

$T_p$  = pad or saddle thickness.

The stress intensification factors from fatigue tests on full size tees may be summarized as:

$$i_f = 0.9/h_e^{2/3}$$

ASA B16.9 tees

$$h_e = 4.4 T/R$$

Fabricated unreinforced tees

$$h_e = T/R$$

Fabricated reinforced tees

$$h_e = (T + T_p/2)^{5/2} / (T^{3/2}R)$$

ASA B31.1 states that stress intensification factors were obtained from tests on full size outlet connections and that, for outlets less than full size, the full size factors should be used until more applicable factors are developed\*. In 1959, Markl prepared a report<sup>(44)</sup> which served as

---

\* However, the required value of the section modulus is not defined.

the basis for ASA B31 Code Case 53, which is reproduced herein as Figure 28. The report considered test data on elastic stresses due to external loads available at that time, plus cyclic bending tests<sup>(45)</sup> on reduced-outlet, saddle reinforced branch connections.

A summary of available fatigue tests on nozzles in cylinders, other than those in Reference (40), is given in Table 23.

Correlation of Elastic Stress Indices with  
Fatigue Stress Intensification Factors

Elastic stresses in welding elbows can be calculated from available theory; which theories have been adequately confirmed by strain-gage measurements on elbows. The elastic stress index for elbows turns out to be almost exactly twice the fatigue stress intensification factor. The reason for this factor of two arises principally from the use of unity for the fatigue stress intensification factor of a "typical" girth butt weld in pipe whereas, as compared to fatigue tests of a polished bar, such welds have fatigue stress intensification factors of around two at  $10^5$  cycles to failure.

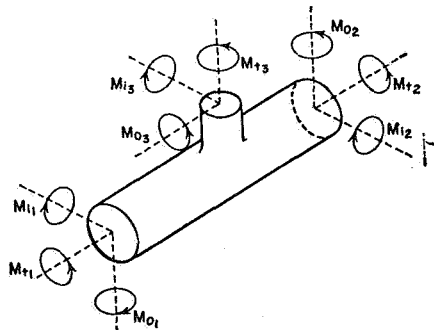
The combination of elastic stress measurements on three test models (L, D, and R) reported in Reference (31) and the bending ( $M_o$ ) fatigue tests on these same three test models reported in Reference (77) gives another correlation between elastic stress indices and fatigue stress intensification factors. The fatigue test results from Reference (47) are summarized in Figure 29. The details of the test specimens, location of fatigue failure and location and magnitude of the maximum measured elastic stress are shown in Figures 30, 31, and 32. A comparison of elastic stress indices with fatigue stress intensification factors is tabulated below.

### INTERPRETATIONS OF CODE FOR PRESSURE PIPING

#### Case 53 Stress Intensification Factor

*Inquiry:* Par. 621 (d) of ASA B31.1-1955, by reference to Fig. 2, provides a direct method for computing stress-intensification factors for full-size tees and fabricated branch connections. Application of the same factor to reducing-outlet connections, as recommended as a pro tem solution in Footnote 6, is believed to lead to gross over-evaluation of the stress range. Clarification and relief from an apparently unnecessarily severe requirement are desired.

*Reply:* The somewhat indefinite and conservative approach recommended by Footnote 6 reflects lack of theoretical or experimental data at the time of its formulation. Isolated test results which have since become available warrant modifying the present rules for full-size tees and branch connections and extending them to cover reducing-outlet tees and branch connections as follows by reference to ASA B31.1-1955:



effective branch section modulus in bending  $Z_0$  used in Equation (53-3) is a fictitious value used for purposes of test correlation:

$$Z_0 = \pi r_B^2 t_0 \dots \dots \dots (53-5)$$

where

- $r_B$  = mean branch cross-sectional radius
- $t_0$  = lesser of  $t_H$  and  $i_0 t_B$  = effective branch wall thickness

Determine in-plane bending moment  $M_i$ , out-of-plane bending moment  $M_o$ , and torsional moment  $M_t$  at the branch junction for each of the three legs and combine the resultant bending stress  $S_b$  and torsional stress  $S_t$  by Equation (13) in Par. 622 (b), where:

$$S_t = \frac{M}{2Z} \text{ for header and branch} \dots (53-1)$$

$$S_b = \frac{[(i_i M_i)^2 + (i_o M_o)^2]^{1/2}}{Z} \text{ for header} \\ \text{(legs 1 and 2)} \dots \dots (53-2)$$

$$S_b = \frac{[(i_i M_i)^2 + (i_o M_o)^2]^{1/2}}{Z_0} \text{ for branch} \\ \text{(leg 3)} \dots (53-3)$$

The value  $i_o$  of the out-of-plane stress-intensification factor appearing in Equations (53-2) and (53-3) equals the value  $i$  presently computed using the dimensions of the pipe matching the run of a tee or the header pipe.\* The value  $i_i$  of the in-plane stress-intensification factor is modified as follows:

$$i_i = 0.75 i_o + 0.25 \dots \dots (53-4)$$

The section modulus  $Z$  in Equations (53-1) and (53-2) is the section modulus of the header or branch pipe, for whichever the stress is being calculated. The

- $t_H$  = thickness of pipe matching run of tee or header exclusive of reinforcing elements
- $t_B$  = thickness of pipe matching branch

\* Note that  $T$  should not be taken as greater than  $1.5t$  in formula for  $h$  for pad or saddle reinforced fabricated tee; this limitation was inadvertently omitted from the Code.

FIGURE 28. REPRODUCTION OF ASA B31 CODE CASE 53

TABLE 23. SUMMARY OF RESULTS OF FATIGUE TESTS OF TEES,  
DATA OTHER THAN GIVEN IN REFERENCE (40)

Ref. No.	Nominal Size	Reinforcing (1)	$\frac{D}{T}$	$\frac{d}{D}$	$\frac{s}{S}$	Load	No. of Specimens	(2)		Code (3)	Case 53 if
								if, Test Data	if		
(45)	12x4	Saddle(a)	67.	.34	.39	Mi Mo	4 2	1.19 4.18	3.70 3.70	2.20 2.65	
(46)	16x6	Pad(b)	31.	.41	.73	Mi Mo	13(f) 4	3.6 2.8	2.85 2.85	1.34 1.60	
	16x6	Saddle(c)	31.	.41	.73	Mi Mo	13 3	2.4 2.8	2.85 2.85	1.34 1.60	
	16x6	None(d)	31.	.41	.73	Mi	7	4.4	{ 2.08(g) 5.60	{ 1.02(g) 3.14	
	16x6	None(d)	15.	.42	1.50	Mi	7	2.4	{ 1.28 3.45	{ 1.00 1.00	
(47)	20x6 (L)	None(d)(e)	19.	.32	.76	Mo	1	1.2	{ 1.50 4.04	{ 1.00 1.77	
	20x12 (D)	None(d)(e)	19.	.63	.92	Mo	1	2.5	{ 1.50 4.04	{ 1.03 2.78	
	20x12 (R)	None(e)	19.	.63	.92	Mo	1	3.9	4.05	2.78	

(1) (a) Saddle dimensions: 0.368" thick x 7.3125" O.D. x 1.25" height above cylinder surface.

(b) Pad dimensions: 0.500" thick x 12.125" O.D.

(c) Saddle dimensions: 0.500" thick x 11.625" O.D. x 1.5" height above cylinder surface.

(d) Drawn outlet tee.

(e) Details of these models are shown in Figures 30, 31, and 32.

(2) Value of if in Equation (6);  $i_{fSN} = 245,000$ .

(3) Values of if from ASA E31.1-1955, with S (nominal stress) taken as M/Zn, Zn = section modulus of nozzle. Limitation that  $T_p$  (reinforcing thickness)  $\leq 1.5 T$  was used.

(f) Part of the fatigue tests were run with 800 psi static internal pressure (nominal pressure stress of 12,500 psi for  $D/T = 31$ ; 6000 for  $D/T = 15$ ). No significant difference in fatigue life was observed between those specimens with pressure and those without pressure.

(g) Top line is if calculated as an ASA B 16.9 tee; bottom line is if calculated as a fabricated, unreinforced tee.

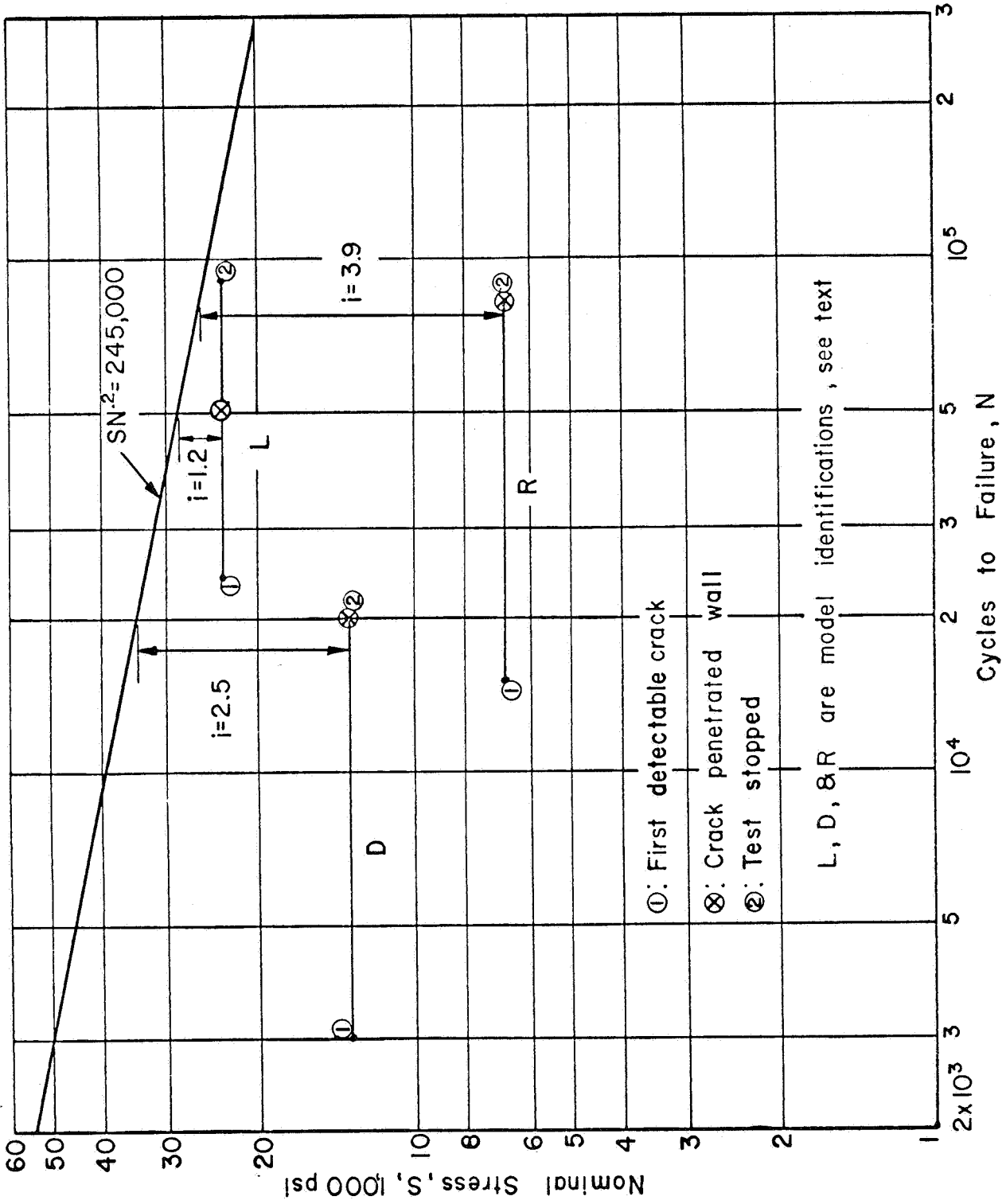


FIGURE 29. RESULTS OF FATIGUE TESTS, 20" x 6" AND 20" x 12" TEES, REFERENCE (47)

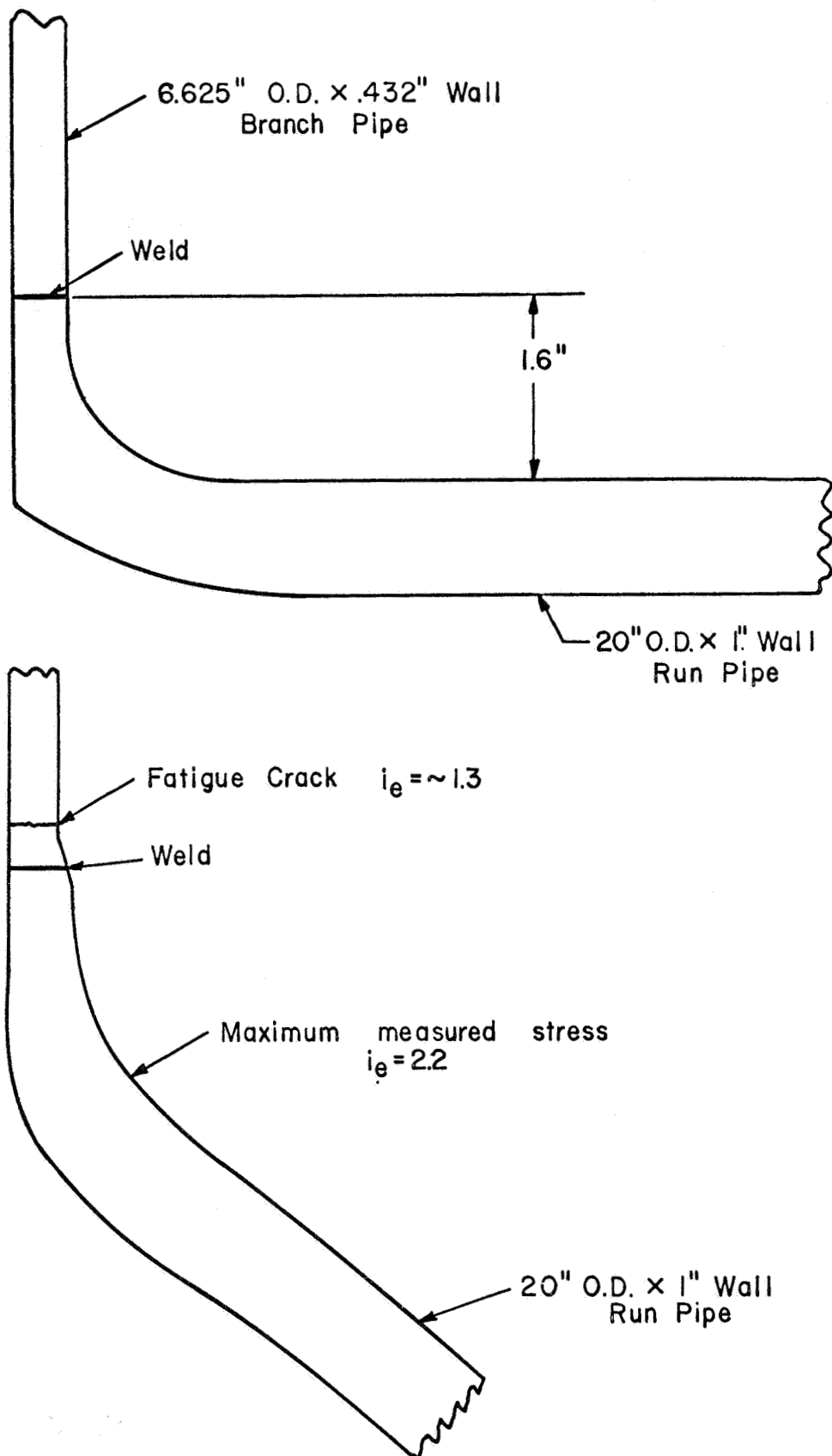


FIGURE 39. DIMENSIONS, FATIGUE FAILURE LOCATION AND MAXIMUM MEASURED STRESS LOCATIONS, REFERENCE (47) MODEL L

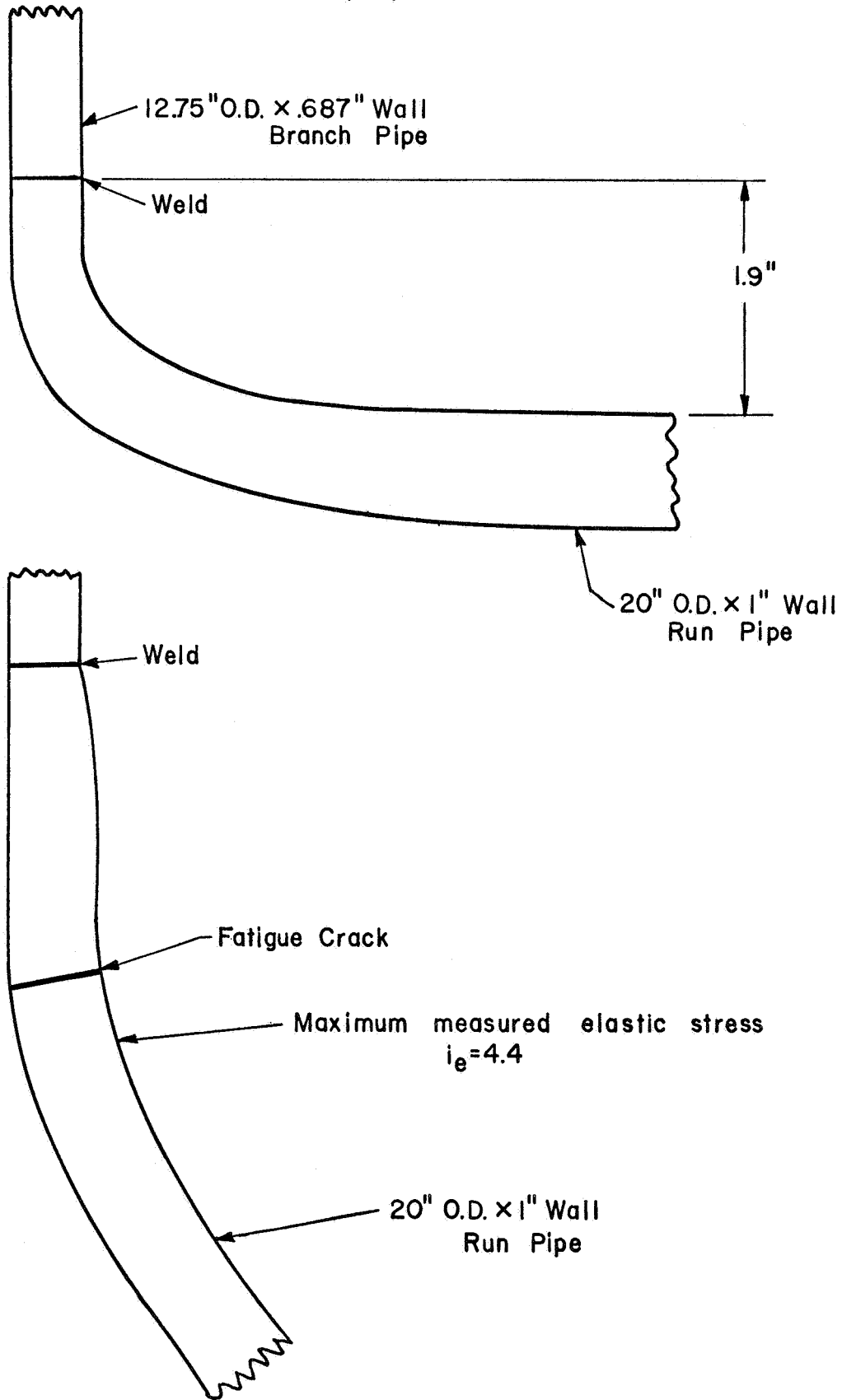


FIGURE 31 . DIMENSIONS, FATIGUE FAILURE LOCATION AND MAXIMUM MEASURED STRESS LOCATIONS, REFERENCE (47) MODEL D



(123)

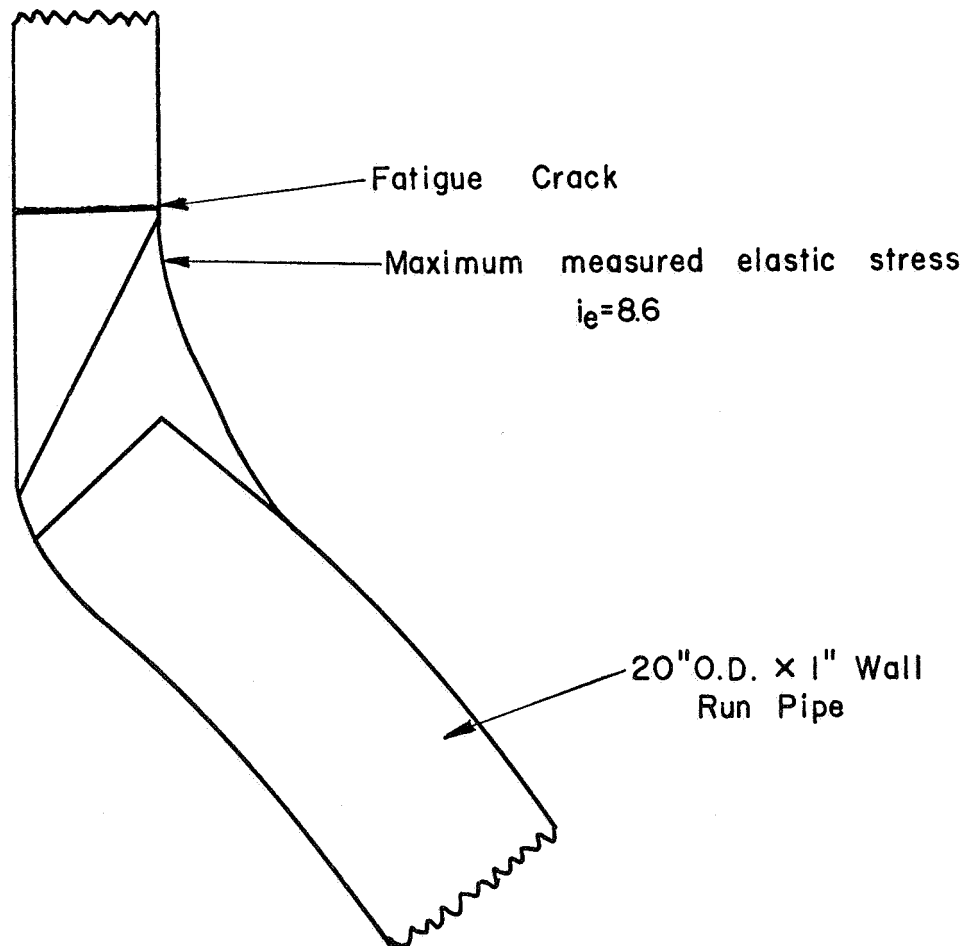
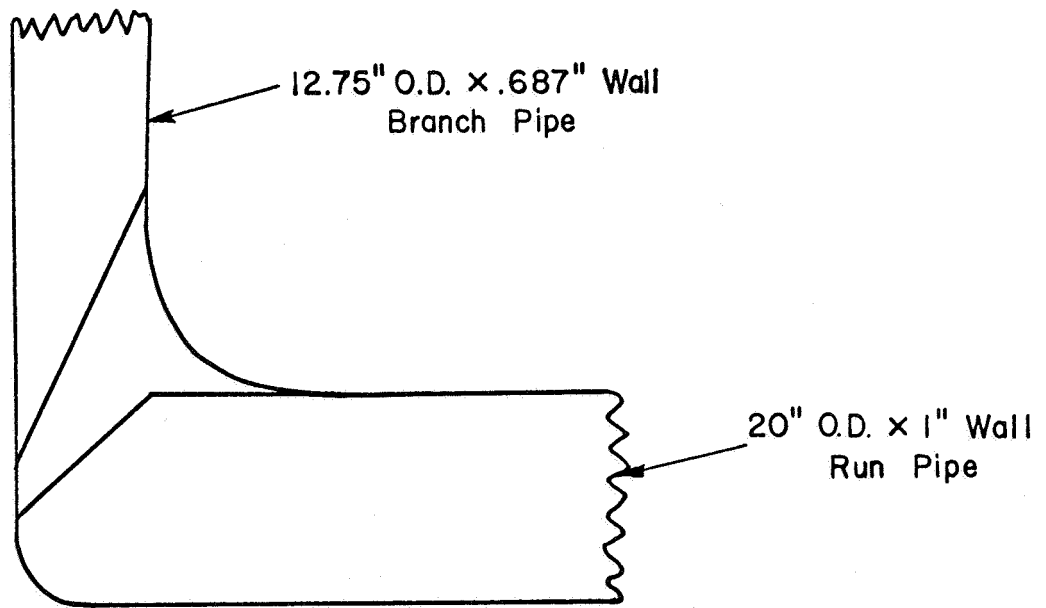


FIGURE 32 . DIMENSIONS, FATIGUE FAILURE LOCATION AND MAXIMUM MEASURED STRESS LOCATIONS, REFERENCE (47) MODEL R

<u>Model</u>	<u><math>i_e</math></u>	<u><math>i_f</math></u>	<u><math>i_e/i_f</math></u>
20 x 6, Drawn Outlet, Model L	2.2	1.2	1.8
20 x 12, Drawn Outlet, Model D	4.4	2.5	1.8
20 x 12, Fabricated, unreinforced, Model R	8.6	3.9	2.2

The ratio of elastic stress indices to fatigue stress intensification factors is approximately equal to two. This is the same ratio found for elbows. In general, therefore, one would expect the fatigue stress intensification factors given by ASA B31.1 and ASA Code Case 53 to be one-half of the measured elastic stress indices.

Failure locations for Models D and R in the fatigue tests were reasonably close to the points of maximum measured stress. In Model L, fatigue cracks started at the location of maximum stress, however, the crack that penetrated the wall first was at the weld. Nominally, the weld was at a lower stress level but the stress intensification due to the weld was sufficiently high to cause failure at the weld.

Before proceeding with comparisons of measured elastic stresses with fatigue test factors, it is pertinent to review certain implications of Table 23. The last two columns of this table show values of  $i_f$  calculated by:

- (1) Equations given in ASA B31.1-1955 (Equations 8 through 12 herein) with (for less than full size nozzles) the nominal stress  $S$  defined as  $S = M/Z_n$ , where  $Z_n$  = section modulus of the nozzle.
- (2) Equations given in ASA B31 Code Case 53.

In comparing  $i_f$  from test data with  $i_f$  by Case 53, it will be noted that (with the exception of Reference (43),  $M_i$ ) Case 53 is unconservative.

With regard to the four "drawn-outlet" tees included in Table 23, it might be noted that such tees are not covered in ASA B31.1-1955. They should be better than fabricated unreinforced tees because they do not have an intersection weld in a zone of high stress. They would not be as good as ASA B16.9 tees (of the type tested by Markl) because they do not have as large a transition radii nor the local reinforcement in the transition zone present in B16.9 tees. Accordingly, one would expect their  $i_f$ -factors to be between those calculated for a fabricated reinforced tee and an ASA B16.9 tee. As shown in Table 23, the test results for drawn outlet tees (with the exception of Reference (47), Model L) do lie between calculated values for fabricated unreinforced tees and ASA B16.9 tees.

Table 24 gives comparisons between measured elastic stresses and ASA B31.1 and ASA B31. Code Case 53. It can be seen in Tables 21 and 22 that, for all tests except References (31) and (33), and the "B16.9 tee" of Reference (36), maximum stresses were not measured; they are estimated by extrapolation of the test data. These extrapolated maximum stresses occur at the toe of a fillet weld which discontinuity itself presumably increases the local elastic stress.

Markl's tests on fabricated branch connections also contained fillet welds and, in most cases, fatigue failure occurred at the toe of these fillet welds. Accordingly, to obtain a valid comparison it is necessary to multiply  $\sigma'/S$  by a factor representing the stress concentration

TABLE 24. COMPARISON OF MAXIMUM MEASURED STRESS INDICES WITH FATIGUE STRESS INTENSIFICATION FACTORS

Ref. No.	Nominal Size (I)	$\frac{D}{T}$	$\frac{d}{D}$	$\frac{s}{S}$	Load	$\frac{\sigma^t}{S}$	$i_e$ Weld (2)	2 if Code	2 if Case 53
(34)	56x12 (T = 1.3")	43	.19	.29	MI	4.1	8.2	14.	7.3
					Mo	6.2	12.4	14.	9.3
(35)	56x12 (T = 2.08")	27	.19	.46	MI	2.1	4.2	10.2	3.4
					Mo	3.8	7.6	10.2	4.3
(35)	24x4	76	.18	.24	MI	4.5	9.0	20.4	12.
					Mo	10.	20.	20.4	15.5
(35)	24x12	76	.53	.66	MI	5.1	10.2	20.4	12.6
					Mo	12.	24.	20.4	16.3
(35)	24x24	76	1.00	1.00	MI	8.4	16.8	20.4	15.8
					Mo	14.	28.	20.4	20.4
(38)	24x4 (a)	76	.18	.24	Mo	4.	8.	9.9	6.0
					Mo	7.	14.	8.4	6.7
(38)	24x12 (a)	76	.53	.66	Mo	7.	14.	8.4	6.7
					Mo	5.	10.	9.2	7.0
(38)	24x4 (b)	76	.18	.24	Mo	6.	12.	9.2	7.4
					Mo	8.	16.	9.2	7.4
(38)	24x8 (b)	76	.35	.44	Mo	2.1	4.2	23.	7.4
					Mo	3.5	7.0	23.	9.7
(18)	36x4 (E)	93	.12	.30	MI	4.7	9.4	23.	13.3
					Mo	10.5	21.	23.	17.2

TABLE 24. (Continued)

Ref. No.	Nominal Size (1)	$\frac{D}{T}$	$\frac{d}{D}$	$\frac{s}{S}$	Load	$\frac{\sigma'}{S}$	$i_e$ WeId (2)	2 if Code	2 if Case 53
(36)	10x10(c)	16	1.00	1.00	Mi	2.2+	4.4+	7.2	5.9
					Mo	3.4+	6.8+	7.2	7.2
	10x10(d)	16	1.00	1.00	Mi	1.7+	3.4+	6.0	5.1
					Mo	2.0+	4.0+	6.0	6.0
Y	8x8(e)	16	1.00	1.00	Mi	1.4	1.4*	1.72	1.54
(37)	48x6 (2)	78	.13	.29	Mi	3.1	6.2	20.6	7.1
					Mo	4.4	8.8	20.6	9.3
	48x6 (3)	78	.13	.29	Mi	1.4	2.8	10.5	3.8
					Mo	4.3	8.6	10.5	4.7
(31)	20x6 (L)	19	.32	.76	Mi	1.7	1.7*	3.0(F)	2.0(F)
								{8.1	{2.8
	20x12 (D)	19	.63	.92	Mo	2.2	2.2*	{3.0	{3.5
								{8.1	{2.0
	20x12 (E)	19	.65	1.74	Mi	2.7	2.7*	{3.0	{4.2
								{8.1	{2.1
	20x12 (R)	19	.64	.92	Mo	4.4	4.4*	{3.0	{5.6
								{8.1	{2.0
	20x20 (S)	19	1.00	1.00	M <sub>t</sub>	3.2	3.2*	{2.0	{2.0
								{2.0	{2.0
	24x12 (C-1)	230	.50	.50	Mi	2.0	2.0*	3.0	2.0
					Mo	8.5	17.	8.1	5.6
(33)	24x12 (C-1)	230	.50	.50	Mi	5.2	10.4	8.1	6.3
					Mo	5.25	10.5	8.1	8.1
	24x12 (C-1)	230	.50	.50	Mi	18.5	37.	42.	32.
					Mo	90.	180.	42.	42.

FOOTNOTES TO TABLE 24.

- (1) Symbols in parentheses under the nominal size give further identification of the test models in accordance with the references cited.
- (a) Saddle reinforced
  - (b) Pad reinforced
  - (c) Unreinforced
  - (d) Pad reinforced
  - (e) Probably a tee typical of ASA B16.9 tees.
- (2) For models in which the maximum measured stress occurred at the toe of a fillet weld, the values of  $\sigma_{\max}/S$  (extrapolated to toe of weld) are multiplied by 2.0 as an approximation of the additional stress due to the fillet weld. Models in which  $\sigma_{\max}/S$  is not associated with a fillet weld are marked with an asterisk.
- (f) Top line is  $2i_f$  calculated as an ASA B16.9 tee; bottom line is  $2i_f$  calculated as a fabricated, unreinforced tee.

due to the weld. In the comparisons of Table 24, a factor of two has been used. This factor gives the elastic stress indices shown in Table 24 under the column " $i_e$ , weld". As discussed previously, agreement between measured stresses and stress intensification factors would be indicated by agreement between the value of  $i_e$ -weld (or  $\sigma'/S$ , where the maximum stress is not at a weld) and two times the code values ( $2i_f$ ). Several observations concerning the correlations of Table 24 are given below.

In-Plane vs Out-of-Plane Moments,  $M_i$  vs  $M_o$

Stress intensification factors given in B31.1-1955 do not differentiate between in-plane and out-of-plane. Actually, Markl's tests (on full-size tees) indicated a relatively small difference between in-plane and out-of-plane; the out-of-plane factor being about 20 percent higher than the in-plane factor for B16.9 tees; around 3 percent higher for fabricated tees. For simplicity, the difference was ignored in B31.1-1955. There are four full size tees listed in Table 24 for which  $M_i$  vs  $M_o$  stresses can be compared. The ratios of out-of-plane to in-plane  $i$ -factors are 1.67, 1.54, 1.18, and 1.05. The best set of data, Reference (31) Model S, agrees with Markl's fatigue data in that there is not much difference in maximum stresses for full size tees and  $D/T$  of around 20.

Case 53, in-so-far as full size tees are concerned, introduces a difference in stress intensification factors depending upon the bending plane. The relationship is:

$$i_i = 0.75 i_o + .25. \quad (13)$$

where

$i_i$  = stress intensification for  $M_i$

$i_o$  = stress intensification for  $M_o$

$i_o$  = value given in ASA B31.1-1955.

For reduced-size nozzles, the data of Table 24 indicates large differences between  $i_i$  and  $i_o$ , particularly for large values of  $D/T$ . The difference is most significant in Reference (33), Model C1, for which the ratio of  $i_o/i_i$  is 4.9. There is some indication from the test data that  $i_o/i_i$  increases as  $D/T$  increases and that for a given  $D/T$  ratio,  $i_o/i_i$  is not constant but rather reaches a maximum value at a  $d/D$  ratio between 0.5 and 1.0.

#### Torsional Moment, $M_t$

Both B31.1-1955 and Case 53 gives a stress intensification factor of unity for torsional moment on the nozzle; i.e.,  $S = M_t/2Z$ . However, if one looks at Figure 27, loading position 2, out-of-plane, it appears that the test represents a torsional moment on the nozzle--for which the stress intensification factor was found to be greater than unity. Table 24 includes two models with  $M_t$ -loading, Reference (31), Models D and E, both tests give a significantly greater than unity stress index for torsional loading.

#### Force Loads

The ASA Code does not give stress intensification factors for force (as distinguished from moment) loads. As shown in Tables 21 and 22, an axial load on the nozzle can produce significantly high stress indices. However, in most piping systems the forces are usually small compared to the moments.



B16.9 Tee

Table 24 includes one "ASA B16.9 tee" similar to those tested by Markl. It is interesting to note that the maximum stress for in-plane bending agrees fairly well with the fatigue stress intensification factor and that the location and direction of that stress (See footnote i of Table 22) agrees with the location and direction of fatigue failures reported by Markl.

B31.1-1955 Factors

Considering the several rough approximations involved in the comparisons shown in Table 24, the agreement between stress indices and stress intensification factors is, for the most part, reasonably good. There are several gross exceptions. For Reference (18) Model E, the Code stress intensification factor is significantly higher than indicated by the stress indices. For Reference (33) Model C-1, the Code stress intensification factor for out-of-plane bending is significantly lower than indicated by the stress indices.

B31.1 Case 53

The maximum stress intensification factor from Case 53 is obtained from Equation (53-3) of Case 53. The relationship between stress factors of B31.1-1955 (with  $S$  defined as  $M/Z_n$ , where  $Z_n$  = section modulus of nozzle) and Case 53 Equation (53-3), can be summarized as follows:

	$(i_i)_{53}$	$(i_o)_{53}$
$T < i_o t$ $(Z_e = \pi r^2 T)$	$(.75 i_o + 0.25) \frac{t}{T}$	$i_o \frac{t}{T}$
$T > i_o t$ $(Z_e = \pi r^2 i_o t)$	$.75 + \frac{0.25}{i_o}$	1.0

In the above:

$t$  = nozzle wall thickness

$T$  = cylinder wall thickness

$i_o$  = stress intensification factor as given in ASA B31.1-1955

$(i_i)_{53}$  = stress intensification factor for  $M_i$  applied to nozzle,  
Case 53

$(i_o)_{53}$  = stress intensification factor for  $M_o$  applied to nozzle,  
Case 53

Case 53 gives stress intensification factors either lower than or equal to those given in B 31.1-1955. The comparisons shown in Table 24 indicate that, on the average, Case 53 factors agree better with measured stress than the B 31.1-1955 factors. However, Case 53 tends to be unconservative in many cases. This may be more apparent for smaller values of  $t/T$  than represented by the test models. A similar tendency of Case 53 to be unconservative is also apparent in Table 23. Accordingly, in the writers' opinion, Case 53 should not be used if a conservative evaluation of stresses is desired.

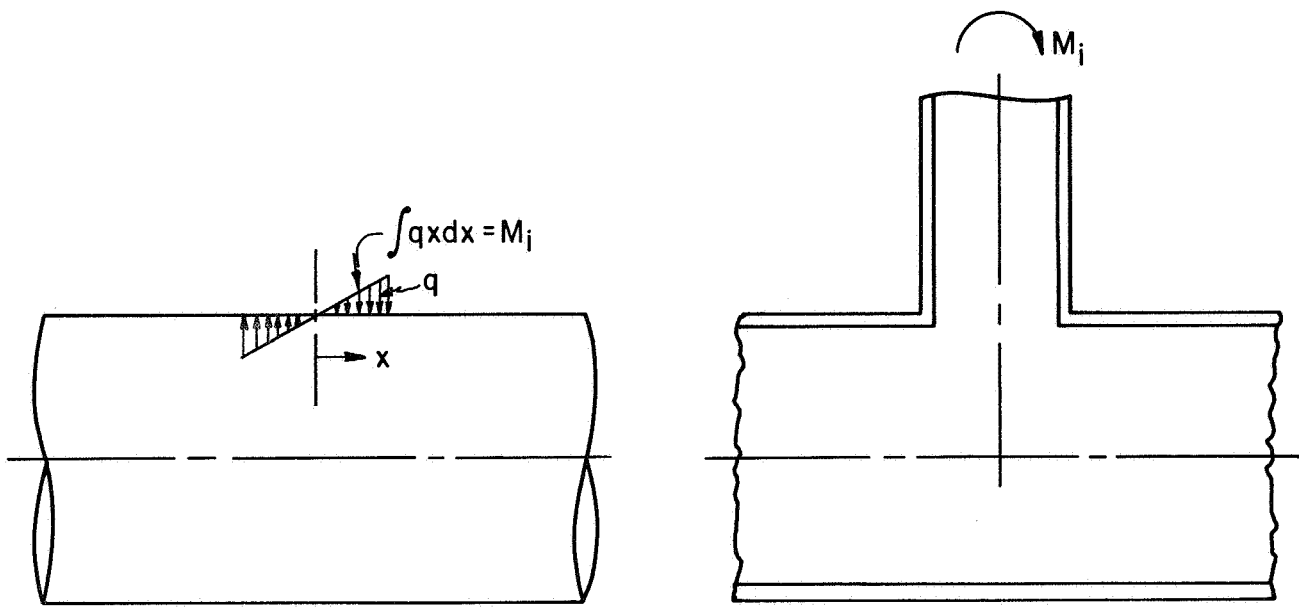
Comparisons of Measured Stresses  
With Calculated Stresses

Bijlaard and Bijlaard-Wichman Comparisons

At present, an accurate analytical method for calculating stresses due to external loads on nozzles is not available. Bijlaard<sup>(3,4,5)</sup> gives an analytical method for calculating stresses in a cylindrical shell due to distributed loads on the surface of the shell, as shown in Figure 33. For lack of a more applicable analysis, Bijlaard's results have been used to compute stresses in a cylindrical shell with a cylindrical nozzle, the nozzle being loaded by a moment or a radial thrust. To the extent that the stiffness of the nozzle is equivalent to the stiffness cut-out by the opening, this analysis might be expected to give some indication of the stresses in the cylindrical shell; of course the analysis does not give any information as to stresses in the nozzle.

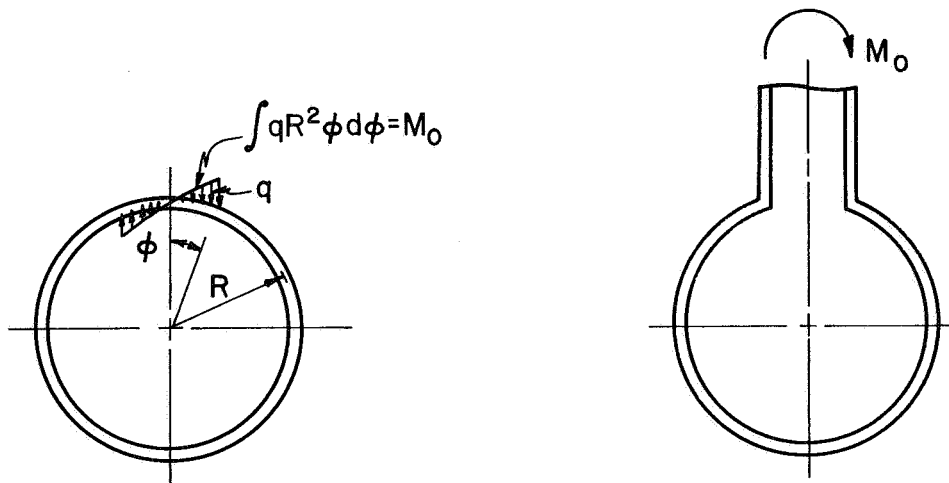
Wichman, Mershon & Hopper<sup>(6)</sup> compared Bijlaard's results with some of the test data listed in Table 21 (in particular, Reference (31) Model R and Reference (33) Model C-1); these comparisons indicated that Bijlaard's results are unconservative when used to predict stresses for nozzles in cylinders with large D/T and/or d/D-ratios. Wichman, et.al. have modified Bijlaard's results, based on test data; in addition to presenting Bijlaard's data in more useable form. Table 25 gives comparisons with Wichman et.al. as well as with stresses obtained directly from a computer program based on Bijlaard's analysis.

With regard to location of the calculated stresses, Bijlaard's stresses are calculated for the following points:



Bijlaard Assumptions

In - Plane Bending



Bijlaard Assumptions

Out-of - Plane Bending

FIGURE 33. COMPARISON OF BIJLAARD'S ASSUMPTIONS WITH ACTUAL GEOMETRY OF NOZZLES IN CYLINDRICAL SHELLS WITH MOMENT LOADING

TABLE 25. COMPARISON OF MEASURED STRESSES (EXTERNAL LOADS ON NOZZLE) WITH CALCULATED STRESSES

Ref. No.	Nominal Size	$\frac{D}{T}$	$\frac{d}{D}$	$\frac{s}{S}$	Load	$\frac{\sigma'}{S}$	Bijlaard (2) Wichman	Bijlaard (3)	Nozzle-in (4) sphere
(34)	56 x 12 (T = 1.3")	43	.19	.29	M <sub>i</sub>	4.1	3.0	4.05	7.81
					M <sub>o</sub>	6.2	4.8	5.92	7.81
					L	9.8	11.8	11.7	9.14
	56 x 12 (T = 2.08")	27	.19	.46	M <sub>i</sub>	2.1	1.6	1.86	5.65
					M <sub>o</sub>	3.8	2.1	2.42	5.65
					L	4.6	5.3	5.43	6.99
(35)	24 x 4	76	.18	.24	M <sub>i</sub>	4.5	6.0	6.02	10.6
					M <sub>o</sub>	10.	9.4	10.5	10.6
	24 x 12	76	.53	.66	M <sub>i</sub>	5.1	7.5	3.53	8.43
					M <sub>o</sub>	12.	23.1	14.2	8.43
(18)	36 x 4 (E)	93	.12	.30	M <sub>i</sub>	2.1	3.5	3.64	12.1
					M <sub>o</sub>	3.5	4.7	5.09	12.1
					L	8.1	11.4	11.7	14.3
	36 x 6 (C)	93	.18	.25	M <sub>i</sub>	4.7	6.6	6.49	12.1
					M <sub>o</sub>	10.5	11.1	12.2	12.1
					L	16.7	22.3	21.5	13.2
(37)	48 x 6 (2)	78	.13	.29	M <sub>i</sub>	3.1	3.2	3.50	11.0
					M <sub>o</sub>	4.4	4.5	4.84	11.0
					L	9.9	10.4	11.3	13.1

TABLE 25. contd.

Ref. No.	Nominal Size	$\frac{D}{T}$	$\frac{d}{D}$	$\frac{s}{S}$	Load	$\frac{\sigma'(1)}{S}$	Bijlaard-Wichman (2)	Bijlaard (3)	Nozzle-in-Sphere (4)
(31)	20 x 6 (L)	19	.32	.76	$M_I$	1.73	1.7	1.77	5.13
					$M_O$	2.19	2.4	2.80	5.13
(D)	20 x 12	19	.63	.92	$M_I$	2.70	2.9	2.43	4.23
					$M_O$	4.36	6.4	5.99	4.23
					L	8.70	-	6.71	4.20
(E)	20 x 12	19	.65	1.74	$M_I$	2.03	1.7	1.30	4.15
					$M_O$	2.33	3.8	3.27	4.15
					L	5.25	-	3.60	4.11
(R)	20 x 12	19	.63	.92	$M_I$	3.53	2.9	2.43	4.23
					$M_O$	8.55	6.4	5.99	4.23
					L	12.5	-	6.71	4.20
(C-1)	24 x 12	230	.50	1.00	$M_I$	18.5	14.5	2.77	14.5
					$M_O$	90.	65.	29.7	14.5
					L	100.	-	21.2	14.7

(1) These stresses are identified in Table 21.

(2) Calculated indices using the graphs of Reference (6) without local stress concentration factor.

(3) Calculated indices using a computer program based on Reference (3).

(4) Calculated indices using a computer program based on a nozzle in a spherical shell. Computed maximum stresses occurred in the nozzle, not the sphere.

<u>Load</u>	<u>Location</u>
$M_i$	$\rho = 0.875r, \theta = 0$
$M_o$	$\rho = 0.875r, \theta = 90^\circ$
L	$\rho = 0$ ---

The signs of the calculated stresses given in Table 25 for  $M_i$  and  $M_o$  loadings are all positive on the outside surface on the side of the nozzle for which  $M_i$  or  $M_o$  gives a nominal tensile stress in the nozzle. The signs of calculated stress for the axial load (which is defined as giving nominal tensile stresses in the nozzle) are also all positive on the outer surface.

The measured stresses and calculated stresses agree as to sign and surface. That is, with one exception, all measured stresses shown in Table 25 are tension on the outside surface. The one exception occurs in Reference (31) Model (L) with axial load on the nozzle, for which the maximum measured stress was on the inside surface.

In-so-far as agreement of stress location and direction, the calculated stresses imply that the maximum stress locations is at  $\theta = 0$  for  $M_i$ ,  $\theta = 90^\circ$  for  $M_o$ . For  $M_i$ , small  $d/D$ ,  $\alpha = 0^*$ ; i.e., the maximum stress is in the  $\rho$ -direction; for large  $d/D$ ,  $\alpha = 90^\circ$ , i.e., the maximum stress is in the  $\theta$ -direction. For  $M_o$ ,  $\alpha = 0$ , i.e., the maximum stress is in the  $\theta$ -direction. Comparison of these directions with the directions shown in Table 21 ( $\theta$ - and  $\alpha$ -columns) indicates a general tendency to agree with the calculated stress location and directions. However, in those models which were more completely strain-gaged (as a function of  $\theta$ ), the maximum stresses were usually found to be located somewhere between  $\theta = 0$  and  $\theta = 90^\circ$ . It might be noted that Markl's fatigue tests, as well as the fatigue tests listed in Table 23, also indicate that the maximum stress does not occur at  $\theta = 0$  or  $90$  for either  $M_i$  or  $M_o$ .

---

\*  $\alpha$  is defined in footnote (3) of Table 21.

In comparing "Bijlaard-Wichman" (Reference 6) stress indices with "Bijlaard" stress indices of Table 25 it should be noted that differences arise from three sources:

- (1) Reference (6) graphs are modified, in a conservative direction, for larger values of  $D/T$  and  $d/D$ .
- (2) Reference (6) procedure is based on using the outside radius of the nozzle. The calculated values (Bijlaard-column) are based on the mean radius of the nozzle--as are all other calculations given in this report.
- (3) The calculated stresses are somewhat dependent upon the assumed ratio of length to radius of the cylindrical shell. Reference (6) graphs are based on a ratio of 4 for  $M_i$  and  $M_o$ ; 8 for  $L$ . The calculated results are based on actual shell lengths where known [Reference (33) and Reference (34) models]; on a ratio of 4 for other models.

For test models within the limits of Phase Report No. 4 rules ( $d/D \sqrt{D/T} < 1.1$ ), Bijlaard's results are in reasonably good agreement with the test data,  $\sigma'/S$ .

For larger values of  $(d/D) \sqrt{D/T}$ , Reference (6) graphs are in better accord with test results ( $\sigma'/S$ ) than Bijlaard's analysis. In addition, Reference (6) method for establishing maximum stresses includes the use of stress concentration factors based on the fillet radius  $r_o$ . In adjusting Bijlaard's theoretical curves, Reference (6) used a stress concentration factor of 1.4 for Reference (31), Model R and Reference (33), Model C-1. Application of this same factor, of course, brings Bijlaard-Wichman into good agreement with the test results; i.e.,



<u>Model Iden.</u>	<u>Load</u>	<u><math>\frac{\sigma'}{S}</math></u>	<u>Bijlaard-Wichman with Stress concentration factor of 1.4</u>
20 x 12	$M_i$	3.53	4.1
(R)	$M_o$	8.55	9.0
24 x 12	$M_i$	18.5	20.3
(C-1)	$M_o$	90.	90.

The fillet radius of the drawn outlet tees (Reference 31, Models L, D, and E) are not well defined, particularly at  $\theta = 90^\circ$ . The effective fillet radius is probably in the range of  $T$  to  $3T$ , implying a stress concentration factor of about 1.4 to 1.2 according to Reference (6), Figure B-2. For the other models considered in Table 25, there was a fillet weld rather than a fillet radius. Following the philosophy of Reference (6), a stress concentration factor for the fillet weld of 2.0 or larger might be used. With these stress concentration factors, the procedure of Reference (6) would give calculated stresses equal to or greater than the values of  $\sigma'/S$  listed in Table 25.

#### Nozzle-in-Sphere Comparisons

Table 25 also shows calculated stress indices for nozzles-in-spheres. Of course, this analytical model cannot differentiate between  $M_i$  and  $M_o$  loadings; however, it does give stresses in the nozzle. For the models of Table 25, the maximum calculated stress was in the nozzle; not in the sphere. It should be noted that measured stresses in the nozzle are not

available except for Reference (31) and Reference (33) models. That calculated stresses are significantly higher than  $\sigma'/S$  for some models [e.g., Reference (37)] may only reflect that maximum stresses actually occurred in the nozzles. If so, the Bijlaard or Bijlaard-Wichman approach must be used with caution in establishing maximum stresses, particularly when the nozzle thickness is small compared to the cylinder thickness.

The very-thin wall model of Reference (33) had high stresses in relation to any of the comparison calculation methods used herein. It was thought that the nozzle-in-sphere analogy might indicate high nozzle stresses for the test model; such is not the case. An additional test on the same cylinder with a smaller nozzle (say  $d/D = .07$ , so that it would be within the range of Eringen's theory for internal pressure) would contribute significantly to available test data.

#### Nonuniform-Wall Models

Table 25 is restricted to "uniform-wall" test models. A few cross-comparisons can be made between the test data of Table 21 and that of Table 22. These are shown in Table 26. In the group "A" models of Table 26, addition of a reinforcing saddle or pad reduced  $\sigma'/S$  in the cylinder. The test data is not sufficient to determine if stresses were also reduced in the nozzle. In the group "B" models of Table 26, addition of local reinforcing reduced  $\sigma_{\max}/S$  significantly. The location of maximum measured stresses are shown in Figure 26. It seems probable that the maximum stresses measured in Group "B" models were highly dependent upon the transition radii and transition tapers used in the models; the reference cited does not specify the transition radii.

TABLE 26. COMPARISON OF UNREINFORCED AND REINFORCED TEST MODELS

Group	Nominal Size (I)	$\frac{D}{T}$	$\frac{d}{D}$	$\frac{s}{S}$	Load	Unreinforced		Reinforced		
						Ref. No.	$\frac{\sigma'}{S}$	Ref. No.	Reinforcing	$\frac{\sigma'}{S}$
A	24 x 4	76	.18	.24	$M_o$	(35)	10.	(38)	Saddle	4.
					$M_o$	(35)	10.	↓	Pad	7.
	24 x 8	76	.35	.44	$M_o$	--	--		Saddle	7.
					$M_o$	--	--		Pad	6.
	24 x 12	76	.53	.66	$M_o$	(35)	12.		Saddle	5.
					$M_o$	(35)	12.		Pad	8.
	48 x 6	78	.13	.29	$M_i$	(37)	3.1	(37)	Pad	1.4
					$M_o$		4.4			4.3
				L		9.9			8.4	
B	20 x 6 (F)	19	.32	.75	$M_i$	(31)	1.73 (a)	(31)	(F) (b)	1.41
					$M_o$		2.19			1.49
	20 x 6 (I)	19	.32	.75	$M_i$		1.73		(I) (b)	1.15
					$M_o$		2.19			1.14
	20 x 6 (J)	19	.32	.75	$M_i$		1.73		(J) (b)	1.42
					$M_o$		2.19			1.18

(1) Further identification of these models is given in Tables 21 and 22.

(a) Comparison is made with the 20 x 6 drawn outlet tee, Model L. As shown in Table 25, the measured stresses agree quite well with Bijlaard's analysis. They do not agree with the nozzle-in-sphere analogy, nozzle stresses, presumably because of the transition radius and gradual change in thickness.

(b) Reinforcing is shown in Figure 26.

STRESSES DUE TO EXTERNAL LOADS ON NOZZLES  
DESIGNED IN ACCORDANCE WITH PHASE REPORT NO. 4

Uniform-Wall Models

It was noted that Bijlaard's analysis for uniform-wall models is in reasonable agreement with measured stresses in the cylinder within the range of  $(d/D)\sqrt{D/T} < 1.1$ . This, of course, is the range covered by Phase Report No. 4, "Proposed Design Procedure for Radial Nozzles in Cylindrical Shells with Internal Pressure". Accordingly, stress indices for external loads  $M_i$  and  $M_o$  were calculated for the nozzle designs covered by Phase Report No. 4.

In these calculations, it should be noted that the stress index is based on the thickness of the nozzle,  $t$ ; where  $t = (d/D)T$ . For designs with reinforcing on the nozzle (Figure 3a of Phase Report No. 4), the use of this stress index assumes that the nozzle thickness  $t' = gt$  extends for a short distance, then tapers down to  $t$ . The index stress is then for the pipe with thickness  $t$  attached to the nozzle; that pipe is assumed to be designed for the same internal pressure as the cylindrical shell; i.e.,  $D/T = d/t$ .

The calculations showed that the stress indices are almost always less than 1.0; for most dimensional parameters the stress indices are much less than 1.0. The few dimensional parameters for which the stress indices are greater than unity are shown in Table 27. For reinforcing on the cylinder (Figure 3b of Phase Report 4), the stress indices are always less than unity. For reinforcing on the nozzle (Figure 3a of Phase Report No. 4), stress indices greater than unity were calculated for the right-hand limit of some of the  $g$ -curves; the largest calculated stress index was 1.52.

TABLE 27. CALCULATED STRESSES IN MODELS AT RIGHT HAND LIMIT OF APPLICABILITY OF PHASE REPORT NO. 4, FIGURE 3b

g (1)	$\frac{D}{T}$	$\frac{d}{D}$	$\sigma_{\max}/S$ (2)		
			Bijlaard (3)		Nozzle-in-Sphere (4)
			$M_i$	$M_o$	Sphere Nozzle
3	15	.29	1.01	1.40	.98 1.38
4	25	.225	1.00	1.38	1.02 1.31
5	40	.18	1.01	1.42	1.06 1.32
6	55	.15	.99	1.34	1.04 1.28
8	90	.12	1.02	1.39	1.11 1.20
10	120	.09	.84	1.10	.90 1.09
10	100	.12	1.09	1.52	1.26 .89
12	150	.07	.68	.82	.72 .98
12	125	.10	1.00	1.37	1.15 .81
16	220	.05	.54	.58	.56 .86
16	155	.09	1.01	1.40	1.19 .59
20	300	.037	.41	0.46	.43 .76

(1)  $g = t'/t$ ;  $t = (d/D)T$

(2)  $\sigma_{\max}$  = maximum calculated stress  
 $S = M/\pi r^2 t$  (not  $t'$ )

(3) Stresses obtained from a computer program based on Bijlaard's analysis for distributed loads on a cylinder.

For  $M_i$ :  $\sigma_{\max}$  at  $\phi = 0$ ,  $\rho = 0.875 r$

$\sigma_{\max}$  is on outside surface in  $\phi$ -direction

For  $M_o$ :  $\sigma_{\max}$  at  $\phi = 0$ ,  $\rho = 0.875 r$

$\sigma_{\max}$  is on outside surface in  $\rho$ -direction

(4) Stresses obtained from analysis of a moment applied to a nozzle in a spherical shell.

Values under "sphere" are for  $\sigma_{\max}$  in the spherical shell.

Values under "nozzle" are for  $\sigma_{\max}$  in the nozzle in the spherical shell.

$\sigma_{\max}$  is on the outside surface in a tangential direction.

Table 27 also gives the stress indices for the same group of models calculated on the nozzle-in-sphere analogy. This group of models is characterized by the relationship  $t \cong T$ . For these models, the stresses calculated by Bijlaard's analysis are not too different than those calculated by the nozzle-in-sphere analogy. However, for models with  $t \ll T$ , the nozzle-in-sphere analogy indicates relatively high stresses in the nozzle. Of course, Bijlaard's analysis does not give any information as to stresses in the nozzles.

Because, for most of the dimensional range covered by Phase Report 4, Bijlaard's analysis gives stress indices significantly less than unity, it is obvious that the analysis does not give maximum stresses; the nominal stress in the pipe attached to the nozzle is never less than unity.

Some guidance on stresses in the nozzles may be obtained from the nozzle-in-sphere analogy. Figures 34 (a) and (b) show the stress indices so calculated. The maximum calculated stress is almost always in the nozzle--not the sphere. The highest stresses occur when reinforcing is placed on the sphere; the nozzle thickness  $t = (d/D)T$  is relatively thin compared to  $T' = hT$  hence high stresses occur in the nozzle. The highest stress index is 3.2, for  $h = 1.5$ ,  $D/T = 300$ ,  $d/D = .07$ .

The above calculations were all based on the assumption that the cylinder thickness was everywhere equal to  $T'$  for Bijlaard's analysis; the sphere thickness was everywhere equal to  $T'$ , nozzle thickness equal to  $t'$  for the nozzle-in-sphere analogy. Phase Report No. 4 requires that these increased thicknesses extend for a distance  $\sqrt{DT'}$  for  $T'$ ,  $\sqrt{dt'}$  for  $t'$ . It is believed that these distances are sufficient so that stresses at the nozzle-cylinder juncture are calculatable as if the increased thickness

Figure 34(a). Reinforcing on Shell,  $h = T'/T$

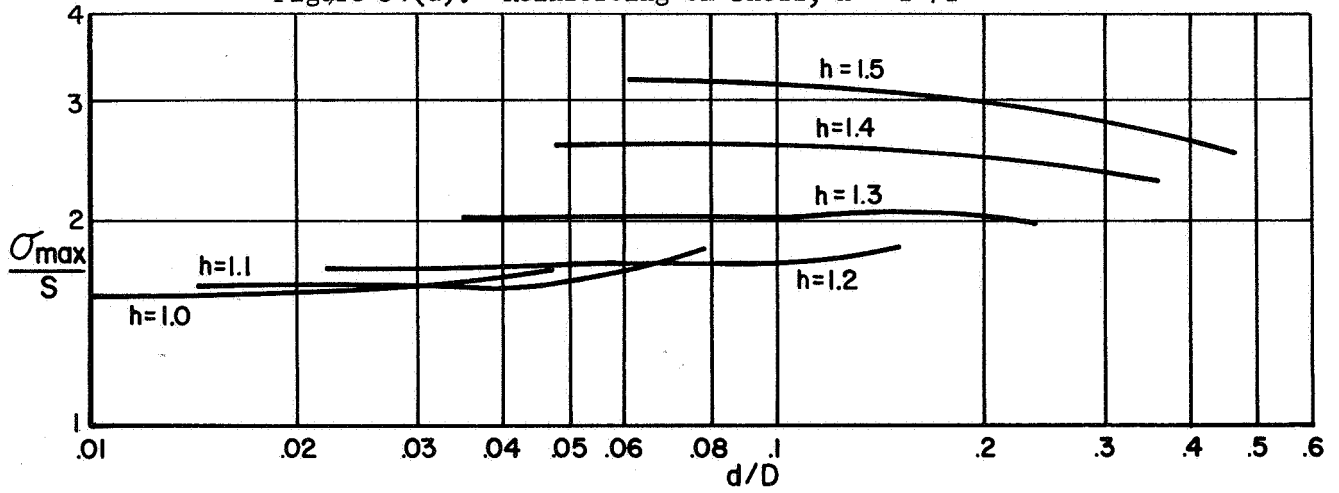


Figure 34(b). Reinforcing on Nozzle,  $g = t'/t$

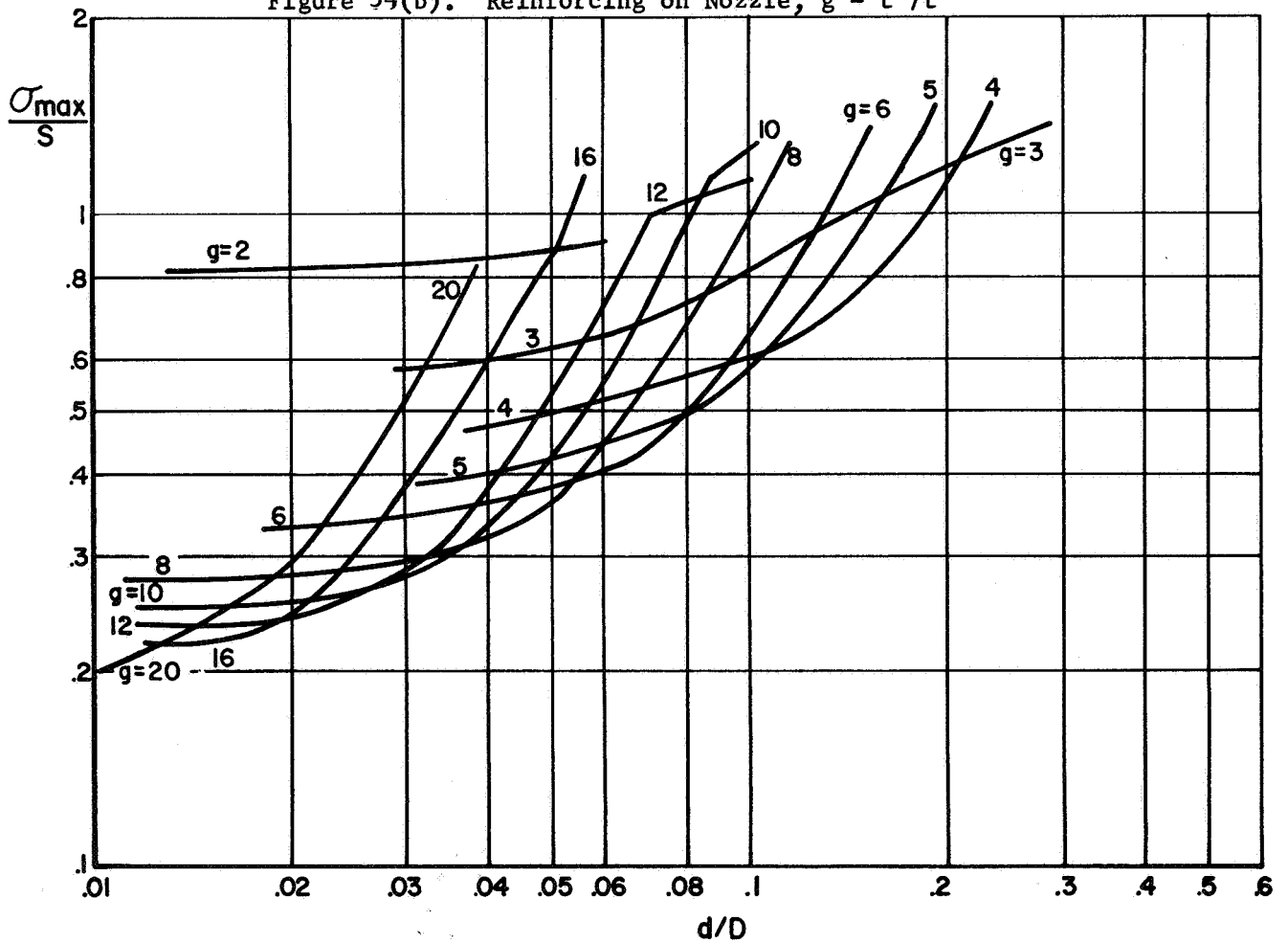


FIGURE 34. MAXIMUM STRESS INDICES FOR DESIGNS OF PHASE REPORT NO. 4, CALCULATED AS A NOZZLE IN A SPHERE

existed everywhere. It is not apparent, however, that the preceding calculations indicate the magnitude of stresses at the juncture of the reinforcing with the shells. For the juncture on the nozzle from  $t'$  to  $t$  (for which a 1:3 transition taper is required), a stress index of 1.5 is believed to be adequate. Stress indices for transition on the cylinder from  $T'$  to  $T$  are discussed in the next section of this report.

#### Nonuniform-Wall Models

The design procedure of Phase Report No. 4 permits the use of compact reinforcing; provided (a) the cross sectional area of the reinforcing meets certain requirements (for larger values of  $(d/D) \sqrt{D/T}$ , the reinforcing area must equal or exceed  $0.75 dT$ ), (b) the reinforcing area be placed within a presented zone given by  $L_c = 0.75 (T/D)^{2/3} D$ , and (c) prescribed transition radii and tapers are used. The test data shown in Table 26, Group B, indicates that local reinforcing is effective in reducing maximum stresses. However, this is an isolated piece of test data, i.e., for  $D/T = 19$ ,  $d/D = 0.32$ ,  $s/S = .75$ .

The test data of Table 26, Group A, is significant with respect to stresses at the edge of a reinforced section on the cylinder. It should be noted that the maximum stresses for the reinforced models in Group A are extrapolated values on the cylinder to the toe of the fillet weld between reinforcement and cylinder. The lengths of reinforcing along the cylinder,  $L_c = 0.75 (T/D)^{2/3} D$  and  $\sqrt{DT'}$  are shown below.



<u>Model</u>	<u>Reinforcing Length on Cylinder</u>	<u>L<sub>c</sub></u>	<u><math>\sqrt{DT'}</math>*</u>
24 x 4, Saddle reinforced	2.31	.98	4.0
24 x 4, Pad reinforced	1.37	.98	4.0
24 x 8, Saddle reinforced	3.56	.98	4.0
24 x 8, Pad reinforced	4.31	.98	4.0
48 x 6, Pad reinforced	1.94	2.0	7.8

The reinforcement lengths used in these models, except for the 24 x 8 models, are significantly less than  $\sqrt{DT'}$ ; the length required by Phase Report 4 for uniform-wall reinforcing on the cylinder. However, the measured stress intensities shown in Table 26 suggest that, for thin-wall cylinders, the maximum stress may occur at the reinforcing-to-cylinder juncture even with a reinforcing length equal to  $\sqrt{DT'}$ . The reinforcing length of the 48 x 6 model happens to be equal to that permitted in Phase Report 4 for compact reinforcing, hence it is a useful guide as to the stress indices for such designs.

Some further information might be obtained by using Bijlaard's<sup>(5)</sup> suggestions for a reinforcing pad; or by using the nozzle-in-sphere analogy, for which the effect of any desired contour of reinforcing can be calculated. Time and funds do not permit investigation along these lines and, in any event, additional confirmation by tests would seem desirable if not essential. Accordingly, it appears necessary to use a conservative approach at this time. It is suggested that, for nozzles designed in accordance with Phase Report No. 4, Figure 2d, 2e, or 2f, the value of  $\sigma_{\max}/S$  for  $M_i$  or  $M_o$  be obtained by the equation:

---

\*  $T'$  is taken as the sum of the cylinder and reinforcing thickness, even though they are not integral.

(148)

$$\sigma_{\max} = \frac{1.8}{h_e^{2/3}} \quad (14)$$

where  $h_e = 3.3 T/R$ .

Comparisons of test data and Equation (14) are shown in Table 28. None of these test models are within the dimensional range covered by Phase Report rules because  $(d/D) \sqrt{D/T}$  is greater than 1.1. Also, models in Group A and C do not meet the rules because the reinforcing is not integral with the shells. It is not known if the transition radii of Group B models meet the Phase Report 4 rules.

In Table 28, Group A, Equation (14) is conservative for measured stresses in the cylinder and probably conservative with respect to stresses in the nozzle. In Table 28, Group B, Equation (14) is conservative. Table 28, Group C, is a comparison of fatigue tests (Table 23) with Equation (14). There are several comparisons which are not conservative, however, these models are not only well beyond the dimensional range of Phase Report 4 rules, but also fatigue failures occurred at the fillet weld between the pad or saddle and the shell.

Equation (14) is, of course, of the same form used in the ASA piping code. The following tabulation may aid in putting Equation (14) in perspective with other components.

<u>Component</u>	<u><math>h_e</math></u>	<u>Relative i-factors</u>
ASA B16.9 Tees	4.4 T/R	1.00
Nozzles per Phase Report 4, Compact Reinforcing	3.3 T/R	1.21
ASA B16.9 Elbows (Bend radius = 3 times cross section radius)	3.0 T/R	1.29
Fabricated, reinforced tees with $T_p = T$	2.76 T/R	1.36
Fabricated, unreinforced tees	T/R	2.68

TABLE 28. COMPARISON OF EQUATION (14) WITH TEST DATA ON REINFORCED NOZZLES

Group	Ref. No.	Nominal Size(l)	$\frac{D}{T}$	$\frac{d}{D}$	$\frac{s}{S}$	Load	$\frac{\sigma^1(2)}{S}$	$\frac{\sigma_{max}}{S}$ Eq. (14)
A	(38)	24 x 4 (Saddle)	76	.18	.24	M <sub>O</sub>	4.	9.2
		24 x 8 (Saddle)	76	.35	.44	M <sub>O</sub>	7.	9.2
		24 x 4 (Pad)	76	.18	.24	M <sub>O</sub>	6.	9.2
		24 x 8 (Pad)	76	.35	.44	M <sub>O</sub>	8.	9.2
		48 x 6 (Pad)	78	.13	.29	M <sub>I</sub> M <sub>O</sub>	1.4 4.3	9.4 9.4
B	(31)	20 x 6 (F)	19	.32	.75	M <sub>I</sub> M <sub>O</sub>	1.41 1.49	3.6 3.6
		20 x 6 (I)	19	.32	.75	M <sub>I</sub> M <sub>O</sub>	1.15 1.14	3.6 3.6
		20 x 6 (J)	19	.32	.75	M <sub>I</sub> M <sub>O</sub>	1.42 1.18	3.6 3.6
		12 x 4 (Saddle)	67	.34	.39	M <sub>I</sub> M <sub>O</sub>	(2 If) 2.4 8.4	8.4 8.4
		16 x 6 (Pad)	31	.41	.73	M <sub>I</sub> M <sub>O</sub>	7.2 5.6	5.1 5.1
C	(46)	16 x 6 (Saddle)	31	.41	.73	M <sub>I</sub> M <sub>O</sub>	4.8 5.6	5.1 5.1

TABLE 28. FOOTNOTES

- (1) These models are further described in the footnotes to Table 22 and 23.
- (2)  $\sigma'/S$  is identified in Table 22. Values of  $i_f$  are derived from fatigue tests as shown in Table 23.
- (3)  $\sigma_{\max}/S = 1.8/h_e^{2/3}$ , where  $h_e = 3.3 T/R$ .

The remaining question to be discussed concerns an appropriate stress index at the edge of the reinforcing-to-cylinder transition for Phase Report 4 designs, Figure 2b, for which the required length of reinforcing is equal to  $\sqrt{DT}$ . No directly applicable test data is available, however, a crude but probably conservative approximation can be developed as follows.

Bijlaard's analysis indicates that maximum stresses can be conservatively estimated as being in inverse ratio to the pad diameter,  $d_p$ . This implies an equation of the form:

$$\frac{\sigma_{\max}}{S} = I_1 \left[ k_1 \frac{d}{d_p} \right] \quad (15)$$

To be consistent with Equation (14),  $k_1$  should be such that when  $d_p$  is equal to  $L_c$ , the quantity  $(k_1 d/d_p)$  should be equal to unity. Since  $d_p$ , for Phase Report 4 Figure 2b designs, is equal to  $\sqrt{DhT}$  and  $L_c = 0.75(T/D)^{2/3}D$ , this leads to the equation:

$$\frac{\sigma_{\max}}{S} = I_1 \left[ \frac{0.75}{h^{1/2} (D/T)^{1/6}} \right] = I_p$$

Values of  $I_p$  are tabulated below

$\frac{D}{T}$	$I_p$ for h of:					
	1.0	1.1	1.2	1.3	1.4	1.5
10	1.21	1.15	1.10	1.06	1.03	.99
20	1.72	1.64	1.57	1.51	1.45	1.40
40	2.42	2.31	2.21	2.12	2.06	1.97
80	3.43	3.27	3.13	3.00	2.92	2.80
100	3.85	3.67	3.35	3.37	3.27	3.14
200	5.45	5.20	4.97	4.78	4.64	4.45
300	6.67	6.36	6.09	5.85	5.68	5.45

Summary

The suggested stress indices for Phase Report No. 4 designs subjected to either  $M_0$  or  $M_1$  loads are:

## (1) Uniform Wall Reinforcing

Nozzle-to-cylinder juncture: Use larger of:

- (a) Stress indices calculated by Bijlaard's analyses, or
- (b) Stress indices calculated from nozzle-in-sphere.

Transition from  $t'$  to  $t$  on nozzle

Stress index = 1.5.

Transition from  $T'$  to  $T$  on cylinder

$$\text{Stress Index} = I_1 \left[ \frac{0.75}{h^{1/2} (D/T)^{1/6}} \right]$$

$$I_1 = 1.8/h_e^{2/3}$$

$$h_e = 3.3 T/R$$

## (2) Compact Reinforcing

Stress Index =  $I_1$ , defined above.

The stress indices are not accurate but are believed to be conservative.

STRESSES DUE TO COMBINED INTERNAL PRESSURE  
AND EXTERNAL LOADS APPLIED TO THE NOZZLE

This section of the report is based on the assumption that stresses due to internal pressure can be linearly combined with the stresses due to external loads. The subject of linear superposition is discussed in Phase Report No. 2 (pp 162-163). It was concluded, on the basis of available theory and test data, that linear superposition is apparently always conservative, and reasonably accurate for  $D/T$  values up to 50 and  $d/D$  up to 0.5. The discussion covers both nozzles in spherical shells and nozzles in cylindrical shells.

Even with linear superposition, the determination of maximum stresses due to combinations of pressure and external loads is difficult. The problem arises, in part, because the pressure and each external load are independent of each other. At a given point on the nozzle-cylinder, both the magnitude and direction of the maximum principal stress varies as a function of the load ratios, i.e.,  $P/M_i$ ,  $P/M_o$ ,  $M_i/M_o$ , etc. Also, of course, the point at which the maximum principal stress occurs is dependent upon these load ratios. If there existed sufficient test data to establish the stress magnitudes and directions at each point on a nozzle-cylinder structure for each of the loads, or if a theory existed which would give such information, it would be a relatively simple task to develop a computer program to compute maximum stresses due to any combination of pressure and external loads. While a theory does exist for internal pressure (limited to small  $d/D$ , uniform-wall nozzle and cylinders), neither the test data nor available theories for external load are adequate.

However, it appears from the preceding section of this report that available test data and theory do give a reasonably good estimate of the magnitude of the maximum stress due to certain types of external loads (with some reservations concerning stresses in the nozzles). The location and direction of those principal stresses is not well established. The only apparent conservative approach at this time, therefore, appears to consist of the assumption that maximum stresses due to pressure and external loads occur at the same point and in the same direction.

For most test models, the maximum stress due to internal pressure occurs at the inside corner,  $\theta = 0$ ,  $\rho = \rho_0$ . Detailed examination of the test data, for models with  $(d/D) \sqrt{D/T} < 1.1$ , indicates that the stresses due to external loads ( $M_i$ ,  $M_o$ ,  $L$ ) are quite small at this particularly location. On the other hand, the stresses due to internal pressure are not negligible at points of maximum stress due to external load. For Reference (33) Model C-1, with  $(d/D) \sqrt{D/T} = 7.6$ , the maximum stress due to pressure occurred at essentially the same location and direction as the maximum stress due  $M_i$ . Accordingly, while this approach usually involves significant conservatism, in some cases the conservatism may not be large.

Whether the degree of conservatism is intolerable may depend upon how the designer estimates the external loads that will be imposed on the nozzle. This estimate is often necessary because the piping system is not laid out at the time the vessel is designed. If the designer assumes that the load on the nozzle will be as much as the pipe can transmit to it, then the designer may indeed find the conservatism intolerable. However, there are several inherent limitations in most piping systems which prevent such loads from being imposed. These are discussed in Phase Report No. 2 (pp 164-171) and are equally applicable to nozzles in cylinders.



LIST OF REFERENCES

- (1) Eringen, A. C., et al., "Analysis of Stress and Deformation in Two Normally Intersecting Cylindrical Shells Subject to Internal Pressure", General Technology Corporation, Technical Report No. 3-8, (Dec. 1965).
- (2) Lind, N. C., "Approximate Stress Concentration Analysis for Pressurized Branch Pipe Connections", Progress Report to the PVRC Subcommittee on Reinforced Openings and External Loadings (Feb. 22, 1967).
- (3) Bijlaard, P. P., "Stresses from Local Loadings in Cylindrical Pressure Vessels", Trans. ASME (August, 1955).
- (4) Bijlaard, P. P., "Stresses from Radial Loads and External Moments in Cylindrical Pressure Vessels", Welding Research Supplement (Dec., 1955).
- (5) Bijlaard, P. P., "Additional Data on Stresses in Cylindrical Shells Under Local Loading", Welding Research Council Bulletin No. 50 (May, 1959)
- (6) Wichman, K. R., Mershon, J. L., and Hopper, A. G., "Local Stresses in Spherical and Cylindrical Shells Due to External Loadings", Welding Research Council Bulletin No. 107 (August, 1965).
- (7) Beskin, Leon, "Strengthening of Circular Holes in Plates Under Edge Loads", J. of App. Mechanics (Sept., 1944).
- (8) Waters, E. O., "Theoretical Stresses Near a Circular Opening in a Flat Plate with a Cylindrical Outlet", Welding Research Council Bulletin No. 51 (June, 1959).
- (9) Lourye, A. I., "Concentration of Stress in the Vicinity of an Aperture in the Surface of a Circular Cylinder", ASTIA AD 250308 (Nov., 1960).
- (10) Withum, D., "The Cylindrical Shell with a Circular Hole under Torsion", Ingr.-Arch., 26, 435-446 (1958).
- (11) Eringen, Naghdi and Thiel, "State of Stress in a Circular Cylindrical Shell with a Circular Hole", Welding Research Council Bulletin No. 102 (January, 1962).
- (12) Lekkerkerker, J. G., "Stress Concentration Around Circular Holes in Cylindrical Shells", Proceedings Applied Mech. Conference, Munich, Germany (1964).
- (13) Savin, G. N., "Concentration of Stresses Around Curvilinear Holes in Plates and Shells", Proceedings Applied Mech. Conference, Munich, Germany (1964).
- (14) Van Dyke, Peter, "Stresses About a Circular Hole in a Cylindrical Shell", AIAA Journal, 3, (9) (Sept., 1965).

LIST OF REFERENCES (contd)

- (15) Reidelbach, W., "The State of Stress at the Perpendicular Intersection of Two Right Circular Tubes", *Ingenieur-Archiv*, 30, (5), 293-296. Translated by M. W. Stamisic, General Technology Corporation, Tech. Note No. 3-1 (April, 1962).
- (16) Eringen, Naghdi, Mahmood, Thiel and Ariman, "Stress Concentrations in Two Normally Intersecting Cylindrical Shells Subject to Internal Pressure", General Technology Corp. Technical Report No. 3-9 (January, 1967).
- (17) Design of Piping Systems, M. W. Kellogg Co., Published by John Wiley & Sons, New York, Second Edition, 1957, page 71.
- (18) Mehringer, F. J., and Cooper, W. E., "Experimental Determinations of Stresses in the Vicinity of Pipe Appendages to a Cylindrical Shell", S.E.S.A. Proceedings, XIV, (2), 1957.
- (19) Cranch, E. T., "An Experimental Investigation of Stresses in the Neighborhood of Attachments to a Cylindrical Shell", Welding Research Council Bulletin No. 60 (May, 1960).
- (20) Berman, I., and Pai, D. H., "An Experimental Investigation of Stresses in an HY-80 Marine Boiler Drum", Welding Research Supplement (July, 1962).
- (21) Berman, I., and Pai, D. H., "An Experimental Investigation of Stresses in an HY-80 Marine Boiler Drum with Added Attachments", Welding Research Supplement (January, 1963).
- (22) Pickett, A. G., and Grigory, S. C., "Studies of the Fatigue Strength of Pressure Vessels, Technical Summary Report, Part I. Cyclic Pressure Tests of Full-Size Pressure Vessels", Southwest Research Institute, San Antonio, Texas (Sept., 1966).
- (23) Wells, Lane & Rose, "Stress Analysis of Nozzles in Cylindrical Pressure Vessels", Proceedings of the Symposium on Pressure Vessel Research Towards Better Design, Published by the Institution of Mechanical Engineers, London (1962).
- (24) Taylor, C. E., and Lind, N. C., "Photoelastic Study of the Stresses Near Openings in Pressure Vessels", Welding Research Council Bulletin No. 113 (April, 1966).
- (25) Leven, M. M., "Photoelastic Determination of the Stresses in Reinforced Openings in Pressure Vessels", Welding Research Council Bulletin No. 113 (April, 1966).
- (26) Mershon, J. L., "PVRC Research on Reinforcement of Openings in Pressure Vessels", Welding Research Council Bulletin No. 77 (May, 1962).
- (27) Stepanek, S., "Stress Concentrations in the Nozzle Ring of a Pressure Vessel", *Nuclear Structural Engineering*, Vol. 2, pp 211-223 (1965).
- (28) Rodabaugh, E. C., and George, H. H., "Design and Strength of Welded Pipe Line Branch Connections", *Proc. ASCE*, 83, No. PL1 (March, 1957).

LIST OF REFERENCES (contd.)

- (29) Babecki, A. J., and Puzak, P. P., "Fabrication and Service Factors Involved in a Failure of Welded Steam Receivers", Welding Research Supplement (July, 1958).
- (30) Puzak, Babecki and Pellini, "Correlations of Brittle-Fracture Service Failures with Laboratory Notch-Ductility Tests", Welding Research Supplement (Sept., 1958).
- (31) Hardenbergh, Zamrik and Edmondson, "Experimental Investigation of Stresses in Nozzles in Cylindrical Pressure Vessels", Welding Research Council Bulletin No. 89 (July, 1963).
- (32) Rose, R. T., "Stress Analysis on Nozzles in Thin-Walled Cylindrical Pressure Vessels", British Welding Research Association Report No. D3/22/63 (March, 1964).
- (33) Riley, W. F., "Experimental Determination of Stress Distributions in Thin-Walled Cylindrical and Spherical Pressure Vessels with Circular Nozzles", Welding Research Council Bulletin No. 108 (Sept., 1965).
- (34) Schoessow, G. J. and Kooistra, L. F., "Stresses in a Cylindrical Shell Due to Nozzle or Pipe Connection", ASME Journal of Applied Mechanics, June, 1945.
- (35) Jackson, et.al., "Stresses in Unreinforced Branch Connections", Battelle Memorial Institute Report to the American Gas Association, September 30, 1953.
- (36) Lane, P.H.R. and Rose, R. T., "Design of Welded Pipe Fittings", British Welding Research Association, Abington Hall, Abington, Cambridge, November, 1959.
- (37) Cranch, E. T., "An Experimental Investigation of Stresses in the Neighborhood of Attachments to a Cylindrical Shell", Welding Research Council Bulletin No. 60, May, 1960.
- (38) McClure, G. M., Sweeney, J. A., and Gross, H. J., "Investigation of Stresses in Pipeline Branch Connections", Battelle Memorial Institute Report to the American Gas Association, March 30, 1956.
- (39) American Standards Association Code for Pressure Piping, ASA B31.1-1955. Published by the American Society of Mechanical Engineers, 345 East 47th Street, New York, N. Y.
- (40) Markl, A.R.C., "Fatigue Tests of Piping Components", Trans. ASME, 1952.
- (41) Markl, A.R.C., "Piping Flexibility Analysis", Trans. ASME, 1955.
- (42) American Standards Association, "Wrought Steel Buttwelding Fittings", ASA B16.9-1964. Published by the American Society of Mechanical Engineers, 345 E. 47th Street, New York, N. Y. 10017

LIST OF REFERENCES (contd)

- (43) Blair, J. S., "Reinforcement of Branch Pieces, Engineering London, England, 1947.
- (44) Markl, A.R.C., "Bending Stress Intensifications in Reducing-Outlet Branch Connections", Tube Turns (Div. of Chemetron), Report No. 8.032, Louisville, Ky., Feb. 1959.
- (45) Rodabaugh, E. C., "Cyclic Bending Tests of a Half-Scale Model of an 8" x 24" Saddle Reinforced Branch Connection", Tube Turns (Div. of Chemetron) Report No. 8.011, Louisville, Ky., 1953.
- (46) Mills, E. J., Atterbury, T. J., and McClure, G. M., "Study of Effects of Cyclic Bending Loads on Performance of Branch Connections", Battelle Memorial Institute Report to the American Gas Association, Columbus, Ohio, May, 1962.
- (47) Pickett, A. G., et.al., "Low Cycle Fatigue Testing of One-Half Scale Model Pressure Vessels", Progress Reports No. 9 through 12, July 1964 through January, 1965. Southwest Research Institute, San Antonio, Texas (Contract No. AT(11-1)-1228, U.S. Atomic Energy Commission)

## APPENDIX A

### STRESSES FROM ERINGEN'S ANALYSIS

#### Stresses at Nozzle-Shell Junctionure

Numerical solutions were obtained\* for the parameters:

D/T from 10 to 250

d/D from .01 to  $(d/D) \sqrt{D/T} \cong 1.1$

s/S from 1/64 to 4.0

The stresses at the nozzle-shell junctionure at  $\phi = 0$  and  $\phi = \pi/2$  obtained from this parametric study are given in Tables A1 through A7. An attempt was made to show these results by means of graphs, however, no accurate way of reducing the dimensional parameters involved was found. In particular, the parameter  $(d/D) \sqrt{D/T}$  does not reduce the dimensional parameters from 3 to 2, except for small values of t/T. Figure 8 shows the  $\sigma_{n\phi}$ -stress at  $\phi = 0$ ,  $\rho = \rho_0$ , plotted against  $(d/D) \sqrt{D/T}$ .

The parametric study gives stresses at  $\phi = 0, \pi/8, \pi/4, 3\pi/8,$  and  $\pi/2$ . Maximums of individual stress components were found to be either at  $\phi = 0$  or  $\phi = \pi/2$ . The minimums of individual stress components may be between  $\phi = 0$  and  $\phi = \pi/2$ .

#### Stresses Away from Junctionure

The parametric study results include stresses as a function of  $\rho$  in the shell, x in the nozzle. While maximum stresses in both the nozzle and the shell occur at the junctionure, maximums of individual stress

---

\* The parametric study includes those cases of the parametric study given in Reference (1) which are within the limitation  $(d/D) \sqrt{D/T} < 1.1$ , plus 68 additional cases within that limitation.

components may not be at the juncture. (See, for example, Figure 15;  $\sigma_{y_0}$  at  $\theta = \pi/2$  is a maximum at  $x/\sqrt{rt} \cong 1.3$ , but the maximum stress in the nozzle is  $\sigma_{y_0}$  at  $\theta = 0$  at the juncture.)

#### Use of Eringen's Computer Program

Eringen's computer program, as modified for use at Battelle, consists of two separate programs, identified as program I and Program II. The input data to program I consists of the values of the three parameters:  $\beta\rho_0$ ,  $t/\rho_0$ , and  $\rho_0/R$ . The output of program I consists of punched cards containing the constants of the analytical series solution. The input to program II is the punched cards from program I. The output from program II consists of:

(a) Eringen's stress resultants for

$$\theta = 0, \pi/8, \pi/4, 3\pi/8, \text{ and } \pi/2.$$

$$\rho/\rho_0 = 1.0, 1.3, 1.6, 2.0, \text{ and } 3.0.$$

$$x/\rho_0 = 0, .3, .6, 1.0, \text{ and } 2.0.$$

(b) Membrane, bending and surface stress indices ( $\sigma/S$ ) for

$$\theta = 0, \pi/8, \pi/4, 3\pi/8, \text{ and } \pi/2.$$

$$(\rho-\rho_0)/\sqrt{RT} = 0, .3, .6, 1.0, 2.0.$$

$$x/\sqrt{rt} = 0, .3, .6, 1.0, 2.0.$$

The relationship between stress indices ( $\sigma/S$ ) and Eringen's stress resultants are summarized in Figure A1.

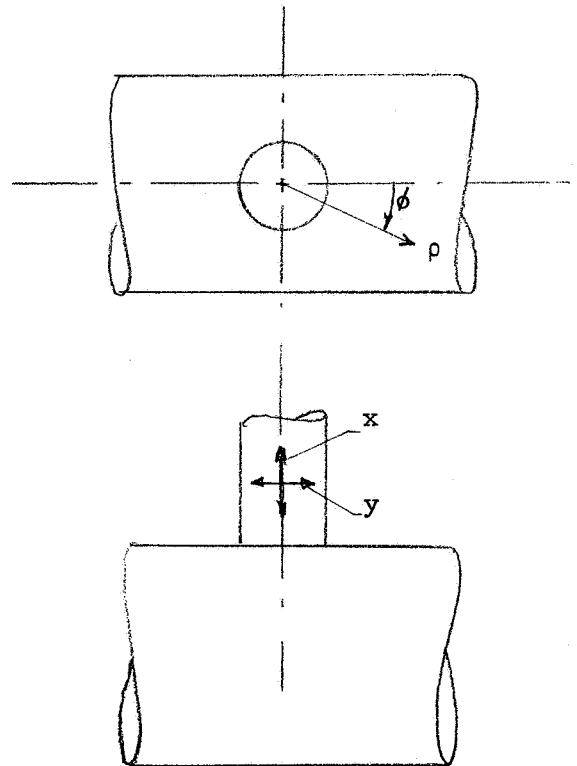
The running time for both programs on a Control Data Model 3400 computer is about 3 minutes per case; on a Control Data 6400 computer the central processor time is about 30 seconds per case, with another 30 secs of peripheral equipment time. For both computers, running times quoted are after compilation and production of a binary deck.

FIGURE A1. EQUATIONS FOR CONVERTING STRESS RESULTANTS OF REFERENCE (1) TO STRESSES

Nomenclature:

- D = cylinder (lower shell) mean diameter
- T = cylinder wall thickness
- d = nozzle (upper shell) mean diameter =  $2\rho_o$
- t = nozzle wall thickness
- P = internal pressure
- S = PD/2T
- s = Pd/2t
- $\nu$  = Poisson's ratio assumed to be 0.3
- n (subscript) = membrane stress
- b (subscript) = bending stress

$\sigma/S$	Equation for Stress	Bending Stress Sign
$\sigma_{n\phi}$	$\frac{\bar{N}_\phi}{2} + \cos^2\phi + 0.5 \sin^2\phi$	
$\sigma_{b\phi}$	$\pm 0.91 \bar{M}_\phi$	+ outside
$\sigma_{n\rho}$	$\frac{\bar{N}_\rho}{2} + 0.5 \cos^2\phi + \sin^2\phi$	
$\sigma_{b\rho}$	$\pm 0.91 \bar{M}_\rho$	+ outside
$\sigma_{nx}$	$\frac{\bar{n}_x}{2} \cdot \frac{T}{t} + 0.5 \frac{s}{S}$	
$\sigma_{bx}$	$\pm 0.91 \left(\frac{T}{t}\right)^2 \bar{m}_x$	+ inside
$\sigma_{ny}$	$\frac{\bar{n}_y}{2} \cdot \frac{T}{t} + \frac{s}{S}$	
$\sigma_{by}$	$\pm 0.91 \left(\frac{T}{t}\right)^2 \bar{m}_y$	+ inside



$\bar{N}_\phi$ ,  $\bar{M}_\phi$ ,  $\bar{N}_\rho$ ,  $\bar{M}_\rho$ ,  $\bar{n}_x$ ,  $\bar{m}_x$ ,  $\bar{n}_y$ , and  $\bar{m}_y$  are stress resultants as defined in Reference (1)

The applicability of the analysis is limited by Eringen to:  $D/T \geq 20$ ,  $d/t \geq 20$  and  $d/D < 1/3$ . These restrictions follow from the use of thin-shell and shallow shell theory. In addition, because of the truncation of the Fourier series in the boundary conditions,  $(d/D)\sqrt{D/T}$  is limited to about 1.1. It will be noted that most of the experimental models used for comparisons have  $D/T$  and  $d/t$  ratios less than 20. Judging by the theory-test comparisons, the  $D/T$  or  $d/t$  restrictions do not appear to be very rigid. However, the necessity of the restriction that  $(d/D)\sqrt{D/T} < 1.1$  is apparent from the computer program output. For values of  $(d/D)\sqrt{D/T}$  of about 1.5, the results appear to be inconsistent with results for lower values of  $(d/D)\sqrt{D/T}$  and at  $(d/D)\sqrt{D/T} = 2.0$ , the program output shows very high stresses at points remote from the juncture, with no evidence of attenuation towards nominal stresses.



TABLE OF STRESSES

The following tables are included in this Appendix.

<u>Table</u>	<u>Title</u>
A1	Membrane Stresses in Cylinder at $\rho = \rho_0$ , $\theta = 0$ , and $\pi/2$ .
A2	Membrane Stresses in Nozzle at $x = 0$ , $\theta = 0$ , and $\pi/2$ .
A3	Bending Stresses in Cylinder at $\rho = \rho_0$ , $\theta = 0$ , and $\pi/2$ .
A4	Bending Stresses in Nozzle at $x = 0$ , $\theta = 0$ , and $\pi/2$ .
A5	Maximum Stress Intensity in Cylinder at $\theta = 0$ and $\pi/2$ .
A6	Maximum Stress Intensity in Nozzle at $\theta = 0$ and $\pi/2$ .
A7	Maximum Surface Stresses in Cylinder and Nozzle

In all of these tables, stresses are shown as divided by the nominal stress,  $S$ . The signs of the bending stresses (Tables A3 and A4) are positive (tension) for the outside surface.

TABLE A1. MEMBRANE STRESSES IN CYLINDER AT  $\rho=\rho_0$ ,  $\phi = 0$  and  $\pi/2$

1 of 5

$\frac{D}{T}$	$\frac{d}{D}$	$\frac{s}{S}$	$\phi = 0$		$\phi = \pi/2$		
			$\sigma_{n\phi}$	$\sigma_{n\rho}$	$\sigma_{n\phi}$	$\sigma_{n\rho}$	
10	.01	1.	2.49	.00	.51	.00	
	.025	.0625	1.34	-.05	.76	.96	
		.125	1.84	-.08	.74	.52	
		.25	2.27	.03	.58	.14	
		.5	2.43	.03	.53	.03	
		1.0	2.48	.01	.52	.00	
		1.5	2.50	.00	.51	.00	
		.05	.0625	1.12	.09	.72	1.05
		.125	1.56	-.02	.76	.71	
		.25	2.10	.05	.64	.26	
		.5	2.38	.05	.56	.05	
		1.	2.48	.02	.53	.00	
		2.	2.52	.00	.52	.00	
		4.	2.54	.00	.51	.00	
		.10	.0625	.93	.23	.69	1.12
		.125	1.32	.08	.77	.83	
		.25	1.87	.11	.70	.42	
		.5	2.33	.10	.59	.11	
		1.	2.54	.04	.55	.02	
		2.	2.61	.01	.52	.00	
		4.	2.64	.00	.51	-.01	
		.25	.25	1.68	.16	.49	.80
		.5	2.34	.23	.52	.36	
		1.	2.89	.13	.51	.11	
		2.	3.16	.04	.49	.02	
	4.	3.26	.00	.47	.01		
	.35	.25	1.67	.20	-.22	1.28	
	.5	2.31	.28	.00	.64		
	1.	3.06	.21	.25	.24		
	1.5	3.44	.13	.36	.11		
	2.	3.63	.08	.38	.07		

TABLE A1. (Continued)

2 of 5

$\frac{D}{F}$	$\frac{d}{D}$	$\frac{s}{S}$	$\phi = 0$		$\phi = \pi/2$	
			$\sigma_{n\phi}$	$\sigma_{n\rho}$	$\sigma_{n\phi}$	$\sigma_{n\rho}$
25	.025	.0625	1.62	.03	.73	.63
		.125	2.13	.09	.60	.21
		.25	2.37	.06	.54	.05
		.5	2.47	.03	.52	.01
		1.	2.50	.01	.51	.00
		1.5	2.51	.00	.51	.00
	.05	.0625	1.36	.12	.76	.75
		.125	1.90	.16	.65	.35
		.25	2.30	.12	.57	.10
		.5	2.48	.05	.54	.02
		1.	2.56	.02	.51	.00
		2.	2.58	.00	.50	.00
	.10	.125	1.71	.23	.67	.49
		.25	2.24	.22	.56	.19
		.5	2.60	.11	.53	.05
		1.	2.77	.04	.51	.01
		2.	2.84	.01	.49	.00
	.25	.125	1.70	.29	-.52	1.29
		.25	2.20	.35	-.40	.58
		.5	2.76	.27	-.02	.25
		1.	3.51	.16	.32	.06
		2.	4.02	.06	.37	.01
		4.	4.20	.01	.27	.01

TABLE A1. (Continued) 3 of 5

$\frac{D}{T}$	$\frac{d}{D}$	$\frac{s}{S}$	$\phi = 0$		$\phi = \pi/2$		
			$\sigma_{n\phi}$	$\sigma_{np}$	$\sigma_{n\phi}$	$\sigma_{np}$	
50	.005	1.	2.50	.00	.50	.01	
	↓	.01	.015625	1.22	.06	.73	.98
		.03125	1.71	.01	.71	.57	
		.0625	2.17	.08	.58	.17	
		.125	2.38	.05	.53	.04	
		.25	2.46	.02	.52	.01	
		.5	2.49	.01	.51	.00	
		1.0	2.50	.00	.50	.00	
		1.5	2.50	.00	.50	.00	
	↓	.025	.03125	1.35	.13	.76	.75
		.0625	1.87	.16	.64	.35	
		.125	2.25	.13	.56	.10	
		.25	2.43	.06	.53	.02	
		.5	2.50	.02	.51	.00	
		1.	2.53	.01	.50	.00	
		2.	2.54	.00	.50	.00	
		4.	2.55	.00	.50	.00	
	↓	.05	.0625	1.64	.24	.70	.46
		.125	2.13	.22	.58	.18	
		.25	2.44	.12	.54	.05	
		.5	2.60	.04	.52	.01	
		1.	2.66	.01	.50	.00	
		2.	2.68	.00	.49	.00	
		4.	2.69	.00	.49	.00	
		↓	.10	.0625	1.68	.24	.27
	.125		2.15	.29	.36	.34	
	.25		2.56	.22	.44	.12	
	.5		2.91	.10	.47	.03	
1.	3.09		.04	.46	.00		
2.	3.15		.01	.44	.00		
4.	3.17		.00	.44	.00		
↓	.15		.125	2.23	.33	-.27	.56
	.25	2.62	.27	.03	.24		
	.5	3.16	.17	.33	.08		
	1.	3.60	.07	.42	.01		
	1.5	3.74	.04	.39	.00		

TABLE A1. (Continued)  
4 of 5

$\frac{D}{T}$	$\frac{d}{D}$	$\frac{s}{S}$	$\phi = 0$		$\phi = \pi/2$		
			$\sigma_{n\theta}$	$\sigma_{np}$	$\sigma_{n\theta}$	$\sigma_{np}$	
100	.01	.015625	1.42	.10	.75	.73	
		.03125	1.94	.14	.62	.30	
		.0625	2.27	.10	.55	.08	
		.125	2.42	.05	.53	.02	
		.25	2.48	.02	.51	.00	
		.5	2.50	.01	.50	.00	
		1.	2.51	.00	.50	.00	
		1.5	2.51	.00	.51	.00	
		.025	.015625	1.12	.26	.75	.87
			.03125	1.61	.24	.71	.46
	.0625		2.07	.21	.58	.18	
	.125		2.36	.12	.54	.05	
	.250		2.50	.05	.52	.01	
	.5		2.61	.02	.50	.00	
	1.		2.58	.00	.50	.00	
	2.		2.59	.00	.49	.00	
	4.		2.60	.00	.49	.00	
	.05		.0625	1.96	.30	.56	.26
		.125	2.34	.21	.52	.10	
		.25	2.64	.10	.51	.03	
		.5	2.78	.04	.49	.01	
		1.	2.84	.01	.48	.00	
		2.	2.86	.00	.47	.00	
		4.	2.86	.00	.47	.00	
		.10	.0625	2.17	.33	-.25	.61
	.125		2.50	.27	.00	.27	
.25	2.89		.19	.28	.12		
.5	3.34		.10	.44	.02		
1.	3.60		.03	.42	.00		
2.	3.70		.01	.38	.00		
4.	3.73		.00	.34	.00		

TABLE A1. (Continued)

5 of 5

$\frac{D}{T}$	$\frac{d}{D}$	$\frac{s}{S}$	$\phi = 0$		$\phi = \pi/2$	
			$\sigma_{n\emptyset}$	$\sigma_{np}$	$\sigma_{n\emptyset}$	$\sigma_{np}$
250	.001	1.	2.50	.00	.50	.00
	.005	.015625	1.99	.17	.60	.24
		.03125	2.29	.10	.55	.07
		.0625	2.42	.05	.53	.02
		.125	2.48	.02	.51	.00
		.25	2.50	.01	.50	.00
		.5	2.51	.00	.50	.00
		1.	2.51	.00	.50	.00
	1.5	2.51	.00	.50	.00	
	.01	.015625	1.75	.24	.67	.34
		.03125	2.15	.18	.57	.12
		.0625	2.37	.09	.54	.04
		.125	2.47	.04	.52	.01
		.25	2.51	.01	.50	.00
		.5	2.53	.00	.50	.00
		1.	2.54	.00	.50	.00
		4.	2.54	.00	.50	.00
	.025	.015625	1.51	.37	.63	.53
		.03125	1.95	.30	.60	.20
		.0625	2.29	.19	.55	.08
		.125	2.54	.09	.52	.03
		.25	2.66	.03	.50	.01
		.5	2.71	.01	.49	.00
		1.	2.73	.00	.48	.00
		4.	2.73	.00	.48	.00
	.05	.0625	2.55	.22	.13	.22
		.125	2.78	.15	.33	.10
		.25	3.05	.07	.45	.00
.5		3.21	.30	.45	.00	
1.		3.27	.00	.43	.00	
4.		3.30	.00	.41	.00	
.07	.0625	2.42	.28	-.04	.27	
	.125	2.71	.20	.22	.14	
	.25	3.21	.13	.44	.05	
	.5	3.63	.06	.50	.00	
	1.0	3.84	.02	.42	.00	
	2.0	3.89	.01	.37	.00	
		2.0	3.92	.01	.35	.00

TABLE A2. MEMBRANE STRESSES IN NOZZLE AT  $x = 0$ ,  $\phi = 0$  and  $\pi/2$

1 of 5

$\frac{D}{T}$	$\frac{d}{D}$	$\frac{s}{S}$	$\phi = 0$		$\phi = \pi/2$		
			$\sigma_{nx}$	$\sigma_{ny}$	$\sigma_{nx}$	$\sigma_{ny}$	
10	.01	1.	.22	2.55	.78	.74	
	↓	.025	.0625	-.09	1.33	.15	.52
		.125	-.16	1.82	.28	.67	
		.25	-.19	2.20	.44	.67	
		.5	-.09	2.39	.59	.70	
		1.0	.20	2.54	.80	.76	
		1.5	.49	2.64	1.01	.82	
	↓	.05	.0625	-.09	1.06	.14	.45
		.125	-.14	1.53	.75	.63	
		.25	-.18	2.02	.43	.69	
		.5	-.10	2.33	.60	.73	
		1.	.18	2.53	.82	.78	
		2.	.75	2.75	1.24	.90	
		4.	1.84	3.09	2.16	1.16	
	↓	.10	.0625	-.06	.84	.12	.40
		.125	-.13	1.26	.24	.61	
		.25	-.16	1.79	.40	.71	
		.5	-.10	2.27	.60	.76	
		1.	.15	2.56	.85	.83	
		2.	.72	2.83	1.28	.93	
		4.	1.98	3.19	2.18	1.20	
	↓	.25	.25	-.04	1.42	.29	1.13
		.5	.06	2.17	.43	1.06	
		1.	.32	2.90	.69	1.01	
2.		.84	3.39	1.19	1.09		
4.		1.89	3.83	2.14	1.33		
↓	.35	.25	.06	1.26	.34	1.80	
	.5	.19	1.97	.41	1.95		
	1.	.49	2.96	.55	1.66		
	1.5	.78	3.54	.80	1.44		
	2.	1.06	3.87	1.06	1.34		

TABLE A2. (Continued)

2 of 5

$\frac{D}{T}$	$\frac{d}{D}$	$\frac{s}{S}$	$\phi = 0$		$\phi = \pi/2$			
			$\sigma_{nx}$	$\sigma_{ny}$	$\sigma_{nx}$	$\sigma_{ny}$		
↓	↓	.025	.0625	-.17	1.56	.23	.61	
		.125	-.22	2.03	.35	.64		
		.25	-.19	2.30	.43	.66		
		.5	-.02	2.45	.52	.68		
		1.	.31	2.59	.69	.72		
		1.5	.61	2.69	.89	.78		
	↓	.05	.0625	-.13	1.29	.19	.60	
		.125	-.17	1.80	.30	.64		
		.25	-.15	2.22	.40	.66		
		.5	-.01	2.46	.51	.69		
		1.	.31	2.64	.69	.73		
		2.	.88	2.85	1.12	.85		
	↓	4.	1.93	3.17	2.07	1.13		
		↓	.10	.125	-.07	1.57	.18	.68
			.25	.00	2.16	.25	.64	
			.5	.12	2.60	.38	.66	
			1.	.39	2.80	.61	.72	
	2.		.94	3.12	1.06	.84		
	↓	4.	1.98	3.45	2.03	1.12		
		↓	.25	.125	.08	.97	.18	1.54
.25			.21	1.53	.14	1.88		
.5			.41	2.33	.12	1.76		
1.			.83	3.56	.16	1.05		
2.	1.57		4.54	.55	.28			
↓	4.	2.70	4.98	1.51	.50			



TABLE A2. (Continued) 3 of 5

$\frac{D}{T}$	$\frac{d}{D}$	$\frac{s}{S}$	$\phi = 0$		$\phi = \pi/2$		
			$\sigma_{nx}$	$\sigma_{ny}$	$\sigma_{nx}$	$\sigma_{ny}$	
50	.005	1.	.40	2.62	.60	.68	
	↓	.01	.015625	-.11	1.17	.12	.48
		.03125	-.18	1.65	.21	.60	
		.0625	-.25	2.07	.31	.62	
		.125	-.24	2.29	.36	.63	
		.25	-.13	2.41	.38	.63	
		.5	.07	2.51	.43	.64	
		1.0	.39	2.62	.61	.68	
	↓	1.5	.67	2.71	.83	.75	
	↓	.025	.03125	-.13	1.27	.16	.59
		.0625	-.19	1.76	.25	.62	
		.125	-.19	2.16	.32	.63	
		.25	-.11	2.38	.36	.64	
		.5	.07	2.52	.42	.64	
		1.	.39	2.65	.61	.69	
		2.	.94	2.82	1.06	.81	
	↓	4.	1.97	3.14	2.03	1.11	
	↓	.05	.0625	-.08	1.53	.14	.62
		.125	-.05	2.04	.18	.60	
		.25	.00	2.41	.25	.60	
		.5	.14	2.62	.36	.63	
		1.	.43	2.78	.57	.68	
		2.	.97	2.97	1.03	.81	
		↓	4.	1.99	3.28	2.01	1.10
	↓	.10	.0625	.01	1.02	.08	1.05
		.125	.06	1.63	.07	1.04	
.25		.17	2.33	.06	.80		
.5		.36	2.92	.13	.64		
1.		.66	3.26	.34	.61		
2.		1.18	3.50	.83	.73		
↓		4.	2.16	3.81	1.85	1.02	
↓	.15	.125	.11	1.26	.08	1.63	
	.25	.23	1.88	.04	1.61		
	.5	.45	2.89	.02	1.14		
	1.	.87	3.85	.12	.47		
	↓	1.5	1.22	4.15	.30	.36	

TABLE A2. (Continued)  
4 of 5

$\frac{D}{T}$	$\frac{d}{D}$	$\frac{s}{S}$	$\phi = 0$		$\phi = \pi/2$	
			$\sigma_{nx}$	$\sigma_{ny}$	$\sigma_{nx}$	$\sigma_{ny}$
100	.01	.015625	-.15	1.34	.17	.58
		.03125	-.22	1.83	.25	.61
		.0625	-.23	2.17	.29	.62
		.125	-.18	2.35	.30	.61
		.25	-.05	2.46	.30	.60
		.5	.15	2.54	.35	.61
		1.	.44	2.64	.56	.67
		1.5	.71	2.73	.79	.74
	.025	.015625	-.05	1.02	.06	.51
		.03125	-.09	1.51	.12	.61
		.0625	-.09	1.98	.15	.58
		.125	-.07	2.30	.19	.59
		.250	.01	2.50	.24	.59
		.5	.18	2.61	.32	.60
		1.	.46	2.72	.54	.66
		2.	.98	2.89	1.02	.80
	.05	.0625	.02	1.71	.04	.72
		.125	.08	2.24	.03	.59
		.25	.17	2.64	.07	.55
		.5	.32	2.86	.18	.55
		1.	.58	3.01	.42	.61
		2.	1.08	3.18	.92	.75
		4.	2.07	3.48	1.93	1.06
		.10	.0625	.05	1.02	.03
	.125		.13	1.50	.01	1.61
	.25		.25	2.27	-.02	1.37
	.5		.50	3.34	-.03	.66
	1.		.91	3.95	.08	.28
2.	1.53		4.20	.49	.40	
4.	2.51	4.49	1.51	.76		

TABLE A2. (Continued)

$\frac{D}{T}$	$\frac{d}{D}$	$\frac{s}{S}$	$\phi = 0$		$\phi = \pi/2$	
			$\sigma_{nx}$	$\sigma_{ny}$	$\sigma_{nx}$	$\sigma_{ny}$
250	.001	1.	.48	2.64	.52	.66
	.005	.015625	-.21	1.88	.22	.60
		.03125	-.22	2.19	.25	.61
		.0625	-.18	2.35	.24	.59
		.125	-.08	2.45	.20	.57
		.25	.04	2.51	.21	.57
		.5	.21	2.57	.29	.59
		1.	.48	2.65	.52	.66
	1.5	.73	2.73	.77	.73	
	.01	.015625	-.11	1.65	.12	.60
		.03125	-.11	2.06	.14	.58
		.0625	-.10	2.31	.17	.58
		.125	-.05	2.45	.17	.57
		.25	.06	2.52	.19	.56
		.5	.21	2.58	.29	.59
		1.	.48	2.68	.52	.66
	2.	.99	2.84	1.01	.80	
	4.	2.00	3.14	2.00	1.10	
	.025	.015625	-.01	1.20	.02	.70
		.03125	.01	1.76	.01	.67
		.0625	.05	2.21	.00	.57
		.125	.10	2.53	.02	.53
		.25	.18	2.70	.07	.52
		.5	.32	2.80	.18	.54
		1.	.56	2.89	.43	.61
	2.	1.05	3.05	.95	.76	
	4.	2.04	3.35	1.96	1.06	
.05	.0625	.07	1.41	.00	1.55	
	.125	.14	2.00	-.02	1.36	
	.25	.27	2.81	-.03	.85	
	.5	.49	3.29	-.06	.54	
	1.	.83	3.52	.16	.50	
	2.	1.35	3.70	.65	.62	
4.	2.30	4.00	1.70	.93		
.07	.0625	.07	1.25	-.01	1.61	
	.125	.14	1.77	-.02	1.63	
	.25	.27	2.89	-.05	.98	
	.5	.54	4.19	-.08	-.29	
	1.0	1.00	4.50	-.02	-.44	
	1.5	1.37	4.50	.13	-.19	
2.0	1.68	4.53	.33	.00		

TABLE A3. BENDING STRESSES IN CYLINDER AT  $\rho = \rho_0$ ,  $\phi = 0$  and  $\pi/2$   
1 of 5

$\frac{D}{T}$	$\frac{d}{D}$	$\frac{s}{S}$	$\phi = 0$		$\phi = \pi/2$	
			$\sigma_{b\phi}$	$\sigma_{bp}$	$\sigma_{b\phi}$	$\sigma_{bp}$
10	.01	1.	.00	.00	.01	.00
	.025	.0625	-.11	.10	-.32	.35
		.125	-.01	.00	-.12	.16
		.25	.00	.00	.01	.04
		.5	.01	.00	.04	.01
		1.0	.02	.00	.04	.00
		1.5	.02	.00	.04	.00
	.05	.0625	-.26	.21	-.51	.59
		.125	-.08	.06	-.31	.42
		.25	-.03	.02	.01	.14
		.5	.01	.01	.12	.03
		1.	.04	.00	.13	.00
		2.	.05	.00	.13	.00
		4.	.06	.00	.12	.00
	.10	.0625	-.28	.13	-.27	.45
		.125	-.25	.12	-.40	.72
		.25	-.17	.08	-.02	.43
		.5	-.08	.05	.34	.10
		1.	.03	.02	.40	.01
		2.	.08	.00	.38	.00
		4.	.10	.00	.37	.00
	.25	.25	-.41	.14	-.04	1.03
		.5	-.48	.28	.62	.63
		1.	-.28	.15	1.23	.14
		2.	-.25	.04	1.38	.00
4.		-.18	.00	1.36	-.02	
.35	.25	-.29	.35	-.14	1.17	
	.5	-.40	.50	.43	1.15	
	1.	-.32	.36	1.50	.41	
	1.5	-.27	.19	1.98	.14	
	2.	-.24	.11	2.16	.04	

TABLE A3. (Continued)

2 of 5

$\frac{D}{T}$	$\frac{d}{D}$	$\frac{s}{S}$	$\phi = 0$		$\phi = \pi/2$	
			$\sigma_{b\phi}$	$\sigma_{b\rho}$	$\sigma_{b\phi}$	$\sigma_{b\rho}$
↓	.025	.0625	-.12	.06	-.31	.44
		.125	-.07	.04	.00	.13
		.25	-.02	.02	.09	.03
		.5	.02	.01	.09	.00
		1.	.04	.00	.09	.00
		1.5	.04	.00	.09	.00
	.05	.0625	-.30	.09	-.39	.75
		.125	-.25	.12	-.04	.42
		.25	-.12	.08	.25	.10
		.5	.01	.03	.29	.01
		1.	.07	.01	.27	.00
		2.	.09	.00	.26	.00
	.10	.125	-.39	.18	-.03	.81
		.25	-.32	.26	.41	.37
		.5	-.12	.12	.69	.08
		1.	.01	.03	.72	.01
		2.	.07	.00	.71	.00
	.25	.125	.10	.76	.02	.93
		.25	.11	1.08	.20	1.21
		.5	.26	.84	.72	.75
1.		.48	.36	1.59	.20	
2.		.40	.09	2.26	.01	
	4.	.08	.01	2.62	-.01	

TABLE A3. (Continued)

$\frac{D}{T}$	$\frac{d}{D}$	$\frac{s}{S}$	$\phi = 0$		$\phi = \pi/2$		
			$\sigma_{b\phi}$	$\sigma_{bp}$	$\sigma_{b\phi}$	$\sigma_{bp}$	
50	.005	1.	.01	.00	.01	.00	
	↓	.01	.015625	-.23	.17	-.51	.59
		.03125	-.09	.04	-.25	.33	
		.0625	-.05	.03	-.02	.09	
		.125	-.02	.01	.04	.02	
		.25	.01	.00	.04	.00	
		.5	.02	.00	.03	.00	
		1.0	.02	.00	.03	.00	
		1.5	.02	.00	.03	.00	
	↓	.025	.03125	-.31	.08	-.43	.75
		.0625	-.26	.12	-.12	.42	
		.125	-.14	.08	.14	.10	
		.25	-.02	.03	.18	.02	
		.5	.04	.01	.16	.00	
		1.	.06	.00	.15	.00	
		2.	.06	.00	.15	.00	
	4.	.07	.00	.14	.00		
	↓	.05	.0625	-.41	.14	-.13	.76
		.125	-.33	.25	.21	.35	
		.25	-.12	.12	.43	.08	
		.5	.03	.03	.45	.01	
1.		.09	.01	.43	.00		
2.		.11	.00	.42	.00		
4.		.12	.00	.42	.00		
↓	.10	.0625	-.16	.14	-.07	.82	
	.125	-.21	.43	.04	.79		
	.25	-.08	.43	.43	.35		
	.5	.07	.17	.79	.08		
	1.	.07	.04	.97	.01		
	2.	.02	.01	1.06	.00		
	4.	-.03	.00	1.10	.00		
↓	.15	.125	.11	.93	-.27	.56	
	.25	.21	.88	.03	.24		
	.5	.43	.46	.83	.28		
	1.	.45	.14	1.36	.04		
	1.5	.34	.05	1.58	.01		

TABLE A3. (Continued)  
4 of 5

$\frac{D}{T}$	$\frac{d}{D}$	$\frac{s}{S}$	$\varphi = 0$		$\varphi = \pi/2$		
			$\sigma_{b\varphi}$	$\sigma_{b\rho}$	$\sigma_{b\varphi}$	$\sigma_{b\rho}$	
100	.01	.015625	-.27	.09	-.47	.69	
		.03125	-.21	.09	-.12	.30	
		.0625	-.11	.05	.06	.07	
		.125	-.03	.02	.08	.01	
		.25	.01	.01	.07	.00	
		.5	.03	.00	.06	.00	
		1.	.03	.00	.06	.00	
		1.5	.03	.00	.06	.00	
		.025	.015625	-.30	-.02	-.16	.57
			.03125	-.42	.11	-.19	.73
			.0625	-.36	.23	.09	.33
			.125	-.15	.12	.27	.08
			.250	.00	.04	.28	.01
			.5	.07	.01	.26	.00
			1.	.09	.00	.25	.00
		2.	.09	.00	.25	.00	
		4.	.09	.00	.25	.00	
		.05	.0625	-.28	.41	.04	.62
			.125	-.15	.40	.24	.29
			.25	.05	.16	.50	.07
	.5		.12	.04	.60	.01	
	1.		.12	.01	.65	.00	
	2.		.10	.00	.68	.00	
	4.	.10	.00	.69	.00		
	.10	.0625	.14	.89	-.04	.70	
		.125	.21	1.04	.02	.75	
		.25	.42	.69	.37	.44	
		.5	.60	.26	.85	.10	
		1.	.51	.06	1.22	.01	
		2.	.23	.01	1.55	.00	
	4.	-.03	.00	1.80	.00		

TABLE A3. (Continued)

5 of 5

$\frac{D}{T}$	$\frac{d}{D}$	$\frac{s}{S}$	$\varphi = 0$		$\varphi = \pi/2$	
			$\sigma_{b\varphi}$	$\sigma_{bp}$	$\sigma_{b\varphi}$	$\sigma_{bp}$
250	.001	1.	.00	.00	.00	.00
	.005	.015625	-.26	.11	-.08	.28
		.03125	-.13	.06	.06	.06
		.0625	-.04	.02	.07	.01
		.125	.00	.01	.05	.00
		.25	.02	.00	.04	.00
		.5	.02	.00	.04	.00
		1.	.02	.00	.04	.00
	1.5	.02	.00	.04	.00	
	.01	.015625	-.45	.15	-.18	.61
		.03125	-.33	.19	.08	.22
		.0625	-.13	.08	.17	.05
		.125	-.01	.02	.15	.01
		.25	.04	.01	.13	.00
		.5	.05	.00	.12	.00
		1.	.06	.00	.12	.00
	2.	.06	.00	.12	.00	
	4.	.06	.00	.12	.00	
	.025	.015625	-.20	.09	-.10	.54
		.03125	-.27	.42	-.09	.48
		.0625	.14	.41	.10	.24
		.125	.06	.16	.31	.08
		.25	.14	.04	.41	.01
		.5	.15	.01	.45	.00
		1.	.13	.00	.47	.00
	2.	.12	.00	.49	.00	
	4.	.12	.00	.49	.00	
.05	.0625	.099	.82	-.09	.59	
	.125	.262	.58	.14	.37	
	.25	.433	.23	.48	.10	
	.5	.408	.06	.72	.02	
	1.	.247	.01	.93	.00	
	2.	.051	.00	1.11	.00	
4.	-.074	.00	1.25	.00		
.07	.0625	.36	1.47	-.10	.48	
	.125	.51	1.18	.07	.58	
	.25	.82	.59	.51	.25	
	.5	.98	.19	.91	.03	
	1.0	.82	.04	1.25	.00	
	1.5	.60	.02	1.49	.00	
	2.0	.42	.01	1.66	.00	



TABLE A4. BENDING STRESSES IN NOZZLE AT  $x=0$ ,  $\varphi=0$  and  $\pi/2$

1 of 5

$\frac{D}{T}$	$\frac{d}{D}$	$\frac{s}{S}$	$\varphi = 0$		$\varphi = \pi/2$		
			$\sigma_{bx}$	$\sigma_{by}$	$\sigma_{bx}$	$\sigma_{by}$	
10	.01	1.	1.53	.06	.83	.65	
	↓	.025	.0625	--	--	--	--
			.125	.07	-1.43	3.92	-2.59
			.25	.47	-1.24	3.87	2.52
			.5	1.33	-.38	2.51	1.53
			1.0	1.53	.06	.84	.65
			1.5	1.20	.09	-.36	.16
	↓	.05	.0625	.33	-.33	.92	.68
			.125	.35	-.87	2.63	1.71
			.25	.53	-1.06	3.46	2.23
			.5	1.33	-.37	2.49	1.51
			1.	1.57	.07	.87	.66
			2.	.74	.02	-1.36	-.20
			4.	-1.94	-.68	-4.86	-1.35
	↓	.10	.0625	-.05	-.31	.18	.35
			.125	.19	-.66	1.13	.98
			.25	.50	-.89	2.67	1.76
			.5	1.37	-.36	2.50	1.51
			1.	2.04	-.20	1.03	.73
			2.	.98	-.08	-1.23	-.16
			4.	-1.67	-.61	-4.79	-1.33
	↓	.25	.25	.14	-.97	1.04	1.30
			.5	1.12	-.55	2.51	1.67
			1.	2.42	.18	2.19	1.27
			2.	2.16	.36	-.11	.30
			4.	-.37	-.26	-3.94	-1.02
	↓	.35	.25	.18	-1.02	.60	1.49
			.5	1.02	-.66	2.35	1.93
		1.	2.89	.26	3.36	1.88	
		1.5	3.51	.62	2.58	1.41	
		2.	3.46	.70	1.44	.93	

TABLE A4. (Continued)

2 of 5

$\frac{D}{T}$	$\frac{d}{D}$	$\frac{s}{S}$	$\varphi = 0$		$\varphi = \pi/2$		
			$\sigma_{bx}$	$\sigma_{by}$	$\sigma_{bx}$	$\sigma_{by}$	
↓	↓	.025	.37	-.90	2.75	1.81	
		.125	.98	-.76	3.35	2.04	
		.25	1.98	.03	2.53	1.38	
		.5	2.54	.44	1.38	.73	
		1.	2.39	.55	.03	.17	
		1.5	1.84	.44	-.96	-.18	
	↓	↓	.05	.14	-.71	1.18	1.07
			.125	.74	-.70	2.59	1.66
			.25	1.92	-.04	2.50	1.36
			.5	2.62	.46	1.48	.77
			1.	2.54	.59	.12	.20
			2.	1.35	.32	-1.79	-.46
	↓	↓	.10	.28	-.77	1.28	1.19
			.25	1.65	-.15	2.30	1.33
			.5	2.91	.51	1.90	.96
			1.	3.07	.73	.55	.36
			2.	1.94	.49	-1.47	-.34
			4.	-1.00	-.35	-4.87	-1.41
	↓	↓	.25	.19	-.95	.23	1.44
			.25	1.08	-.44	1.21	1.55
.5			3.35	.53	3.00	1.60	
1.			5.82	1.48	3.28	1.38	
2.			5.75	1.59	.66	.41	
4.			2.47	.64	-3.17	-.88	

TABLE A4. (Continued) 3 of 5

$\frac{D}{T}$	$\frac{d}{D}$	$\frac{s}{S}$	$\varphi = 0$		$\varphi = \pi/2$		
			$\sigma_{bx}$	$\sigma_{by}$	$\sigma_{bx}$	$\sigma_{by}$	
50	.005	1.	2.68	.72	-.31	-.01	
	↓	.01	.015625	.41	-.43	1.43	.97
		.03125	.39	-1.01	3.22	2.09	
		.0625	1.07	-.76	3.55	2.14	
		.125	2.16	.03	2.71	1.43	
		.25	2.89	.55	1.75	.84	
		.5	3.12	.77	.79	.40	
		1.0	2.69	.73	-.31	-.01	
		1.5	2.03	.56	-1.19	-.30	
	↓	.025	.03125	.12	-.70	1.17	1.07
		.0625	.73	-.67	2.60	1.66	
		.125	1.61	.00	2.58	1.37	
		.25	2.65	.54	1.80	.86	
		.5	3.18	.79	.85	.42	
		1.	2.78	.75	-.26	.00	
		2.	1.40	.38	-1.98	-.56	
		4.	-1.61	-.52	-5.12	-1.54	
	↓	.05	.0625	.22	-.72	1.18	1.12
		.125	1.45	-.13	2.16	1.24	
		.25	2.93	.54	1.99	.93	
		.5	3.45	.86	1.11	.51	
		1.	3.10	.84	-.08	.06	
		2.	.73	.47	-1.86	-.52	
		4.	-1.30	-.41	-5.12	-1.51	
		↓	.10	.0625	.05	-.92	.32
.125	.75		-.47	1.23	1.13		
.25	1.74		.42	2.18	1.09		
.5	4.21		1.05	1.96	.82		
1.	4.13		1.13	.74	.35		
2.	2.75		.77	-1.24	-.31		
4.	-.33		-.12	-4.65	-1.36		
↓	.15		.125	.65	-.58	.68	1.28
	.25	2.46	.29	2.11	1.23		
	.5	5.08	1.28	3.12	1.25		
	1.	6.13	1.71	1.85	.72		
	1.5	5.53	1.57	.63	.30		

TABLE A4. (Continued)

4 of 5

$\frac{D}{T}$	$\frac{d}{D}$	$\frac{s}{S}$	$\varphi = 0$		$\varphi = \pi/2$		
			$\sigma_{bx}$	$\sigma_{by}$	$\sigma_{bx}$	$\sigma_{by}$	
100	.01	.015625	.22	-.73	1.68	1.29	
		.03125	.88	-.67	2.94	1.81	
		.0625	2.10	.03	2.69	1.41	
		.125	3.02	.59	1.94	.90	
		.25	3.49	.89	1.20	.52	
		.5	3.47	.96	.48	.22	
		1.	2.87	.82	.47	.10	
		1.5	2.16	.62	-1.30	-.36	
		.025	.015625	-.01	-.60	.22	.66
			.03125	.16	-.71	1.14	1.09
	.0625		1.46	-.14	2.08	1.19	
	.125		2.89	.55	2.01	.92	
	.250		3.61	.91	1.36	.58	
	.5		3.65	1.01	.61	.27	
	1.		3.07	.88	-.38	-.07	
	2.		1.60	.46	-2.04	-.59	
	4.		-1.47	-.44	-5.13	-1.56	
	.05		.0625	.63	-.40	.97	.89
		.125	2.52	.41	1.80	.90	
		.25	4.00	1.02	1.83	.74	
		.5	4.29	1.19	1.12	.43	
1.		3.68	1.06	.02	.05		
2.		2.20	.63	-1.76	-.50		
4.		-.91	-.28	-4.01	-1.49		
.10	.0625	.35	-.65	.28	1.08		
	.125	1.63	.05	1.17	.91		
	.25	4.31	1.05	2.73	1.11		
	.5	6.55	1.84	.257	.93		
	1.	6.38	1.85	1.15	.43		
	2.	4.40	1.28	-.69	-.18		
4.	1.10	.26	-3.96	-1.22			

TABLE A4. (Continued)

5 of 5

$\frac{D}{T}$	$\frac{d}{D}$	$\frac{s}{S}$	$\varphi = 0$		$\varphi = \pi/2$	
			$\sigma_{bx}$	$\sigma_{by}$	$\sigma_{bx}$	$\sigma_{by}$
250	.001	1.	2.94	.87	-.57	-.16
	.005	.015625	1.11	-.48	2.75	1.64
		.03125	2.41	.24	2.47	1.23
		.0625	3.31	.74	1.83	.80
		.125	3.80	1.01	1.26	.51
		.25	3.91	1.11	.80	.30
		.5	3.66	1.07	.27	.11
		1.	2.96	.87	-.57	-.15
		1.5	2.21	.65	-1.37	-.40
	.01	.015625	.38	-.60	1.48	1.15
		.03125	1.90	.10	2.11	1.10
		.0625	3.17	.70	1.86	.81
		.125	3.81	1.01	1.34	.53
		.25	3.97	1.13	.86	.32
		.5	3.73	1.09	.30	.12
		1.	3.02	.89	-.55	-.15
		2.	1.49	.44	-2.18	-.62
	.025	.015625	.03	-.67	.21	.74
		.03125	.66	.27	.75	.70
		.0625	2.55	.50	1.50	.71
		.125	4.07	1.09	1.69	.65
		.25	4.50	1.28	1.27	.46
		.5	4.26	1.24	.66	.24
		1.	3.50	1.04	-.29	-.07
		2.	1.96	.51	-1.98	-.57
	.05	.0625	1.27	.03	.92	.69
		.125	3.61	.90	2.31	.90
.25		5.71	1.62	2.54	.86	
.5		5.94	1.73	1.76	.56	
1.		4.95	1.46	.58	.20	
2.		3.17	.94	-1.24	-.36	
.07	.0625	1.17	.01	.38	.55	
	.125	3.76	.94	1.85	.78	
	.25	7.52	2.16	3.22	1.08	
	.5	9.57	2.82	1.55	.52	
	1.0	8.19	2.43	.23	.10	
	1.5	6.59	1.96	-.36	-.09	
2.0	5.31	1.58	-1.03	-.29		

TABLE A5. MAXIMUM STRESS INTENSITY\* IN CYLINDER AT  $\phi = 0$   
AND  $\pi/2$  (1 of 6)

$\frac{D}{T}$	$\frac{d}{D}$	$\frac{s}{S}$	$\phi = 0$		$\phi = \pi/2$		
			$\bar{\sigma}$	Iden.	$\bar{\sigma}$	Iden.	
10	.01	1.	2.68	$\phi_i$	0.69	$\phi_i$	
	↓	.025	.0625	1.65	$\phi_i$	1.39	$\rho_o$
			.125	2.05	$\phi_i$	1.05	$\phi_i$
			.25	2.46	$\phi_i$	.77	$\phi_i$
			.5	2.61	$\phi_i$	.69	$\phi_i$
			1.0	2.66	$\phi_i$	.67	$\phi_i$
			1.5	2.67	$\phi_i$	.67	$\phi_i$
	↓	.05	.0625	1.58	$\phi_i$	1.64	$\rho_o$
			.125	1.84	$\phi_i$	1.27	$\phi_i$
			.25	2.32	$\phi_i$	.83	$\phi_i$
			.5	2.57	$\phi_i$	.68	$\phi_o$
			1.	2.64	$\phi_i$	.66	$\phi_o$
			2.	2.67	$\phi_i$	.65	0-0
			4.	2.68	$\phi_i$	.64	0-0
	↓	.10	.0625	1.41	$\phi_i$	1.56	$\rho_o$
			.125	1.77	$\phi_i$	1.55	$\rho_o$
			.25	2.24	$\phi_i$	.92	$\phi_i$
			.5	2.61	$\phi_i$	.93	$\phi_o$
			1.	2.71	$\phi_i$	.95	$\phi_o$
			2.	2.73	$\phi_i$	.91	0-0
			4.	2.74	$\phi_i$	.88	0-0
	↓	.25	.25	2.30	$\phi_i$	1.84	$\rho_o$
			.5	3.02	$\phi_i$	1.14	$\phi_o$
			1.	3.47	$\phi_i$	1.74	$\phi_o$
			2.	3.62	$\phi_i$	1.87	$\phi_o$
		4.	3.64	$\phi_i$	1.83	$\phi_o$	
↓	.35	.25	2.16	$\phi_i$	2.81	0-0	
		.5	2.91	$\phi_i$	1.78	$\rho_o$	
		1.	3.59	$\phi_i$	1.75	$\rho_o$	
		1.5	3.90	$\phi_i$	2.33	$\phi_o$	
		2.	4.07	$\phi_i$	2.56	$\phi_o$	

\* See footnote on Sheet 6.

TABLE A5. (Continued)

(2 of 6)

$\frac{D}{T}$	$\frac{d}{D}$	$\frac{s}{S}$	$\phi = 0$		$\phi = \pi/2$	
			$\bar{\sigma}$	Iden.	$\bar{\sigma}$	Iden.
25	.025	.0625	1.82	$\emptyset i$	1.12	$\emptyset i$
		.125	2.27	$\emptyset i$	.68	$\emptyset i$
		.25	2.47	$\emptyset i$	.63	$\emptyset o$
		.5	2.52	$\emptyset i$	.61	$\emptyset o$
		1.	2.55	$\emptyset i$	.60	$\emptyset o$
		1.5	2.55	$\emptyset i$	.59	$\emptyset o$
	.05	.0625	1.75	$\emptyset i$	1.50	$\rho o$
		.125	2.22	$\emptyset i$	1.37	$\emptyset o$
		.25	2.49	$\emptyset i$	.81	$\emptyset o$
		.5	2.55	$\emptyset i$	.82	$\emptyset o$
		1.	2.62	$\emptyset o$	.78	$\emptyset o$
		2.	2.67	$\emptyset o$	.76	$\emptyset o$
	.10	.125	2.18	$\emptyset i$	1.30	$\rho o$
		.25	2.64	$\emptyset i$	.98	$\emptyset o$
		.5	2.80	$\emptyset i$	1.22	$\emptyset o$
		1.	2.84	$\emptyset i$	1.23	$\emptyset o$
		2.	2.91	$\emptyset o$	1.20	$\emptyset o$
		4.	2.94	$\emptyset o$	1.18	$\emptyset o$
	.25	.125	1.80	$\emptyset o$	2.72	0-0
		.25	2.31	$\emptyset o$	1.99	0-0
		.5	3.02	$\emptyset o$	1.00	$\rho o$
		1.	3.99	$\emptyset o$	1.91	$\emptyset o$
		2.	4.42	$\emptyset o$	2.63	$\emptyset o$
		4.	4.28	$\emptyset o$	2.89	$\emptyset o$

TABLE A5. (Continued)  
(3 of 6)

$\frac{D}{T}$	$\frac{d}{D}$	$\frac{s}{S}$	$\phi = 0$		$\phi = \pi/2$	
			$\bar{\sigma}$	Iden.	$\bar{\sigma}$	Iden.
50	.005	1.	2.53	$\phi_0$	.53	$\phi_0$
	.01	.015625	1.56	i-i	1.57	$\rho_0$
		.03125	1.83	$\phi_i$	1.01	$\phi_i$
		.0625	2.27	$\phi_i$	.64	$\phi_i$
		.125	2.44	$\phi_i$	.57	$\phi_0$
		.25	2.49	$\phi_i$	.55	$\phi_0$
		.5	2.52	$\phi_i$	.54	$\phi_0$
		1.0	2.52	$\phi_i$	.54	$\phi_0$
		1.5	2.53	$\phi_i$	.53	$\phi_0$
	.025	.03125	1.70	$\phi_i$	1.23	$\phi_i$
		.0625	2.17	$\phi_i$	.83	i-i
		.125	2.43	$\phi_i$	.71	$\phi_0$
		.25	2.49	$\phi_i$	.71	$\phi_0$
		.5	2.54	$\phi_0$	.68	$\phi_0$
		1.	2.59	$\phi_0$	.66	$\phi_0$
		2.	2.61	$\phi_0$	.65	$\phi_0$
		4.	2.61	$\phi_0$	.64	$\phi_0$
	.05	.0625	2.04	$\phi_0$	1.22	$\rho_0$
		.125	2.50	$\phi_i$	.78	$\phi_0$
		.25	2.60	$\phi_i$	.96	$\phi_0$
		.5	2.63	$\phi_0$	.96	$\phi_0$
		1.	2.75	$\phi_0$	.93	$\phi_0$
		2.	2.79	$\phi_0$	.92	0-0
		4.	2.80	$\phi_0$	.91	0-0
	.10	.0625	1.89	$\phi_i$	1.64	$\rho_0$
		.125	2.56	i-i	1.12	$\rho_0$
		.25	2.86	i-i	.87	$\phi_0$
.5		2.97	$\phi_0$	1.26	$\phi_0$	
1.		3.16	$\phi_0$	1.43	$\phi_0$	
2.		3.17	$\phi_0$	1.50	$\phi_0$	
4.		3.19	$\phi_i$	1.54	$\phi_0$	
.15	.125	2.73	i-i	1.79	0-0	
	.25	3.04	i-i	1.00	$\rho_0$	
	.5	3.58	$\phi_0$	1.16	$\phi_0$	
	1.	4.05	$\phi_0$	1.78	$\phi_0$	
	1.5	4.08	$\phi_0$	1.98	$\phi_0$	



TABLE A5. (Continued)  
(4 of 6)

$\frac{D}{T}$	$\frac{d}{D}$	$\frac{s}{S}$	$\phi = 0$		$\phi = \pi/2$		
			$\bar{\sigma}$	Iden.	$\bar{\sigma}$	Iden.	
100	.01	.015625	1.71	$\phi_i$	1.41	$\rho_o$	
		.03125	2.17	$\phi_i$	.76	$\phi_i$	
		.0625	2.40	$\phi_i$	.62	$\phi_o$	
		.125	2.46	$\phi_i$	.61	$\phi_o$	
		.25	2.49	$\phi_i$	.58	$\phi_o$	
		.5	2.53	$\phi_o$	.57	$\phi_o$	
		1.	2.54	$\phi_o$	.56	$\phi_o$	
	v	1.5	2.55	$\phi_o$	.56	$\phi_o$	
	.025	.015625	.015625	1.43	$\phi_i$	1.44	$\rho_o$
			.03125	2.05	$\phi_i$	1.18	$\rho_o$
			.0625	2.45	$\phi_i$	.67	$\phi_o$
			.125	2.53	$\phi_i$	.82	$\phi_o$
			.250	2.53	$\phi_i$	.80	$\phi_o$
			.5	2.68	$\phi_o$	.77	$\phi_o$
			1.	2.67	$\phi_o$	.75	$\phi_o$
			2.	2.69	$\phi_o$	.74	$\phi_o$
	v	4.	2.69	$\phi_o$	.74	$\phi_o$	
	.05	.0625	.0625	2.34	i-i	.96	i-i
			.125	2.68	i-i	.76	$\phi_o$
			.25	2.69	$\phi_o$	1.00	$\phi_o$
			.5	2.91	$\phi_o$	1.09	$\phi_o$
1.			2.96	$\phi_o$	1.13	$\phi_o$	
2.			2.96	$\phi_o$	1.15	$\phi_o$	
v	4.	2.96	$\phi_o$	1.16	$\phi_o$		
.10	.0625	.0625	2.58	i-i	1.60	0-0	
		.125	3.06	i-i	1.01	$\rho_o$	
		.25	3.31	$\phi_o$	.65	$\phi_o$	
		.5	3.94	$\phi_o$	1.29	$\phi_o$	
		1.	4.12	$\phi_o$	1.65	$\phi_o$	
		2.	3.93	$\phi_o$	1.92	0-0	
v	4.	3.79	$\phi_i$	2.14	0-0		

TABLE A5. (Continued)

(5 of 6)

$\frac{D}{T}$	$\frac{d}{D}$	$\frac{s}{S}$	$\phi = 0$		$\phi = \pi/2$	
			$\bar{\sigma}$	Iden.	$\bar{\sigma}$	Iden.
250	.001	1.	2.51	$\phi_i$	.51	$\phi_i$
	.005	.015625	2.26	$\phi_i$	.73	i-i
		.03125	2.42	$\phi_i$	.61	$\phi_o$
		.0625	2.46	$\phi_i$	.59	$\phi_o$
		.125	2.48	$\phi_i$	.56	$\phi_o$
		.25	2.52	$\phi_o$	.55	$\phi_o$
		.5	2.53	$\phi_o$	.54	$\phi_o$
		1.	2.53	$\phi_o$	.54	0-0
	.01	1.5	2.53	$\phi_o$	.54	0-0
		.015625	2.21	$\phi_i$	1.11	i-i
		.03125	2.49	i-i	.65	$\phi_o$
		.0625	2.50	$\phi_i$	.71	$\phi_o$
		.125	2.49	$\phi_i$	.67	$\phi_o$
		.25	2.55	$\phi_i$	.64	$\phi_o$
		.5	2.58	$\phi_i$	.62	$\phi_o$
	1.	2.59	$\phi_i$	.62	0-0	
	.025	2.	2.60	$\phi_i$	.62	$\phi_o$
		4.	2.60	$\phi_i$	.62	0-0
		.015625	1.71	$\phi_i$	1.07	$\rho_o$
		.03125	2.35	i-i	.98	i-i
		.0625	2.65	i-i	.64	$\phi_o$
		.125	2.60	$\phi_o$	.83	$\phi_o$
		.25	2.80	$\phi_o$	.90	$\phi_o$
	.5	2.85	$\phi_o$	.94	$\phi_o$	
	1.	2.86	$\phi_o$	.95	0-0	
	.05	2.	2.85	$\phi_o$	.97	0-0
4.		2.85	$\phi_o$	.97	0-0	
.0625		3.05	i-i	.82	$\rho_o$	
.125		3.05	$\phi_o$	.49	$\rho_o$	
.25		3.48	$\phi_o$	.93	$\rho_o$	
.5		3.63	$\phi_o$	1.17	$\rho_o$	
1.		3.52	$\phi_o$	1.37	$\rho_o$	
2.	3.35	$\phi_o$	1.55	$\rho_o$		
.07	4.	3.38	$\phi_i$	1.66	$\rho_o$	
	.0625	3.26	i-i	.88	0-0	
	.125	3.22	$\phi_o$	.72	$\rho_o$	
	.25	4.03	$\phi_o$	.94	$\phi_o$	
	.5	4.60	$\phi_o$	1.41	$\phi_o$	
	1.0	4.65	$\phi_o$	1.67	$\phi_o$	
	1.5	4.49	$\phi_o$	1.86	$\phi_o$	
2.0	4.34	$\phi_o$	2.01	$\phi_o$		

## TABLE A5. (Continued)

(6 of 6)

 $\bar{\sigma}$  = stress intensity

$$\bar{\sigma} = \text{maximum of: } \left| \sigma_{\phi i} - p \right|, \left| \sigma_{\rho i} - p \right|, \left| \sigma_{\phi i} - \sigma_{\rho i} \right| \\ \left| \sigma_{\phi o} \right|, \left| \sigma_{\rho o} \right|, \left| \sigma_{\phi o} - \sigma_{\rho o} \right|$$

$p$  = radial stress due to internal pressure,  $p = -2/(D/T)$

Identification:

$$\phi i = \left| \sigma_{\phi i} - p \right|$$

$$\phi o = \left| \sigma_{\phi o} \right|$$

$$\rho o = \left| \sigma_{\rho o} \right|$$

$$o-o = \left| \sigma_{\phi o} - \sigma_{\rho o} \right|$$

$$i-i = \left| \sigma_{\phi i} - \sigma_{\rho i} \right|$$

\*  
 TABLE A6. MAXIMUM STRESS INTENSITY IN NOZZLE  
 AT  $\phi = 0$  AND  $\pi/2$   
 (1 of 6)

$\frac{D}{T}$	$\frac{d}{D}$	$\frac{s}{S}$	$\phi = 0$		$\phi = \pi/2$		
			$\bar{\sigma}$	Iden.	$\bar{\sigma}$	Iden.	
10	.01	1.	3.81	i-i	1.62	xo	
	↓	.025	.0625	2.50	i-i	2.31	xo
		.125	3.48	i-i	4.19	xo	
		.25	4.10	i-i	4.31	xo	
		.5	4.20	i-i	3.09	xo	
		1.0	3.81	i-i	1.64	xo	
		1.5	3.26	i-i	1.57	xi	
	↓	.05	.0625	1.81	i-i	1.14	yo
		.125	2.89	i-i	2.88	xo	
		.25	3.81	i-i	3.89	xo	
		.5	4.14	i-i	3.09	xo	
		1.	3.86	i-i	1.69	xo	
		2.	2.76	yo	2.60	xi	
		4.	3.77	yo	7.02	xi	
	↓	.10	.0625	1.26	i-i	0.75	yo
		.125	2.23	i-i	1.59	yo	
		.25	3.35	i-i	3.07	xo	
		.5	4.11	i-i	3.10	xo	
		1.	4.06	i-i	1.88	xo	
		2.	3.01	i-i	2.51	xi	
		4.	3.80	yo	6.97	xi	
	↓	.25	.25	2.56	i-i	2.42	yo
		.5	3.78	i-i	2.94	xo	
		1.	4.82	i-i	2.88	xo	
		2.	4.36	i-i	1.39	yo	
		4.	4.08	yo	6.08	xi	
	↓	.35	.25	2.40	i-i	3.29	yo
		.5	3.47	i-i	3.88	yo	
1.		5.11	i-i	3.92	xo		
1.5		5.66	i-i	3.38	xo		
2.		5.58	i-i	2.50	xo		

\* See footnote on Sheet 6.

TABLE A6. (Continued)  
(2 of 6)

$\frac{D}{T}$	$\frac{d}{D}$	$\frac{s}{S}$	$\phi = 0$		$\phi = \pi/2$	
			$\bar{\sigma}$	Iden.	$\bar{\sigma}$	Iden.
25	.025	.0625	3.00	i-i	2.98	xo
		.125	3.99	i-i	3.69	xo
		.25	4.49	i-i	2.96	xo
		.5	4.57	i-i	1.90	xo
		1.	4.12	i-i	.89	yo
		1.5	3.49	i-i	1.94	xi
	.05	.0625	2.27	i-i	1.67	yo
		.125	3.41	i-i	2.89	xo
		.25	4.32	i-i	2.90	xo
		.5	4.63	i-i	1.99	xo
		1.	4.28	i-i	.93	yo
		2.	3.17	yo	2.91	xi
	.10	.125	2.68	i-i	1.87	yo
		.25	3.96	i-i	2.54	xo
		.5	4.88	i-i	2.28	xo
		1.	4.82	i-i	1.16	xo
		2.	3.63	i-i	2.54	xi
	.25	.125	2.02	i-i	2.98	yo
		.25	2.85	i-i	3.43	yo
		.5	5.80	i-i	3.37	yo
		1.	7.08	i-i	3.44	xo
2.		7.32	xo	1.21	xo	
4.		5.62	yo	4.67	xi	

TABLE A6. (Continued)  
(3 of 6)

$\frac{D}{T}$	$\frac{d}{D}$	$\frac{s}{S}$	$\phi = 0$		$\phi = \pi/2$	
			$\bar{\sigma}$	Iden.	$\bar{\sigma}$	Iden.
50	.005	1.	4.17	i-i	.95	xi
	.01	.015625	2.12	i-i	1.55	xo
		.03125	3.23	i-i	3.43	xo
		.0625	4.15	i-i	3.86	xo
		.125	5.07	i-i	3.07	xo
		.25	4.88	i-i	2.12	xo
		.5	4.78	i-i	1.22	xo
		1.0	4.19	i-i	.95	xi
	1.5	3.51	i-i	2.06	xi	
	.025	.03125	2.24	i-i	1.66	yo
		.0625	3.31	i-i	2.84	xo
		.125	4.34	i-i	2.89	xo
		.25	4.82	i-i	2.16	xo
		.5	4.84	i-i	1.27	xo
		1.	4.29	i-i	.69	yo
		2.	3.20	yo	3.04	xi
	4.	3.65	yi	7.16	xi	
	.05	.0625	2.56	i-i	1.74	yo
		.125	3.78	i-i	2.34	xo
		.25	4.80	i-i	2.24	xo
		.5	5.07	i-i	1.47	xo
		1.	4.60	i-i	.74	yo
		2.	3.44	yo	2.90	xi
	4.	3.70	yi	7.14	xi	
	.10	.0625	2.00	i-i	2.16	yo
.125		2.79	i-i	2.16	yo	
.25		4.46	i-i	2.24	xo	
.5		5.73	i-i	2.09	xo	
1.		5.60	i-i	1.08	xo	
2.		4.31	i-i	2.07	xi	
4.	3.94	yi	6.49	xi		
.15	.125	2.38	i-i	2.91	yo	
	.25	3.83	i-i	2.84	yo	
	.5	6.23	i-i	3.14	xo	
	1.	7.40	i-i	1.96	xo	
	1.5	6.89	i-i	.93	xo	

TABLE A6. (Continued)

(4 of 6)

$\frac{D}{T}$	$\frac{d}{D}$	$\frac{s}{S}$	$\phi = 0$		$\phi = \pi/2$	
			$\bar{\sigma}$	Iden.	$\bar{\sigma}$	Iden.
100	.01	.015625	2.45	i-i	1.87	yo
		.03125	3.60	i-i	3.19	xo
		.0625	4.47	i-i	2.98	xo
		.125	4.96	i-i	2.24	xo
		.25	5.11	i-i	1.49	xo
		.5	4.90	i-i	.83	yo
		1.	4.25	i-i	1.04	xi
	1.5	3.54	i-i	2.09	xi	
	.025	.015625	1.66	i-i	1.17	yo
		.03125	2.48	i-i	1.70	yo
		.0625	3.66	i-i	2.23	xo
		.125	4.72	i-i	2.20	xo
		.250	5.18	i-i	1.60	xo
		.5	5.07	i-i	.93	xo
		1.	4.46	i-i	.92	xo
		2.	3.35	yo	3.06	xo
	4.	3.64	yi	7.13	xi	
	.05	.0625	2.73	i-i	1.61	yo
		.125	4.27	i-i	1.83	xo
.25		5.46	i-i	1.90	xo	
.5		5.64	i-i	1.30	xo	
1.		5.04	i-i	.66	yo	
2.		3.81	yo	2.68	xi	
4.	3.76	yi	6.94	xi		
.10	.0625	1.97	i-i	2.53	yo	
	.125	2.96	i-i	2.52	yo	
	.25	5.26	i-i	2.75	xo	
	.5	7.55	i-i	2.64	xi	
	1.	7.56	i-i	1.24	xo	
	2.	5.93	xo	1.18	xi	
	4.	4.75	yo	5.47	xi	

TABLE A6. (Continued)  
(5 of 6)

$\frac{D}{T}$	$\frac{d}{D}$	$\frac{s}{S}$	$\phi = 0$		$\phi = \pi/2$		
			$\bar{\sigma}$	Iden.	$\bar{\sigma}$	Iden.	
250	.001	1.	4.24	i-i	1.10	xi	
	↓	.005	.015625	3.68	i-i	2.97	xo
		.03125	4.58	i-i	2.73	xo	
		.0625	5.10	i-i	2.07	xo	
		.125	5.31	i-i	1.47	xo	
		.25	5.26	i-i	1.01	xo	
		.5	4.96	i-i	.70	yo	
		1.	4.26	i-i	1.09	xi	
		1.5	3.55	i-i	2.13	xi	
	↓	.01	.015625	2.73	i-i	1.75	yo
		.03125	3.96	i-i	2.25	xo	
		.0625	4.89	i-i	2.03	xo	
		.125	5.30	i-i	1.51	xo	
		.25	5.31	i-i	1.05	xo	
		.5	5.02	i-i	.71	yo	
		1.	4.33	i-i	1.11	yi	
		2.	3.27	yo	3.18	xi	
	↓	.025	.015625	1.91	i-i	1.44	yo
		.03125	2.68	i-i	1.37	yo	
		.0625	4.21	i-i	1.50	xo	
		.125	5.42	i-i	1.71	xo	
		.25	5.75	i-i	1.36	xo	
		.5	5.50	i-i	.84	xo	
		1.	4.80	i-i	.68	yi	
		2.	3.62	yo	2.92	xi	
	↓	.05	.0625	2.59	i-i	2.24	yo
		.125	4.58	i-i	2.82	i-i	
.25		6.60	i-i	2.56	i-i		
.5		7.01	i-i	1.70	xo		
1.		6.17	i-i	.74	xo		
↓	2.	4.64	yo	1.89	xi		
	4.	4.02	yi	6.30	xi		
↓	.07	.0625	2.34	i-i	2.16	yo	
	.125	4.44	i-i	2.41	yo		
	.25	7.97	i-i	3.27	xi		
	.5	10.40	i-i	1.63	xi		
	1.0	9.25	i-i	.54	yi		
	1.5	7.76	i-i	.49	xi		
	2.0	6.58	i-i	1.36	xi		



TABLE A6. (Continued)

6 of 6

 $\bar{\sigma}$  = stress intensity
$$\bar{\sigma} = \text{maximum of: } \left| \sigma_{xi} - p \right|, \left| \sigma_{yi} - p \right|, \left| \sigma_{xi} - \sigma_{yi} \right|$$

$$\left| \sigma_{xo} \right|, \left| \sigma_{yo} \right|, \left| \sigma_{xo} - \sigma_{yo} \right|$$

$p$  = radial stress due to internal pressure;  $p = -2/(D/T)$

## Identification:

$$x_o = \left| \sigma_{x_o} \right|$$

$$x_i = \left| \sigma_{x_i} - p \right|$$

$$y_o = \left| \sigma_{y_o} \right|$$

$$y_i = \left| \sigma_{y_i} - p \right|$$

$$i-i = \left| \sigma_{x_i} - \sigma_{y_i} \right|$$

TABLE A7. MAXIMUM SURFACE STRESSES IN CYLINDER AND NOZZLE.\*

(1 of 6)

$\frac{D}{T}$	$\frac{d}{D}$	$\frac{s}{S}$	Cylinder		Nozzle			
			$\sigma_m$	Iden.	$\sigma_m$	Iden.		
10	.01	1.	2.49	$\emptyset_o$	2.61	yo		
	↓	.025	.0625	1.45	$\emptyset_i$	--	--	
		.125		1.85	$\emptyset_i$	4.19	xo †	
		.25		2.27	$\emptyset_o$	4.31	xo †	
		.5		2.44	$\emptyset_o$	3.09	xo †	
		1.0		2.50	$\emptyset_o$	2.60	yo	
		1.5		2.52	$\emptyset_o$	2.73	yo	
	↓	.05	.0625	1.38	$\emptyset_i$	1.39	yi	
		.125		1.64	$\emptyset_i$	2.88	xo †	
		.25		2.12	$\emptyset_i$	3.89	xo †	
		.5		2.39	$\emptyset_o$	3.09	xo †	
		1.		2.52	$\emptyset_o$	2.60	yo	
		2.		2.58	$\emptyset_o$	2.76	yo	
	↓	↓	4.	2.59	$\emptyset_o$	7.02	xi †	
			.10	.0625	1.21	$\emptyset_i$	1.15	yi
			.125		1.57	$\emptyset_i$	1.91	yi
			.25		2.04	$\emptyset_i$	3.07	xo †
			.5		2.41	$\emptyset_i$	3.10	xo †
			1.		2.56	$\emptyset_o$	2.67	yo
	↓	↓	2.	2.70	$\emptyset_o$	2.91	yo	
			4.	2.74	$\emptyset_o$	6.97	xi †	
			.25	.25	2.10	$\emptyset_o$	2.42	yo †
			.5		2.82	$\emptyset_o$	2.94	xo †
			1.		3.27	$\emptyset_o$	3.08	yo
	↓	↓	2.	3.42	$\emptyset_o$	3.75	yo	
			4.	3.44	$\emptyset_o$	6.08	xi †	
			.35	.25	2.45	$\rho_o$ †	3.29	yo †
.5				2.72	$\emptyset_i$	2.76	xo †	
↓	↓	1.	3.39	$\emptyset_i$	3.91	xo †		
		1.5	3.70	$\emptyset_i$	4.29	xo		
		2.	3.87	$\emptyset_i$	4.57	yo		

\* See footnote on Sheet 6.

TABLE A7. (Continued)

(2 of 6)

$\frac{D}{T}$	$\frac{d}{D}$	$\frac{s}{S}$	Cylinder		Nozzle	
			$\sigma_m$	Iden.	$\sigma_m$	Iden.
25	.025	.0625	1.74	$\emptyset_i$	2.98	xo <sup>†</sup>
		.125	2.19	$\emptyset_i$	3.69	xo <sup>†</sup>
		.25	2.39	$\emptyset_i$	2.96	xo <sup>†</sup>
		.5	2.49	$\emptyset_o$	2.89	yo
		1.	2.54	$\emptyset_o$	3.15	yo
		1.5	2.56	$\emptyset_o$	3.14	yo
	.05	.0625	1.67	$\emptyset_i$	2.00	yi
		.125	2.14	$\emptyset_i$	2.89	xo <sup>†</sup>
		.25	2.41	$\emptyset_i$	2.90	xo <sup>†</sup>
		.5	2.49	$\emptyset_o$	2.92	yo
		1.	2.62	$\emptyset_o$	3.23	yo
		2.	2.67	$\emptyset_o$	3.17	yo
		4.	2.69	$\emptyset_o$	7.13	xo <sup>†</sup>
	.10	.125	2.10	$\emptyset_i$	2.34	yi
		.25	2.56	$\emptyset_i$	2.54	xo <sup>†</sup>
		.5	2.72	$\emptyset_i$	3.11	yo
		1.	2.79	$\emptyset_o$	3.61	yo
		2.	2.91	$\emptyset_o$	3.60	yo
		4.	2.94	$\emptyset_o$	6.89	xi
	.25	.125	2.23	$\rho_o$ <sup>†</sup>	2.98	yo <sup>†</sup>
		.25	2.31	$\emptyset_o$	3.43	yo <sup>†</sup>
		.5	3.02	$\emptyset_o$	3.76	xo
		1.	4.00	$\emptyset_o$	6.65	xo
		2.	4.42	$\emptyset_o$	7.32	xo
		4.	4.28	$\emptyset_o$	5.62	yo

TABLE A7. (Continued)  
(3 of 6)

$\frac{D}{T}$	$\frac{d}{D}$	$\frac{s}{S}$	Cylinder		Nozzle		
			$\sigma_m$	Iden.	$\sigma_m$	Iden.	
50	.005	1.	2.51	∅o	3.34	yo	
	↓	.01	.015625	1.57	∅o <sup>†</sup>	1.60	yi
		.03125	1.79	∅i	3.44	xo <sup>†</sup>	
		.0625	2.23	∅i	3.86	xo <sup>†</sup>	
		.125	2.40	∅i	3.07	xo <sup>†</sup>	
		.25	2.46	∅o	-3.02	xi	
		.5	2.51	∅o	3.28	yo	
		1.0	2.52	∅o	3.35	yo	
		1.5	2.52	∅o	3.26	yo	
	↓	.025	.03125	1.66	∅i	1.98	yi
		.0625	2.13	∅i	2.84	xo <sup>†</sup>	
		.125	2.39	∅i	2.89	xo <sup>†</sup>	
		.25	2.45	∅i	-2.99	xi	
		.5	2.54	∅o	3.31	yo	
		1.	2.59	∅o	3.40	yo	
		2.	2.61	∅o	3.20	yo	
		4.	2.61	∅o	7.16	xo <sup>†</sup>	
	↓	.05	.0625	2.04	∅o	2.26	yi
		.125	2.46	∅i	2.34	xo <sup>†</sup>	
		.25	2.56	∅i	2.95	yo	
		.5	2.63	∅o	3.59	xo	
		1.	2.75	∅o	3.62	yo	
		2.	2.79	∅o	3.45	yo	
		4.	2.80	∅o	7.14	xi <sup>†</sup>	
	↓	.10	.0625	1.85	∅i	2.16	yo <sup>†</sup>
		.125	2.36	∅i	2.17	yo <sup>†</sup>	
		.25	2.64	∅i	2.91	xo	
		.5	2.97	∅o	4.57	xo	
		1.	3.16	∅o	4.79	xo	
		2.	3.17	∅o	4.27	yo	
	↓	.15	.125	2.34	∅i	1.84	yi
		.25	2.83	∅o	2.84	yo <sup>†</sup>	
		.5	3.58	∅o	5.53	xo	
		1.	4.05	∅o	7.01	xo	
		1.5	4.08	∅o	6.76	xo	

TABLE A7. (Continued)

(4 of 6)

$\frac{D}{T}$	$\frac{d}{D}$	$\frac{s}{S}$	Cylinder		Nozzle		
			$\sigma_m$	Iden.	$\sigma_m$	Iden.	
100	.01	.015625	1.69	$\emptyset i$	2.07	yi	
		.03125	2.15	$\emptyset i$	3.19	xo †	
		.0625	2.38	$\emptyset i$	2.98	xo †	
		.125	2.44	$\emptyset i$	-3.20	xi	
		.25	2.49	$\emptyset o$	-3.54	xi	
		.5	2.53	$\emptyset o$	3.61	xo	
		1.	2.54	$\emptyset o$	3.46	yo	
		1.5	2.55	$\emptyset o$	3.35	yo	
	.025	.015625	1.44	po †	1.62	yi	
		.03125	2.03	$\emptyset i$	2.22	yi	
		.0625	2.43	$\emptyset i$	2.23	xo †	
		.125	2.51	$\emptyset i$	-2.96	xi	
		.250	2.51	$\emptyset o$	3.61	xo	
		.5	2.68	$\emptyset o$	3.83	xo	
		1.	2.67	$\emptyset o$	3.60	yo	
		2.	2.69	$\emptyset o$	3.35	yo	
	.05	.0625	1.	2.69	$\emptyset o$	7.13	xi †
			2.	2.69	$\emptyset o$	7.13	xi †
			4.	2.69	$\emptyset o$	7.13	xi †
			1.	2.24	$\emptyset i$	2.11	yi
2.			2.49	$\emptyset i$	2.65	yo	
4.			2.69	$\emptyset o$	4.17	xo	
.10	.0625	1.	2.91	$\emptyset o$	4.61	xo	
		2.	2.96	$\emptyset o$	4.26	xo	
		4.	2.96	$\emptyset o$	6.94	xi †	
		1.	2.32	$\emptyset o$	2.53	yo †	
		2.	2.72	$\emptyset o$	2.52	yo †	
		4.	3.31	$\emptyset o$	4.56	xo	
		1.	3.94	$\emptyset o$	7.05	xo	
		2.	4.12	$\emptyset o$	7.29	xo	
.10	.0625	2.	3.93	$\emptyset o$	5.93	xo	
		4.	3.77	$\emptyset i$	5.47	xi †	

TABLE A7. (Continued)

(5 of 6)

$\frac{D}{T}$	$\frac{d}{D}$	$\frac{s}{S}$	Cylinder		Nozzle	
			$\sigma_m$	Iden.	$\sigma_m$	Iden.
250	.001	1.	2.50	$\emptyset o$	3.51	yo
	.005	.015625	2.26	$\emptyset i$	2.98	xo †
		.03125	2.42	$\emptyset i$	2.73	xo †
		.0625	2.46	$\emptyset i$	-3.49	xi
		.125	2.48	$\emptyset o$	-3.88	xi
		.25	2.52	$\emptyset o$	3.95	xo
		.5	2.53	$\emptyset o$	3.87	xo
		1.	2.53	$\emptyset o$	3.52	yo
		1.5	2.53	$\emptyset o$	3.38	yo
	.01	.015625	2.21	$\emptyset i$	2.25	yi †
		.03125	2.48	$\emptyset i$	2.25	xo †
		.0625	2.50	$\emptyset i$	-3.28	xi
		.125	2.48	$\emptyset i$	-3.86	xi
		.25	2.55	$\emptyset o$	4.03	xo
		.5	2.59	$\emptyset o$	3.95	xo
		1.	2.59	$\emptyset o$	3.57	yo
		2.	2.60	$\emptyset o$	3.27	yo †
	.025	.015625	1.71	$\emptyset i$	1.87	yi
		.03125	2.22	$\emptyset i$	2.03	yi
		.0625	2.44	$\emptyset i$	2.71	yo
		.125	2.60	$\emptyset o$	4.17	xo
		.25	2.80	$\emptyset o$	4.68	xo
		.5	2.86	$\emptyset o$	4.58	xo
		1.	2.86	$\emptyset o$	4.07	xo
		2.	2.85	$\emptyset o$	3.62	yo †
	.05	.0625	2.65	$\emptyset o$	2.24	yo †
		.125	3.05	$\emptyset o$	3.76	xo
		.25	3.48	$\emptyset o$	5.98	xo
.5		3.63	$\emptyset o$	6.44	xo	
1.		3.52	$\emptyset o$	5.78	xo	
2.		3.35	$\emptyset o$	4.64	yo †	
.07	.0625	2.78	$\emptyset o$	2.16	yo †	
	.125	3.22	$\emptyset o$	3.90	xo	
	.25	4.03	$\emptyset o$	7.80	xo	
	.5	4.60	$\emptyset o$	10.11	xo	
	1.0	4.65	$\emptyset o$	9.19	xo	
	1.5	4.49	$\emptyset o$	7.96	xo	
	2.0	4.34	$\emptyset o$	6.99	xo	

## TABLE A7. (Continued)

(6 of 6)

$\sigma_m$  = maximum surface stress.

Maximum surface stress is at  $\phi = 0$ , except where an  $f$  is shown,  
for which maximum surface stress is at  $\phi = \pi/2$ .

## Identification:

$\phi_o$  = stress in  $\phi$ -direction, outside surface

$\phi_i$  = stress in  $\phi$ -direction, inside surface

$\rho_o$  = stress in  $\rho$ -direction, outside surface

$\rho_i$  = stress in  $\rho$ -direction, inside surface

$x_o$  = stress in x-direction, outside surface

$x_i$  = stress in x-direction, inside surface

$y_o$  = stress in y-direction, outside surface

$y_i$  = stress in y-direction, inside surface.

PHASE REPORT No. 6

on

FLEXIBILITY OF NOZZLES IN CYLINDRICAL SHELLS

December 22, 1967

to

UNITED STATES ATOMIC ENERGY COMMISSION

E. C. Rodabaugh and T. J. Atterbury

Contract No. W-7405-eng-92  
Task 16

BATTELLE MEMORIAL INSTITUTE  
Columbus Laboratories  
505 King Avenue  
Columbus, Ohio 43201

Section 6



TABLE OF CONTENTS

	<u>Page</u>
INTRODUCTION . . . . .	1
SUMMARY . . . . .	3
NOMENCLATURE. . . . .	4
DEFINITION OF FLEXIBILITY FACTOR . . . . .	5
TEST DATA . . . . .	7
THEORY. . . . .	10
COMPARISON OF TEST DATA WITH BIJLAARD'S THEORY . . . . .	12
EMPIRICAL EQUATION. . . . .	15
SIGNIFICANCE OF FLEXIBILITY OF NOZZLES. . . . .	25
REFERENCES . . . . .	28

## FLEXIBILITY OF NOZZLES IN CYLINDRICAL SHELLS

### INTRODUCTION

Nozzles in pressure vessels are quite often attached to a piping system; the loads applied to the nozzle by that piping system depend upon the flexibility of the piping system. At present it is customary to assume that the nozzle in the vessel forms a rigid anchor to the end of the piping system. This assumption is conservative but, in some cases, it may be highly overconservative and lead to unnecessary cost in the piping system. This point arises because the nozzle in a pressure vessel is not a rigid anchor; its flexibility may contribute significantly to the overall flexibility of the piping system, thereby reducing the loads in the piping system arising from thermal expansion of the piping or movement of end connections to the piping system.

Phase Report No. 3, "Flexibility of Nozzles in Spherical Shells", gives a definition of flexibility factors for nozzles in spherical shells for either moment or thrust loads. Factors are calculated and results given in graphical form for a range of dimensional parameters. The factors are based on Bijlaard's<sup>(1)\*</sup> theoretical analysis of a nozzle in a spherical shell. The present Phase Report is intended to provide analogous data for nozzles in cylindrical shells. However, at this time no theoretical analysis is available for nozzles in cylindrical shell with moment or

---

\* References are listed on page 28.

thrust loads applied to the nozzle. In this report, an empirical equation is derived from test data, guided by Bijlaard's<sup>(2)</sup> analysis for distributed load on the surface of a cylinder. Because test data is almost all limited to moment loads applied to the nozzle, only such loads are considered herein.

SUMMARY

Available test data on the flexibility of nozzles in cylindrical shells are presented in the form of flexibility factors. Test data are almost entirely limited to in-plane or out-of-plane bending moments applied to the nozzle. For nozzles with small  $d/D$  ratios, the flexibility under such loading is probably the only significant flexibility in-so-far as the contribution of the nozzle to the attached piping system.

An empirical equation is given which follows the same general trends as given by Bijlaard's theory for distributed loads on a cylinder shell but gives lower flexibility. The empirical equation for the flexibility factor of nozzles in cylinders gives flexibility factors which are:

- (a) For in-plane bending, lower than for a nozzle in a sphere,
- (b) For out-of-plane bending, higher than for a nozzle in a sphere.

The significance of the flexibility of nozzles in cylinders is relatively small for thick-wall cylinders but can become large for thin-wall cylinder. For "tight" piping system, examples are cited in which, if the nozzle flexibility is ignored, moments at the nozzle can be over-estimated by factors of 10 to 30.

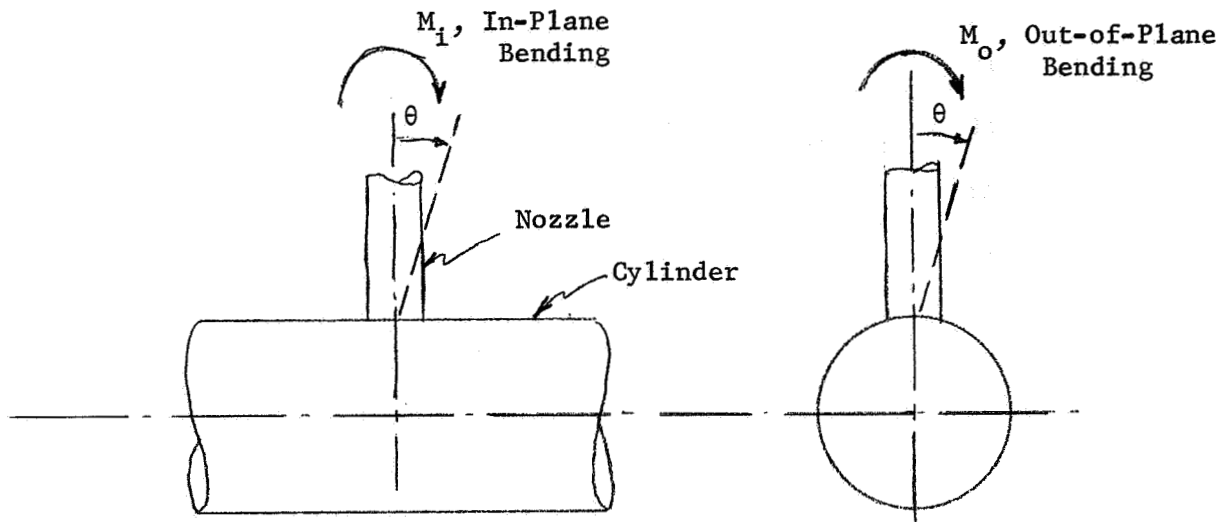
NOMENCLATURE

FIGURE 1. NOMENCLATURE ILLUSTRATION

$D$  = mean diameter of cylinder, in.

$T$  = wall thickness of cylinder, in.

$d$  = mean diameter of nozzle, in.

$t$  = wall thickness of nozzle, in.

$k$  = flexibility factor  $\theta / (Md/EI_n)$

$\theta$  = rotation in direction of applied moment, radians

$M$  = moment applied to nozzle, in-lb

$E$  = modulus of elasticity, psi

$I_n$  = moment of inertia of nozzle =  $\pi d^3 t / 8$ , in<sup>4</sup>.

Other symbols defined in the text where used

DEFINITION OF FLEXIBILITY FACTOR

For small nozzles ( $\frac{d}{D} < 1/3$ ) in pressure vessels, application of a moment to the nozzle produces local displacements in the shell and nozzle near the shell-nozzle juncture. These local displacements result in a rotation of the nozzle axis with respect to the shell surface. For small nozzles, the displacements of the shell remote from the nozzle can be disregarded since their contribution to the movement of the nozzle will be small. Accordingly, it is convenient to define an angle  $\theta$  as:

$\theta$  = rotation of axis of nozzle (in the direction of the applied moment) with respect to the surface of the shell, radians

and a flexibility factor  $k$  as

$$k = \frac{\theta}{Md/EI_n} \quad (1)$$

where

$M$  = moment applied to nozzle, in-lb

$d$  = mean diameter of nozzles, inches

$E$  = modulus of elasticity, psi

$I_n$  = moment of inertia of nozzle cross section, in<sup>4</sup>.

The quantity  $(Md/EI_n)$  in Equation (1) is simply the rotation of a nozzle of one-diameter length loaded by a moment  $M$ . The utility of a flexibility factor as defined by Equation (1) arises from two considerations:

- (1) The value of  $k$ , for a given nozzle and piping system, immediately indicates whether the flexibility of the nozzle is significant. For example, if  $k = 2$  and the length

of the pipe attached to the nozzle is  $50d$ , then the local flexibility of the nozzle will have only a small effect on the flexibility of the piping system. If, on the other hand,  $k = 10$ , and the length of pipe attached to the nozzle is  $2d$ , then the local flexibility of the nozzle may have a very significant effect on the flexibility of the piping system.

- (2) The use of a flexibility factor as defined by Equation (1) is analogous to the flexibility factor for elbows or curved pipe presently given in the ASA Code for Pressure Piping and generally used in piping flexibility analyses.

While the flexibility factor for a nozzle in a cylinder, as defined by Equation (1) is analogous to the flexibility factor of an elbow, it should be noted that the flexibility of the nozzle is inherently a lumped parameter. The flexibility of an elbow or curved pipe is inherently a distributed parameter associated with a unit length and, for accurate results, an integration over the elbow or curved pipe length must be carried out. The rotation  $\theta$ , as defined and used herein, arises from local deformations at the nozzle-cylinder juncture. For small values of  $d/D$ ,  $\theta$  is independent of the reaction loads on the cylinder, provided only that those reaction loads are applied at a sufficient distance from the nozzle-cylinder juncture such that the local displacements at the juncture are not influenced by the reaction loads.

TEST DATA

Available data on displacements of nozzles in cylinders are relatively limited. Available data are summarized in Table 1. All of the data were obtained as incidental measurements taken as part of other test data; as a preliminary to fatigue tests in Reference (3) and as a part of obtaining measured strains in the other references.

All of the references except (7) and (9) provide measurements of the displacement of the branch pipe as a function of the load applied to the nozzle. The displacement zero point for the measurements is not clearly indicated in all test data, however, in all cases it was assumed that zero displacement was at an anchor of the cylinder.

The value of  $\theta$ , where displacements of the nozzle are given, was obtained by subtracting out that part of the displacement attributable to nominal displacements of the cylinder and nozzle between the anchor point (or points) and point of nozzle displacement measurement. Where the  $d/D$  is small (e.g.  $< 0.5$ ) and  $t$  is not greater than  $T$ , the contribution of nominal displacements of the cylinder to the measured displacements of the nozzle are small because the rotation (torsional or bending) is inversely proportional to the cylinder radius cubed.

It should be noted that  $\theta$  represents the rotation of the nozzle due to local displacements of the cylindrical shell and nozzle and hence  $\theta$  is not dependent upon the cylinder length or nozzle length used in the test models; provided only that those lengths were sufficient to avoid end effects from anchors or load applicative points on the behavior of the nozzle-cylinder junction region.



TABLE 1. SUMMARY OF DIMENSIONAL RATIOS & TEST DATA, FLEXIBILITY FACTORS OF NOZZLES

Ref. No.	Nom. Size	$\frac{D}{T}$	$\frac{d}{D}$	$\frac{t}{T}$	T, in.	Type of Nozzle	T <sub>P</sub> in.	D <sub>P</sub> in.	In-Plane	Out-of-Plane	$k = \theta / (Md) / EI_n$
(3)	12x 4	68	.35	.88	.188	Saddle Reinforced	.368	7-5/16	4.5	18.	
(4)	24x 4	76	.18	.76	.312	Fabricated, unreinforced	--	--	17.	31.	
	24x12		.53	.80		"	--	--	8.4	44.	
	24x24		1.00	1.00		"	--	--	17.	16.	
(5)	24x 4		.18	.76		Saddle Reinforced	.344	9-5/8	1.5	15.	
	24x 8		.53	.80		"	.437	17-1/4	2.1	22.	
	24x12		1.00	.80		"	.437	25-1/2	2.8	12.	
	24x 4		.18	.76		Pad Reinforced	.375	7-3/4	4.7	20.	
	24x 8		.35	.80		"	.375	15-3/4	3.6	28.	
	24x12		.53	.80		"	.375	25	5.6	18.	
(6)	16x 6	31	.41	.56	.5	Drawn Outlet	--	--	2.7	11.8	
	16x 6	31	.41	.56	.5	Pad Reinforced	.500	12-1/8	1.5	8.4	
	16x 6	31	.41	.56	.5	Saddle Reinforced	.500	11-5/8	1.3	3.0	
	16x 6	15	.42	.28	1.0	Drawn Outlet	--	--	1.1	1.7	
(7)	48x 6	78	.13	.45	.625	Fabricated, unreinforced	--	--	5.6	11.	
	48x 6	78	.13	.45	.625	Pad Reinforced	.625	10-1/2	1.6	10.	
(8)	20x 6	19	.33	.43	1.0	Drawn Outlet (L)	--	--	1.1	2.3	
	20x12	19	.64	.69	1.0	Drawn Outlet (D)	--	--	1.8	3.5	
	20x12	19	.64	.69	1.0	Fabricated, unreinforced (R)	--	--	1.8	--	
(9)	36x 4	93	.12	.42	.375	Fabricated, unreinforced	--	--	4.0	10.	
	36x 6	93	.18	.75	.375	"	--	--	8.0	27.	

T<sub>P</sub> = thickness of pad or saddle  
D<sub>P</sub> = diameter of pad or saddle

References (7) and (9) provide measurements of the local displacement of the cylindrical shell near the nozzle when moments were applied to the nozzle. With some extrapolation of these displacements to the edge of the nozzle, and assuming the nozzle itself has negligible displacements along its axis, these measurements can be converted to the rotation  $\theta$  by  $\theta = \delta / r$ , where  $\delta$  = measured shell displacement at the edge of the nozzle and  $r$  = radius of the nozzle.

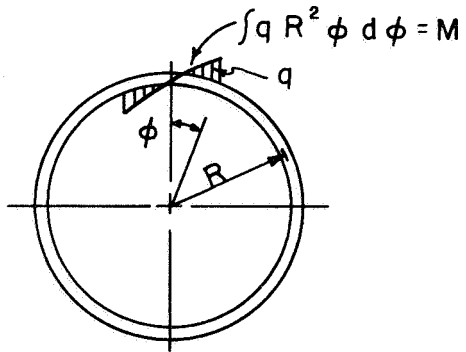
The load applied, in Reference (7), (8), and (9) tests, was a pure moment. In the other references, the load applied was a force, however, the point of load application was sufficiently remote from the nozzle-shell juncture so that the forces at the juncture were negligible compared to the moments at the juncture.

The last two columns of Table 1 summarize the available test data on flexibility or nozzles in cylinders in the form of flexibility factors.

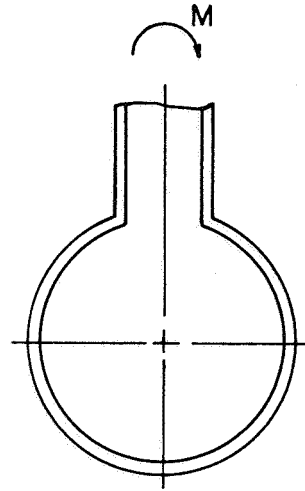
THEORY

An adequate theory for nozzles in cylinders with bending loads applied to the nozzle is not available at this time. Dr. A. C. Eringen's analysis is understood to be complete, however, the theory must be programmed for a digital computer to obtain numerical results and this programming is not completed.

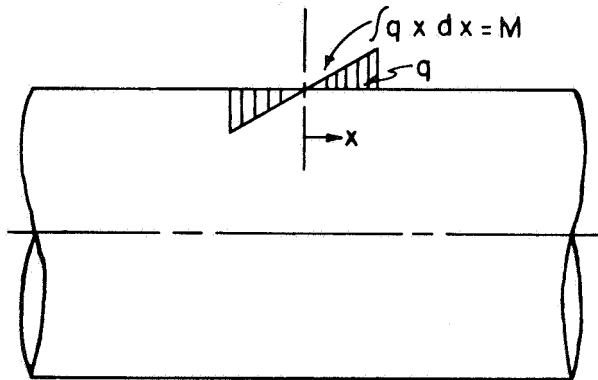
In view of the similar results obtained for nozzles in spheres as compared to nozzles in cylinders for internal pressure loading (see Phase Report No. 5), some guidance may be obtained from the theory for nozzles in spheres with moment loading. Also, Bijlaard's<sup>(2)</sup> theory for a distributed load on a cylinder may provide guidance. Figure 2 shows Bijlaard's loadings on the surface of a cylinder and the analogous moment loading of a nozzle in a cylinder. To the extent that the nozzle stiffness replaces the stiffness of the cut-out, Bijlaard's theory might reasonably predict the flexibility on the nozzle.



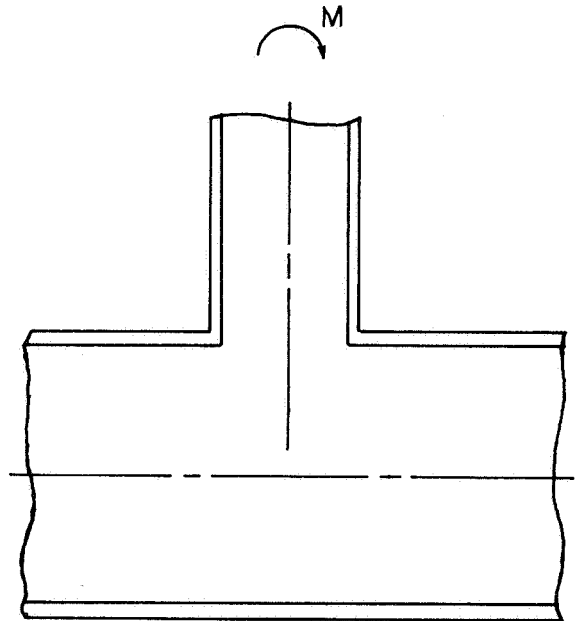
Bijlaard's Assumptions



Out-of Plane Bending



Bijlaard's Assumptions



In-Plane Bending

FIGURE 2. COMPARISON OF BIJLAARD'S ASSUMPTIONS WITH ACTUAL GEOMETRY OF NOZZLES IN CYLINDRICAL SHELLS WITH MOMENT LOADING

COMPARISON OF TEST DATA WITH BIJLAARD'S THEORY

Test data for uniform-wall\* test models is plotted in Figures 3 and 4. The test data is in qualitative agreement with Bijlaard's theory in that:

1. The flexibility factor increases as  $D/T$  increases,
2. The flexibility factors are larger for out-of-plane bending than for in-plane bending,
3. There appears to be a maximum in the value of  $k/(t/T)$  as a function of  $d/D$ ; at  $d/D$  in the general range of 0.2 to 0.5, depending upon  $D/T$  and the bending plane.

In a quantitative sense, Bijlaard's theory consistently over-predicts the actual flexibility factors as compared to available test data.

---

\* The term "unreinforced" is used here as referring to test models which consisted of a uniform-wall nozzle welded into a uniform-wall cylinder without local reinforcing other than that provided by the fillet welds. This includes the "drawn-outlet" models of Table 1.

Bijlaard Theory —————

Symbol	D/T	Ref. No.
○	93	9
□	78	7
△	76	4
x	31	6
+	19	8
●	15	6

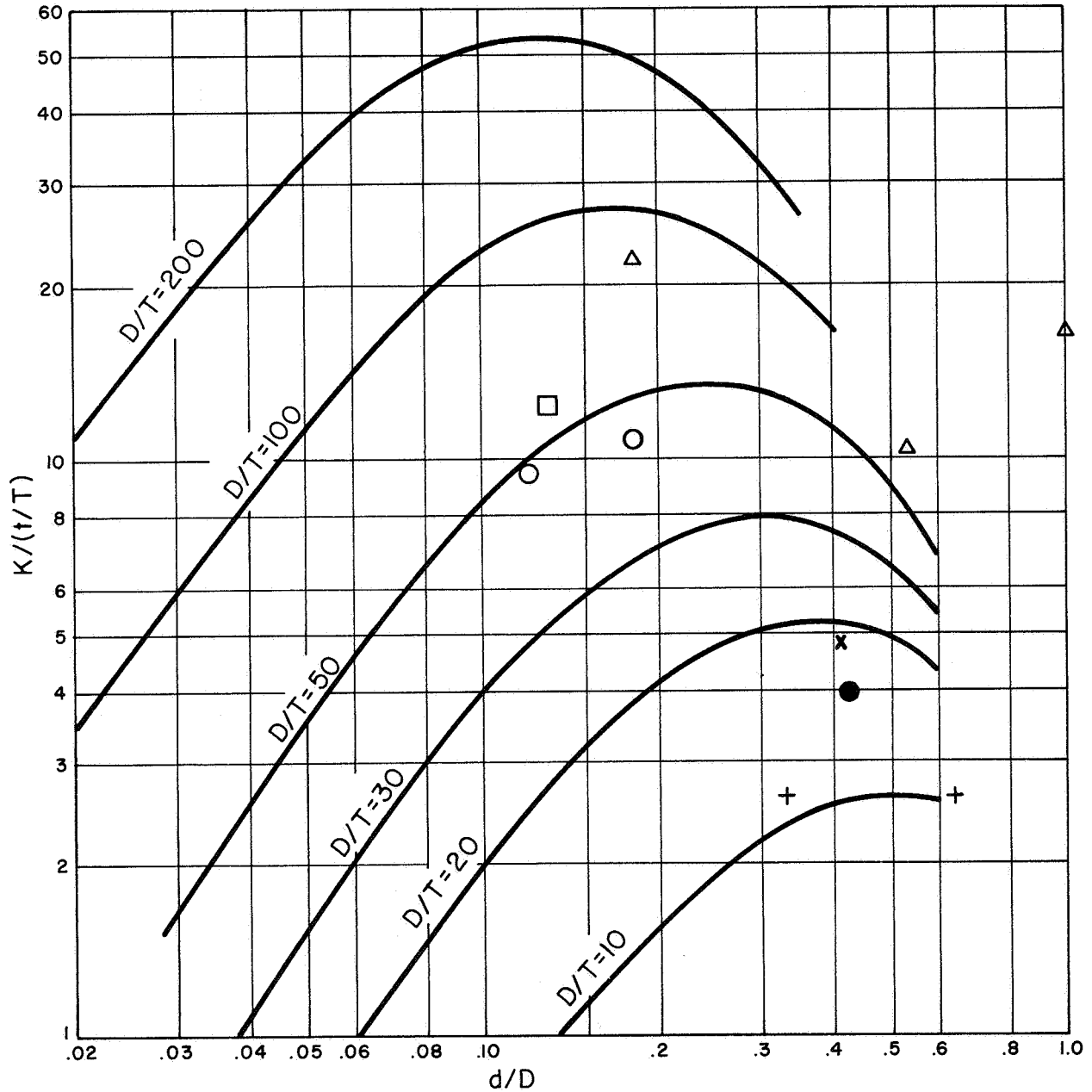


FIGURE 3. COMPARISON OF BIJLAARD THEORY AND TEST DATA, FLEXIBILITY FACTORS FOR IN-PLANE BENDING

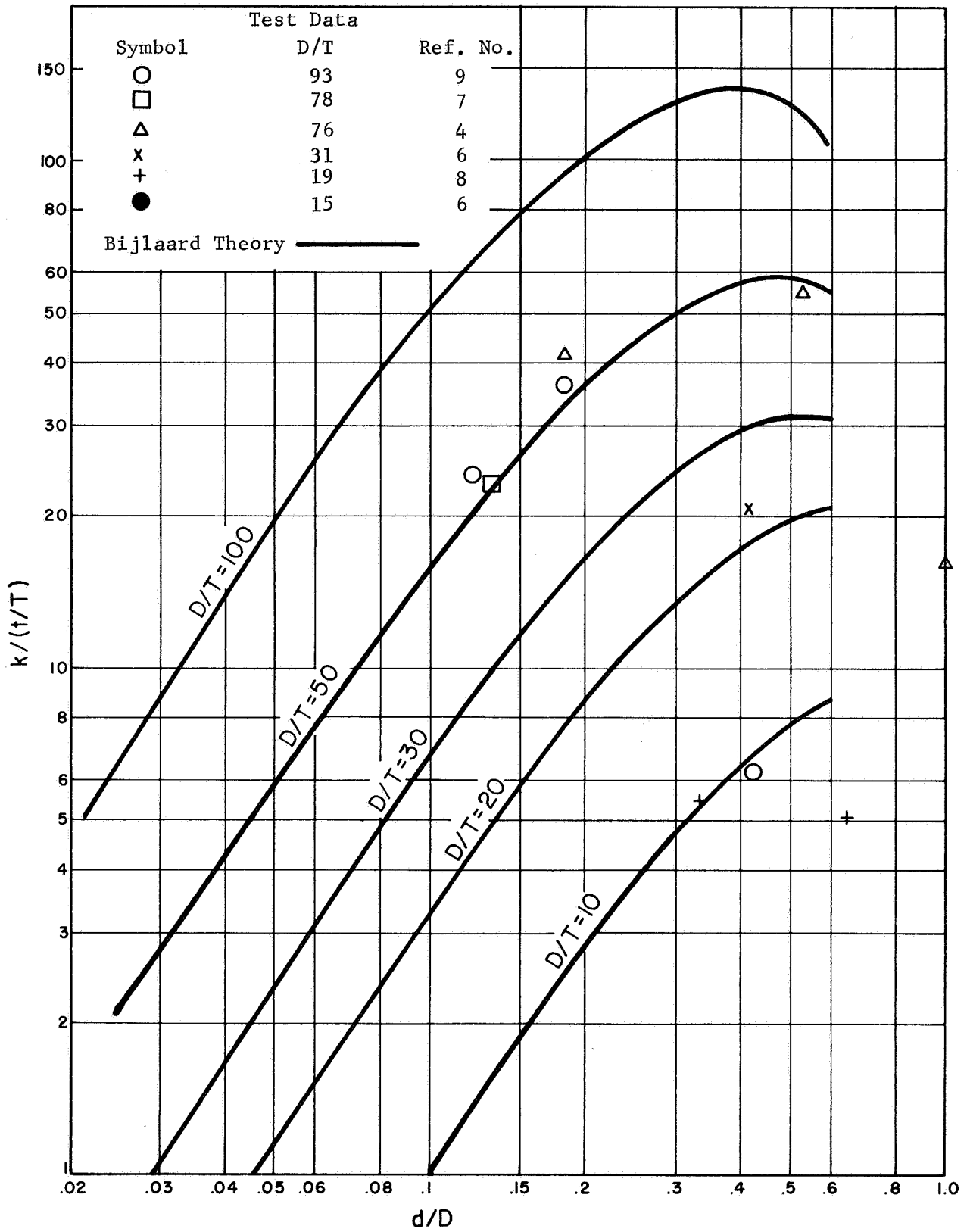


FIGURE 4. COMPARISON OF BIJLAARD THEORY AND TEST DATA, FLEXIBILITY FACTORS FOR OUT-OF-PLANE BENDING

EMPIRICAL EQUATION

While the available test data represents a rather motley array of sizes, dimensions, and types of reinforcing, in conjunction with Bijlaard's analysis certain consistent trends in the data for small  $d/D$  appear. Bijlaard's theory indicates that, for small  $d/D$ ,  $k/(t/T)$  is roughly proportional to  $(D/T)^{3/2}$  and is also roughly proportional to  $d/D$ . A simple equation that fits the data for uniform-wall test models is:

$$k = C (D/T)^{3/2} (t/T)(d/D) \quad (2)$$

$$C = 0.09 \text{ for in-plane bending}$$

$$C = 0.27 \text{ for out-of-plane bending}$$

The test models with saddle or pad reinforcing can be included in Equation (2) if the run thickness  $T$  in the  $(D/T)^{3/2}$  term is replaced by an equivalent thickness,  $T_e$ .  $T_e$  is defined as:

$$T_e = T + \frac{A}{d} \text{ for in-plane bending, in.}$$

$$T_e = T + \frac{A}{2d} \text{ for out-of-plane bending, in.}$$

$A$  = cross sectional area of reinforcing (in the plane containing the nozzle and cylinder axes) provided by the pad or saddle,  $\text{in}^2$ .

The empirical Equation (2) is compared with the test data of Table 1 (for all models with  $d/D$  less than 0.5), in Figures 5 and 6. As



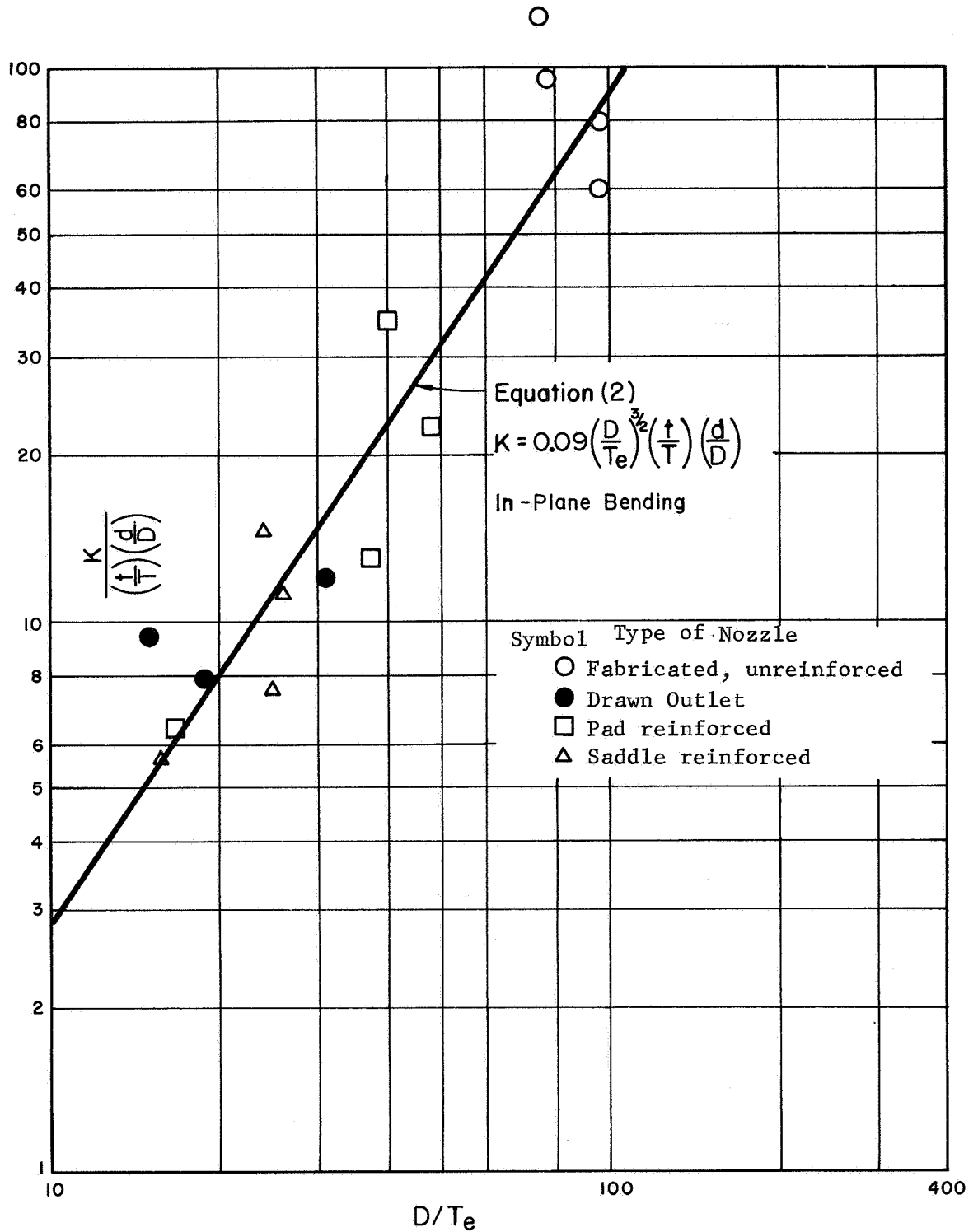


FIGURE 5. COMPARISON OF TEST DATA WITH EQUATION (2), FLEXIBILITY FACTORS FOR IN-PLANE BENDING

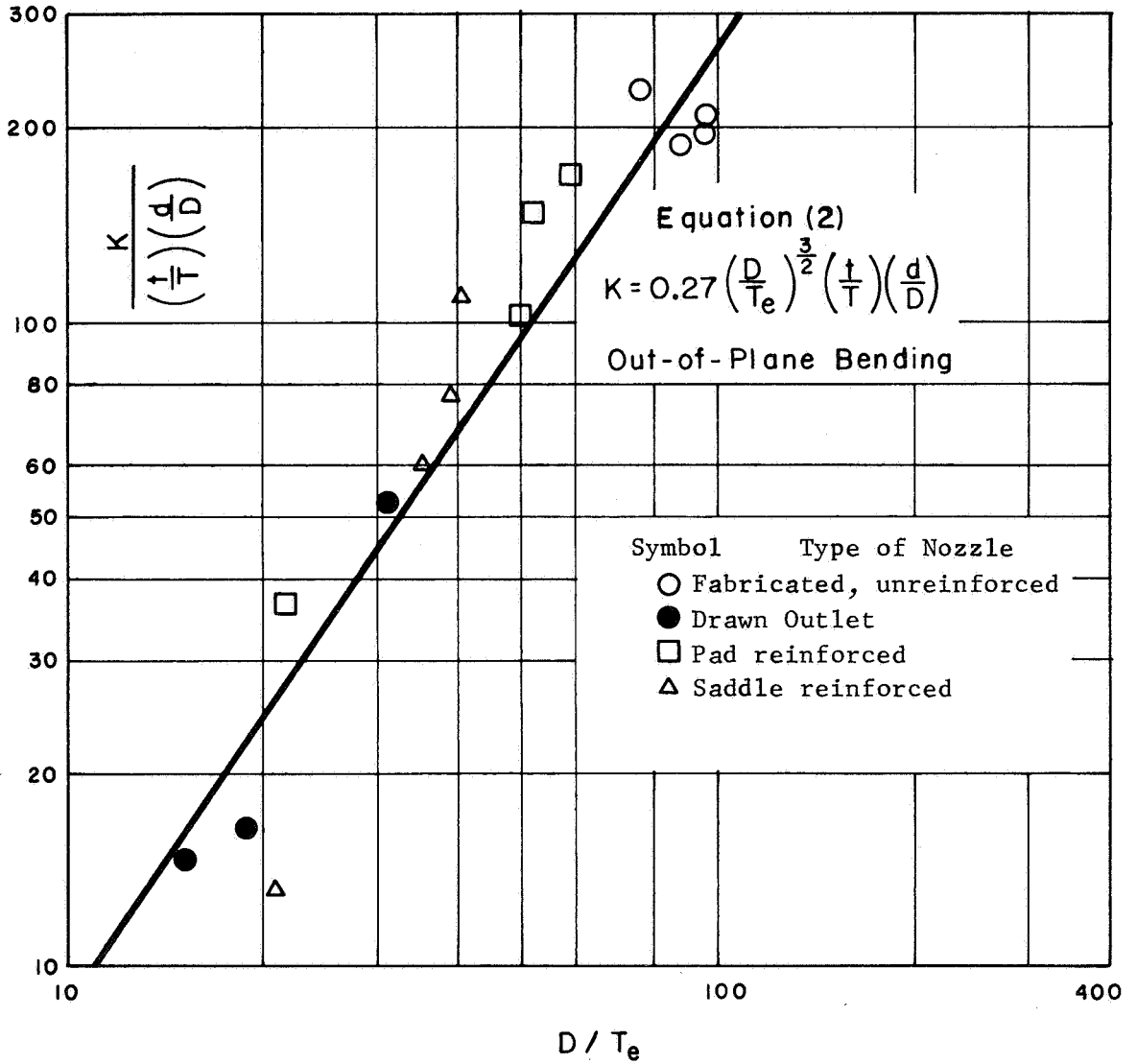


FIGURE 6. COMPARISON OF TEST DATA WITH EQUATION (2), FLEXIBILITY FACTORS FOR OUT-OF-PLANE BENDING

can be seen in these Figures, Equation (2) is a fairly good average of the test data and, considering the variety of test data involved, the scatter is fairly small.

Equation (2) is compared with Bijlaard's theory for distributed loads on a cylinder in figures 7 and 8. As necessary to conform with the test data, Equation (2) gives lower values than Bijlaard's theory but otherwise has the same trends for small  $d/D$  as exhibited by the theory.

Equation (2) is compared with flexibility factors for nozzles in spheres in Figures 9 through 12. The dashed lines in Figures 9 through 12 are from Phase Report No. 3, "Flexibility of Nozzles in Spherical Shells". For most of the dimensional parameters covered in Figures 9 through 12, the flexibility of a nozzle in a sphere is bracketed by flexibility factors for in-plane and out-of-plane bending of a nozzle in a cylinder; i.e., the flexibility of a nozzle in a cylinder with in-plane bending is lower than for a nozzle in a sphere while the flexibility of a nozzle in a cylinder with out-of-plane is higher than for a nozzle in a sphere.

- - - - Bijlaard Theory, distributed load on cylinder  
 ——— Empirical Equation:  $k = 0.09 \left(\frac{D}{T}\right)^{3/2} \left(\frac{t}{T}\right) \left(\frac{d}{D}\right)$   
 (for  $d/D < 1/3$ )

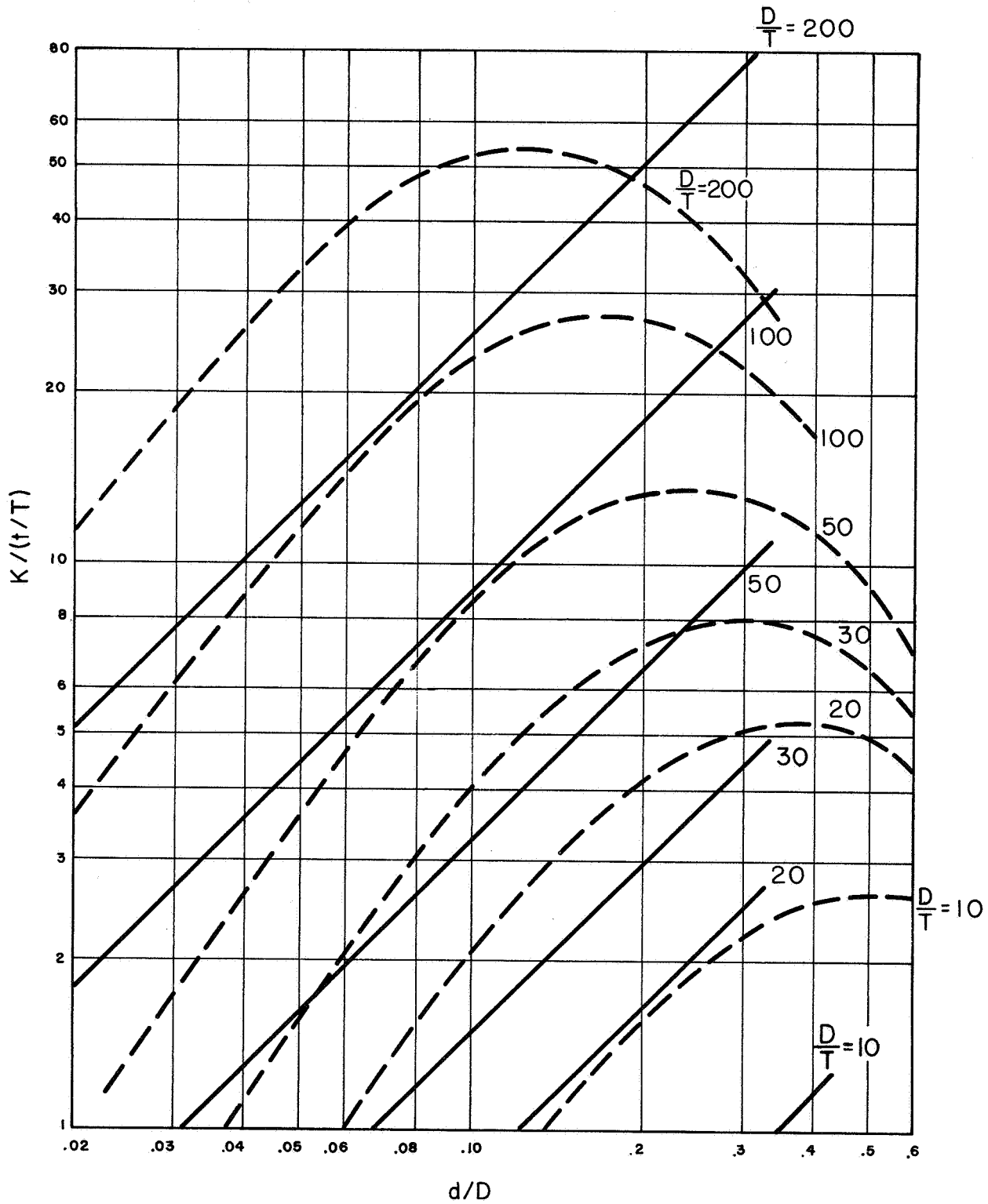


FIGURE 7. COMPARISON OF IN-PLANE FLEXIBILITY FACTORS; EQUATION (2) WITH BIJLAARD THEORY FOR DISTRIBUTED LOAD ON A CYLINDER

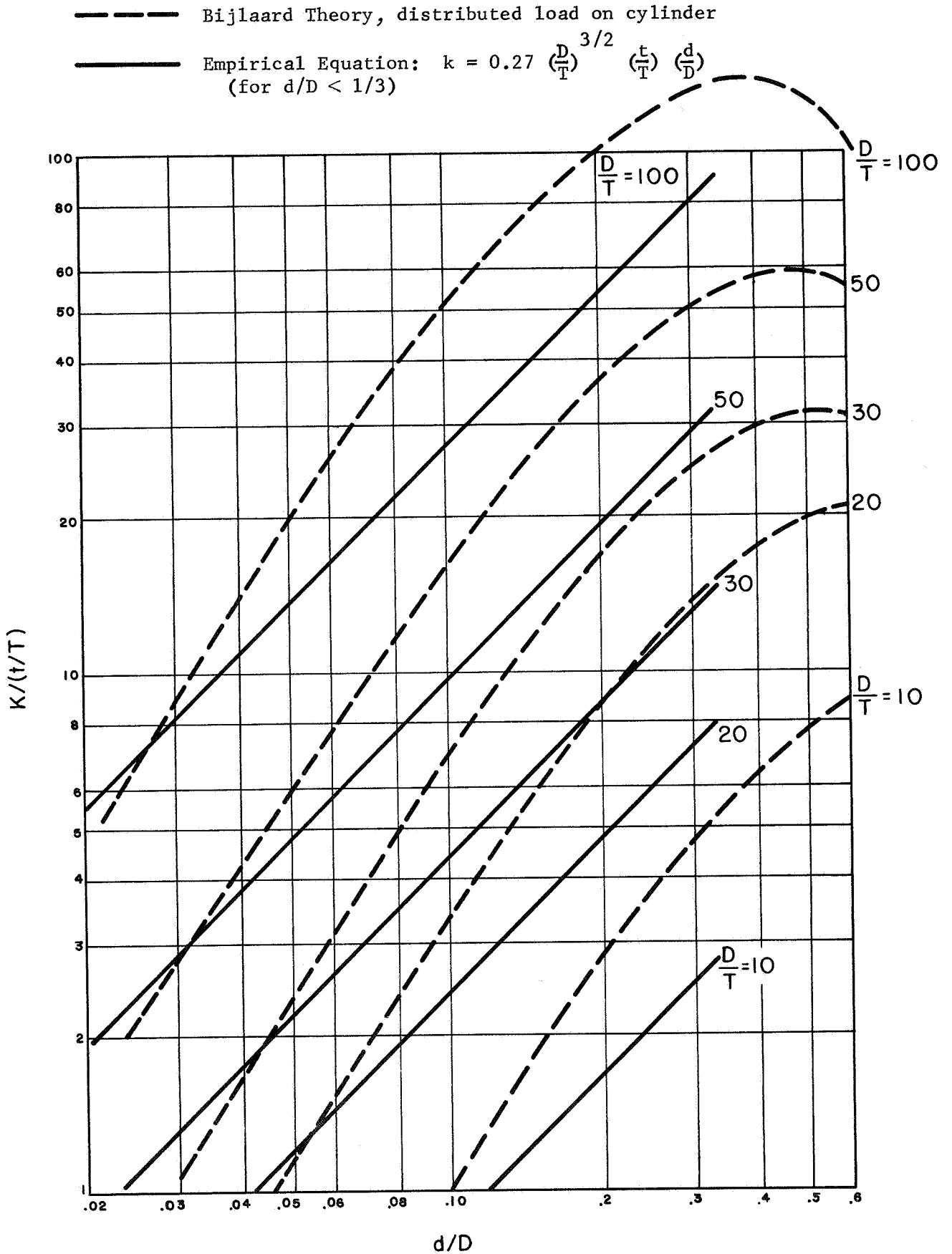


FIGURE 8. COMPARISON OF OUT-OF-PLANE FLEXIBILITY FACTORS; EQUATION (2) WITH BIJLAARD THEORY FOR DISTRIBUTED LOAD ON A CYLINDER

— In-Plane,  $c = 0.09$       Empirical Equation:  $k = c \left(\frac{D}{T}\right)^{3/2} \left(\frac{t}{T}\right) \left(\frac{d}{D}\right)$   
 - - - Out-of-Plane,  $c = 0.27$       (for  $d/D < 1/3$ )  
 - - - Nozzle in a Sphere

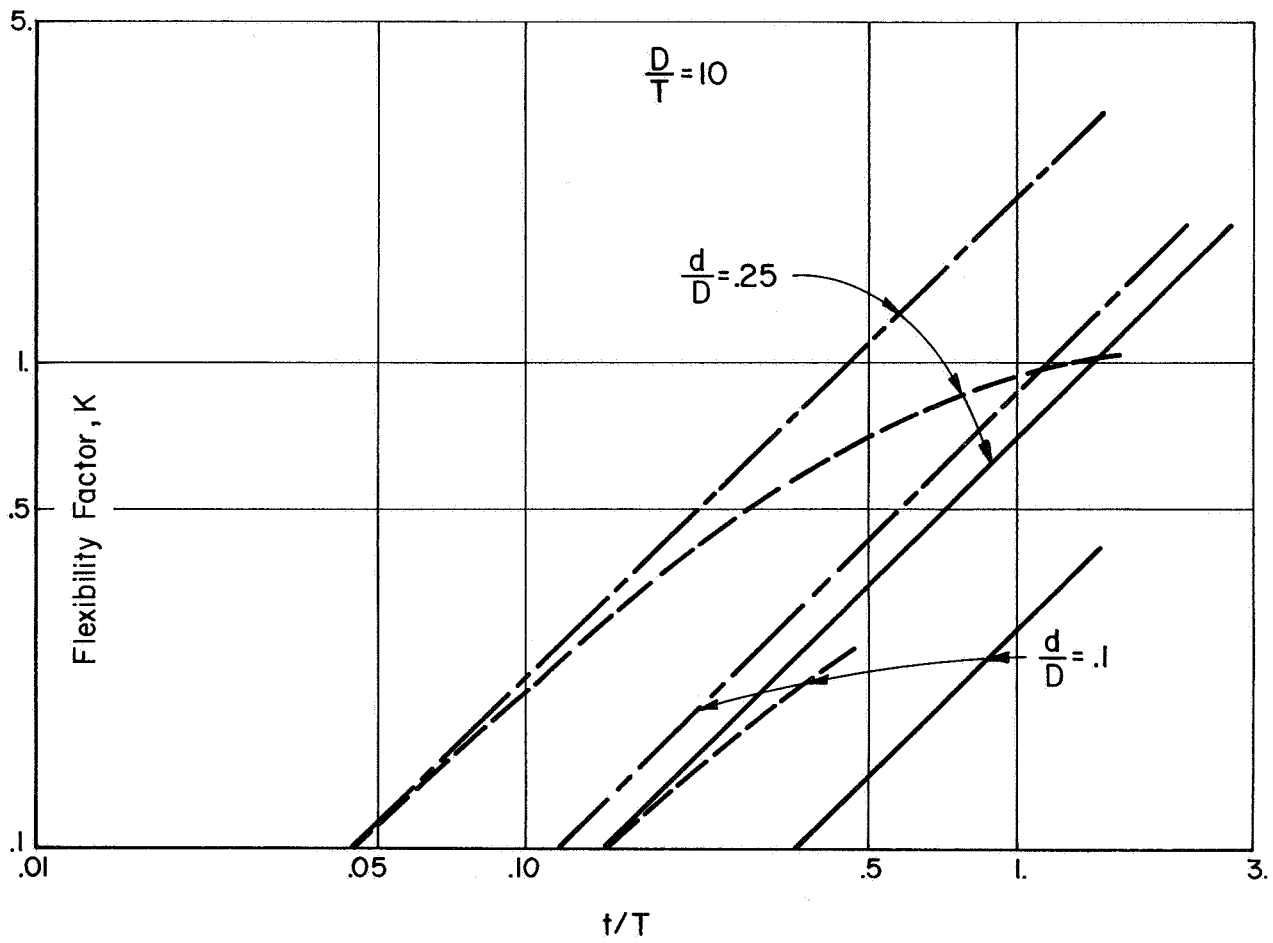


FIGURE 9. COMPARISON OF FLEXIBILITY FACTORS, EQUATION (2) WITH THEORY FOR A NOZZLE IN A SPHERE,  $D/T = 10$ .

————— In-Plane,  $c = 0.09$       Empirical Equation:  $k = c \left(\frac{D}{T}\right)^{3/2} \left(\frac{t}{T}\right) \left(\frac{d}{D}\right)$   
 - - - - - Out-of-Plane,  $c = 0.27$       (for  $d/D < 1/3$ )  
 - - - - - Nozzle in a Sphere

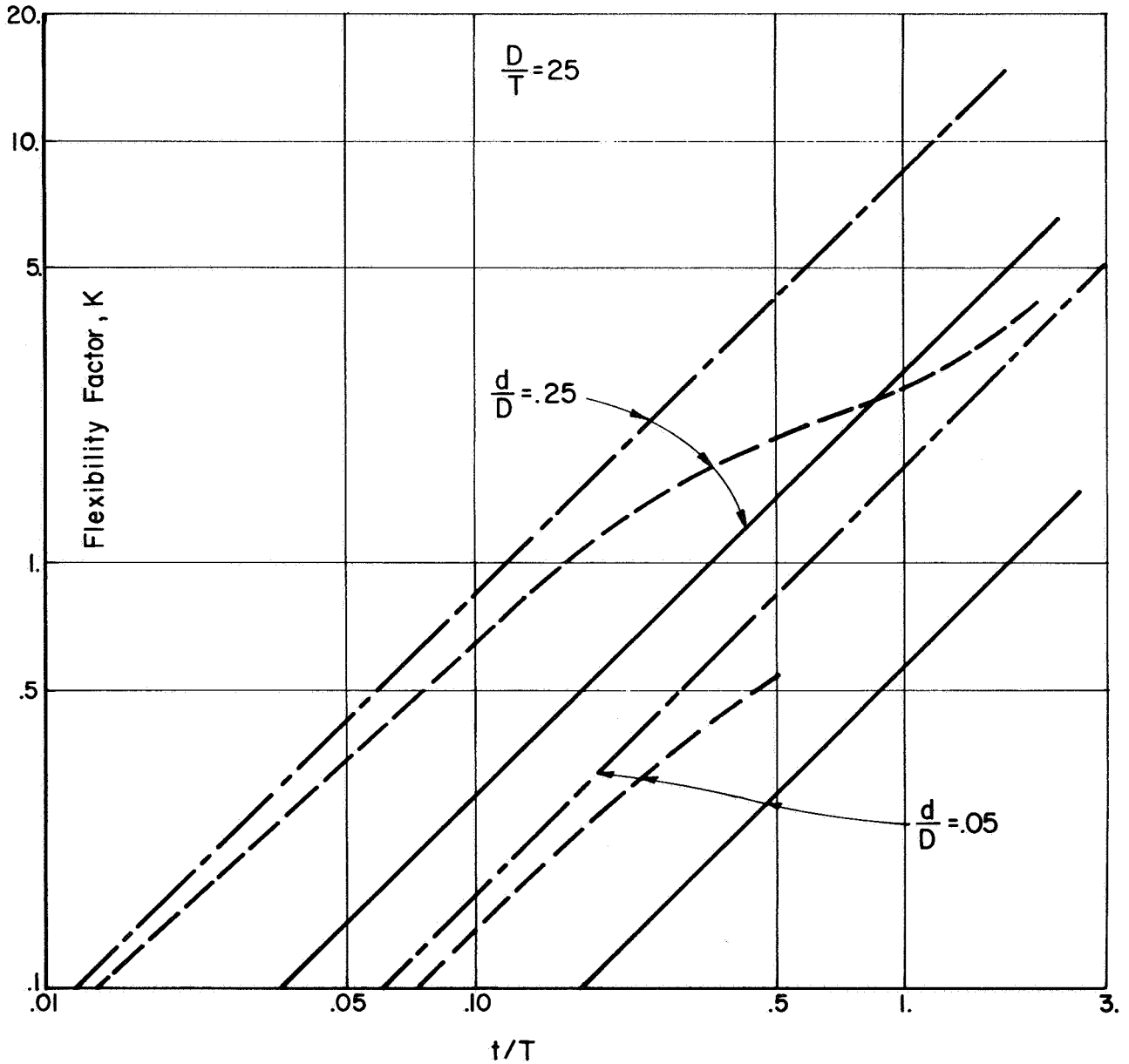


FIGURE 10. COMPARISON OF FLEXIBILITY FACTORS, EQUATION (2) WITH THEORY FOR A NOZZLE IN A SPHERE,  $\frac{D}{T} = 25$ .

— In-Plane,  $c = 0.09$

Empirical Equation:  $k = c \left(\frac{D}{T}\right)^{3/2} \left(\frac{t}{T}\right) \left(\frac{d}{D}\right)$

- - - Out-of-Plane,  $c = 0.27$

(for  $d/D < 1/3$ )

- · - · - Nozzle in a Sphere

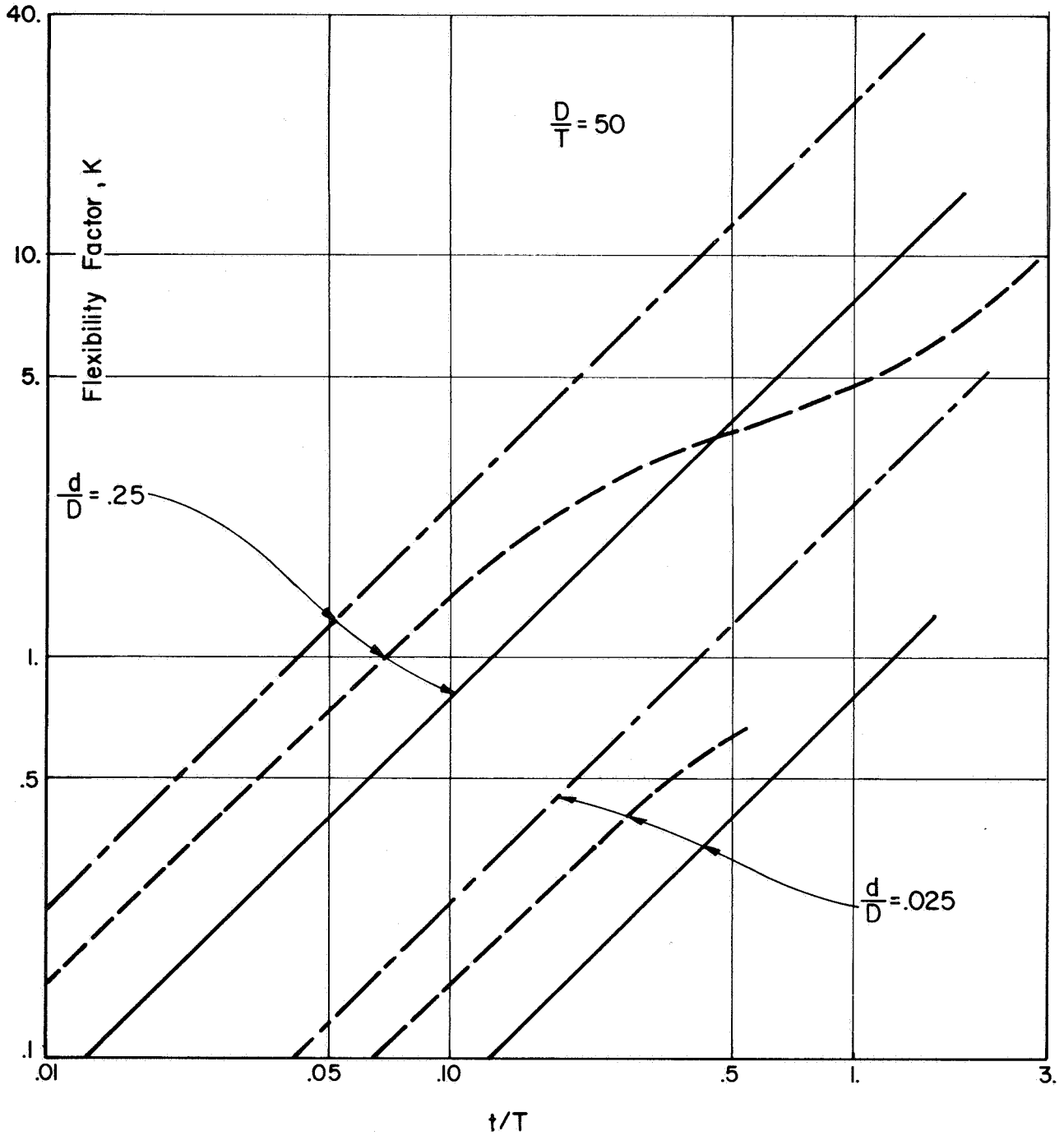


FIGURE 11. COMPARISON OF FLEXIBILITY FACTORS, EQUATION (2) WITH THEORY FOR A NOZZLE IN A SPHERE,  $D/T = 50$ .



————— In-Plane,  $c = 0.09$       Empirical Equation:  $k = c \left(\frac{D}{T}\right)^{3/2} \left(\frac{t}{T}\right) \left(\frac{d}{D}\right)$   
 - - - - - Out-of-Plane,  $c = 0.27$       (for  $d/D < 1/3$ )  
 - - - - - Nozzle in a Sphere

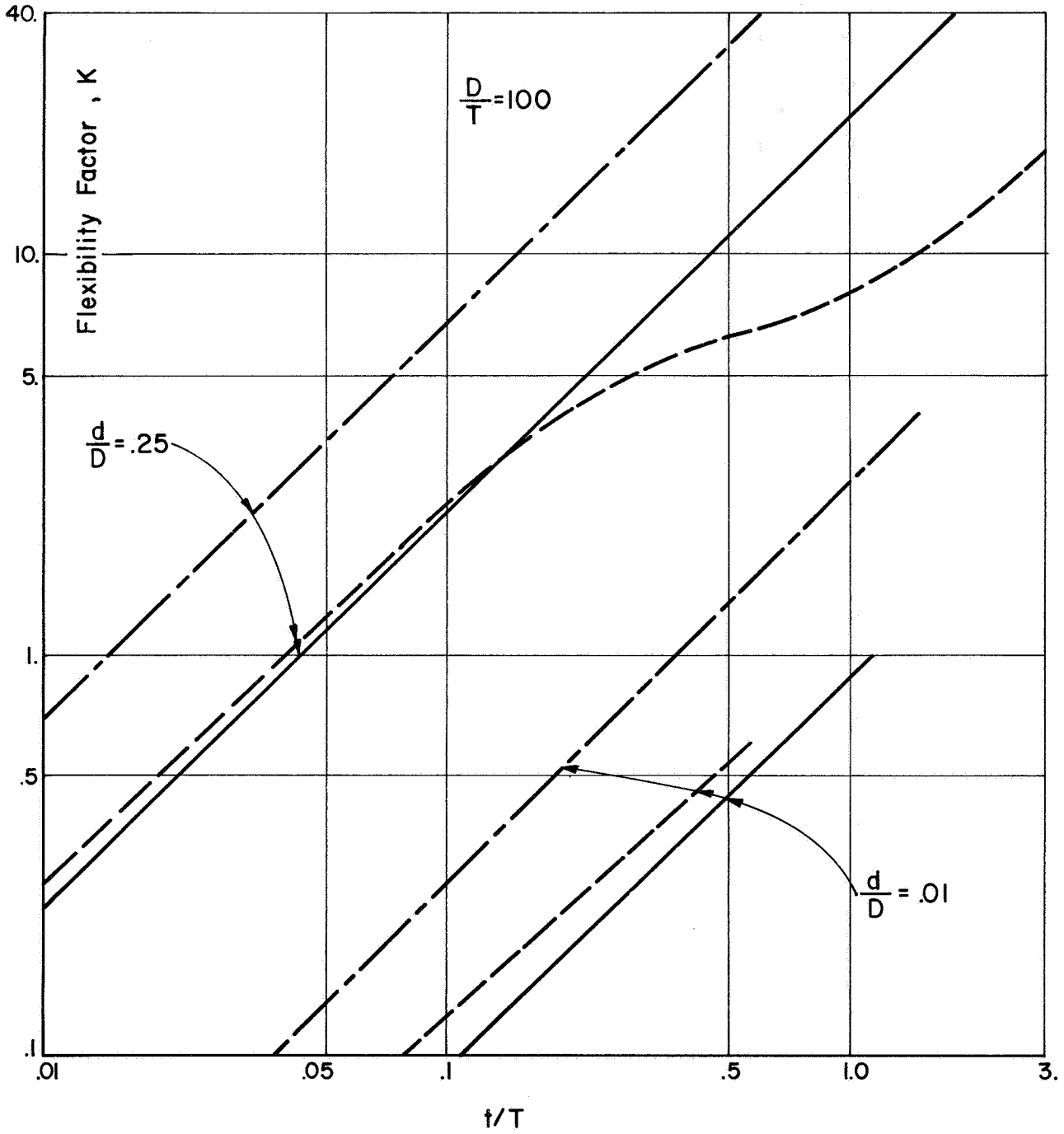


FIGURE 12. COMPARISON OF FLEXIBILITY FACTORS, EQUATION (2) WITH THEORY FOR A NOZZLE IN A SPHERE,  $D/T = 100$ .

SIGNIFICANCE OF FLEXIBILITY OF NOZZLES

Phase Report No. 3, "Flexibility of Nozzles in Spherical Shells" shows that in "tight" piping systems, the moment on a nozzle may be over-estimated by a factor of six or more if the flexibility of the nozzle is ignored. Table 2 shows calculated results\* for a "tight" piping system involving out-of-plane bending of a nozzle. For these systems, the moment at the nozzle could be over-estimated by a factor of 12 if the nozzle flexibility factor is ignored. These examples are, of course, for extremely tight systems and illustrate, more-or-less, the maximum errors introduced by ignoring the nozzle flexibility.

(10)

Stevens, Groth, and Bell illustrate the affect of nozzle flexibility for two sample piping systems. The two examples given involve flexibility of nozzles in heads and in cylinders. The flexibility for a nozzle in a head used in the examples is based on Bijlaard's theory; which is the same as given in Phase Report No. 3. Flexibility of a nozzle in cylinders is also based on Bijlaard's theory; for the particular parameters and bending plane involved in the examples, Bijlaard's theory and Equation (2) are in fairly close agreement. With respect to moments at the nozzles, the results are:

	Example 1	Example 2
	$(M_n)_o / (M_n)_k$	$(M_n)_o / (M_n)_k$
Nozzle in cylinder	4.35	29.1
Nozzle in head	1.44	--

---

\* Calculations are based on a k-factor of 11.8 taken directly from test data. By Equation (2),  $k = 10.7$ .

where  $(M_n)_o$  = calculated moment at nozzle with nozzle flexibility factor ignored.

$(M_n)_k$  = calculated moment at nozzle with nozzle flexibility factor included.

Example 1 represents a comparatively "loose" piping system, while Example 2 represents a "tight" piping system. For Example 2, the actual moment of the nozzle would theoretically be over-estimated, ignoring the flexibility of the nozzle, by a factor of 29. It might be noted that the examples given by Stevens, et al, involved thin wall vessels ( $D/T \sim 215$ ) and fairly large nozzles ( $d/D \sim .25$ ). The flexibility factor for the nozzle is around 175. The pipe was 36 inches O.D.; therefore, the equivalent length of pipe (lumped at the nozzle) was about 520 ft. The total length of the pipe in the piping system was about 31 ft, hence the pronounced effect of the nozzle flexibility.

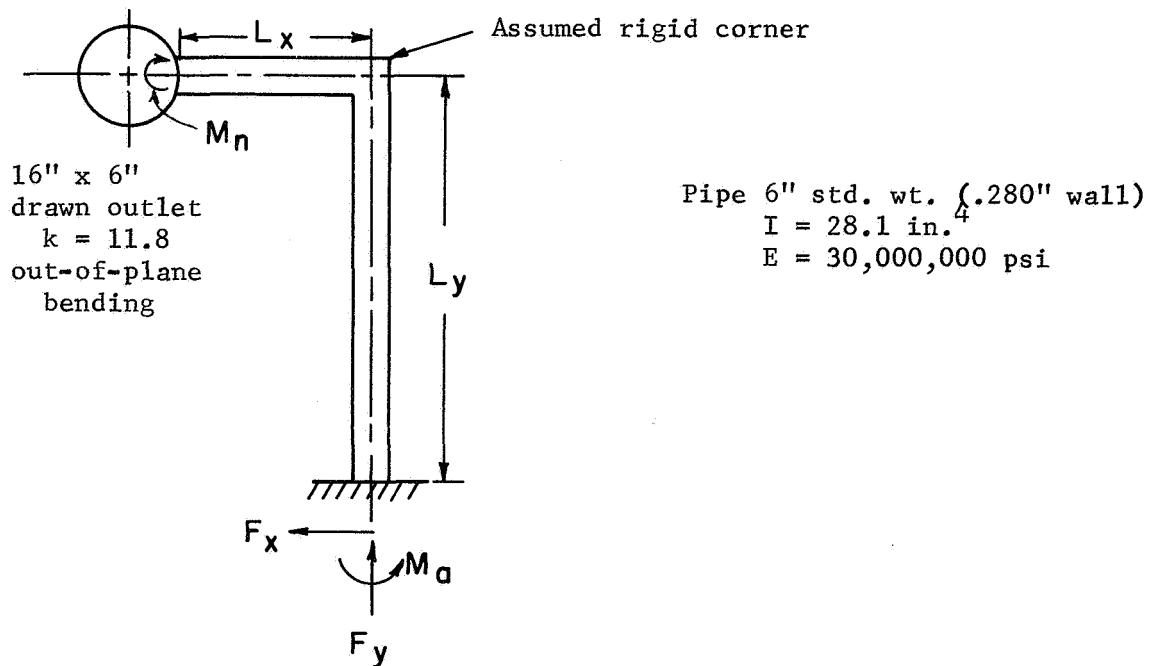
TABLE 2. EFFECT OF THE FLEXIBILITY OF A NOZZLE ON THE CALCULATED END FORCES OF A PIPING SYSTEM

$L_x$ , in.	$L_y$ , in.	$\frac{(F_x)_o}{(F_x)_k}$	$\frac{(F_y)_o}{(F_y)_k}$	$\frac{(M_a)_o}{(M_a)_k}$	$\frac{(M_n)_o}{(M_n)_k}$
120	24	1.06	1.54	1.02	3.50
96	24	1.07	1.60	1.03	4.08
72	24	1.09	1.68	1.04	5.07
48	24	1.12	1.85	1.06	6.97
24	24	1.24	2.45	1.15	12.4
24	48	1.39	3.25	1.32	11.8
24	72	1.45	3.77	1.40	11.6
24	96	1.47	4.17	1.44	11.4
24	120	1.47	4.50	1.45	11.3

$(F_x)_o = F_x$  calculated with flexibility of nozzle ignored

$(F_x)_k = F_x$  calculated with flexibility of nozzle included

Other force ratios are analogous to  $(F_x)_o / (F_x)_k$



16" pipe is assumed to be anchored sufficiently close to the 6" branch so that torsional displacements of the 16" run pipe are negligible.

REFERENCES

- (1) Bijlaard, P. P., "Stresses in a Spherical Vessel from Radial Loads Acting on a Pipe"; "Stresses in a Spherical Vessel from External Moments Acting on a Pipe"; "Influence of a Reinforcing Pad in the Stresses in a Spherical Vessel Under Local Loading", Welding Research Council Bulletin No. 49 (April, 1959).
- (2) Bijlaard, P. P., "Stresses from Local Loadings in Cylindrical Pressure Vessels", ASME Transactions (August, 1955).
- (3) Rodabaugh, E. C., "Cyclic Bending Tests of a Half-Scale Model of an 8" x 24" Saddle Reinforced Branch Connection", Tube Turns (Division of Chemetron) Report No. 8.011, Louisville, Kentucky (1953).
- (4) Jackson, L. R., et al. "Stresses in Unreinforced Branch Connections", Battelle Memorial Institute, Columbus, Ohio (September, 1953).
- (5) McClure, G. M., Sweeney, J. A. and Gross, H. J., "Investigation of Stresses in Pipeline Branch Connections", Battelle Memorial Institute, Columbus, Ohio (March, 1956).
- (6) Mills, E. J., Atterbury, T. J., and McClure, G. M., "Study of Effects of Cyclic Bending Loads on Performance of Branch Connections", Battelle Memorial Institute, Columbus, Ohio (May, 1962).
- (7) Cranch, E. T., "An Experimental Investigation of Stresses in the Neighborhood of Attachments to a Cylindrical Shell", Welding Research Council Bulletin No. 60 (May, 1960).
- (8) Pickett, A. G., et al, "Low Cycle Fatigue Testing of One-Half Scale Model Pressure Vessels", Progress Reports 9 through 12, Southwest Research Institute, San Antonio, Texas (July, 1964 through January, 1965).
- (9) Mehringer, F. J., and Cooper, W. E., "Experimental Determinations of Stresses in the Vicinity of Pipe Appendages to a Cylindrical Shell", S.E.S.A. Proceedings, XIV, No. 2.
- (10) Stevens, P. G., Groth, V. J., and Bell, R. B., "Vessel Nozzles and Piping Flexibility Analysis", Trans. ASME, Series B, 84 (1962).